

UNCLASSIFIED

AD NUMBER
ADB089975
NEW LIMITATION CHANGE
TO Approved for public release, distribution unlimited
FROM Distribution authorized to U.S. Gov't. agencies and their contractors; Critical Technology; MAY 1984. Other requests shall be referred to US Army Medical Research Institute of Chemical Defense, Aberdeen Proving Ground, MD.
AUTHORITY
USAMRICD ltr, 30 Nov 1994

THIS PAGE IS UNCLASSIFIED

AD-B089 975

Proceedings
of the
Fourth Annual Chemical
Defense Bioscience Review

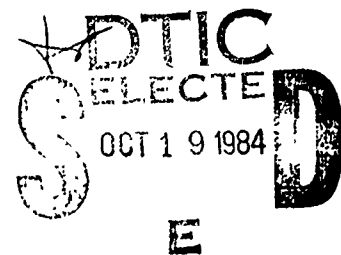
US Army
Medical Research and Development
Command



DTIC FILE COPY

US Army Medical Research
Institute of Chemical Defense

Aberdeen Proving Ground, Maryland 21010
30 May - 1 June 1984



84 10 16 14 5

FOREWORD

In conducting the research described in these proceedings, the investigators adhered to the "Guide for the Care and Use of Laboratory Animals," prepared by the Committee on Care and Use of Laboratory Animals of the Institute of Laboratory Animal Resources, National Research Council.

The views expressed in these proceedings are those of the authors and do not reflect official policy or position of the Department of the Army, Department of Defense, or the U.S. Government.

Distribution Statement C. Distribution limited to US Government agencies and their contractors; ~~proprietary information~~, May 1981. Other requests for this document shall be referred to: Commander, US Army Medical Research Institute of Chemical Defense, Aberdeen Proving Ground, MD 21010-5425. **CT**

DISPOSITION INSTRUCTIONS

Destroy this report when no longer needed. Do not return to the originator.

Unclassified

SECURITY CLASSIFICATION OF THIS PAGE (When Data Entered)

REPORT DOCUMENTATION PAGE		READ INSTRUCTIONS BEFORE COMPLETING FORM
1. REPORT NUMBER USAMRICD-P-88-84	2. GOVT ACCESSION NO. AD-B089 97	3. RECIPIENT'S CATALOG NUMBER
4. TITLE (and Subtitle) Fourth Annual Chemical Defense Bioscience Review	5. TYPE OF REPORT & PERIOD COVERED Review Proceedings 30 May-1 June, 1984	
7. AUTHOR(s) COL Richard E. Lindstrom, Editor	6. PERFORMING ORG. REPORT NUMBER	
9. PERFORMING ORGANIZATION NAME AND ADDRESS US Army Medical Research Institute of Chemical Defense, Bldg. E3100, APG, MD 21010	10. PROGRAM ELEMENT, PROJECT, TASK AREA & WORK UNIT NUMBERS 3M161102B-S11-00-000 3M162734A-875-00-000 3M463751D-993-00-000	
11. CONTROLLING OFFICE NAME AND ADDRESS US Army Medical Research and Development Command Ft. Detrick, MD 21701	12. REPORT DATE 1 June 1984	
14. MONITORING AGENCY NAME & ADDRESS (if different from Controlling Office) N/A	13. NUMBER OF PAGES XXX	
	15. SECURITY CLASS. (of this report) Unclassified	
	15a. DECLASSIFICATION/DOWNGRADING SCHEDULE	
16. DISTRIBUTION STATEMENT (of this Report) Distribution C: Distribution limited to US Government agencies and their contractors; proprietary information , May 1984. Other requests for this document shall be referred to: Commander, US Army Medical Research Institute of Chemical Defense, Aberdeen Proving Ground, MD 21010-5425.		
17. DISTRIBUTION STATEMENT (of the abstract entered in Block 20, if different from Report) Same as above.		
18. SUPPLEMENTARY NOTES N/A		
19. KEY WORDS (Continue on reverse side if necessary and identify by block number) Nerve agents; soman intoxication; cyanide intoxication; animal models; chemical casualties; human cyanide poisoning; chemoprophylaxis; blood-brain barrier; monoclonal antibodies; acetylcholinesterase; acetylcholine receptor; chemical warfare agents; pyridostigmine; <i>nerve agents, soman, cyanide, animal models, chemical casualties, human cyanide poisoning, chemoprophylaxis, blood-brain barrier, monoclonal antibodies, acetylcholinesterase, acetylcholine receptor, chemical warfare agents, pyridostigmine, medical research, drug research.</i>		
20. ABSTRACT (Continue on reverse side if necessary and identify by block number) The Fourth Annual Chemical Defense Bioscience Review was held at Aberdeen Proving Ground, Maryland on 30 May-1 June, 1984. The objective of this review was to present selected research findings in the area of medical defense against chemical warfare agents. This document constitutes the proceedings of that review.		

Preface

The 1984 US Army Medical Research and Development Command Bioscience Review was an unqualified success. It represented the fourth consecutive year of growth in terms of both quantity and quality of the presentations. Moreover, the Review retained its status as a major forum for military/civilian scientist and government/management information interchange among the many organizations involved in medical chemical defense research in the Department of Defense.

The level of maturity of the total in-house and extramural Army medical research and development efforts in chemical defense were reflected in this review. For those involved in planning, programming, and execution of a relatively young rejuvenated medical chemical defense research program over the past five years, it was gratifying to see the enthusiasm and dedication of experienced and new scientists support or refute old concepts and find new answers that may yield real progress for a number of nagging, difficult, biomedical scientific questions.

Summaries contained herein report a fraction of the research that is now underway to address the chemical agent threat. Total in-house and contract efforts are aimed at a large array of questions, most of which were not addressed just a few years ago. It is the purpose of the annual Bioscience Review to keep the medical chemical defense workers and interested DOD managers abreast of those efforts. A new and expanded review format for 1985 is being planned to help meet the need and increased interest in this subject.

Accession For	
NTIS GRA&I	<input type="checkbox"/>
DTIC TAB	<input checked="" type="checkbox"/>
Unannounced	<input type="checkbox"/>
Justification	
By	
Distribution/	
Availability Codes	
Dist	Avail and/or Special
C-2	

Duane E. Hilmas

Duane E. Hilmas, DVM, Ph.D.
Colonel, Veterinary Corps
Commander, US Army Medical Research
Institute of Chemical Defense



Contents

Preface.	iii
Agenda	ix
I. STANDARDIZED EFFICACY MODELS	
Models for Assessing Efficacy of Therapy Compounds Against Organophosphates (OP's)	1
<i>MAJ Dennis E. Jones</i>	
Models for Assessing Efficacy of Pretreatment Compounds Against Organophosphates (OP's)	39
<i>Dr. Irwin Koplovitz</i>	
Guinea Pig Model for Correlating Efficacy with Pralidoxime Chloride (2-PAM) Plasma Levels.	71
<i>MAJ(P) Martin D. Green</i>	
Correlation of Interspecies Variation in Treatment Efficacy with Endogenous Nonspecific Agent Binding.	97
<i>Donald M. Maxwell</i>	
II. PYRIDOSTIGMINE: UPDATE ON NERVE AGENT PRETREATMENT	
Status of the Pyridostigmine Development Effort.	107
<i>LTC Gerald L. Wannarka</i>	
Oral Dose Effects of Pyridostigmine on Human Performance	121
<i>Dr. Charles Graham</i>	
Ultrastructural Pathology in Mammalian Skeletal Muscle Following Acute and Subacute Exposure to Pyridostigmine. Studies of Dose-Response and Recovery	131
<i>Dr. C. Sue Hudson</i>	
<u>In Vivo</u> and <u>In Vitro</u> Pathophysiology of a Mammalian Skeletal Muscle Following Acute and Subacute Exposure to Pyridostigmine. Studies on Muscle Contractility and Cellular Mechanisms	173
<i>Dr. Michael Adler</i>	



III. SKIN INJURY AND PROTECTION

- Noninvasive Methods for Assessing Skin Trauma. 193
Dr. Robert E. Baier
- The Use of Human Leukocytes as a Model for Studying the
Biochemical Effects of Chemical Warfare (CW) Agents 233
Dr. Henry Louis Meier
- Solution Hydrolysis and Sorption Kinetics of CW Agents
by Polymeric Resins: Evaluation for Decontamination
Applications. 259
Dr. Philip S. Hammond
- Modification of DNA by the Sulfur Mustards 281
Dr. David B. Ludlum

IV. BIOTECHNOLOGY: ADVANCES IN MOLECULAR BIOLOGY

- Molecular Cloning of Acetylcholine Receptor. 299
Dr. James W. Patrick
- Expression of Acetylcholinesterase Gene(s) in Human
Brain Tissues 313
Dr. Hermona Soreq
- Monoclonal Antibody Affinity Purification of Human
Acetylcholinesterase. 327
Dr. J. Thomas August
- Anti-Soman Monoclonal Antibodies; Structural and
Stereochemical Specificity. 335
Dr. David E. Lenz
- Design and Synthesis of Peptides Mimicking the Active Site
of a Serine Esterase with Covalent Binding to
Organophosphorus Inhibitors 355
Dr. M. Zouhair Atassi
- Molecular and Structural Bases for the Polymorphic
Forms of Acetylcholinesterase 369
Dr. Palmer Taylor

V. ORGANOPHOSPHATES: CNS TOXICITY AND THERAPEUTIC APPROACHES

- Intravenous Soman Intoxication of Awake Cats—Model
Development, Laboratory Findings, and Neuropathology. 377
LTC James B. Moe
- Pathology of Organophosphorus Compounds in Various
Animal Species: Comparison with Seizure-Related
Pathology in Man. 391
Dr. James S. Nelson
- A Study on the Effect of Soman on the Rat Blood-Brain
Barrier 395
Dr. John P. Petralli
- Brain Pathology Induced by Organophosphate Poisoning
with the Nerve Agent Soman. 407
Dr. James M. Petras
- Anticonvulsant Therapy for OP-Induced Lethality. 415
MAJ Dennis E. Jones
- Effect of Valium and Atropine on Soman-Induced
Neuropathology in Guinea Pigs 433
MAJ Allen W. Singer
- Brain Regional Energy Flow: Effects of Pretreatment
with Valium in Soman-Exposed Rats 437
Dr. Thomas L. Pazdernik

VI. CYANIDE: INTOXICATION, PROPHYLAXIS, AND THERAPY

- Toxicodynamic Basis of Cyanide Intoxication and Its
Antagonism. 451
Dr. James L. Way
- Chemoprophylaxis of Cyanide Intoxication 461
COL David E. Davidson, Jr.
- Comparative Acute Toxicity of Hydrogen Cyanide and Its Salts . . . 477
Dr. Bryan Ballantyne
- Roles of Divalent Sulfur in the Biological Detoxication
of Cyanide. 503
Dr. John L. Westley

VI. CYANIDE: INTOXICATION, PROPHYLAXIS, AND THERAPY (continued)

Interaction of Carbon Monoxide and Cyanide 513
Dr. Arthur S. Hume

Mechanisms of Cyanide Inhibition by Scavengers 525
Dr. Peter Hambright

USAMRDC Advisory Subcommittee on Medical Defense Against
Chemical Agents 541

Registrants 543

Distribution. 579

FOURTH ANNUAL CHEMICAL DEFENSE BIOSCIENCE REVIEW

Post Theatre, Aberdeen Proving Ground (Edgewood Area), Maryland

30 May - 1 June 1984

Agenda

Wednesday, 30 May 1984

0830 REGISTRATION Post Theatre

0900 WELCOMING REMARKS

MG Garrison Rapmund, Commander
US Army Medical Research and Development Command

COL Duane E. Hilmas, Commander/Director
US Army Medical Research Institute of Chemical Defense

COL Richard E. Lindstrom, Associate Director
US Army Medical Research Institute of Chemical Defense

I. Standardized Efficacy Models

Moderator: MAJ D.E. Jones

0915 Introduction: Efficacy Models MAJ D.E. Jones

0920 Models for Assessing Efficacy of Therapy MAJ D.E. Jones
Compounds Against OP's

0945 Models for Assessing Efficacy of Pretreatment Dr. I. Koplovitz
Compounds Against OP's

1010 BREAK

1020 Guinea Pig Model for Correlating Efficacy CPT M.D. Green
with 2-PAM Plasma Levels

1045 Correlation of Inter-Species Variation in Mr. D.M. Maxwell
Treatment Efficacy with Endogenous Non-Specific
Agent Binding

1110 QUESTIONS/DISCUSSION

Wednesday, 30 May 1984

II. Pyridostigmine: Update on Nerve Agent Pretreatment

Moderator: LTC G.L. Wannarka

- | | | |
|------|---|--------------------|
| 1120 | Status of the Pyridostigmine Development Effort | LTC G. L. Wannarka |
| 1145 | Oral Dose Effects of Pyridostigmine on Human Function | Dr. C. Graham |
| 1210 | QUESTIONS/DISCUSSION | |
| 1215 | LUNCH | |
| 1315 | Ultrastructural Pathology in Mammalian Skeletal Muscle Following Acute and Subacute Exposure to Pyridostigmine. Studies of Dose-Response and Recovery. | Dr. C.S. Hudson |
| 1340 | <u>Ir Vivo</u> and <u>In Vitro</u> Pathophysiology of Mammalian Skeletal Muscle Following Acute and Subacute Exposure to Pyridostigmine. Studies on Muscle Contractility and Cellular Mechanisms. | Dr. M. Adler |
| 1405 | QUESTIONS/DISCUSSION | |

III. Skin Injury and Protection

Moderator: LTC M.C. Powanda

- | | | |
|------|---|------------------|
| 1415 | Noninvasive Methods for Assessing Skin Trauma | Dr. R.E. Baier |
| 1440 | Solution Hydrolysis and Sorption Kinetics of CW Agents by Polymeric Resins: Evaluation for Decontamination Applications | Dr. P.S. Hammond |
| 1505 | QUESTIONS/DISCUSSION | |
| 1515 | BREAK | |
| 1530 | The Use of Human Leukocytes as a Model for Studying Biochemical Effects of CW Agents | Dr. H.L. Meier |
| 1555 | Modification of DNA by Sulfur Mustards | Dr. D.B. Ludlum |

Wednesday, 30 May 1984

1620 QUESTIONS/DISCUSSION
1630 CLOSING REMARKS
1645 ADJOURN

Thursday, 31 May 1984

IV. Biotechnology: Advances in Molecular Biology
Moderator: COL J.C. Sadoff

0830	Cloning of the Acetylcholine Receptor	Dr. J.W. Patrick
0855	Expression of Acetylcholinesterase Gene(s) in Human Brain Tissue	Dr. H. Soreq
0920	QUESTIONS/DISCUSSION	
0930	Affinity Purification of Human Acetylcholinesterase	Dr. J.T. August
0955	Anti-Soman Monoclonal Antibodies: Structural and Stereochemical Specificity	Dr. D.E. Lenz
1020	QUESTIONS/DISCUSSION	
1030	BREAK	
1045	Design and Synthesis of Peptides Mimicking the Active Site of Trypsin with Covalent Binding Activity for Organophosphates	Dr. M.Z. Atassi
1110	Molecular and Structural Basis for the Polymorphic Forms of Acetylcholinesterase	Dr. P. Taylor
1135	QUESTIONS/DISCUSSION	
1200	LUNCH	

Thursday, 31 May 1984

V. Organophosphates: CNS Toxicity and Therapeutic Approaches

Moderator: LTC C.G. McLeod

1300	Introduction	LTC C.G. McLeod
1305	Intravenous Soman Intoxication of Awake Cats: Model Development, Laboratory Findings, and Neuropathology	LTC J.B. Moe
1330	Pathology of Organophosphorus Compounds in Various Animal Species: Comparison with Seizure-Related Pathology in Man	Dr. J.S. Nelson
1400	QUESTIONS/DISCUSSION	
1410	A Study on the Effects of Soman on the Rat Blood-Brain Barrier	Dr. J.P. Petralli
1435	Brain Pathology Induced by Organophosphate Poisoning with the Nerve Agent Soman	Dr. J.M. Petras
1500	Anticonvulsant Therapy for OP-Induced Lethality	MAJ D.E. Jones
1525	QUESTIONS/DISCUSSION	
1535	BREAK	
1550	Effect of Valium and Atropine on Mortality and Pathology in Guinea Pigs Exposed to Soman	MAJ A.W. Singer
1615	Brain Regional Energy Flow: Effects of Pretreatment with Valium in Soman-Exposed Rats	Dr. T.L. Pazdernik
1640	QUESTIONS/DISCUSSION	
1650	CLOSING REMARKS	
1700	ADJOURN	

Friday, 1 June 1984

VI. Cyanide: Intoxication, Prophylaxis, and Therapy

Moderator: LTC H.H. Newball

0830	Toxicodynamic Action of Cyanide Intoxication and Its Antagonism	Dr. J.L. Way
0850	Comparitive Toxicity of Hydrogen Cyanide and Its Salts	Dr. B. Ballantyne
0910	QUESTIONS/DISCUSSION	
0920	Roles of Divalent Sulfur in Biological Detoxication of Cyanide	Dr. J.L. Westley
0940	Interaction of Carbon Monoxide and Cyanide	Dr. A.S. Hume
1000	QUESTIONS/DISCUSSION	
1010	BREAK	
1020	Mechanisms of Cyanide Inhibition by Scavengers	LTC H.H. Newball Dr. P. Hambright
1100	QUESTIONS/DISCUSSION	
1110	Human Cyanide Poisoning	Dr. B.H. Rumack
1130	Chemoprophylaxis of Cyanide Intoxication	COL D.E. Davidson
1150	QUESTIONS/DISCUSSION	
1200	CLOSING REMARKS	
1215	ADJOURN	

I. Standardized Efficacy Models

MODELS FOR ASSESSING EFFICACY OF THERAPY COMPOUNDS
AGAINST ORGANOPHOSPHATES (OP)

D.E. JONES*, I. KOPLOVITZ, D.G. HARRINGTON, D.E. HILMAS
US Army Medical Research Institute of Chemical Defense
Aberdeen Proving Ground, MD 21010

and

C.J. CANFIELD
Walter Reed Army Institute of Research
Washington, DC

*Mailing Address: Commander
US Army Medical Research Institute
of Chemical Defense
ATTN: SGRD-UV-DD/Major Dennis E. Jones
Aberdeen Proving Ground, MD 21010

ABSTRACT

Mouse and guinea pig models have been developed to identify and evaluate treatment compounds with greater nerve agent antidotal efficacy than that afforded by the standard therapy of atropine sulfate (ATS) and pralidoxime chloride (2-PAM). The full range of protective efficacy has been defined for combination therapies of ATS/2-PAM against soman (GD), tabun (GA), and sarin (GB). Optimal treatment doses of ATS/2-PAM and corresponding maximum nerve agent challenge doses have been selected from these studies and used as referenced standards for screening and evaluating candidate treatment compounds. Compounds (at doses equivalent to non-lethal fractions of the test compound LD50) are initially screened in mice against GD. Those compounds identified as more efficacious than ATS/2-PAM are further screened and validated in guinea pigs for efficacy against GD. To insure that compounds identified in the mouse and guinea pig screen are not restricted to efficacy against GD, they are also screened in both the mouse and guinea pig against GA and GB. Compounds which are found to be more efficacious than ATS/2-PAM against these agents are then tested alone and with appropriate adjunct against multiple agent challenge doses (GD, GA, and GB). These standardized methods provide an efficient, reliable means to identify and rank order nerve agent antidotes more efficacious than ATS/2-PAM.

Introduction

Drug screening programs have historically proven to be one of the preferred methods for identifying pharmacologically active compounds. Such programs have been utilized to evaluate the activity of structural analogues of proven, active compounds, as well as to evaluate novel, newly synthesized chemical structures. Drug screens are generally designed to evaluate a singular pharmacological drug property, with the intent being to both identify active compounds and eliminate inactive ones. The published literature abounds with numerous in vitro, in situ, and in vivo drug screening techniques (1,2,3). The preferred type of screen for evaluating compounds for clinical use potential has been to use animal model correlations of the specific human condition being investigated.

It would, therefore, seem logical to utilize in vivo drug screening programs to identify and evaluate potential nerve agent antidotes. This approach has been utilized in the past by several different investigators (4,5,6). These investigators have utilized numerous animal models, including the mouse, rat, guinea pig, rabbit, dog, and monkey and have further utilized vastly differing evaluation techniques (4,5,6,7). This, of course, has resulted in differing results and interpretations among the various investigating laboratories. Our intent has been to develop and implement a standardized in vivo screening and evaluation program to identify and evaluate compounds which provide greater protection against nerve agent-induced lethality than that afforded by the standard therapy of atropine sulfate (ATS) and pralidoxime chloride (2-PAM).

Materials and Methods

The basic methodologies for our testing program are outlined in Figure 1. Two animal models were developed; an ICR male mouse model, and a Duncan Hartley, mixed sex, guinea pig model. These two species were chosen because they are both readily available in inbred strains, thereby reducing the chance for intraspecies variability. In addition, the literature has shown a marked difference between these two species in magnitude of response to both agent challenge and traditional oxime/cholinolytic therapy (4,5).

As shown in Figure 1, the mouse was chosen as the primary test species. This is because the mouse is one of the least responsive laboratory animals to treatment with traditional oxime/cholinolytic therapy (4,5). The premise here is that compounds which prove efficacious in the mouse model would have the greatest probability of being efficacious in other species, including man. The guinea pig was chosen for a secondary validation species, primarily because this species is more responsive to therapy (4,5) and would, therefore, provide a greater margin for evaluation and eventual comparison of therapies.

The choice of agent challenge route was based on logistics and practicality. Although the anticipated route of nerve agent exposure in a field situation would be via inhalation (8), such a route is impractical for precise dosing of such large numbers of animals as would be required for a drug screening program. For this reason, the intramuscular (IM) route of agent exposure was chosen for the mouse model. This route allows precisely controlled administration of agent to large numbers of animals, with a relatively rapid absorption and distribution of agent. The subcutaneous (SC) route of agent exposure was chosen for the guinea pig model because this route also allows the precise administration of agent to large numbers of animals, but provides a somewhat delayed absorption and distribution (i.e., onset). This delay in onset allows further latitude in the evaluation and comparison of candidate treatment antidotes.

The route selected for administration of candidate treatment compounds was IM. This route was chosen as it is the current route of administration of antidotes in the field (9). The preferred dose volume selected for candidate treatment compounds was 0.5 ml/kg. A volume of 1.0 ml/kg was utilized, if so dictated, by low solubility of the candidate compound.

All candidate therapy compounds were first toxicity tested to determine the range and limits of acute (24 hour) IM lethality. Compounds were then screened for efficacy at one-quarter fractions of their acute LD50 as determined by probit analysis (10). Those compounds for which the solubility limits or toxicity were too low to allow assessment of the acute IM LD50 (within the physiologically acceptable limits, 1.0 ml/kg maximum volume) were efficacy tested at quarter fractions of the compound solubility limits. Candidate treatment compounds were administered at 10 seconds post agent challenge in the mouse and at 60 seconds post agent challenge in the guinea pig.

The nerve agents of concern for our screening and evaluation programs were soman (GD), tabun (GA), sarin (GB), and VX. The agent VX is not listed in Figure 1 because data will not be presented here on efficacy testing of treatment compounds against this agent. As indicated in Figure 1, GD is the primary agent of concern. This is because GD is one of the most rapidly aging and, therefore, least responsive agents to therapy (11). Compounds were, therefore, screened initially against GD in the mouse model. Those compounds which provided greater protective efficacy than ATS/2-PAM were further screened in the guinea pig model. Compounds which were thus validated as providing greater protective efficacy against GD than ATS/2-PAM were then screened and evaluated for protective efficacy against the other nerve agents. This, of course, was to preclude selection of an antidote for field development which may have limited efficacy against a nerve agent other than GD.

Results and Discussion

As previously indicated, our intent has been to develop a standardized screening program for identifying and evaluating nerve agent antidotes. One of the primary concerns for a standardizing program of this sort is that of test animal response to agent challenge. If a candidate compound is to be selected for or eliminated from further testing based on results of an agent challenge screen, one must be certain that the agent challenge doses used and the animal response falls within some acceptable limits. Although the agent stock that we use for our testing is evaluated for agent concentration by gas chromatographic (GC) analysis, animal response to agent challenge has been shown to vary according to daily circadian rhythm, seasonal variability, isomerization, and, of course, dilution error (12,13,14). Since agent potency is a directly comparative measure of response to a particular drug/compound dose, we utilize a daily agent potency check in the particular animal species being tested to assure that both the agent concentration and the animal response for that particular study are within acceptable limits.

An additional concern for these types of conclusions is that the biological response to agent-induced lethality, i.e., agent potency, follows a Gaussian frequency distribution (15). If responses to an agent were found to be skewed or otherwise nonnormality distributed, because of slight differences in agent concentration or animal variability, evaluation of results and comparison of compounds would be greatly complicated. For these reasons, we have compiled the lethality data from multiple, daily agent potency checks for GD, GA, and GB in both mice and guinea pigs. This has allowed us to assess the frequency distribution of agent-induced lethality in these two species and to further insure that the response to an agent for each particular study falls within statistically acceptable limits.

The next six figures illustrate the results of these assessments. Figure 2 shows the frequency distribution of the acute LD50 of GD in mice. The mean LD50, variance, standard deviation, range, standard error of the mean, coefficient of variation, degree of skewness, and degree of kurtosis were determined for all the frequency distributions shown in Figures 2 through 7. As shown in Figure 2, the ordinate indicates the log LD50 of GD and the abscissa indicates both the number of LD50 data points for each LD50, as well as the percent relative frequency. The data in Figure 2 are representative of 65 consecutive GD LD50 determinations in mice. As can be seen from the illustration, GD lethality in mice is perfectly lognormally distributed (16), with a mean LD50 of 97.70 ug/kg. Figure 3 illustrates that GD-induced lethality in guinea pigs is also lognormally distributed, with a mean LD50 of 28.00 ug/kg. These calculations are also based on the results of 65 different GD LD50 studies. Figure 4, based on only 14 different data sets, illustrates the frequency distribution of the LD50 for tabun in mice, with a calculated mean LD50 of 304.16 ug/kg. It is apparent that the data do not fit a lognormal frequency distribution curve as perfectly as did the GD data for both mice and guinea pigs. This is most probably because fewer data points (14 compared to 65) were used for this plot. It has been our experience that as more data points are added to the frequency distribution curve (from daily experiments), the more precise the lognormal fit becomes. As new experiments are conducted, the new LD50 data will be added to the data shown here to update the assessment of the frequency distribution.

Figure 5, based on the data from 21 daily agent potency checks, illustrates the cumulative frequency distribution of tabun lethality in guinea pigs. The calculated mean LD50 is 118.48 ug/kg. Figure 6, based on 24 LD50 studies, illustrates the cumulative frequency distribution of sarin lethality in mice. The calculated mean LD50 is 178.75 ug/kg. Figure 7, based on 22 LD50 studies, illustrates the cumulative frequency distribution of sarin lethality in guinea pigs, with a calculated mean LD50 of 42.72 ug/kg.

These data calculations indicate that agent-induced lethality (for GD, GA, and GB) is lognormally distributed, thus allowing comparisons of agent lethality data for different agent concentrations and for studies conducted on separate days. These data also permit daily agent potencies to be compared to a standard cumulative frequency distribution curve of agent potency to assess whether or not the agent response for each individual study conducted is within acceptable limits. For results of a study to be valid in our laboratory, we have determined that the agent potency for each study must be within the 99 percent tolerance limit of the 95 percent confidence interval of the data presented in Figures 2 through 7. These limits have allowed us to reject screening and evaluation results based on assessments made when the agent dilutions used were of greater or lesser potency than acceptable. In addition, these selection methods have provided the means to identify statistically valid experimental results.

As previously stated, the purpose of developing a standardized screening and evaluation program is to identify compounds with greater efficacy than ATS/2-PAM. Efficacy of nerve agent antidotes is most often assessed as protective ratio (PR) (4). Figure 8 illustrates a hypothetical example of PR, calculated by the agent LD50 following treatment divided by the untreated control agent LD50. As an example, a PR of 2.0 would indicate that a treatment compound would double the population mean LD50.

Drug efficacy is defined as the maximum response that a drug can provide (17). The efficacy response that we are looking for in potential nerve agent antidotes is the ability to increase PR. This does not mean that compounds should be evaluated on an equivalent molar basis, for this would provide only an assessment of relative potency, not efficacy (17). This further indicates that to identify compounds which provide greater efficacy against agent-induced lethality than ATS/2-PAM, the full range and limits of protective efficacy of ATS/2-PAM therapy must be assessed for each nerve agent of concern and for animal models to be used. The purpose of such an assessment would be to determine both the optimal combination therapy of ATS and 2-PAM for treatment of each of the nerve agents, as well as the greatest degree of protection (maximum efficacy) provided by that dose combination.

We conducted studies to determine the optimal dose combination of ATS and 2-PAM for treatment of GD, GA, and GB-induced toxicity in both mice and guinea pigs. Figure 9 shows the results of an ATS/2-PAM optimum dose study in GD-challenged mice. Note that although several dose combinations of ATS/2-PAM provided similar levels of protection, efficacy did not exceed a PR of 2.0, irregardless of treatment dosage used. This figure shows a plot of the actual data points. A dose of 11.2 mg/kg ATS combined with 25.0 mg/kg 2-PAM gave a protective ratio equivalent to greater than 90 percent of the maximal attainable protective response. This dose combination was selected as the standard

optimal ATS/2-PAM dose for testing and comparing other candidate antidotal compounds.

Similar studies were conducted in GA- and GB-challenged mice and in GD-, GA-, and GB-challenged guinea pigs. Figure 10 shows the results of a similar ATS/2-PAM optimal dose study in guinea pigs. Again, actual data points are plotted, not calculated, "best-fit" curves. It can be noted from this graph that, as previously indicated, the guinea pig is more responsive to therapy than the mouse, with achievable protective ratios greater than 3.7. This value is almost double that attainable with ATS/2-PAM therapy in the mouse. Also, note that much higher ATS/2-PAM doses are required to achieve maximum protective efficacy.

Figure 11 shows still another ATS/2-PAM optimal dose study. This one is in GA-challenged guinea pigs. Here we see that GA-induced lethality is even more amenable to treatment with ATS/2-PAM than was GD in either the mice or the guinea pig. We see here an achievable PR of greater than 4.6.

Rather than demonstrating the composite ATS/2-PAM optimal dose plots for each of the G-class nerve agents in both the mouse and the guinea pig, a composite graph of these data has been compiled. Figure 12 illustrates the computed optimal combination therapy dose of ATS and 2-PAM for treatment of each of the G-agents (in the mouse and guinea pig) and the corresponding protective ratios. Note that, in both animal species, GD is least amenable to therapy, whereas GB is most amenable to therapy. Also note that, for each agent, the guinea pig is more responsive to therapy than the mouse. One additional comment should be made here in regards to therapy, and that is the magnitude of the response of GB-challenged guinea pigs to ATS/2-PAM therapy. Note the PR of 56.0 in GB-challenged guinea pigs compared to a PR of only 2.2 in GB-challenged mice. Although I cannot, at this time, tell you the exact reason for this large interspecies disparity, basic research into this phenomenon could answer some important questions regarding the mechanisms of both agent-induced toxicity and response to therapy.

Refer to the optimal dose column. These doses are used to screen and compare other candidate treatment compounds. As previously stated, candidate compounds are first toxicity tested to determine acute 24-hour lethality and are screened at 1/4 fractions of their calculated LD50, usually at 1/4 and 1/8 fractions. Candidate oximes are screened alone and in combination with the optimal ATS dose. Candidate chol'olytics are screened alone and in combination with the optimal 2-PAM dose. Candidate third component compounds such as anticonvulsants, non-oxime reactivators, and sympathomimetics are screened alone, in combination with ATS, 2-PAM, and ATS plus 2-PAM.

The last column in Figure 12 shows the LD90 dose. That is the agent challenge dose that would result in 90-100 percent mortality in animals treated with the optimal dose of ATS/2-PAM. The number on the left indicates the actual challenge dose in ug/kg. The number on the right indicates the equivalent LD50 multiple for untreated animals. To illustrate, for mice treated with 11.2 mg/kg ATS and 25.0 mg/kg 2-PAM, a challenge dose of 196 ug/kg would result in 90-100 percent mortality. This dose, 196 ug/kg, is equivalent to twice the GD LD50 in untreated mice, that being 98.0 ug/kg. Note that the LD90 dose for GB-challenged guinea pigs has not been accurately

determined yet. This is because this model is so responsive to therapy that extremely high levels of neat, that is non-exempt (or dilute), agent must be used to accurately assess this value and must, therefore, be done in the BA or neat agent laboratory. Logistically, we have not as yet been able to compare the necessary experiments to accurately assess this value.

The value of this LD90 challenge dose is that this is the agent challenge dose used in screening candidate compounds. The premise is that if animals are challenged with this dose of agent, only 0-10 percent will survive, even if treated with the optimal dose of ATS/2-PAM. Likewise, if a candidate compound does not provide greater protective efficacy than ATS/2-PAM, only 0-10 percent of these animals will survive a similar agent challenge. If, however, a candidate compound provides greater protective efficacy than ATS/2-PAM, more than 0-10 percent of those challenged with the LD90 agent dose will survive.

Figure 13 will serve to clarify how these therapy and agent challenge doses are used to screen potential treatment antidotes. Figure 13 shows the screening results of the oxime TMB-4 against GD-challenge in mice. This oxime has been reported to be equal to or slightly more efficacious than 2-PAM against GD (18). Each bar represents 10 mice challenged with 2 x LD50 of GD. The bars with mice treated on the left represent the optimal dose of 2-PAM, 25 mg/kg or with doses of TMB-4 equivalent to 1/8 and 1/4 of the LD50 of TMB-4. Note there are no survivors with 2-PAM alone or with the 1/8 LD50 fraction of TMB-4. The 1/4 LD50 fraction, however, shows slightly greater efficacy with 10 percent surviving. The bars on the right represent the same oxime doses combined with the optimal dose of 11.2 mg/kg ATS. Again we see no survivors with 2-PAM plus ATS or with the 1/8 x LD50 fraction of TMB-4 plus ATS, but we see a 10 percent survival rate with the 1/4 x LD50 fraction of TMB-4 plus ATS. Although the difference here is not statistically significant, it does indicate that TMB-4 is equal to and perhaps slightly more efficacious than 2-PAM. A repeat of this study did, in fact, reconfirm these findings.

Figure 14 illustrates the screening results of another oxime, toxogonin, in GD-challenged mice. This oxime has also been reported to be equal to or slightly more efficacious than 2-PAM against GD-induced lethality (19). Here again we see the results of 1/8 and 1/4 fraction of toxogonin screened alone and in combination with ATS. Again we see indication that toxogonin is only slightly more efficacious than 2-PAM against GD-challenge, with no survivors with 2-PAM alone or combined with ATS. We see, however, a 10 percent survival rate with 1/4 LD50 of toxogonin alone and with 1/8 and 1/4 LD50 dose of toxogonin plus ATS.

Figure 15 illustrates the screening results of the oxime HI-6, in GD-challenged mice. This oxime has previously been reported to be much more efficacious against GD in both in vitro reactivation studies and in vivo screening and evaluation studies (20). Here we see these results validated in our screen. Note that we get 30 percent survival with the 1/8 LD50 fraction of HI-6 without ATS. This has been the only oxime we have screened, thus far, that has provided greater efficacy by itself, that is without adjunct therapy, than the optimal dose of ATS/2-PAM. Note that when combined with ATS, HI-6 provides much greater protection than that afforded by the optimal dose of

ATS/2-PAM, providing, in fact, 100 percent survival at the 1/8 LD50 fraction. The slightly lesser protection attained with the 1/4 fraction compared to the 1/8 fraction is, most probably, due to the fact that 153.4 mg/kg of HI-6 is near the LD01 dose for HI-6 and may, in fact, be slightly toxic, especially when combined with GD-challenge.

As stated earlier, candidate compounds are also screened in guinea pigs. Figure 16 illustrates the screening results of TMB-4 in GD-challenged guinea pigs. Here again, each bar represents 10 animals. Note the higher GD LD90 challenge and the higher optimal ATS/2-PAM doses. The results here indicate that TMB-4 is not more efficacious than 2-PAM against GD-challenge in the guinea pig.

Figure 17 illustrates the screening results of toxogonin in GD-challenged guinea pigs. Here, again, we see no indication that toxogonin is more efficacious than 2-PAM against GD.

Figure 18 shows the screening of HI-6 in GD-challenged guinea pigs. Here we can see, as in the mouse, that HI-6, when combined with ATS, provides greater protective efficacy than the optimal ATS/2-PAM therapy.

I do not intend to present you with a periodic table of all compounds we have screened against agents in both mice and guinea pigs. I would, however, like to show you the screening results of these three oximes, TMB-4, toxogonin, and HI-6 against GA. These results are important for two reasons; first, because of the recent interest in tabun due to the confirmed use of it in the Iraq-Iran conflict (21) and second, because the results tend to validate our screening model.

The literature reports an inverse in the order in the efficacy for TMB-4, toxogonin, and HI-6 for treatment of GA as compared to treatment of GD (22). That is, TMB-4 and toxogonin have been shown to be more efficacious than HI-6 against GA.

Figure 19 shows the screening results of TMB-4 in GA-challenged mice. Note that greater protection is provided by 1/4 LD50 TMB-4 alone and with 1/8 and 1/4 LD50 TMB-4 plus ATS as compared to the optimal dose of ATS plus 2-PAM. In fact, a level of 100 percent survival has been achieved with the higher dose of TMB-4 plus ATS.

Figure 20 shows the screening results of toxogonin in GA-challenged mice. Again, we see significantly greater protection with both doses of toxogonin plus ATS than was provided by the optimal dose of ATS/2-PAM. This compares to a maximum percent survival of only 10 percent with toxogonin treatment in GD-challenged mice.

Figure 21 shows the screening results of HI-6 in GA-challenged mice. We see confirmation of the previous reports that HI-6 is much less efficacious against GA than TMB-4 and toxogonin. Again, this also confirms the literature which reports HI-6 to be more effective against GD than against GA. If you will recall, the previous slides showing the HI-6/GD screening results also verified this.

The next three figures illustrate similar screening results for TMB-4, toxogonin, and HI-6 in GA-challenged guinea pigs. Figure 22 illustrates TMB-4 screening results in GA-challenged guinea pigs. Note the greater percent survival with TMB-4, as compared to the optimal ATS/2-PAM dose, with 100 percent survival achieved with the 1/4 LD50 fraction of TMB-4 plus ATS.

Figure 23 shows the screening results of toxogonin in GA-challenged guinea pigs. Greater protection is provided by both doses of toxogonin combined with ATS as compared to the optimal ATS/2-PAM dose. This, again, corresponds to the mouse GA screening data and to the previous literature reports (22).

This procedure, then, typifies the screening program developed for evaluating potential nerve agent antidotes. Although I have shown only the results of screening oximes, these procedures have also proven valuable for screening cholinolytics as well as other, third component adjuncts. As stated earlier, cholinolytics are screened alone and in combination with the optimal 2-PAM dose. Third components are screened alone, in combination with 2-PAM, ATS, and ATS plus 2-PAM. Compounds that do not provide greater protection than ATS/2-PAM are eliminated from further testing. Those which prove more efficacious are subjected to optimal dose studies, as was done for ATS and 2-PAM, to define both the maximum efficacy afforded by that compound and the corresponding optimal dose.

Behavioral tests are currently being developed and implemented to evaluate identifiable efficacious compounds for cognitive and performance incapacitation. Those compounds which are identified as providing greater protection than ATS/2-PAM at non-incapacitating doses will be subjected to further developmental testing in the primate model.

To date, we have tested and evaluated more than 80 compounds in more than 250 separate efficacy tests. The published literature reports efficacy data on 15 of those compounds we have, thus far, tested in the mouse and/or guinea pig against GD, GA, and/or GB. The screening results we have obtained, thus far, correspond completely with results reported in the literature. It appears that these factors tend to verify and validate the standardized screening and evaluation program developed.

References

1. Gillespie, J.S. and T.C. Muir, Br. J. Pharmacol., 30:78-87, 1967.
2. Lewin, J. and D.W. Esplin, J. Pharmacol, Exp. Ther., 132:245-250, 1961.
3. Dewey, W.L., L.S. Harris, J.F. Nowes, and J.A. Nuite, J. Pharmacol. Exp. Ther., 175:435-442, 1970.
4. Boskovic, B., V. Kovacevic, and D. Jovanovic, Fundamental and Applied Toxicol., 4:S106-S115, 1984.
5. Green, D.M., A.W. Muir, J.A. Stratton, and T.D. Inch, J. Pharm. Pharmacol., 29:62-64, 1977.
6. Berry, W.K., D.R. Davies, and J.J. Gordon, Biochem. Pharmacol., 20:125-134, 1971.
7. Gordon, J.J. and L. Leadbeater, Toxicol. Appl. Pharmacol., 40:109-114, 1977.
8. Introduction: Defences Against Chemical Warfare Agents, in Medical Protection Against Chemical Warfare Agents, Stockholm International Peace Research Institute, Almquist and Wiskell International, Stockholm, Sweden, 22-35, 1976.
9. Sidell, F.R., Medical Protection Against Chemical Warfare Agents, Stockholm International Peace Research Institute, Almquist and Wiskell International, Stockholm, Sweden, 22-35, 1976.
10. Finney, D.J., Probit Analysis, 3rd Ed., Cambridge University Press, 1971.
11. Michel, H.D., B.E. Hockley, Jr., L. Berkowitz, G. List, E.B. Hackley, W. Gillilan, and M. Pankau, Archives of Biochem. and Biophysics, 121:29-34, 1967.
12. Elsmore, T.F., Fundamental and Applied Toxicology, 1,2:238-241, 1981.
13. Mayersbach, H.V., Chronobiology, Igaku Shoin Ltd., Tokyo, 191-196, 1974.
14. Benschop, H.P., F. Berends, and L.P.A. deJong, Fundamental and Applied Toxicology, 1,2:177-182 1981.
15. Daniel, W.W., Biostatistics: A Foundation for Analysis in the Health Sciences, 2nd Ed., John Wiley and Sons, Toronto, Canada, 1978.
16. Tallardia, R.J. and L.S. Jacob, The Dose-Response Relation in Pharmacology, Springer-Verlag, New York, New York, 1979.
17. Gilman, A.G., S.E. Mayer, and K.L. Melmon, Goodman and Gilman's The Pharmacological Basis of Therapeutics, 6th Ed., MacMillan Publishing Co., Inc., New York, New York, 1980.

18. Schoene, K., Medical Protection Against Chemical Warfare Agents, Stockholm International Peace Research Institute, Almquist and Wiskell International, Stockholm, Sweden, 88-100, 1976.
19. Bruener, H., I. Gandawidjaja, H. Hettwer, and H. Oldiges, *Arzneim.-Forsch. Drug Res.* 27(II), Nr. 10, 1983-1988, 1977.
20. Smith, A.P., H.J. Van Der Weil, and O.L. Wolthuis, *European J. Pharmacol.*, 70:371-379, 1981.
21. *Chemical and Engineering News*, 2 April, 4, 1984.
22. Inns, R.H. and L. Leadbeater, *J. Pharm. Pharmacol.*, 35:427-433, 1983.

DRUG TESTING & EVALUATION METHODOLOGY

- I. Test Species
 - A. Mouse - Primary Test Species
 - B. Guinea Pig: Secondary Test and Validation Species
- II. Agent Challenge Route
 - A. Mouse: Intramuscular (0.5 ml/kg)
 - B. Guinea Pig: Subcutaneous (1.0 ml/kg)
- III. Candidate Compound Dosing
 - A. Dose Route: Intramuscular (IM)
 - B. Dose volume: 0.5-1.0 ml/kg
 - C. Dose: Based on one-quarter fractions of the test compound acute (24 hr) IM LD₅₀; those compounds for which the LD₅₀ cannot be determined are tested at quarter fractions of the compound solubility limits
 - D. Time
 - 1. Mouse: 10 seconds post-agent challenge
 - 2. Guinea Pig: 60 seconds post-agent challenge
- IV. Organophosphate Nerve Agents
 - A. Soman (GD): Primary Agent of Concern
 - B. Tabun (GA)
 - C. Sarin (GB)

Figure 1

Soman Lethality in Mice Cumulative Frequency Distribution

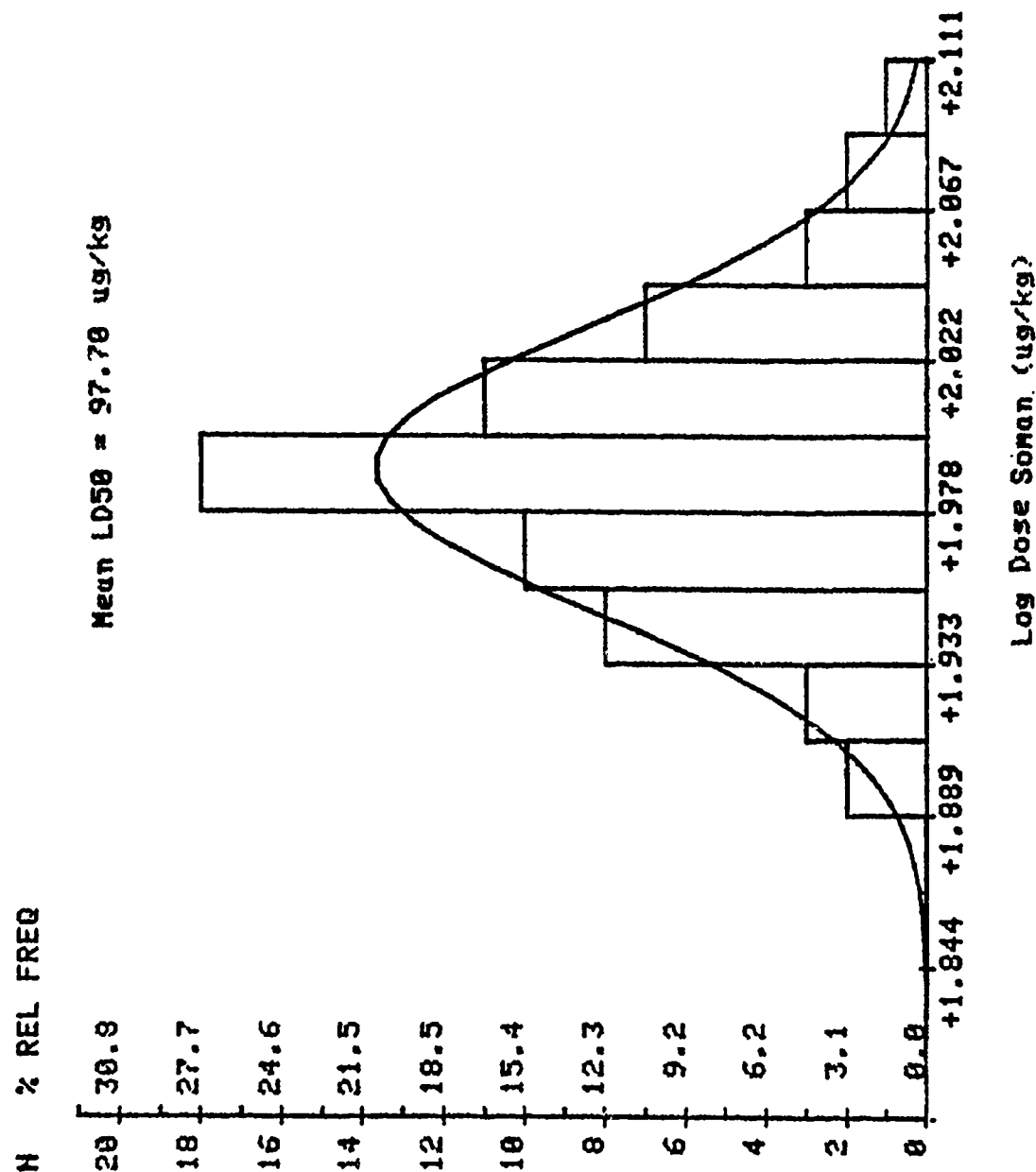


Figure 2

Soman Lethality in Guinea Pigs
Cumulative Frequency Distribution

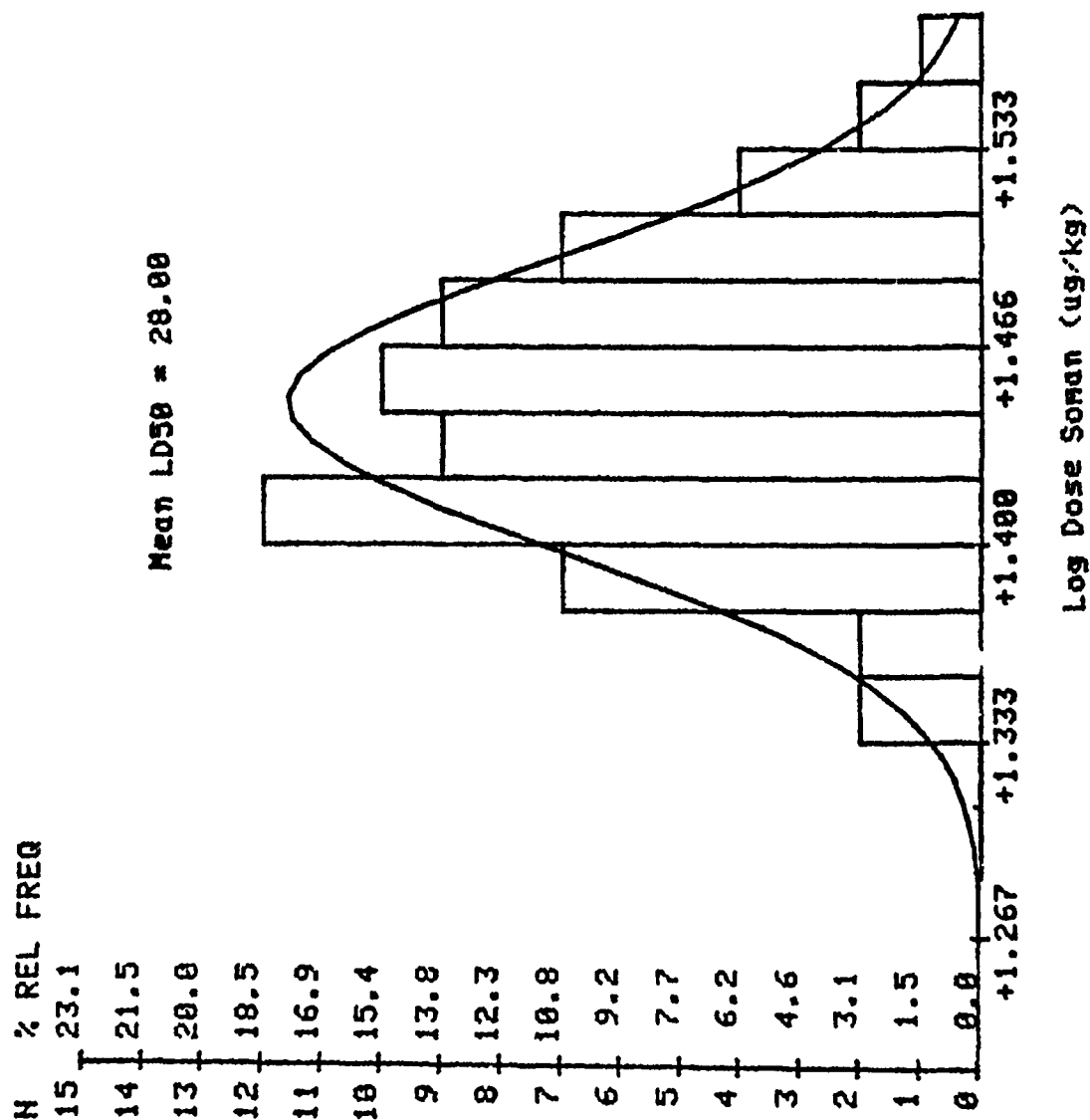


Figure 3

Tabun Lethality in Mice Cumulative Frequency Distribution

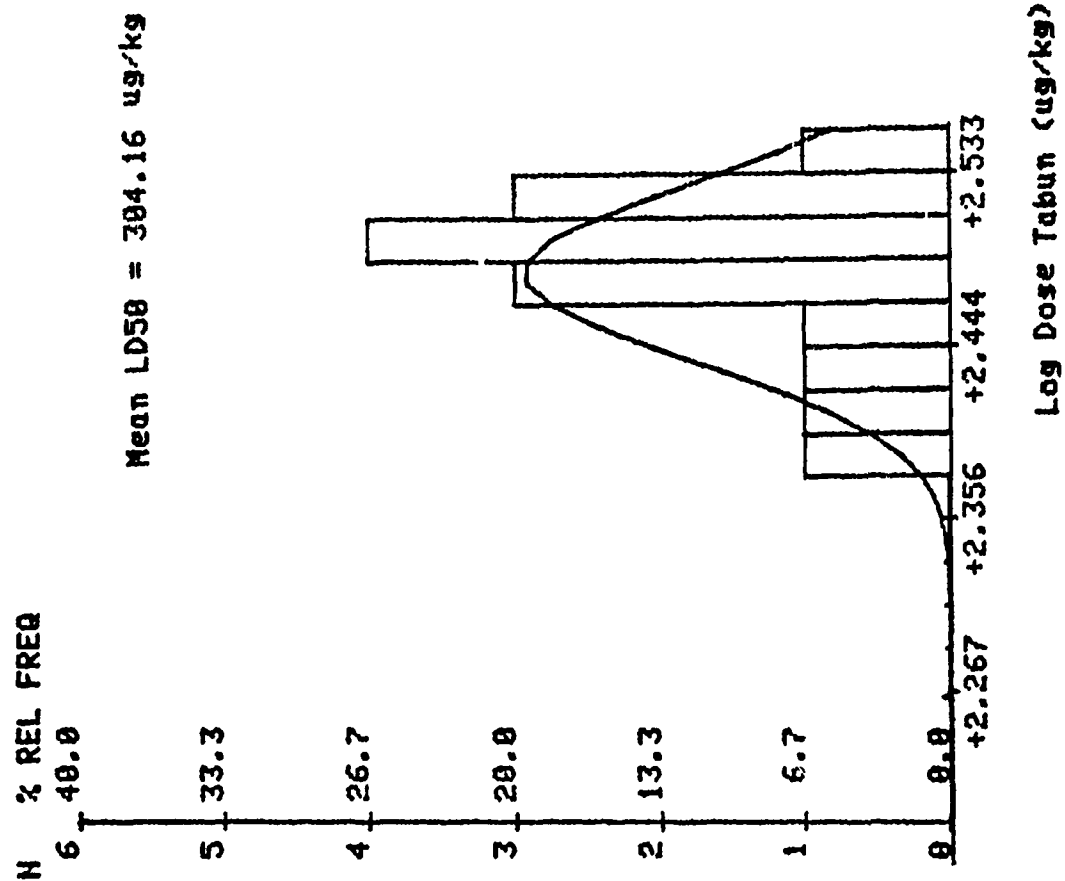


Figure 4

Tabun Lethality in Guinea Pigs
Cumulative Frequency Distribution

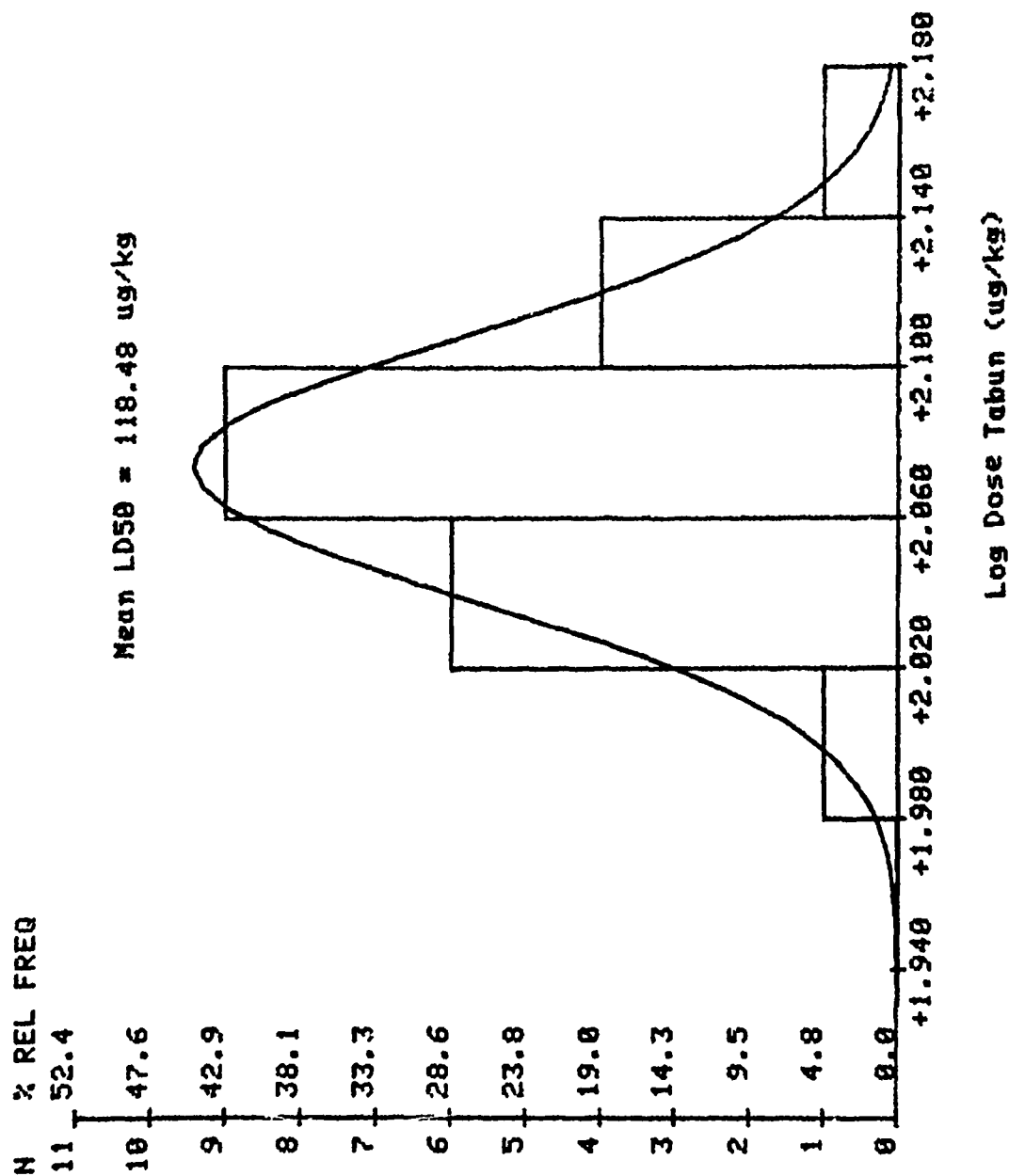


Figure 5

Sarin Lethality in Mice Cumulative Frequency Distribution

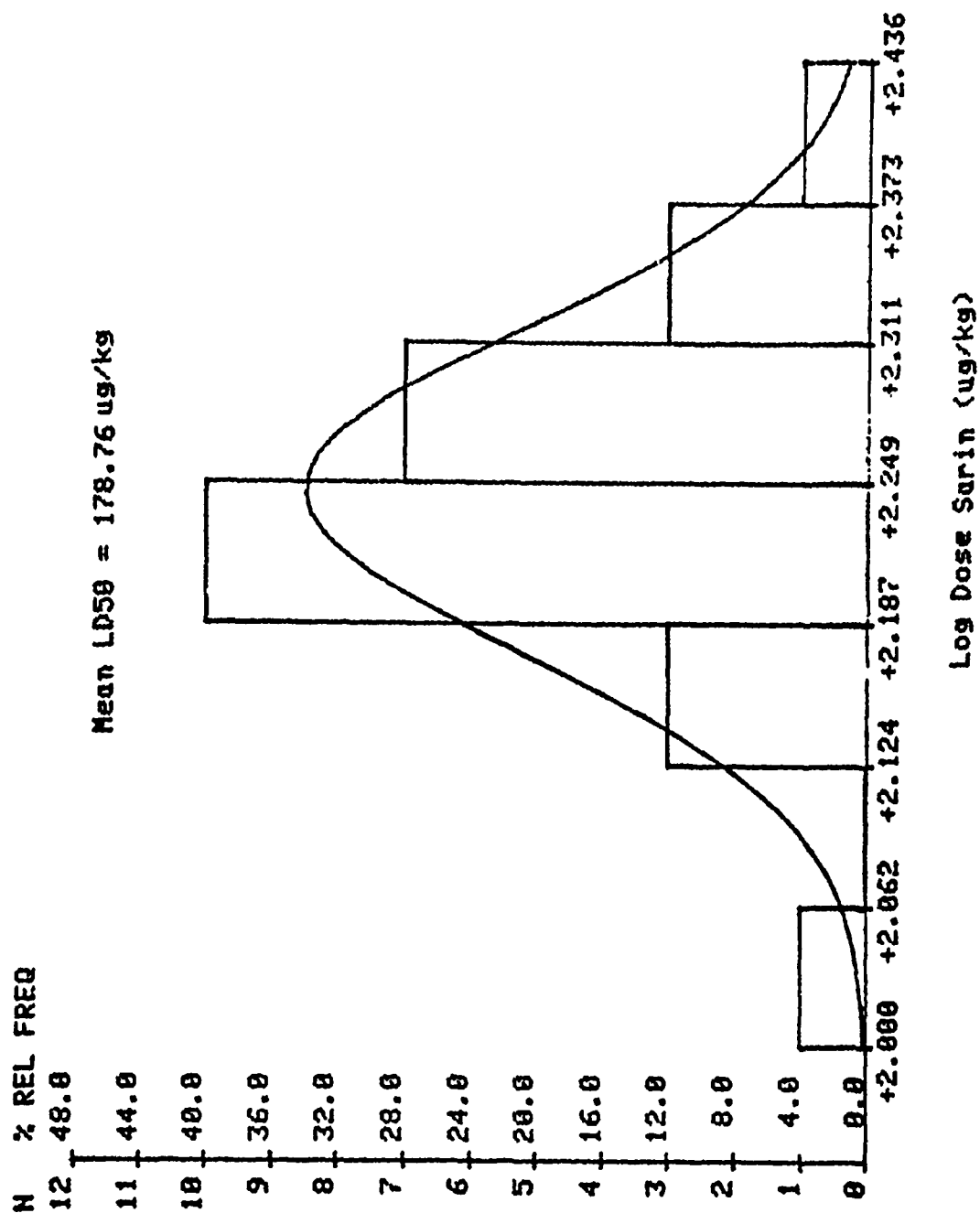


Figure 6

Sarin Lethality in Guinea Pigs Cumulative Frequency Distribution

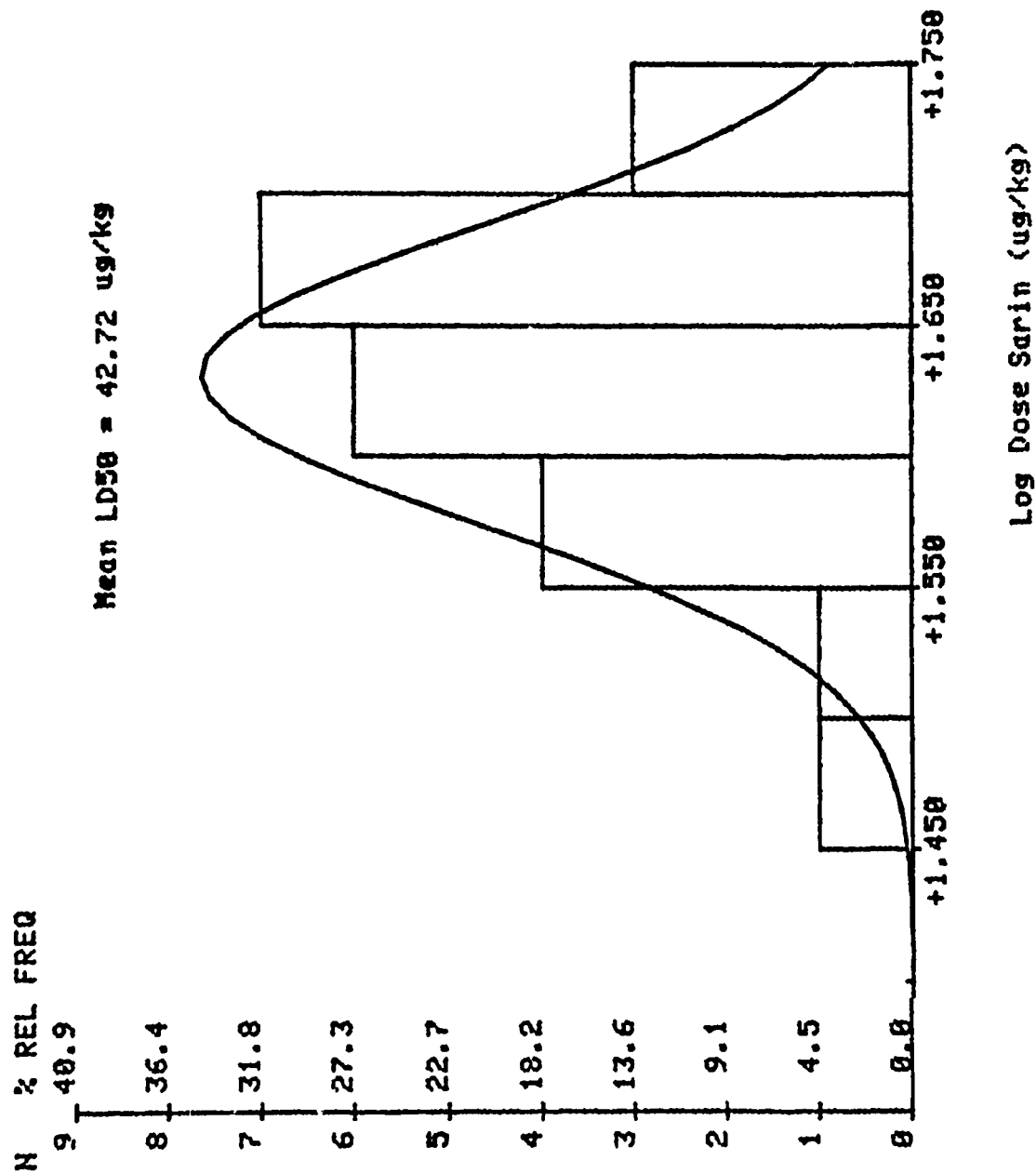
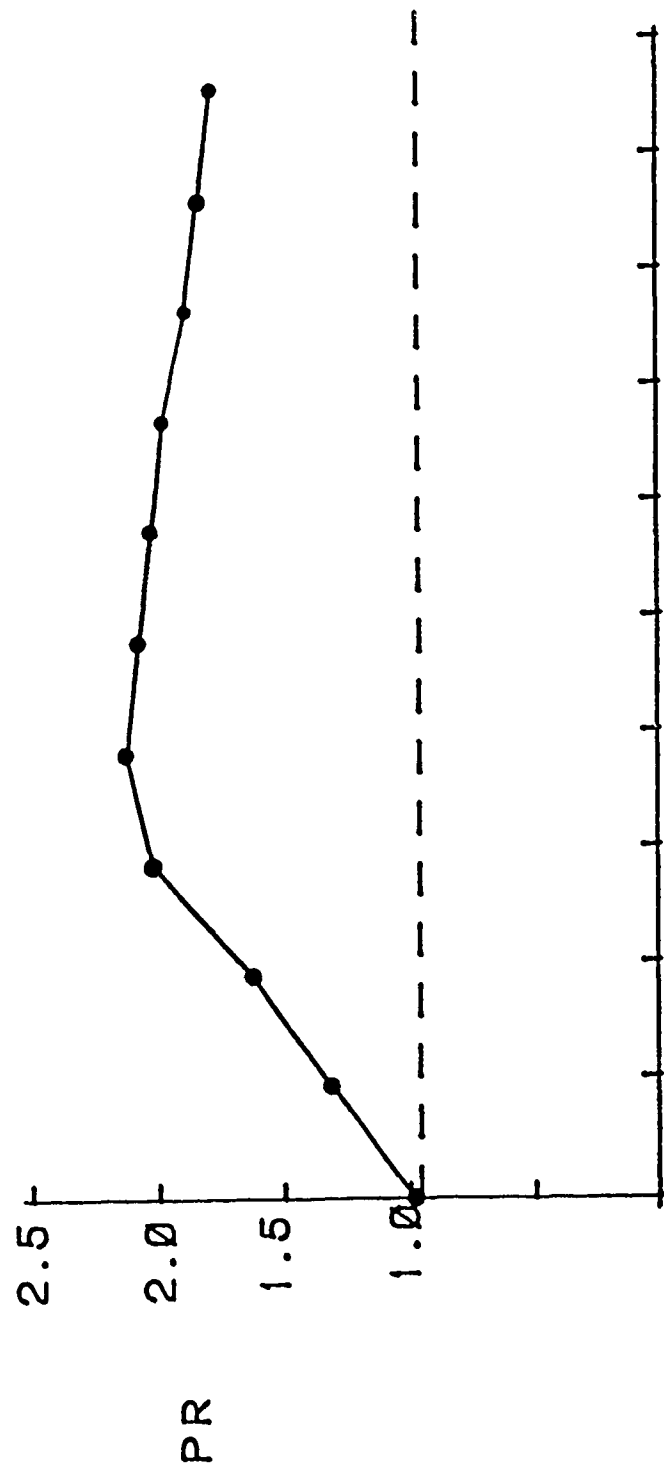


Figure 7

Response to Drug Therapy = Protective Ratio (PR)

$$PR = \frac{\text{Agent LD50 for Treated Group}}{\text{Agent LD50 for Untreated Group}}$$



Drug Dose

Figure 8

Protection Afforded by Various Doses of Atropine Sulfate and Pralidoxime Chloride Against Soman(GD) Poisoning in Mice

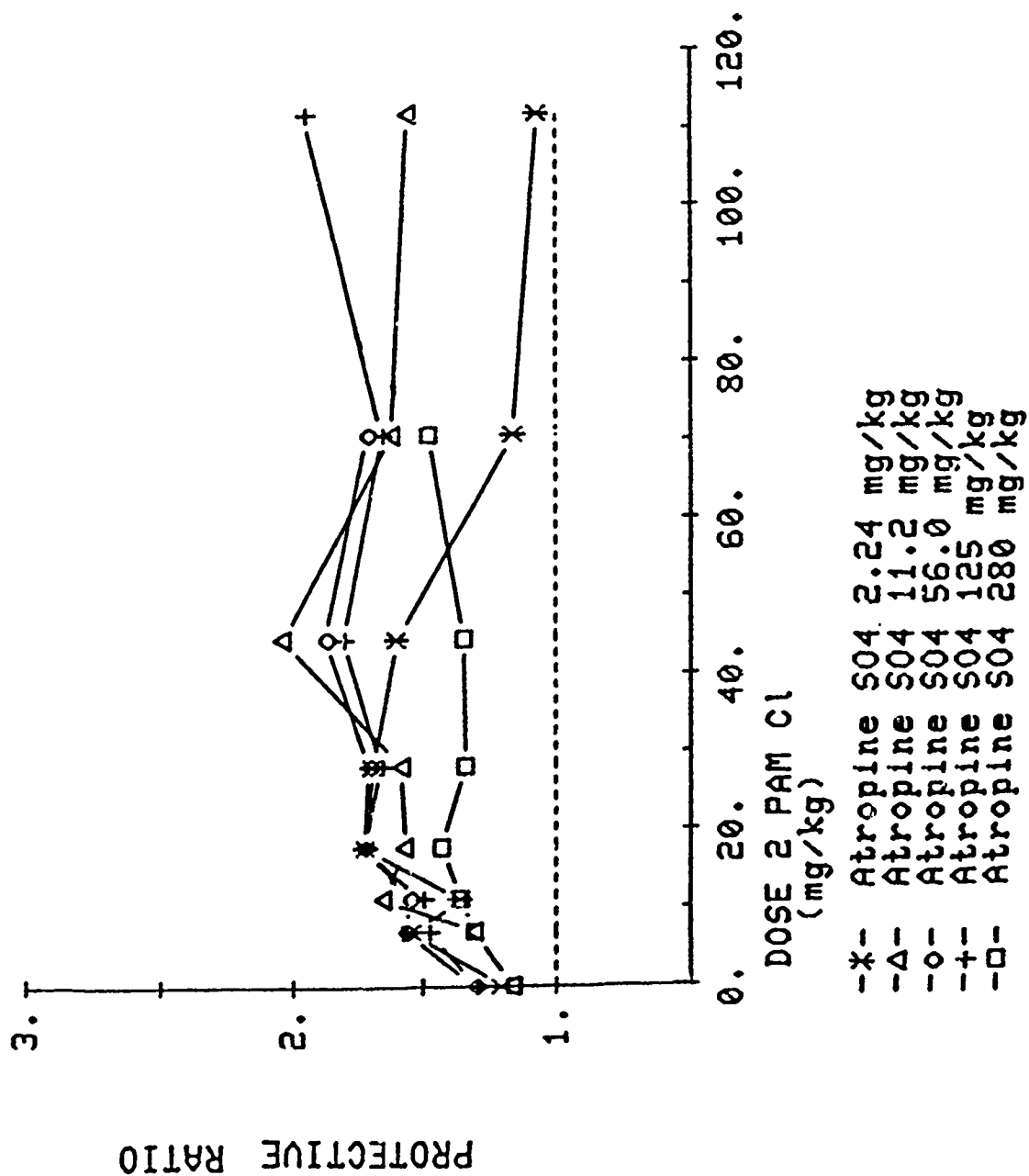


Figure 9

Efficacy of Various Doses of 2PAMCI + Atropine 904 vs GD in Guinea Pigs

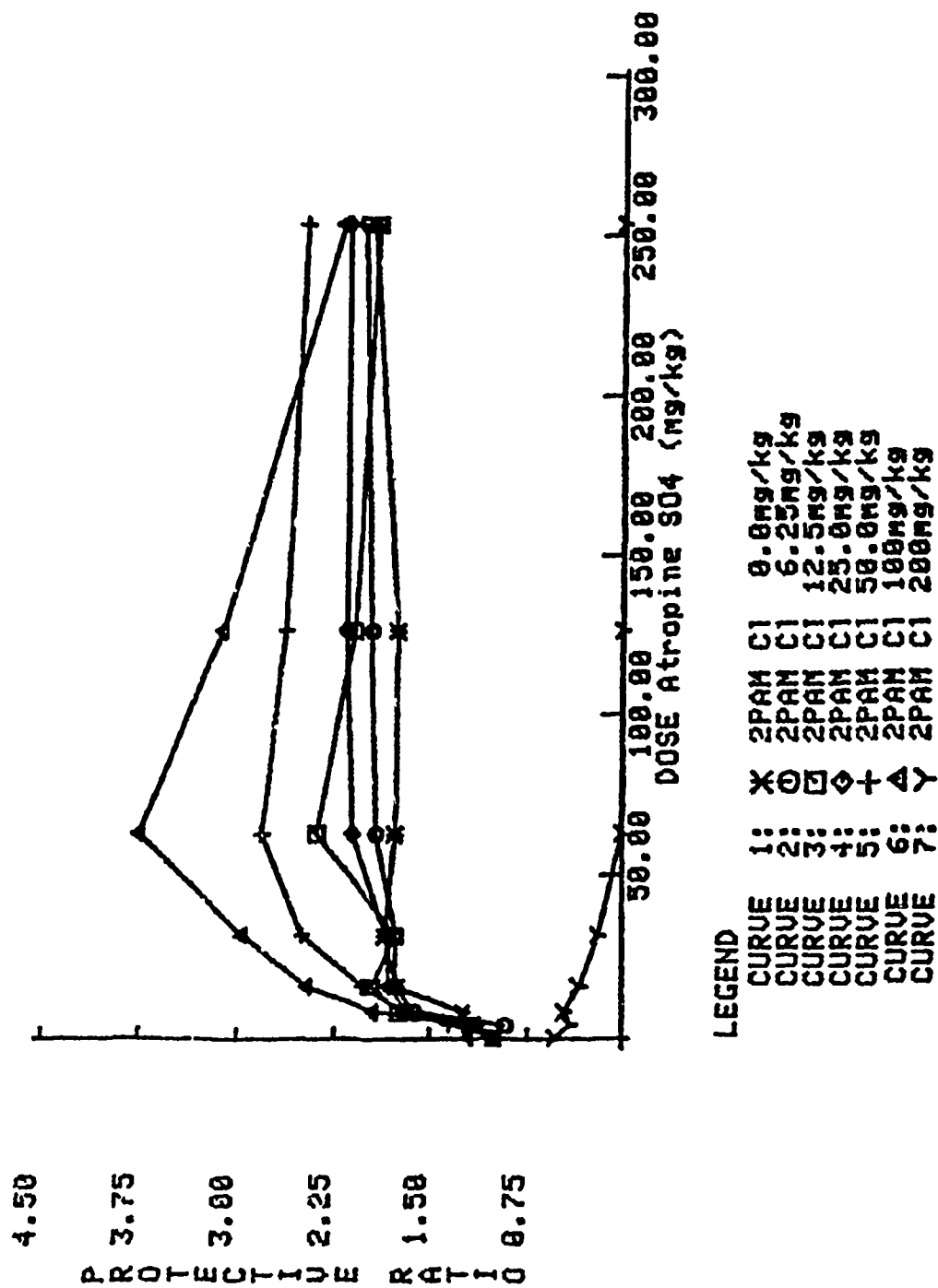


Figure 10

Efficacy of Atropine S04 + 2PAM Cl vs GA in Guinea Pigs

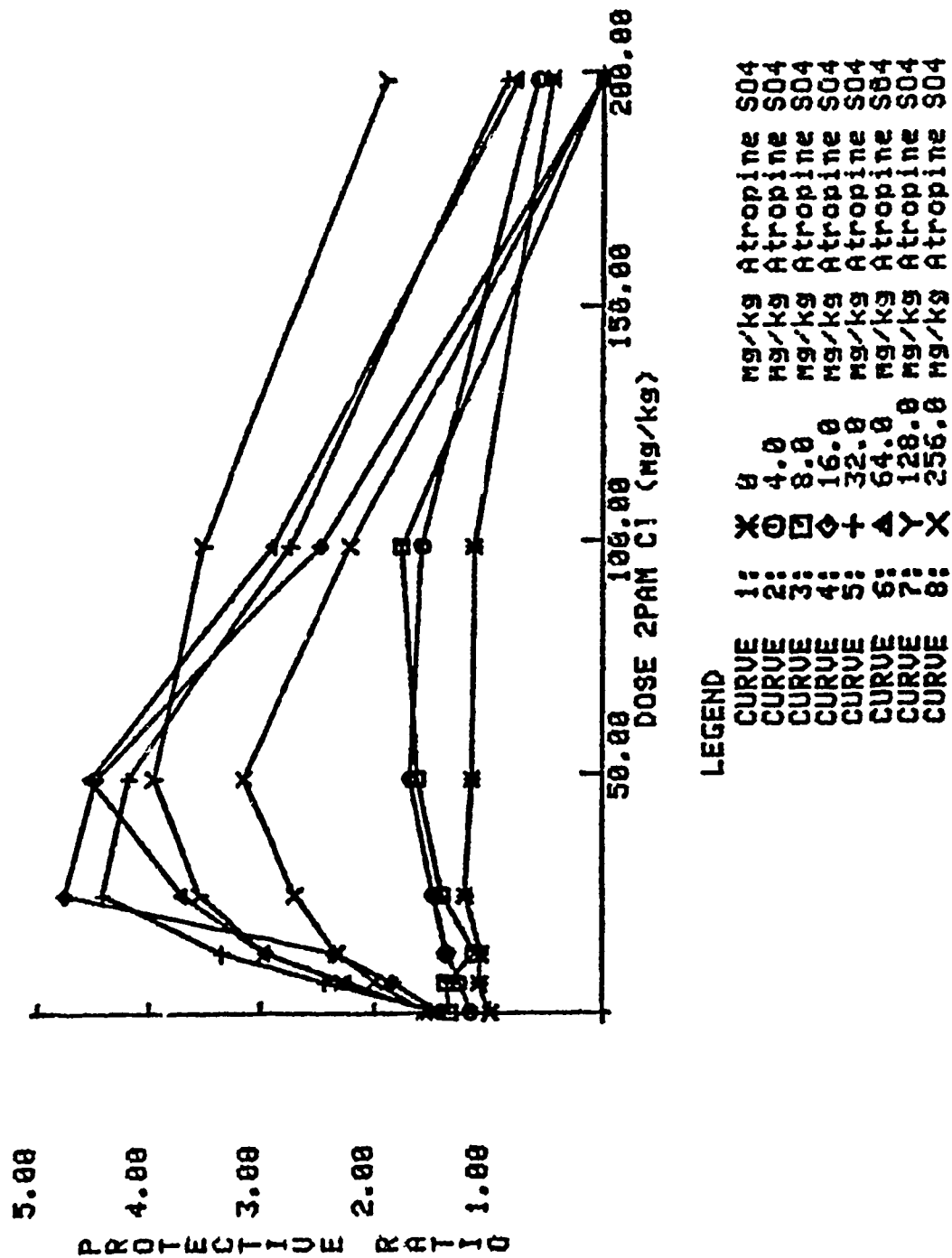


Figure 11

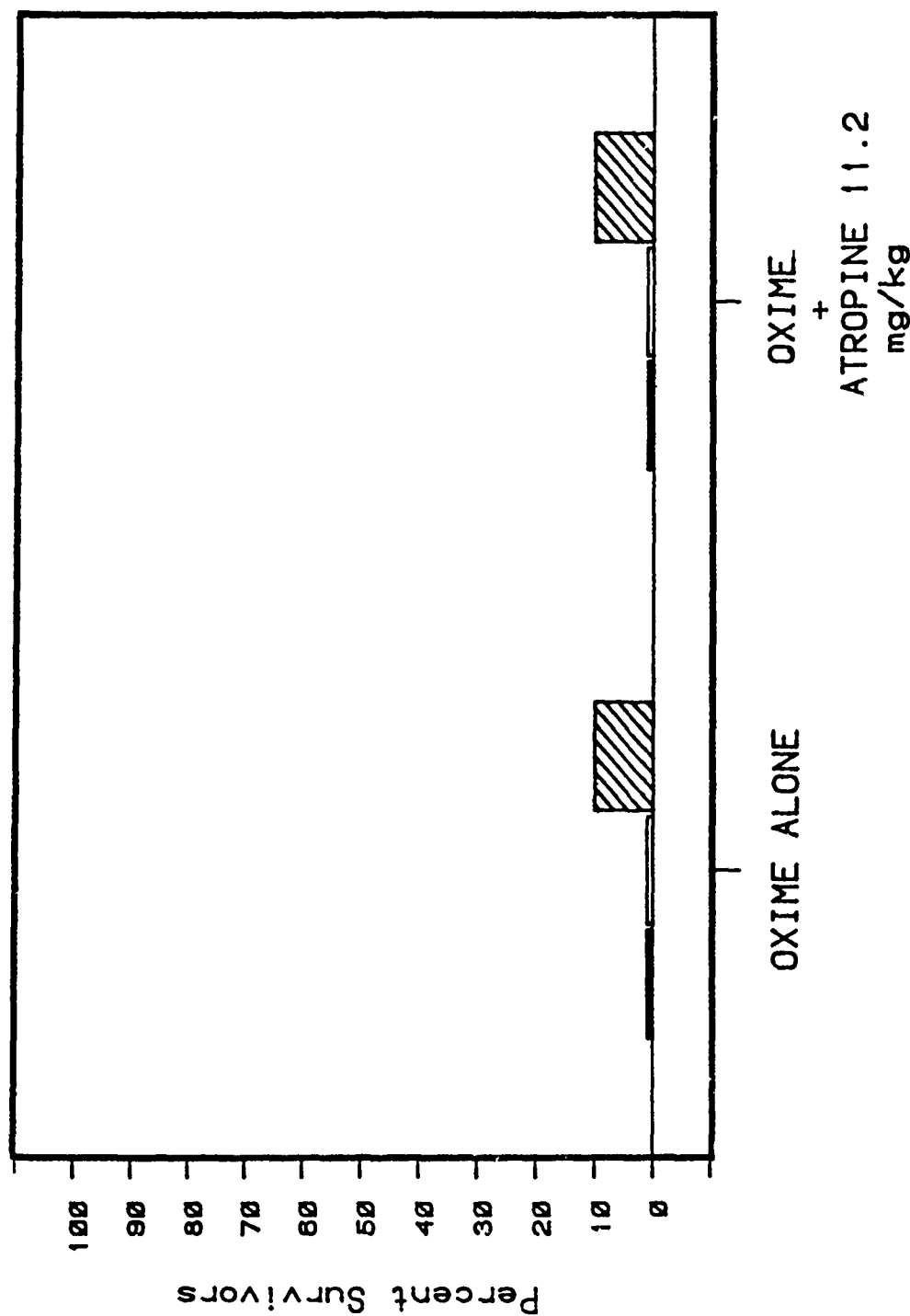
Optimal Atropine Sulfate/Pralidoxime Chloride Therapy
for GD, GA, and GB Poisoning in Mice and Guinea Pigs

Animal Model	Agent	Optimal Dose ATS/2-PAM(mg/kg)	Protective Ratio Afforded	LD90 Challenge Dose (ug/kg; LD50 Multiple)
Mouse	GD	11.2/25.0	1.9	196 ; 2.0xLD50
Mouse	GA	56.0/44.6	1.9	748 ; 2.46xLD50
Mouse	GB	25.0/28.0	2.2	468 ; 2.61xLD50
Guinea Pig	GD	64.0/100	3.7	129 ; 4.30xLD50
Guinea Pig	GA	32.0/50.0	4.6	638 , 5.36xLD50
Guinea Pig	GB	16.0/40.0	56.0	N.D.

N.D. Indicates not determined

Figure 12

Initial Efficacy of TMB-4 Alone and with Atropine Against (2.0xLD50) GD in Mice






 2-PAM 25.0 mg/kg
 TMB-4 11.8 mg/kg
 TMB-4 23.5 mg/kg

Figure 13

Initial Efficacy of Toxogonin Alone and with Atropine Against (2.0xLD50) GD in Mice

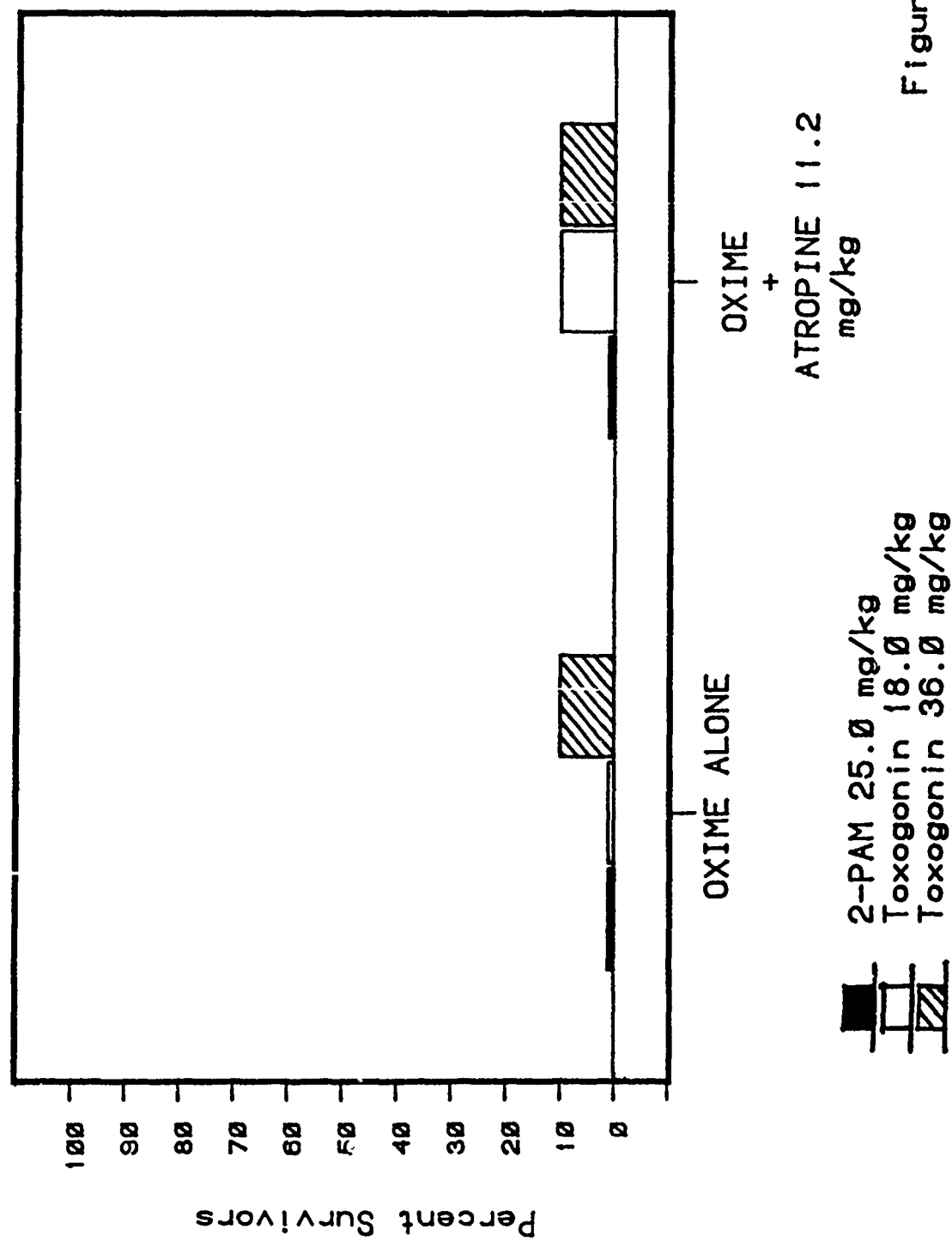
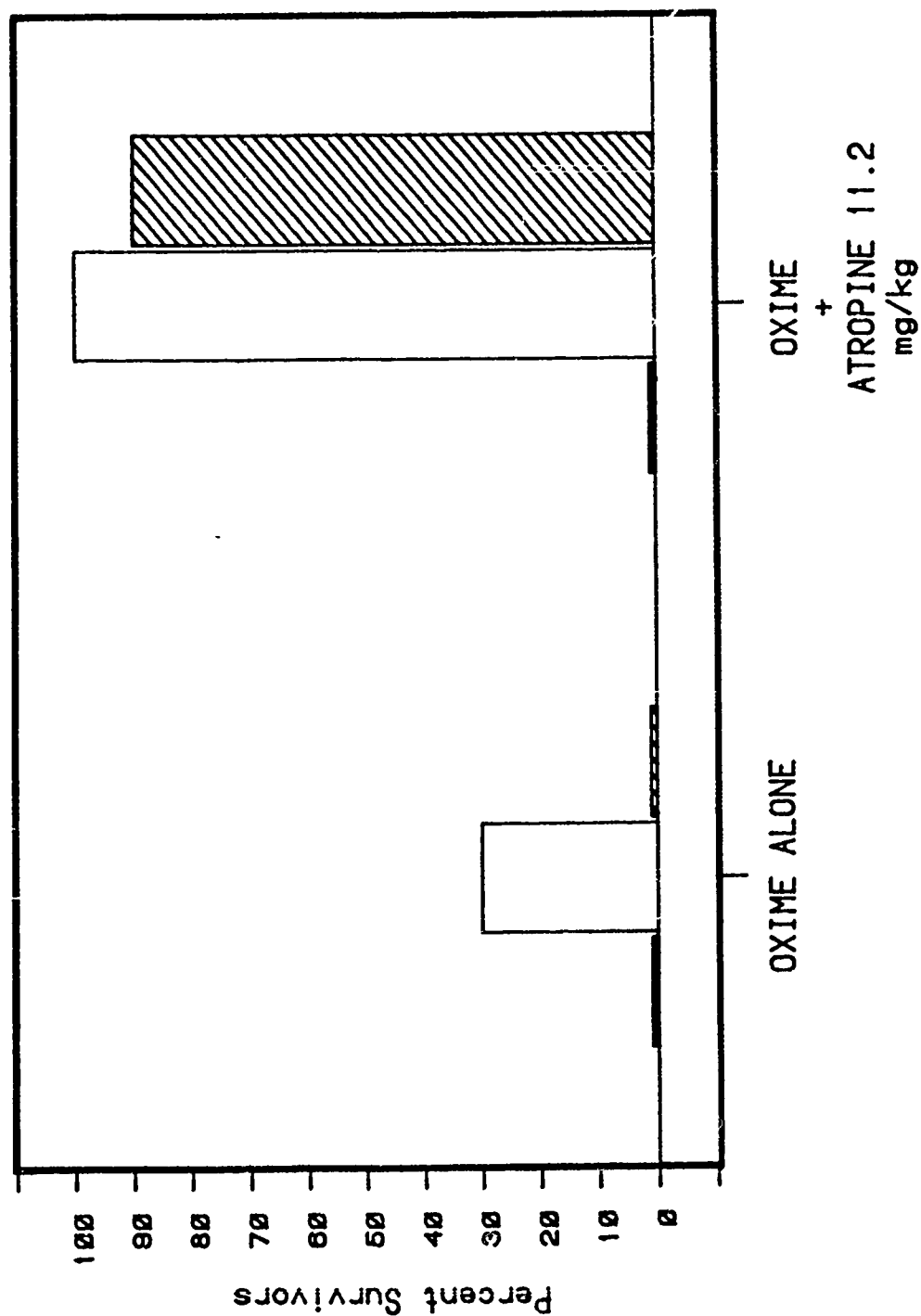


Figure 14

Initial Efficacy of HI-6 Alone and with Atropine Against (2.0xLD50) GD in Mice






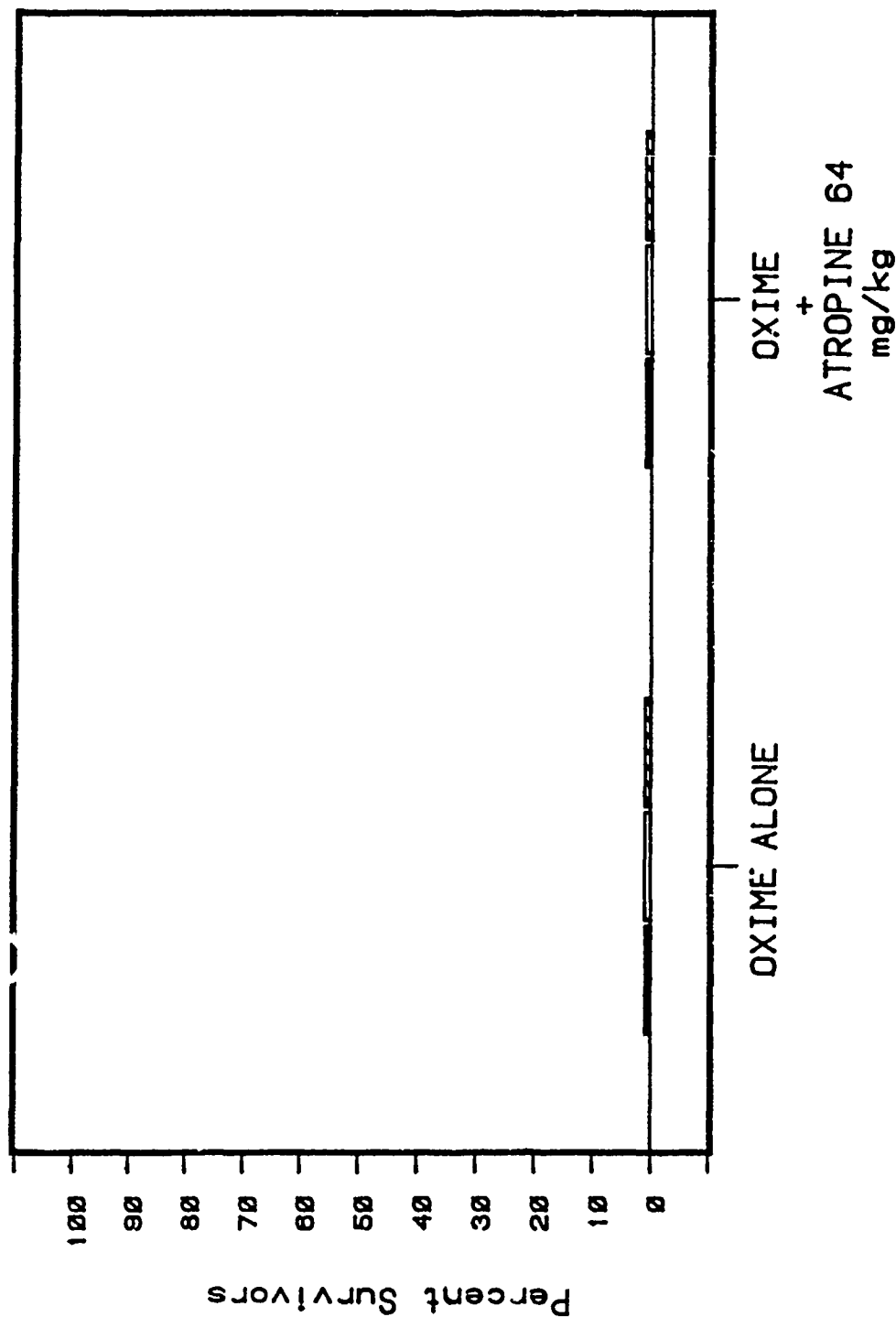
 2-PAM 25.0 mg/kg
 HI-6 76.6 mg/kg
 HI-6 153.4 mg/kg

Figure 15

Initial Efficacy of TMB-4 Alone and with Atropine Against (4.3xLD50) GD in Guinea Pigs






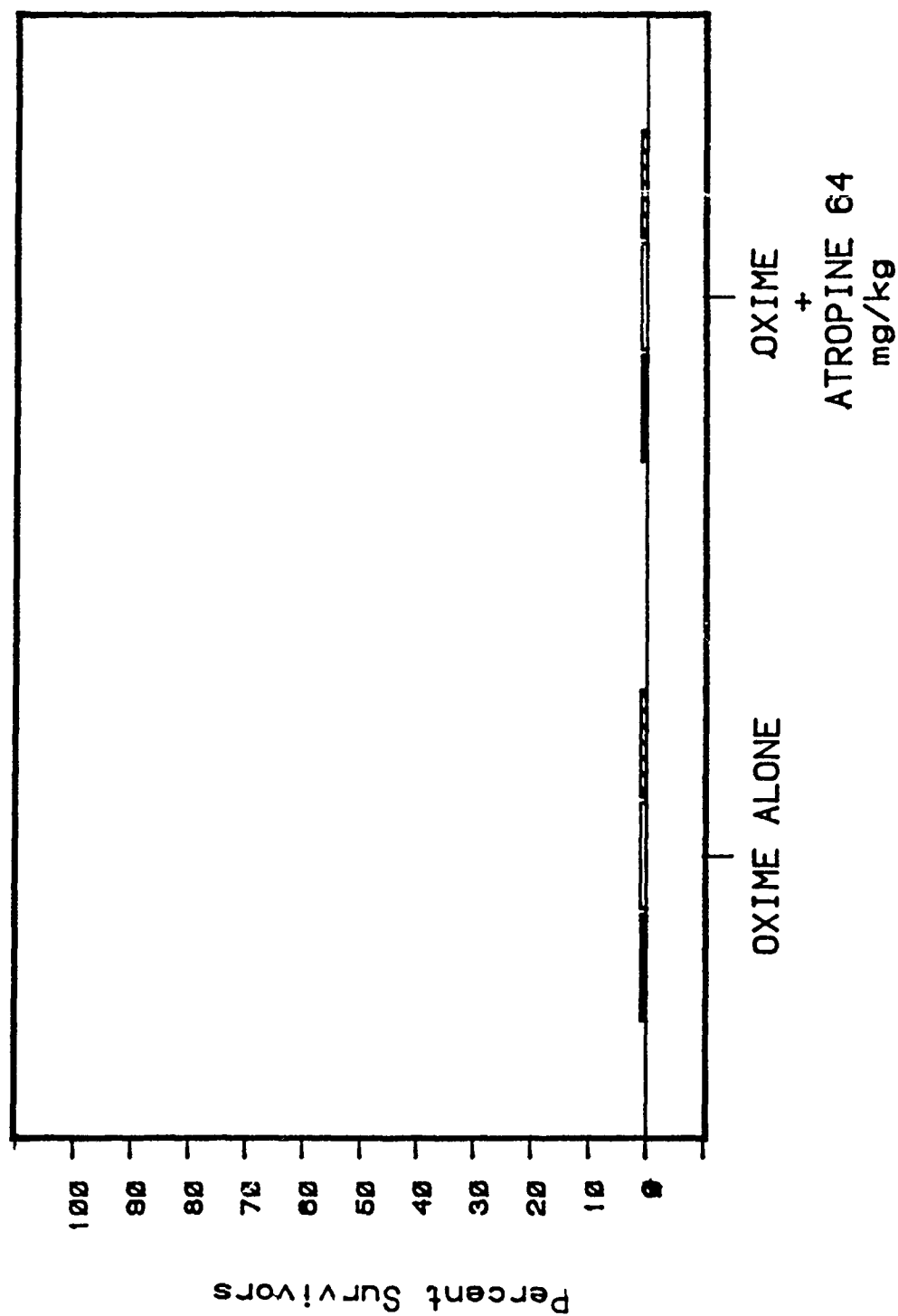
 2-PAM 100 mg/kg
 TMB-4 10.0 mg/kg
 TMB-4 20.0 mg/kg

Figure 16

Initial Efficacy of Toxogonin Alone and with Atropine Against (4.3xLD50) GD in Guinea Pigs






 2-PAM 50.0 mg/kg
 Toxogonin 13.1 mg/kg
 Toxogonin 26.3 mg/kg

Figure 17

Initial Efficacy of HI-6 Alone and with Atropine Against (4.3xLD50) GD in Guinea Pigs

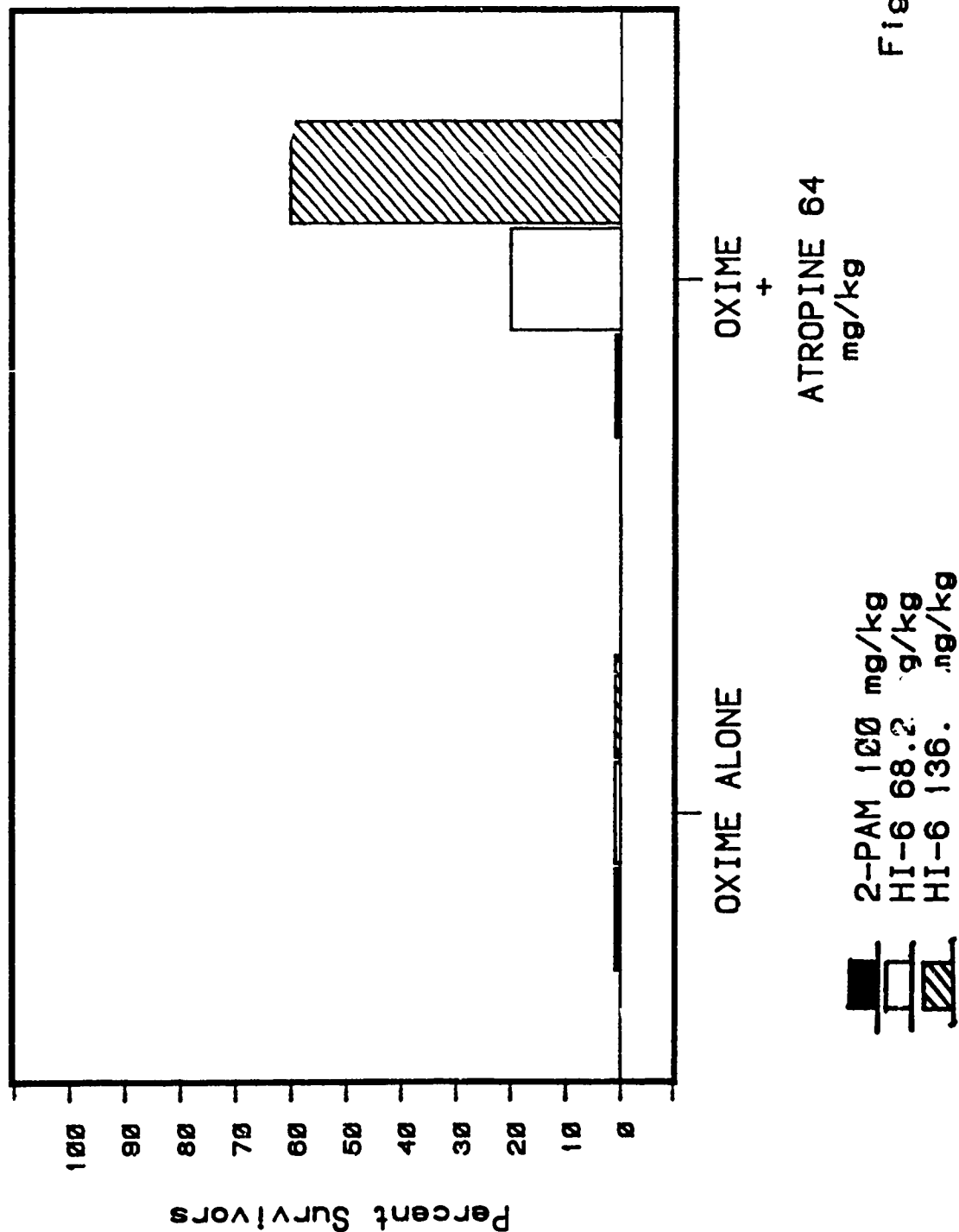


Figure 18

Initial Efficacy of TMB-4 Alone and with Atropine Against (2.46xLD50) GA in Mice

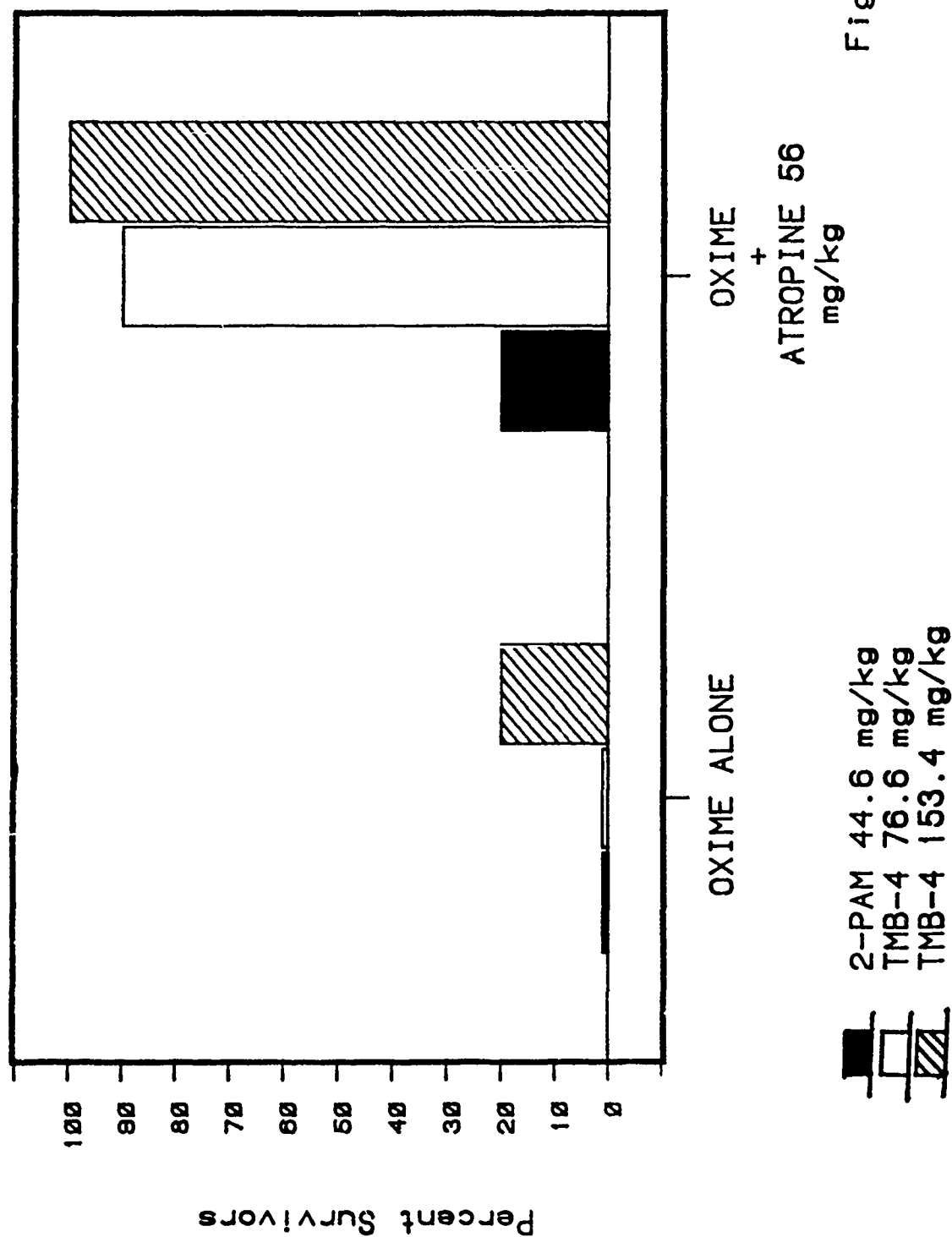
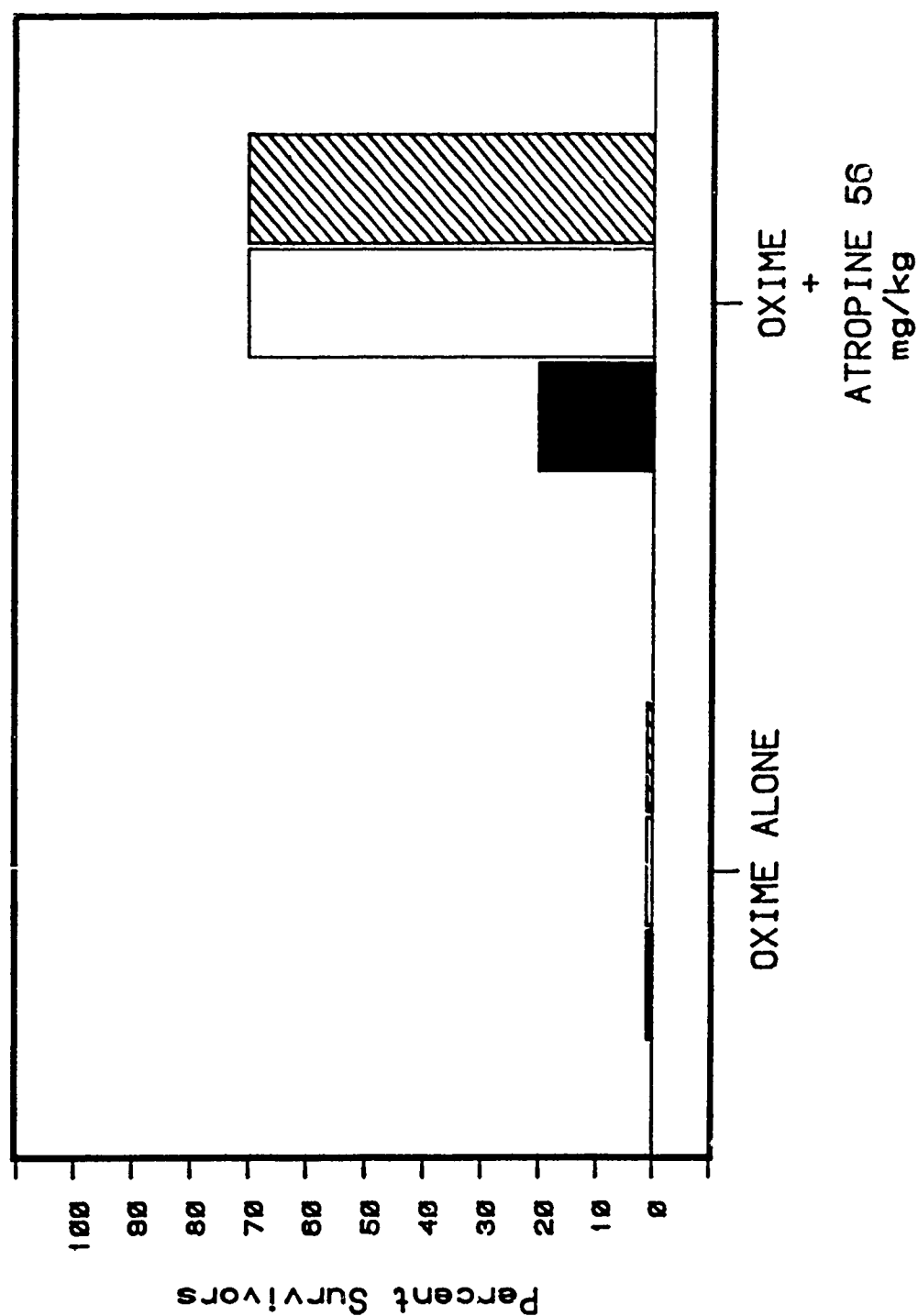


Figure 19

Initial Efficacy of Toxogonin Alone and with Atropine Against (2.46xLD50) GA in Mice






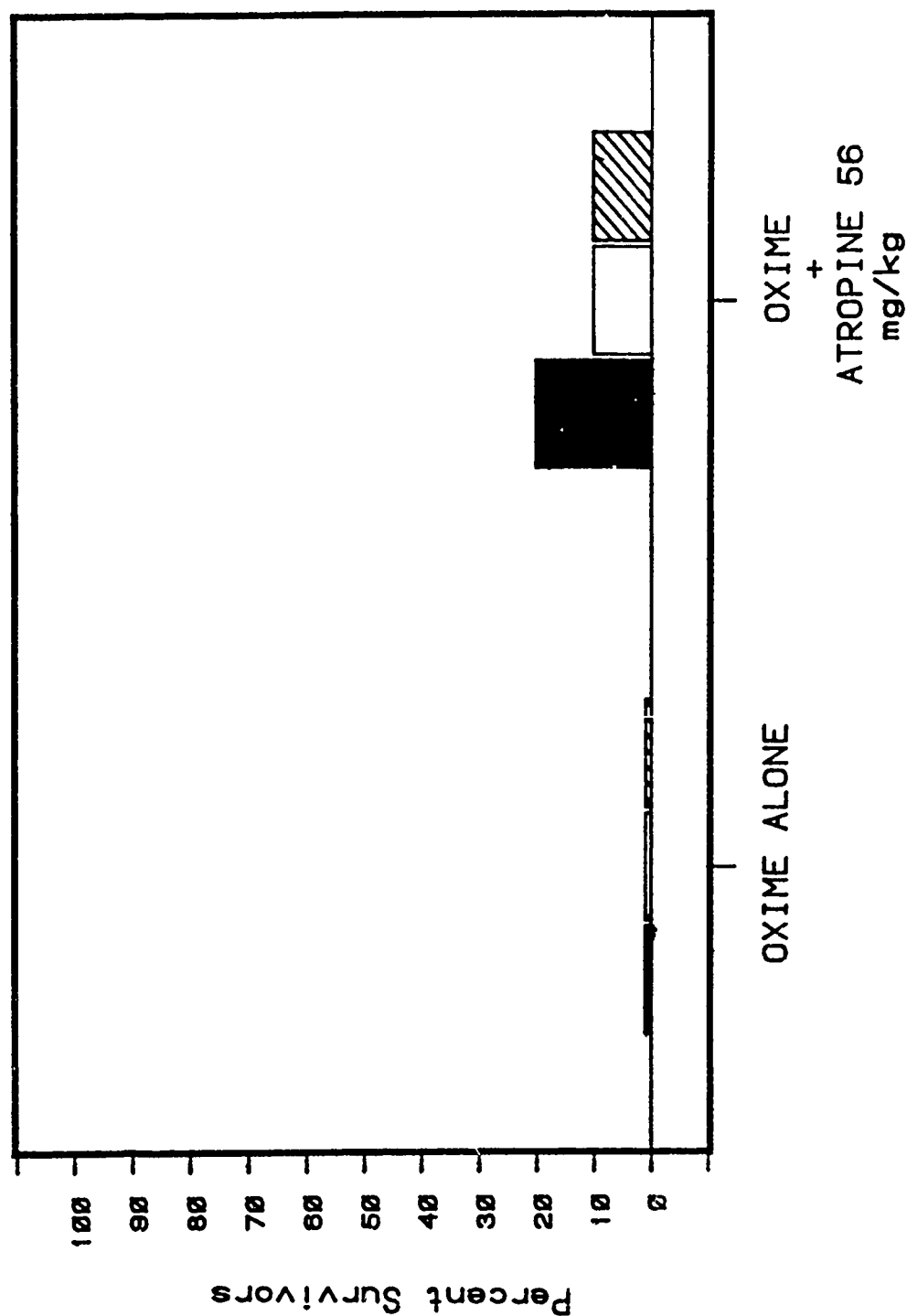
 2-PAM 44.6 mg/kg
 Toxogonin 19.5 mg/kg
 Toxogonin 39.1 mg/kg

Figure 20

Initial Efficacy of HI-6 Alone and with Atropine Against (2.46xLD50) GA in Mice



2-PAM 44.6 mg/kg
 HI-6 76.6 mg/kg
 HI-6 153.4 mg/kg

Figure 21

Initial Efficacy of TMB-4 Alone and with Atropine Against (5.36xLD50) GA in Guinea Pigs

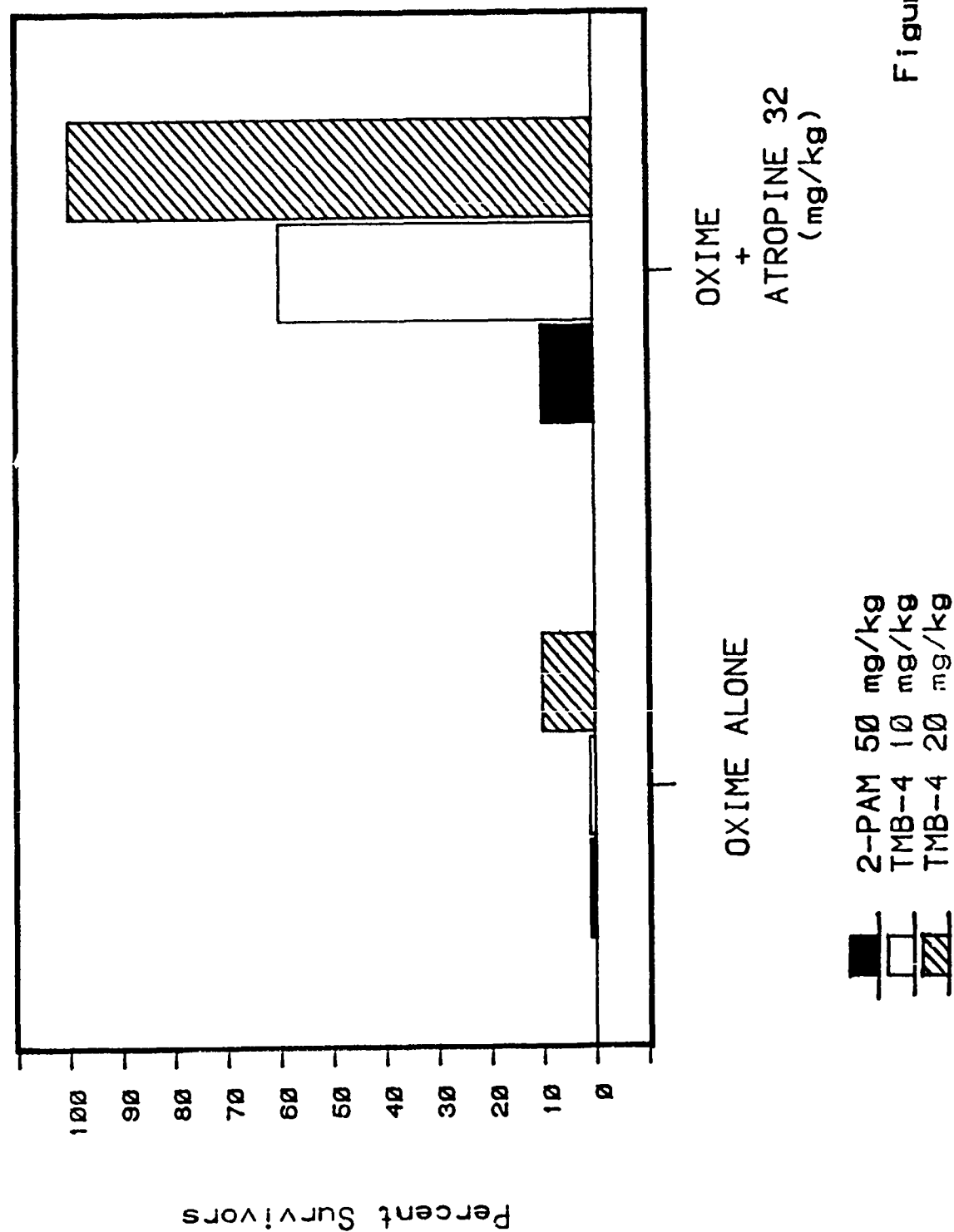


Figure 22

Initial Efficacy of Toxogonin Alone and with Atropine Against (5.36xLD50) GA in Guinea Pigs

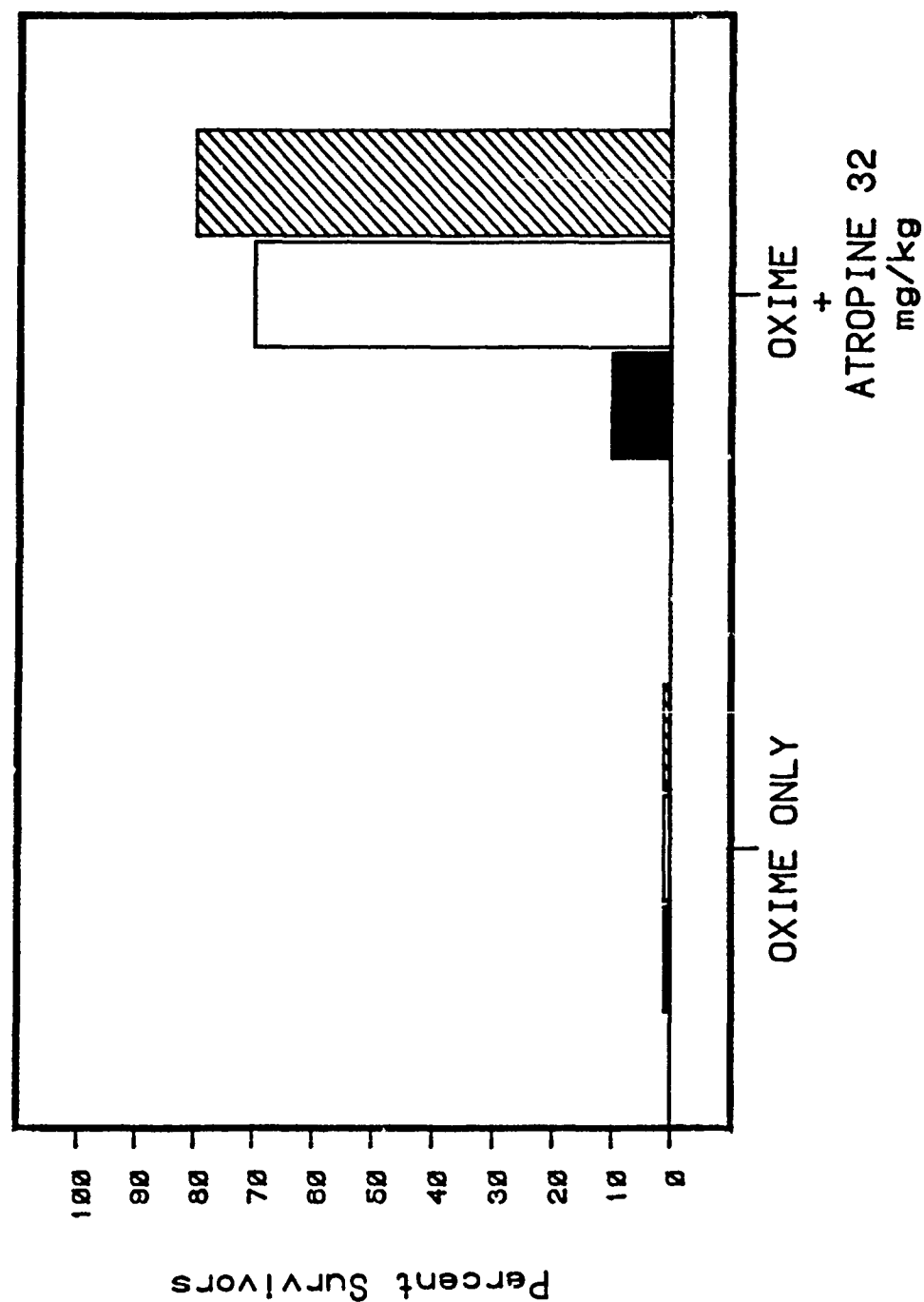


Figure 23

Initial Efficacy of HI-6 Alone and with Atropine Against (5.36xLD50) GA in Guinea Pigs

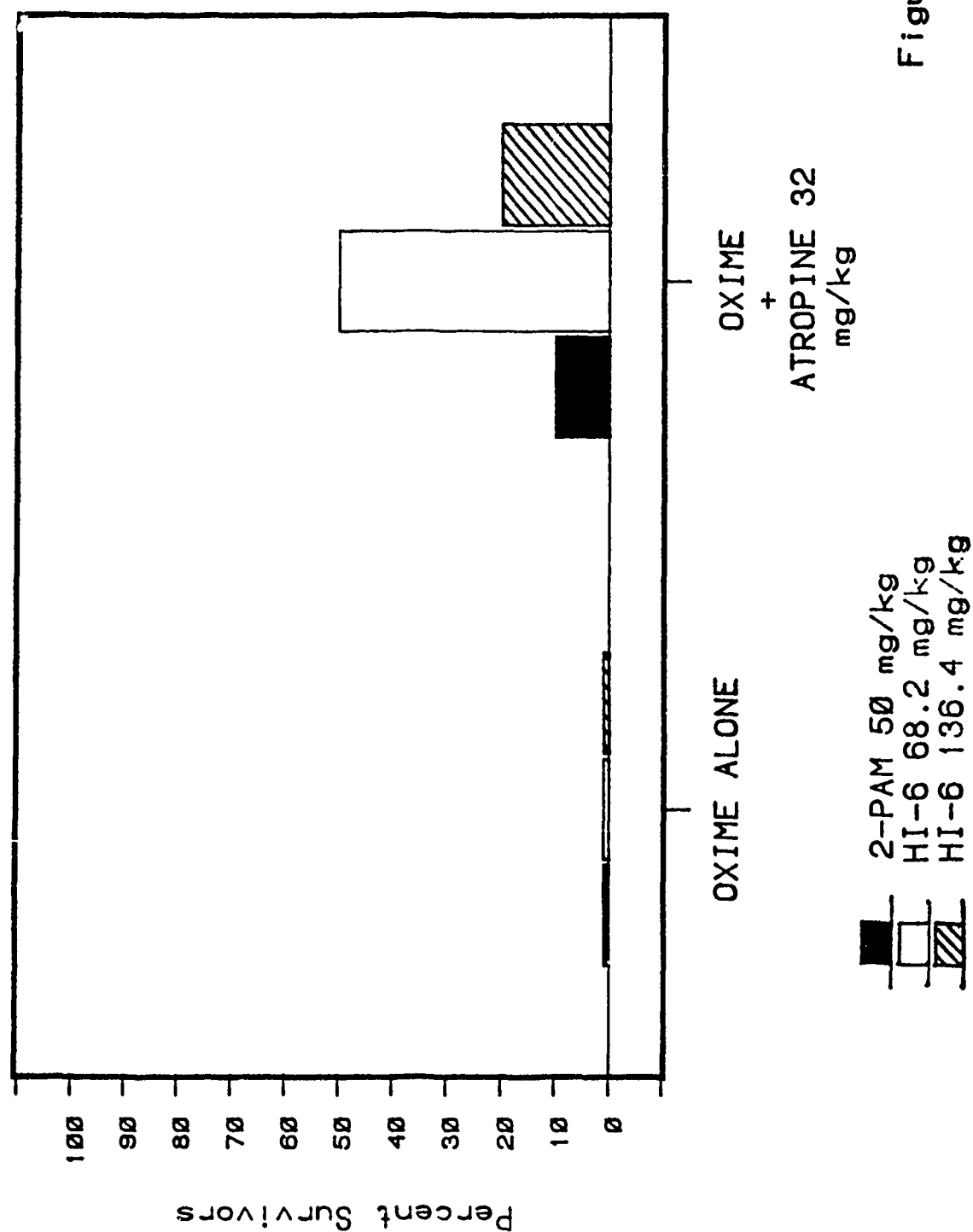


Figure 24

MODELS FOR ASSESSING EFFICACY OF PRETREATMENT COMPOUNDS
AGAINST ORGANOPHOSPHATES (OP'S)

I. KOPLOVITZ*, D.E. JONES, D.G. HARRINGTON, D.E. HILMAS
US Army Medical Research Institute of Chemical Defense
Aberdeen Proving Ground, MD 21010

and

C.J. CANFIELD
Walter Reed Army Institute of Research
Washington, DC

*Mailing Address: Commander
US Army Medical Research Institute of Chemical Defense
ATTN: SGRD-UV-DD/Dr. Irwin Koplovitz
Aberdeen Proving Ground, MD 21010

Abstract

A drug screening and evaluation program has been developed for the purpose of identifying and comprehensively evaluating pretreatment compounds to be used in combination with supporting treatment for efficacy against soman lethality in the mouse. We have defined and standardized the route of drug administration, a method for determining pretreatment time interval, and the test drug dosages to be used. These criteria have been used to standardize a pretreatment initial efficacy screen, a model which allows both the identification of efficacious compounds, and selection of the optimal pretreatment time interval for administration of each compound. Methods have also been developed and standardized for assessing the optimal pretreatment dose and corresponding protective level afforded by those identified efficacious compounds. The utility and reproducibility of these models have been validated through screening and evaluation of the carbamate pyridostigmine. Additional methods have also been developed and standardized for evaluating the critical range of acetylcholinesterase inhibition produced by this class of compounds (reversible cholinesterase inhibitors). These procedures have been extended to evaluate pretreatment compound efficacy against other organophosphorous compounds and have been adapted for similar use in the guinea pig. These methods should provide the means for accurate and efficient screening and evaluation of any combination of multiple pretreatment/treatment drug therapies.

Introduction

We have developed, standardized, and validated in vivo methods for the screening and evaluation of pretreatment compounds to be used in combination with supporting treatment for efficacy against soman-induced lethality in the mouse. These procedures have been extended to the guinea pig and adapted for use against other organophosphorous (OP) anticholinesterase agents. Our intent has been to interface these methods with the treatment models described by Major Jones in the preceding presentation, enabling evaluation and optimization of combination therapy with both pretreatment and treatment compounds.

In developing these methods, several questions or problems unique to the pretreatment test mode were readily apparent. These questions primarily concerned the rationale for pretreatment of agent intoxication, the selection of a reference drug for standardizing the methods, selection of a route for pretreatment drug administration, selection of pretreatment time intervals, and drug doses to be tested.

The rationale for a pretreatment mode for OP intoxication is based on results of several published studies which have shown that pretreatment can, indeed, provide protection against OP-induced lethality. In 1946, Koster showed that cats could be protected against the lethal effects of diisopropyl fluorophosphate (DFP) by pretreatment with the carbamate physostigmine (1). Subsequently, Gordon, et al. (2), found that treatment of the lethal effect of soman with atropine and pialidoxime chloride (2-PAM) in guinea pigs could be significantly enhanced by the intramuscular (IM) administration of physostigmine or pyridostigmine prior to agent challenge. Similar results have been reported in a number of species by several other investigators (3,4). It has been proposed that the protection seen in these studies is a result of spontaneous decarbamylation of acetylcholinesterase (AChE), thereby providing a constant, albeit low, level of AChE, which is both protected from irreversible agent inhibition and sufficient to maintain vital cholinergic function (5).

Pyridostigmine bromide was selected as the prototype drug to initiate development and standardization of the pretreatment test models. This carbamate was chosen rather than physostigmine for several reasons. It has both a longer half-life and a wider margin of safety than physostigmine (3,6). Most importantly, however, pyridostigmine is already approved for oral human use by the Food and Drug Administration, although not for the intended use described here (7). This fact, however, means that a great deal of preclinical and clinical test data are already available regarding pyridostigmine; an important point for future drug development considerations.

As described by Major Jones in the preceding paper, treatment compounds are all tested IM in the mouse screening model (8). This route of administration was chosen as it most closely parallels the present route of antidote

administration in the field, i.e., deep IM injection of atropine/2-PAM. In a field situation, however, parenteral administration of prophylactic compounds is infeasible, particularly if repeated self-administration is required. These constraints, therefore, dictate that dosing by the oral route would be most practical. For these reasons, we elected to screen and evaluate compounds for pretreatment efficacy following oral drug administration only.

An additional area of consideration for pretreatment drug screening was that of time of test compound administration. Although the optimal time for administration of treatment compounds is as soon after agent challenge as possible (atropine/2-PAM and all test compounds are administered at 10 seconds post-agent challenge in the mouse therapy models), no such corollary is true regarding optimal time for administration of pretreatment compounds. Time to peak activity in mice following oral drug administration can vary from as rapid as 10 minutes (9) to as long as 4 hours or more (10). Since our intent was to utilize this pretreatment test system to evaluate all types of compounds, the pretreatment test time must, therefore, coincide with time to peak drug effect for the particular drug being tested. Because this information is unknown for many of the compounds we intend to evaluate, the only alternative was to test compounds at multiple times prior to agent challenge using time points, which would hopefully encompass time to peak drug effect for any drug tested. Based on these considerations and the results of the literature review of orally administered compounds, we elected to initially screen pretreatment drugs at 7.5, 15, 30, 60, 120, 240, and 480 minutes prior to agent challenge.

The final area of consideration for testing of pretreatment compounds was that of selection of test drug dosage. It was imperative that the dose or doses tested not be, of themselves, toxic, yet high enough to provide effective drug levels at the necessary site of action. The first step for evaluating test compounds, therefore, had to be the determination of the range and limits of oral lethality. Once the acute (24 hour) oral LD₁ through LD₉₉ (with 95 percent confidence limits) were determined, it was further decided that compounds would be tested at fractions of their oral LD₅₀ ranging from a maximum of $1/4 \times \text{LD}_{50}$. With these considerations and limits thus decided, the initial step was to assess the pretreatment efficacy of our selected standard drug, pyridostigmine.

The Oral Toxicity of Pyridostigmine

Figure 1 shows the results of the oral lethality determination for pyridostigmine in the mouse. As standard procedure for all phases of model development, mice were fasted overnight. Doses of pyridostigmine were randomly allocated to groups of 10 mice and administered by gavage at a volume of 10 ml/kg in a vehicle consisting of 0.2 percent methylcellulose + 0.4 percent Tween 80. This vehicle was used rather than water to anticipate future compounds which might not be water soluble and would have to be given orally as a suspension. Pyridostigmine readily dissolved in this vehicle. The 24-hour oral LD₅₀ of pyridostigmine was calculated by probit analysis to be 26.2 mg/kg.

Initial Efficacy and Optimal Pretreatment Time

The initial efficacy and optimal pretreatment time for oral pyridostigmine were determined in 3 studies using doses ranging from 1/4 (6.55 mg/kg) to 1/512 (0.051 mg/kg) of the pyridostigmine LD50. Pretreatment times ranged from 7.5 min. to 48 hours. Ten mice were used for each time interval and dose of pyridostigmine tested. Doses of pyridostigmine were allocated to the mice randomly. At the appropriate time after pretreatment, soman was injected intramuscularly at 2 x LD50, followed 10 seconds later by treatment with a mixture of atropine (11.2 mg/kg) and 2-PAM (25.0 mg/kg). The rationale for this challenge level and treatment regimen was previously described and discussed by Major Jones. Some animals received pyridostigmine and soman without therapy. Control groups were included in which mice received vehicle as a pretreatment, followed by soman challenge and then therapy with atropine and 2-PAM.

The results of the first study are shown in Figure 2. Pyridostigmine was evaluated in this initial screen only at 1/4 and 1/8 x LD50. Pretreatment with either 1/8 (3.3 mg/kg) or 1/4 (6.55 mg/kg) LD50 afforded significant protection against soman-induced lethality at 24 hours in mice treated with atropine and 2-PAM. Thirty percent survival at 24 hours was observed following 1/8 x LD50 pyridostigmine administration as early as 7.5 minutes prior to agent challenge. In addition, 60 percent survival was observed as early as 15 minutes after the 1/4 LD50 dose. Peak protection afforded by either dose was 70 percent observed at the 8-hour interval. No survivors were observed in mice that received atropine and 2-PAM therapy alone, thus validating both the agent challenge dose and the protection observed following pyridostigmine pretreatment. Pyridostigmine alone at either dose was ineffective in preventing lethality from soman at any pretreatment time interval. An optimal pretreatment time could not be determined from this study because the protective effects of pyridostigmine were maintained throughout the duration of the experiment.

In an effort to further elucidate the efficacy and time course of the protective effects of oral pyridostigmine pretreatment, this study was repeated using lower doses of pyridostigmine and longer pretreatment time intervals. The doses of pyridostigmine tested in this study ranged from 1/4 LD50 to 1/64 LD50, while pretreatment time intervals were extended out to 48 hours. Again, mice were challenged with 2 x LD50 of soman IM at the appropriate time and treated with atropine (11.2 mg/kg) and 2-PAM (25.0 mg/kg) 10 seconds later. The results are shown in Figure 3. Pyridostigmine exhibited a protective effect at all the dose levels tested when combined with atropine and 2-PAM therapy. The onset of activity ranged from 15 to 60 minutes and was not dose related. Peak response was also not dose related with the lowest dose (1/64 x LD50; 0.41 mg/kg) showing almost as much protection (50 percent) as higher doses. Although the percent response was not directly dose related, the peak effect appeared to occur between 30 minutes and 120 minutes.

Again, the test data indicate that oral pretreatment of mice with pyridostigmine augments the therapeutic efficacy of atropine and 2-PAM. The data also suggest that very low oral doses of pyridostigmine are able to exert

a protective effect. In the third study, we evaluated oral doses of pyridostigmine as low as 1/512 LD50 and were still able to observe efficacy when combined with atropine/2-PAM therapy.

Individually, these studies did not define a precise optimal time for pyridostigmine pretreatment. We pooled the survival data for the three studies according to time interval, irrespective of the dose of pyridostigmine given. The results are shown in Figure 4. The numbers in parentheses indicate the total number of animals pretreated at each time interval. The highest survival occurred in a broad peak between 15 and 480 minutes. From this plot of the data, the 60-minute time interval was selected as the optimal pretreatment time.

Pyridostigmine Optimal Dose

Studies were next conducted to determine the oral dose of pyridostigmine affording the greatest protection against the lethal effects of soman in mice receiving atropine/2-PAM therapy. Based on results of the preceding studies, pyridostigmine was administered 1 hour prior to agent challenge. Pyridostigmine was administered orally to fasted mice at 1 of 9 doses ranging from 13.1 mg/kg (or 1/2 x LD50) to 0.013 mg/kg (or 1/2048 x LD50). Two vehicle control groups were also included. Pyridostigmine and vehicle dose groups were randomly allocated to the mice. One hour after pretreatment, mice (10 per group) were challenged IM with one of 5 doses of soman for each pretreatment dose, thereby providing a singular agent lethality dose response curve for each pretreatment dose tested (5 soman challenge doses x 10 mice per agent challenge group = 50 mice/agent LD50 curve).

Atropine (11.2 mg/kg) and 2-PAM (25 mg/kg) therapy was administered IM at 10 seconds postagent challenge to the 9 pyridostigmine pretreatment groups and to one of the control (no pyridostigmine) groups. The second control group (no pyridostigmine) was sham treated (IM) with saline rather than atropine/2-PAM. Mortality counts were taken at 24 hours and the 24-hour soman LD50 for each pretreatment group was calculated by probit analysis (11) or Thompson-Weil (12). Protective ratios (PR) for each pretreatment group were calculated by dividing the soman LD50 for untreated mice into the soman LD50 for each pretreatment group. Results of this study are shown in Figure 5. Note that the PR achieved with all doses of pyridostigmine tested up to 13.1 mg/kg (1/2 x LD50 of pyridostigmine) was greater than that achieved with atropine/2-PAM alone. The greatest PR was achieved with a dose of 0.82 mg/kg pyridostigmine. In order to further validate the results and reproducibility of the model, this procedure was repeated again in its entirety.

Results of this second study duplicated, almost exactly, results of the first optimal dose study. Note that the data are consistent and reproducible and that optimal protection is achieved with a pyridostigmine pretreatment dose of 0.82 mg/kg, a dose equivalent to 1/32 of the pyridostigmine oral LD50. This pyridostigmine dose affords a mean PR of 2.30 compared to a mean PR of 1.66 with atropine/2-PAM therapy alone. Although this increase in PR may appear slight, it represents a doubling of the protection afforded by atropine/2-PAM therapy alone.

We were satisfied from the results of these experiments that we had developed reliable, reproducible, and standardized methods to screen and evaluate the efficacy of pretreatment compounds against soman-induced lethality in mice. We had examined a number of criteria important for development of a valid model. The major areas of consideration were: rationale for the pretreatment test mode, selection of a standard pretreatment compound, selection of test compound administration, and selection of test compound dosage and pretreatment time intervals. Each of these considerations was achieved and appropriate test systems developed.

Table 1 shows a summary of the components of our model. As indicated, the initial experiments define the limits of candidate drug toxicity. Next, candidate drugs are screened for pretreatment efficacy against a single agent challenge dose. This method determines not only efficacy but also optimal pretreatment time. With pyridostigmine, we tested a wide range of drug doses and many pretreatment time intervals to fully explore the behavior of the model. To speed up the process for evaluating other pretreatment compounds, we decided to initially screen test compounds only at 1/4, 1/8 or 1/16, or 1/64, and 1/256 fraction of their oral LD50. These doses were selected because they encompass a range extending from a maximum non-lethal dose (1/4 x LD50) down through a very nominal drug dose (1/256 x LD50). We further decided to limit the pretreatment time intervals to 30, 60, 120, and 240 minutes. We felt that these intervals should encompass the time to peak drug activity for most orally administered drugs in mice.

If the candidate drug proved efficacious in the initial screen, it was then evaluated in the optimal dose study to assess the maximum attainable protective level, as well as the corresponding dose at which this level of protection was achieved. This entire screening process was then repeated in the guinea pig to confirm efficacy in a more responsive species.

Oral Toxicity of Pyridostigmine in Guinea Pigs

Our next objective was to extend the model just described for pyridostigmine in the mouse to the guinea pig. For experiments in guinea pigs, both male and female animals (300-450 grams) were used. As in mice, the animals were fasted overnight prior to use.

Figure 6 shows the oral toxicity of pyridostigmine in guinea pigs. The doses of pyridostigmine were randomly allocated to groups of 10 animals. The 24-hour oral LD50 was calculated to be 29.8 mg/kg and was very similar to that found in the mouse (Figure 1).

Pyridostigmine Initial Efficacy and Optimal Pretreatment Time in Guinea Pigs

The initial efficacy of oral pyridostigmine pretreatment in guinea pigs is shown in Figure 7. As described earlier, doses of pyridostigmine ranging from 1/4-1/256 fraction of the oral LD50 were administered to groups of 10 animals at pretreatment times of 30, 60, 120, and 240 minutes. At the appropriate time, each group of animals was challenged with subcutaneously

administered soman ($4.3 \times \text{LD}_{50}$) and treated intramuscularly 1.0 minute later with atropine (64.0 mg/kg) and 2-PAM (100.0 mg/kg). The rationale for this soman challenge level and treatment regimen for guinea pigs was previously described and discussed by Major Jones in the preceding presentation.

Protection against soman-induced lethality at 24 hours was observed at all pretreatment times in guinea pigs which received the 0.47, 3.75, and 7.5 mg/kg doses of pyridostigmine. The 0.12 mg/kg dose showed activity only at the 240-minute time period. Peak protection of 66 percent was observed at the 30-minute pretreatment interval for $1/4 \times \text{LD}_{50}$. No survivors were observed in guinea pigs receiving atropine/2-PAM alone or in animals pretreated with pyridostigmine alone. This validates both the agent dose and the protection observed. Plotting the survival data versus time (Figure 8) for all doses of pyridostigmine showed that the highest survival occurred between 30-240 minutes with a small peak at 30 minutes. This broad peak, if your recall, was also observed with pyridostigmine in the mouse. Optimal dose studies are currently in progress using 30, 60, and 120 minutes pretreatment intervals.

The data from the guinea pigs confirm that oral pyridostigmine pretreatment is effective against soman lethality when used in combination with atropine/2-PAM treatment. Pyridostigmine exhibited similar efficacy and time course against soman in both the mouse and guinea pig.

Having established the methodology using pyridostigmine as the prototype to screen for pretreatment efficacy against soman in the mouse and extending these procedures to evaluate pyridostigmine in the guinea pig, we were then interested in evaluating another candidate pretreatment compound, the carbamate physostigmine.

Oral Toxicity of Physostigmine

Table 2 shows the oral LD_{50} of physostigmine in mice and guinea pigs. Physostigmine was 6.7 times more toxic than pyridostigmine in the mouse with an LD_{50} of 3.9 mg/kg and 4.4 times more toxic than pyridostigmine in the guinea pig with an LD_{50} of 6.8 mg/kg.

Initial Efficacy of Physostigmine Pretreatment in Mice and Guinea Pigs

The initial efficacy of oral physostigmine pretreatment was performed in both mice and guinea pigs using $1/4$, $1/16$, $1/64$, and $1/256$ fractions of their respective oral LD_{50} . These doses were administered at 30, 60, 120, and 240 minutes prior to soman. The challenge level of soman and the atropine/2-PAM doses for each species were the same as those used for the pyridostigmine studies. The results of the physostigmine initial efficacy in the mouse are shown in Figure 9.

In the mouse, oral physostigmine was an effective pretreatment against soman-induced lethality at all doses tested when combined with atropine and 2-PAM treatment. Peak survival at 24 hours was observed for 3 of 4 doses at the 30-minute pretreatment interval. Peak activity at this time ranged from

50 percent for 0.015 mg/kg ($1/256 \times \text{LD50}$) to 100 percent for 0.975 mg/kg ($1/4 \times \text{LD50}$). A plot of the survival data versus time for all doses of physostigmine (Figure 10) shows that peak survival occurred at the 30-minute pretreatment interval.

Figure 9 shows that the duration of the protective effect of oral physostigmine was dose related. The highest dose ($1/4 \times \text{LD50}$) exhibited activity for 4 hours. Protection declined after 60 minutes for the $1/256 \times \text{LD50}$ dose and after 120 minutes for the $1/16$ and $1/64 \times \text{LD50}$ doses. The short duration of action of the lower doses of physostigmine is in contrast to pyridostigmine pretreatment in the mouse, which showed significant amounts of protection at 4 hours with low ($1/256$, $1/512 \times \text{LD50}$) doses.

Oral physostigmine was also an effective pretreatment against soman lethality in guinea pigs when combined with atropine/2-PAM treatment (Figure 11). All pretreatment doses evaluated were protective. Peak protection at 24 hours ranged from 30 percent survival for $1/256 \times \text{LD50}$ at 30 minutes to 90 percent survival for $1/16 \times \text{LD50}$ at 60 minutes. At the 4 hour pretreatment time the $1/64$, $1/16$, and $1/4 \text{ LD50}$ doses still showed 30-60 percent protection. A plot of total survivors versus time for all doses of physostigmine (Figure 12) showed that peak survival in the guinea pig occurred at the 60-minute pretreatment time.

Oral Efficacy of Pyridostigmine Pretreatment Against Tabun Poisoning

Soman is the OP agent against which the efficacy of all pretreatment and treatment compounds are evaluated first, since this agent is considered the primary threat agent and the most difficult to treat. It is, however, also important that pretreatment, as well as treatment compounds, exhibit efficacy against other OP's. For this reason, we evaluated the efficacy of oral pyridostigmine against Tabun poisoning in mice and guinea pigs. Tabun was selected because it is also difficult to treat and has recently gained public attention because of its use in the Iraq-Iran war.

The efficacy of oral pyridostigmine pretreatment was evaluated against Tabun poisoning in mice and guinea pigs using previously described pyridostigmine doses and pretreatment time intervals. Mice were challenged at the appropriate time after pretreatment with $2.46 \times \text{LD50}$ of Tabun injected intramuscularly followed 10 seconds later with intramuscular atropine (56 mg/kg) and 2-PAM (44.6 mg/kg). The rationale for the Tabun challenge level and the atropine/2-PAM doses was described in the previous paper by Major Jones. The results are shown in Figure 13. Oral pyridostigmine was an effective pretreatment against the lethal actions of Tabun in mice receiving treatment with atropine and 2-PAM. Peak survival at 24 hours occurred at the 120-minute pretreatment interval and ranged from 60 percent for the $1/256$ dose to 100 percent for the $1/16$ dose. This pretreatment time period was clearly the optimal time for oral pyridostigmine pretreatment against Tabun poisoning in mice. At four hours, 3 of the 4 doses still showed 30-40 percent protection.

The efficacy of oral pyridostigmine pretreatment against Tabun poisoning in guinea pigs is shown in Figure 14. Doses of pyridostigmine and pretreatment times were as described. At the appropriate time after pretreatment, the guinea pigs were challenged with $5.36 \times \text{LD}_{50}$ of Tabun subcutaneously and treated 1.0 minute later with atropine (32 mg/kg) and 2-PAM (50 mg/kg). The rationale for this challenge dose and treatment regimen was described by Major Jones in the preceding paper. Oral pretreatment with pyridostigmine was very effective in augmenting the activity of atropine/2-PAM therapy in guinea pigs poisoned with Tabun. Sustained and dose-related protection was observed at all time periods and dose levels tested. Peak activity ranged from 30 percent survival for the $1/256 \times \text{LD}_{50}$ dose to 90 percent for the $1/8 \times \text{LD}_{50}$ dose and was still present 4 hours after pretreatment. No precise optimal pretreatment time could be determined from this study.

Acetylcholinesterase Inhibition

As previously stated, the protective action of carbamates against poisoning by organophosphate cholinesterase inhibitors is presumably due to the ability of the carbamate to reversibly bind to acetylcholinesterase (13). The carbamylated enzyme subsequently undergoes spontaneous breakdown to liberate the free enzyme. The portion of the enzyme in tissues that was carbamylated would be protected against phosphorylation by organophosphates. Gradual decarbamylation of the enzyme in parallel with relatively rapid removal or destruction of the organophosphate would release sufficient acetylcholinesterase to maintain life (14). To more fully examine this premise, we decided to examine the relationship between AChE inhibition following oral pyridostigmine and the protection afforded against soman lethality.

Mice were treated orally with pyridostigmine (6 mice per treatment group) at the same doses used in the optimal dose studies. One hour later, blood was collected from the medial canthus of the eye and whole blood AChE levels measured using methods described by Siakotos et al. (15). Results are shown in Figure 15.

At 1 hour postpyridostigmine oral dosing, AChE inhibition ranged from a mean of 3 percent at the low dose of 0.013 mg/kg to a mean of 91 percent at the high dose of 13.1 mg/kg. The computed dose for 50 percent AChE was 0.46 mg/kg. Probit transformation analysis (16), not shown here, indicated that the increase in AChE inhibition corresponded to the increase in pyridostigmine dose (log dose) with a correlation coefficient of 0.988.

A comparison of these results with those of the pyridostigmine optimal dose studies, Table 3, indicated that the optimal dose of pyridostigmine, 0.82 mg/kg, produced a 66 percent inhibition of AChE at one hour after dosing. A one hour post-treatment time was also the time point chosen for soman challenge in the optimal dose studies.

Table 3 shows that relatively large changes in AChE inhibition resulted in only relatively small increases in protective ratios. Whereas the optimal

dose of 0.82 mg/kg produced a 66 percent inhibition of AChE with a corresponding PR of 2.30, a much lower dose of pyridostigmine, 0.026 mg/kg, produced a corresponding lower (9 percent) inhibition of AChE but only a slightly lower PR of 2.03.

It is readily apparent from these studies that the degree of pretreatment efficacy in mice is not solely dependent on amount of AChE inhibitor in whole blood. The data provided by these studies should, however, serve as a useful reference for comparing and, hopefully, further elucidating the exact mechanism of action of other similarly acting pretreatment compounds yet to be tested.

Summary and Conclusions

We have described standardized methods to screen and evaluate pretreatment compounds orally for efficacy against OP-induced lethality. These methods were developed for use in combination with treatment models, enabling simultaneous evaluation and optimization of both pretreatment and treatment compounds.

We gave careful consideration to a number of questions or problems we felt were important to the development of a valid pretreatment model. We provided answers to each of these questions and developed the appropriate test system.

Using the methods developed, we have demonstrated the oral pretreatment efficacy of pyridostigmine and physostigmine in mice and guinea pigs against soman-induced lethality when combined with supporting atropine/2-PAM therapy. The protection afforded by both carbamates occurred over a wide range of oral doses. The protection observed at small doses ($1/256 \times \text{LD}_{50}$) is indicative of the high potency of these compounds. In addition, oral pyridostigmine was equally effective as a pretreatment in both species against the lethal effect of tabun. Without supporting treatment, however, neither carbamate was effective against soman or tabun.

The optimal pretreatment time varied with the individual carbamate, the dose administered, the species, and the OP used. Both pyridostigmine and physostigmine were capable of exhibiting activity for at least 4 hours following single oral doses.

Optimal protection afforded by oral pyridostigmine administered one hour prior to soman occurred at a dose of 0.82 mg/kg. This dose resulted in a mean protective ratio of 2.30. Lower doses (0.026 mg/kg), however, were almost as effective (PR=2.03).

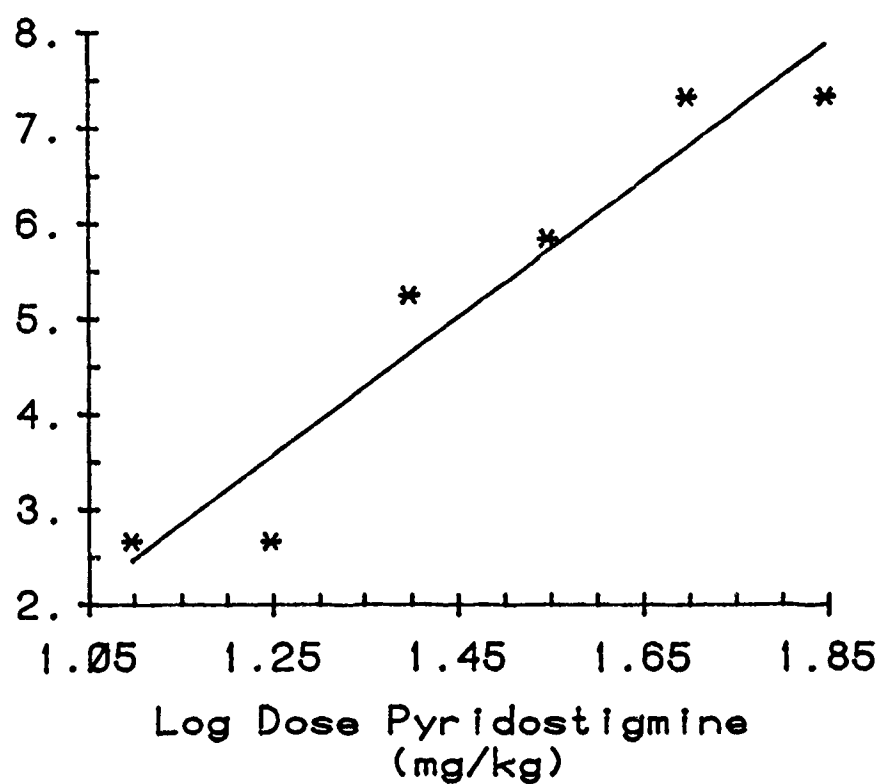
The methods described provide a reliable and reproducible means of evaluating the efficacy of all classes of compounds.

Comparison of acetylcholinesterase inhibition at one hour after oral pyridostigmine in mice with protection against soman-induced lethality showed that relatively large changes in acetylcholinesterase inhibition resulted in only small increases in protective ratios. This suggests that the degree of pretreatment efficacy afforded by oral pyridostigmine in the mouse is not solely dependent on the amount of acetylcholinesterase inhibition in whole blood.

/

References

1. Koster, R., J. Pharm. Exp. Ther., 88:39-46, 1946.
2. Gordon, J.J., L. Leadbeater, and M.P. Maidment, Toxicol. and App. Pharm., 43:207-216, 1978.
3. Berry, W.K. and D.R. Davies, Biochem. Pharmacol., 19:927-934, 1970.
4. Dirnhuber, P., M.C. French, D.M. Green, L. Leadbeater, and J.A. Stratton, J. Pharm. Pharmacol., 31:295-299, 1979.
5. Green, A.L., Biochem. Pharmacol., 32:1717-1722, 1983.
6. Deyi, X., W. Linxiu, and P. Shuqiu, Fundamental and Appl. Tox., 1:217-221, 1981.
7. Baker, C.E., Jr., Pub., Physicians Desk Reference, 36th Ed., 1982.
8. Jones, D.E. and D.E. Hilmas, NATO Panel VIII RSG-3 Proceedings, Oslo, Norway, 10-14 Oct 1983.
9. Kissel, J.W., J.R. Albert, and G.C. Boxhill, J. Exp. Ther., 134:332-340, 1961.
10. Fink, G.B. and E.A. Swinyard, J. Pharm. Exp. Ther., 127:318-324, 1954.
11. Finney, D.J., Probit Analysis, 3rd Ed., Cambridge University Press, 1971.
12. Thompson, W.R. and C.S. Weil, Biometrics 8, 51-58, 1952.
13. Wilson, I.B., M.A. Hatch, and S. Ginsburg, J. Biol. Chem., 236:1498-1500, 1961.
14. Wilson, I.B., M.A. Hatch, and S. Ginsburg, J. Biol. Chem., 235:2512-2515, 1960.
15. Siakotos, A.N., M. Filbert, and R. Hester, Biochem., 3:1, 1969.



0 Percent Mortality	1 DOSE (mg/kg)	2 95% Conf. Limits
1. 1.0	14.7	9.8-21.9
2. 16.0	20.4	16.4-25.4
3. 50.0	26.2	22.5-30.4
4. 84.0	33.6	26.9-41.7
5. 99.0	46.7	31.2-69.9

Figure 1. Acute (24 hour) Oral LD50 of Pyridostigmine Bromide in Mice. Top - A probit plot of the oral pyridostigmine dose-lethality curve. N=10 at each point. Bottom - Computed oral pyridostigmine doses and 95 percent confidence limits for various percent mortalities.

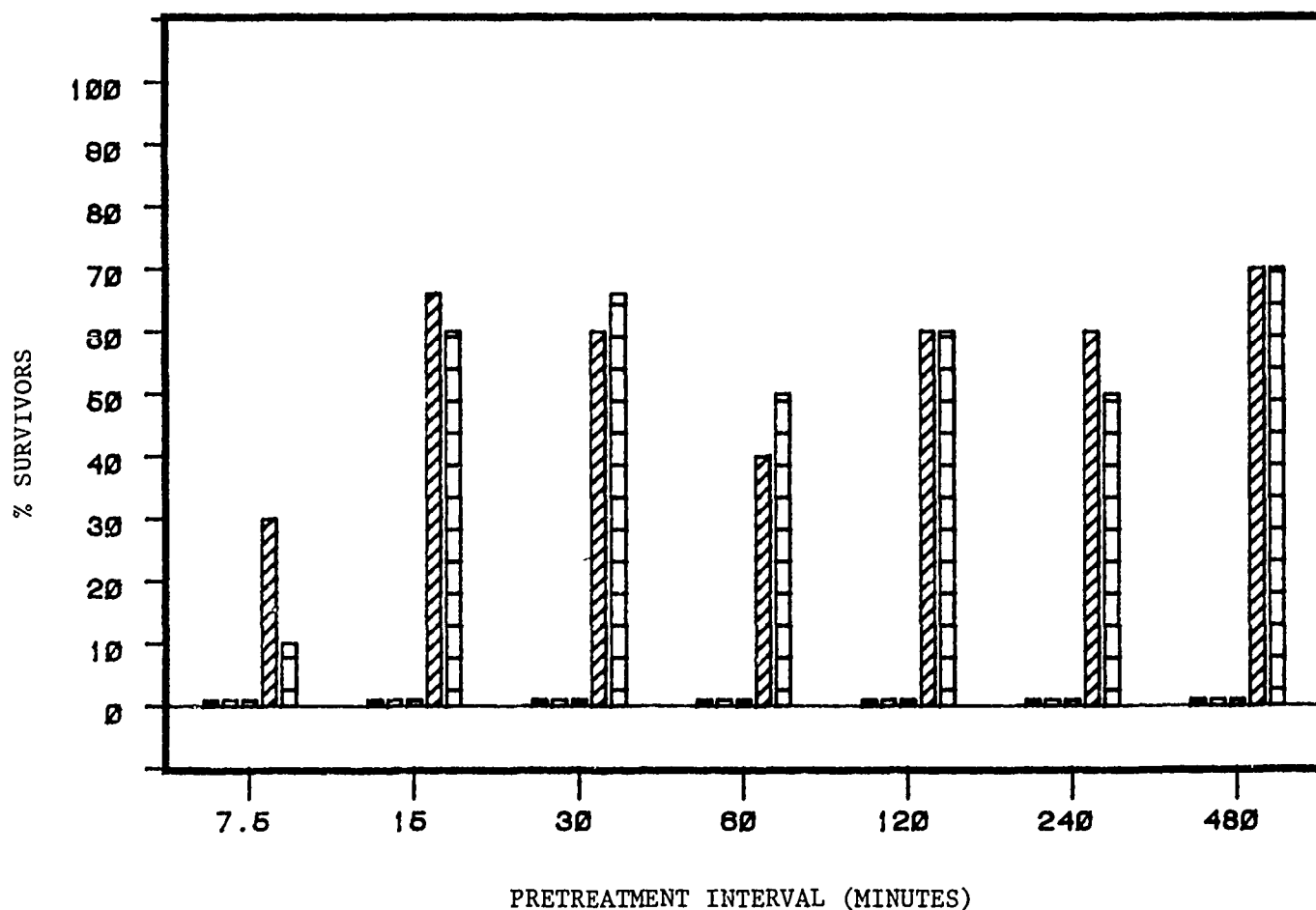


Figure 2. The Efficacy of Oral Pyridostigmine Pretreatment in Mice Challenged with Soman (2 x LD50, IM). Bars represent 24-hour survival at the pretreatment intervals indicated.

■ = therapy alone (atropine (11.2 mg/kg) and 2-PAM (25 mg/kg));
 □ = pyridostigmine alone at 3.3 mg/kg (1/8 x LD50);
 ▨ = pyridostigmine alone at 6.55 mg/kg (1/4 x LD50);
 ▩ = pyridostigmine 1/8 x LD50 + therapy;
 ▪ = pyridostigmine 1/4 x LD50 + therapy. N=10 1/8 x LD50 for each bar.

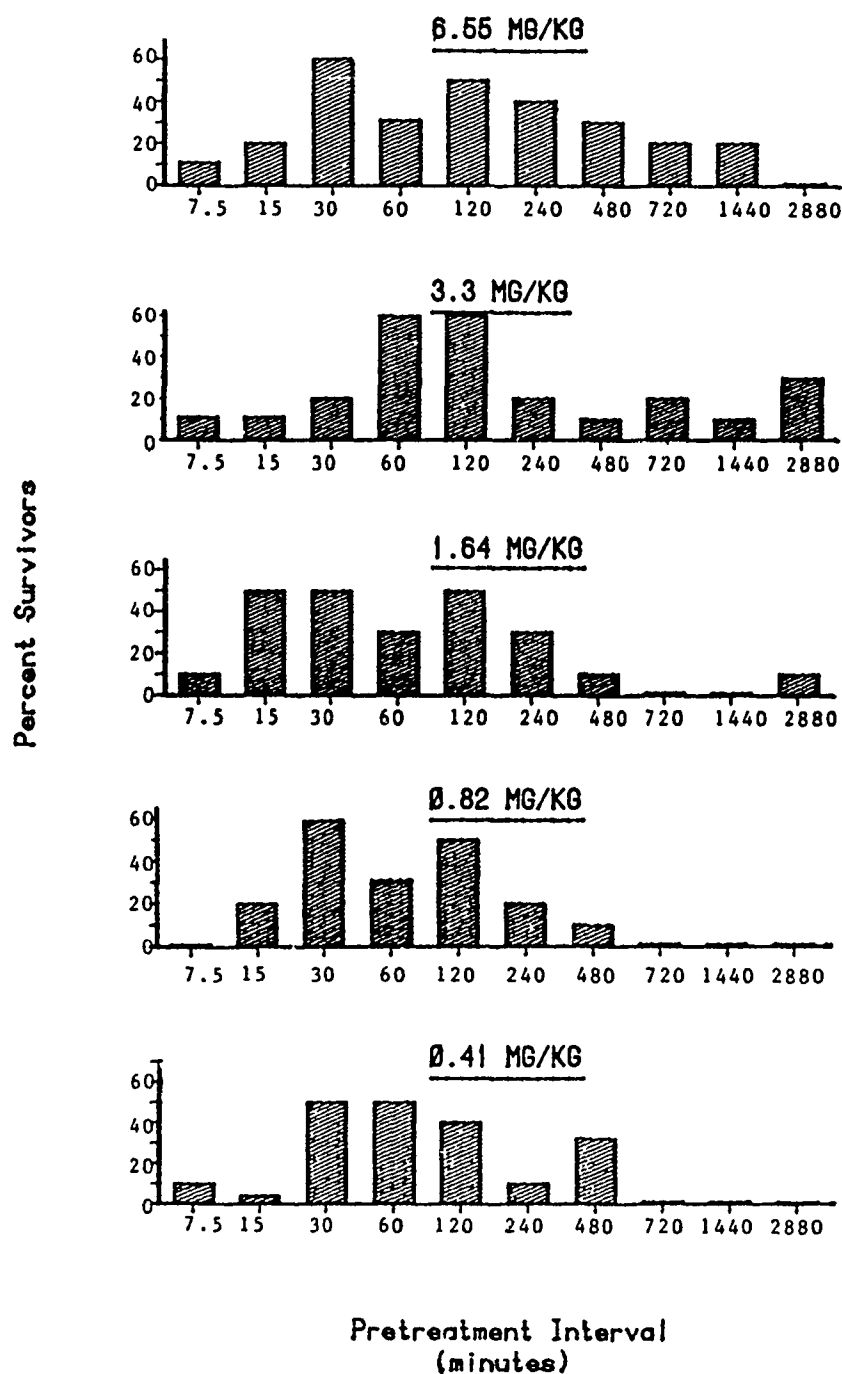


Figure 3. Dose and Time Related Effects of Oral Pyridostigmine Pretreatment in Mice Challenged with Soman (2 x LD50) and Treated with Atropine (11.2 mg/kg) and 2-PAM (25 mg/kg). N=10 at each bar.

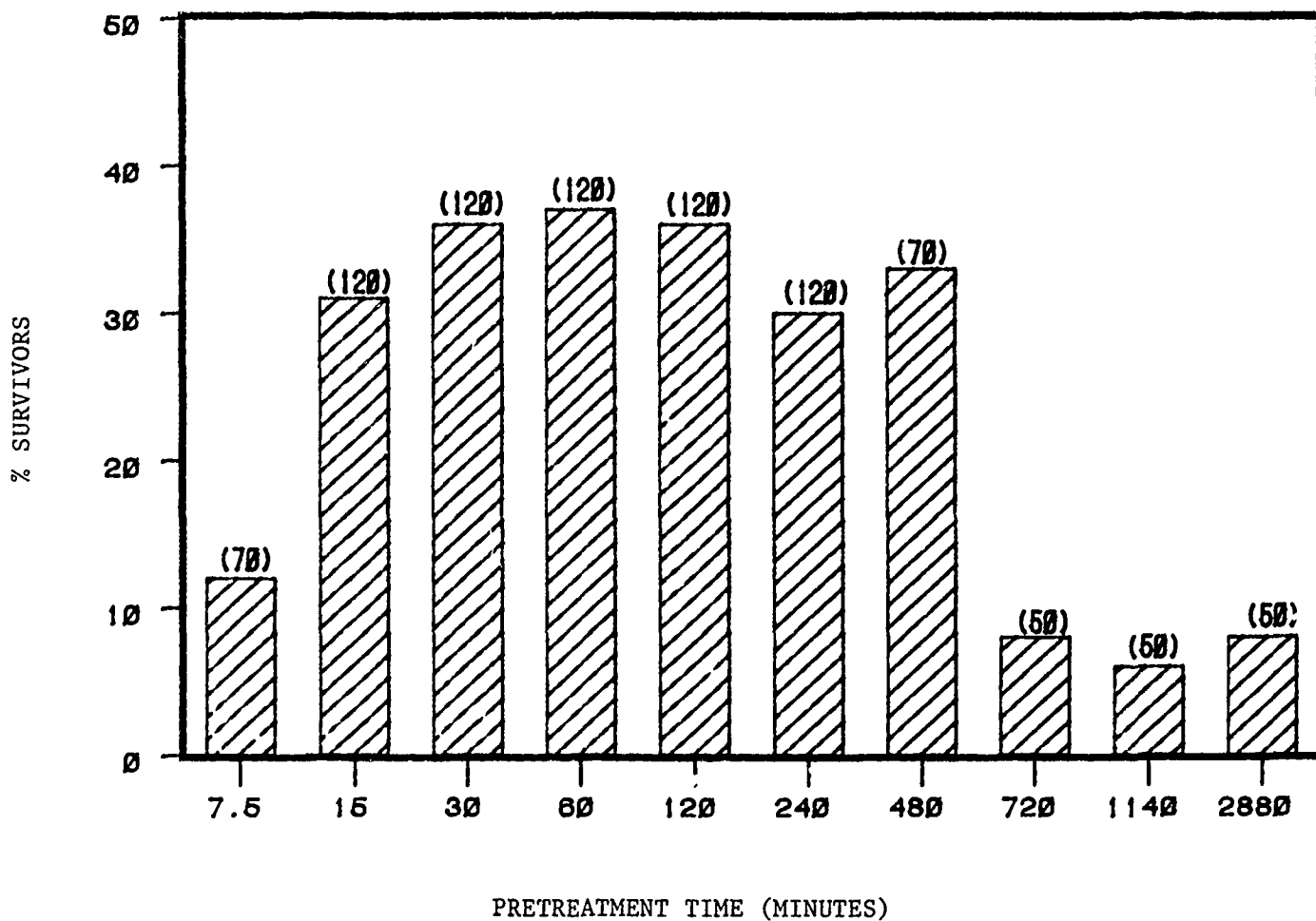


Figure 4. 24-Hour Survival in Mice Pretreated with Oral Pyridostigmine at Various Time Intervals Prior to Soman ($2 \times \text{LD}_{50}$) and Treated with Atropine (11.2 mg/kg) and 2-PAM (25.0 mg/kg). Bars represent mean survival for all doses of pyridostigmine at each time period. The numbers in parentheses indicate the number of animals sampled.

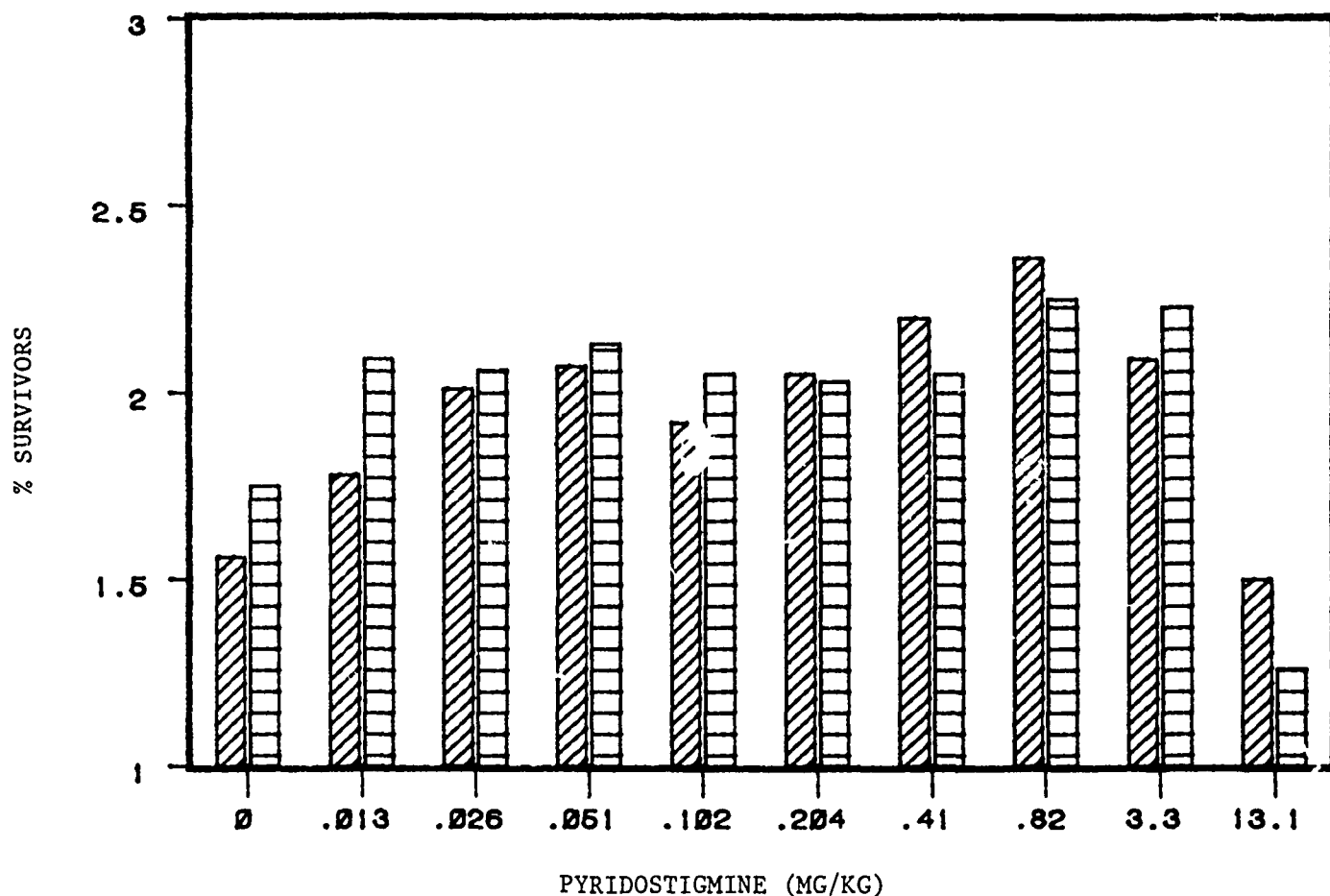
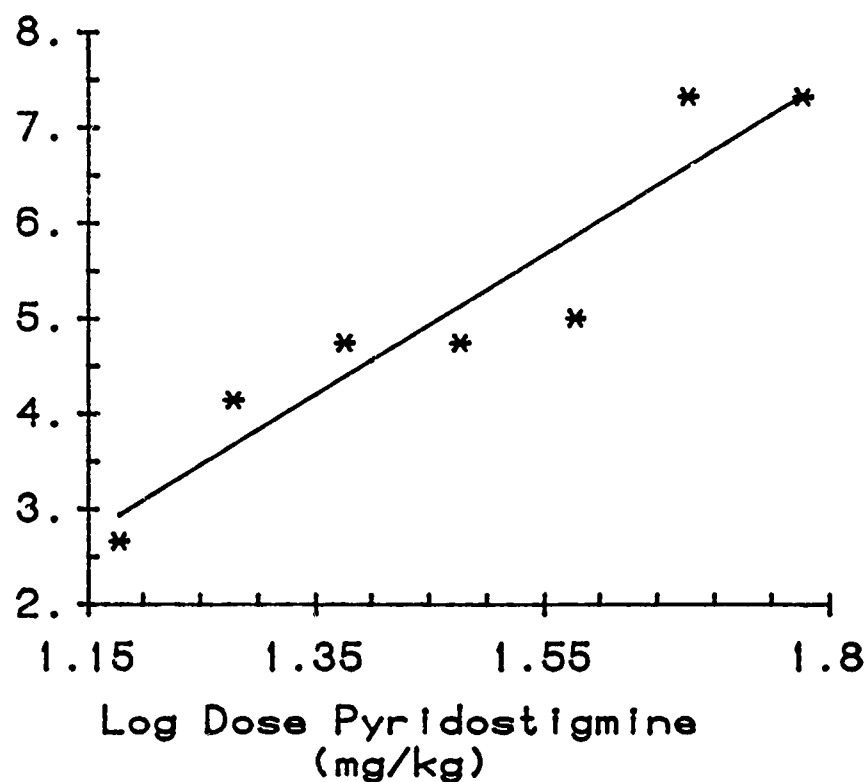


Figure 5. The Protection Afforded by Oral Pyridostigmine Administered 1 Hour Prior to Soman in Mice Treated with Atropine (11.2 mg/kg) and 2-PAM (25.0 mg/kg). The different bars at each dose represent the protective ratio (95 percent CI) achieved in 2 separate studies. Control animals receiving no pyridostigmine prior to soman are represented by the zero (0) dose.



Percent Mortality	DOSE (mg/kg)	95% Conf. Limits
1.0	12.3	8.1-18.6
15.0	20.4	16.4-25.4
50.0	29.8	25.7-34.5
84.0	43.6	34.9-54.3
99.0	72.4	47.9-109.3

Figure 6. Acute (24 hour) Oral LD50 of Pyridostigmine in Guinea Pigs. Top - A probit plot of the oral pyridostigmine dose-lethality curve. N=10 at each point. Bottom - Computed oral pyridostigmine doses and 95 percent confidence limits for various percent mortalities.

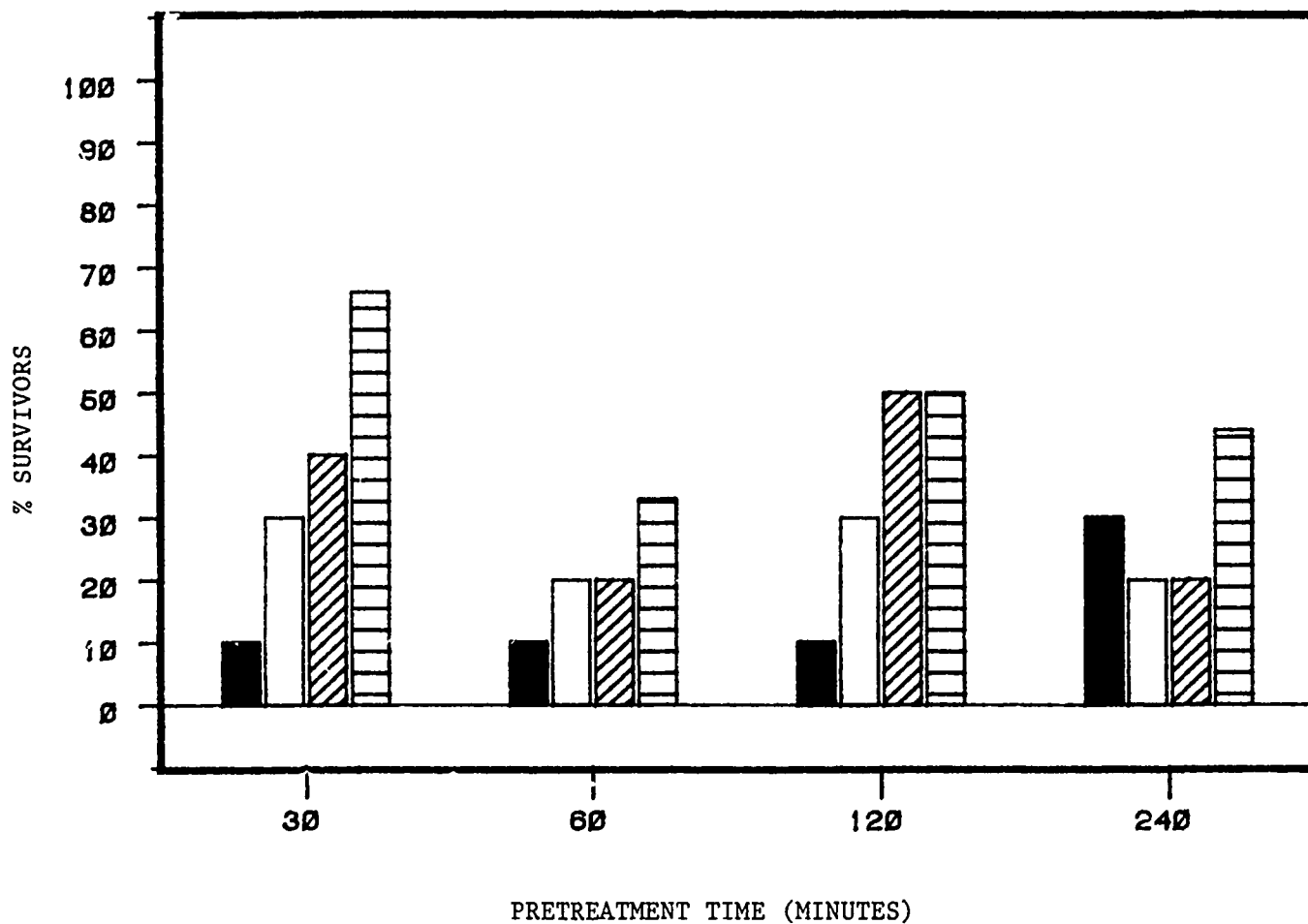






Figure 7. The Efficacy of Oral Pyridostigmine Pretreatment in Guinea Pigs Challenged with Soman (4.3 LD₅₀, s.c.) and Treated with Atropine (64.0 mg/kg) and 2-PAM (100 mg/kg) at 1.0 Minute. The bars represent 24-hour survival at the pretreatment times indicated. The oral doses of pyridostigmine were as follows:  = 0.12 mg/kg (1/256 x LD₅₀);  = 0.47 mg/kg (1/64 x LD₅₀);  = 3.75 mg/kg (1/8 x LD₅₀);  = 7.5 mg/kg (1/4 x LD₅₀).

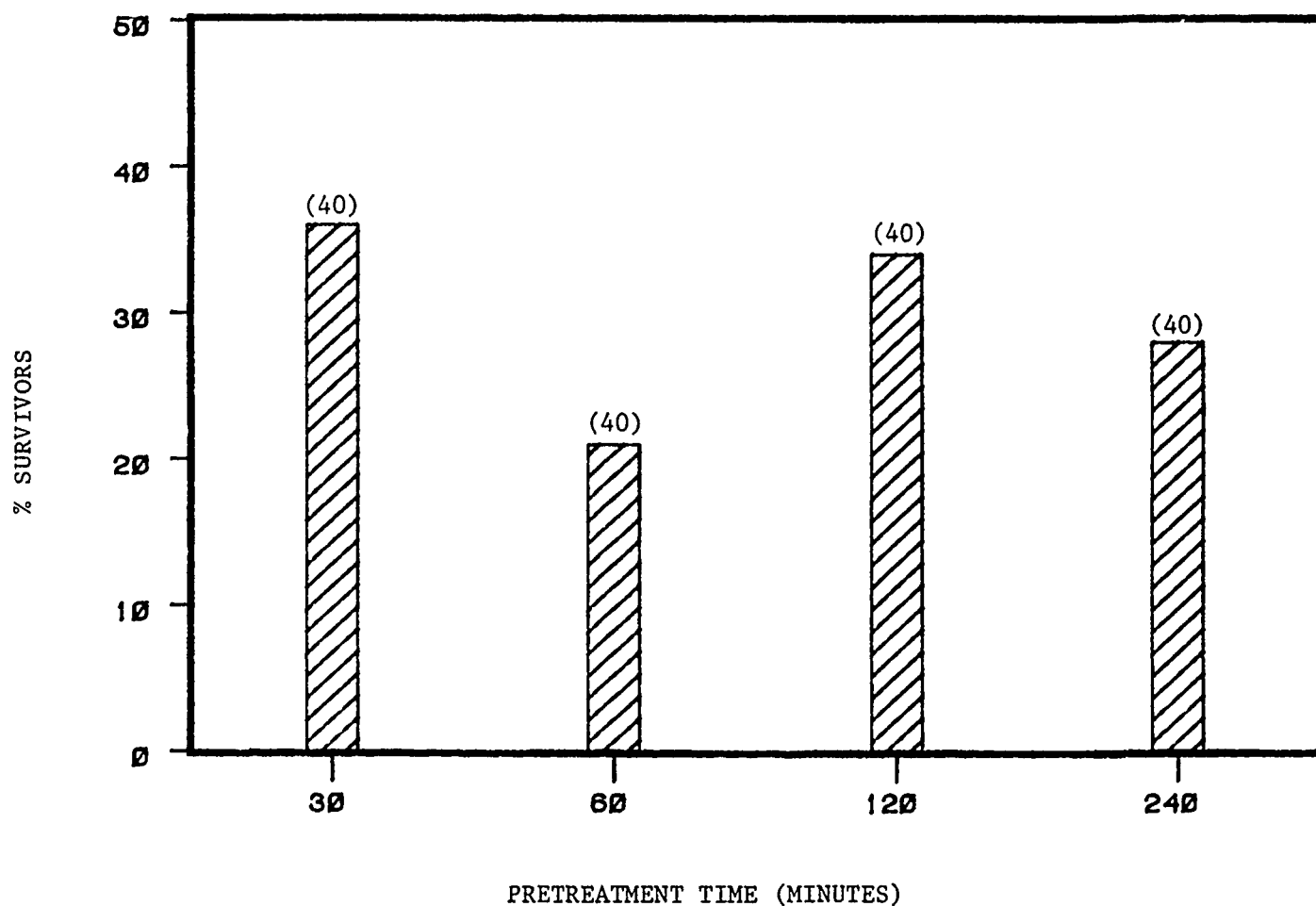


Figure 8. 24-Hour Survival in Guinea Pigs Pretreated with Oral Pyridostigmine at Various Time Intervals Prior to Soman ($4.3 \times \text{LD}_{50}$, s.c.) and Treated with Atropine (64.0 mg/kg) and 2-PAM (100 mg/kg). Bars represent mean survival for all doses of pyridostigmine at each time period. The numbers in parentheses indicate the number of animals sampled.

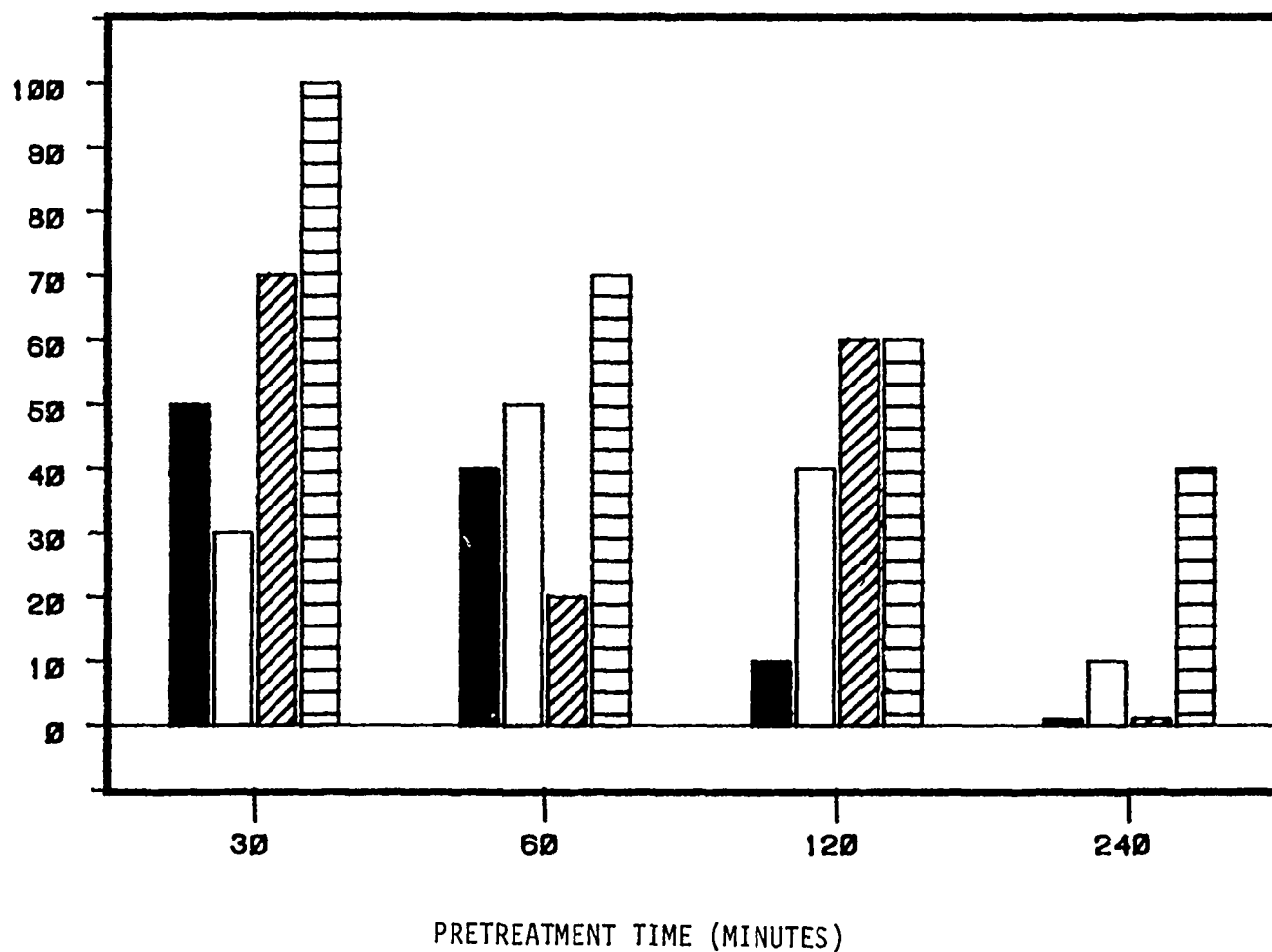






Figure 9. The Efficacy of Oral Physostigmine Pretreatment in Mice Challenged with Soman (2 x LD50, IM) and Treated with Atropine (11.2 mg/kg) and 2-PAM (25.0 mg/kg) at 10 Seconds. Bars represent 24-hour survival at the pretreatment time intervals indicated. The oral physostigmine doses were as follows:  = 0.015 mg/kg (1/256 x LD50);  = 0.061 mg/kg (1/64 x LD50);  = 0.244 mg/kg (1/16 x LD50);  = 0.975 mg/kg (1/4 x LD50).

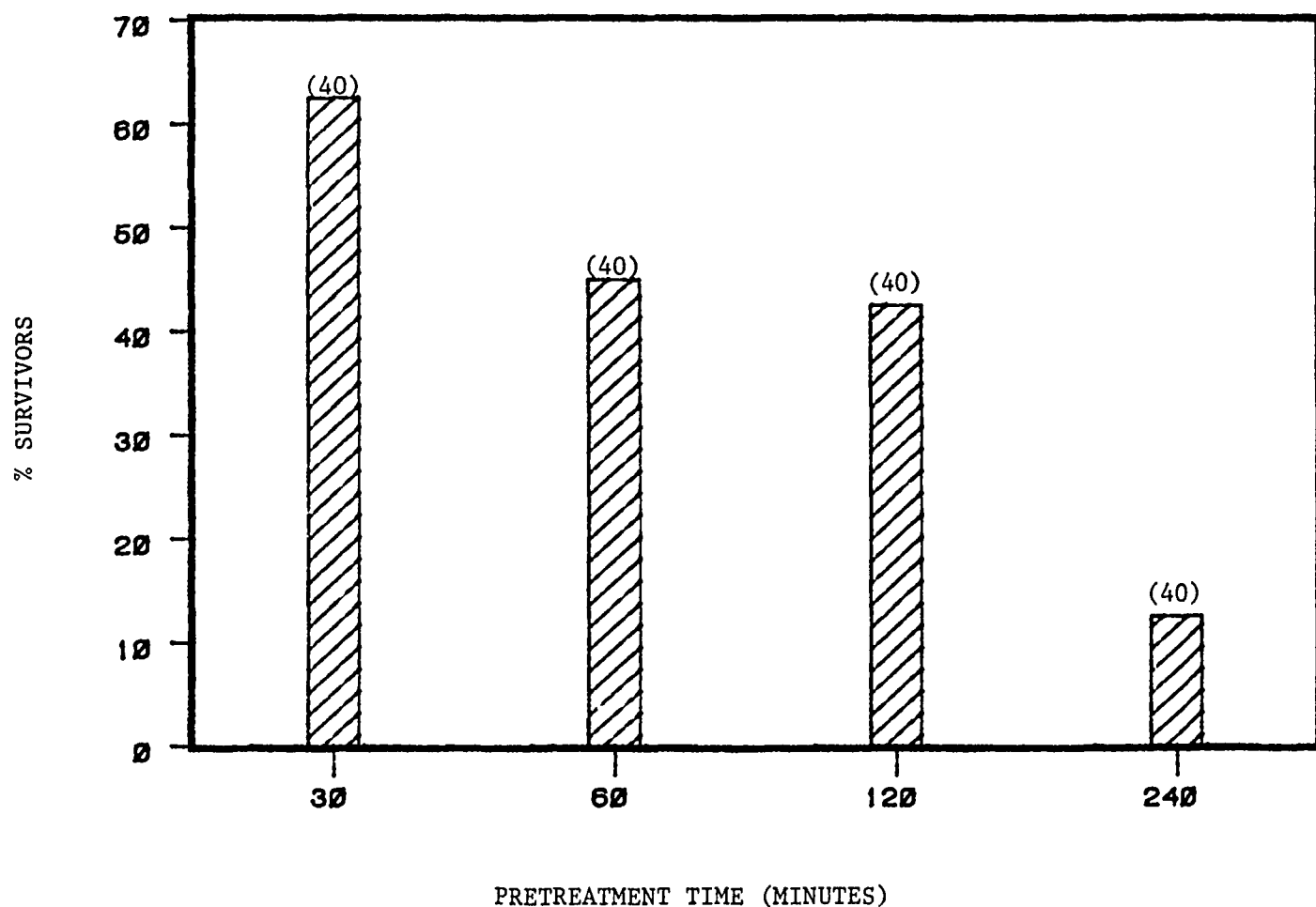


Figure 10. 24-Hour Survival in Mice Pretreated with Oral Physostigmine at Various Times Prior to Soman ($2 \times \text{LD}_{50}$, IM) and Treated with Atropine (11.2 mg/kg) and 2-PAM (25.0 mg/kg). Bars represent mean survival for all doses of physostigmine at each time period. The numbers in parentheses indicate the number of animals sampled.

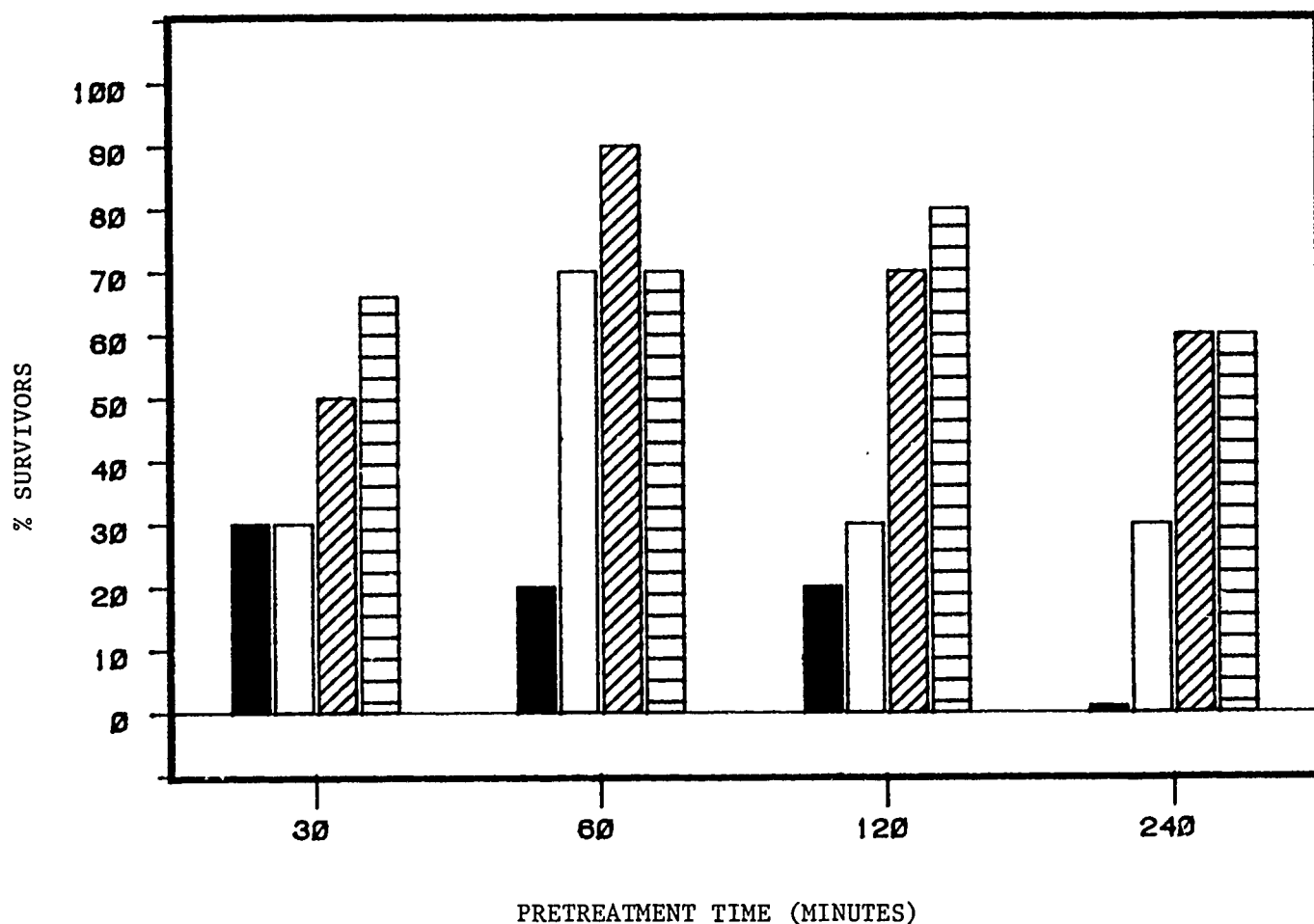






Figure 11. The Efficacy of Oral Physostigmine Pretreatment in Guinea Pigs Challenged with Soman ($4.3 \times \text{LD}_{50}$, s.c.) and Treated with Atropine (64.0 mg/kg) and 2-PAM (100 mg/kg) at 1.0 Minute. Bars represent 24-hour survival at the pretreatment times indicated. The oral doses of physostigmine were as follows:  = 0.03 mg/kg ($1/256 \times \text{LD}_{50}$);  = 0.11 mg/kg ($1/64 \times \text{LD}_{50}$);  = 0.43 mg/kg ($1/16 \times \text{LD}_{50}$);  = 1.705 mg/kg ($1/4 \times \text{LD}_{50}$).

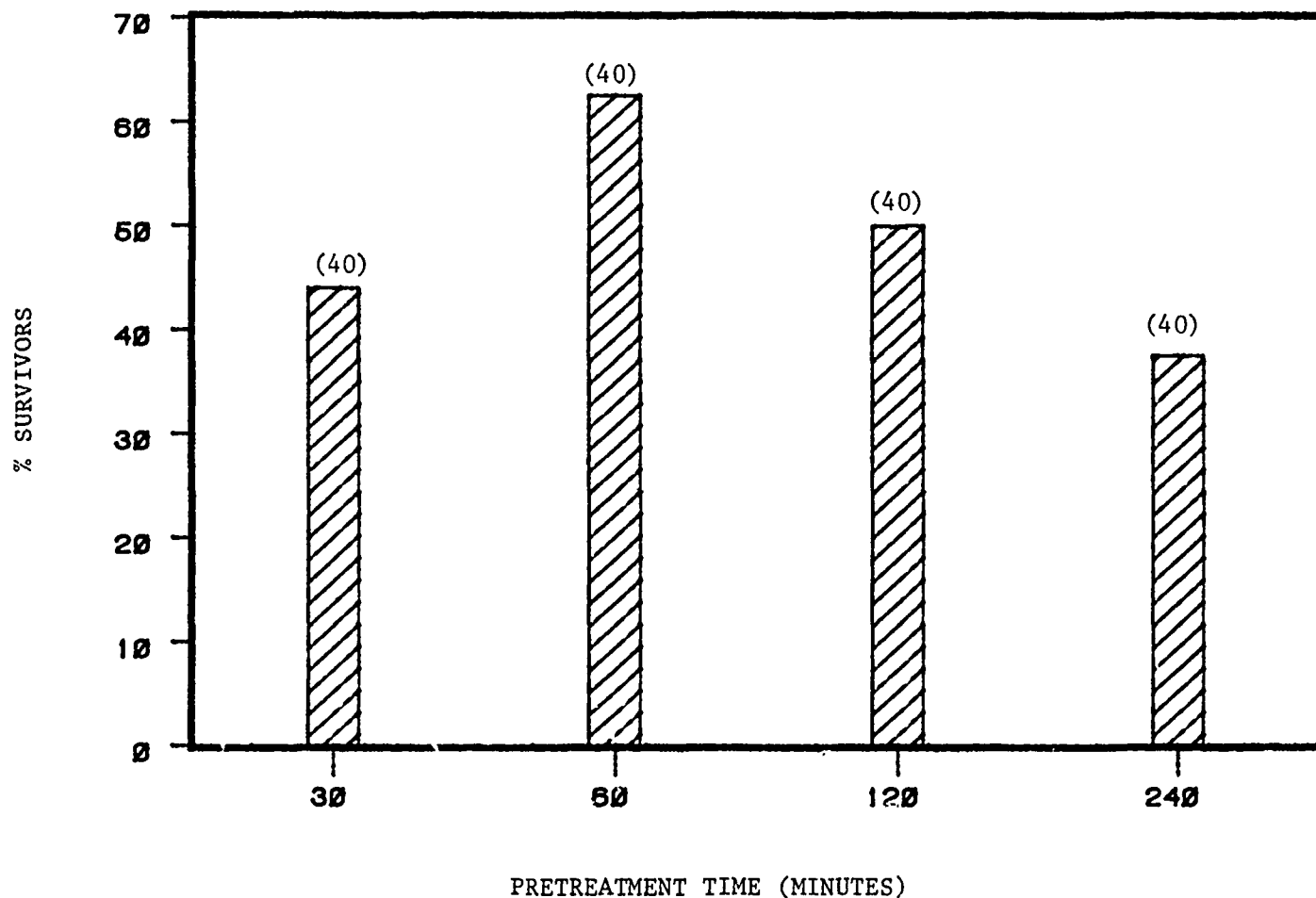


Figure 12. 24-Hour Survival in Guinea Pigs Pretreated with Oral Physostigmine at Various Time Intervals Prior to Soman ($4.3 \times \text{LD}_{50}$, s.c.) and Treated with Atropine (64.0 mg/kg and 2-PAM (100 mg/kg). Bars represent mean survival for all doses of physostigmine at each time period. The numbers in parentheses indicate the number of animals sampled.

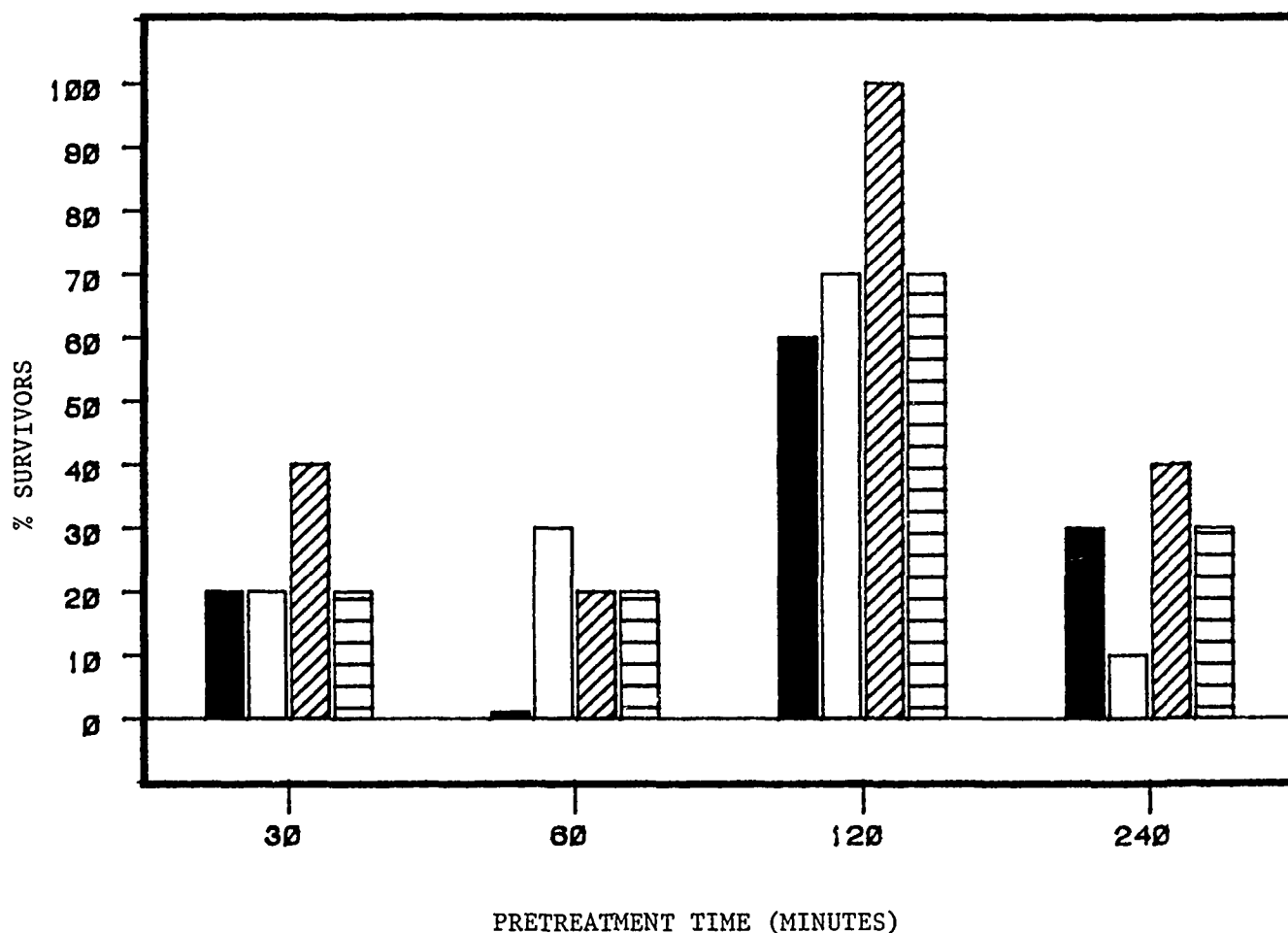


Figure 13. The Efficacy of Oral Pyridostigmine in Mice Challenged with IM Tabun ($2.45 \times \text{LD}_{50}$) and Treated with IM Atropine (56.0 mg/kg) and 2-PAM (44.6 mg/kg) at 10 Seconds. Bars represent 24 hour survival at the pretreatment intervals indicated. The pyridostigmine oral doses were as follows:
 ■ = 0.102 mg/kg ($1/256 \times \text{LD}_{50}$); □ = 0.41 mg/kg ($1/64 \times \text{LD}_{50}$), ▨ = 1.64 mg/kg ($1/16 \times \text{LD}_{50}$);
 ▤ = 6.55 mg/kg ($1/4 \times \text{LD}_{50}$).

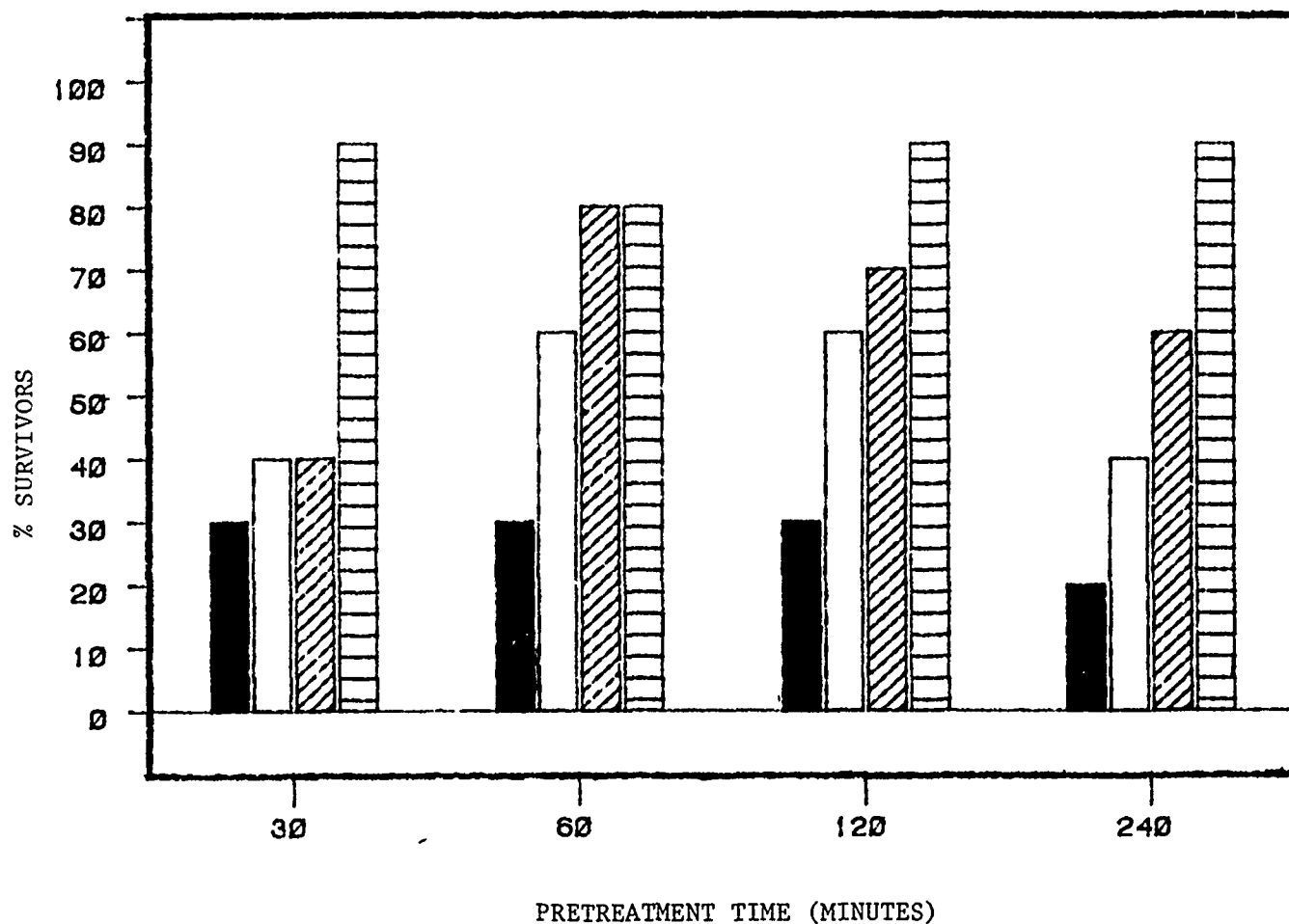






Figure 14. The Efficacy of Oral Pyridostigmine Pretreatment in Guinea Pigs Challenged with Tabun ($5.36 \times \text{LD}_{50}$, s.c.) and Treated with Atropine (32.0 mg/kg) and 2-PAM (50 mg/kg) at 1.0 Minute. Bars represent 24-hour survival at the pretreatment intervals indicated. Pyridostigmine oral doses were as follows:
 = 0.12 mg/kg ($1/256 \times \text{LD}_{50}$);  = 0.47 mg/kg ($1/64 \times \text{LD}_{50}$);  = 1.88 mg/kg ($1/16 \times \text{LD}_{50}$);  = 3.75 mg/kg ($1/8 \times \text{LD}_{50}$).

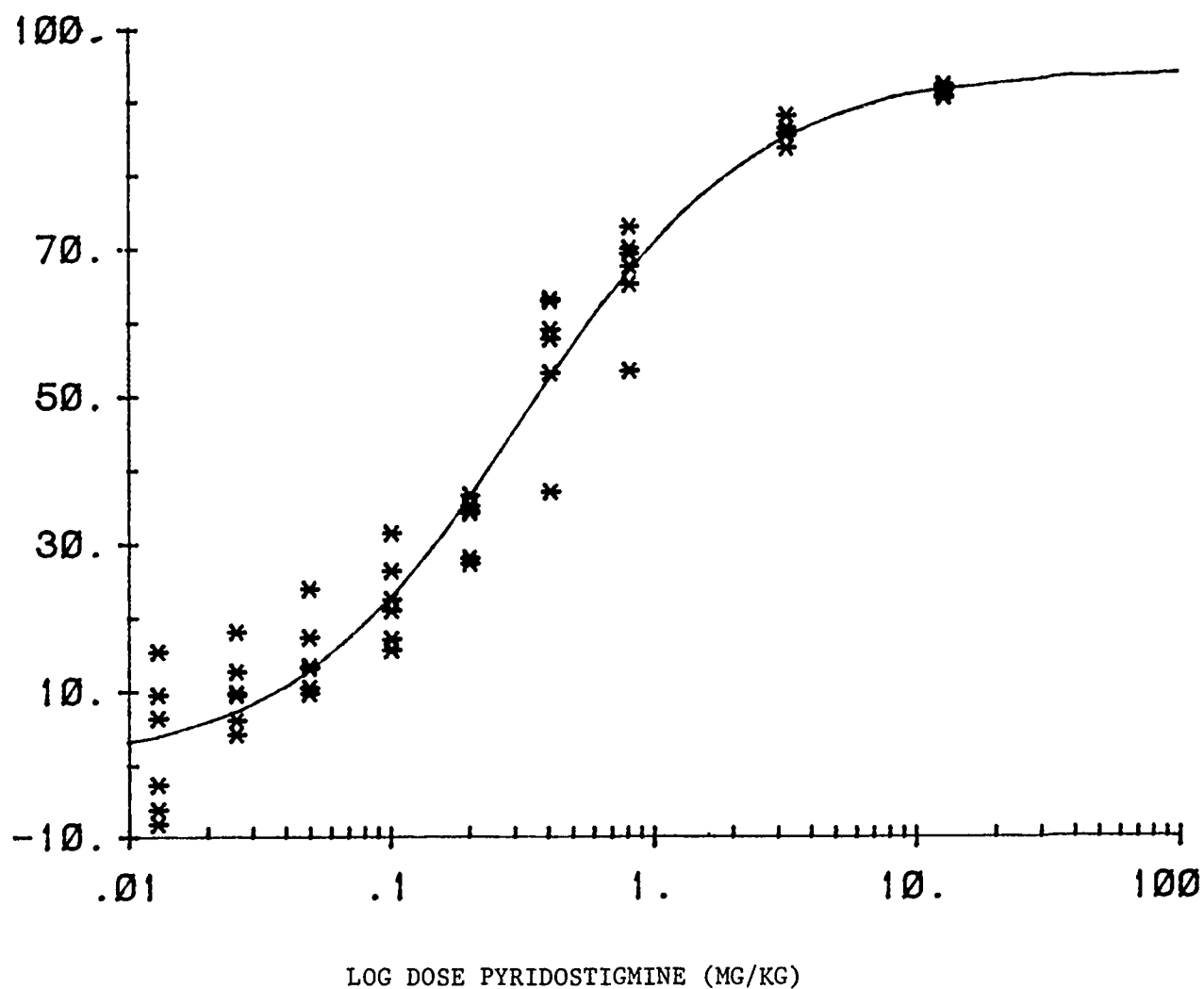


Figure 15. Inhibition of Whole Blood Acetylcholinesterase Activity One Hour After Oral Pyridostigmine in Mouse. Each point represents an individual animal. N=6 at each dose.

Table 1

Components of Oral Pretreatment Model

I Acute Oral Toxicity in Mice

- 5-7 doses;
- 5 or 10 ml/kg
- Calculate 24 hour LD1-LD99

II Initial Oral Efficacy/Optimal Pretreatment Time

- Doses: 1/4, 1/16, 1/64, 1/256
fraction of oral LD50
- Times: 30, 60, 120, 240 minutes
- Single agent challenge dose
- Treat with optimal Atropine/2-PAM
dose, I.M.
- 24 hour survival assessed
 - if > 10% select optimal pre-
treatment time and proceed to III

III Optimal Protection Studies

- 7-9 pretreatment doses
- 5 agent challenge levels/pretreat-
ment dose
- Dose at optimal pretreatment time
- Controls randomized into study
- Treat with optimal Atropine/2-PAM
dose, I.M.
- Calculate 24 hour Soman LD50 for
each pretreatment dose
- Calculate Protective Ratio
- Select optimal dose and highest
Protective Ratio

IV Repeat I-III in Guinea Pigs

V Enzyme Studies

Table 2

ACUTE ORAL TOXICITY OF CARBAMATES

CARBAMATE	24HR LD50 (mg/kg) (95% CI)	
	MICE	GUINEA PIG
PHYSOSTIGMINE	3.9 (3.5-4.3)	6.8 (5.6-8.3)
PYRIDOSTIGMINE	26.2 (22.5-30.4)	29.8 (25.7-34.6)

Table 3

Comparison of Acetylcholinesterase Inhibition
and Mean Protective Ratio (PR) with Oral Dose
of Pyridostigmine in Mice

Dose Pyridostigmine (mg/kg)	% inh AChE (Mean \pm S.D.)	Mean PR
0.013	2.14 \pm 9.4	1.94
0.026	10.0 \pm 4.9	2.04
0.051	14.6 \pm 5.2	2.10
0.102	22.3 \pm 5.9	1.99
0.204	32.6 \pm 4.0	2.04
0.410	55.6 \pm 9.8	2.13
0.82	66.4 \pm 6.8	2.30
3.3	85.8 \pm 1.5	2.16
13.1	91.3 \pm 0.7	1.38

GUINEA PIG MODEL FOR CORRELATING EFFICACY
WITH PRALIDOXIME CHLORIDE (2-PAM) PLASMA LEVELS

by

Martin D. Green

U.S. Army Medical Research Institute of Chemical Defense
Aberdeen Proving Ground, Maryland 21010



That the plasma content of an oxime like 2-PAM is related to its effectiveness is tacitly accepted as a general therapeutic principle. The higher the plasma content of 2-PAM the better is its antagonism of Sarin's toxicity. This has been demonstrated by experiments relating the effectiveness of 2-PAM to the time of challenge by agent. The longer a time after a standard dose of 2-PAM is given, the less effective it is, provided it is not toxic to begin with.

The problem of determining a mathematical relationship between the plasma content of 2-PAM and its efficacy against Sarin as measured by the LD50 has been examined in relatively few experiments. This background is important to the presentation, so let us take a moment to review the findings of others in this regard. (Figure 1)

One of the earliest references to this problem is that of Sundwall (Biochem. Pharmacol. 8:413, 1961). He initiated a blockade of the neuromuscular junction, produced bradycardia, hypotension, and respiratory failure, and then injected sufficient oxime (the sulphonate salt of pralidoxime, P2S) to restore diminished activity to control levels. His experiments were done without injecting atropine and using an organophosphate inhibitor of cholinesterase, 37 S-N⁺. In these experiments Sundwall defined two functional ranges in terms of plasma oxime concentration. The first range was one of therapeutic success, 4 to 12 µg/ml of plasma, which reversed the toxic signs in three cats. The second range was one of therapeutic failure in which the plasma concentration was 2-4 µg/ml of plasma. In the latter group of animals recovery was not achieved or was not permanently established. From these experiments, therefore, 4 µg/ml was considered the minimum therapeutic concentration of P2S.

At about the same time O'Leary et al. (J. Pharmacol. Exp. Ther. 132: 50, 1961) performed experiments on rabbits which indicated that a non-linear relationship existed between the log of the LD50 of Sarin and the log of 2-PAM. These animals were administered various doses of 2-PAM along with a standard dose of atropine sulfate to determine the LD50 of Sarin. All chemicals were given intravenously and the therapeutic compounds were given 30 seconds after Sarin. Approximately a 2.5, 8.5 and 40 mg/kg dose of 2-PAM was used (Figure 2). These authors observed that there was a point of therapeutic maximum beyond which there was less protection than before. These authors ascribed this effect to the toxic properties of the oxime overcoming its beneficial effects.

Two additional contributors to this area of research were Zvirblis and Kondritzer (J. Pharm. Exp. Ther. 157:432, 1967). (Figure 1). These investigators used 2-PAM as a pretreatment compound against Sarin's toxicity in rats. They studied the effects of two doses of 2-PAM, i.e. 30 and 60 mg/kg, at two time points. (Figure 3). They formulated a linear relationship between the log of the LD50 of Sarin and the log of the plasma concentration for 2-PAM. The dynamic range of their response was only 2.3 to 2.5 LD50. This short dynamic range limits the useful information which can be derived, since the two therapeutic end points are probably not significant from each other.

Before proceeding further let me explain in a general way the method by which the correlation experiments were conducted and the questions toward which they were directed. The questions central to these experiments were:

- (1) Is there a linear or nonlinear relationship between the LD50 of Sarin and the plasma level of oxime?
- (2) Is there a significant and predictable influence of poisoning on the plasma-time relationship?

Generally the experimental method was as follows:

First, a suitable range of 2-PAM dosage was selected for study. In this case an upper limit of 25 mg/kg was used in the analysis of the data, since a higher level of oxime, 50 mg/kg, was found to yield protective ratios below the therapeutic maximum.

LD50 determinations were made for each dose of Sarin studied, or they were interpolated from a large set of data gathered from similar experiments done under exactly the same conditions.

The plasma level for each dose of 2-PAM was determined at an appropriate time, using a spectrophotometric method. Samples were obtained from guinea pigs following decapitation. Sarin was injected subcutaneously; atropine and 2-PAM were injected intramuscularly in the same hind limb.

Lastly, the plasma level was correlated with the LD50 of Sarin for both pretreatment and therapeutic modes of administration.

In the pretreatment experiments, selected doses of 2-PAM were examined for their relationship to plasma content. In the first group of guinea pigs different doses of 2-PAM were injected and successive time points were selected to determine the plasma oxime content. (Figures 4 and 5). In a different group of guinea pigs the efficiency of antagonizing Sarin at the LD50 was determined at the chosen point of 4 minutes. (Figure 6). The experimental results were plotted against the dose of Sarin (Figure 7) and plasma level of 2-PAM. (Figure 8).

In the next series of experiments the relationship between the plasma levels of 2-PAM and the LD50 of Sarin was determined for the antidote given in the therapeutic mode. In these experiments the time to maximum plasma concentration for the highest and lowest doses of 2-PAM was determined. The results are shown in the next two figures (Figures 9 and 10). As one can observe from these figures, an apparent interaction was found between Sarin and 2-PAM at 3.12 and 25.0 mg/kg of the oxime. This interaction was most often statistically significant at the lower dose of the oxime.

Although the apparent time to the maximum level of plasma oxime

remains unchanged, as does the general shape in the rising and falling phases, successively higher doses of Sarin are associated with successively higher levels of 2-PAM in plasma. A rigorous pharmacokinetic analysis of the data in terms of the various rate constants was not possible in these experiments. This was due to an insufficient number of sampling points and the inherent dispersion in the data arising from a destructive sampling technique. However, some simpler analysis of the data was possible. Both the peak plasma content and the area under the curve were correlated to the dose of Sarin. Areas under the curve were computed, using the trapezoidal rule between 1 to 10 minutes after therapy. (Figure 11). These results were found to correlate in the case of the 3.12 mg/kg dose. Also the change in peak height at 2 minutes was found to correlate at the 3.12 mg/kg dose. (Figure 12).

These correlations were not found at the higher dose of the oxime. With the 25 mg/kg dose of 2-PAM, the higher concentration at the site of injection may have offset any interaction. Further correlation at the higher dose of the oxime may have been complicated by the nonlinear nature of the plasma concentration curve for pralidoxime, as reported by Benschoep (SIPRI 120).

In the experiments conducted in the therapeutic mode, 2 minutes was chosen as the apparent time to maximum plasma content based on the previously shown experimental data.

The next figure shows the correlation between the LD50 value obtained for Sarin and the dose of 2-PAM given therapeutically. (Figure 13). The regression coefficient is quite high, and inspection of the curve reveals a linear relationship between the two variables. Next the LD50 values were correlated with the plasma concentrations of 2-PAM at two minutes after poisoning with Sarin. (Figure 14).

Although a high correlation coefficient was found, the correspondence between the variables in this case appeared less consistent than had been observed for the previous pretreatment case; further, a negative intercept was found. The divergence at the lower end of the curve suggested that a transformation might improve the fit. Further, a linear analysis suggested a continuous, non-ending increase in therapeutic benefit.

Intuitively, the problem seemed to hinge on the plasma content of the oxime, which was dependent on the dose. Hence the relationship between these two variables was examined. (Figure 15). A simple linear regression yielded similar concerns as that considered earlier; that is, although the line of regression was highly correlated, it seemed a deficient explanation in terms of accounting for dispersion in the data, particularly since the two variables did not intersect at 0. A search for an empirically derived mathematical relationship which might better account for the data was sought. This search ended with a fitting of the data to a rectangular hyperbola following a natural logarithmic transformation of the plasma oxime content. (Figure 16).

Remembering that both the plasma content and dose of oxime are relative to an LD50 value for Sarin, relating the LD50 value of Sarin to the therapeutic plasma concentration becomes a two-step process by the non-linear method. (Figure 17). First, the LD50 value of Sarin is used to determine the apparent dose of oxime; second, the apparent dose of oxime is related to the predicted plasma content of the oxime. Thus two models could be examined for the relationship of the plasma level to the LD50 value: a linear and a non-linear model. A summary of predicted and observed values is presented in the next figure. (Figure 18).

A chi-square comparison of the two types of analysis is shown in the next slide. A comparison of the linear and non-linear models through a chi-square analysis suggested that the non-linear model is a better fit of the data. Although the linear model has an acceptable level of significance, its chi-square term is much larger than that of the non-linear case. Therefore, the non-linear model is in better agreement with the data. (Figure 19).

From the relationship derived, a minimum therapeutic level of 2-PAM may be determined. (Figure 20). As you may recall, the work of Sundwall suggested a functional minimum of 4 $\mu\text{g/ml}$ of P2S to antagonize the lethal effects of Sarin. His experiments were conducted to determine an absolute plasma level of oxime, 100% effective in reversing the signs of toxicity. From the experiments I just described, a threshold value for the oxime content in plasma may be found, one that estimates a minimum dose of 2-PAM which gives a just meaningful difference in the efficacy estimate as measured at the LD50. In the estimate of the LD50, confidence limits were found for that point estimate. This particular estimate and its 95% confidence limits suggest an upper limit for the efficacy of atropine alone. Therapeutic benefit found beyond this upper limit may be considered as resulting from the addition of other therapeutic compounds such as 2-PAM.

Using the two-step process referred to earlier, a value of 3 $\mu\text{g/ml}$ was computed which would yield a detectable difference in the LD50 of Sarin due to the use of 2-PAM. This value is identical with the suggested value for 2-PAM in dogs reported by Crook *et al.* (J. Pharmacol. Exp. Ther. 136, 1962) to protect against Sarin poisoning. It differs from the value of Sundwall, whose work suggested a value of 5.2 $\mu\text{g/ml}$ PAM as a minimum therapeutic level (4 $\mu\text{g/ml}$ of P2S is the equivalent of 5.2 $\mu\text{g/ml}$ of PAM when converted on a molar basis). Further, these results are consistent with the value of 4.3 $\mu\text{g/ml}$ as found by Fleisher *et al.* (Toxicol. Appl. Pharmacol. 16:40-47, 1970) in *in vitro* experiments, who found that this level of 2-PAM reactivated 88% of Sarin-inhibited RBC-AChE.

Returning to our original questions: This research has demonstrated (1) The relationship between the lethal dose values for Sarin and the plasma content of 2-PAM are best expressed through a non-linear relationship, and (2) a significant, predictable influence is exerted by Sarin on the plasma concentration of 2-PAM.

Figure 1

LEVELS OF PRALDOXIME IN RELATIONSHIP TO EFFICACY

AUTHOR (SPECIES)	OXIME, LEVEL (μ G/ML)	EFFECT IN RELATION TO AGENT
SUNDWALL (CAT)	P2S, 4 - 12	THERAPEUTIC SUCCESS vs 37 S - N+
	P2S, 2 - 4	THERAPEUTIC FAILURE vs 37 S - N+
	P2S, 4	MINIMUM THERAPEUTIC vs 37 S - N+
O'LEARY, et.al. (RABBIT)	2 PAM	APPARENT MAXIMUM RESPONSE \sim 40 MG/KG vs SARIN
ZVIRBLIS AND KONDRITZER (RAT)	2 PAM	LOG LD50 SARIN = 2.207 + 0.33 LOG OXIME (μ G/ML)

Figure 2

WORK OF O'LEARY ET. AL., 1961

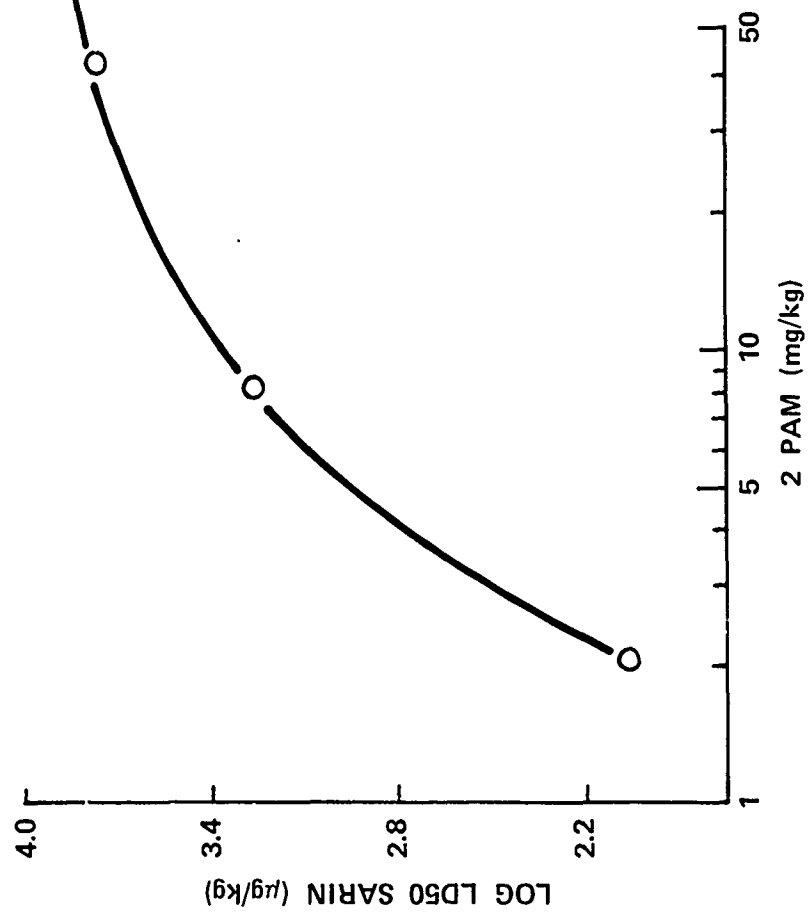


Figure 3

WORK OF ZVIRBLIS AND KONDRITZER, 1967

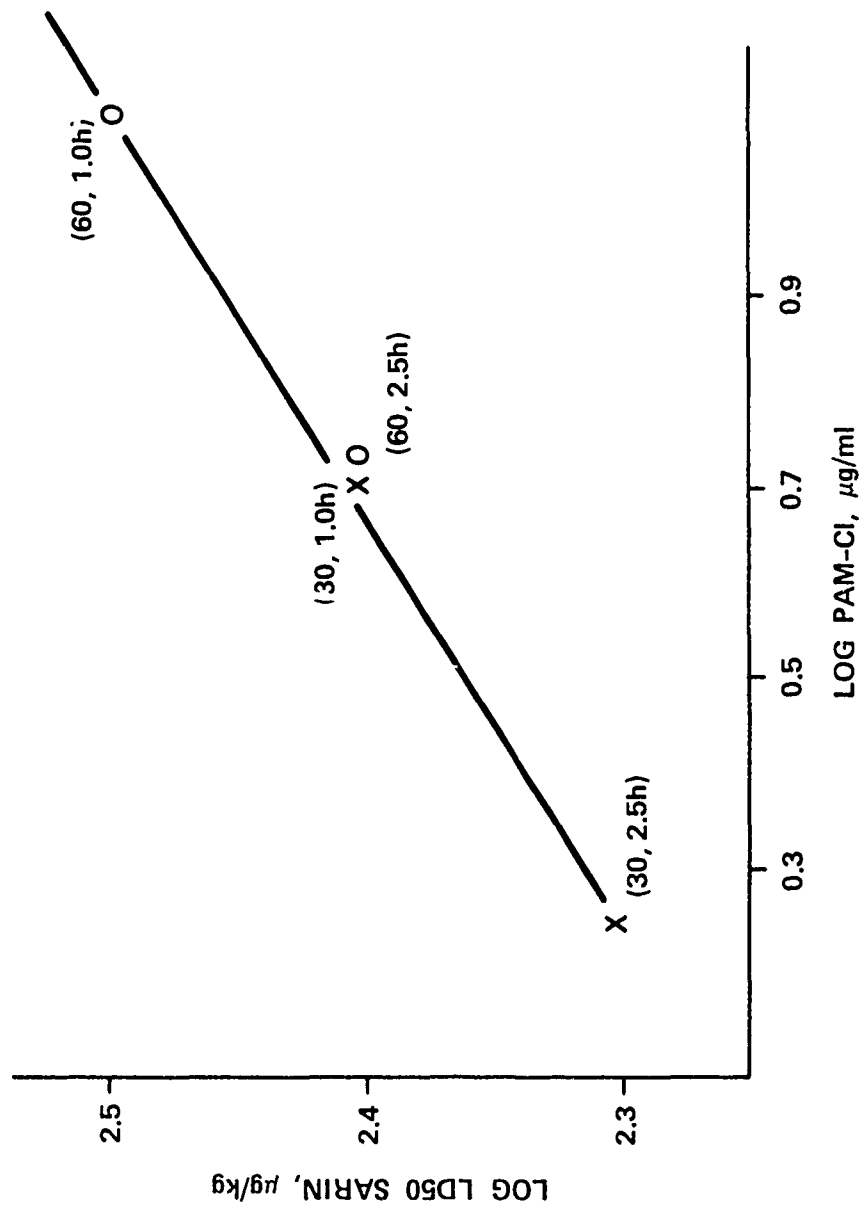


Figure 4

CP OXIME PRETREATMENT

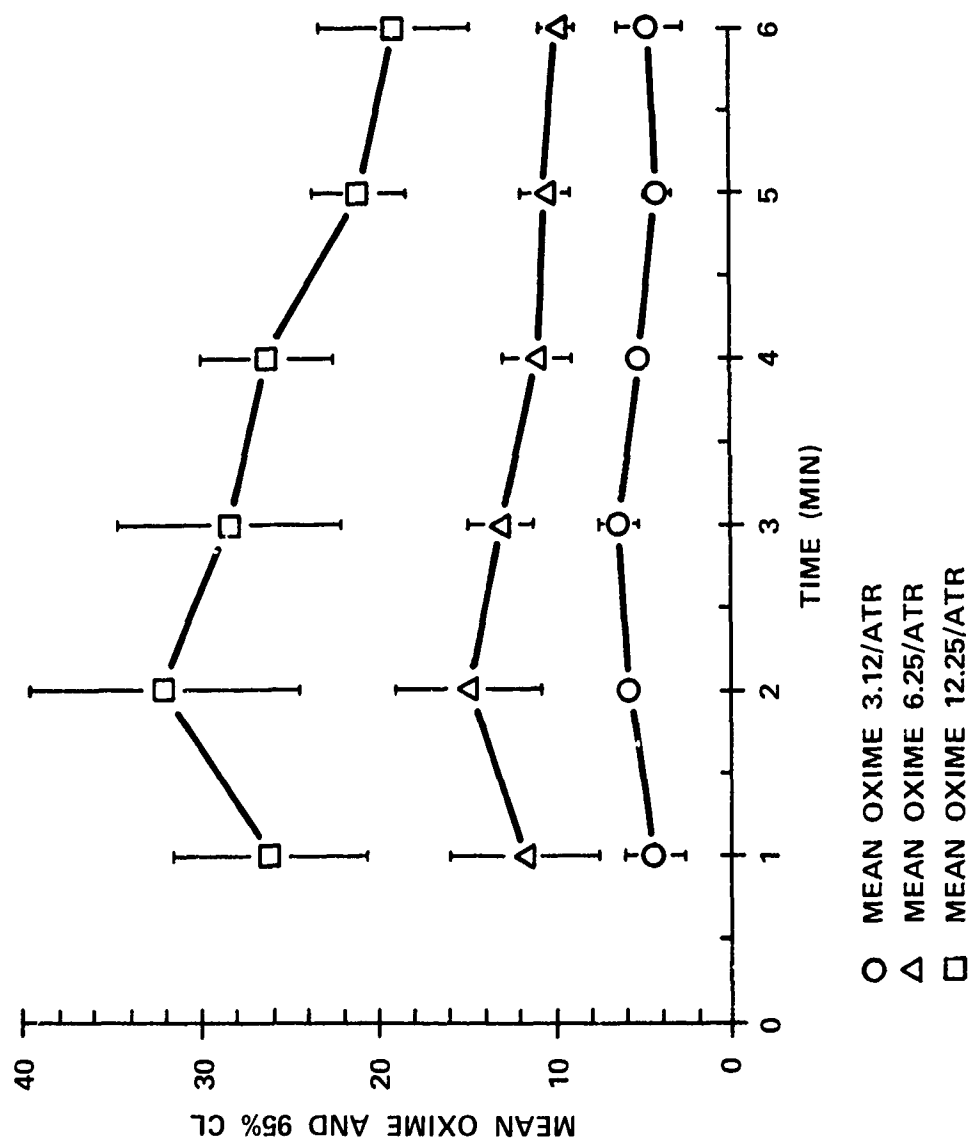


Figure 5

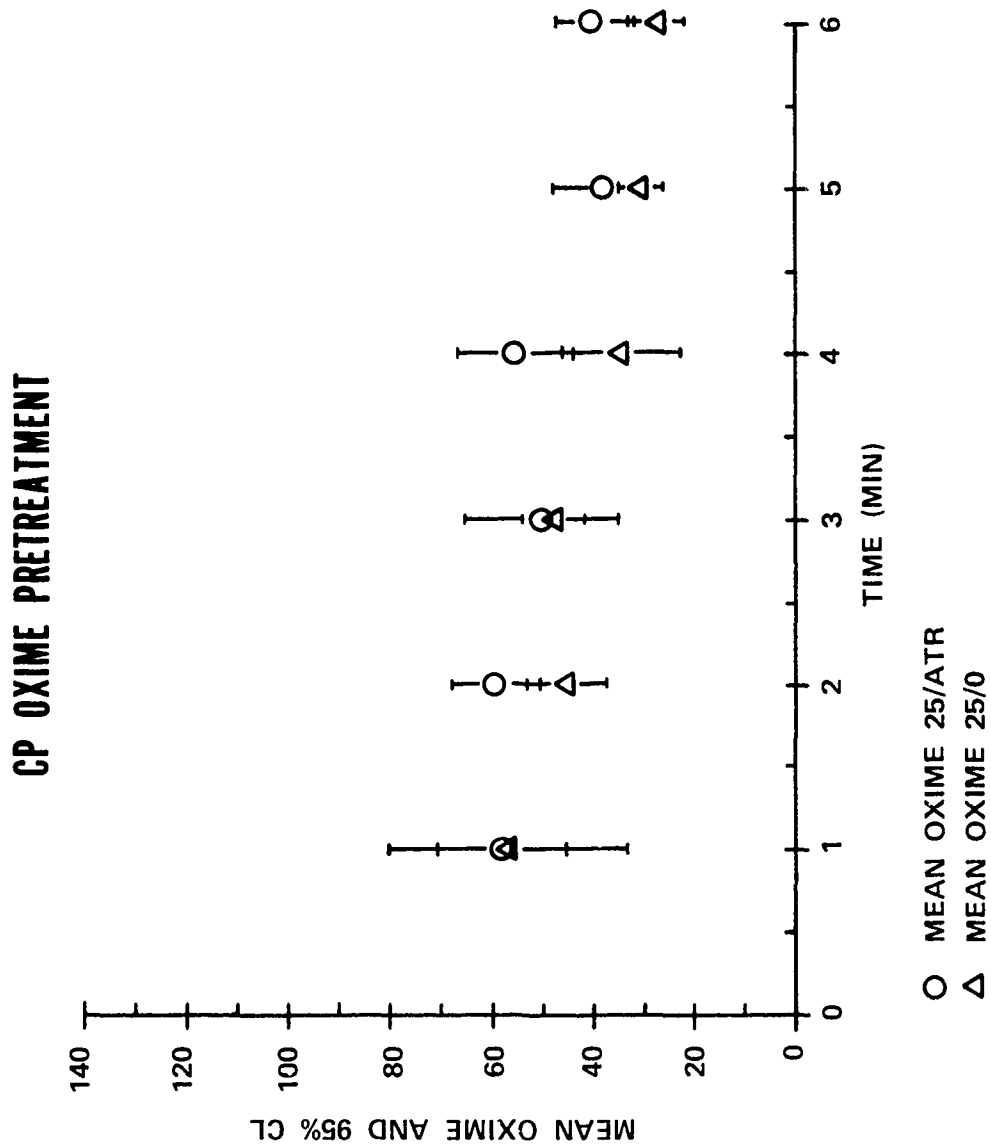


Figure 6

EXPERIMENTAL PARADIGM FOR PRETREATMENT MODE

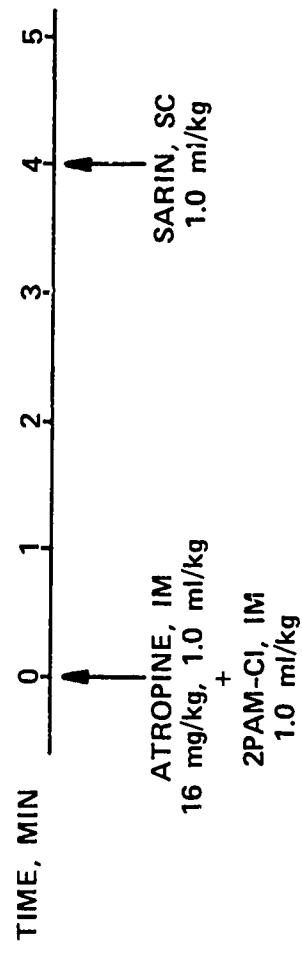


Figure 7

REGRESSION OF DOSE ON LD50 MEASURE

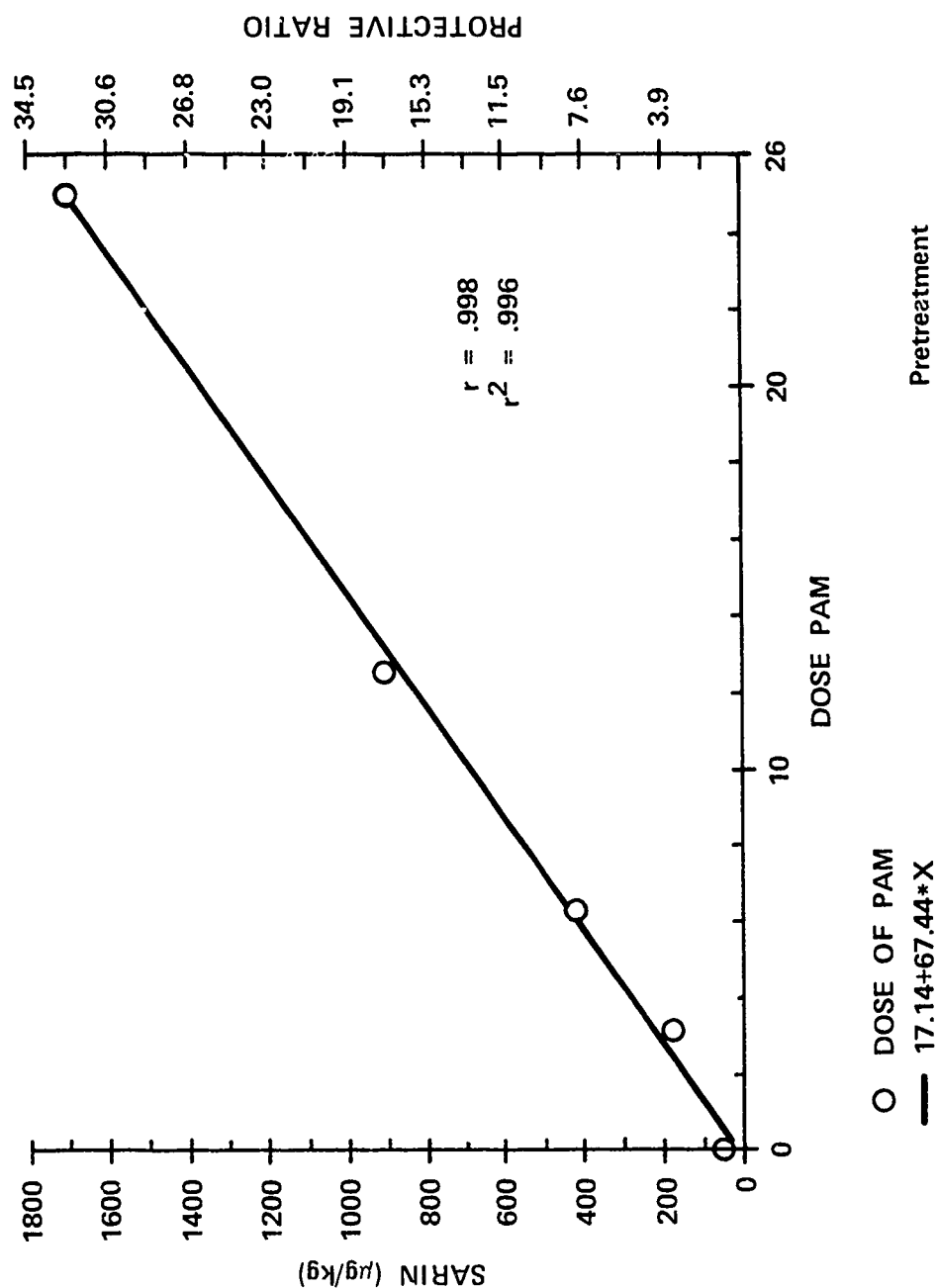


Figure 8

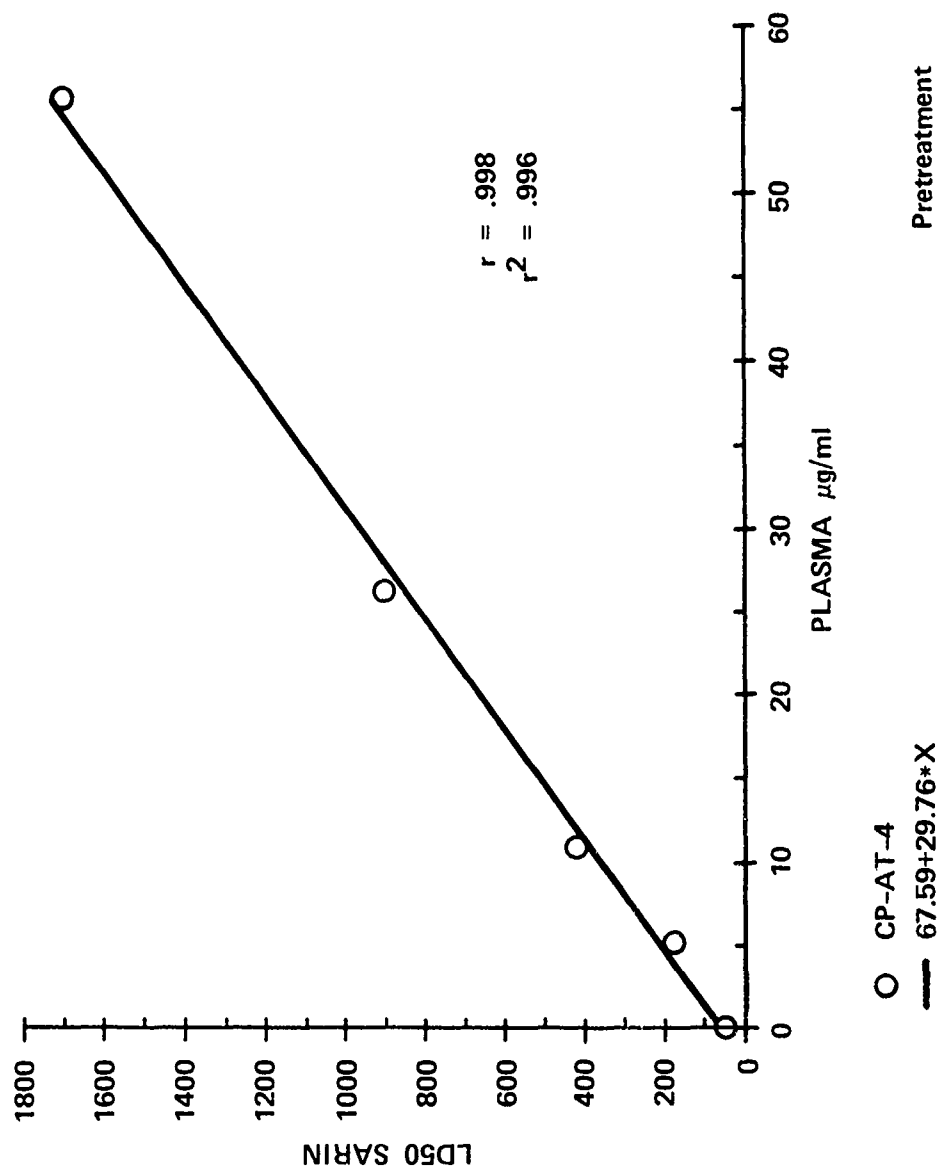
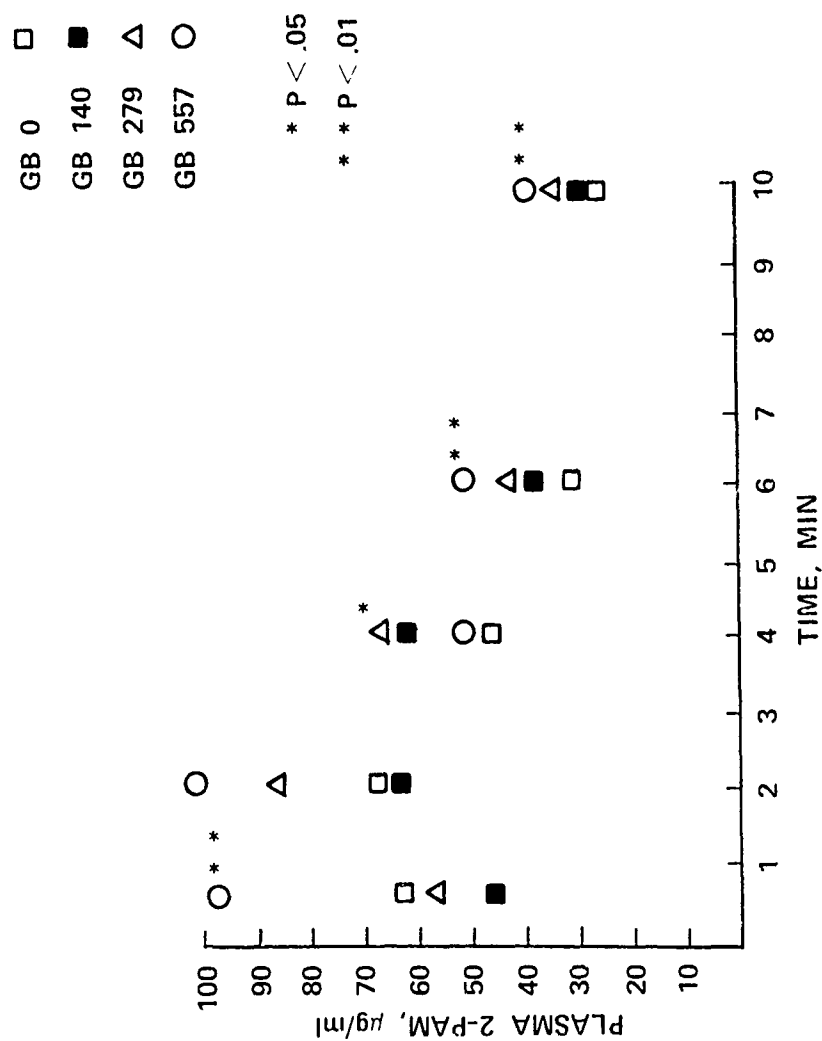


Figure 9



MEAN PLASMA CONTENT OF 2PAM AFTER SARIN INJECTION IN GUINEA PIGS GIVEN 25 mg/kg 2 PAMCI (IM) THERAPEUTICALLY. ANALYSIS BY DUNNETT'S TEST. GROUPS COMPARED TO GB 0 AS CONTROL.

Figure 10

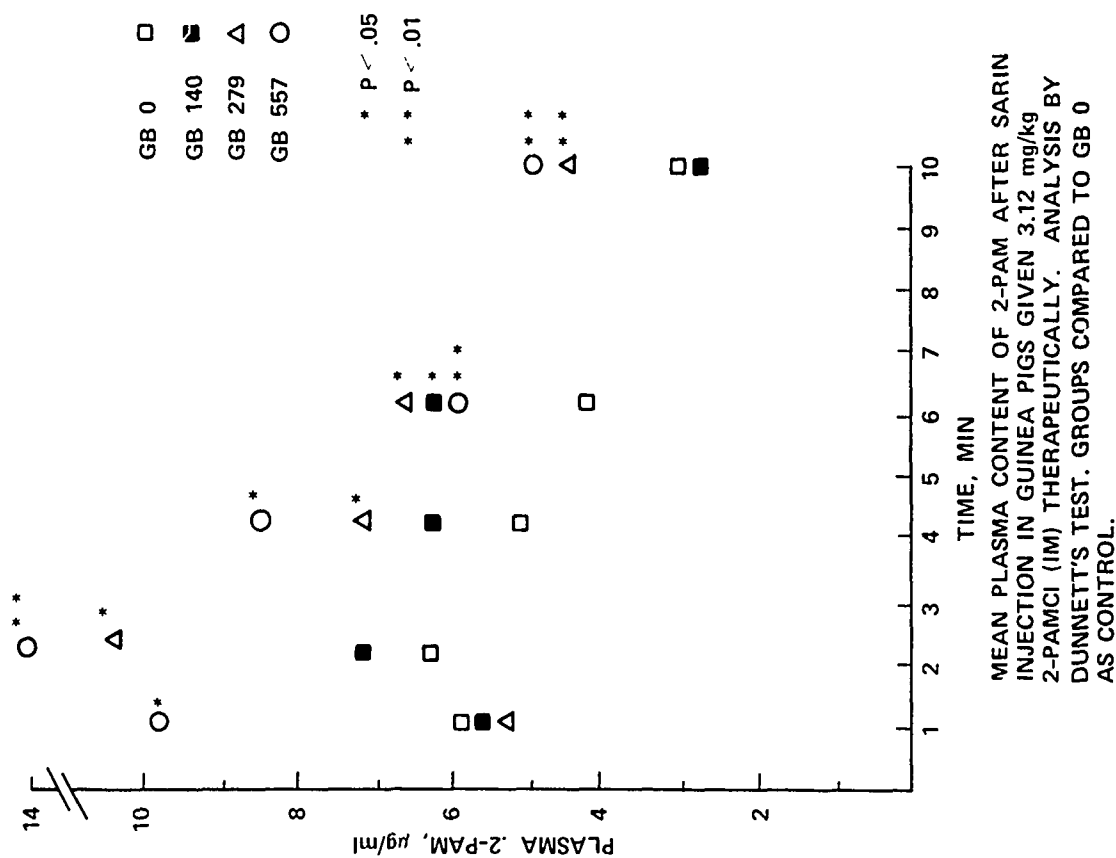


Figure 11

$\text{AUC}_{1 \rightarrow 10} \left(\frac{\text{mg} \cdot \text{min}}{\text{ml}} \right)$ FOR 2-PAM, 3.12 mg/kg

<u>SARIN</u>	<u>AUC</u>	<u>% CONTROL</u>
0	41.4	100
140	54.6	132
279	66.7	161
557	80.8	195

Figure 12

PERCENTAGE CHANGE FROM 0 SARIN PEAK LEVEL

<u>SARIN ($\mu\text{g/kg}$)</u>	<u>DOSE 2-PAM (mg/kg)</u>	
	<u>3.12</u>	<u>25</u>
140	18	-2.4
279	65	26
557	123	44

Figure 13

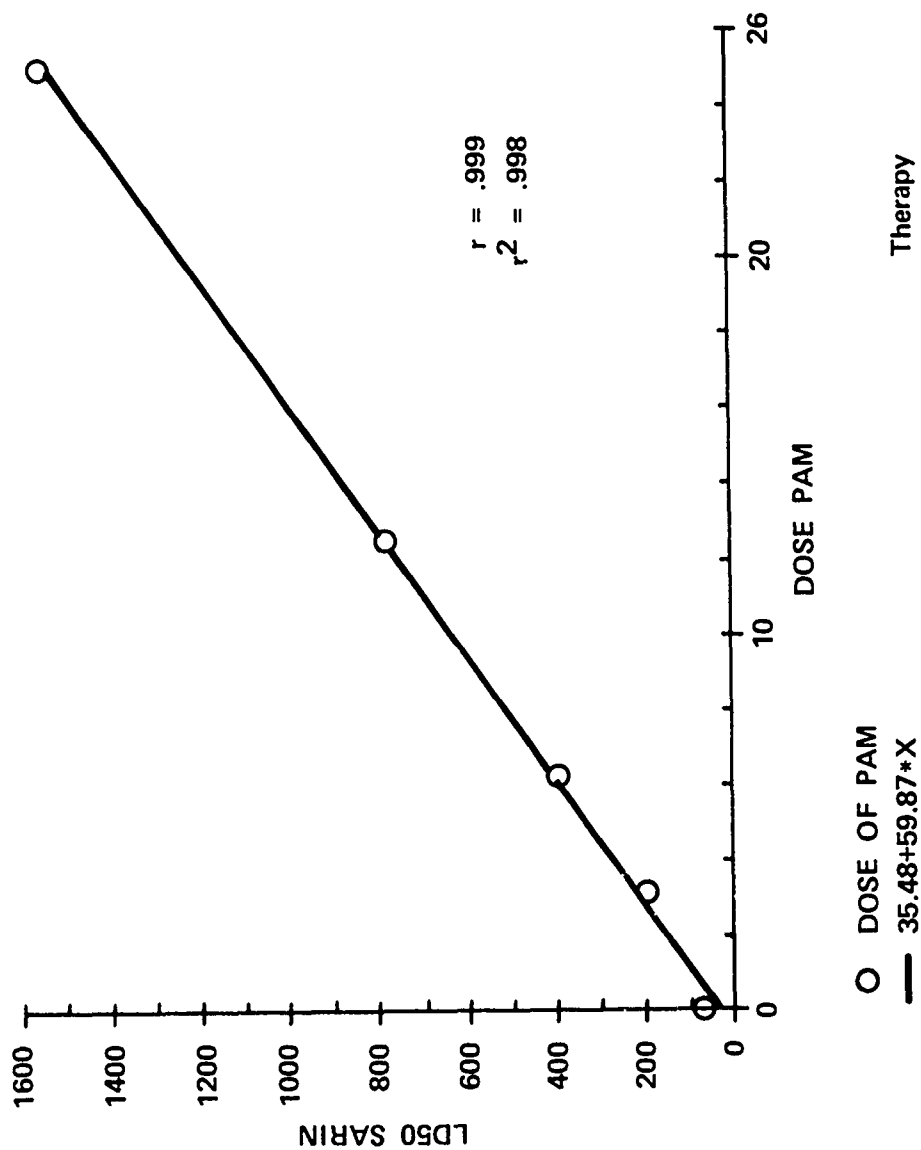


Figure 14

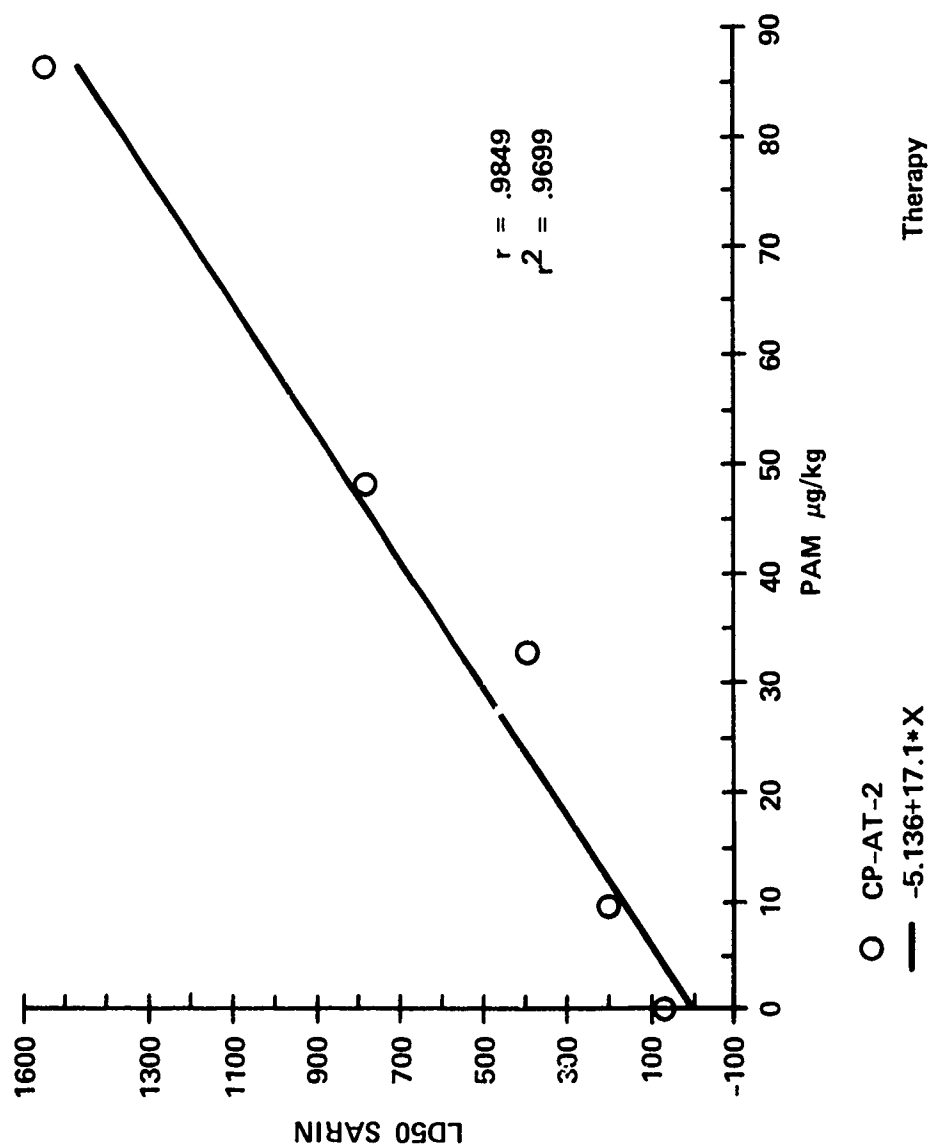


Figure 15

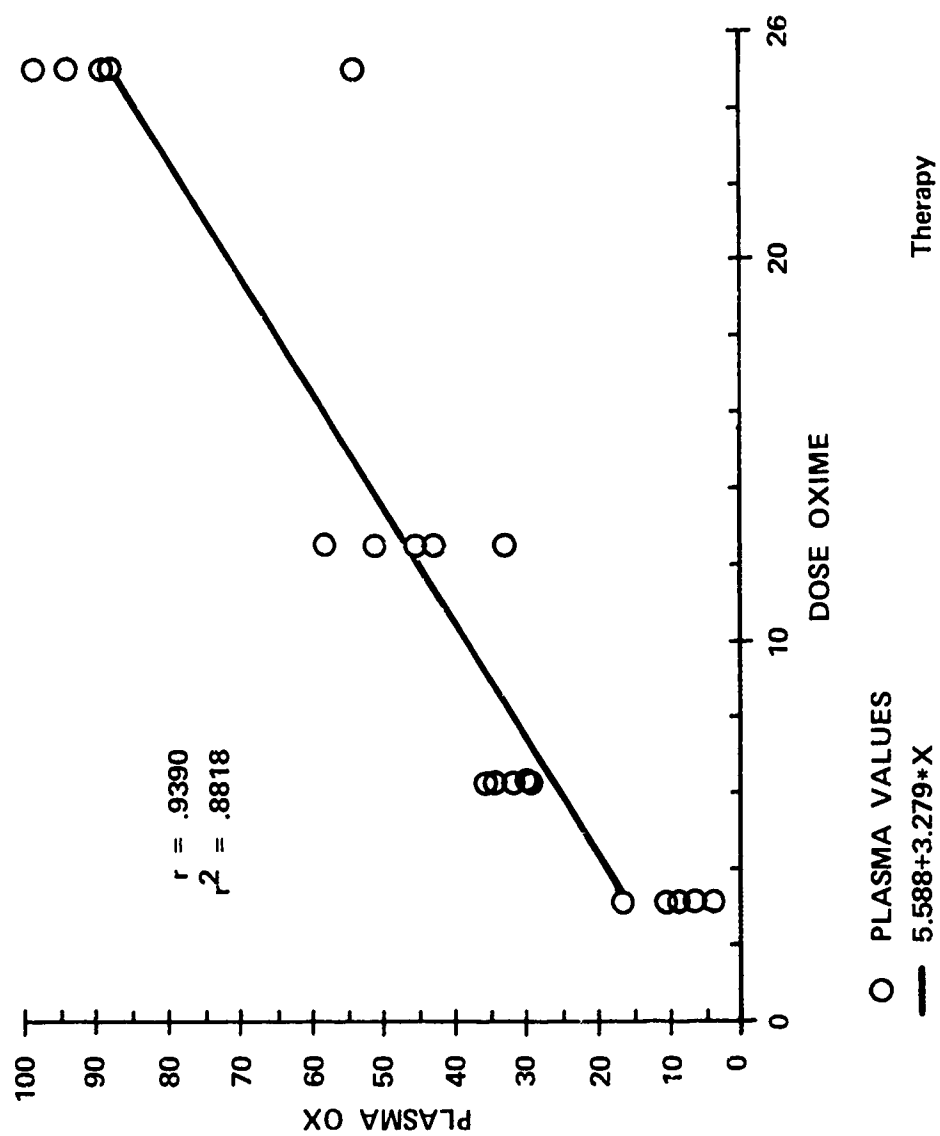


Figure 16

NONLINEAR REGRESSION OF DATA

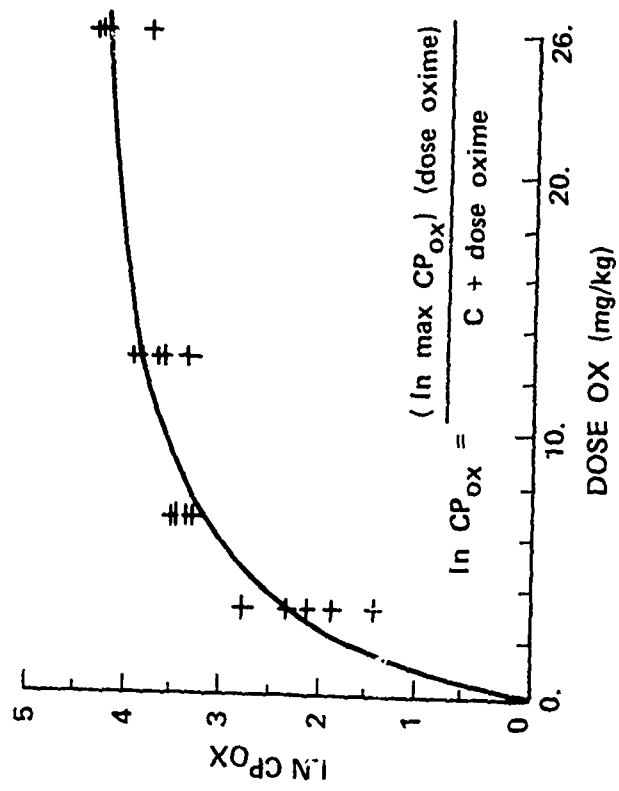


Figure 17

TWO STEP METHOD FOR THE NON-LINEAR MODEL

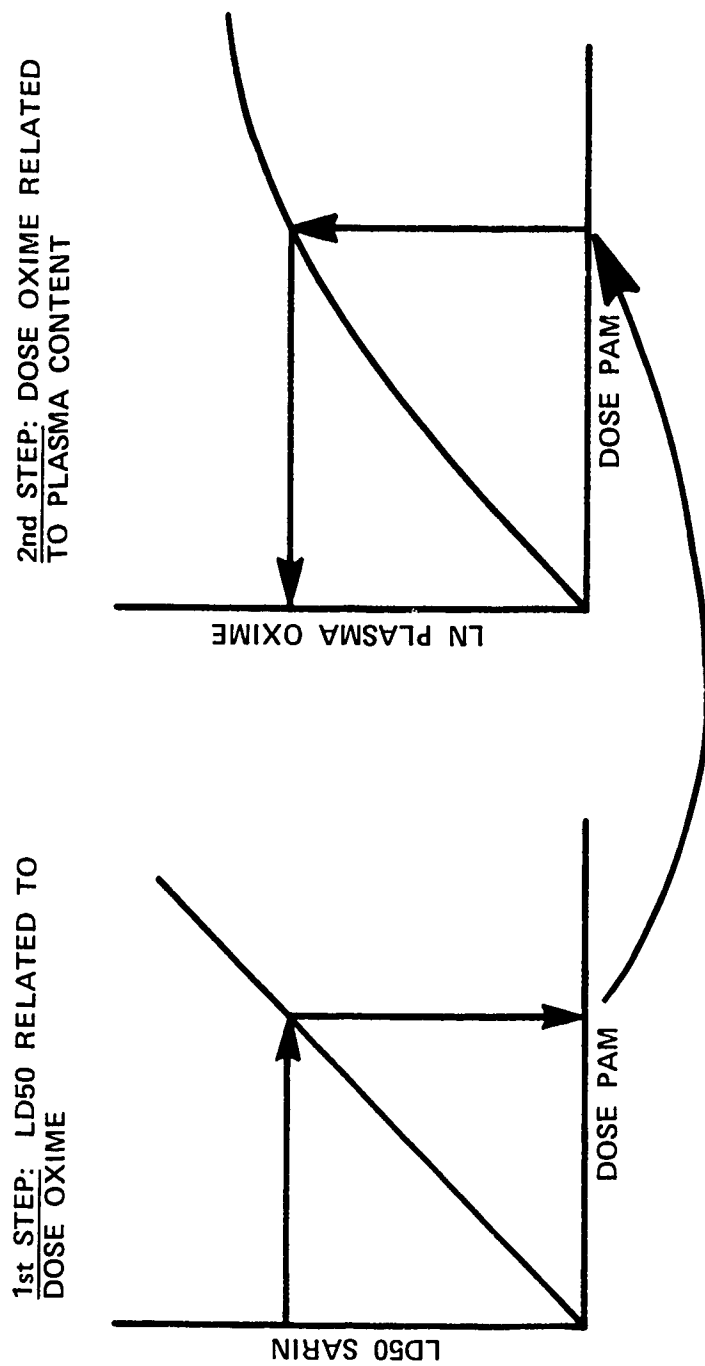


Figure 18

COMPARISON OF PREDICTED VALUES BY MODELS

DOSE SARIN $\mu\text{g/kg}$	OBSERVED PAM* $\mu\text{g/ml}$	PREDICTED BY LINEAR MODEL $\mu\text{g/ml}$	PREDICTED BY NON-LINEAR MODEL $\mu\text{g/ml}$
76.24	0**	4.16	2.2
196.2	9.38	11.17	10.43
390.6	32.58	22.54	24.95
776.6	48.08	45.11	51.92
1544	85.98	89.99	86.26

* MEAN OF EXPERIMENTAL VALUES

** NOT DETERMINED EMPIRICALLY

Figure 19

ANALYSIS OF CHI-SQUARE DETERMINATION

<u>MODEL</u>	<u>CHI-SQUARE</u>	<u>DF</u>
LINEAR	9.293	4
NON-LINEAR	2.724	4

Figure 20

SUMMARY OF FINDINGS BY INVESTIGATORS

AUTHOR (SPECIES)	OXIME, LEVEL (μ G/ML)	EFFECT IN RELATION TO AGENT
SUNDWALL (CAT)	P2S, 4 - 12 P2S, 2 - 4 P2S, 4	THERAPEUTIC SUCCESS THERAPEUTIC FAILURE MINIMUM THERAPEUTIC CONCENTRATION
GREEN NON-LINEAR MODEL (GUINEA PIG)	2 PAM, 3	DETECTABLE DIFFER- ENCE AT LD50
CROOK, et.al. (DOG)	2 PAM, 3	EFFECTIVE AGAINST SARIN
FLEISHER, et.al.	2 PAM, 4.8	IN VITRO, 88% REACTI- VATION

Correlation of Interspecies Variation in Treatment Efficacy with Endogenous
Nonspecific Agent Binding

Donald M. Maxwell, Frances M. Reid, and Dennis E. Jones

US Army Medical Research Institute of Chemical Defense,
Aberdeen Proving Ground, Maryland 21010

One of the major difficulties in assessing an antidote's efficacy against organophosphorous agents is the interspecies variation in efficacy which is generally observed. This problem is illustrated in Figure 1, which is a compilation on the efficacies of various drug combinations against soman as measured in several species. Antidote efficacy in this table is expressed as the protective ratio, which is the ratio of the soman LD50 in animals receiving antidote divided by the soman LD50 in untreated animals. The magnitude of the problem of interspecies variation is clearly evident from the data in Figure 1. Such variation creates considerable uncertainty with regard to the predicted efficacy in humans of antidotes whose efficacy is measured in animal models. Consequently, the development of a logical procedure to extrapolate antidote efficacy between species is a critical problem in the evaluation of antidotes intended for eventual use in humans.

Resolution of the problem of interspecies variation in antidote efficacy focuses on two hypotheses which are illustrated in Figure 2. Soman is a racemic mixture of two types of stereoisomers: P(-), which are highly toxic and P(+), which are nontoxic. The P(-) isomers, in addition to being toxic, are also less susceptible to enzymatic hydrolysis by somanase, which has a substrate specificity for the nontoxic P(+) isomers. The major means of in vivo detoxification of P(-) isomers is to bind to nonspecific tissue binding sites, which react irreversibly with both P(+) and P(-) isomers. Antidotes produce their pharmacological effects by interaction with one of the three components of the cholinergic complex. Oximes reactivate the inhibited acetylcholinesterase (AChE), anticholinergic drugs block the excess acetylcholine, stimulating acetylcholine receptors (AChR), carbamates protect AChE, and all of these drugs may interact with the ion channel. Some workers have hypothesized that the interspecies variation of antidote efficacy is the result of differences in the responsiveness of the cholinergic complex of various species to antidotes. However, the small pharmacological differences which have been demonstrated in vitro do not explain the large differences in antidote efficacy. An alternative hypothesis is that the apparent interspecies differences in antidote efficacy are the result of interspecies variation in soman metabolism and disposition. To examine this hypothesis, it is necessary to alter the detoxification of soman in vivo, which can be accomplished by blocking the nonspecific tissue binding of soman with an inhibitor known as cresylbenzodioxaphosphorin oxide (CBDP). The structure of CBDP is shown in Figure 3.

CBDP possesses the ability to specifically block the tissue binding sites for soman without inhibiting acetylcholinesterase. CBDP reacts 133,000 times faster with tissue binding sites than AChE. In contrast, soman is more specific for AChE than tissue binding sites. The bimolecular rate constant for the reaction of soman with nonspecific tissue binding sites is only 1/100 of its reaction rate constant with AChE. Thus, it is possible to administer an in vivo dose of CBDP, which blocks the nonspecific tissue binding of soman without inhibiting AChE.

In Figure 4, the soman LD50's in control animals and animals receiving CBDP are presented. The soman LD50's in control animals vary considerably from near 100 ug/kg in mice and rats to near 30 ug/kg in rabbits and guinea pigs. When animals are pretreated with CBDP at doses which block nonspecific

binding sites for soman without inhibiting AChE, the LD50's of all species are reduced to the same level (8-13 ug/kg). Thus, the difference in the LD50's in various species appears to result from species differences in the quantity of tissue binding sites for soman. The soman LD50 in nonhuman primates is also 8-13 ug/kg, which may indicate an absence of nonspecific binding sites in primates.

Since the interspecies variation in soman toxicity can be eliminated by CBDP treatment of animals, it was hypothesized that interspecies variation in antidote efficacy could be reduced or eliminated by CBDP treatment. Also supporting the idea that nonspecific binding sites may alter the apparent antidote efficacy observed in different species is the correlation between maximal antidote efficacy in mice and guinea pigs as shown on Figure 5. In these studies, the doses of each drug (pyridostigmine given as oral pretreatment, atropine and PAM given i.m., postchallenge) to produce maximal antidotal effect against soman were determined in each species. Antidote efficacy is expressed as the soman LD50 in mice or guinea pigs receiving each antidote regimen. A perfect correlation between mice and guinea pig models for the optimized antidote efficacies presented in this graph would be observed if the slope = 1, the intercept = 0, and the correlation coefficient (r) = 1. In this graph, the slope is 1.06 and $r = 0.95$, but the intercept is 65 ug/kg. The intercept describes a consistent 65 ug/kg difference in LD50 between mice and guinea pigs, which is exactly the difference in soman LD50's between the two species and, thus, equal to the difference in nonspecific binding sites in these species. In Figure 6, the difference in the levels of nonspecific binding sites between mice and guinea pigs has been eliminated by treatment with CBDP. The antidotes were administered at the same dose levels as in the previous slide. However, the intercept is now 6 ug/kg, the slope is 0.7 and $r = 0.99$. CBDP treatment has eliminated nonspecific binding sites as a factor in antidote efficacy and greatly reduced the interspecies differences in antidote efficacy, as demonstrated by a high correlation coefficient, an intercept near zero, and a slope near one.

It should not be inferred from this study that all testing should be done in CBDP-treated animals to eliminate interspecies variation. However, if an antidote looks promising, an evaluation of antidote efficacy in CBDP-treated rodents can suggest what degree of maximal efficacy is possible in species of limited availability (e.g., nonhuman primates) or nonavailability (e.g., humans). A summary of the results of this study is provided in the final Figure.

Figure 1

PROTECTIVE RATIO AGAINST SOMAN (S.C.)

DRUGS	SPECIES					
	MOUSE	RAT	RABBIT	GUINEA PIG	DOG	MONKEY
ATROPINE	1.4	-	1.9	-	-	3.5
PAM + ATROPINE	1.1	-	2.2	1.8	-	-
TMB-4 + ATROPINE + BENACTYZINE	2.0	-	2.9	-	-	3.9
HS-6 + ATROPINE + BENACTYZINE	-	3.8	10.0	-	6.5	-
PHYSOSTIGMINE + ATROPINE	2.8	2.0	4.5	8.2	6.3	-
PYRIDOSTIGMINE + ATROPINE	2.0	-	-	3.9	-	15.0
PYRIDOSTIGMINE + ATROPINE + P2S	-	1.7	2.7	5.3	-	-
TEPP + ATROPINE + P2S	-	1.5	3.7	7.1	-	-

Figure 2

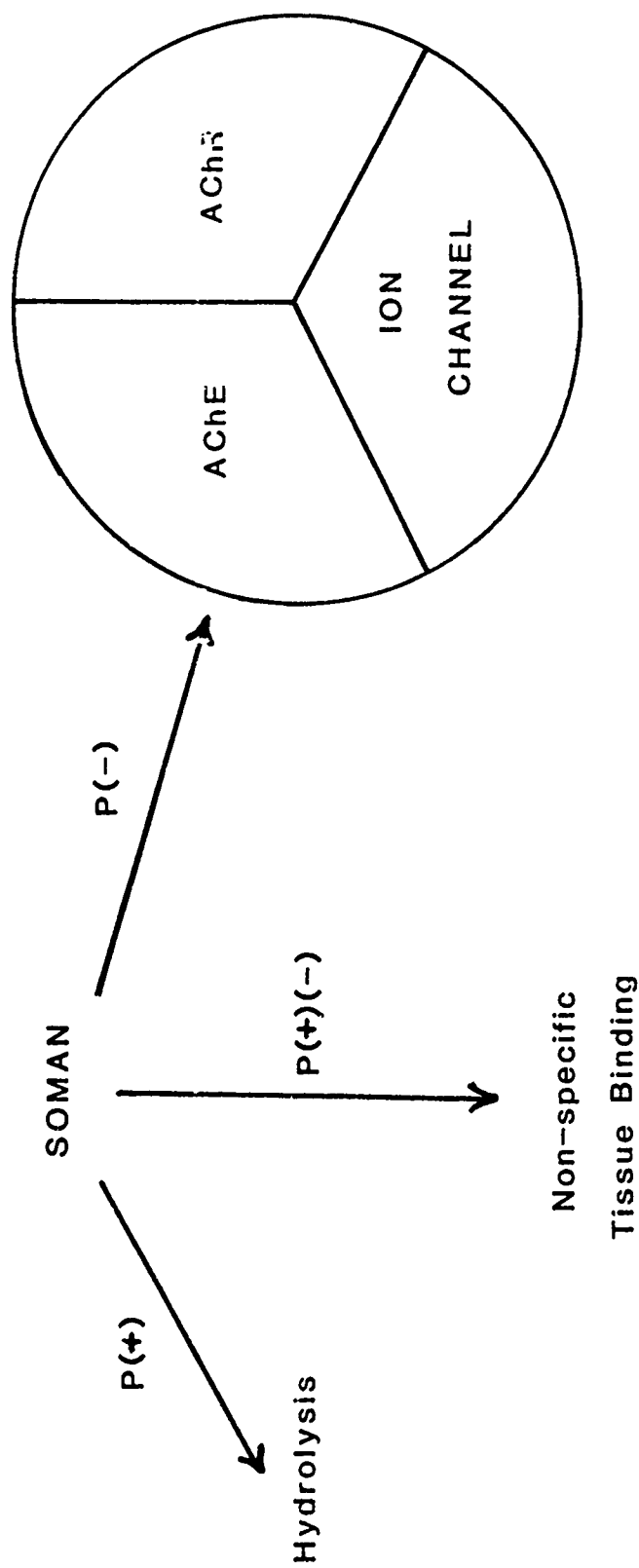
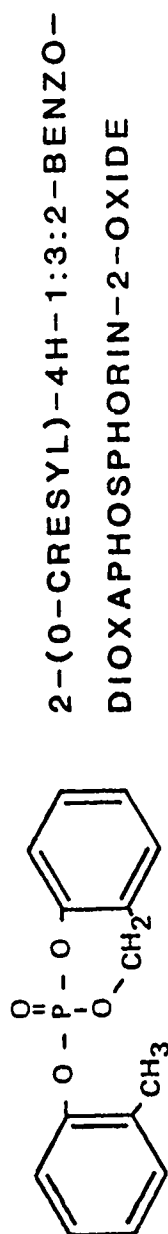


Figure 3



BIMOLECULAR RATE CONSTANT ($M^{-1} \text{min}^{-1}$)

	NON-SPECIFIC TISSUE BINDING SITES	AChE	BINDING SITES AChE
CBDP	2.0×10^8	1.5×10^3	133,000
SOMAN	1.4×10^6	1.2×10^8	0.012

Figure 4

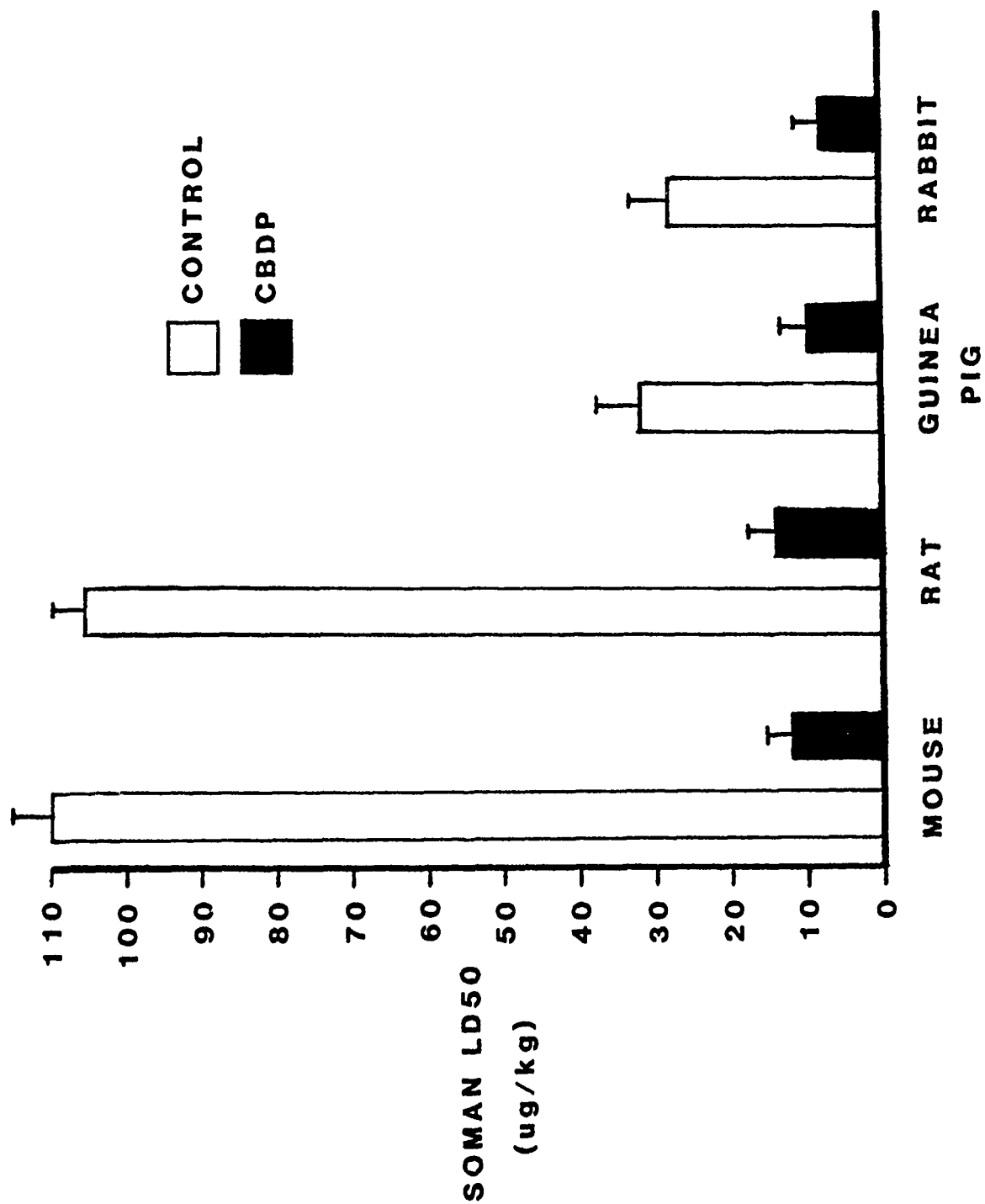


Figure 5

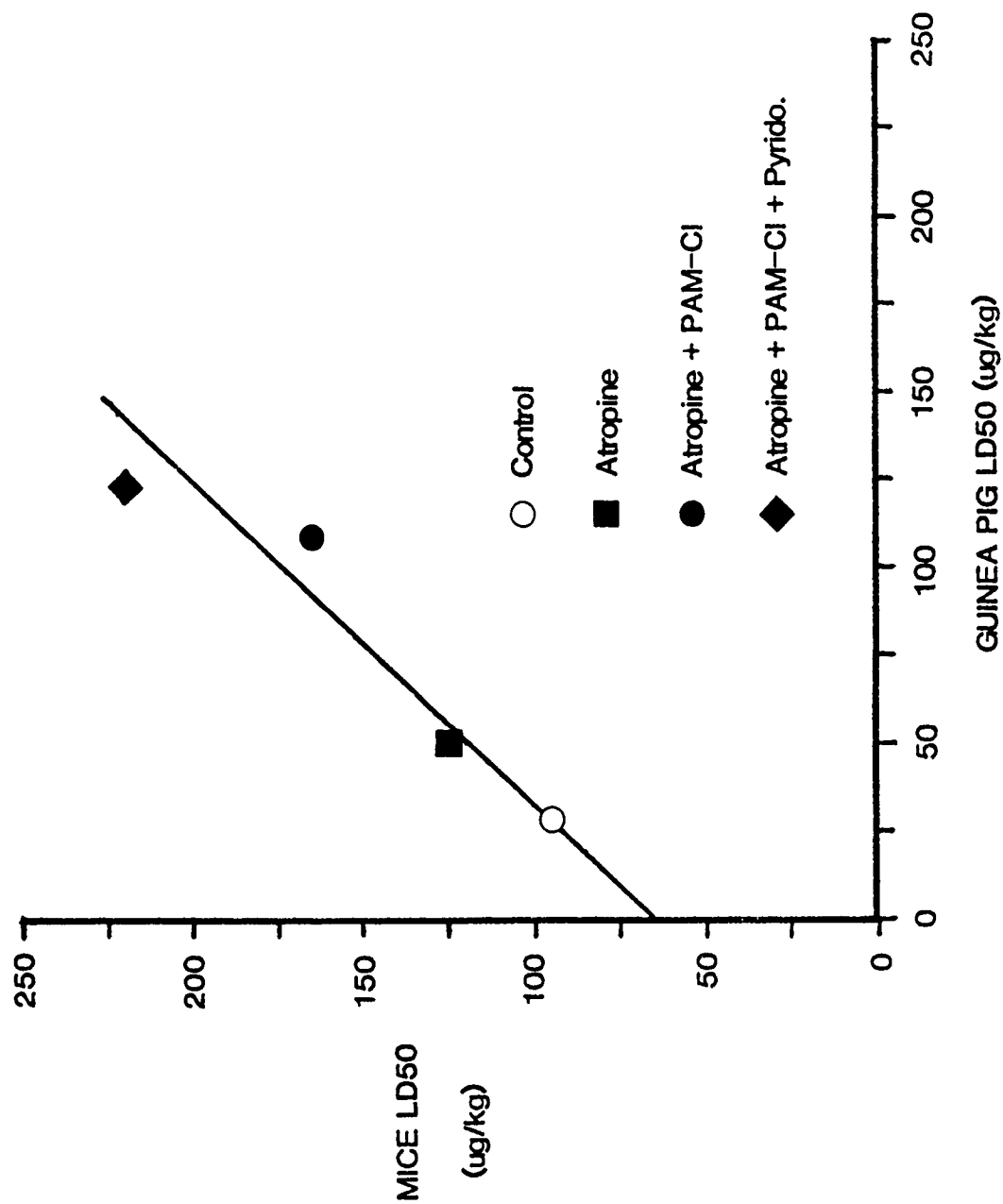


Figure 6

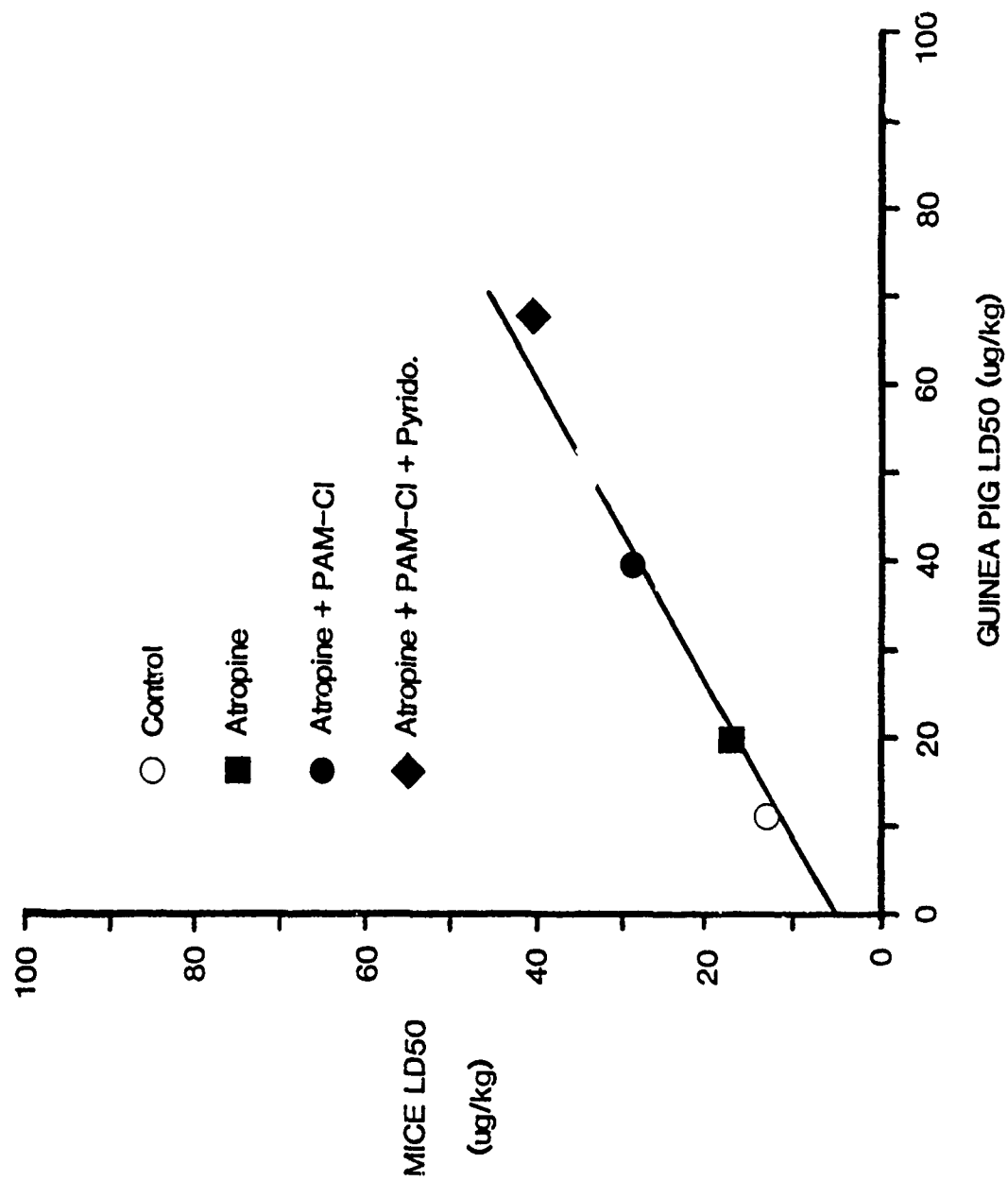


Figure 7

SUMMARY

INTER-SPECIES VARIATION IN SOMAN TOXICITY RESULTS FROM DIFFERENCES IN NON-SPECIFIC TISSUE BINDING OF SOMAN, WHICH CAN BE SELECTIVELY BLOCKED BY CBDP.

INTER-SPECIES VARIATION IN MAXIMAL ANTIDOTE EFFICACY IS ALSO PRIMARILY THE RESULT OF NON-SPECIFIC TISSUE BINDING OF SOMAN.

IN CONJUNCTION WITH ANTIDOTE EFFICACY OPTIMIZATION PROCEDURES AND PHARMACOKINETIC STUDIES, THE REDUCTION OF INTER-SPECIES VARIATION IN ANTIDOTE EFFICACY BY CBDP ALLOWS RATIONAL EXTRAPOLATION OF ANTIDOTE EFFICACY TO OTHER SPECIES INCLUDING MAN.

II. Pyridostigmine: Update on Nerve Agent Pretreatment

Status of the Pyridostigmine Development Effort

by

LTC Gerald L. Wannarka, Ph.D.
HQ, US Army Medical Research and Development Command
ATTN: SGRD-DPM
Ft. Detrick, Frederick, MD 21701

It is my intention to discuss the recent progress in developing a pretreatment compound to be used to protect soldiers against the effects of CW nerve agents. This review will be slanted more toward program issues rather than science. While the latter are not of lesser importance, restrictions affecting non-science issues tend to make non-science issues more difficult to resolve.

FIRST VIEWGRAPH

The concept which calls for the use of a pretreatment compound to protect the soldier during exposure to organophosphorus nerve agents has been around for some time.

The first generation pretreatment compound which was identified by the USARMDC for development was the quaternary carbamate, pyridostigmine. This compound was introduced in the US during the late 40's as a treatment for a degenerative neuro-muscular disease called myasthenia gravis. It has since been marketed in most, if not all, countries in the free world. Its use as a pretreatment compound is not new or novel, and, in fact, it was considered a candidate drug for this indication as early as the mid 50's. Interest increased over the years, and a major initiative to develop a useful formulation of the drug was underway in the early 70's at the Biomedical Laboratory at Edgewood, MD. The decreased emphasis in medical chemical defense that occurred in the mid 70's stopped the initiative until its rather recent revival.

A sufficient amount of quality data now exists to safely conclude that the pretreatment or prophylactic administration of pyridostigmine will enhance the efficacy, at least several fold, of the currently fielded atropine/2 PAM-Cl regimen against soman exposure. Soman is considered one of the organophosphorous compounds most difficult to protect against. It should be remembered, however, that pyridostigmine is an adjunct to the atropine/2PAM-Cl regimen, and is without protective effect in itself.

There are two theories currently in existence which describe how pyridostigmine exerts its mechanism of action. The traditional theory states that pyridostigmine reversibly inhibits AChE. Therefore, when an individual is exposed to an irreversible inhibitor such as a soman, a certain amount of AChE is protected by pyridostigmine from binding with soman. The reversibly bound enzyme spontaneously regenerates from its complex with pyridostigmine, thus allowing some degree of normal neural function to return. An emerging theory states that pyridostigmine has a direct effect on the post-synaptic membrane. Thus, it appears to be a partial agonist to soman and exerts this effect directly on the membrane in at least one of several ways.

SECOND VIEWGRAPH

Most of the countries in the free world that have a chemical defense program have investigated the concept of a pretreatment compound, and specifically, pyridostigmine.

The United Kingdom has recently fielded pyridostigmine in a 30mg tablet. The drug is packaged in a 21 tablet blister pack--enough for seven days--and one package is issued to the soldier at a time. The soldier is instructed, upon command, to take one tablet every eight hours when an attack is deemed imminent.

Several other allies are considering fielding the UK product, and another has decided to field a shorter regimen of 30mg tablets. Additionally, the US Air Force (USAF) has decided to obtain the UK formulation for emergency use by its forces.

THIRD VIEWGRAPH

Individuals at the USAF Surgeon General Office reviewed the data on pyridostigmine, and recommended to their Surgeon General that the USAF should purchase the UK product. This recommendation was accepted by the USAF staff, and action has been initiated to purchase this drug from Roche of England. The USAF has coordinated this action with the FDA who posed no objection to stockpiling the drug for emergency use only at USAF medical logistic and treatment facilities in CONUS and Europe.

While the data base is deficient in many of the areas normally included in an NDA, it does, however, support both the premise of safety and efficacy for this indication.

FOURTH VIEWGRAPH

Some shortcomings exist in the current data base which has led to the Army's decision to initiate an effort to develop an optimized pyridostigmine formulation.

The Army's position is that:

- The potential utility of this compound has caused it to be identified as a high priority development effort by the USAMRDC.
- The data base is adequate to support the initiation of full scale development.
- The principle emphasis of this development effort would be to determine the optimal dose and delivery system, or systems.

Accordingly, a multi-organization management structure was established and full scale pyridostigmine development initiated in August 1983.

FIFTH VIEWGRAPH

For this discussion, the issues being addressed in the pyridostigmine development effort are divided into Science/Technology and Development/Production.

Most of the science and technology efforts are currently being undertaken at the Walter Reed Army Institute of Research (WRAIR) or the US Army Medical Research Institute of Chemical Defense (USAMRICD). While some of these issues are being pursued in-house, most will be pursued by outside contractors supporting these laboratories.

The development and production efforts are being addressed by the Directorate of Development and Production Management at HQ, USAMRDC with assistance from the Division of Experimental Therapeutics, WRAIR.

SIXTH VIEWGRAPH

The science and technology issues are divided into four major categories as shown on this viewgraph. They include toxicity, pharmacology, formulation and, usage considerations.

In spite of the fact that pyridostigmine has been on the market over 35 years, much of the safety data usually associated with an FDA approved drug has not been generated. Consequently, this development effort must ensure that the necessary data is generated to update the compound in order to meet the safety standards currently accepted.

Recent preliminary laboratory data has alerted us to the pyridostigmine's potential to damage certain muscle tissue. Therefore, the questions which must be answered are: is the observed muscle damage real or an artifact; if it is real, is it reversible; if it is reversible, then what is the short term or long term impact; is the effect clinically relevant.

Efforts are underway under the auspices of the USAMRICD to investigate this observation, and we will hear more about their findings this afternoon.

Since carcinogenicity and teratology studies were rarities in the 40's, these additional issues must be addressed today. The current national pastime of searching for potential carcinogens has made the fielding of an untested drug unrealistic. Of course, with Army female strength around 15-20% of the total force, the appropriate teratology studies have to be completed.

Arriving at an appropriate dose is less straightforward. First of all, since efficacy testing can never be done in man with these compounds, efficacy must be demonstrated in animals and the results then extrapolated to man. This is further complicated by current limitations for determining blood levels of pyridostigmine following dosing.

The most common procedure used to determine blood levels is to assay the extent of inhibition of red blood cell acetylcholinesterase (RBC AChE). This has limitations because the assay has some exacting requirements for consistency. Depending on the theory you subscribe to for how pyridostigmine works, the assay may be only a casual indicator of drug available at the receptor site. Attempts to develop an assay which determines actual blood levels of the drug are nearing completion, but these have not been validated yet.

In using the RBC AChE assay, one notices that considerable variation exists between individuals as to the degree of drug-induced enzyme inhibition observed at the same dose level. This may be a result of the assay, the formulation, compliance with the dosing regimen, or to individual variation as to how the drug is handled in the body.

The early literature suggests that the compound is about 40% absorbed following oral administration, and that which is absorbed is about 90% metabolized by the liver on the first pass. Thus, individual variation may be a critical factor following administration of a solid oral dosage form. Clinical studies will be conducted in the next few months in an attempt to obtain more definitive information on this issue.

While recognizing the desirability of an assay to directly measure pyridostigmine in body fluids, the decision was made to validate the red cell cholinesterase assay for use in the upcoming clinical studies. Work will continue on a direct assay, however.

The first step in optimizing the formulation and dosing regimen for pyridostigmine is to obtain pharmacokinetic data for the currently available formulations of this compound. Formulations to be evaluated are 30 and 60 mg tablets, an oral syrup, and a 180 mg sustained release tablet. These Phase I pharmacokinetic studies will be initiated this June under an Army sponsored IND. The results of these studies will provide the basis for optimizing the drug delivery system. The objective is to provide a formulation which will deliver the desired blood level of the drug, but minimize or simplify the dosing procedure by the soldier. Both sustained release dosage forms and transdermal delivery systems hold considerable promise in this area. The latter is especially appealing and preliminary efforts are underway to involve this technology.

Very little stability data currently exists for pyridostigmine. Consequently, when a candidate dosage form is identified, product stability testing of the formulation in its package must then be initiated. Basic data of this nature is an essential part of the new drug application (NDA), and is required by the logisticians in programming for supply needs.

As with any drug that will be administered to ambulatory subjects, the potential impact that the drug has on the routine performance of the subject must be determined. This information can be obtained from the observed side effects of the drug in Phase I and Phase II clinical evaluation, and by a behavioral pharmacology work-up. The latter will be addressed in a Request for Proposals (RFP) that is to be advertised later

this summer. The USAF has sponsored a study to evaluate the effects, or lack of effects, of the UK formulation on volunteers' ability to execute a battery of performance oriented tasks. The results of this study will be discussed by the following speaker, Dr. Graham.

Another concern under active discussion is, "How long should the planned pretreatment period be?" The extent and duration of safety studies in animals is dictated by the length of time the drug is to be administered in humans. In addition, the knowledge of the length of time the drug is to be administered must be known to plan for availability of adequate quantities of the drug, and to budget for monies to procure it.

SEVENTH VIEWGRAPH

Since this is a science review, I will not dwell on development/production issues, but will highlight several general problems or challenges involved. Unfortunately, these issues tend to involve more bureaucracy, and frequently have more restraints which limit approaches for resolution of these issues.

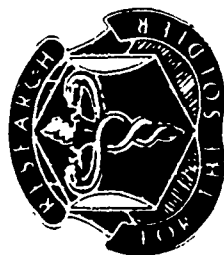
The requirements for competition between contractors is extremely difficult to meet in the drug development process. Additionally, the recent implementation of the Federal Acquisition Regulation has gone on to place additional restrictions on obtaining contractual support. This becomes substantially more difficult when attempting to contract for development efforts that lead to initial procurement.

As a candidate product is identified and moves through the basic research phase, hundreds of potential contractors exist who can support the basic research. However, when this candidate graduates to the development stage, time and cost restrictions dictate that the contractor who supported the development effort also have the capability to produce the item. If the pharmaceutical is produced by someone other than the one who developed it, much of the data such as stability and bioavailability will have to be repeated. In addition, the present system for procurement of medical items does not facilitate the follow-on procurement of developed items. As you can see, all of this tends to slow the process and increase the cost.

Another challenge in development has to do with funding. An item which is under evaluation in the science base can be funded under general science and technology programs. When it moves to development, the funding becomes specific for the development of that item only. At that time, the requirement documents, that is, the Army's need statement document, must support the development effort. These documents are dynamic and become more detailed as the item moves through the development process.

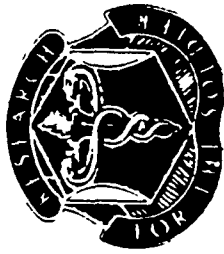
EIGHTH VIEWGRAPH

This last viewgraph summarizes the major development milestones for the pyridostigmine effort. The IND was filed in February; the FDA subsequently concurred with the document and proposed plan of study. The Phase I pharmacokinetic studies considered critical for the development effort will begin in June. The Request for Quotations (RFQ) for performance impact evaluation is being prepared and should be advertised in late summer. The pharmacokinetic data will then be evaluated and appropriate doses selected for incorporation into the performance study. When all these data are accumulated, decisions can then be made to develop an appropriate drug delivery system. Since efficacy cannot be established in man, drug level data in humans must be extrapolated back to animals to verify efficacy. It is hopeful that a final product configuration can be decided upon in the second quarter of FY 86 which will permit an NDA soon thereafter.



U. S. ARMY

MEDICAL RESEARCH & DEVELOPMENT COMMAND



PYRIDOSTIGMINE AS A NERVE AGENT PRETREATMENT

- MARKETING DRUG
- OLD CONCEPT
- ADJUNCT
- MECHANISM OF ACTION



U. S. ARMY

MEDICAL RESEARCH & DEVELOPMENT COMMAND

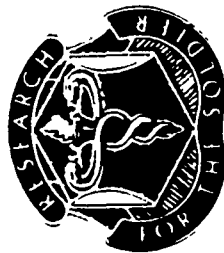


INTEREST IN PYRIDOSTIGMINE AS A NERVE

AGENT PRETREATMENT

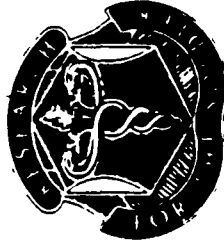
- ALLIES
 - UNITED KINGDOM
 - OTHERS
- UNITED STATES
 - US AIR FORCE
 - US ARMY

Viewgraph #2



U. S. ARMY

MEDICAL RESEARCH & DEVELOPMENT COMMAND



US INTEREST IN PYRIDOSTIGMINE

USAF POSITION

- SURGEON GENERAL RECOMMENDATION TO PROCURE UK
PRODUCT
- TO BE MAINTAINED AT USAF MEDICAL LOGISTIC/
TREATMENT FACILITIES
- ACTION COORDINATED WITH THE FDA
- DATA SUPPORT PREMISE OF SAFETY AND EFFICACY

Viewgraph #3



U. S. ARMY

MEDICAL RESEARCH & DEVELOPMENT COMMAND



US INTEREST IN PYRIDOSTIGMINE

US ARMY POSITION

- CONCEPT VALID FOR DEVELOPMENT
- NEED TO DETERMINE OPTIMAL DOSE AND
DELIVERY SYSTEM
- MANAGEMENT STRUCTURE FOR DEVELOPMENT ESTABLISHED
- IDENTIFIED AS A HIGH PRIORITY DEVELOPMENT EFFORT

Viewgraph #4



U. S. ARMY

MEDICAL RESEARCH & DEVELOPMENT COMMAND



ISSUES

- SCIENCE/TECHNOLOGY
- DEVELOPMENT/PRODUCTION

Viewgraph #5



U. S. ARMY

MEDICAL RESEARCH & DEVELOPMENT COMMAND



SCIENCE/TECHNOLOGY ISSUES

- TOXICITY
 - MUSCLE DAMAGE
 - CARCINOGENICITY/TERATOLOGY
- PHARMACOLOGY
 - APPROPRIATE DOSE
 - INDIVIDUAL VARIABILITY
- FORMULATION
 - BLOOD LEVEL ASSAY
 - PHARMACOKINETICS
 - ROUTE OF ADMINISTRATION
 - STABILITY
- USAGE CONSIDERATIONS
 - PERFORMANCE ALTERATIONS
 - DURATION OF PRETREATMENT PERIOD

Viewgraph #6



U. S. ARMY



MEDICAL RESEARCH & DEVELOPMENT COMMAND

DEVELOPMENT/PRODUCTION ISSUES

- FEDERAL CONTRACT REQUIREMENTS
 - RESTRAINTS
 - COMPETITION
- MANUFACTURING CAPABILITY
- FUNDING
 - REQUIREMENTS DOCUMENT
 - INDIVIDUAL ITEM ACCOUNTABILITY



U. S. ARMY
MEDICAL RESEARCH & DEVELOPMENT COMMAND



DEVELOPMENT MILESTONES

IND FILED	FEB 84
PHARMACOKINETIC STUDIES	JUN 84
RFQ FOR PERFORMANCE IMPACT	4TH QTR FY84
FORMULATION ASSESSMENT	1ST QTR FY85
EXTRAPOLATE DRUG LEVELS IN HUMANS TO	
EFFICACY IN ANIMALS	2ND QTR FY85
FINAL PRODUCT CONFIGURATION DECISION	1ST QTR FY86
SUBMIT NDA	---

Viewgraph #8

12 Jun 1984

Oral Dose Effects of Pyridostigmine on Human Performance

Charles Graham, Mary R. Cook, Mary M. Gerkovich,
Harvey D. Cohen, James W. Phelps and Sophia S. Fotopoulos

Midwest Research Institute
Kansas City, Missouri 64110

Charles Graham, Ph.D.
Midwest Research Institute
425 Volker Boulevard
Kansas City, Mo. 64110

A. INTRODUCTION

Pyridostigmine is a reversible anticholinesterase inhibitor long used in the medical treatment of the neuromuscular disorder myasthenia gravis. Due to the site and the reversible nature of its action, this drug is currently being considered by the USAF for field use as a pretreatment medication to aid pilot survival in the event of a chemical attack. Medical reports indicate that high daily oral doses (600 mg/day) are well tolerated in patient populations. Recent NATO studies also suggest that lower dose regimens (30 mg, 3 x day, 30 days) can provide enhanced survival protection in nonclinical populations, with only minor gastric upset reported in a few individuals.

Although health risks appear minimal, there exists a significant need to evaluate the impact of the drug on human functions important in pilot operations. The present study addressed this need. A double-blind, cross-over experimental design was used to evaluate the effects of an oral regimen of pyridostigmine (30 mg, 3 x day, 5 days) on the performance, physiology, and subjective state of 24 paid, male volunteers.

B. METHOD

1. EXPERIMENTAL DESIGN

There were two identical drug testing weeks, separated by a week of no drug administration. Half the subjects (N=12) were assigned at random to the test sequence drug (week-1) followed by placebo (week-2); the remaining subjects (N=12) participated in the reverse sequence. Pills were given under double-blind conditions (i.e., pills were marked "Subject 1, pill 1; subject 1, pill 2"). At the end of each test week, subjects and experimenters judged whether the drug or the placebo had been administered.

In each test week, pills were administered daily at 0700-0800, 1600-1700 and 2300-2400 for 5 days. Blood samples were taken on days 3 and 5 of the test week, and 3 days after intake ceased (day 8). Performance was tested at the same time of day for each subject on days 4, 5 and 8. In addition, a subgroup (N=12), was also tested on day 2 to provide information on the early effects of drug intake.

2. SUBJECTS

Volunteers were solicited by means of advertisements posted at local universities and colleges. Subjects had to be males in good physical and mental health between the ages of 21 and 35 years, with normal vision (corrected) and hearing, and not currently taking any medication or using illicit drugs. They also had to agree not to use alcohol or drugs during the testing weeks. After informed consent

was obtained according to policies outlined in FR45CFR46, subjects received a comprehensive medical examination, and provided urine and blood samples for drug screen analysis and determination of baseline plasma cholinesterase levels.

A total of 33 subjects participated in the study. Of these, 8 were dropped for failure to meet various study criteria before starting the drug regimen. One other subject, however, was discontinued after ingesting 120 mg of pyridostigmine (4, 30 m^c pills over 2 days). This subject, after reading the PDR, reported what he believed were drug-related symptoms (excessive physical fatigue and malaise). Drug intake was stopped immediately. The subject's vital signs, subjective symptoms and plasma cholinesterase level were monitored during the following 3 days. The subject reported "feeling completely normal" within 24 hours after drug cessation. After examining all available data, the reactions of this subject were not considered to be drug-related. The remaining 24 subjects completed all study requirements. Subjects were paid approximately \$250.00 for the 40-50 hours of participation required.

3. PROCEDURES

A comprehensive battery of tasks and measures was designed and implemented by MRI in coordination with USAF personnel. The primary goal was to ensure that a broad spectrum of capabilities related to pilot performance and/or drug action would be sampled. TABLE 1 summarizes all of the measures obtained. The various tasks were performed at 4 different work stations. Multiple subjects were tested simultaneously, with each requiring approximately 2 hours to complete the entire battery.

Prior to drug testing, subjects were trained to performance criteria on the various battery tasks, and baseline values were established for the physiological and subjective measures. At the end of the baseline period, a second urine and blood sample was obtained.

During each test week, 3 pills per day were administered by project staff at MRI. Due to unavoidable schedule conflicts, some subjects had to take one of their daily pills away from the laboratory. In such cases, the subject was instructed to call a staff member at a specified time to verify pill ingestion; if no call was received within 15 minutes of the time set, the subject was contacted by the staff. Analysis of cholinesterase levels revealed no differences between the two pill administration procedures.

Vital signs and subjective data were collected each day; blood samples and performance/physiological data were obtained on the schedule

described above. After completion of the study, subjects received a second medical examination and group debriefings were conducted by an independent interviewer.

C. RESULTS

The drug regimen produced the expected mean level of inhibition (8.1%) in plasma cholinesterase, with values returning to baseline when sampled 64 hours after intake ceased. However, unexpectedly large individual differences in inhibition under drug conditions were observed (range= -21.7% to +8.3%).

Experimenters were not able to judge at better than chance levels whether subjects received the drug or the placebo. During week 1 of the drug regimen, the subjects' ratings were also no better than chance. At the end of week 2, however, no subject taking the placebo judged it to be pyridostigmine; thus, subject ratings were significantly better than chance ($p < .05$).

No evidence of adverse health effects were associated with participation, or found in daily vital sign data. Measures of subjective state and daily life and work activities also failed to distinguish between conditions.

Although few performance differences were observed, those differences that did occur were in particularly significant areas. Early effects were evaluated using day 2 data. Subjects performed significantly more poorly on the visual probability monitoring task under pyridostigmine (17.6 sec. vs. 13.9 sec., $p < .05$); no other effects were significant.

The effects of chronic intake were evaluated using day 4 and 5 test data. Performance under pyridostigmine improved significantly on tests of depth perception, visual contrast sensitivity at 3 c/d, and hand steadiness (see TABLE 2). However, under the drug a decrement was found on some aspects of dual task performance. For example, as FIGURE 1 indicates, when the Stroop and the Two-Digit Addition tasks were performed simultaneously, greater performance decrements in addition accuracy were found under the drug condition ($F=5.39$, $p=.03$). Similarly, as shown in FIGURE 2, when the visual tracking task was performed simultaneously with the Sternberg Memory Task, there was a strong trend for the memory task to be more disrupted under pyridostigmine than under placebo conditions ($F=3.15$, $p=.09$).

These data clearly point to the value of using the dual task strategy in studies of this type. Under single task conditions, no decrements in central processing functions were found. Under dual task conditions, performance on the primary tasks was maintained well under drug conditions, but secondary tasks showed decrements. This suggests that pyridostigmine may have a negative influence on the reserve capacity used by an individual when performing tasks requiring rapid attention sharing.

Regression analyses were performed to determine the performance consequences of individual differences in cholinesterase inhibition. As inhibition increased, performance on tests of visual acuity decreased. Differences in cholinesterase inhibition explained 32% of the variance in visual acuity ($p=.004$). In contrast, depth perception improved as inhibition increased; 21% of the variance was explained ($p=.02$). Finally, the analyses indicated that, the greater the inhibition, the greater the increase in oral temperature while ingesting pyridostigmine (24% of the variance was explained, $p=.02$).

D. DISCUSSION

The pyridostigmine regimen followed in this study was well tolerated by the healthy male participants; no apparent adverse health effects were observed, and no disruption of daily life or work activities was reported. However, the unexpected finding that subjects show large individual differences in plasma cholinesterase inhibition raises interesting questions about the biochemical efficacy of this particular regimen. The inhibition differences observed could be due to dietary influences, individual metabolic differences, or the route and type of drug administration used. This finding should be replicated and the underlying mechanisms investigated in future research.

Few performance decrements were observed; however, those that did occur were in areas of particular military importance, and included visual acuity, temperature regulation, and the ability to perform simultaneous tasks. Future research should be conducted to provide a more detailed evaluation of the effects of pyridostigmine on these specific performance parameters.

Care must be taken, however, in extrapolating from the significant laboratory results reported here to real-world military operations. On the one hand, given the large number of statistical tests performed, some of the findings may simply be due to chance. In contrast, strict reliance on statistical significance levels may serve to provide only a limited view of the effects of pyridostigmine. For example, if one-third of personnel have a 30% reduction in reserve capacity, and the rest are unaffected, the result is not likely to be statistically significant. The consequences for long-term military operations, however, could be considerable. In this context, it should be noted that performance decrement "trends" were observed in several additional tasks. These included: Target Identification (dual task); Stroop (dual task-% correct); Blinking Light Monitoring; and Grip Strength (interaction effect).

Finally, it is important to note that the data reported here were collected under the conditions of pressure, temperature and humidity typically found in indoor laboratory settings. Additional research should be conducted on the effects of pyridostigmine under selected environmental conditions of specific interest. This study was supported by USAF Contract No. F33615-80-C-0606.

TABLE 1

TASK BATTERY SUMMARY TABLE

<u>Variable</u>	<u>Assessment Method</u>
<u>Physiological Measures</u>	
Blood pressure	Auscultation
Oral Temperature	Oral Thermometer
Pulse Rate	Palpation
Cholinesterase	Dietz modification, Ellman procedure
Pyridostigmine	GC-Mass Spectrometer
<u>Visual Function</u>	
Spatial Resolution	Contrast Sensitivity Task
Neural Transit Time	Steady State VER Task
Visual Acuity	Snellen Eye Chart
Depth Perception	Biopter Test
<u>Psychomotor Function</u>	
Eye-Hand Coordination	Tracking Task (single axis)
Coordination	Two-Hand Coordinator Task
Precision	Stabilimeter Task
Speed	Simple Reaction Time Task
Strength	Grip Strength Task
Perceived Exertion	Exertion Scale Rating Task
<u>Central Processing</u>	
Internal Timing	Interval Production Task
Memory - Span	Digit Span Task
- Processing Time	Sternberg Memory Task (set sizes 3, 4, and 6)
Attention - Monitoring	3 Meter Monitoring Task
- Interference	Stroop Color/Word Task
- Perseveration	Reverse Tapping Task
Information Processing	
- Symbolic	Two Digit Addition Task
Decision Making	
- Integrated/complex	Baddely Grammatical Reasoning Task
- Choice	Forced Choice Reaction Time Task
<u>Simultaneous Central Processing</u>	
Eye-Hand Coordination with Memory Processing Time	Tracking Task (primary) with Sternberg Memory Task (set size 6) (secondary)
Attention with Information Processing (symbolic)	Stroop Color Task (primary) with Two Digit Addition Task (secondary)
Attention with Information Processing (spatial)	3 Meter Monitoring Task (primary) with Target Identification Task (secondary)
<u>Subjective Effects</u>	
Symptom Checklist	General Response Questionnaire
Fatigue	SAM Fatigue Scale
	MARI Fatigue Scale
Workload	SAM Workload Scale
	Subjective Workload Assessment Technique (SWAT)
Depression	Depression Adjective Check List (DACL)

TABLE 2

SUMMARY OF SIGNIFICANT EFFECTS **VISUAL AND PSYCHOMOTOR TASKS**

Variable	Mean Performance Score		F	p <
	Pyridostigmine	Placcbo		
Depth Perception — mm error	14.2	17.9	7.54	.05
Contrast Sensitivity Index at 3 cycles/degree	376.6	326.9	4.28	.05
Hand Steadiness seconds of error	Day 4 Day 5 Day 8	6.4 6.8 6.6	3.65	.05

TWO DIGIT ADDITION TASK
MAIN EFFECT for DRUG $F = 5.39$, $p = .03$

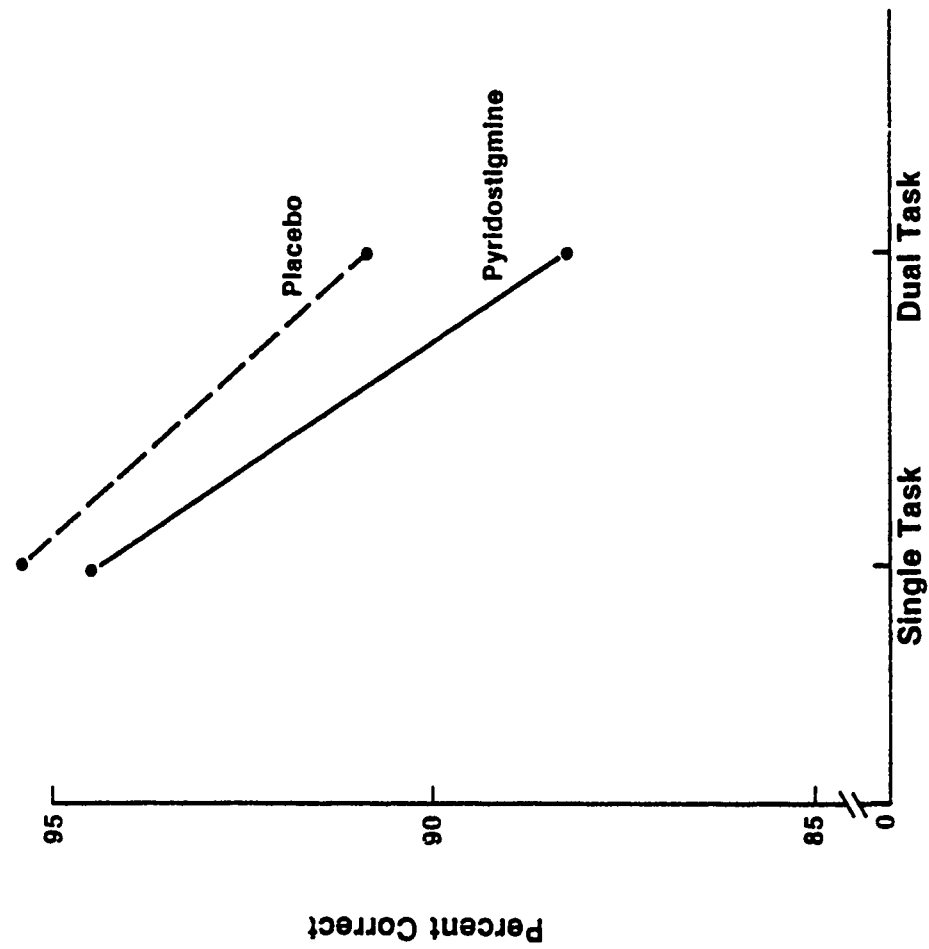


FIGURE 1

STERNBERG MEMORY TASK
DRUG by TASK INTERACTION, $F = 3.15$, $p = .09$

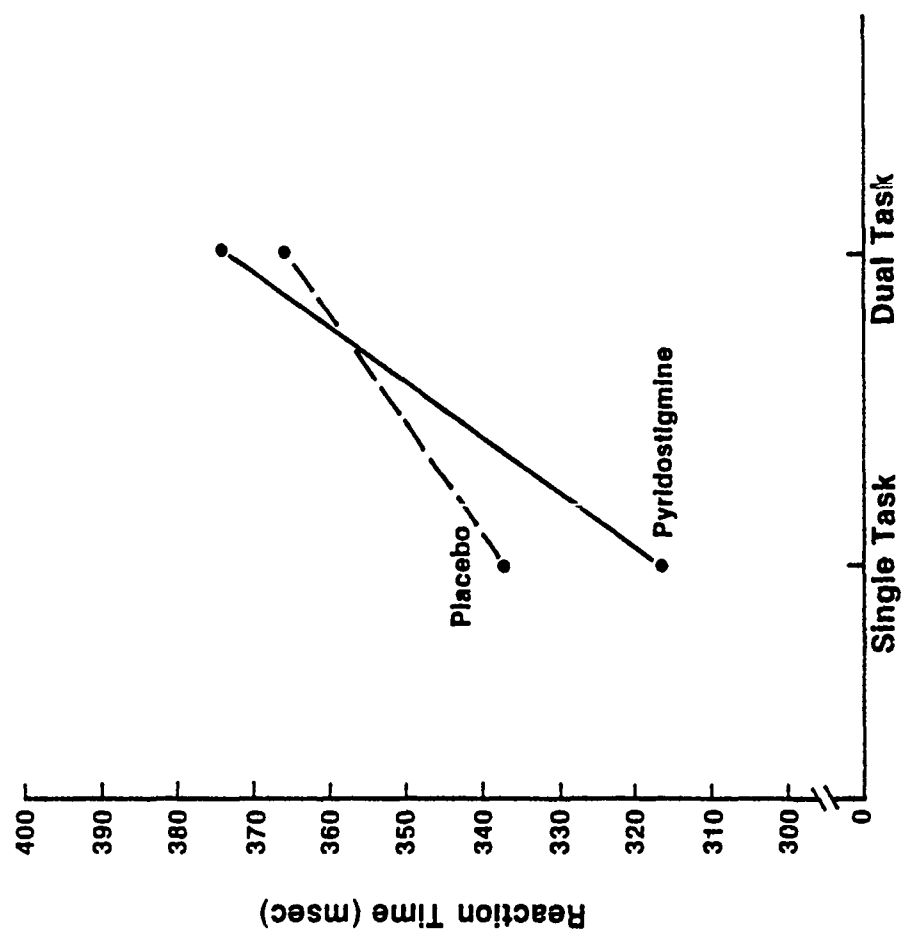


FIGURE 2

ULTRASTRUCTURAL PATHOLOGY IN MAMMALIAN SKELETAL MUSCLE FOLLOWING ACUTE
AND SUBACUTE EXPOSURE TO PYRIDOSTIGMINE.
STUDIES OF DOSE-RESPONSE AND RECOVERY

C. Sue Hudson¹ and Robert E. Foster²

¹ Department of Pharmacology and Experimental Therapeutics, University of
Maryland School of Medicine, Baltimore, MD 21201

and
² Neurotoxicology Branch, U.S. Army Medical Research Institute of Chemical
Defense, Aberdeen Proving Ground, MD 21010

ABSTRACT

Diaphragms from male albino, Charles River or Edgewood rats were assessed for morphological alterations following acute or subacute exposures to pyridostigmine bromide. Acute doses of pyridostigmine bromide in Mestinon[®]-equivalent buffer were administered by single subcutaneous injection in doses that ranged from 0.0036 to 3.6 mg/kg (0.001 - 1.0 LD50). Tissues were analyzed in the acute experiments 10 - 30 minutes, 24 hrs., and one week postinjection. Subacute exposures were administered by subcutaneously implanted Alzet[®] osmotic minipumps that contained either 3.0 or 20 mg pyridostigmine in Mestinon[®]-equivalent buffer. Tissues were analyzed after subacute exposures of 3, 7 or 14 days and with post-exposure recovery times of 7, 14, or 23 days. In select animals, whole blood cholinesterase activity was measured by radiometric assay. The morphological effects of the drug were localized predominantly at the neuromuscular junction (NMJ) with both pre- and postsynaptic regions involved. The data indicated that there was a variation in the extent of the damage between different muscle fibers and between different areas of an individual NMJ. With acute doses, there was a dose dependent response which was manifest in terms of the location of the pathology. Low doses (threshold ~ 0.001 LD50) seemed to affect the presynaptic area with no apparent effects on the muscle cell. At higher doses (0.01 - 1.0 LD50), both pre- and postsynaptic elements became involved. The subacute doses examined also created dose dependent lesions in the diaphragm. At 14 days, the 20 mg dose group exhibited pre- and postsynaptic alterations which were more extensive than those seen in the 3 mg group although no subacute dose created damage equivalent to that seen 30 minutes after a single LD50 dose. Presynaptic alterations included withdrawal of the terminal from the junctional folds, invasion of the synaptic cleft with Schwann cell processes, and disruption of axon terminal organelles. Postsynaptic alterations included subjunctional supercontraction, disruption of myofibrillar apparatus with the z-lines apparently being the most sensitive element, and disruption of subjunctional mitochondria. Ultrastructural recovery of the diaphragm after acute or subacute exposure to the drug varied. The evidence suggests that subacute exposure had the greatest effect within the first week of exposure with the damage being sustained for the duration of exposure but not increasing in severity. In contrast, diaphragms subjected to acute doses (e.g., 0.72 LD50) exhibited a progression in the degenerative process for at least one week post-exposure. Evidence of recovery from the drug-induced effects included reinnervation of junctional areas and the replacement or repair of subcellular elements. In conclusion, the data indicates a dose-dependent effect of pyridostigmine on muscle ultrastructure with subsequent recovery.

INTRODUCTION

In a variety of experimental animals, pyridostigmine has been shown to be an effective prophylactic against systemic exposure to irreversible cholinesterase inhibitors (e.g., Berry and Davies, 1970; Gordon et al., 1978; Dirnhuber et al., 1979). The clinical use of pyridostigmine in humans has been largely limited to patients with neuromuscular disorders, such as myasthenia gravis, or to patients under curariform neuromuscular blockade. While there is a dearth of clinical literature on the toxicology of pyridostigmine, it has been known for at least 17 years that acute and subacute intoxication with cholinesterase inhibitors (e.g., Preusser, 1967; Ariens, 1969; Engel et al., 1973; Fenichel et al., 1972, 1974; Laskowski and Dettbarn, 1975; Laskowski, et al., 1975; Wecker and Dettbarn, 1976; Wecker et al., 1979; Salpeter et al., 1979, 1982) including the tertiary carbamate physostigmine (Wecker et al., 1979) and the quaternary carbamate neostigmine (Engel and Santa, 1973; Kawabuchi et al., 1976; Ward et al., 1975; Hudson et al., 1978) cause myopathies and/or neuropathies and produce abnormal physiology at the mammalian neuromuscular junction (NMJ).

Previous morphological studies have placed major emphasis on the postsynaptic myopathic alterations which appear more severe than the alterations to the presynaptic apparatus. However, presynaptic changes have been demonstrated following acute, subacute, and/or chronic exposure to cholinesterase inhibitors. Morphologically, increased numbers of coated vesicles, swollen mitochondria (Laskowski, et al., 1975; Hudson et al., 1978), increased nerve terminal size (Engel et al., 1973) and reduced numbers of nerve terminal endings (Glazer et al., 1978) have been noted. The functional correlates of either the pre- or postsynaptic damage are not clear. Reports of abnormal miniature end-plate potential amplitude and frequency (Tiedt et al., 1978; Laskowski and Dettbarn, 1975) and antidromic activity of the motorneuron (Laskowski and Dettbarn, 1975) might be related, in part, to the drug-induced presynaptic alterations. The postsynaptic damage could be a contributing factor to the muscle weakness reported for pyridostigmine treated rats by Gillies and Allen (1977).

This study was undertaken to assess the potential neuro- and myotoxicity of pyridostigmine bromide. Acute (single injection) and subacute (up to 14 days) exposures to various doses of the drug were utilized to examine drug affects in dose-response and drug-recovery studies. Regions of phrenic nerve-neuromuscular junctions in rat diaphragm were analyzed for drug-induced structural alterations at the ultrastructural level. Preliminary results from these studies have been presented in abstract form (Foster and Hudson, 1983).

MATERIALS AND METHODS

Male albino rats (Edgewood or Charles River strains) weighing 180 to 250 gms received subcutaneous, acute and subacute exposures to pyridostigmine bromide. All acute exposures were by single syringe injections under the skin of the midback region and all subacute exposures (maximum 14 days) were via osmotic minipump (Alzet[®] 2ML2 minipump; ALZA Corp., Palo Alto, Ca.) implanted under the skin of the midback. Pyridostigmine bromide was administered in a Mestinox[®]-equivalent diluent composed of 1.30 mg/ml citric acid monohydrate, 4.10 mg/ml sodium citrate dihydrate, 0.50 mg/ml methyl paraben, 0.05 mg/ml propyl paraben and 7.40 mg/ml sodium chloride in sterile water at pH 5.1.

Acute Drug Exposure. Acute doses of pyridostigmine ranged from 0.0036 mg/kg to 3.6 mg/kg (1 LD50 subcutaneous injection = 3.6 mg/kg determined by Probit analysis). Animals in the acute control group received a single injection of the Mestionon®-equivalent diluent. A minimum of 3 experimental and 2 control animals were prepared for each dose level analyzed. For the acute dose-response studies, animals were sacrificed under deep barbiturate anesthesia by transcardiac vascular perfusion 10 - 30 minutes after the pyridostigmine injection. For the acute dose-recovery study, animals were perfused 24 hours or 7 days after the single pyridostigmine injection (other survival times are currently being examined).

Subacute Drug Exposure. Subacutely treated animals had 2 ml osmotic minipumps implanted subcutaneously to provide continuous infusion of pyridostigmine. The rationale for using continuous infusion of the drug rather than multiple acute doses (e.g., Hudson et al., 1978) hinges on our attempt to hold constant the cholinesterase (ChE) depression and the tissue concentration of the drug. Since pyridostigmine is a reversible inhibitor of ChE, maintaining a constant depression of ChE via subcutaneous injections would have required approximately 4 -10 injections per day for up to 14 days. Presumably, each injection would have produced a drastic decrease (enzyme carbamylation) then increase (enzyme decarbamylation) of ChE level with the attendant single-dose acute effects. It was also important to maintain a constant tissue concentration of the drug during long term exposure without the variables of metabolism inherent in a multiple injection paradigm. Use of osmotic minipumps allowed continuous release of the drug which presumably maintained both tissue-ChE and tissue-drug levels as constant as possible.

Subacute doses were studied using minipumps loaded with 1.5 or 10.0 mg/ml pyridostigmine bromide in the Mestionon®-equivalent buffer. Control animals were implanted with minipumps containing the Mestionon®-equivalent buffer. The morphological effects of chronic infusion of pyridostigmine were evaluated after periods of 2, 7 and 14 days exposure. Morphological recovery from a 14 day exposure was examined after 7, 14 and 23 days of withdrawal from the drug. A minimum of 3 experimental and 2 control animals were prepared and analyzed for each dose at each exposure and each recovery period. Since the Alzet® pumps utilized in this study released their contents at approximately 5.9 μ l/hr, the low dosage group animals (pumps containing 1.5 mg/ml pyridostigmine) were exposed to an approximate total of 0.43, 1.5 and 3.0 mg of drug on 2, 7 and 14 days respectively. Animals in the high dosage group (pumps containing 10 mg/ml pyridostigmine) had total exposures of 2.8, 10.0 and 20 mg of drug after 2, 7 and 14 days, respectively. Blood ChE levels of each drug-treated and control animal were analyzed (Siakotos et al., 1969, see below) periodically (at least twice) during the course of the experiment.

Preparation for Electron Microscopy. All animals were prepared by whole body perfusion through the left ventricle using an initial perfusate of oxygenated, rat Ringer's solution (millimolar concentrations were NaCl, 135.0; KCl, 5.0; MgCl₂, 1.0; CaCl₂, 2.0; NaHCO₃, 15.0; and Na₂HPO₄, 1.0) containing 10 units/ml of heparin followed by the fixation perfusate containing 2.5% glutaraldehyde in 0.1M sodium cacodylate buffer (pH 7.4). The perfusates were maintained at room temperature. The diaphragm of each animal was immediately removed and fixed for an additional hour in cold 2.5% glutaraldehyde. NMJs were identified by staining for ChE in a solution of 5 mg acetylthiocholine iodide, 6.5 ml 0.1M sodium cacodylate buffer (pH 7.4) with 0.2 M sucrose,

0.5 ml 0.1M sodium citrate, 1.0 ml 30 mM copper sulfate and 1.0 ml ddH₂O (modified from Karnovsky and Roots, 1964). End-plate regions and tissue remote from the end-plates were removed by careful dissection, postfixed in 1% OsO₄, stained en bloc in aqueous uranyl acetate or 2% uranyl acetate in 70% ethyl alcohol, embedded in an Epon-Araldite mixture (10% Polybed 812, 20% Araldite 6005, 70% dodecenyl succinic anhydride with 1.5% DMP-30) and polymerized at 70°C for 24 hours. Ultrathin sections were cut with a diamond knife using an LKB III or IV ultramicrotome, poststained with lead citrate (Venable and Coggeshall, 1965) and aqueous or methanolic uranyl acetate and examined with a JEOL 100 B or 100 CX electron microscope.

Cholinesterase Assay. The radiometric method of Siakotos et al. (1969) using ¹⁴C-acetylcholine as the ChE substrate was utilized throughout. The relative ChE depression in whole blood (i.e., percent carbamylation of the enzyme) produced by acute or subacute exposure to pyridostigmine was determined. Blood (100 µl) was drawn from the tail into heparinized capillary tubes and processed for an immediate assay or frozen in liquid nitrogen for subsequent assay. In order to test for the effects of freezing whole blood on the assay results, the 100 µl of blood was divided into two 50 µl aliquots, one used for immediate assay and the other frozen for later assay. Freezing prior to assay resulted in a variation of approximately 5% of the ChE depression established by immediate assay. This was within an acceptable range for the purposes of the present studies.

Since it was not practical to gather the ChE values for all of the acutely treated animals, a parallel study (using a group of rats not utilized in the morphological study) established a dose-response curve of enzyme carbamylation at the time point of 30 minutes post-injection (single subcutaneous). The dose range utilized in this determination was 0.005 - 3.2 mg/kg. A minimum of three drug treated and one control animal was used for the determination of total whole blood ChE depression at each dose.

For the animals which were in the subacute exposure groups, ChE levels were assayed before and periodically after the implantation of the osmotic minipump. The assay was performed on these animals (a) to confirm that each minipump was releasing the drug and (b) to establish the general dose/ChE depression relationship for each dose and each animal.

RESULTS

GENERAL OBSERVATIONS

Considerable individual variation was observed in the behavioral response of rats during the 30 minutes following a single injection of 3.2 or 3.6 mg/kg (0.9 or 1.0 LD₅₀) pyridostigmine. Initially, all animals exhibited increased oral and ocular secretions simultaneous with rapid fasciculations and tremor of superficial muscle groups. An increased sensitivity to sounds (startle to hands claps) was also noted. As intoxication progressed, some animals displayed no additional behavioral responses (usually the survivors). Other animals (usually those which died before 30 minutes post-injection) exhibited whole body piloerection, periods of ballistic kicking movements of the fore- and hindlimbs, continued gross muscle fasciculations, tremor and breathing difficulties.

Animals which received 2.6 mg/kg (0.72 LD₅₀) pyridostigmine generally displayed fewer and less intense reactions although several animals did not

survive 30 minutes. No deaths resulted from any of the lower acute doses. Rats given single injections of 0.36 mg/kg (0.1 LD50) pyridostigmine or less and those injected with diluent (control group) displayed no outward signs of anticholinesterase intoxication.

Similarly animals implanted with the osmotic pumps containing 20 mg or 3 mg of pyridostigmine or diluent exhibited no obvious behavioral signs of pyridostigmine intoxication over a 14 day period of observation with the exception of four animals. These 4 of the 24 animals that received high dose Alzet[®] pumps exhibited increased ocular secretions (chromodacryorrhea) within the initial several hours of pyridostigmine exposure, but displayed no other typical sign of anticholinesterase intoxication. The chromodacryorrhea cleared within the first 24 hours and did not reappear. These animals as well as the rest of the experimental animals remained symptom free for the duration of the experiment.

Since irreversible ChE inhibitors have been reported to effect weight gain in rats under subacute exposure conditions, the question arose as to the effect of a reversible inhibitor on weight gain. All rats in the 7 and 14 day subacute exposure groups were weighed at least three and six times, respectively, during the drug exposure period. No consistent effect of drug exposure on weight gain was detected.

WHOLE BLOOD ChE LEVELS

Acute Exposures to Pyridostigmine. Animals were exposed to various doses of pyridostigmine to determine the average inhibition (enzyme carbamylation) of whole blood ChE activity after 30 minutes exposure. The data plotted as the percent of ChE activity inhibited vs. log dose resulted in a S-shaped curve with a steep log-linear midregion between doses of 0.01 mg/kg ($22 \pm 1.9\%$ inhibition) and 1.0 mg/kg ($71 \pm 1.0\%$ inhibition). With regard to the doses used in the present study, the following whole blood ChE depression (inhibition) values were determined: 0.0036 mg/kg (0.001 LD50) - 10% depression; 0.036 mg/kg (0.01 LD50) - 25% depression; 0.36 mg/kg (0.1 LD50) - 55% depression; 2.6 mg/kg (0.72 LD50) - 70% depression; 3.24 mg/kg (0.9 LD50) - 78% depression; and, 3.6 mg/kg (1.0 LD50) - 80% depression.

Subacute Exposures to Pyridostigmine. The whole blood ChE levels of subacutely treated animals were also monitored. At the low and high ends of the dosage spectrum, animals exposed to 1.5 mg/ml pyridostigmine were maintained at an average ChE depression of $23.4 \pm 4.0\%$ while rats in the 10 mg/ml group had a much larger, $65.9 \pm 3.5\%$ depression of ChE. An observation worth noting is that ChE activity levels in some of the low dose animals began returning toward control values by day 14 of exposure. Whether this result indicates osmotic pump failure or development of drug tolerance is unresolved. However, those low dose subacute animals which demonstrated this phenomenon have been excluded from our description.

ULTRASTRUCTURAL OBSERVATIONS

Neuromuscular Junction Morphology of Control Animals. Animals which[®] received a single injection of diluent, or which were implanted with Alzet pumps containing diluent, served as controls for the acute and subacute experimental groups. Ultrastructural morphology of NMJs from rats treated by the two methods appeared similar (figs. 1 & 2). Nerve terminal plasma membranes were separated from the crests of the postsynaptic junctional folds by a 50 nm wide primary cleft with basement membrane evenly interposed

between the pre- and postsynaptic elements. The nerve terminals contained various numbers of mitochondria, numerous clear synaptic vesicles, a few coated vesicles and occasional smooth endoplasmic reticulum cisternae and coated pits. In fortuitous sections, nerve terminals could be observed in continuity with the innervating myelinated nerve (fig. 1). The nerve terminals were overlain by Schwann cells with processes that extended to the margins of the primary cleft but not into the cleft (see arrowhead, fig. 1 & 2). Thus, the NMJs of the control animals presented no sign of any untoward effect of the Mestinon[®]-equivalent buffer alone.

Presynaptic Effects of Acute Exposure to Pyridostigmine. All acute doses employed resulted in morphological alterations ranging from slight to pronounced in all of the diaphragmatic NMJs analyzed. Nonetheless, it is important to keep in mind that 1) different NMJs from the same animal were affected to different degrees and 2) that different presynaptic areas within the same NMJ frequently were affected to varying extent (figs. 4 & 5). In general, alterations were observed in mitochondria, vesicles or in the spatial relationship of the nerve terminal both to its overlying Schwann cell and to the junctional folds of the innervated muscle cell.

Changes in presynaptic organelle ultrastructure were dose-dependent. Nerve terminals exposed to the lowest acute doses (0.0036 and 0.036 mg/kg) possessed mitochondria with small rarefied areas (figs. 3 & 4) in the matrix. At higher doses, mitochondrial alterations varied from small rarefactions in the matrix (fig. 5) to complete disruption of the cristae or absence of the matrix altogether (fig. 6). The latter, more extreme and probably irreversible alterations were not always observed in terminals even at the highest doses (3.6 mg/kg; fig. 8). Vesicles two or more times the average diameter of synaptic vesicles were present, as were occasional vesicles with denser than normal contents (figs. 4, 5 & 6). Whether these large vesicles represent abnormal synaptic vesicles or originate from another source is unresolved.

The shape and spatial geometry of nerve terminals were also altered following pyridostigmine exposures. In all experimental groups, all NMJs sampled possessed at least small areas of terminal membrane which were no longer closely apposed to the basement membrane. In these regions, the width of the primary cleft was highly variable and frequently exceeded twice the cleft width observed in control preparations. Within the primary synaptic clefts, finger-like processes (apparently from the Schwann cells) were commonly seen separating areas of the nerve terminal from postsynaptic folds (figs. 3, 5 & 6). The Schwann cell overlying the nerve terminal remained in close apposition to the nonsynaptic terminal membrane surface (figs. 3, 4, 6 - 8) but sometimes invaded the nerve terminal with processes (figs. 4, 7 & 8). Figure 8 illustrates how some invading Schwann processes interdigitate with and sequester portions of the nerve terminal. Profiles of both Schwann cell and nerve terminal projections appeared finger-like in longitudinal section (figs. 4 & 8). In cross section, the nerve terminal projections appeared as separate vesicle-containing, membrane bound structures within the nerve terminal or within Schwann cell processes (figs. 4 & 7). No evidence indicated that the nerve terminal projections were physically separated from the body of the nerve terminal.

Presynaptic effects of Subacute Exposure to Pyridostigmine. Neuro-muscular junctions of animals implanted with Alzet[®] pumps containing 1.5 mg/ml

or 10 mg/ml pyridostigmine were assessed for damage 2, 7 and 14 days following implantation of the pumps. Both dose levels induced alterations at all time intervals analyzed. However, the extent of the damage varied with the duration of exposure. In general, the alterations from subacute dosages (figs. 9 - 12) were qualitatively similar to the observations in acutely treated rats (figs. 3 - 8), i.e., nerve terminal organelles were altered and the spatial geometry of the NMJ was affected. Reminiscent of acute exposures, the extent of nerve terminal damage (figs. 9 - 12) from any subacute exposure varied within a single muscle and varied within individual NMJs.

Figures 9 - 12 illustrate organelle alterations which resulted from subacute pyridostigmine exposure. Several presynaptic mitochondria possessed rarefied areas in their matrices and nerve terminal vesicles exhibited an unusual range of diameters. The organelle alterations following subacute exposure never progressed to the degree of severity observed following acute exposures. Complete disruption of mitochondria was not observed and the numbers of abnormal vesicles were lower.

Alteration of the spatial relationship of the nerve terminal and muscle cell was the most obvious effect of subacute drug exposure. The most subtle, observable changes occurred following a low dose exposure to pyridostigmine for 2 days. This treatment resulted in regional separation of the nerve terminal from the junctional fold crests (fig. 9 & 10). This phenomenon was present in every NMJ analyzed following 2 or more days of low or high dose exposure. In some NMJs, processes of overlying Schwann cells were interposed between the nerve terminal and the junctional fold crests (fig. 10 & 11) which also resulted in separation of presynaptic transmitting surface from the postsynaptic receptor-containing junctional fold crests. Following 7 and 14 days of subacute exposure, similar alterations were observed. Although quantitation of the severity of changes between low and high dose exposures was not performed, animals exposed to the higher dose of pyridostigmine appeared to possess more obvious and extensive alterations. In general, longer exposure resulted in continued invasion of primary synaptic clefts by Schwann cells (fig. 11), regional withdrawal of some nerve terminal membranes (fig. 12), and complete absence (withdrawal) of some nerve terminal portions as evidenced by vacant positions adjacent to postsynaptic folds (fig. 11). Membrane fragments near the crests of folds indicated degeneration of the missing segments of nerve terminal. Finally, NMJs with many terminal branches that appeared morphologically similar to those from control preparations sometimes possessed a single branch that exhibited drug-induced alterations (fig. 11).

Postsynaptic Effects of Acute and Subacute Exposure to Pyridostigmine.

At low acute doses (0.0036 and 0.036 mg/kg) minimal alteration of postsynaptic organelles and myofibrils was detected (figs. 13 - 15). Occasional fibers possessed some swollen mitochondria and sarcoplasmic reticulum elements (fig. 13). No other changes were observed. All higher acute doses consistently produced subjunctional damage in all fibers analyzed. Following an acute injection of 0.36 mg/kg, mitochondria displayed alterations ranging from matrix rarefactions to matrix dissolution (figs. 16 & 17). Subjunctional endoplasmic reticulum and nuclei were also affected. These organelles displayed swelling of cisternae and the paranuclear space, respectively (fig. 17). At this dose, sarcomeres often lacked distinct striation patterns and the z-lines frequently lacked typical uniformity (fig. 16). These abnormalities were pronounced in the immediate subjunctional region but

decreased in severity and finally disappeared with increasing distance from the NMJ.

Acute doses of 2.6 mg/kg or greater resulted in dramatic changes in end-plate morphology of many fibers. The most severe postsynaptic damage included complete disruption of mitochondria and other membranous organelles and extreme supercontraction of the sarcomeres (fig. 18). In cases of extreme supercontraction, synaptic components were pushed out of the normal muscle contour, z-line morphology was obliterated and the organized orientation of thick and thin filaments was lost (figs. 18 & 19). These changes to sarcomere structure, as well as those to membranous organelles, were graded with distance from the junction. At the margins of the muscle cell damage, disrupted myofibrillar components blended into normal sarcomeres (fig. 19).

In comparison, even high dose subacute exposure to the drug produced less severe postsynaptic changes. Swelling of subjunctional membranous organelles was minimal when present (fig. 20), but was generally absent even following exposure to 20 mg of pyridostigmine over a 14 day period (fig. 21). Disruption of myofibrillar components was observed in a few fibers (fig. 20). When present, the sarcomere damage was limited to a small subjunctional region (fig. 20) or to small, randomly restricted regions of non-subjunctional sarcomeres in contrast to the extensive areas affected by high acute doses. Although myofibrillar disruption by subacute dosage was not widespread or frequent, drug effects on sarcomere length were still obvious (fig. 21). Subjunctional sarcomeres were often shorter in length (arrowheads, fig. 21) than sarcomeres in control muscles or sarcomeres distal to the affected NMJ (fig. 21, lower right) or sarcomeres from adjacent muscle fibers (fig. 21, left). Thus, even fibers which appeared minimally altered revealed some pyridostigmine-induced effects, with the most notable changes being localized to the immediate subjunctional region.

Recovery from Acute and Subacute Pyridostigmine Exposure. A limited number of NMJs at two recovery intervals have been analyzed in a preliminary assessment of the recovery of pre- and postsynaptic NMJ components following acute and subacute drug exposures. Seven days following a single injection of 2.6 mg/kg pyridostigmine, NMJ morphology was variable. Some NMJs demonstrated degenerative phenomena (fig. 22) not observed in tissues gathered 30 minutes after a single injection. Specifically, abundant debris was present in the primary and secondary synaptic clefts which indicated degeneration of junctional folds and/or presynaptic elements (fig. 22). In addition, profuse Schwann cell processes were present and some nerve terminal portions were widely separated from the junctional folds. Pre- and postsynaptic membranous organelles appear minimally affected. In contrast, other NMJs subjected to identical exposures reflected minimal damage to postsynaptic myofibrillar components and minimally altered pre- and postsynaptic spatial relationships.

Seven days of recovery from a 14 day subacute exposure to 20 mg of pyridostigmine revealed NMJs with no additional and many fewer residual drug effects than acute dosing. NMJs recovering from subacute exposure had few abnormal pre- or postsynaptic membranous organelles (figs. 24 & 25). However, Schwann cell processes remained abundant between some nerve terminal branches and remained in the primary synaptic clefts of some NMJs (fig. 25). Other NMJs and portions of NMJs were free of structural alterations in the synaptic region (figs. 24 & 25).

Twenty three days of recovery from a 14 day subacute exposure to 20 mg of pyridostigmine revealed only a few NMJs with a structural abnormality (fig.

27) and many with no apparent residual affects of the drug (fig. 26). The pre- and postsynaptic cellular compartments of all NMJs analyzed were normal in appearance. Only in the spatial relationship of the pre- and postsynaptic elements were residual drug affects noted. Thus even with 23 days recovery, some NMJs retained Schwann cell processes in the primary synaptic cleft (fig. 27). Results from other recovery intervals after either acute or subacute drug are being analyzed.

DISCUSSION

Administration of pyridostigmine, in quantities capable of producing a short- or long-term whole blood ChE depressions of approximately 10% or more resulted in morphological alterations to rat diaphragm NMJs. Both low and high doses of acute and subacute exposure induced changes in NMJ organelle ultrastructure and/or alterations in the spatial relationships of the presynaptic nerve terminal to the overlying Schwann cell and to the postsynaptic folds. It was clear that the severity of both types of ultrastructural modifications were dose dependent within a given experimental regimen (i.e., acute exposure via injection or subacute exposure via osmotic pump). Comparison of NMJ morphology following injections of 0.0036 mg/kg pyridostigmine (~10% ChE depression; figs. 3,16,17) and 2.6 mg/kg pyridostigmine (~70% ChE depression; figs. 6,18,19) revealed greater damage following the larger acute dose. Similarly, comparison of low and high subacute doses of drug revealed less extensive alterations following exposure to 1.5 mg/ml pyridostigmine (~25% ChE depression; figs. 9,10) than exposure to 10 mg/kg of drug (~65% ChE depression; figs. 11,12,20,21).

Similar ChE depressions produced at low doses by different methods of administration (i.e., acute injection versus subacute infusion) resulted in alterations of the same type. An acute injection of 0.036 mg/kg and subacute exposure of 1.5 mg/ml both produced ChE depressions of approximately 25% with correspondingly similar ultrastructural modifications (compare acute effects-figs. 4, 14, 15 to subacute effects-figs. 9 & 10). In contrast, high acute doses had a greater impact on pre- and postsynaptic membranous organelles while high subacute exposures resulted in more prominent alterations to presynaptic geometry. For example, comparison of NMJs exposed to an acute dose of 2.6 mg/kg (figs 6, 18, 19) and a subacute dose of 10 mg/ml (0.4 LD50/day; figs. 11, 12, 20, 21) revealed more striking damage to pre- and postsynaptic organelles and myofibrillar apparatus following the acute exposure. On the other hand, changes in the geometric relationships of the nerve terminals with the adjacent Schwann and muscle cells were more notable after 7 or 14 days of subacute exposure to pyridostigmine or 7 days following the single acute exposure (fig. 22).

These observed differences in pathology resulting from acute or subacute dosing require us to consider what intrinsic differences in drug dosage regimen would be responsible since the resultant ChE depressions are similar. Inherent in the two modes of drug administration (i.e., single injection and osmotic minipump) are markedly different times to maximum enzyme carbamylation. Acute drug injection results in abrupt ChE inhibition which is maximum during the first 30 minutes following injection (L. Harris, personal communication). This is followed by normal decarbamylation of the enzyme during the period of recovery of ChE levels. In contrast, subacute exposure by minipump results in slow release of drug (5.9 μ l/hr) and consequent slow

rate of ChE carbamylation. Maximum depression occurs only after several hours with sustained depression for up to 14 days. Therefore, the severity of organelle damage following acute ChE depression may be related to the rate of ChE inhibition and attendant rapid physiological responses, rather than the level of ChE depression.

With regard to organelle damage, the most notable change was expressed in the mitochondria as a rarefaction or disruption of the matrix. In addition, presynaptic vesicle profiles of unusual diameters and densities were present. These abnormalities could reflect an unusual level of mitochondrial activity and/or an irregularity in the membrane recycling/vesicle formation system. An alternative cause could be related to swelling due to shifts in ion concentrations. Such ionic imbalances could be influenced by direct action of the drug on the presynaptic membrane, or by unusually high levels of acetylcholine (ACh) in the primary cleft. Either condition could presumably alter presynaptic structure and function. A definitive answer can not be formulated from these data. However, it is important to note that other studies have shown that some anticholinesterase agents can alter function by inducing presynaptic activation (Laskowski and Dettbarn, 1975).

Dramatic changes in geometric relationships of the cells, such as elimination of nerve terminal branches, apparently require more than 30 minutes to be accomplished. Thus, extensive changes of this nature were observed only after 7-14 days of subacute exposure to pyridostigmine or after several days following an acute exposure (fig. 22). Indeed, analysis of acutely treated animals in an extended time frame (7-14 days postinjection, i.e., recovery) also reflected extensive alterations in cellular geometric relationships (fig. 22). This observation supports the suggestion that the severity of altered spatial relationships may be a function of time.

For purposes of discussion, several possible reasons for the two types of drug-induced morphological presynaptic alterations (i.e., organelle versus spatial relationship) can be proposed. An initial possibility is that pyridostigmine may have direct chemical actions on the terminal membranes. We cannot presently contribute to the discussion of this idea. A second possibility is that pyridostigmine generates terminal activation and antidromic axonal firing akin to the effects of paraoxon (Laskowski and Dettbarn, 1975). This drug action has been reported for other ChE inhibitors. In a study of the effects of ChE inhibition on the mammalian NMJ, paraoxon induced presynaptic activation which was demonstrable with physiological and morphological techniques. Paraoxon-induced presynaptic effects are manifest electrophysiologically as antidromic activation and increased miniature end-plate potential frequencies and amplitudes (Laskowski and Dettbarn, 1975). Morphologically the effects of paraoxon are demonstrated by decreased numbers of synaptic vesicles and increased amounts of clathrin coat material as well as increased numbers of coated pits, coated vesicles and elongated cisternae (Laskowski et al., 1975). Since, in the present study only occasional NMJs exhibited characteristics associated with nerve hyperactivity, no substantive morphological evidence suggests presynaptic activation by pyridostigmine. Since both paraoxon and pyridostigmine inhibit junctional ChE, the differences in their presynaptic action at the morphological level is unresolved.

As a third possibility, nerve terminals may withdraw as a result of attempted neuronal autoregulation of agonist levels, which is followed by appropriate Schwann cell reaction. It is obvious that carbamylation of acetylcholinesterase (AChE) by pyridostigmine can create levels of acetylcholine in the cleft of the NMJ which are greater than normal and

possibly greater than that which can be induced by high frequency nerve stimulation. The question arises, does the nerve terminal autoregulate the levels of junctional agonist by altering normal junctional morphology? Clearly, prolonged nerve stimulation produces little alteration of the normal nerve-muscle cell contact region (Heuser and Reese, 1973). However, junctional ACh levels in stimulation experiments might not be as high as those resulting from AChE inhibition. While it is beyond the scope of the present observations, the hypothesis of autoregulation can be tested morphologically by utilizing nerve-muscle preparations exposed to high levels of ACh with and without AChE inhibition.

A fourth idea concerning presynaptic alteration deals with the possible loss of trophic relations (Brimijoin, 1983; Guth, 1968; Massoulié and Bon, 1982) between junctional AChE and the nerve terminal; i.e., normal levels of junctional AChE may be required to maintain the normal cell-to-cell contact. Perturbation of the trophic relationship would be followed by nerve terminal withdrawal coincident with or followed by a reaction of the Schwann cell. A corollary to this fourth idea is that the Schwann cell initiates the alteration due to its reaction to inhibition of the AChE inserted in the junctional basal lamina, a structure which the Schwann cell shares with the muscle cell. An argument against this notion is the observation that there are regions of normal nerve terminal apposition and regions of terminal withdrawal devoid of intervening Schwann cell fingers.

To complete the discussion of possible reasons for pyridostigmine-induced neuromuscular pathology, the postsynaptic effects need to be considered. Since all ChE inhibitors studied to date can cause myopathy, commonality in the etiology of the pathology may be inferred. Indeed, Salpeter and co-workers (1982) have proposed an attractive hypothesis for the cause of ChE inhibitor-induced myopathies. They argue that the myopathy may be an agonist-induced phenomenon. Thus, excess agonist (ACh) caused by enzyme (AChE) inhibition causes calcium ion imbalances in the subjunctional muscle cell which in turn trigger calcium-activated proteases. These proteases, then, would be responsible for the disruption of the z-lines and myofibrils that is typical of the drug-induced myopathy. While there is evidence to support the Salpeter hypothesis, the experimental evidence is indirect and not altogether compelling. Studies have been initiated to examine calcium ion distribution in NMJs from pyridostigmine treated animals utilizing electron probe analysis.

As is the nature of ultrastructural analyses, we can not approximate the percentage of muscle fibers in the diaphragm that were affected. However, all acute and subacute doses employed induced alterations in every NMJ analyzed. This suggests that the neuro- and myopathies were common under the drug conditions studied. On the other hand, a consistent feature of the damage was the variation in severity which was present within a NMJ and between NMJs from a single muscle. This is not a unique phenomenon since such variation is commonly observed in mammalian NMJs affected by myasthenia gravis (Engel and Santa, 1973), interrupted axoplasmic transport (Hudson et al., 1984), or NMJs undergoing normal synaptic turnover (Cotman et al., 1981; Mark, 1980). Assuming that sampling bias caused by electron microscopic examination of only a small portion (several thin sections) of each NMJ from a limited number of fibers is not the reason for the observed variability, the mechanism underlying variable effects could be attributed to a number of factors including localized differences in drug concentration, differences in the distribution of AChE, differences in the innervating axon, and/or differences in muscle fiber type. While variability in the drug-induced effects exists,

at every dose, under both drug administration conditions, the overall effect was that the percentage of nerve terminal contact with junctional folds decreases.

While the precise reason underlying the variation in structural modification is not within the realm of this study, the presence of the variable morphological alteration is of great importance if one attempts to predict the pathophysiological effects of pyridostigmine in relation to dose and duration of exposure. It is not altogether clear that the morphological effects of pyridostigmine could or should be manifest in results from standard electrophysiological studies (e.g., Tiedt et al., 1978) of drug treated muscles or muscle fibers. Since Gillies and Allen (1977) have reported pyridostigmine-induced muscle weakness in behaving rats, it is tempting to predict that the structural effects of the drug would be most apparent in exercising animals or in muscles from physically stressed subjects. This prediction is being tested in other laboratories and the results will be of significant military interest.

REFERENCES

- Ariens, A.T., E. Meeter, O.L. Wolthuis, and R.M.J. VanBenthem. 1969. Reversible necrosis at the end-plate region in striated muscles of the rat poisoned with cholinesterase inhibitors. *Experientia*. 25:57-59.
- Berry, W.K. and D.R. Davies. 1970. The use of carbamates and atropine in the protection of animals against poisoning by 1,2,2-trimethylpropyl methylphosphonofluoridate. *Biochem. Pharmac.* 19:927-934.
- Brimijoin, S. 1983. Molecular forms of acetylcholinesterase in brain, nerve and muscle: Nature, localization and dynamics. *Prog. Neurobiol.* 21:291-322.
- Cotman, C.W., M. Nieto-Sampedro and E.W. Harris. 1981. Synapse replacement in the nervous system of adult vertebrates. *Physiol. Rev.* 61:684-784.
- Dirnhuber, P., M.C. French, D.M. Green, L. Leadbeater and J.A. Stratton. 1979. The protection of primates against soman poisoning by pretreatment with pyridostigmine. *J. Pharm. Pharmacol.* 31:295-299.
- Engel, A.G., E.H. Lambert and T. Santa. 1973. Study of the long-term anticholinesterase therapy: Effects on neuromuscular transmission and on motor and end-plate fine structure. *Neurology* 23:1273-1281.
- Engel, A.G. and T. Santa. 1973. Motor end-plate fine structure: Quantitative analysis in disorders of neuromuscular transmission and prostigmine-induced alterations. In: Developments in Electromyography and Clinical Neurophysiology, ed. J.E. Desmedt. 1:196-228. S. Karger, Basel.
- Fenichel, G.M., W.D. Dettbarn and T.M. Newman. 1974. An experimental myopathy secondary to excessive acetylcholine release. *Neurology* 24:41-45.

- Fenichel, G.M., W.B. Kibler, W.H. Olson and W.D. Dettbarn. 1972. Chronic inhibition of cholinesterase as a cause of myopathy. *Neurology* 22:1026-1033.
- Foster, R.E. and C.S. Hudson. 1983. The effect of pyridostigmine bromide on the morphology of the rat diaphragm. *J. Cell Biol.* 97:237a.
- Gillies, J.D. and J. Allen. 1977. Effects of neostigmine and pyridostigmine at the neuromuscular junction. *Clin. Exp. Neurol.* 14:271-279.
- Glazer, E.J., T. Baker and W.F. Riker, Jr. 1978. The neuropathology of DFP at cat soleus neuromuscular junction. *J. Neurocytology.* 7:741-758.
- Gordon, J.J., L. Leadbeater and M.P. Maidment. 1978 The protection of animals against organophosphate poisoning by pretreatment with a carbamate. *Toxicol. Appl. Pharmacol.* 43:207-216.
- Guth, L. 1968 "Trophic" influences of nerve on muscle. *Physiol. Rev.* 48:645-687.
- Heuser, J.E. and T.S. Reese. 1973. Evidence for recycling of synaptic vesicle membrane during the transmitter release at the frog neuromuscular junction. *J. Cell Biol.* 57:315-344.
- Hudson, C.S., S.S. Deshpande and E.X. Albuquerque. 1984. Consequences of axonal transport blockade by batrachotoxin on mammalian neuromuscular junction. III. An ultrastructural study. *Brain Res.* 296:319-332.
- Hudson, C.S., J.E. Rash, T.N. Tiedt and E.X. Albuquerque. 1978. Neostigmine-induced alterations at the mammalian neuromuscular junction. II. Ultrastructure. *J. Pharmacol. Exp. Ther.* 205:340-356.
- Karnovsky, M.J. and L. Roots. 1964. A direct coloring thiocholine method for cholinesterases. *J. Histochem. Cytochem.* 12:219-221.
- Kawabuchi, M., M. Osame, S. Watanabe, A. Igata and T. Kanaseki. 1976. Myopathic changes at the end-plate region induced by neostigmine methylsulfate. *Experientia (Basel)* 32:623-625.
- Laskowski, M.B. and W-D. Dettbarn. 1975. Presynaptic effects of neuromuscular cholinesterase inhibition. *J. Pharmacol. Exp. Ther.* 194:351-361.
- Laskowski, M.B., W.H. Olson and W-D. Dettbarn. 1975. Ultrastructural changes at the motor end-plate produced by an irreversible cholinesterase inhibitor. *Experimental Neurol.* 47:290-306.
- Mark, R.F. 1980. Synaptic repression at neuromuscular junctions. *Physiol. Rev.* 60:355-395.
- Massoulie, J. and S. Bon. 1982. The molecular forms of cholinesterase and acetylcholinesterase in vertebrates. *Ann. Rev. Neurosci.* 5:57-106.

- Preusser, H. 1967. Ultrastruktur der Motorischen Endplatte in Zwerchfell der Ratte und Veränderungen nach Inhibierung der Acetylcholinesterase. Z. Zellforsch. 80:436-457.
- Salpeter, M.M., H. Kasprzak, H. Feng and H. Fertuck. 1979. End-plates after esterase inactivation in vivo: correlation between esterase concentration, functional response and fine structure. J. Neurocytol. 8:95-115.
- Salpeter, M.M., J.P. Leonard and H. Kasprzak. 1982. Agonist-induced postsynaptic myopathy. Neurosci. Commentaries. 1:73-83.
- Siakotos, A.N., Filbert, M. and Hester, R. 1969. A specific radioisotopic assay for acetylcholinesterase and pseudocholinesterase in brain and plasma. Biochem. Med. 3:1-12, 1969.
- Tiedt, T.N., E.X. Albuquerque, C.S. Hudson, and J.E. Rash. 1978. Neostigmine-induced alterations at the mammalian neuromuscular junction. I. Muscle contraction and electrophysiology. J. Pharmacol. Exp. Ther. 205:326-339.
- Venable, J.H. and Coggeshall, R.A. 1965. A simplified lead citrate stain for use in electron microscopy. J. Cell Biol. 25:407-408.
- Ward, M.D., M.S. Forbes and T.R. Johns 1975. Neostigmine methylsulfate: Does it have a chronic effect as well as a transient one? Arch. Neurol. 32:808-814.
- Wecker, L. and W-D. Dettbarn. 1976. Paraoxon induced myopathy: muscle specificity and acetylcholine involvement. Exp. Neurol. 51:281-291.
- Wecker, L., T. Kiauta and W-D. Dettbarn. 1979. Relationship between acetylcholinesterase inhibition and the development of a myopathy. J. Pharmacol. Exp. Ther. 206:97-104.

ACKNOWLEDGMENTS:

Supported in part by Contract #DAMD 17-83-C-3126 (CSH) from the U.S. Army Medical Research and Development Command and by USAMRICD Protocol #1-05-2-03-A-073 (REF). We gratefully acknowledge the technical assistance of Susan K. Cameron, Karen Olson and M.A. Khang, and the photographic expertise of Eric Hudson and Perry Comegys.

FIGURES

Figure 1. Preterminal myelinated axon and neuromuscular junction from an acute control rat diaphragm. This electron micrograph illustrates the relationship between an innervating myelinated axon (ax) and the junctional folds (jf) of a muscle cell from an animal injected with Mestimon[®]-equivalent buffer 30 minutes prior to fixation. The myelin sheath ends with typical paranodal loops (pn) bounding the terminal heminode. The nerve terminal (nt) of this axon possesses mitochondria with normal matrices and numerous clear synaptic vesicles of uniform diameter. The 50 nm primary synaptic cleft (bounded by arrowheads) has evenly distributed basal lamina. The nonsynaptic surface of the nerve terminal is overlain by Schwann cell (sc) processes which terminate at the margins (arrowheads) of the primary synaptic cleft.

Figure 2. Neuromuscular junction from a control rat subacutely exposed to Mestimon[®]-equivalent buffer for 14 days prior to fixation. The relationship of the nerve terminal (nt), Schwann cell (sc) and postsynaptic junctional folds (jf) appears normal and comparable to the acute control junction illustrated in fig. 1. This electron micrograph illustrates several cellular features of the subjunctional region. The muscle cell nucleus (n), sarcomere myofibrillar thick and thin filaments (mf), dense z-line (z) and subjunctional folds (jf) appear normal. The nerve terminal is evenly apposed to the junctional folds and separated by the typical 50 nm primary cleft (bounded by arrowheads) which contains a typical basal lamina. Note that the overlying Schwann cell processes (sc) do not enter the primary cleft (arrowheads).

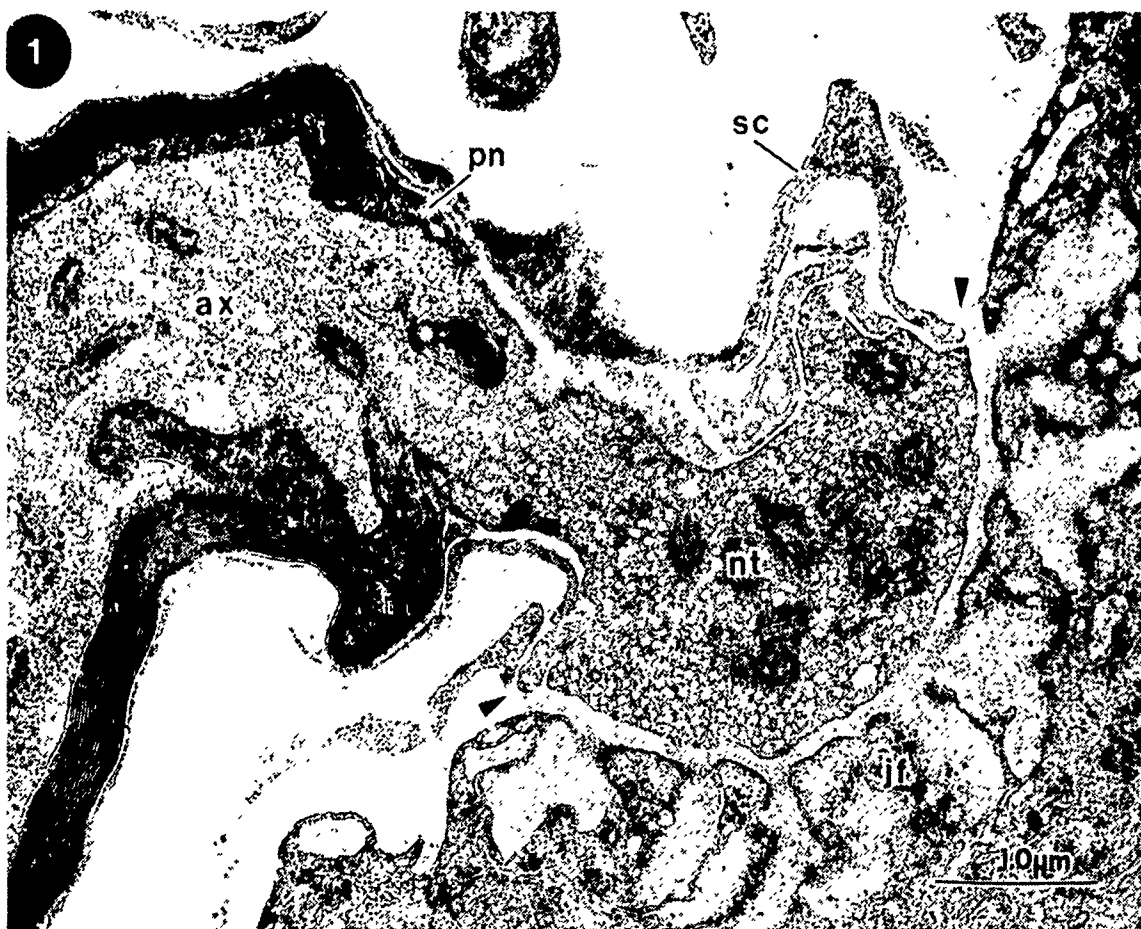


Figure 3. Acute dose-response: Presynaptic effects of pyridostigmine on rat diaphragm neuromuscular junction with fixation 30 minutes after a single, subcutaneous injection of drug (0.0036 mg/kg; 0.001 LD50 ; ~10% whole blood ChE depression). This electron micrograph illustrates the effects of the lowest drug dose used in the study. Even at this dose, the nerve terminal morphology and spatial relationship of the nerve terminal (nt) to the junctional folds (jf) are altered. Within the nerve terminal, only the mitochondria appear effected with rarefied areas in the matrix of some. The other organelles of the terminal appear normal including the synaptic vesicles which remain clear and normally sized. Regional withdrawal of the nerve terminal from the junctional folds is evident in this electron micrograph (between arrowhead & small arrow). At upper right (between asterisk & open asterisk), an area of junctional folds is devoid of nerve terminal and invaded by Schwann cell processes (sc). Also at upper right, a portion of nerve terminal (nt) is completely sequestered by a Schwann cell process. Where the nerve terminal has withdrawn, normal basal lamina remains (small arrows). Postsynaptically, the myofibrillar apparatus (mf) of the muscle cell appears mostly normal although some mitochondria (m) have been effected in this cell. This electron micrograph represents the greatest damage seen at the lowest drug dose.

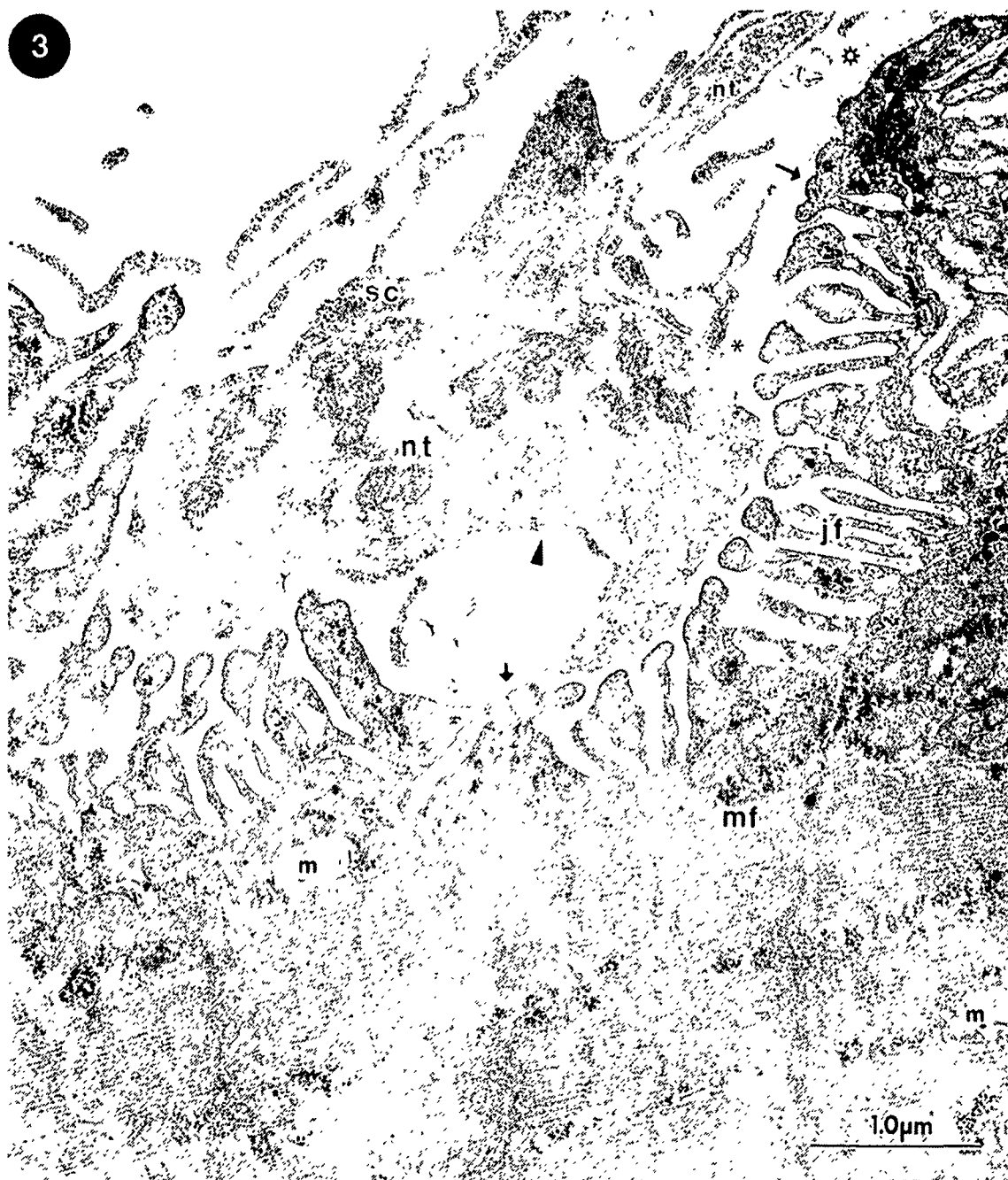


Figure 4. Acute dose-response: Presynaptic effects of pyridostigmine on rat diaphragm neuromuscular junction with fixation 30 minutes after a single, subcutaneous injection of drug (0.036 mg/kg; 0.01 LD50; ~25% whole blood ChE depression). While the postsynaptic morphology in this electron micrograph exhibits normal junctional folds (jf) and myofibrillar apparatus (mf), the presynaptic ultrastructure is altered. The nerve terminal (nt) is normally apposed to the junctional folds over much of this field. At the asterisk, however, there is evidence of terminal withdrawal from the junctional folds. Damage appears in the form of multiple membranous layers (arrow) some of which sequester vesicle containing nerve terminal portions (see right of arrow). Abnormally large diameter vesicles are evident in the nerve terminal. The arrowhead points to a Schwann cell process which has invaded the nerve terminal from the nonsynaptic side.

Figure 5. Acute dose-response: Presynaptic effects of pyridostigmine on rat diaphragm neuromuscular junction with fixation 30 minutes after a single, subcutaneous injection of drug (0.36 mg/kg; 0.1 LD50; ~55% whole blood ChE depression). All compartments in this neuromuscular junction are obviously effected at this dose. The nerve terminal (nt) contains altered mitochondria (m) and abnormal vesicular inclusions. The nerve terminal is withdrawn from various regions (asterisks) of the junctional folds while in other areas normal synaptic morphology is preserved. In regions of withdrawal vesicular debris, Schwann cell processes and small nerve terminal profiles are evident. Postsynaptically, the mitochondria are most obviously effected.

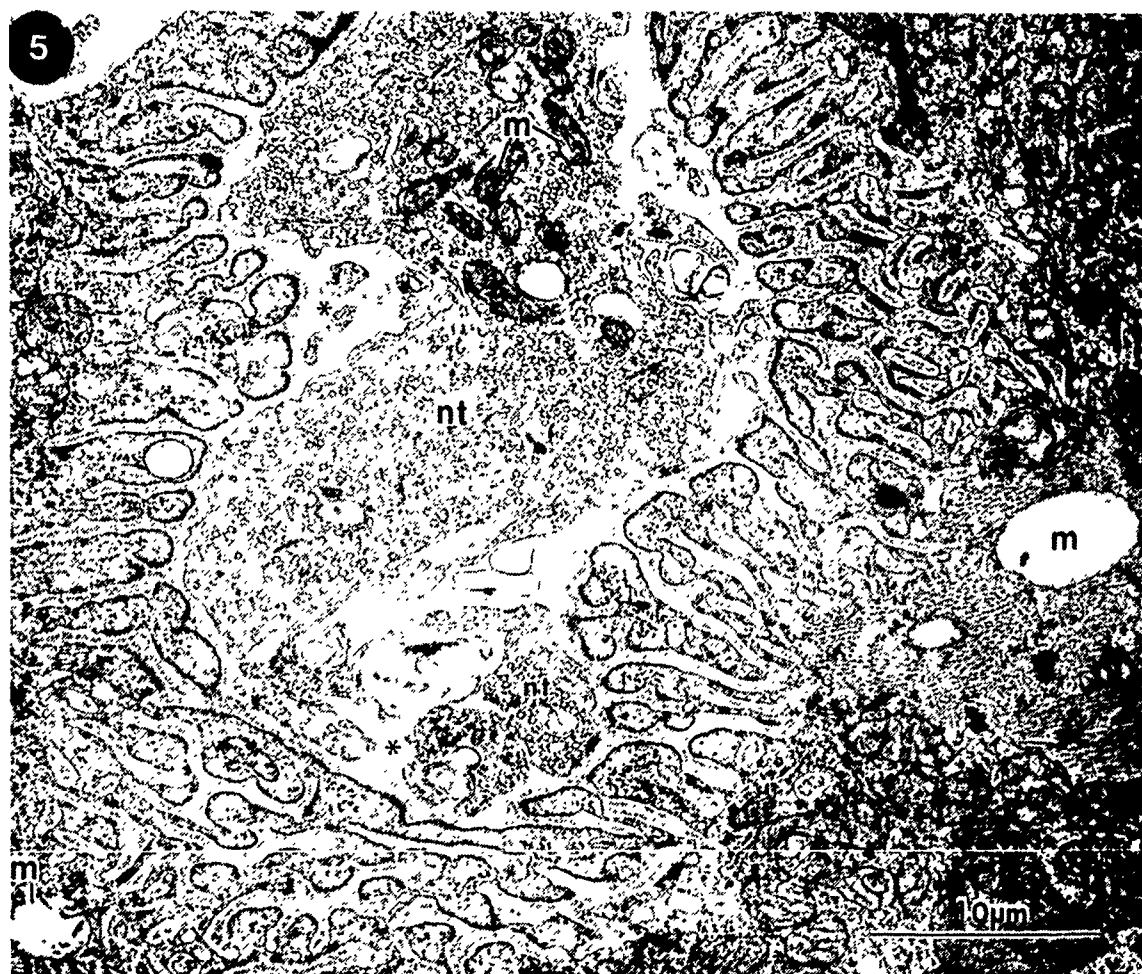
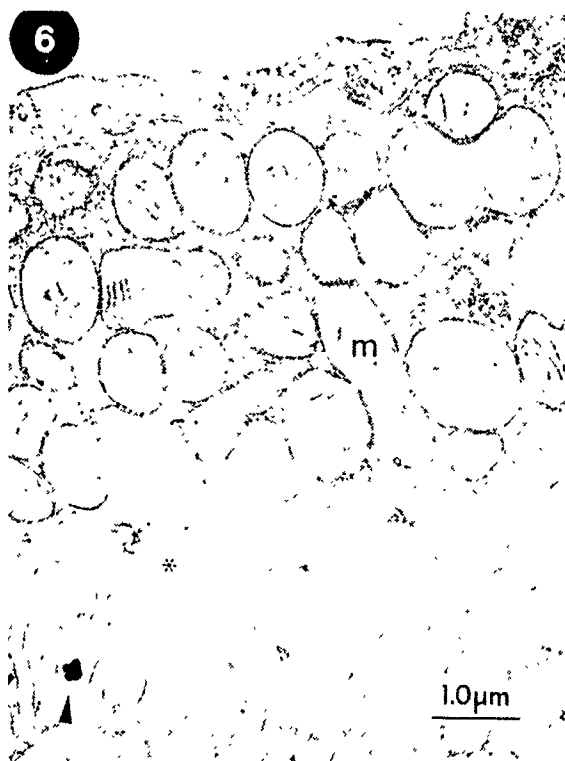


Figure 6. Acute dose-response: Presynaptic effects of pyridostigmine on rat diaphragm neuromuscular junction with fixation 30 minutes after a single, subcutaneous injection of drug (2.6 mg/kg; 0.72 LD50; ~70% whole blood ChE depression). A high magnification electron micrograph illustrates altered presynaptic mitochondria (m) and a Schwann cell process (asterisk) separating the pre- and postsynaptic membranes. An occasional membrane bound inclusion (arrowhead) is present in the junctional folds.

Figure 7. Acute dose-response: Presynaptic effects of pyridostigmine on rat diaphragm neuromuscular junction with fixation 30 minutes after a single, subcutaneous injection of drug (0.036 mg/kg; 0.01 LD50; ~25% whole blood ChE depression). An electron micrograph to illustrate the sequestration of nerve terminal (nt) by Schwann cell processes (arrowheads). These abnormally sequestered vesicle containing profiles appear different as a function of plane of section (e.g., see dotted line in fig. 8).

Figure 8. Acute dose-response: Presynaptic effects of pyridostigmine on rat diaphragm neuromuscular junction with fixation 17 minutes after a single, subcutaneous injection of drug (3.6 mg/kg; 1.0 LD50; ~80% whole blood ChE depression). This figure illustrates 1) alterations similar to those in figs. 3 - 7 occur relatively rapidly after drug administration; 2) that there is not always more damage with higher dose; and 3) the Schwann cell sequestration of nerve terminal portions is a consistent feature of the drug-induced alterations. In this electron micrograph, a Schwann cell process has invaded the primary synaptic cleft (two arrowheads at bottom). The nerve terminal (nt) contains abnormal vesicular profiles and has withdrawn from the junctional folds (asterisk). The nonsynaptic side of the nerve terminal has been invaded by a Schwann cell process (three arrowheads). The dotted line indicates a plane of section which would demonstrate a nerve terminal profile sequestered within a Schwann cell process similar to those seen in figs. 4 and 7.



Figures 9 and 10. Subacute dose-response: Presynaptic effects of a 2 day exposure to pyridostigmine on rat diaphragm neuromuscular junction (0.43 mg total drug exposure; sustained ~24% whole blood ChE depression). Both electron micrographs illustrate the predominance of the drug-induced presynaptic alterations regardless of dosage method. Regional withdrawal (asterisks) of the nerve terminal (nt) from the junctional folds is apparent. Schwann cell processes (sc) have invaded both the nonsynaptic regions of the nerve terminal and the primary cleft (arrowheads, fig. 10). Presynaptic organelle alteration is variable as illustrated in fig. 9 by the difference in the matrices of the various mitochondria (m).

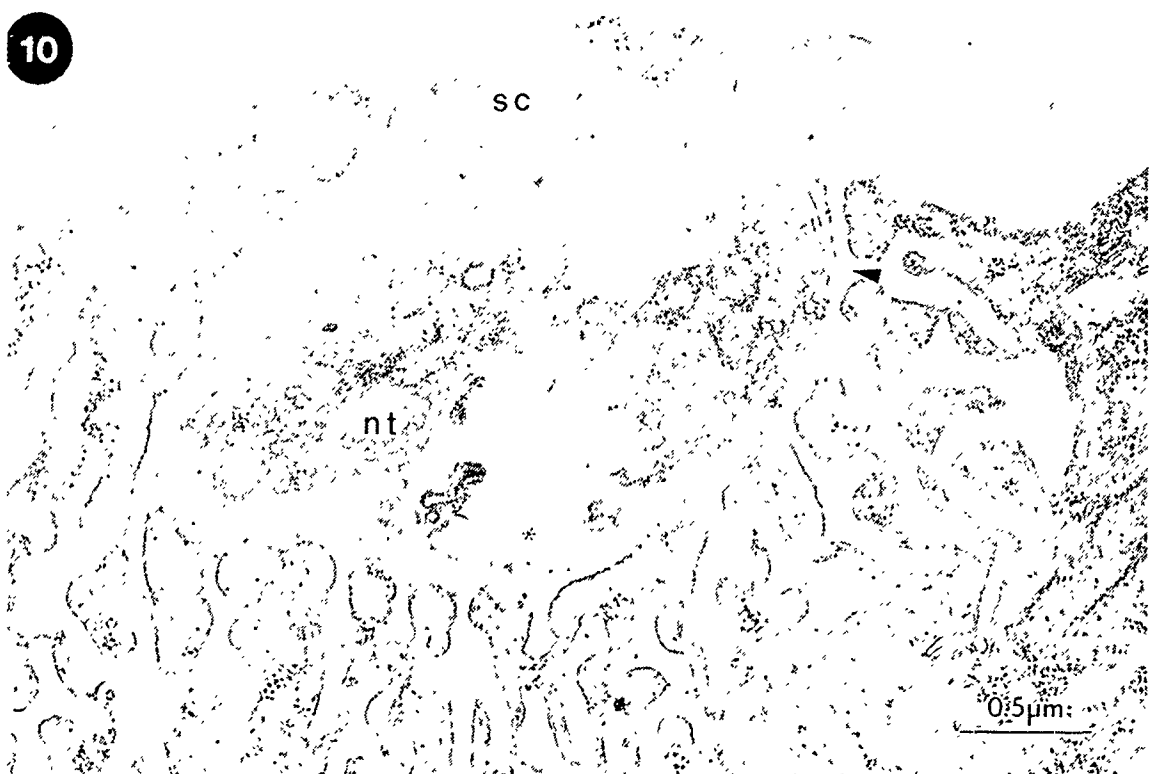
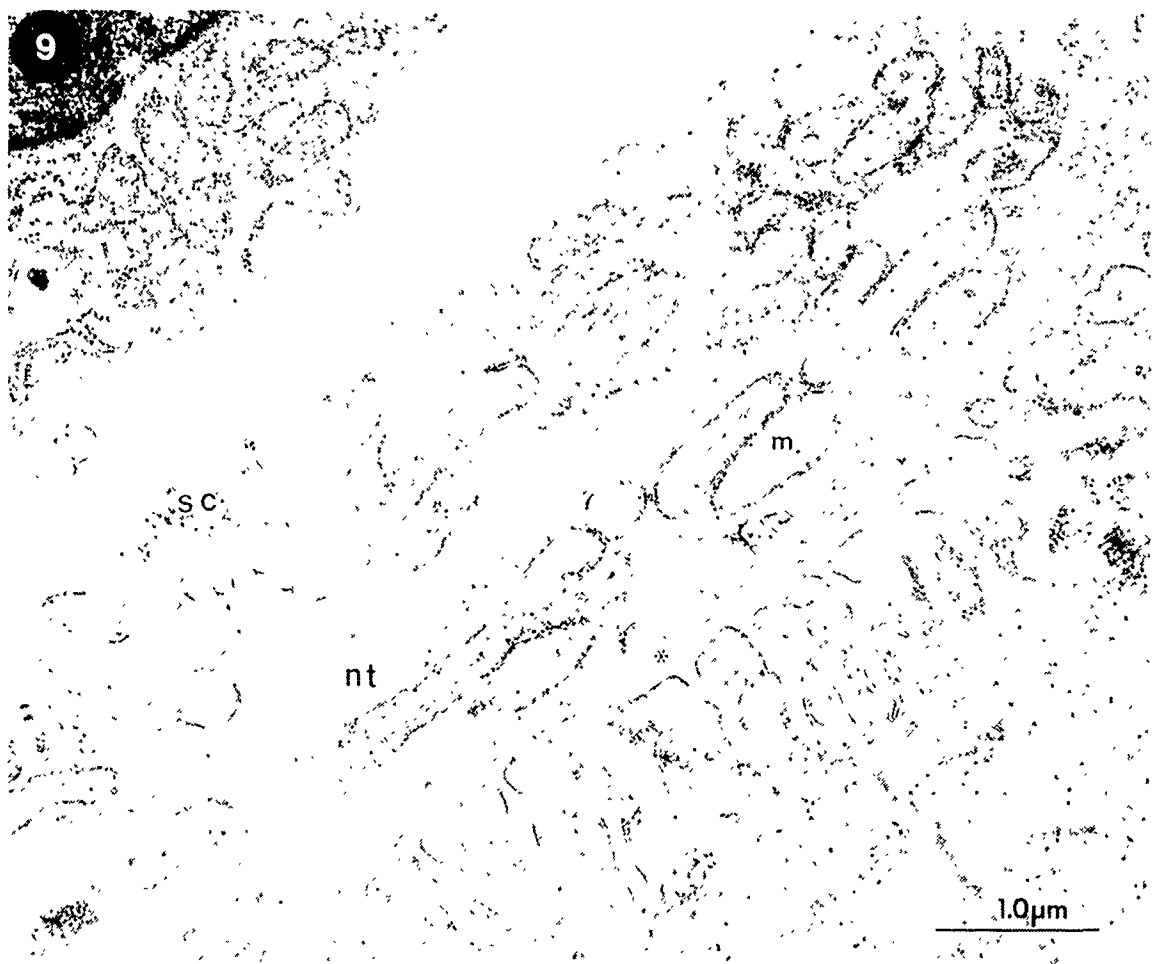


Figure 11. Subacute dose-response: Presynaptic effects of a 7 day exposure to pyridostigmine on rat diaphragm neuromuscular junction (10 mg total drug exposure; sustained ~65% whole blood ChE depression). Both pre- and postsynaptic alterations are evident in this electron micrograph. A portion of the neuromuscular junction (between arrows) is devoid of nerve terminal while Schwann cell processes (arrowheads) have invaded another portion. The nerve terminal has abnormal vesicular debris and abnormal mitochondria. The subjunctional myofibrillar apparatus (mf) is disrupted to the point of complete disorganization in contrast to the junctional folds which appear relatively normal.

Figure 12. Subacute dose-response: Presynaptic effects of a 14 day exposure to pyridostigmine on rat diaphragm neuromuscular junction (20 mg total drug exposure; sustained ~65% whole blood ChE depression). This electron micrograph illustrates gross presynaptic alterations with minor postsynaptic involvement. Schwann cell (sc) fingers have invaded the primary cleft and the nerve terminal has withdrawn (asterisks) from the junctional folds. Some nerve terminal mitochondria (m) are abnormal. The subjunctional myofibrillar apparatus (mf) is abnormally contracted. In this field, the muscle cell nucleus (n) appears unaffected.

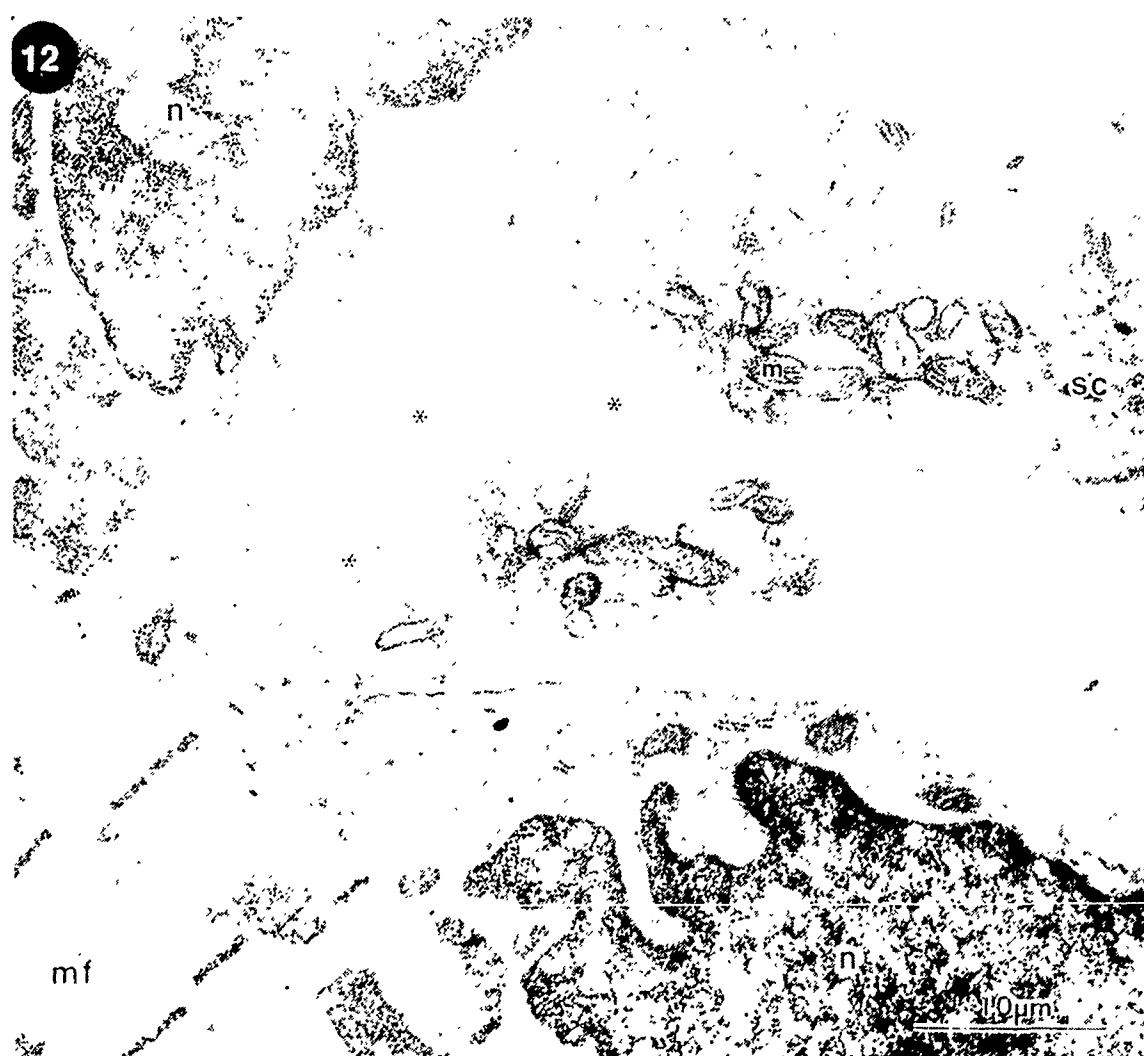
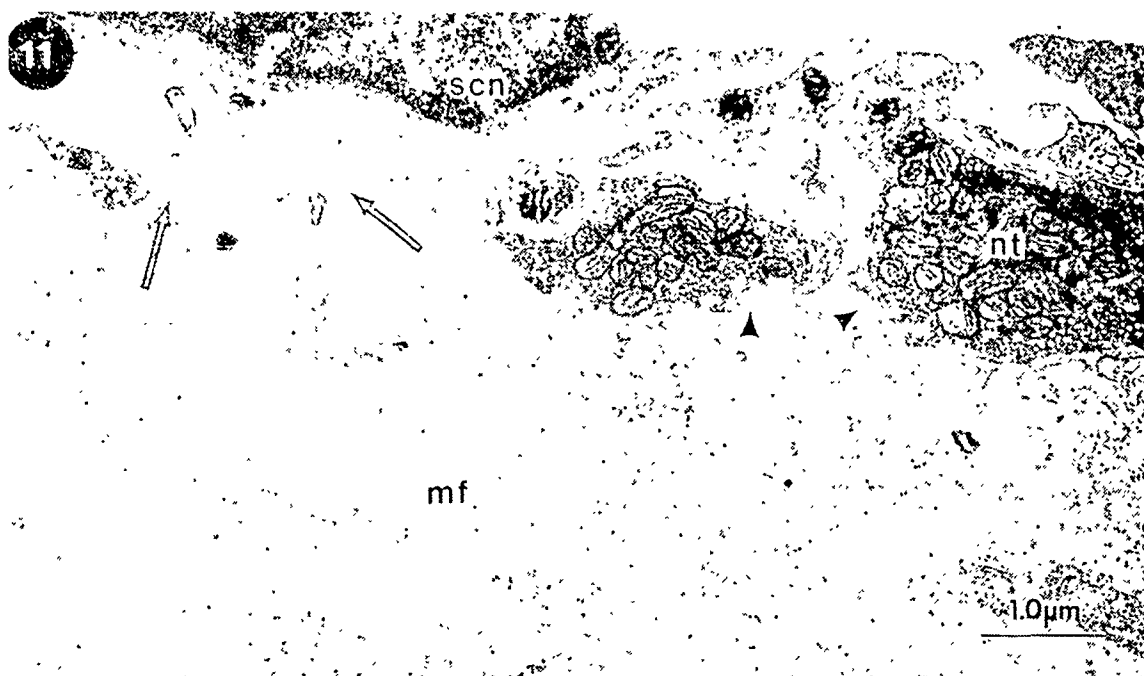
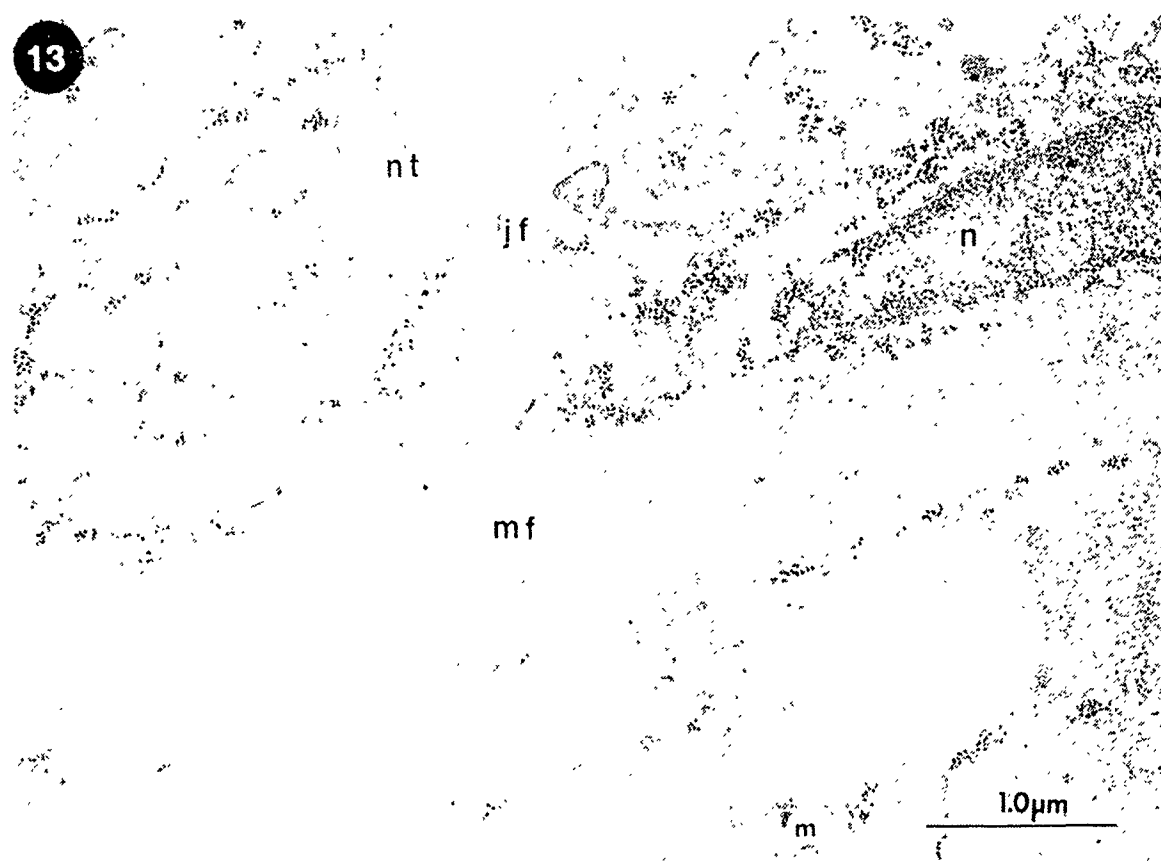


Figure 13. Acute dose-response: Postsynaptic effects of pyridostigmine on rat diaphragm neuromuscular junction with fixation 30 minutes after a single, subcutaneous injection of drug (0.0036 mg/kg; 0.001 LD50; ~10% whole blood ChE depression). The postsynaptic effects at this dose are minimal and usually manifest as mitochondrial (m) alterations. As in fig. 3, nerve terminal (nt) withdrawal (asterisk) is present. The postsynaptic myofibrillar apparatus (mf) appears normal as does the muscle cell nucleus (n).

Figures 14 and 15. Acute dose-response: Postsynaptic effects of pyridostigmine on rat diaphragm neuromuscular junction with fixation 30 minutes after a single, subcutaneous injection of drug (0.036 mg/kg; 0.01 LD50; ~25% whole blood ChE depression). Low and high magnification electron micrographs illustrate relatively normal muscle cell morphology at a dose higher than that in fig. 13. A mitochondrion (m) in fig. 14 is labelled for orienting reference to the same organelle in fig. 15. While some muscle cell mitochondria exhibit rarefied matrices, the sarcomere length and myofibrillar apparatus (mf) appears normal. As in fig. 4, the presynaptic compartment is altered with nerve terminal withdrawal (asterisk, fig. 14) and Schwann cell invasion of the primary cleft (arrowhead, fig. 14).

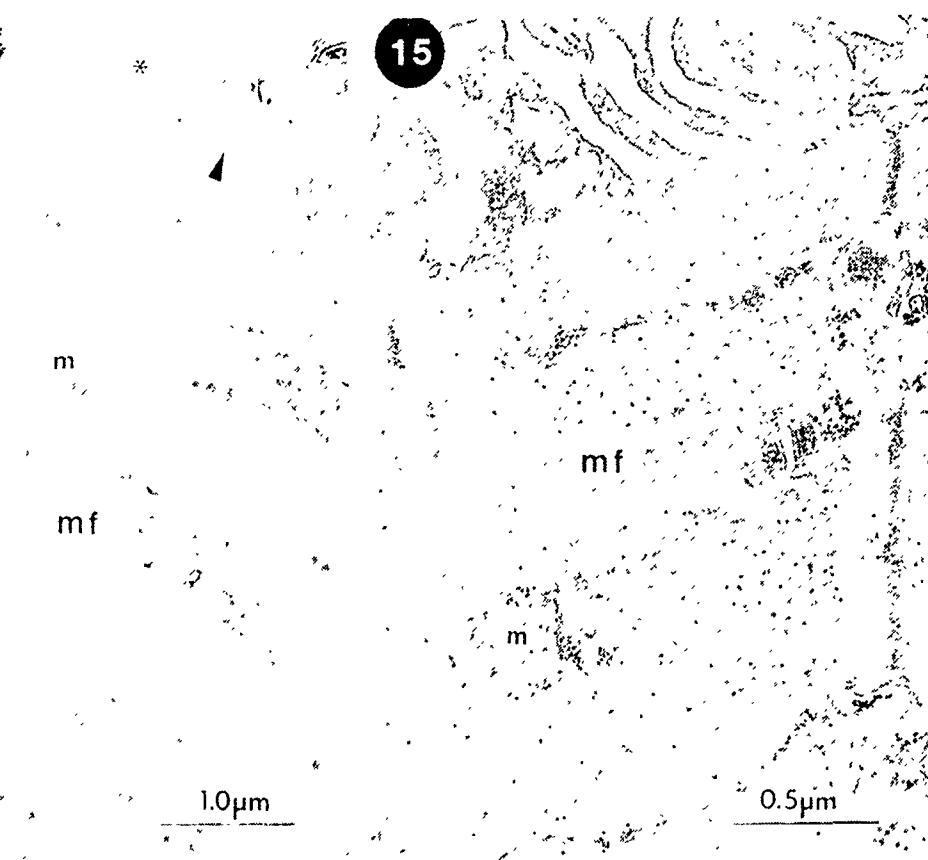
13



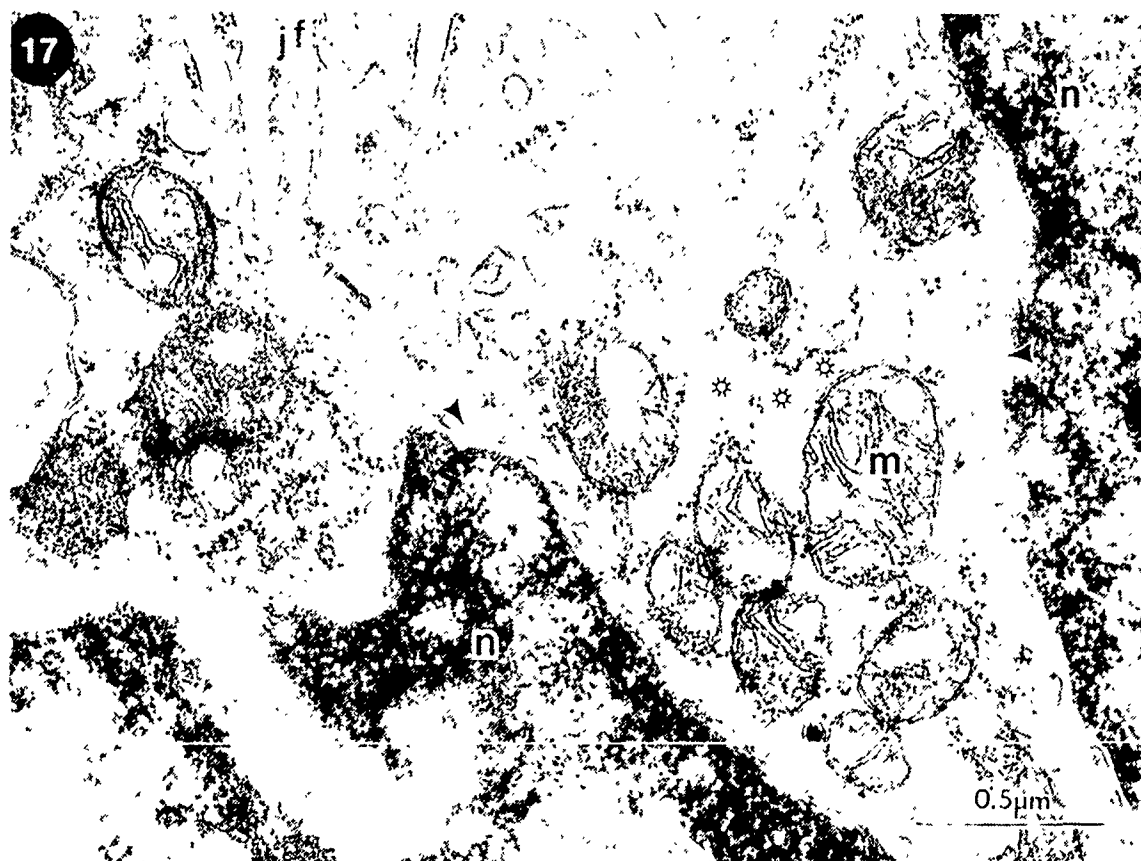
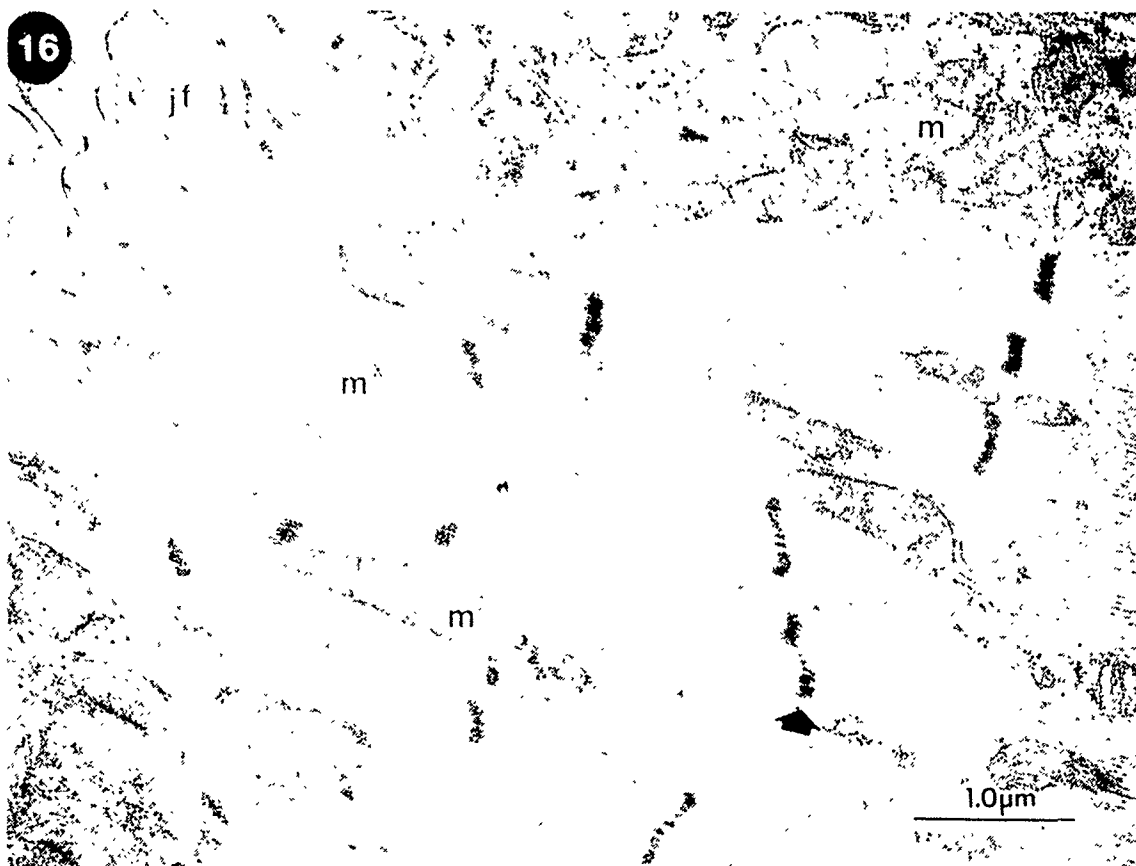
14



15



Figures 16 and 17. Acute dose-response: Postsynaptic effects of pyridostigmine on rat diaphragm neuromuscular junction with fixation 30 minutes after a single, subcutaneous injection of drug (0.36 mg/kg; 0.1 LD50; ~55% whole blood ChE depression). Low and high magnification electron micrographs illustrating some of the most severe effects of this acute dose. Fig. 16 illustrates mitochondrial damage which varies from rarefaction of the matrix (m) to complete disruption (m*). The subjunctional (note junctional folds, jf) z-lines begin to look abnormally diffuse (large arrow) at this dose. At higher magnification, fig. 17 illustrates alterations near the muscle cell nucleus (n). Abnormal mitochondria (m) and swollen endoplasmic reticulum (open asterisks) are evident. Note the increase in paranuclear space (arrowhead) in this field.



Figures 18 and 19. Acute dose-response: Postsynaptic effects of pyridostigmine on rat diaphragm neuromuscular junction with fixation 30 minutes after a single, subcutaneous injection of drug (2.6 mg/kg; 0.72 LD50; ~70% whole blood ChE depression). The most severe postsynaptic alterations were seen with doses between 0.1 and 1.0 LD50. At 0.72 LD50, fig 18 illustrates supercontraction (between open arrows) of the subjunctional sarcomeres with attendant gross mitochondrial (m) and myofibrillar (mf) damage. The nerve terminal (nt) and its subjunctional area have been pushed out of position in this field. The myofibrillar damage is graded with distance from the junction area. Fig. 19 illustrates gradation of the sarcomere damage in a non-subjunctional area. The mitochondria (m) in this field are relatively normal. From upper right to lower left, the myofibrillar apparatus (mf) and sarcomere (arrowheads) morphology ranges from completely abnormal to normal. Note the graded effect on z-line (z) ultrastructure.

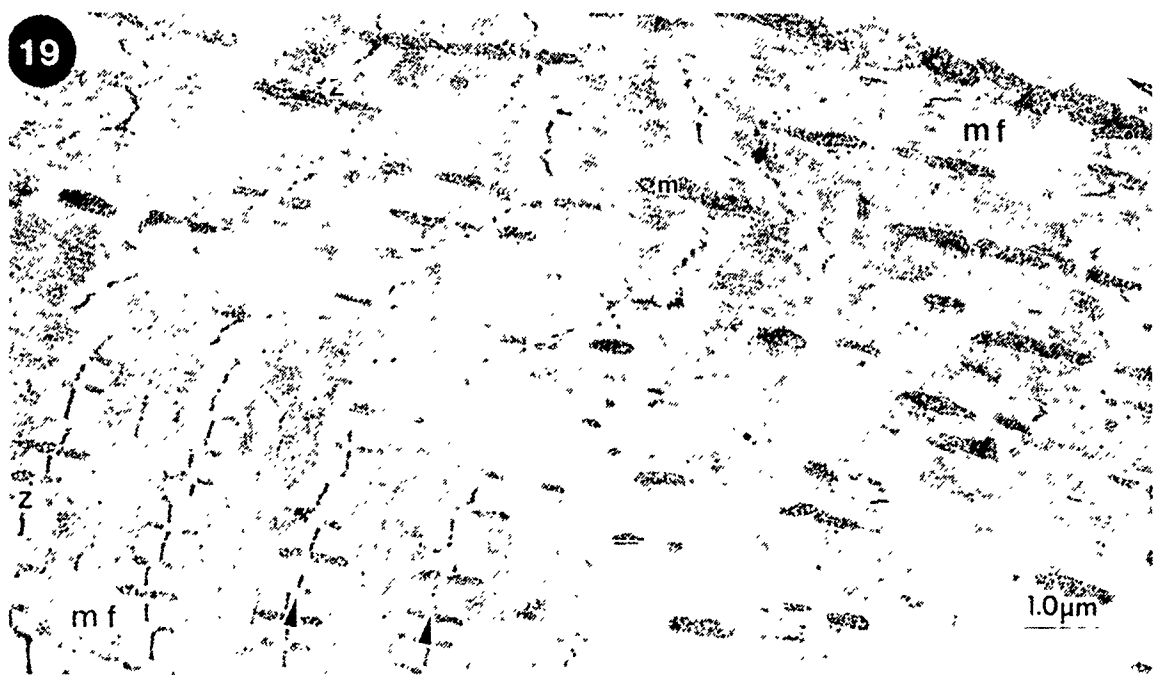
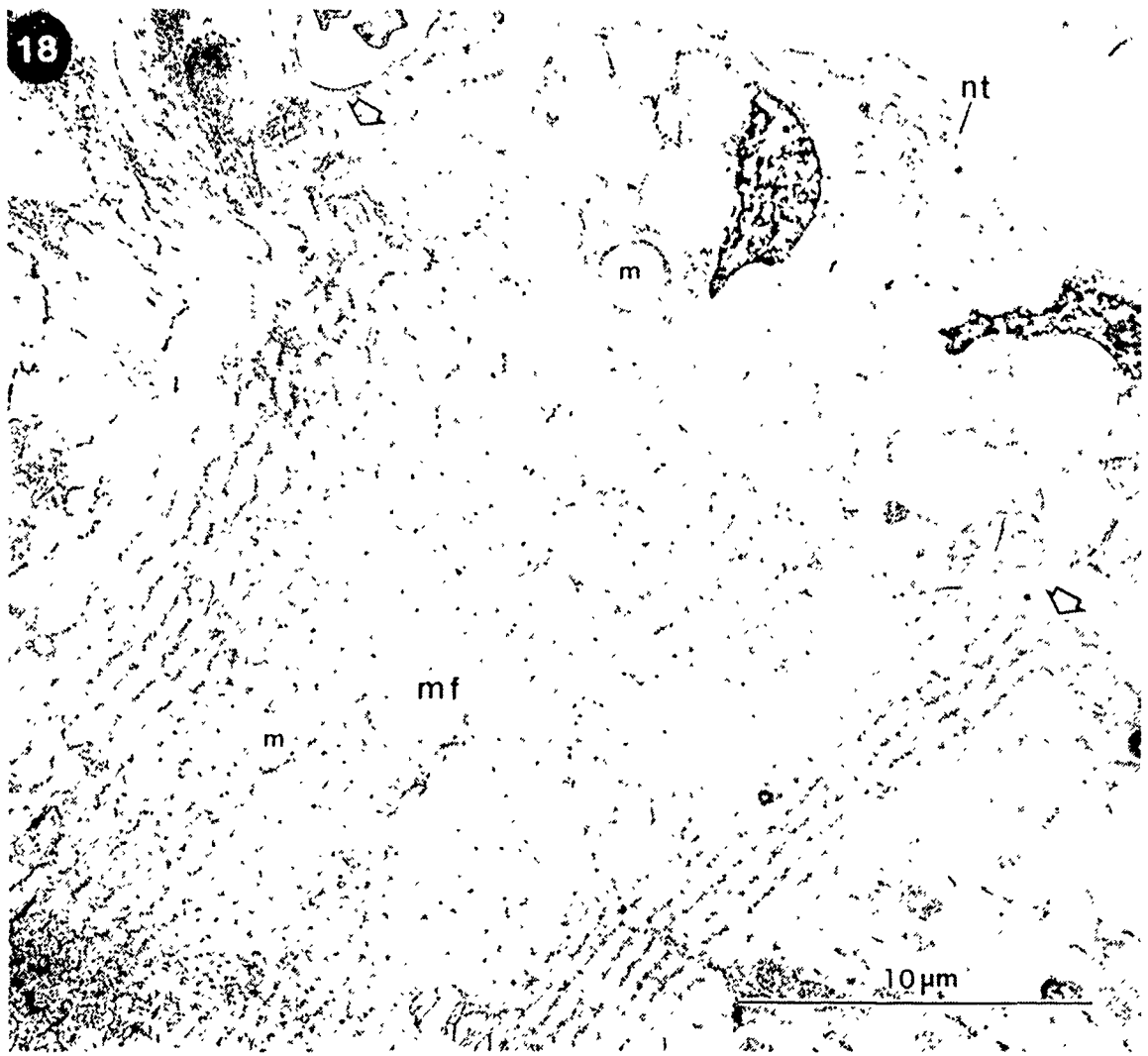
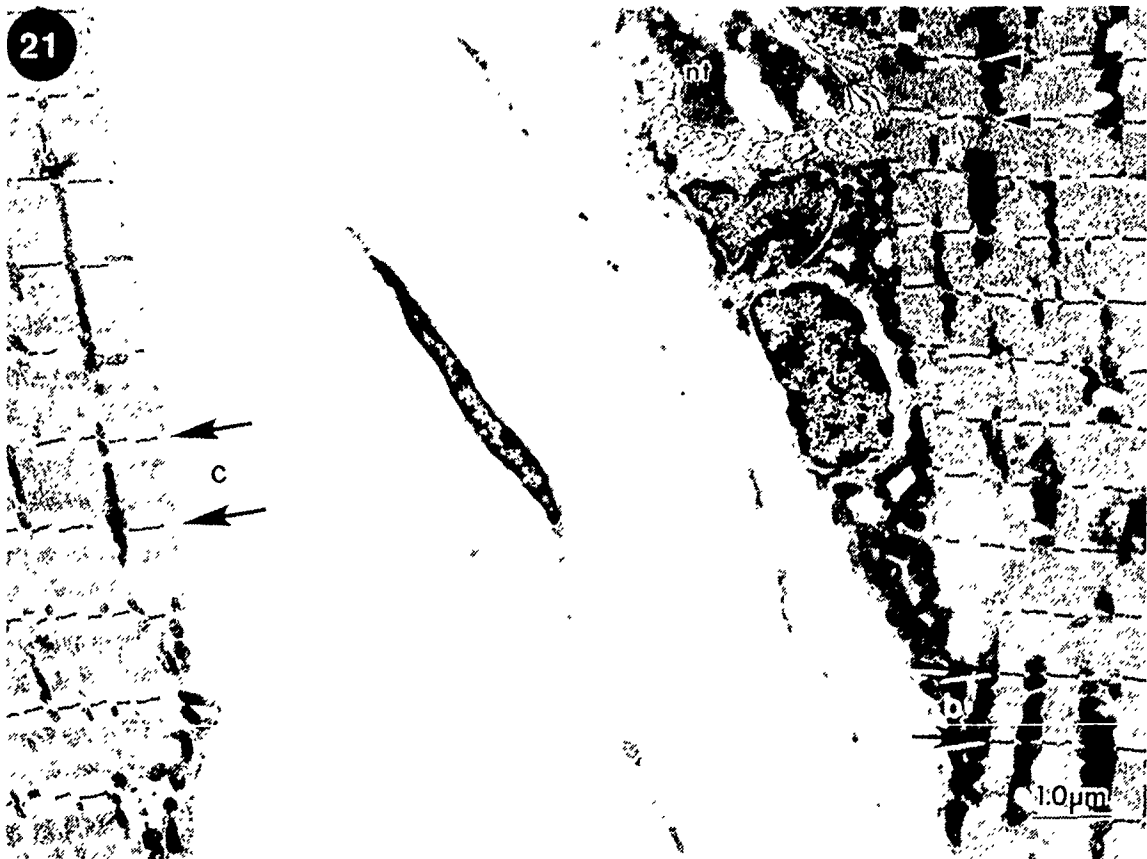
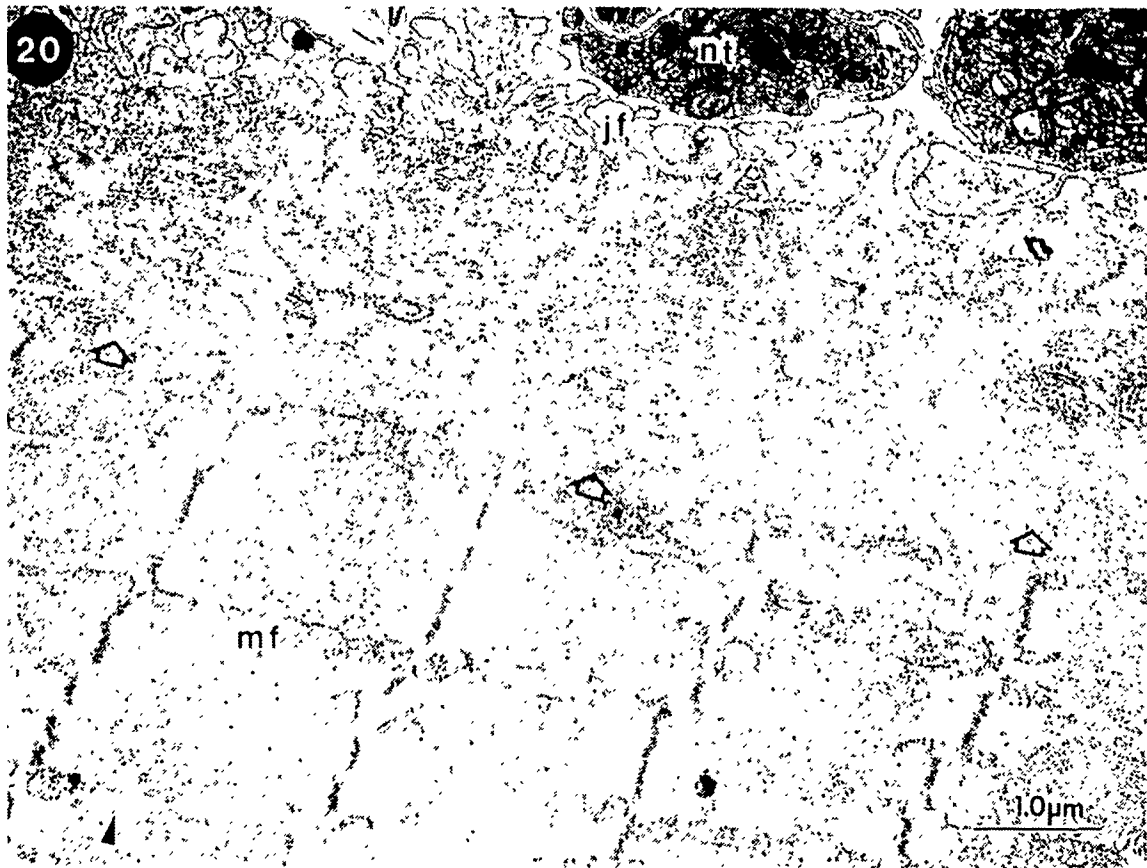


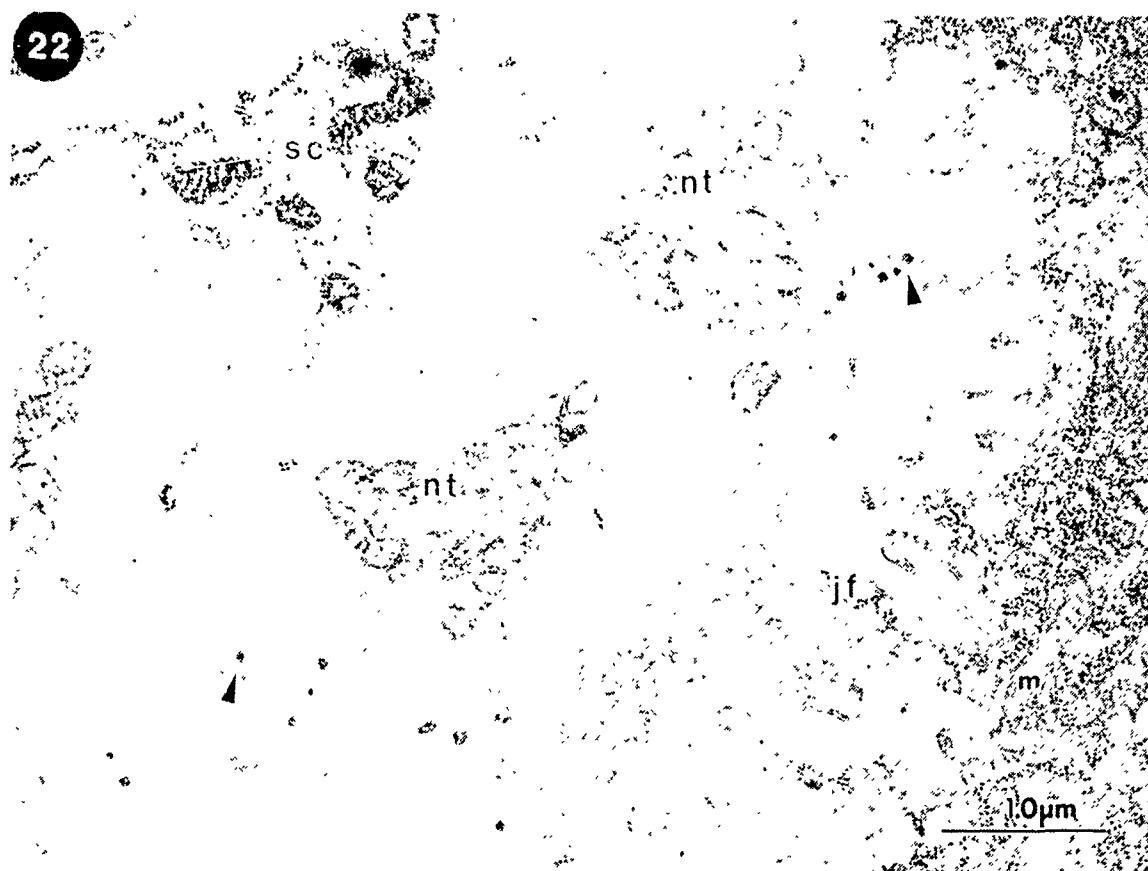
Figure 20. Subacute dose-response: Postsynaptic effects of a 7 day exposure to pyridostigmine on rat diaphragm neuromuscular junction (10 mg total drug exposure; sustained ~65% whole blood ChE depression). This electron micrograph illustrates the most severe postsynaptic damage encountered with subacute dosing. The open arrows mark the boundary of myofibrillar (mf) damage which is manifest as disruption of sarcomere structure. Subjunctional sarcoplasmic reticulum appears slightly swollen (arrowhead). While the junctional folds (jf) appear normal, the relationship of the nerve terminal (nt) to the junctional folds is altered as described in fig. 11. This electron micrograph also illustrates that the drug induced damage is graded with distance from the junctional area.

Figure 21. Subacute dose-response: Presynaptic effects of a 14 day exposure to pyridostigmine on rat diaphragm neuromuscular junction (20 mg total drug exposure; sustained ~65% whole blood ChE depression). This electron micrograph illustrates the variability in the nature and extent of drug induced damage when compared to fig. 20. While the two muscle cells in this field are relatively unaffected, note the typical nerve terminal (nt)/presynaptic alterations (see also fig. 12). Postsynaptically, the drug effect is manifest in subjunctional shortening of sarcomere length -- compare sarcomeres a, b & c (length= a- subjunctional, arrowheads $\frac{1}{4}$ b- non-subjunctional, arrows at lower right $\frac{1}{4}$ c- another cell, arrows at left).

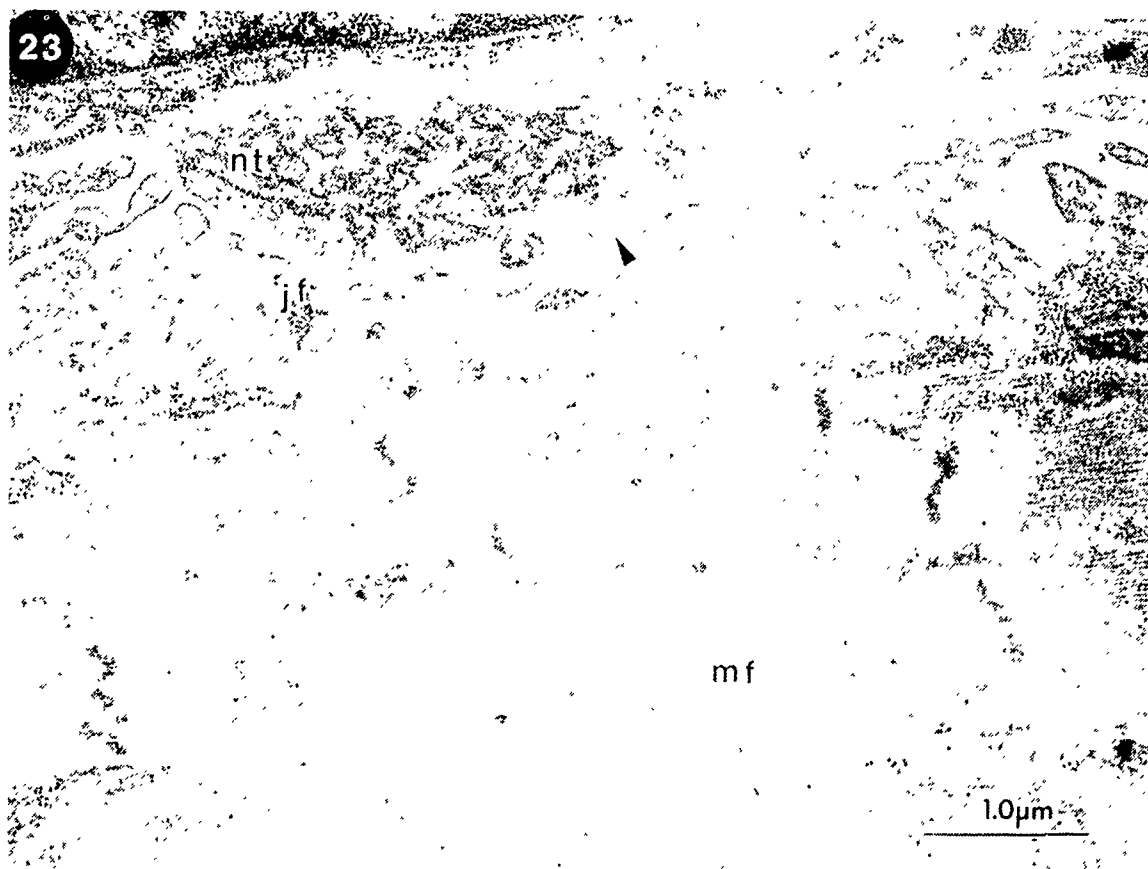


Figures 22 and 23. Acute dose recovery: Recovery of rat diaphragm neuromuscular junction from a single dose of pyridostigmine (2.6 mg/kg; 0.72 LD50; ~70% whole blood ChE depression) administered 7 days prior to fixation. These electron micrographs illustrate the variability in the process of recovery following a single drug exposure. Unlike the 30 minute image in fig. 6, the drug effect shown in fig. 22 has progressed to include junctional fold (jf) breakdown, further withdrawal of the nerve terminal (nt) profile, profuse Schwann cell processes (sc), and abnormal debris (arrowheads) in the primary and secondary clefts. The remaining mitochondria are normal in appearance. This field is reminiscent of a neuromuscular junction from a human patient with myasthenia gravis. In contrast, fig. 23 illustrates a neuromuscular junction which is minimally abnormal under the same recovery conditions. While a Schwann cell process (arrowhead) can be seen in the primary cleft, the junctional folds (jf) appear normal (compare to fig. 22). The subjunctional myofibrillar apparatus (mf) is minimally altered with the z-lines being slightly diffuse.

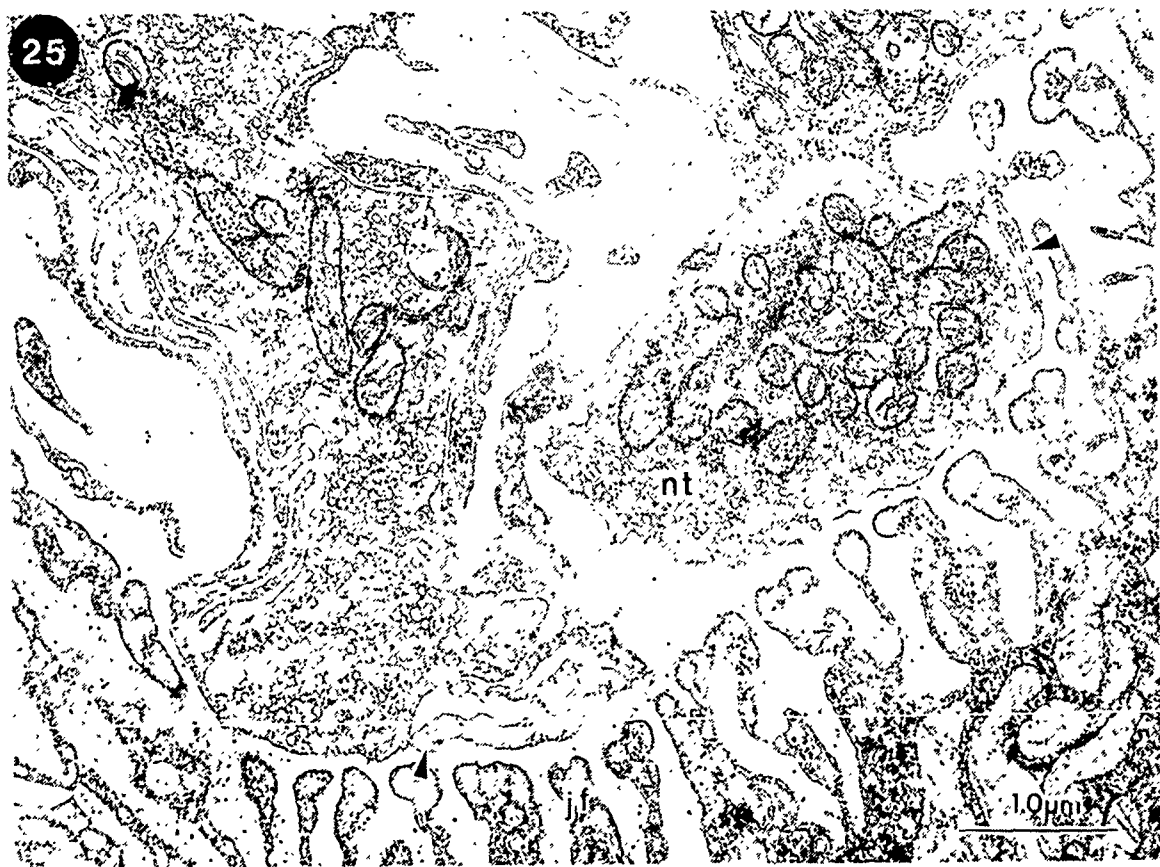
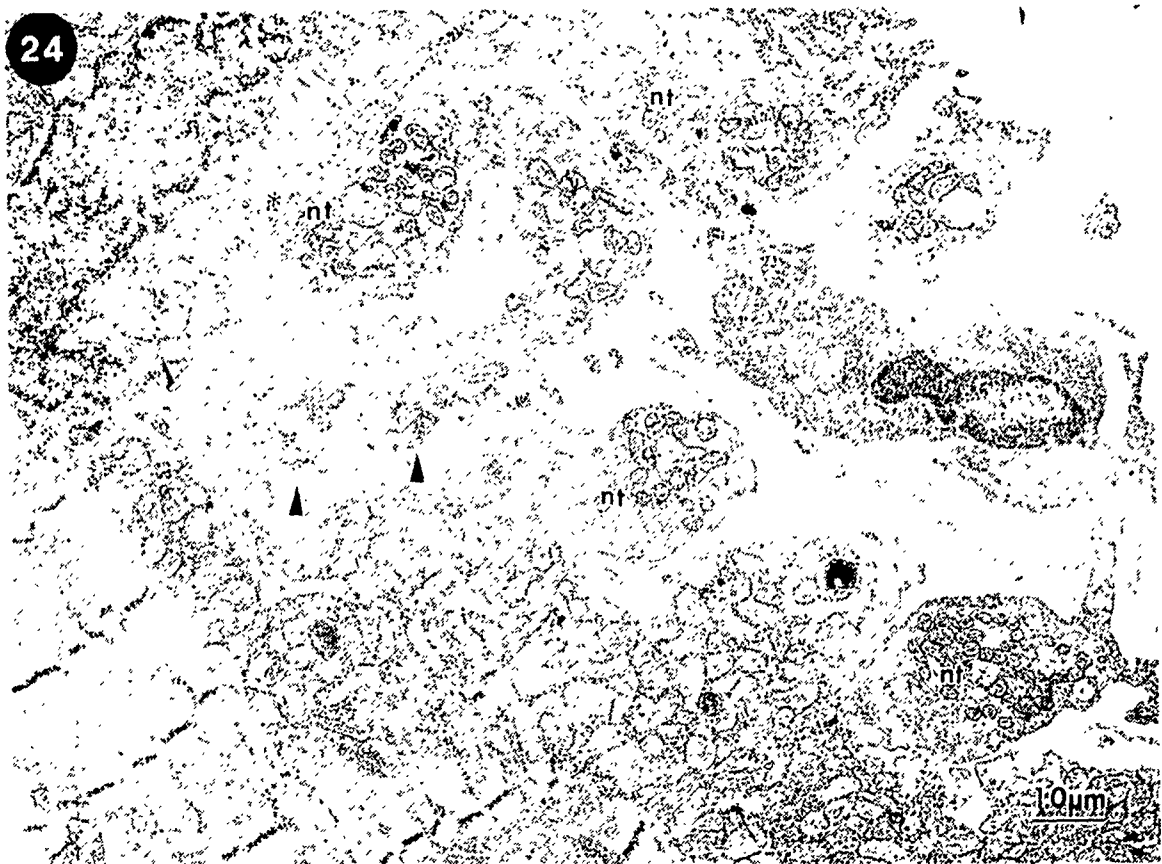
22



23

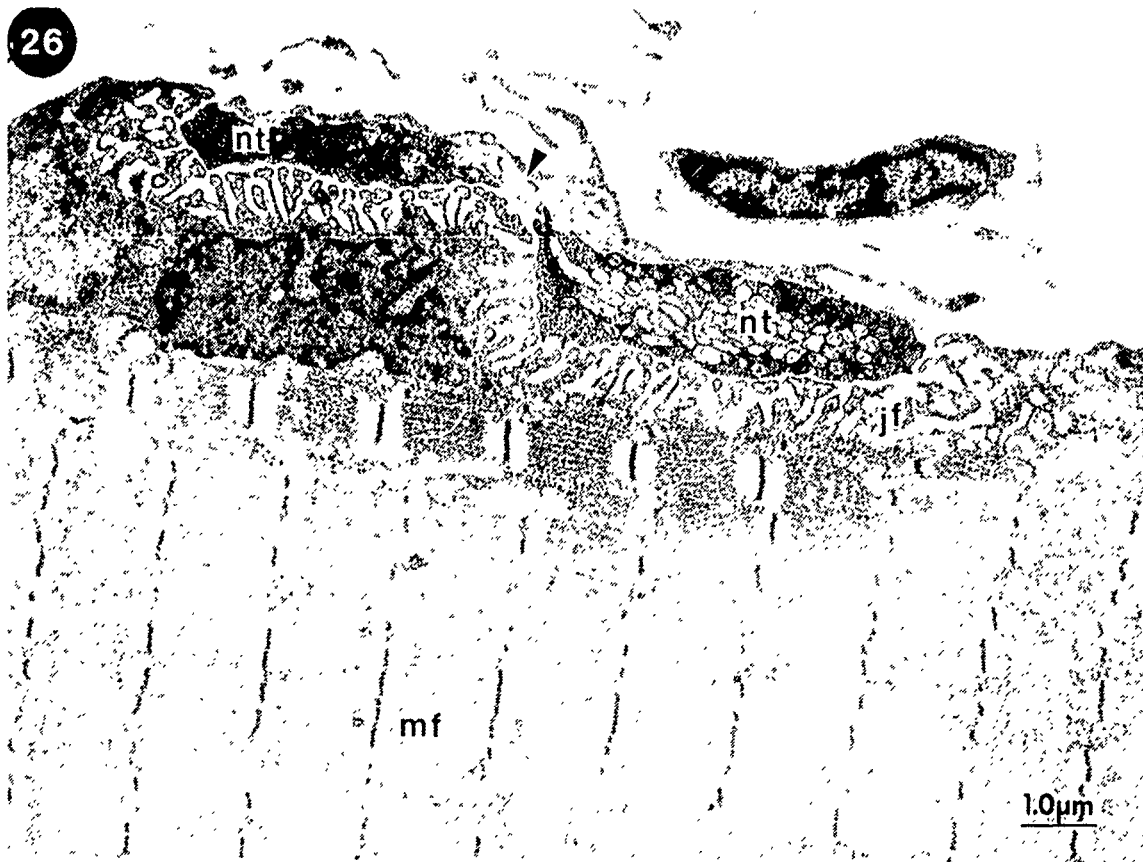


Figures 24 and 25. Subacute dose recovery: Seven days recovery of rat diaphragm neuromuscular junction from a 14 day exposure to pyridostigmine (20 mg to 1 exposure; sustained ~65% whole blood ChE depression). At low magnification, fig. 24, parts of the nerve terminal (nt) appear in normal apposition to the junctional folds while other parts are simply separated (asterisk) or completely altered (arrowhead). The subjunctional muscle cell has little alteration. Thus, seven days of recovery are not sufficient to completely reverse the presynaptic effects of subacute drug exposure. At higher magnification, fig. 25, illustrates the lack of recovery of the presynaptic alterations. Schwann cell processes (arrowheads) are present in the primary cleft. While the nerve terminal is normally a continuous structure overlying a contiguous portion of junctional fold, the drug effects include partitioning of the terminal into smaller bouton-like endings separated by abnormal Schwann cell processes.

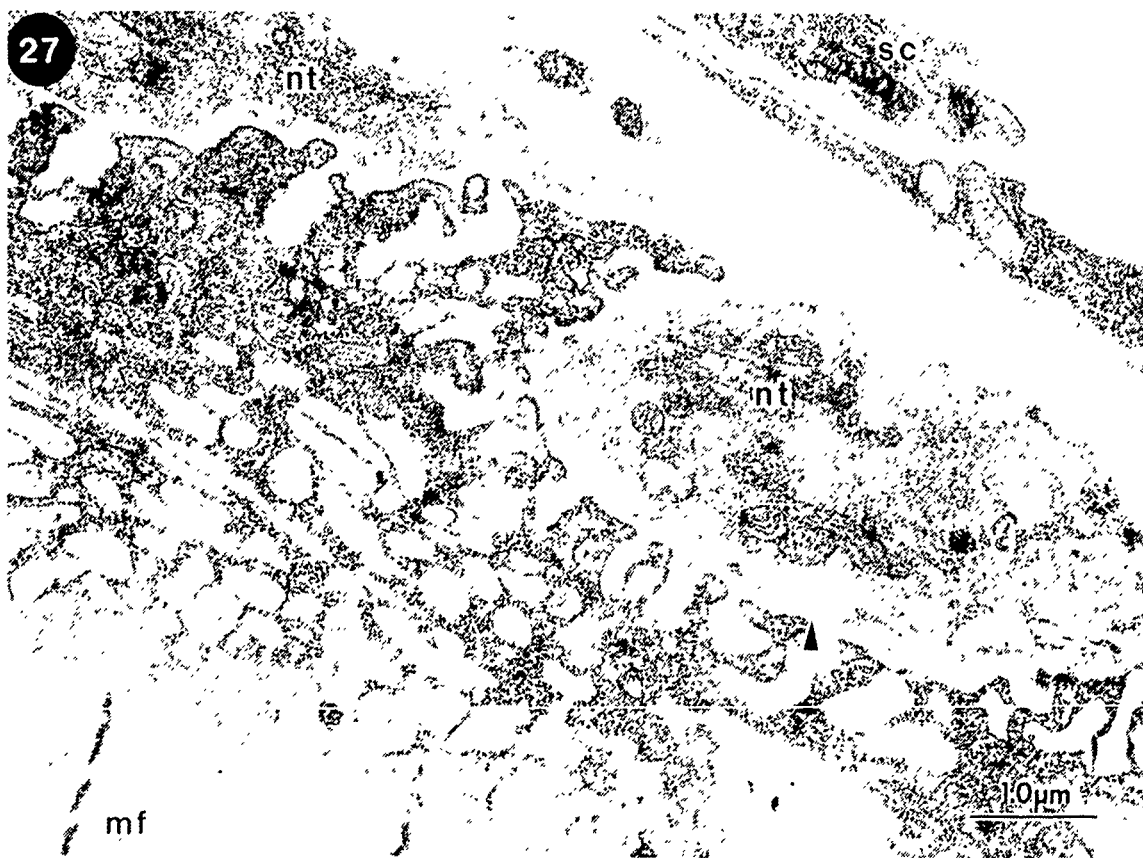


Figures 26 and 27. Subacute dose recovery: Twenty three days recovery of rat diaphragm neuromuscular junction from a 14 day exposure to pyridostigmine (20 mg total exposure; sustained ~65% whole blood ChE depression). The diaphragm neuromuscular junction in fig. 26 exhibits relatively normal junctional fold (jf) and myofibrillar apparatus (mf) ultrastructure. The overlying Schwann cell is in normal apposition to the nerve terminal (nt) in the nonsynaptic region with the exception of a region (arrowhead) between two nerve terminal profiles. Figure 27 illustrates the variability of recovery from subacute dosing. While the neuromuscular junction is not as fully recovered as that in fig. 26, the only remarkable alteration remaining is the interposition of Schwann cell processes (arrowhead) in the primary cleft. As in fig. 26, the myofibrillar apparatus is unaffected.

26



27



In vivo and In Vitro Pathophysiology of Mammalian Skeletal Muscle

Following Acute and Subacute Exposure to Pyridostigmine.

Studies on Muscle Contractility and Cellular Mechanisms.

Michael Adler, Donald Maxwell, Robert E. Foster.

Neurotoxicology Branch, Physiology Division
U.S. Army Medical Research Institute of Chemical Defense
Aberdeen Proving Ground, MD 21010

and

Sharad S. Deshpande and Edson X. Albuquerque

Department of Pharmacology and Experimental Therapeutics
University of Maryland School of Medicine
Baltimore, MD 21201

ABSTRACT

The subacute effects of pyridostigmine bromide on rat extensor digitorum longus (EDL) and diaphragm were investigated utilizing nerve-muscle preparations and standard electrophysiological techniques. Pyridostigmine was delivered at 5.93 μ l/hr via subcutaneously implanted Alzet[®] osmotic minipumps containing 4 mg (low dose) or 20 mg (high dose) drug in 2 ml of Mestimon[®] equivalent buffer. Control rats were implanted with minipumps containing buffer alone. Blood acetylcholinesterase (AChE) activities were depressed by 25% (low dose) and 68% (high dose) of control within 6 hr of minipump implantation.

In vivo studies. Indirect isometric twitch tensions from EDL muscles of chloral hydrate anesthetized rats were recorded after 1, 3, 7 and 14 days of drug exposure. Supramaximal stimuli were applied to the isolated peroneal nerve at frequencies of 1, 5, 10 and 20 Hz for 10 sec trials, between which the nerve was stimulated at 0.1 Hz. Rats implanted with low dose pyridostigmine pumps showed little or no alteration of twitch tensions for up to 14 days of treatment. Animals receiving high dose pyridostigmine pumps exhibited marked alterations in muscle properties within the first day of exposure that persisted for the remaining 13 days. With 0.1 Hz stimulation, EDL twitch tensions of treated animals were potentiated relative to control. Repetitive stimulation at ≥ 1 Hz led to a frequency-dependent depression in the amplitudes of successive twitches during the train. At 20 Hz, the final tensions were reduced on average to 35% of initial levels between days 1 and 14. Recovery from the high dose of pyridostigmine was rapid, and essentially complete by 1 day of withdrawal.

In Vitro studies: Tensions were recorded from diaphragm and EDL muscles isolated from animals receiving subacute doses of pyridostigmine in order to test for adaptive change in muscle properties. Experiments were performed after 1, 3, 7 and 14 days of pyridostigmine exposure and after 1, 3, 7 and 14 days of withdrawal from drug. When tested at room temperature after 1 hr of equilibration with physiological solution, these muscles had twitch tensions comparable to control, showed no frequency-dependent decrements in amplitude and were able to maintain a 10 sec tetanus. Acute pyridostigmine challenges were carried out by bath application to determine if alterations in sensitivity to the carbamate occurred during subacute treatment or recovery. The results indicate that no significant changes in sensitivity to pyridostigmine developed with either long-term exposure or upon withdrawal of treatment. Thus, there was no demonstrable persistent effect of the drug. Finally, the data demonstrate that the threshold concentration for obtaining frequency-dependent decrements in twitch and tetanic tensions was ≥ 5 μ M under control conditions and for all drug exposure/withdrawal conditions.

Additional in vitro studies, utilizing intracellular recordings of evoked endplate potentials (EPPs), indicate that the frequency-dependent effects of pyridostigmine result from a progressive decline in the EPP amplitude during repetitive stimulation. A similar decline in amplitudes of focal junctional acetylcholine potentials suggests that the depression is due, at least in part, to an enhancement in desensitization.

INTRODUCTION

Pretreatment by the carbamate acetylcholinesterase (AChE) inhibitor, pyridostigmine, can decrease the lethality associated with organophosphorus nerve agent exposure when combined with therapy by antimuscarinic compounds and oximes (Gall, 1981). The optimal dose of pyridostigmine is one which reduces whole blood AChE by approximately 30%. Some of the beneficial effects of pyridostigmine appear to be mediated by protection of a critical pool of AChE from irreversible phosphorylation (Berry and Davies, 1970). Other effects of pyridostigmine, unrelated to its inhibition of AChE, are also known to occur and have recently been well characterized. By use of voltage-clamp and ligand binding studies, Pascuzzo *et al.* (1984) have shown that pyridostigmine can enhance endplate desensitization rates in vertebrate skeletal muscle. The underlying mechanism involves an increase in the affinity between acetylcholine (ACh) and its recognition site on the receptor macromolecule. This mechanism would be expected to act in conjunction with accumulated ACh following inhibition of transmitter hydrolysis to produce a profound desensitization of the ACh receptor. Application of the gigaohm seal patch-clamp technique has revealed a weak agonist action of pyridostigmine (Akaike *et al.*, 1984). The channels activated by pyridostigmine have a mean lifetime similar to that observed with channels gated by ACh but have a lower unitary conductance. Activation of endplate channels by pyridostigmine may be expected to interfere with synaptic transmission since such channels are not synchronized with nerve impulses.

In addition to these effects, pyridostigmine has also been found to produce ultrastructural lesions of the synaptic membranes of mammalian skeletal muscle (Hudson and Foster, 1984; Meshul *et al.*, 1983). Ultrastructural abnormalities can be detected within 30 min of carbamate treatment, are dose-dependent and in extreme cases can lead to muscle fiber degeneration.

The pharmacological and morphological actions of pyridostigmine may be expected to impair neuromuscular transmission and skeletal muscle contractility. To determine whether pyridostigmine alters skeletal muscle function, we have examined the effects of the carbamate on nerve elicited twitch tensions, endplate potential (EPP) generation and microiontophoretic ACh sensitivities in rat extensor digitorum longus (EDL) and diaphragm nerve-muscle preparations. Several routes of administration were used and both acute and subacute actions were investigated.

METHODS

Subacute experiments:

Animals and preparation. Alzet® osmotic minipumps were implanted subcutaneously in three groups of adult albino rats (200-250 g) under ketamine anesthesia. The first group of animals (high dose) received 20 mg of pyridostigmine bromide in 2 ml of Mestinon® equivalent buffer; the second group of animals (low dose) received 3 mg of pyridostigmine and the third group (control) received only the Mestinon® buffer vehicle. Pyridostigmine was released continuously at 5.93 μ l/hr for 14 days making the effective

delivery rates 60 and 9 $\mu\text{g/hr}$ for the high and low dose pumps, respectively. Whole blood AChE activities were determined periodically to ensure accurate delivery.

In vivo contractility measurements. To determine the actions of pyridostigmine on skeletal muscle contractility, in vivo twitch tensions were recorded from EDL muscles in rats anesthetized with chloral hydrate (400 mg/kg i.p.). The distal tendon was freed at its insertion and secured to a Grass FT.03 force-displacement transducer while the paw and femur were immobilized in a stereotaxic apparatus. The peroneal nerve was isolated, sectioned and placed on bipolar stimulating electrodes. The exposed nerve and muscle tissues were kept moist, and the core temperature of the animal was maintained at physiological levels by application of surface heat. Muscle tensions were elicited by supramaximal pulses of 0.1 msec duration. The nerve was stimulated for 10 sec trials at frequencies of 1, 5, 10, and 20 Hz and at 0.1 Hz between trials. These frequencies are within the physiological range for locomotion (Grimby, 1984). Resting tensions were adjusted to 4 g prior to data collection.

The effects of pyridostigmine were assessed 1, 3, 7, and 14 days after osmotic minipump implantation and 1, 3, 7, and 14 days after removal of pumps. The animals were sign-free during the course of subacute pyridostigmine treatment but approximately 70% of the high dose group exhibited fasciculations of the facial muscles and forelimbs after injection of chloral hydrate. Experiments were also performed to determine the sensitivity of muscles from treated rats to an acute pyridostigmine challenge by testing the response of isolated EDL and diaphragm to bath applied pyridostigmine in vitro.

In vitro contractility measurements. Sciatic nerve-EDL and phrenic nerve-diaphragm muscles were removed and mounted in a tissue bath for recording of muscle contractions using an isometric force displacement transducer. The bath contained oxygenated (95% O_2 and 5% CO_2) Krebs-Ringer solution (pH 7.2-7.4) of the following composition (mM): NaCl, 135; KCl, 5.0; CaCl_2 , 2.0; NaHCO_3 , 15; Na_2HPO_4 , 1.0 and glucose, 11. Recordings were performed at room temperature following a 60 min equilibration with physiological solution. Drugs were dissolved in saline and were introduced by several changes of the bathing media. Resting tensions for EDL and diaphragm were 4 and 2 g respectively. Stimulation parameters were similar to those used for the in vivo studies.

Intracellular recordings. EPPs were recorded in the cut muscle preparation of the rat diaphragm according to the procedure described by Barstad and Lillheil (1968). The muscles were cut transverse to the fiber axis, close to the endplate zone, to minimize or abolish contractions following nerve stimulation. Junctional ACh potentials were elicited by microinotophoretic application of ACh from a high resistance (150-300 megohm) pipette filled with 2 M ACh and positioned near the edge of a nerve terminal. ACh responses were recorded by an intracellular microelectrode (filled with 3M KCl and having 15-20 megohm resistance) placed in the synaptic region. Complete details of this technique are published elsewhere (Albuquerque and McIsaac, 1970).

Acetylcholinesterase determinations. AChE activity was measured by the radiometric method of Siakotas et al. (1969). Blood: Blood samples were collected in tubes containing citrate buffer from a separate group of subacutely-treated rats during and after pyridostigmine exposure. Samples were assayed within 1 min after collection for AChE activity at 25°C using ^{14}C -acetyl β -methylcholine as substrate.

Tissue: Rat hemidiaphragms were homogenized in phosphate buffered saline (5% w/v). Samples of homogenate (25 μl) were incubated for 30 min with pyridostigmine at 25° C and assayed for cholinesterase activity (10 min) using ^{14}C -ACh as substrate. The reaction was quenched by addition of Amberlite in dioxane. The homogenates were centrifuged at 700 rpm for 1 min and enzyme activity determined in a scintillation counter.

RESULTS AND DISCUSSION

In vivo muscle contractions during subacute pyridostigmine treatment. Supramaximal stimulation of the peroneal nerve (0.1 Hz) in rats implanted with control minipumps produced single twitch tensions in the EDL muscle of 37.4 ± 2.5 g (mean \pm SEM, $n=10$). With repetitive nerve stimulation, muscle contractions generally showed a triphasic profile consisting of an initial rise in tension, followed by a brief relaxation and a secondary development of tension during 10 sec stimulation periods (Fig. 1). Initial tension

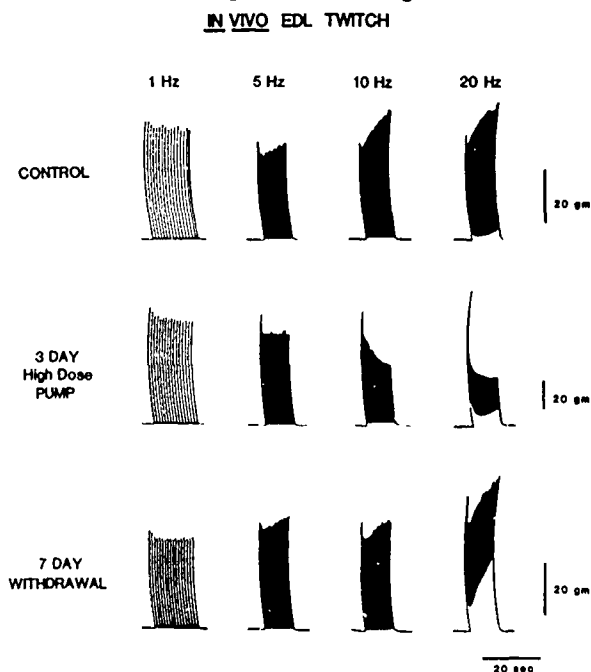


Fig. 1

Typical polygraph records illustrating the alteration of in vivo tensions in EDL muscles following subacute administration of pyridostigmine (60 $\mu\text{g/hr}$) via osmotic minipumps. Muscle contractions were elicited by supramaximal stimulation of the peroneal nerve in anesthetized rats (chloral hydrate 400 mg/kg, i.p.). Twitch tensions were well maintained under control conditions and during recovery but underwent frequency dependent decreases in the presence of pyridostigmine. Note the differences in the vertical calibration.

amplitudes were comparable to those of single twitches for stimulation frequencies of 1-10 Hz and augmented at 20 Hz; final tensions were elevated at frequencies above 1 Hz (Fig. 2). These characteristics of control EDL muscle are in accord with those reported by other investigators (Tiedt *et al.*, 1978).

EDL muscles from rats treated subacutely with a high dose of pyridostigmine delivered via minipumps (60 μ g/hr) showed altered contractile properties. Single twitch tensions were potentiated by an average of 114% between 1 and 14 days of exposure to pyridostigmine. Twitch potentiation by anticholinesterase agents results from the generation of multiple muscle action potentials following a single nerve impulse due to the prolonged nature of the EPP (Clark *et al.*, 1984). With repetitive stimulation, twitch tensions from pyridostigmine-treated rats were progressively depressed during the 10 sec trains. Depression was evident even at 1 Hz and became more marked with increases in stimulation frequency (Figs. 1 and 2). Because of the underlying

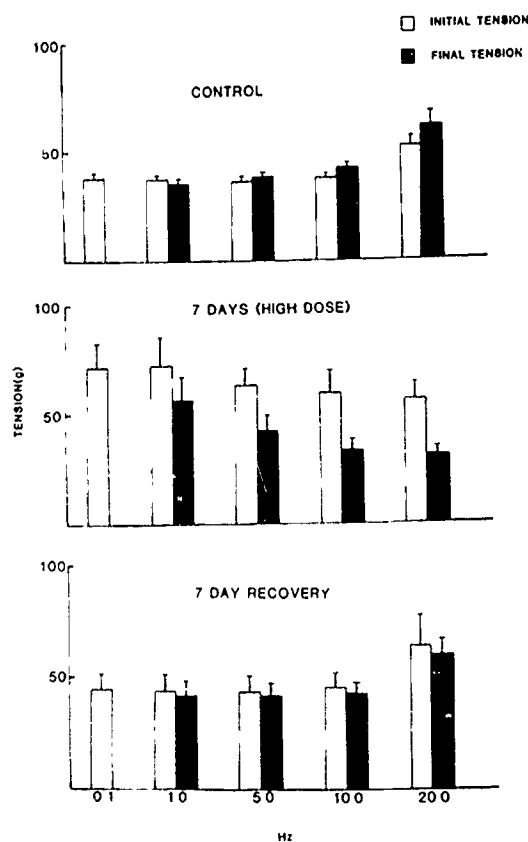


Fig. 2

Histograms illustrating the frequency-dependent action of subacutely administered pyridostigmine (60 μ g/hr) on *in vivo* EDL muscle tensions. The conditions depicted are control (top), 7 days after implantation of osmotic minipumps containing pyridostigmine (middle) and 7 days after removal of minipumps in rats exposed to pyridostigmine for the previous 14 days. The initial and final tension were measured at the beginning and end of a 10 sec duration train. The data represent the mean \pm SEM from 3-7 muscles.

potentiation, initial tensions during the train were equal to or greater than those recorded from control animals. Final tensions, however, were depressed relative to control at 10 and 20 Hz (Fig. 2). Restoration of initial tensions occurred within 10-20 sec of cessation of repetitive stimulation.

The time course for the onset and recovery from pyridostigmine treatment is shown in Fig. 3. As illustrated, both the depression during a 20 Hz train (top) and potentiation of single twitch tensions (bottom) were fully developed

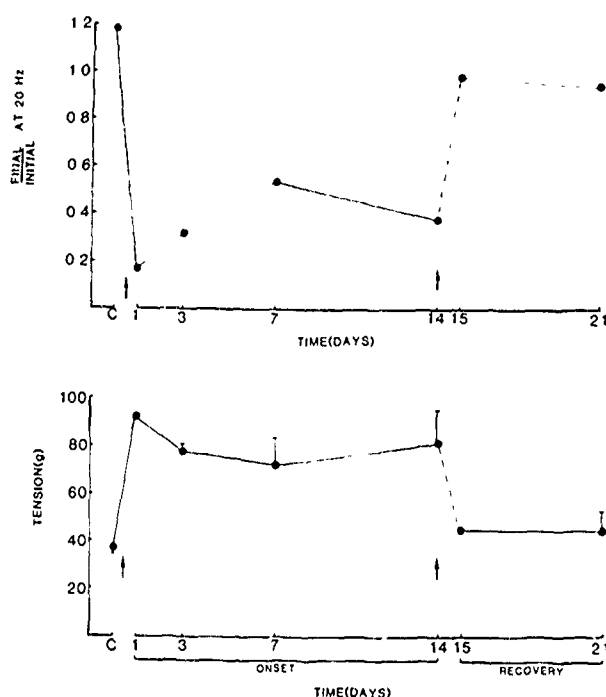


Fig. 3

Time course of pyridostigmine-induced alterations of EDL twitch tensions during subacute administration of pyridostigmine (60 μ g/hr). Upper graph shows the ratio of final to initial tension during a 10 sec train at 20 Hz. Lower graph shows twitch tensions elicited by 0.1 Hz nerve stimulation illustrating potentiation of the single twitch. The onset of pyridostigmine's action is fully developed within 1 day of administration and is not progressive; recovery is essentially complete within 1 day of withdrawal. Qualitatively similar results were obtained with stimulation frequencies of 1, 5 and 10 Hz.

1 day after minipump implantation. These effects persisted without increasing in severity for the entire 14 day treatment period. The data in fact indicate a trend towards decreases in the magnitude of depression during the 3rd and 7th day of treatment but these were not significantly different from the level of depression obtained on days 1 or 14. To monitor recovery, minipumps were removed after 14 days of subacute pyridostigmine exposure and muscle tensions were determined 1, 3 and 7 days after withdrawal. Recovery of both twitch potentiation at 0.1 Hz and depression during repetitive stimulation (1-20 Hz,

10 sec) was observed 1 day after removal of pyridostigmine containing minipumps (Fig. 3). In one experiment, in vivo tensions were recorded continuously, before, and up to 105 min after removal of the pyridostigmine minipump. In another experiment recording of twitches was begun 2 hr after removal of the pump and continued for 2 hr. Both rats had received pyridostigmine (60 $\mu\text{g/hr}$) for 3 days. Little or no recovery was detected in either animal. Thus, recovery from the effects of subacute pyridostigmine treatment occurs between 4 and 24 hr of drug withdrawal. The persistence of pyridostigmine's effects after subacute administration contrasts with its rapid termination following acute application (Fig. 6).

EDL muscles of rats implanted with minipumps containing 3 mg pyridostigmine (9 $\mu\text{g/hr}$) failed to show either potentiation of single twitch tensions or depression of successive twitches during repetitive stimulation. No significant departure from control values was observed during 14 days of treatment or during 14 days following pyridostigmine withdrawal (Fig. 4). These results are of interest since the inhibition of whole blood AChE (about 25%) in animals with low dose pyridostigmine pumps approximates the levels considered optimal for protection against organophosphorus nerve agent toxicity (Gall, 1981).

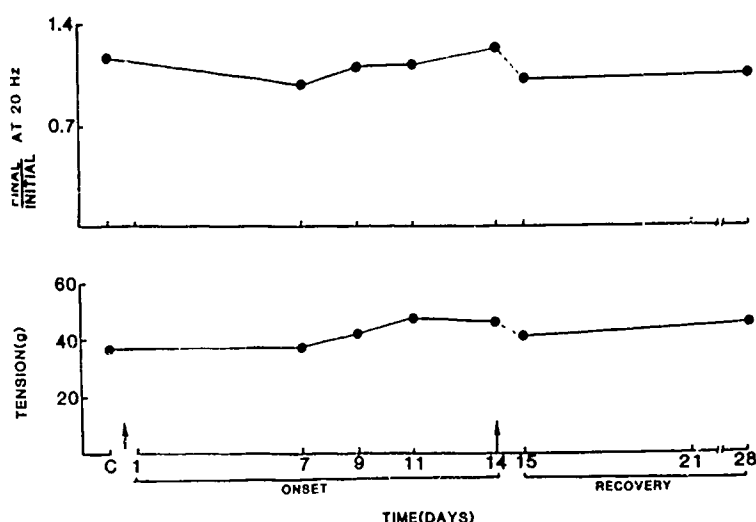


Fig. 4

In vivo twitch tensions in EDL muscle during and following subacute treatment with 9 $\mu\text{g/hr}$ of pyridostigmine. Exposure to the lower dose of pyridostigmine did not cause significant alterations in single twitch tension (bottom) or lead to frequency-dependent depression (top).

Determination of whole blood AChE activities. Fig. 5 shows the time course for inhibition of whole blood AChE levels during and after subacute pyridostigmine treatment via implanted osmotic minipumps. The experimental

conditions were similar to those used for the contractility studies except that the low dose pumps contained a total of 4 rather than 3 mg of pyridostigmine. Inhibition of AChE was complete by the first time point, measured 2 days after minipump implantation. AChE levels were depressed on average to 60% and 32% of control for the low and high dose of pyridostigmine, respectively for the entire 14 day period. Fluctuations in AChE activity in pyridostigmine-treated rats were similar to those observed in control animals ($\pm 10\%$). AChE activities recovered to control levels within one day of exhaustion of pyridostigmine, coinciding with the time course of recovery for the alterations in muscle contractility.

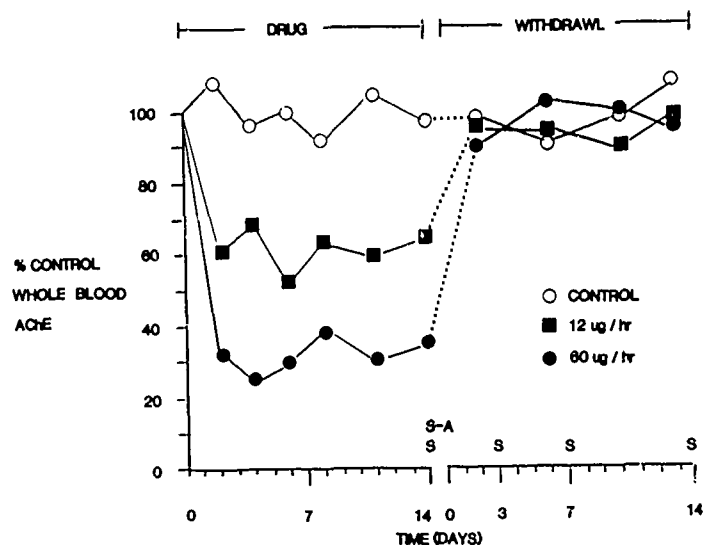


Fig. 5

Time course for inhibition of whole blood AChE activities during and following subacute treatment with 12 $\mu\text{g/hr}$ or 60 $\mu\text{g/hr}$ of pyridostigmine delivered via osmotic minipumps. Control animals were implanted with minipumps containing buffer. These experiments were conducted in parallel with the electrophysiological study. Soman challenge(s) were performed at the indicated times. S-A represents a soman challenge accompanied by atropine 16 mg/kg, s.c.) therapy (see text). Note that the low dose of pyridostigmine (12 $\mu\text{g/hr}$) is higher than 9 $\mu\text{g/hr}$ used elsewhere.

Intravenously applied pyridostigmine. The actions of pyridostigmine on twitch potentiation (0.1 Hz) and depression (1-20 Hz) are not confined to subacute treatment, but can be demonstrated by all routes of administration. The results from a rapid intravenous injection of pyridostigmine on in vivo tensions in EDL muscle are depicted in Fig. 6. The top trace shows single twitches elicited at 0.1 Hz. At the time indicated by the arrow, 0.1 ml of a 20 μg pyridostigmine (80 $\mu\text{g/kg}$) solution was injected into the external jugular vein. Single twitch tensions were potentiated within 30 sec of injection and continued to increase over the next 3 min. A 20 Hz train elicited during the period of maximum potentiation resulted in a marked depression in muscle tension during the 10 sec repetitive stimulation (middle trace). The depression was similar to that observed when the drug was applied by means of the minipump. Recovery from the effects of intravenously administered

pyridostigmine occurred rapidly, and by 23 min after injection both single and repetitive twitch tensions were restored nearly to control levels (bottom trace). Similar increases in single twitch tension and depression during repetitive stimulation were observed after a subcutaneous injection of 0.1 mg/kg pyridostigmine. The time course of drug action was somewhat slower, however. The onset, peak and total duration required 8, 25 and 45 min respectively.

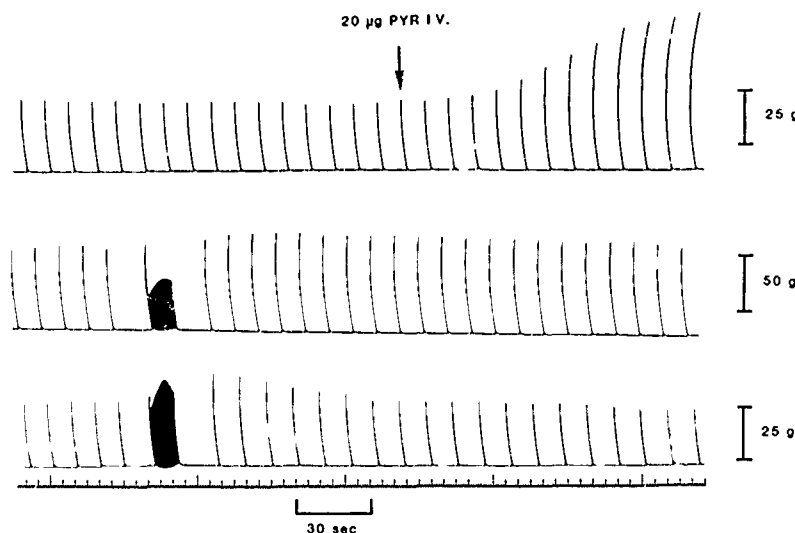


Fig. 6

Typical experiment showing the effect of pyridostigmine on the in vivo contractions elicited by indirect stimulation in control EDL muscle at 0.1 and 20 Hz. Pyridostigmine was injected into the external jugular vein as indicated by the arrow in the first trace. The onset of potentiation of the single muscle twitch tensions occurred within 30 sec. As the stimulation rate was increased from 0.1 to 20 Hz, there was a significant depression of muscle tension during the 10 sec high frequency train (middle trace). The first two traces are continuous; the bottom trace was obtained 23 min after initial injection of the drug and shows recovery of muscle function. Note the differences in the vertical calibrations.

Examination of adaptive changes following subacute pyridostigmine treatment. One of the consequences of long-term exposure to AChE inhibitors is an apparent progressive adaptation to the drug. Resistance to the drug or tolerance is manifest as a decrease in the severity of the signs and symptoms of anticholinesterase toxicity with continued administration of the AChE inhibitor (Costa et al. 1982). Although tolerance is generally associated with organophosphorus AChE inhibitors, it may occur with subacute pyridostigmine administration since the AChE activities are depressed continuously during the treatment period (Fig. 5). To examine this possibility, muscles were removed during and following subacute pyridostigmine treatment (60 µg/hr) and challenged with acute pyridostigmine exposure in vitro. The results for EDL muscle are shown in Fig. 7. In rats, treated only with vehicle, little or no depression in muscle tension was observed during a 20 Hz train in the presence of pyridostigmine concentrations below 5 µM.

Raising the pyridostigmine concentration to 10 and 100 μM resulted in depression of final tensions by 70 and 90% respectively relative to initial tensions.¹ As indicated in Fig. 7, the sensitivity of EDL muscle to pyridostigmine was essentially unchanged when tested after 7 days of treatment or 1 and 14 days after withdrawal. Similar results were obtained for all treatment and withdrawal times examined on both EDL and diaphragm muscles. Moreover, no significant differences were detected in the 24 hr LD50 of subcutaneously injected soman either during or following exposure to pyridostigmine. Thus, on day 14 of pyridostigmine treatment the LD50 dose of soman was 129 $\mu\text{g/kg}$ (113 $\mu\text{g/kg}$ in control rats). Prior administration of atropine sulfate (16 mg/kg) increased LD50 of soman from 140 $\mu\text{g/kg}$ (atropine alone) to 234 $\mu\text{g/kg}$ (atropine + 14 days of pyridostigmine treatment). Withdrawal of pyridostigmine for 3-14 days resulted in no significant deviation in LD50 dose of soman (93-114 $\mu\text{g/kg}$) from that observed for control animals (Maxwell and Foster, unpublished observation). These results indicate

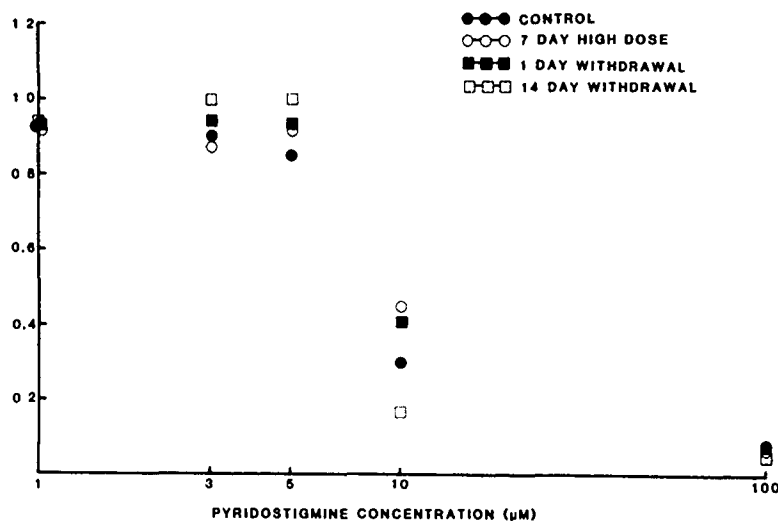


Fig. 7

In vitro concentration effect curves determined during acute bath application of pyridostigmine on isolated EDL nerve-muscle preparations. Muscles were obtained from animals after the indicated subacute treatments. Recordings were performed at room temperature in Krebs-Ringer solution. Muscles were equilibrated for at least 60 min with physiological solution prior to recording and 30 min to each pyridostigmine concentration. It should be noted that (1) recovery from subacute pyridostigmine was complete within 1 hr when muscles were removed and placed in drug free solution, and (2) no systematic alteration in acute sensitivity to pyridostigmine was apparent in either treated or recovered animal. Each point represents an average of values obtained from two muscles.

¹However, blockade of single twitches elicited by nerve stimulation required 16 mM pyridostigmine and depression of directly elicited muscle tensions was not observed with either single or repetitive stimulation up to the highest concentration examined (2 mM).

that pyridostigmine treatment under the conditions used in the present study does not alter sensitivities to either carbamate or organophosphate AChE inhibitors.

In vitro studies. One of the goals of the present investigation is to determine whether the ultrastructural alterations that pyridostigmine provokes at the motor endplate could lead to deficits in contractile strength. The results from the early recovery times following 14 days of (60 μ g/hr) pyridostigmine treatment indicate no residual impairment in muscle function when tested in vivo. Subacutely administered pyridostigmine should be excreted completely by 3 days of drug withdrawal (Birtley *et al.*, 1966), but the myopathies are still severe at this time (Hudson and Foster, 1984). Thus, the absence of residual deficits in contractility indicates that the muscle can compensate for the ultrastructural lesions.

Similar finding from in vitro contractility studies in diaphragm muscle is presented in Table 1. Indirect twitch and tetanic tensions were recorded at room temperature after removal of diaphragm muscles during and following subacute pyridostigmine treatment (60 μ g/hr). The muscles were washed extensively with control physiological solution for at least one hour to remove pyridostigmine and to allow for partial decarbamylation (Heyl *et al.*, 1980). As shown in Table 1, no significant reduction in contractile strength was detected on either pyridostigmine-treated or recovered animals. Results similar to these were found for all treatment and recovery times and for all stimulation frequencies examined.

TABLE 1

CONTRACTILE TENSION IN DIAPHRAGM OF RATS IMPLANTED WITH HIGH DOSE PYRIDOSTIGMINE

TREATMENT	MUSCLE TENSION (g)		
	0.1 Hz	20 Hz	
		INITIAL	FINAL
NONE	17.2 \pm 2.2 ^A (7/7)	45.1 \pm 3.2	48.2 \pm 5.6
3 DAY	17.0 \pm 2.2 (5/5)	53.0 \pm 8.6	55.8 \pm 7.4
7 DAY	17.4 \pm 0.7 (5/5)	52.6 \pm 2.8	57.8 \pm 1.4
14 DAY	20.3 (3/2)	52.5	51.3
1 DAY RECOVERY	15.1 (2/2)	41.1	43.0
14 DAY RECOVERY	21.5 (2/2)	59.5	57.7

NUMBER OF MUSCLES/NUMBER OF RATS SHOWN IN PARENTHESES.

^A MEAN \pm S.E.M.

Mechanisms underlying depression of muscle tension during repetitive stimulation. The characteristic actions of pyridostigmine on skeletal muscle function described in this study are an increase in single twitch tensions and depression of muscle tensions during high frequency nerve stimulation. The potentiation in the amplitude of single twitches appears to be a consequence of AChE inhibition (Clark *et al.* 1984). It is not clear, however, whether the depression during repetitive stimulation can be accounted for entirely on the basis of AChE inhibition. One way to investigate this problem is to examine the actions of pyridostigmine under conditions of normal AChE activity and

after AChE activity is abolished by pretreatment with the irreversible AChE inhibitor diisopropylfluorophosphate (DFP). The results of one such experiment are shown in Fig. 8. The records are from a diaphragm muscle stimulated indirectly at frequencies of 0.1 Hz and 20 Hz (center of each trace). In control solution a 20 Hz pulse gave rise to a sustained tetanic contraction. Tetanic tension was reduced after a 30 min exposure to 5 μ M pyridostigmine and depressed further after incubation with 10 μ M pyridostigmine. The preparation was then washed in drug free solution for 20 min which led to full recovery of tetanic tension. Next, the muscle was bathed in a solution containing 500 μ M DFP which led to a pronounced fade in tetanic tension such that the 10 sec tetanus appeared almost as brief as a single twitch. Restoration of tetanic tension after removal of excess DFP was seen 60 min after repeated washing of the preparation. Subsequent

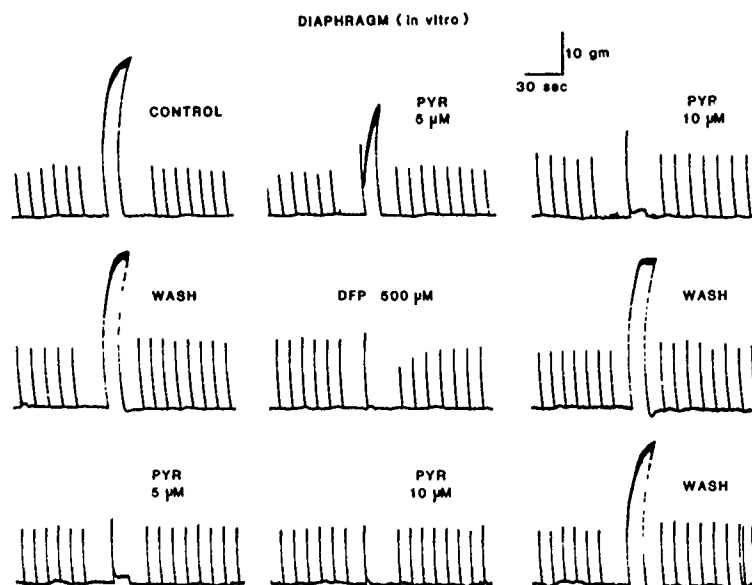


Fig. 8

Effect of pyridostigmine on in vitro twitch (0.1 Hz) and tetanic (20 Hz 10 sec) tensions in diaphragm muscle prior to and following exposure to DFP. Addition of 5 and 10 μ M pyridostigmine produced a concentration-dependent tetanic depression that was rapidly reversible (20 min) by washout. The addition of 500 μ M DFP, a concentration in excess of that required for complete AChE inhibition, produced a similar tetanic fade and subsequent depression of single twitch tensions. Washout of DFP for 60 min led to restoration of tetanic tension. Readmission of pyridostigmine still caused tetanic depression. These findings suggest that AChE inhibition alone is not sufficient to produce depression of tetanic tensions under the present experimental conditions. Note that the duration was 10 sec for all trains. This may not be evident during the presence of DFP and after the second exposure to 10 μ M pyridostigmine due to the rapid muscle relaxation in spite of continued nerve stimulation.

administration of pyridostigmine resulted in even more pronounced tetanic fade than that observed during the first application. A sustained tetanic contraction at 20 Hz was recorded after removal of pyridostigmine from the bath by repeated washing of muscle with drug-free physiological solution.

These results may be subject to two possible interpretations: first, since DFP was added 20 min after washout of 10 μ M pyridostigmine, only a fraction of the AChE sites would have been accessible to phosphorylation; the remainder would still be carbamylated and therefore protected from irreversible DFP action. During washout of DFP, spontaneous decarbamylation could generate sufficient AChE molecules to restore tetanic contractions. The reinduction of tetanic fade upon addition of pyridostigmine after washout of DFP would then result from inhibition of the newly decarbamylated AChE molecules.

Although the events outlined above no doubt occur, it is not clear that tetanic fade is caused solely by excess ACh. An alternative interpretation is that depression of muscle tension during high frequency repetitive stimulation results from a combination of excess ACh that accumulates during the train and a direct desensitizing action of the AChE inhibitor on the endplate receptor-ion channel complex. Thus the recovery from the effects of DFP may be the consequence of removal of the direct action of the organophosphate (Kuba *et al.*, 1974), while the reinduction of tetanic fade after addition of pyridostigmine may reflect the contribution of a direct desensitizing action of pyridostigmine (rather than the effect of additional AChE inhibition) (Pascuzzo *et al.*, 1984; Akaike *et al.*, 1984; Albuquerque *et al.*, 1984).

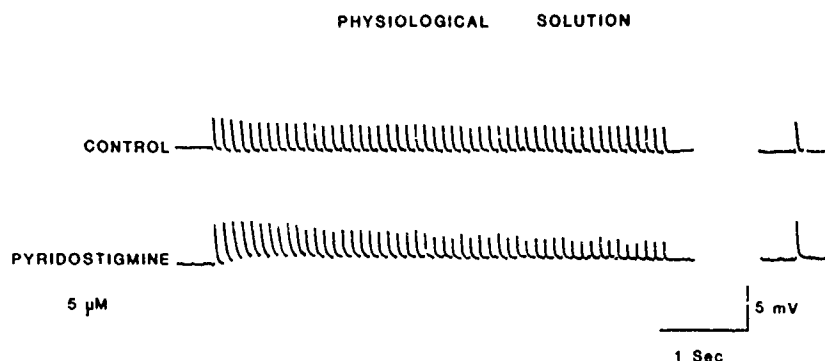


Fig. 9

Effect of pyridostigmine on EPP generation in a cut diaphragm nerve-muscle preparation. Under control conditions the EPP amplitude showed little or no decrement during a 10 Hz train. In the presence of 5 μ M pyridostigmine, the initial EPP amplitude was larger than control due to AChE inhibition, but successive EPP amplitudes became progressively depressed. The depression was accompanied by a persistent depolarization of the endplate region. Recovery from depression was observed after a 10 sec quiescent period as indicated by the isolated traces on the right.

To distinguish between these possibilities, the effects of pyridostigmine and DFP were examined on EPPs in the cut muscle preparation of the rat diaphragm by intracellular microelectrode techniques. Cut muscles were used in this case since their low resting potentials (-30 to -50 mV) ensure that the EPP amplitudes remain below the threshold for the generation of action potential and muscle contractions. Under control conditions, EPP amplitudes exhibited a slight depression during repetitive stimulation at a frequency of 10 Hz (Fig. 9). In the presence of $5 \mu\text{M}$ pyridostigmine the EPP amplitudes underwent a progressive desensitization, accompanied by a sustained endplate depolarization. The single trace following the train was recorded after a 10 sec quiescent period and shows restoration of the EPP amplitude. Desensitization could be reinstated, however, by repetition of the 10 Hz train, indicating that the phenomenon is frequency-dependent. Fig. 10 shows

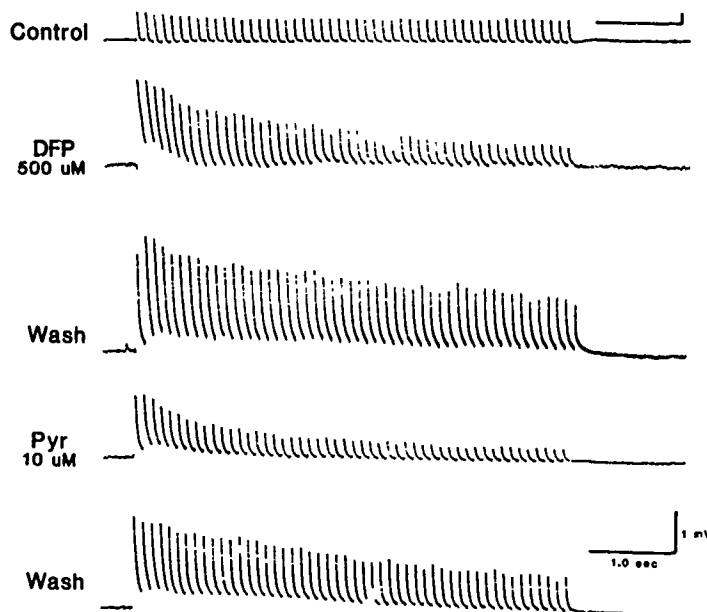


Fig. 10

Effects of pyridostigmine on EPPs recorded from transversely cut diaphragm muscle preparations. In control solution (top trace) a train of 50 EPPs at 10 Hz showed a slight depression in amplitude with no endplate depolarization. After a 30 min exposure to DFP there was a gradual decline in amplitude of EPPs throughout the train. This decline was accompanied by a large initial endplate depolarization with repolarization towards the end of 50 pulse train. Upon washout of DFP for 120 min (trace 3) the decline in the amplitude of successive EPPs was significantly reduced. At this point presumably all of AChE was still inhibited by the irreversible agent. When the preparation was subsequently exposed for 30 min to pyridostigmine (trace 4) results similar to those recorded in the presence of DFP were observed. The response to a 10 Hz train 30 min after removal of pyridostigmine is shown in the last trace. Note that although the rate of desensitization is reduced the concomitant endplate depolarization (presumably due to irreversible inhibition of AChE by DFP) still persists.

the effects of pyridostigmine on a preparation pretreated with DFP. In the presence of DFP (500 μ M), the EPP amplitudes underwent a marked desensitization during the 10 Hz train. The desensitization rate was substantially reduced after a 2 hr wash with physiological solution. It is unlikely that spontaneous dephosphorylation can account for the observed recovery (Kuba *et al.*, 1974). More likely, the recovery is due to removal of a direct desensitizing effect of DFP as demonstrated by Adler *et al.* (1984). The addition of 10 μ M pyridostigmine after washout of DFP caused an increase in the desensitization rate. Whereas washout of pyridostigmine resulted in a reduction in the desensitization kinetics. Since AChE is completely and irreversibly phosphorylated after addition of DFP, the partial recovery observed after washout of DFP and pyridostigmine must reflect the contributions of the direct effects of these inhibitors on the endplate receptor. The residual desensitization that persists after washout should then indicate the contributions of excess ACh in the desensitization process. The synergy between excess ACh and direct effects on desensitization produced by AChE inhibitors was initially proposed by Karczmar and Ohta (1981) and confirmed by Albuquerque and colleagues (Pascuzzo *et al.*, 1984; Akaike *et al.*, 1984). The latter authors have shown that pyridostigmine can convert nicotinic ACh receptors to a state where they bind agonists with higher than normal affinity. The excess ACh resulting from AChE inhibition during repetitive stimulation coupled with the increased binding affinity of the receptor for transmitter, appear to produce a desensitization rate that is sufficiently rapid to cause neuromuscular failure and hence a depression in nerve elicited muscle contractions.

Additional evidence that AChE inhibition alone is not sufficient to produce neuromuscular failure is provided in Fig. 11. The symbols denote the inhibition in AChE activity of rat diaphragm homogenates incubated with pyridostigmine. Inhibition can be detected in the presence of 10 nM pyridostigmine and is complete at 50 μ M ($IC_{50} = 0.18 \mu$ M). The EPP decay undergoes the first detectable prolongation in the presence of 1 μ M pyridostigmine (by 30%) and near maximal prolongation when the concentration of inhibitor is raised to 5 μ M. Further increases in pyridostigmine concentration produce little additional prolongation. If only AChE inhibition were responsible for neuromuscular failure, the summation of the EPP decays should be the sole determinant of the depolarization and desensitization observed during repetitive stimulation. Accordingly, the desensitization rates as well as the depression of muscle tensions during tetanic stimulation should be maximal with 5 μ M pyridostigmine. However, the data clearly show that the fade in tetanic tension is greater when the pyridostigmine concentration was raised from 5 to 10 μ M (Fig. 8).

The desensitizing effect of pyridostigmine can also be studied on ACh potentials elicited by brief (100 μ sec) microiontophoretic application of agonist on the junctional membrane. This technique has the advantage of allowing for controlled and accurate delivery of ACh. Fig. 12 shows the effects of pyridostigmine on 1 Hz trains of ACh potentials. The upper panel was obtained from one muscle fiber and shows the desensitization produced by 10 and 25 μ M pyridostigmine as well as recovery after wash. The lower panel shows data from another cell after addition of 2 and 5 μ M pyridostigmine.

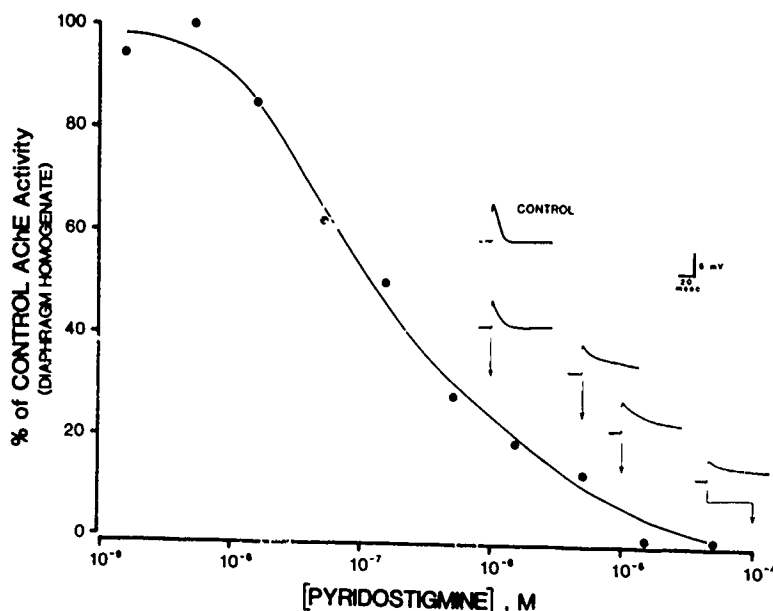


Fig. 11

Comparison of the muscle AChE inhibition induced by pyridostigmine with the effect of the drug on EPPs evoked in cut diaphragm nerve-muscle preparations. Each EPP was obtained from a separate muscle fiber. Pyridostigmine concentrations are indicated by the arrows. The solid circles represent means of triplicate determinations for inhibition of AChE activity in diaphragm muscle homogenates following 30 min incubations with pyridostigmine at 25°C.

In more recent work, using pulse frequencies up to 16 Hz, desensitization was found to occur with pyridostigmine concentrations as low as 1 μ M (Deshpande, Adler and Albuquerque, unpublished observations). The ability to elicit desensitization by exogenous application of ACh suggests that the depression in the EPP amplitude during repetitive stimulation (Fig. 10) is due to postsynaptic rather than presynaptic alterations.

SUMMARY AND CONCLUSIONS

1. Pyridostigmine produces an increase in the amplitude of single twitches and depresses the amplitude of contractions elicited by repetitive stimulation in mammalian skeletal muscle. The depression is produced by a depolarization and desensitization of the postjunctional membrane and results from a combination of accumulated ACh and a conversion of the ACh receptor to a high affinity agonist binding state.
2. The effects of pyridostigmine were qualitatively similar regardless of the route of administration or time of exposure. Recovery from subacute pyridostigmine treatment was complete within one day of withdrawal and no residual impairment of muscle contractility or sensitization to subsequent exposure to AChE inhibitors was observed.

RESPONSE AT 1 Hz ACh PULSE

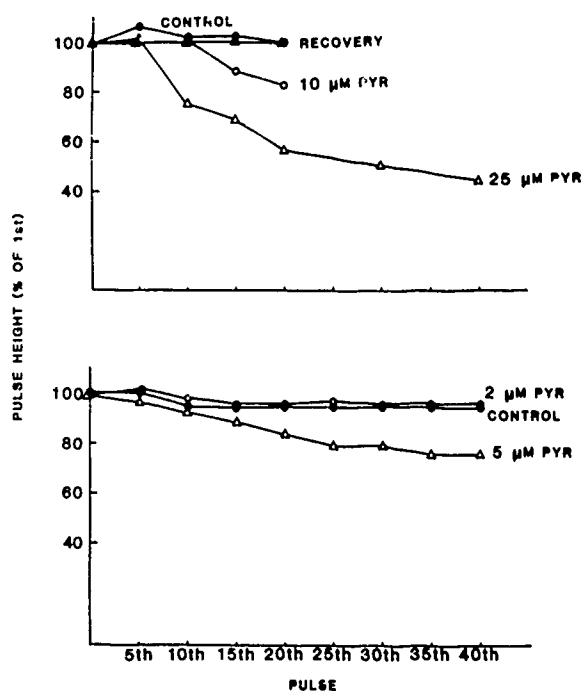


Fig. 12

Effect of pyridostigmine on junctional ACh potentials recorded by iontophoretic application of ACh in diaphragm muscle. Desensitization, as revealed by a decline in the ACh response during a train of 40 pulses, was evident after superfusion with 5 μ M pyridostigmine (lower panel). This desensitization was dependent on pyridostigmine concentration as shown by the large decline in successive ACh potential amplitudes with 10 and 25 μ M pyridostigmine exposure. Recovery from desensitization was observed after the muscle was bathed in physiological solution for 30-60 min. Note that pyridostigmine-induced desensitization was also accompanied by endplate depolarization (not shown).

ACKNOWLEDGEMENT

We are specially grateful to Dr. M. Filbert for allowing us to use her data on the effects of pyridostigmine on AChE activity in the diaphragm muscle. This enabled us to correlate changes in EPP time course with the changes in pyridostigmine concentration. The authors would like to thank Mrs. Deborah Green for assistance in analysis of data. This work was supported, in part, by the US Army Medical Research and Development Command Contract # DAMD 17-81-C-1279 (S.S.D. and E.X.A.) and by USAMRICD Protocol #1-05-2-03-A-073 (M.A., D.M. and R.E.F.).

REFERENCES

- Adler, M., Chang, F.-C. T., Maxwell, D., Mark, G., Glenn, J.F. and Foster, R.E. (1984) Effect of diisopropylfluorophosphate on synaptic transmission and acetylcholine sensitivity in neuroblastoma-myotube co-culture. In: Dynamics of Cholinergic Function, Plenum, N.Y., in press.
- Albuquerque, E.X. and McIsaac, R.J. (1970) Fast and slow mammalian muscles after denervation. *Exp. Neurol.* 26:183-202.
- Albuquerque, E.X., Akaike, A., Shaw, K.-P. and Rickett, D.L. (1984) The interaction of anticholinesterase agents with the acetylcholine receptor-ion channel complex. *Fund. Appl. Toxicol.* 4:527-533.
- Akaike, A., Ikeda, S.R., Brookes, N., Pascuzzo, G.J., Rickett, D.L. and Albuquerque, E.X. (1984) The nature of the interactions of pyridostigmine with the nicotinic acetylcholine receptor-ionic channel complex. II. Patch clamp studies. *Mol. Pharmacol.* 25: 102-112.
- Barstad, J.A.B. and Lillekeil, G. (1968) Transversely cut diaphragm preparation from rat. *Arch. Int. Pharmacodyn.* 175:373-390.
- Berry, W.K. and Davies, D.R. (1970) The use of carbamates and atropine in the protection of animals against poisoning by 1,2,2-trimethylpropyl-methylphosphonofluoridate. *Biochem. Pharmacol.* 19:927-934.
- Birtley, R.D.N., Roberts, J.B., Thomas, B.H. and Wilson, A. (1966) Excretion and metabolism of [14 C]-Pyridostigmine in the rat. *Brit. J. Pharmacol.* 26:393-402.
- Clark, A.L., Hobbiger, F. and Terrar, D.A. (1984) Nature of the anticholinesterase-induced repetitive response of rat and mouse striated muscle to single nerve stimuli. *J. Physiol. (Lond.)* 349:157-166.
- Costa, L.G., Schwab, B.W. and Murphy, S.D. (1982) Tolerance to anticholinesterase compounds in mammals. *Toxicol.* 25:79-97.
- Gall, D. (1981) The use of therapeutic mixtures in the treatment of cholinesterase inhibition. *Fund. Appl. Toxicol.* 1:214-216.
- Grimby, L. (1984) Firing properties of human motor units during locomotion. *J. Physiol. (Lond.)* 346:195-202.
- Heyl, W.C., Harris, L.W., and Stitcher, D.L. (1980) Effects of carbamates on whole blood cholinesterase activity: chemical protection against soman. *Drug and Chem. Toxicol.* 3:319-332.
- Hudson, C.S. and Foster, R.E. (1984) Ultrastructural pathology in mammalian skeletal muscle following acute and subacute exposure to pyridostigmine. Studies of dose-response and recovery. (This volume).
- Karczmar, A.G. and Ohta, Y. (1981) Neuromyopharmacology as related to anticholinesterase action. *Fund. Appl. Toxicol.* 1:135-142.

- Kuba, K., Albuquerque, E.X., Daly, J. and Barnard, E.A. (1974) A study of the irreversible cholinesterase inhibitor, diisopropylfluorophosphate, on time course of endplate currents in frog sartorius muscle. *J. Pharmacol. Exp. Ther.* 189:499-512.
- Meshul, C.K., Deshpande, S.S., Boyne, A.F. and Albuquerque, E.X. (1983) Effects of chronic administration of pyridostigmine at the neuromuscular junction. *Abs. Soc. Neurosci.* 9:1026.
- Pascuzzo, F.J., Akaike, A., Maleque, M.A., Shaw, K.-P., Aronstam, R.S., Rickett, D.L. and Albuquerque, E.X. (1984) The nature of the interactions of pyridostigmine with the nicotinic acetylcholine receptor-ionic channel complex. I. Agonist, desensitizing, and binding properties. *Mol. Pharmacol.* 25:92-101.
- Siakotas, A.N., Filbert, M. and Hester, R. (1969) A specific radioisotopic assay for acetylcholinesterase and pseudocholinesterase in brain and plasma. *Biochem. Med.* 3:1-12.
- Tiedt, T.N., Albuquerque, E.X., Hudson, C.S. and Rash, J. E. (1978) Neostigmine-induced alterations at the mammalian neuromuscular junction. I. Muscle contraction and electrophysiology. *J. Pharmacol. Exp. Ther.* 205:326-339.

III. Skin Injury and Protection

NONINVASIVE METHODS FOR ASSESSING SKIN TRAUMA

A.E. Meyer, B.S.⁺, R.E. Baier, Ph.D.⁺, H.B. Hammili, M.S.⁺,
C.K. Akers, Ph.D.⁺, and A.A. Kyriakopoulos, M.D.^{*}

Advanced Technology Center, Calspan Corporation⁺,
and Bristol Myers Research (Dermatology)^{*},
Buffalo, NY

Introduction

We are engaged in an interdisciplinary research effort to establish a series of complementary noninvasive and, in some cases, noncontacting tools for assessing skin trauma in relevant clinical or field circumstances. This manuscript briefly introduces the successful methods already identified and provides typical data from preliminary experiments with human subjects.

Building from an extensive data base developed earlier for the in situ analysis of protective creams and ointments applied to human skin, the method of internal reflection infrared spectroscopy is first introduced and exemplified, comparing its yield with that reflective UV/visible measurements and scanning electron microscopy. Then, using the model of sunburned human skin as a typical example of erythema that might characterize other cases of skin trauma, measurements by infrared, UV/visible, replication, photogrammetric, and remote sensing methods are presented and compared. Considerable promise is indicated for the noncontacting, remote radiometric technique utilizing a device called a Spotmeter for first assessment and subsequent monitoring of erythematous responses of human skin. A significant collection of data is included to illustrate these results.

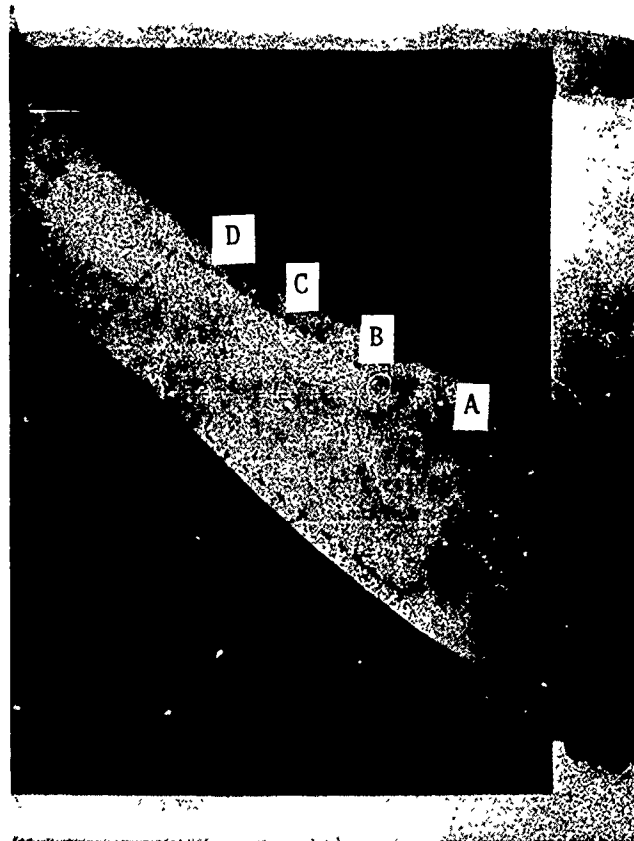
Finally, future research needs are highlighted regarding the objective characterization of traumatized skin, assessment of protective lotion effectiveness, differentiation of traumatized skin states, image processing for skin texture analysis, and automation of spectral record analysis. An appendix briefly reviews the relevant photometric theory and color analytics utilized.

Methods

The analytical techniques utilized for this ongoing study include internal reflection infrared spectroscopy, ultraviolet and visible spectroscopy, spot meter reflectance ratios, photogrammetry, and skin replication followed by scanning electron microscopy. All measurements are made according to a timed schedule and the measurements can be completed, after careful planning and instrument calibration, within the course of one workday for each subject.

Typically, one forearm of the subject is marked into separate areas for the purpose of making a particular type of measurement on the same area through time. Figure 1 is a photograph of the subject area, showing the different measurement sectors. The spot meter, UV, and visible spectrometer methods are remote (i.e., both noninvasive and noncontacting); the IR spectrometer and replication techniques, while noninvasive, do require contact of the subject area with the analytical device.

Prior to application of protective lotions, all measurements are made on the subject area to serve as "baseline" data.



A: SPOT METER
B: IR SPECTRA

C: VISIBLE & UV SPECTRA
D: REPLICAS (4 DIFFERENT AREAS)

Figure 1 MEASUREMENT SECTORS

Typical Results

Protective Lotion Studies:

As documented in Figures 2 and 3, the UV and visible spectroscopic data obtained do not usually show significant changes in skin surface reflectance as the experiment proceeds. Similarly, spot meter measurements are not influenced by application of the lotion. These preliminary results are encouraging in that they demonstrate that simple "glint" of the smoothed lotion-modified skin does not affect the quality of the spectrophotometric measurements expected to be important in later analyses of protective effects.

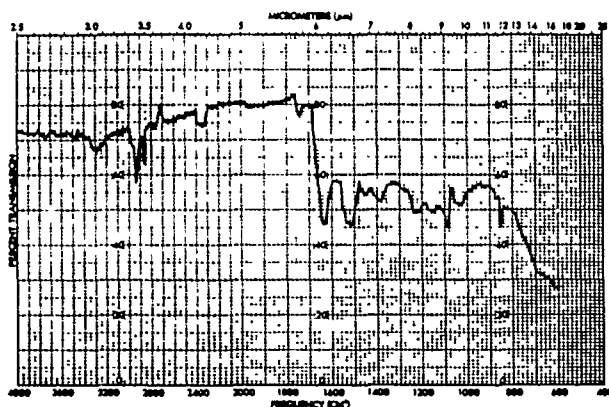
The data of most interest are those obtained from infrared spectroscopy. The raw data shown in Figure 4 demonstrate a decrease with time in the amount of lotion on the surface of the skin. The absorption band in the 3300 cm^{-1} region is not attributable to excess lotion.

The computer-aided technique of "spectrum subtraction" is most useful for the skin/lotion experiments. Point-by-point subtracting of one spectrum from another allows one to define significant areas of change. Figure 5 illustrates a series of such subtractions ("deltas") all derived in the same manner. The deltas resulted from subtracting the spectrum of the residue on the analytical prism (after a skin measurement) from the spectrum of the skin. The residue is the unassociated material that was "on" the skin rather than "in". Therefore, the deltas in Figure 5 represent the skin as fortified by materials closely associated with it (absorbed lotion, retained water, etc.).

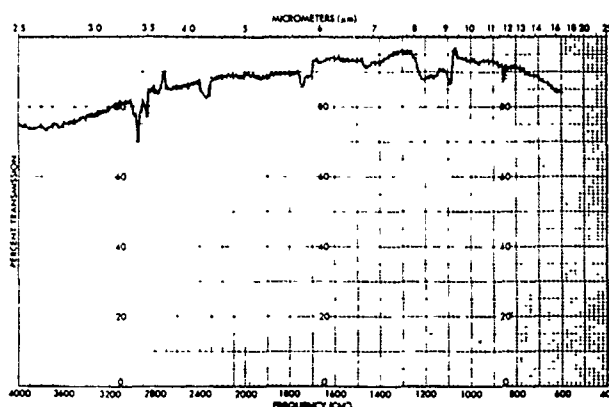
Another set of subtraction results is shown in Figure 6, as obtained by subtracting Scan A (Figure 5) from Scans B, C, D (Figure 5). In effect, the deltas in Figure 6 represent only the extraneous or excess materials most closely associated with the skin, the skin signature itself having been subtracted. Although the results are preliminary, the absorption in the 3300 cm^{-1} region indicates that water is being held at the surface or within the epidermal layer of the skin.

Replicas of control and treated areas were obtained using a replicating material selected after a careful series of comparative studies of replication fidelity. Scanning electron microscope photomicrographs of the replicas are given in Figure 7. Within one hour of lotion application, the replicas showed the skin to have retained excess lotion as unspread globules; the epidermal grooves in the skin were not well-defined. Four hours after lotion application, there was little excess lotion present and the skin "pads" appeared to be plump and smooth. The skin grooves were better defined than at 0.7 hr, but less "stressed" than before lotion application.

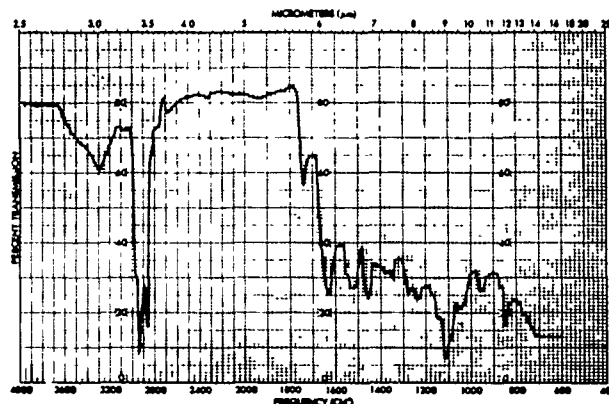
The "globules" of lotion on the skin can be explained by the results of separate surface tension analyses of the lotion. The lotion, as a whole, has an apparent surface tension of approximately 50 dynes/cm. Clean human skin generally has a critical surface tension less than 38 dynes/cm. Because the lotion has a higher surface tension than normal skin, the lotion will not spontaneously spread on skin, but will spontaneously retract with time into



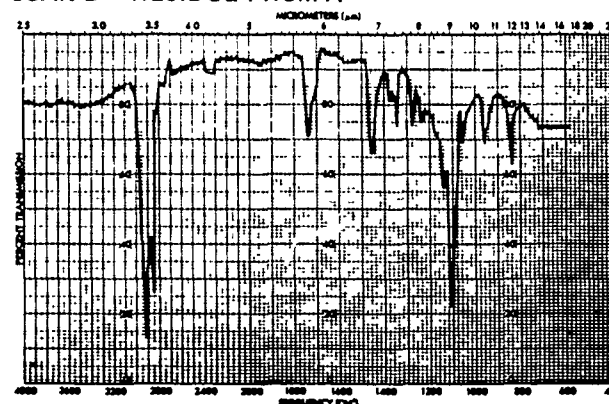
SCAN A - NO LOTION



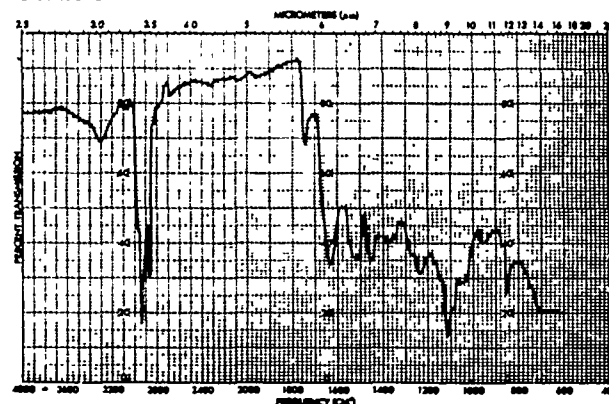
SCAN B - RESIDUE FROM A



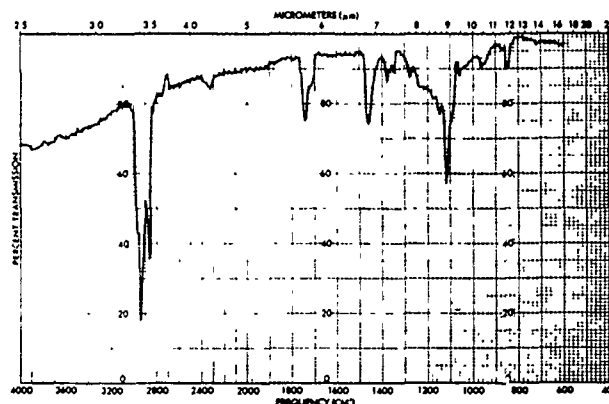
SCAN C - 0.6 HR AFTER LOTION APPLICATION



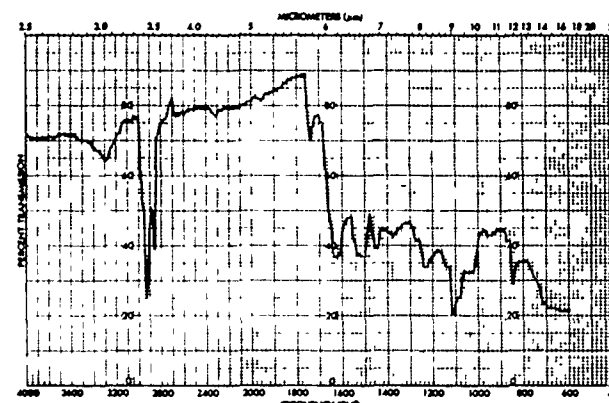
SCAN D - RESIDUE FROM C



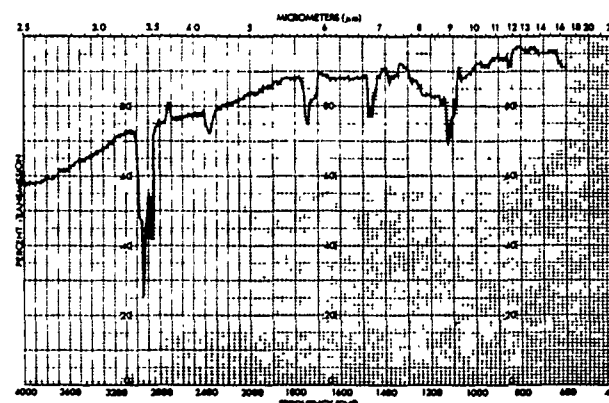
SCAN E - 3.7 HRS AFTER LOTION APPLICATION



SCAN F - RESIDUE FROM E

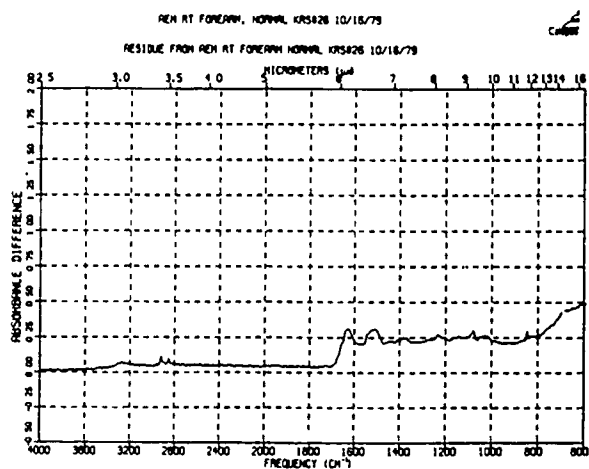


SCAN G - 5.6 HRS AFTER LOTION APPLICATION

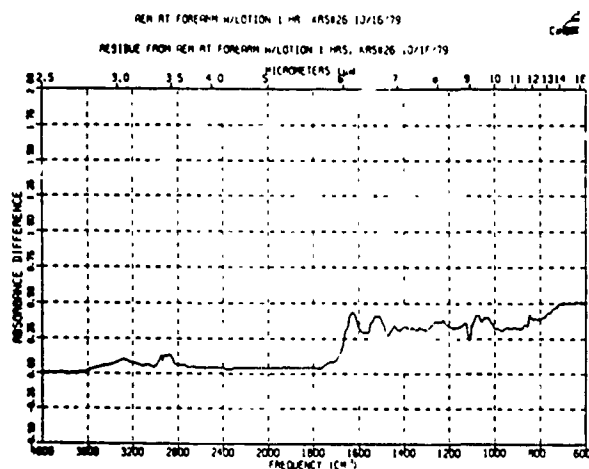


SCAN H - RESIDUE FROM G

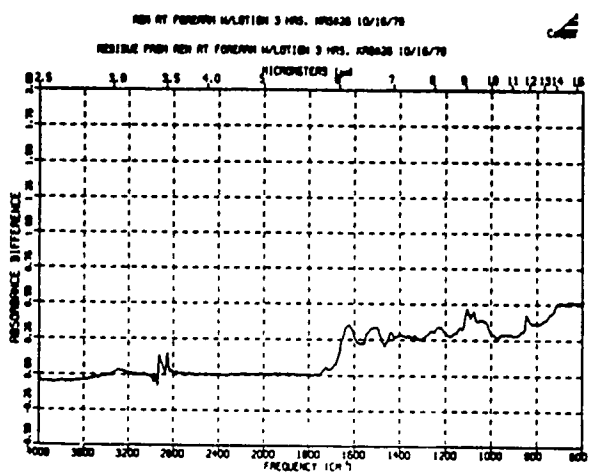
Figure 4 PROTECTIVE LOTION STUDY - INFRARED SPECTRA OF SKIN AND RESIDUE



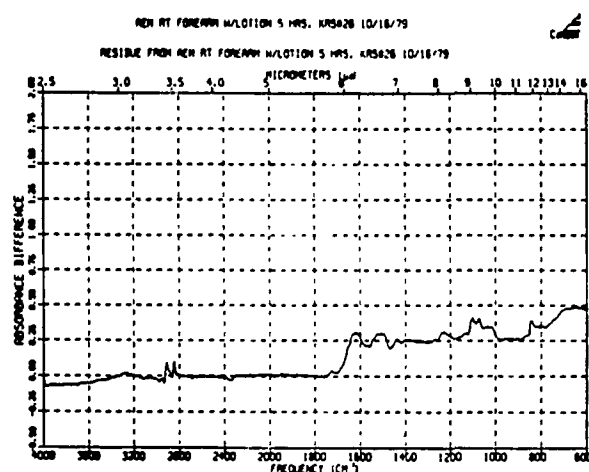
DELTA A - NO LOTION



DELTA B - 0.6 HR AFTER LOTION APPLICATION



DELTA C - 3.7 HRS AFTER LOTION APPLICATION



DELTA D - 5.6 HRS AFTER LOTION APPLICATION

Figure 5 PROTECTIVE LOTION STUDY - INITIAL SPECTRUM SUBTRACTIONS, RESULTING IN "SKIN + ASSOCIATED MATERIALS"

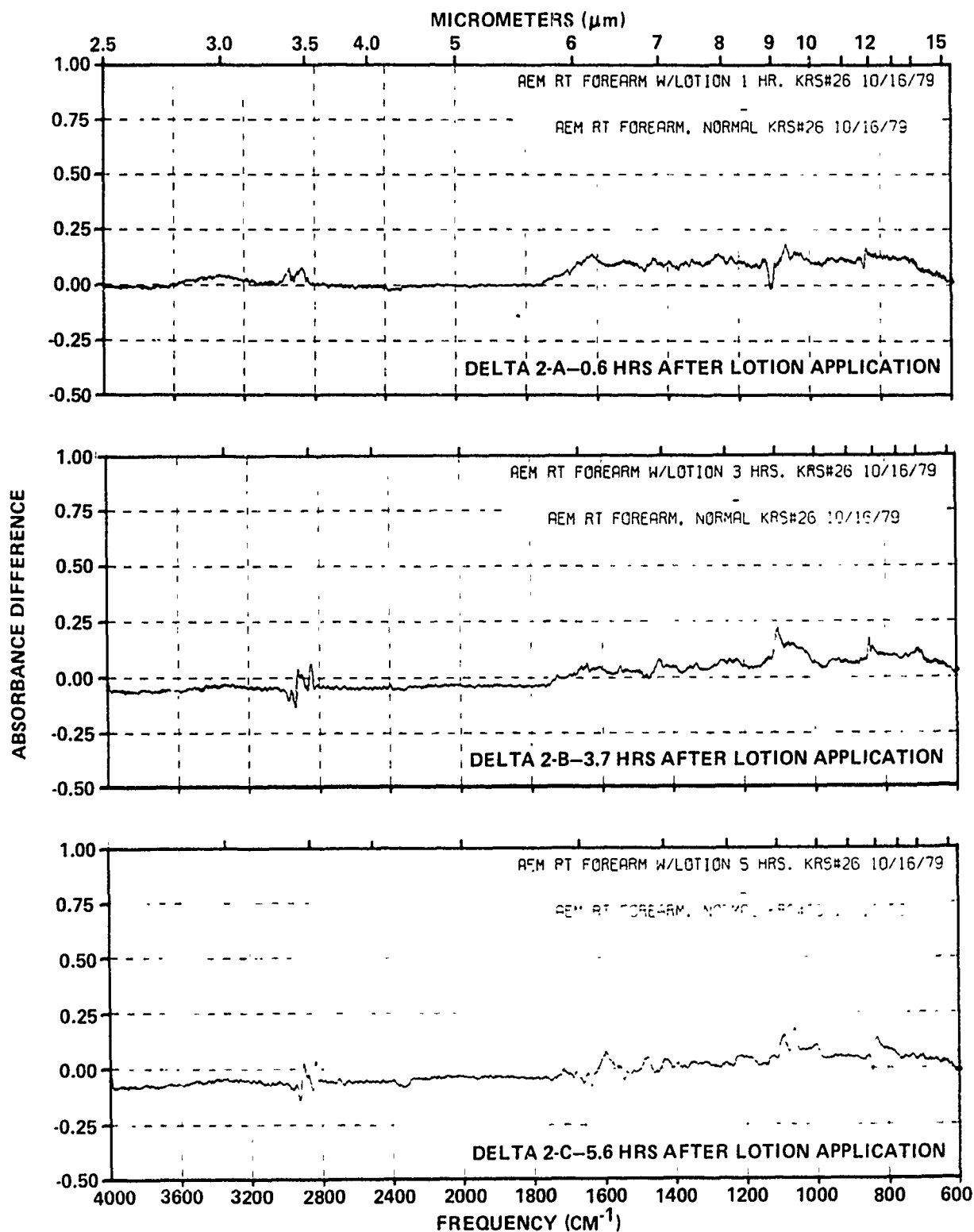
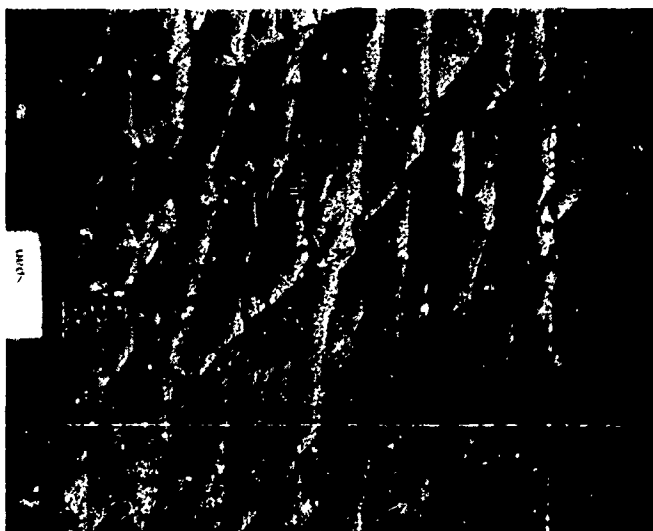


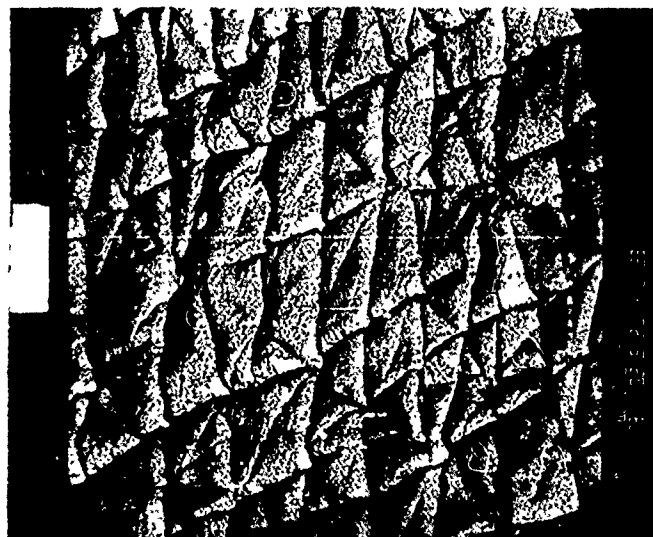
Figure 6 PROTECTIVE LOTION STUDY - FINAL SPECTRUM SUBTRACTIONS, RESULTING IN "ASSOCIATED MATERIALS"



AEM R FOREARM-NO LOTION-10/16/79-30X



AEM R FOREARM-0.7 HR AFTER LOTION -
10/16/79-30X



AEM R FOREARM-4 HRS AFTER LOTION -
10/16/79-30X

Figure 7 DRY SKIN/LOTION STUDY — SEM PHOTOMICROGRAPHS OF SKIN REPLICAS

globules, like those observed. Reformulation of such lotions to exhibit slightly lower operational surface tensions should result in more effective, uniform, and permanent spreading on skin surfaces.

In earlier Calspan research efforts, the persistence of moisturizing preparation applied to human skin was assessed using the internal reflection infrared spectroscopic technique. One interesting result was objective demonstration of the product's presence in the epidermal zone of a female volunteer for at least 3 days. This objective demonstration of product retention, coupled with the subject's impression of continued efficacy over the same period, is especially noteworthy when the additional fact is considered that two regular morning showers intervened between product application and the final skin analysis.

Contrary to expectation, our spectroscopic signatures of "dry" skin in situ on three male volunteers (one with simple Winter scaling and itching, one with ichthyosis, and one with keratosis) revealed the average condition of 10 cm² surface zones to be more "moist" than the skin of both normal control subjects and subjects having used "moisturizing" preparations. This judgment is based on the appearance of substantial absorption bands for water's hydroxyl groups, revealing apparently "dry" skin to be -- at least -- transpiring moisture at higher rates than normal or treated skin. It is of great importance to determine, in future work, the micro-architecture of "dry" skin zones to assess the nature of structural defects which might be responsible for the anomalous high water content. Our novel surface texture determinations, using Calspan's patented SCRIMAGE technique, will be of considerable help in this regard.

Erythema Studies:

The measurements from this study were taken primarily on two areas of a subject's right forearm: (1) an "unexposed" middle area which was shielded from the direct rays of the sun by a deliberately located wristwatch and (2) an exposed area on the forearm between the protected area and the elbow (see Figure 8). Some photometric, spot meter, remote sensing, and surface texture data were also taken on the exposed forearm area between the wristwatch and the hand, as well as on the exposed forehead, abdominal, and chest areas. All measurements on the forearm were taken on the relatively hairless, inside surface of the arm, which was deliberately positioned during the exposure period to receive continuous direct illumination from the nearly vertical sun.

The infrared and ultraviolet spectroscopic records showed only minor sensitivity to changes in the "sunburned" skin. Internal reflection IR spectroscopy revealed only a slight loss of natural "oils" from the exposed skin surface, which slowly recovered its natural (control) condition during the recovery phase. The methods based on the visible portions of the electromagnetic spectrum (spot meter, densitometer, and visible spectrometer) provided the most meaningful data on erythema. Scanning electron microscopy of routine skin replicas was also rewarding.



Figure 8 ERYTHEMA STUDY - REB RIGHT FOREARM

Figures 9-12, show a variety of the SEM photomicrographs obtained. The whiter areas in the photomicrographs are desquamated cells that adhered to the replicating material when it was removed from the skin. In Figure 9, the unexposed and exposed areas are compared 24 hours after exposure. Of greatest interest is the difference shown between the epidermal grooves in the exposed and unexposed areas. The grooves in the exposed skin appear to be more wrinkled and stressed, perhaps due to microedema or swelling of the skin pads. In Figure 10, showing exposed and unexposed areas three days after the burn, it appears that the grooves are approaching a more normal state. Figure 11 gives a view of the forehead skin one day after exposure. At this magnification level, the forehead skin does not appear to be as stressed as the forearm skin; in all likelihood this is due to the productivity of the sebaceous glands in the forehead, which lubricate and keep the skin relatively smooth, and to the protective effect of previously developed melanin pigment in an area more often exposed to the sun's rays. Figure 12 compares the exposed skin on the abdomen at two days and 13 days after exposure. At 13 days, the epidermal cells are peeling away, giving the replica a flat, "crinkled" look.

Of great potential use to the research project is a Calspan-patented technique called "Scrimage". In this technique, SEM micrographs are used to produce true-height measurements. Roughness, height frequency, and height probability are some of the quantities that can be derived from the method. An example of the Scrimage technique using a skin replica is given in Figure 13. Because the technique is non-contacting, time-consuming secondary replication with hard materials is not necessary in the Calspan process as it is in all prior-art techniques that use mechanical profiling with stylus probes.

Photometric Data:

A sensitometric wedge was placed on each roll of film used in the study and photographs were taken at days 1, 2, 3 and 13 after exposure to the sun. The various areas of the arm were analyzed in three bands (red, green and blue) using a Macbeth Quantalogue densitometer with a 1 micron probe, as was the step wedge on each roll of film.

From the step wedge densities and exposures, the D-log E curve was developed for each roll of film. The readings on the various areas of the skin were converted to absolute exposures. Since there was no way to calibrate the film for camera flare, transmission or amount of incident light, all data reduction was done in exposure space as opposed to reflectance space.

In order to account for overall brightness of the skin, a type of ratio was developed and defined as "Relative Exposure". This ratio was defined as:

$$\text{RELATIVE RED EXPOSURE} = \text{RED EXPOSURE} / \sum \text{EXPOSURES}$$

$$\text{RELATIVE GREEN EXPOSURE} = \text{GREEN EXPOSURE} / \sum \text{EXPOSURES}$$

$$\text{RELATIVE BLUE EXPOSURE} = \text{BLUE EXPOSURE} / \sum \text{EXPOSURES}$$

Where $\sum \text{Exposures} = \text{Red Exposure} + \text{Green Exposure} + \text{Blue Exposure}$



REB R FOREARM/UNBURNED-09/26/79-30X



REB R FOREARM/UNBURNED-09/26/79-100X



REB R FOREARM/SUNBURN
AFTER 1 DAY-09/26/79-30X



REB R FOREARM/SUNBURN
AFTER 1 DAY-09/26/79-100X

Figure 9 SEM PHOTOMICROGRAPHS OF R FOREARM - 24 HOURS AFTER EXPOSURE



REB R FOREARM/UNBURNED-09/28/79-30X



REB R FOREARM/UNBURNED-09/28/79-100X



REB R FOREARM/SUNBURN AFTER 3 DAYS -
09/18/79-30X



REB R FOREARM/SUNBURN AFTER 3 DAYS -
09/28/79-100X

Figure 10 SEM PHOTOMICROGRAPHS OF R FOREARM - 3 DAYS AFTER EXPOSURE



REB FOREHEAD-09/26/79-30X



REB FOREHEAD-09/26/79-100X

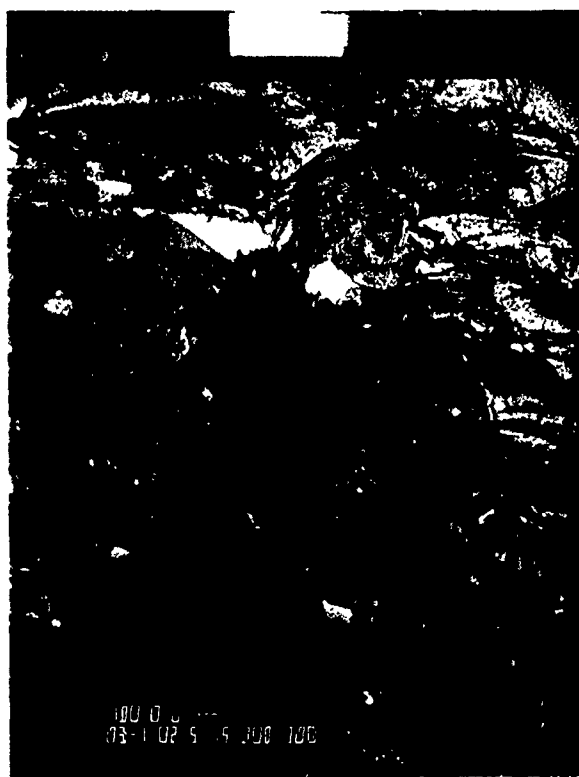
Figure 11 SEM PHOTOMICROGRAPHS OF FOREHEAD – 24 HOURS AFTER EXPOSURE



REB ABDOMEN/SUNBURN AFTER 2 DAYS -
09/27/79-30X



REB ABDOMEN/SUNBURN AFTER 2 DAYS -
09/27/79-100X



REB ABDOMEN/SUNBURN AFTER 13 DAYS
(PEELING) - 10/08/79-30X



REB ABDOMEN/SUNBURN AFTER 13 DAYS
(PEELING) - 10/08/79-100X

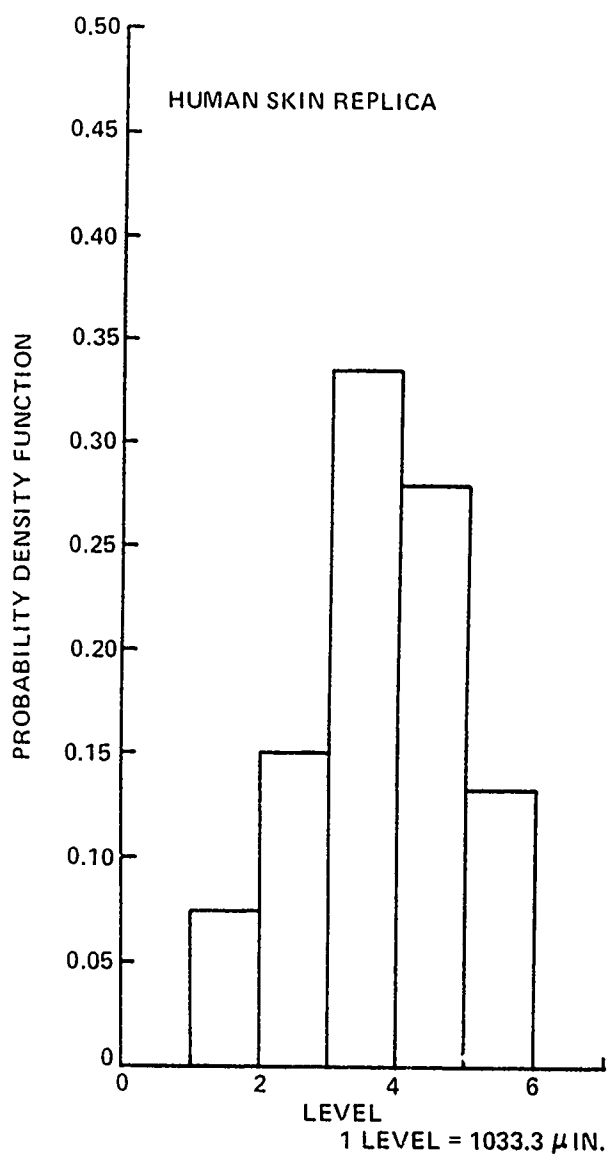
Figure 12 SEM PHOTOMICROGRAPHS OF ABDOMEN – 2 AND 13 DAYS AFTER EXPOSURE

No. 6 @ 30X

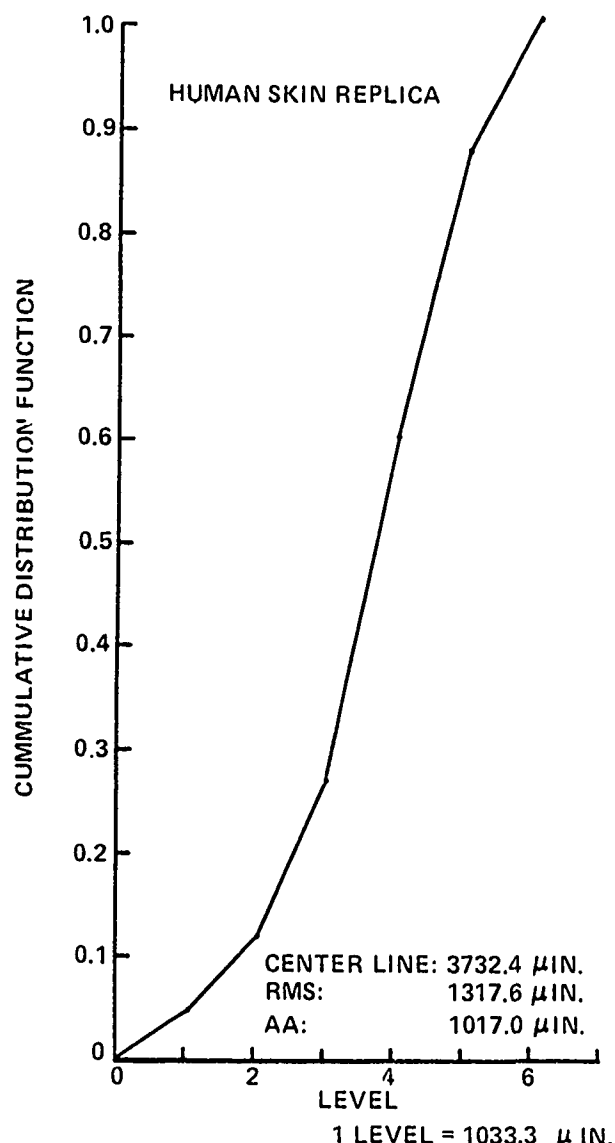


100.0 0 H
03-1 30.0 20 212 33-

PROFILE FROM SKIN REPLICA



RESULT: PROBABILITY DENSITY FUNCTION



RESULT: CUMULATIVE DISTRIBUTION FUNCTION

Figure 13 SEM SCRIMAGE TECHNIQUE

The absolute exposures for this study are recorded in Table 1. The control area of Subject 1 (REB) was the area previously discussed as being shaded from the sun by a wrist watch. The elbow area and wrist area were burned areas. For the sake of comparison, a fairer-skinned person with no sun exposure was included as Subject 2.

Plots of these absolute exposures against time can be seen in Figure 14 for the red band, Figure 15 for the green band and Figure 16 for the blue band. The plots indicate that a general darkening of the skin is a result of sunburn, and that recovery back to "normal" is a slow process. However, since lighting and film conditions may have altered through the study period, no absolute conclusions may be made from this preliminary experiment.

Table 2 contains the relative exposures for all of areas of Subjects 1 and 2. Figure 17 contains the plots of this data for Subject 1 against time. These plots reveal some very interesting phenomena.

The relative value of the red band is, as expected, much higher in the sunburned areas than in the control area, i.e., the area is reflecting proportionally more red light. Even though the sunburned areas may be reflecting less total light (i.e., are darker), they appear "bright red" to the human eye. The red ratio "recovers" by returning over time to the red ratio of the unexposed area. Recovery of the ratio begins at day 1. It is interesting to note that the wrist area, which is exposed more consistently to light throughout the year recovers more quickly than the area on the inside of the elbow.

The green band ratio, as well as the blue band ratio, is reduced by the sunburn. This means that the percent of total reflectivity attributable to those wavelengths is decreased. Again both bands recover with time, the green band more quickly than the blue.

Finally it is interesting to note on Table 2 that, despite Subject 2's greater overall brightness, the ratios are very similar to Subject 1.

Visible Spectrometry Data:

Some overlays of the visible spectra that were obtained from Calspan's Beckman DK2A reflectance spectrometer (with integrating sphere) are given in Figure 18. In each view, the solid line is the scan of the exposed forearm (between wristwatch and elbow) and the dashed line is the scan of the unexposed area (under the wristwatch). It is apparent that, except for Day 1, the "red" areas of the spectra (600-700 mμ) remain fairly constant. The "green" and "blue" areas (400-600 mμ), however, change considerably in the two weeks following exposure with respect to overall % reflectance and to the strong absorbances at 530 and 570. The trends in these data parallel those in the data from the spot meter and remote sensing/photometer methods.

Figure 19 is a plot of the % reflectance values at specific wavelengths (600 mμ-"red", 560 mμ-"green", 440 mμ-"blue") for both the burned and unburned skin through time. Figure 19 (spectrometric data) can be compared

TABLE 1
REB POST-EXPOSURE
ABSOLUTE EXPOSURE

		<u>RED</u>	<u>GREEN</u>	<u>BLUE</u>
<u>Control</u>				
(Subject 1)	Day 1	122.1	106.8	109.8
	Day 2	111.0	99.2	100.5
	Day 3	106.1	92.3	93.5
	Day 13	110.2	97.0	100.5
<u>Elbow Area</u>				
(Subject 1)	Day 1	69.0	40.3	39.1
	Day 2	56.3	37.0	34.0
	Day 3	49.7	34.2	31.2
	Day 13	62.8	46.2	38.9
<u>Wrist Area</u>				
(Subject 1)	Day 1	70.6	42.0	40.6
	Day 2	67.6	45.2	41.0
	Day 3	59.5	41.4	37.6
	Day 13	66.2	68.7	41.4
(Subject 2)	Average	114.0	101.5	112.0

TABLE 2
REB POST-EXPOSURE
RELATIVE EXPOSURE

		<u>RED</u>	<u>GREEN</u>	<u>BLUE</u>
<u>Control</u>				
(Subject 1)	Day 1	.361	.315	.324
	Day 2	.357	.319	.324
	Day 3	.364	.316	.320
	Day 13	.353	.315	.327
<u>Elbow Area</u>				
(Subject 1)	Day 1	.465	.272	.263
	Day 2	.440	.292	.268
	Day 3	.432	.297	.271
	Day 13	.425	.312	.263
<u>Wrist Area</u>				
(Subject 1)	Day 1	.461	.274	.265
	Day 2	.440	.294	.266
	Day 3	.430	.299	.271
	Day 13	.375	.390	.235
(Subject 2)	Average	.349	.310	.341

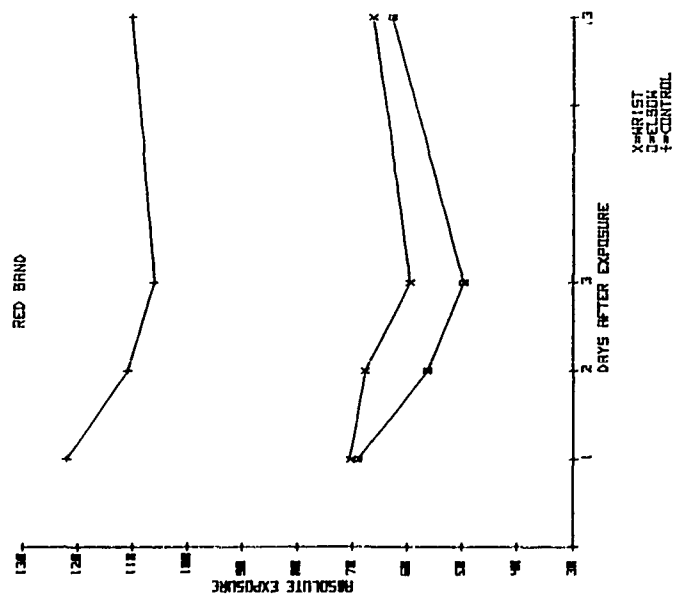


Figure 14 REB POST-EXPOSURE, RED BAND

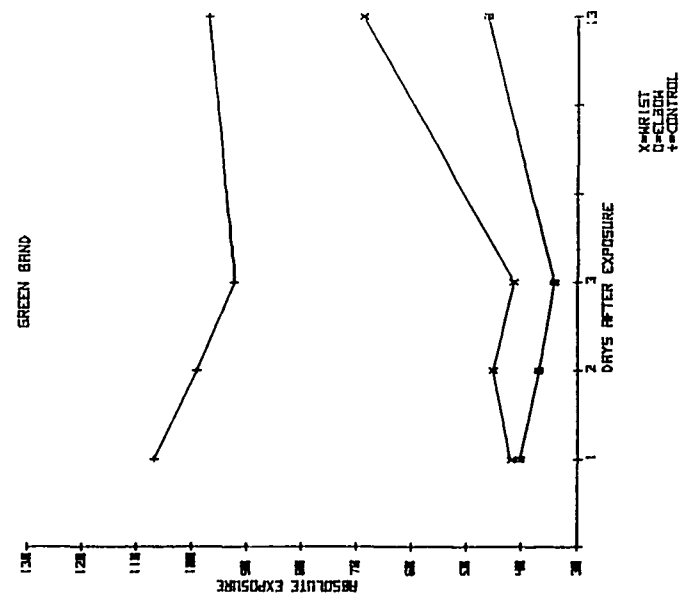


Figure 15 REB POST-EXPOSURE, GREEN BAND

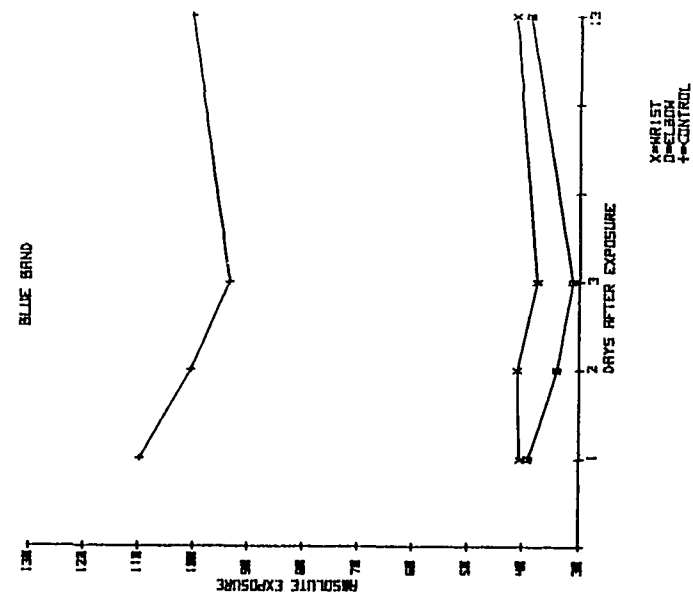
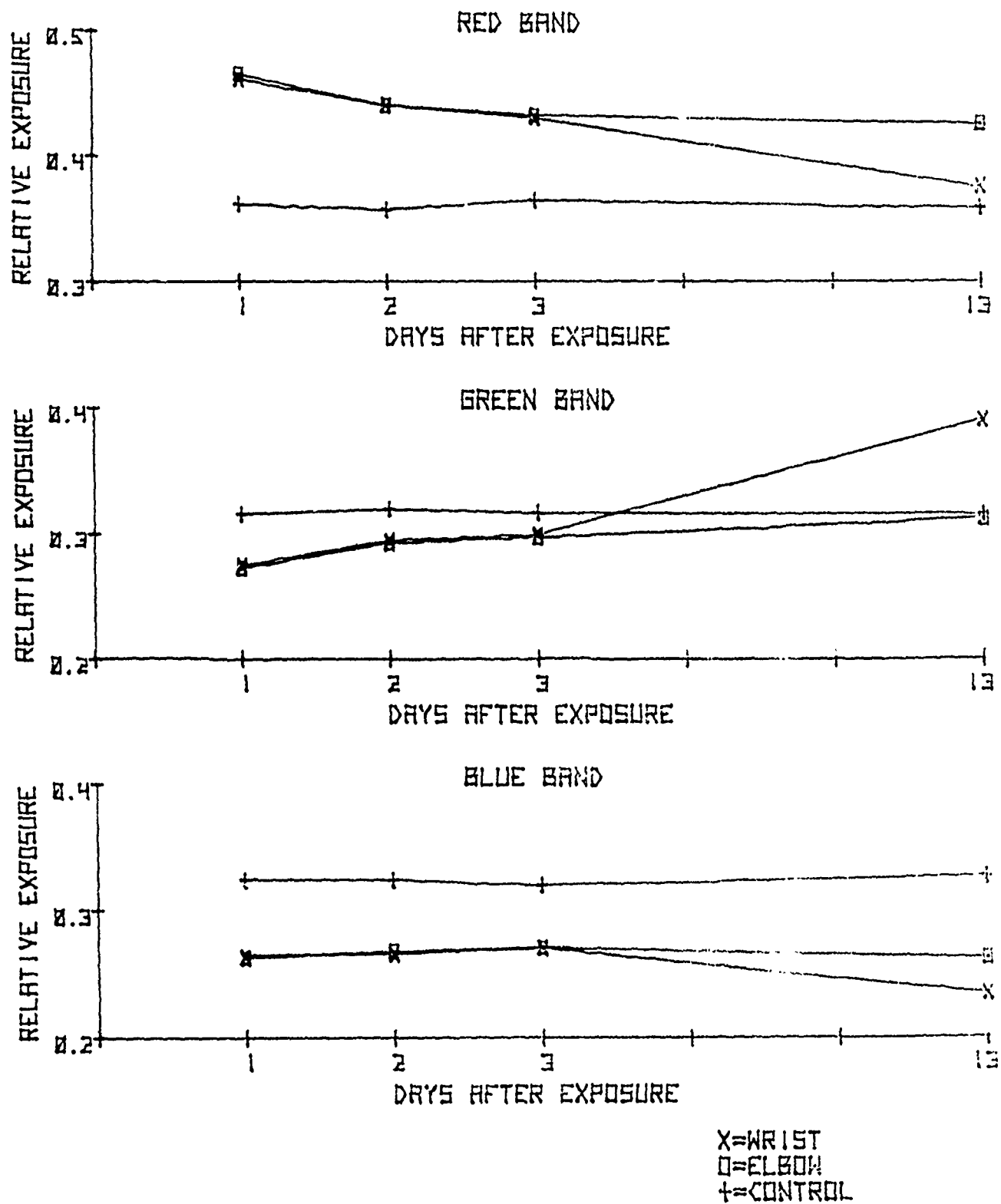


Figure 16 REB POST-EXPOSURE, BLUE BAND

Figure 17 REB POST-EXPOSURE, RELATIVE EXPOSURE



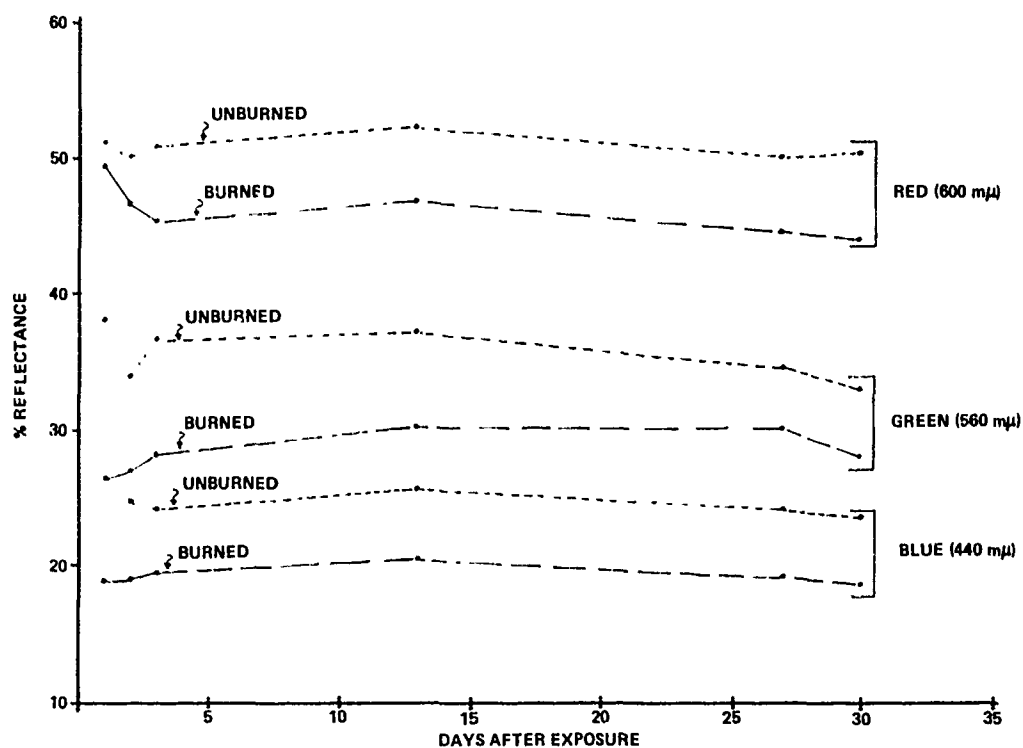


Figure 19 VISIBLE DATA - % REFLECTANCE - REB R FOREARM - EXPOSED AND UNEXPOSED

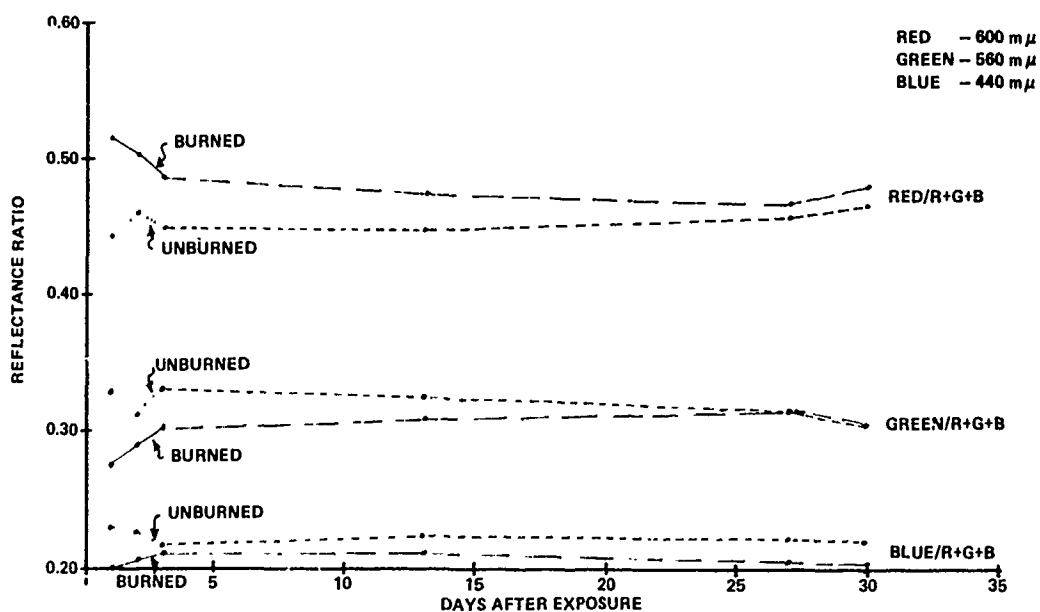


Figure 20 VISIBLE DATA - REFLECTANCE RATIOS - REB R FOREARM - EXPOSED AND UNEXPOSED

with Figures 14-16 (photometric data). Figure 20 plots the reflectance ratios at the specific wavelengths through time and can be compared with Figure 17. It is apparent that the "green" portion of the spectrum "recovers" more quickly than the "red" or "blue." Figure 21 is a planar plot of all of the reflectance ratios obtained from the spectrometric data and can be compared to the chromaticity plot of the spot meter data (Figure 26).

All these data verify the supposition that "sunburn" is associated with increased blood flow in the near-surface skin. One would expect that the additional blood would increase reflectivity in the red portion of the spectrum for as long as the sunburn persists; the data presented above show that this is not the case. Instead, the sunburn response is primarily greater absorption at certain wavelengths in the blue and green portions of the spectrum. Figure 22 is an overlay of visible spectra of fresh blood; the similar undulations to those seen in the blue-green area when erythema is present are obvious.

Figure 23 is a visible spectrum of a blister cap that was removed from the body. The isolated-skin spectrum does not contain the strong absorptions in the blue-green areas that are seen for fresh blood or for in vivo skin spectra.

"Tanning" is characterized by increased melanin pigmentation in the epidermis. Figure 24 is an overlay of visible spectra of various amounts of melanin prepared as control specimens. The spectra are remarkably parallel and nearly flat. Thus, the increasingly parallel behavior of the spectra (exposed vs. unexposed) in Figure 18 can be used as an indicator for the events and rates of tanning processes. When the visible absorption spectra are effectively parallel throughout their entire range, uniform differences in intrinsic pigmentation among different individuals can be readily quantitated and clearly differentiated from erythematous events. Conversely, non-parallel spectral records for a single individual can reveal early activation of melanin precursors while the slower approach to parallel spectral signature reflects the rate of de novo melanin synthesis. Fading of the "tan" is shown by a re-merging of the "control" and "exposed" spectra.

The data from these preliminary studies indicate that, given uniformly colored skin, responses to radiation show a definite dose-response curve in photometrically obtained data. This correlation is strongest for fairer skin, and is most pronounced in the red and green bands.

Spotmeter Data:

In conjunction with direct spectral scans and photographic recording, the color of human skin in erythematic response to intense sunlight exposure was also measured over the same period of 30 days using a spectral integrating radiometer (spotmeter). The radiometer possesses self-contained spectral filters especially tuned to be compatible with human color vision, originally for reasons apart from the present application.

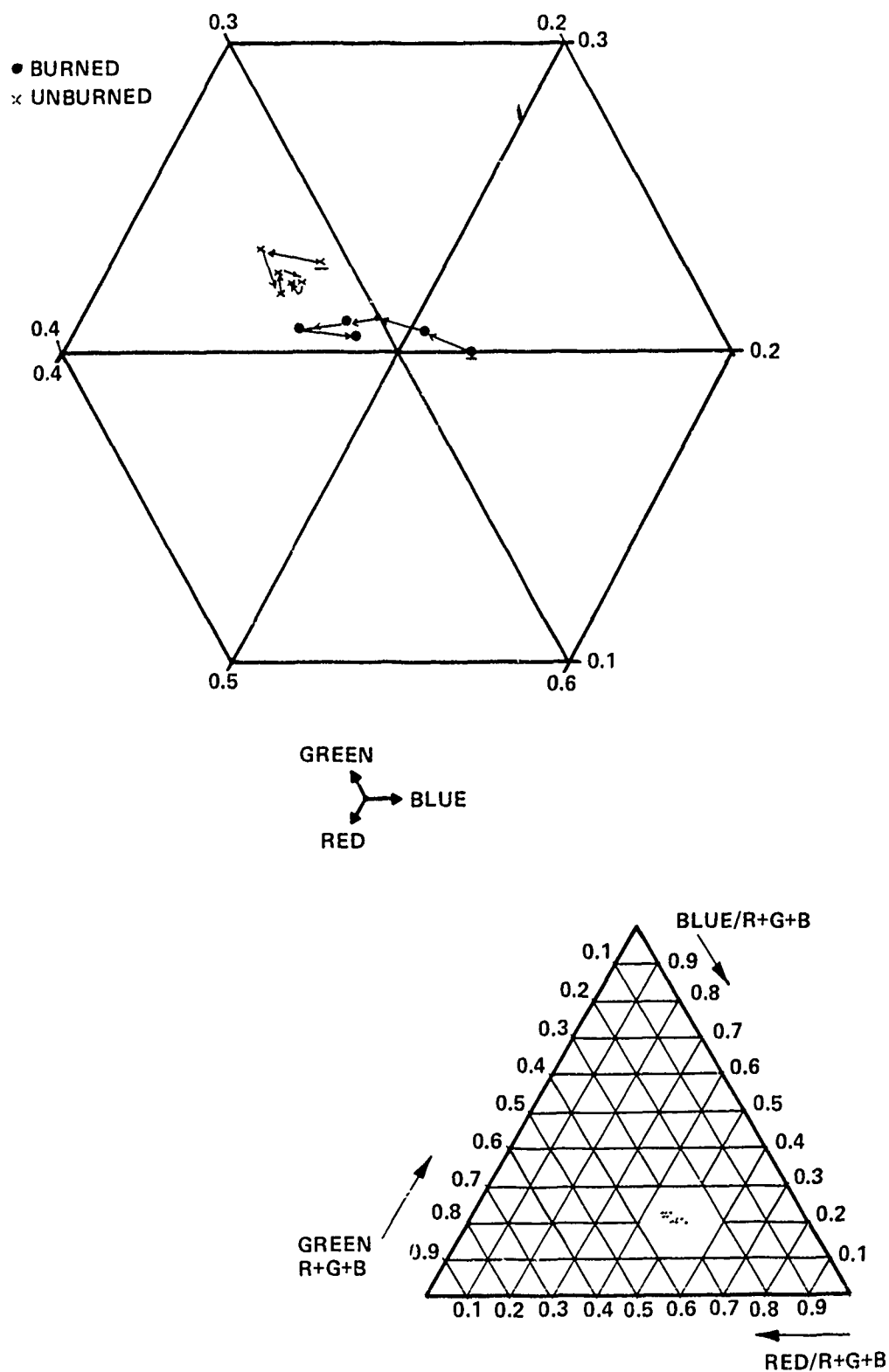


Figure 21 VISIBLE DATA – PLANAR PLOT OF REFLECTANCE RATIOS –
REB R FOREARM – EXPOSED AND UNEXPOSED

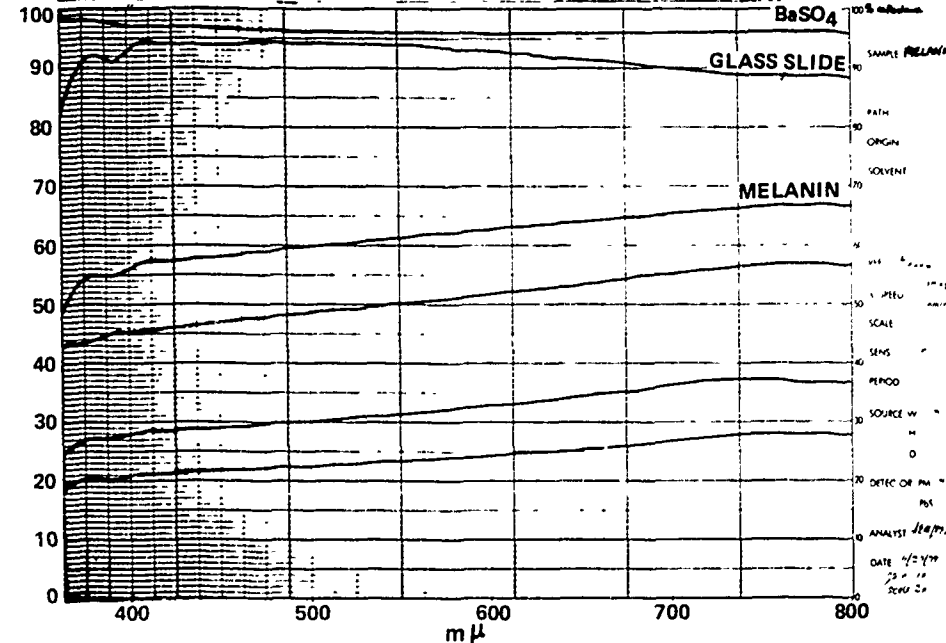
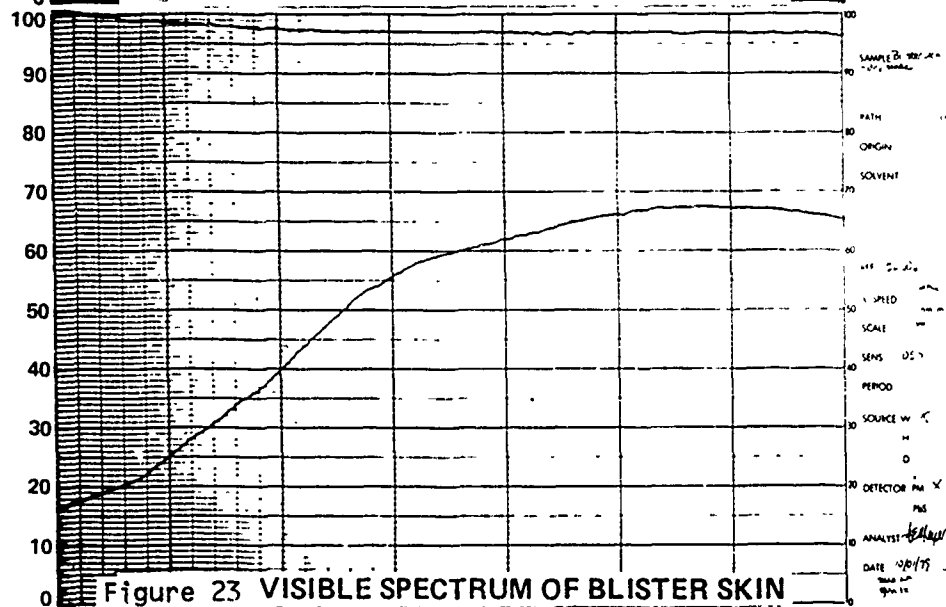
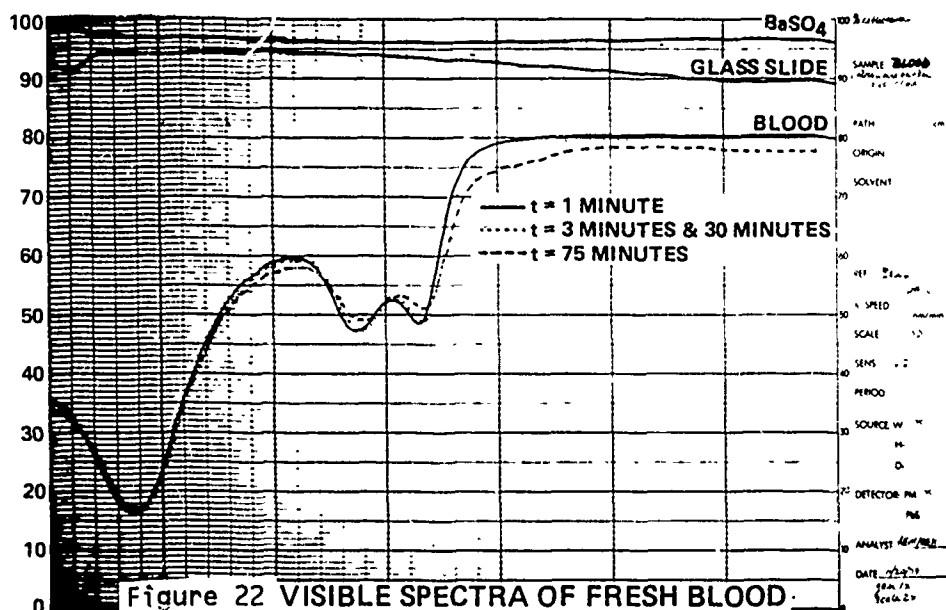


Figure 24 VISIBLE SPECTRA OF MELANIN

The measurements were "remote;" radiometer/subject separation was approximately one meter. The illumination was incandescent, thereby precluding the temporal oscillations often associated with fluorescent lamps. Bulb voltage was constantly monitored and adjusted as needed. The radiometer allows simultaneous reflex viewing of the measured area thereby assuring correct positioning. With the standard Spotmeter optics, sample size was about 0.2 inches.

The Spotmeter was operated in a differential mode in that every sample measurement was immediately accompanied with a measurement of a standard. This for the most part eliminated errors due to source positioning, bulb voltage and Spotmeter drift. The B (blue), R (red) and P (photopic) readings from the spotmeter were incorporated into the analytic framework given in the Appendix. Both the raw spotmeter data and the numerical results of the analysis follow.

The following figures present the results in different ways, although each does not necessarily give a new perspective. First, Figure 25 shows the time course of luminous reflectance (lightness or darkness) for four test areas (UN-unexposed, El-elbow, WR-wrist, ST-stomach) of different apparent "sunburn" intensity. For all areas, including the "unexposed" area, a strong change within the first 24 hours is indicated. No explanation is at hand as to why the curves cross, but in regard to the upswing near day 30, it was noted by the subject that moderate skin "peeling" had occurred by that time.

Figure 26 presents the same time course in the chromaticity diagram. Beyond a reasonably monotonic trend away from red, no other significant features are observed.

In order to learn how the data were arranged in tristimulus space, a principal component analysis was undertaken. It was learned the data lay primarily along a straight line in X, Y, Z space having these direction cosines: (-0.4964, -0.8387, -0.2239). The line, of course, passes through the data centroid at (34.0, 42.5, 8.9). The straight line character of the data was confirmed when the analysis showed that 98% of the data variance was in the stated direction.

The time course of the data was again replotted in terms of this principal component, and is shown in Figure 27. The colorimetric characteristic of this component is "redder and darker" for increasing value, and there is no behavior present that has not already been observed in the equivalent curves for luminous reflectance.

One final time course of the Spotmeter findings was plotted as a result of an observation regarding the photographic data. It was noted that the red-sensitive layer of color film predicted an erythema maximum after the first 24 hours, which appears contrary to the Spotmeter data already presented. To compare, $\bar{X}(\lambda)$, which yields the "reddest" tristimulus value X, was isolated by plotting the time course of X itself (Figure 28). With the exception of a slight reversal for the stomach at day three, maximum erythema is still indicated within the first 24 hours. However, all this does not imply an

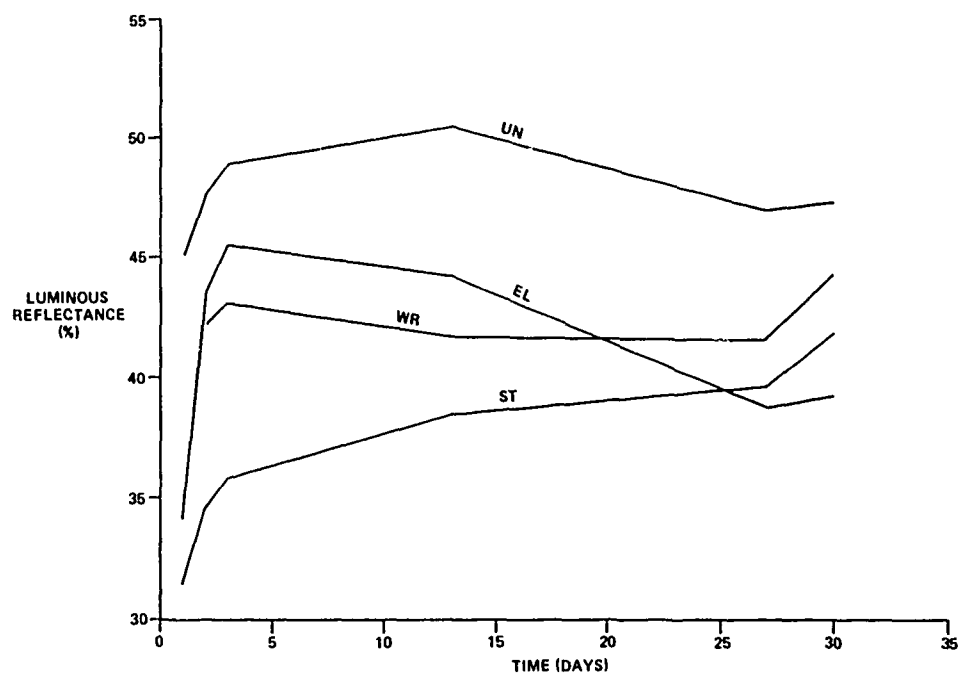


Figure 25 TIME COURSE OF LUMINOUS REFLECTANCE FOR FOUR EXPOSED AREAS

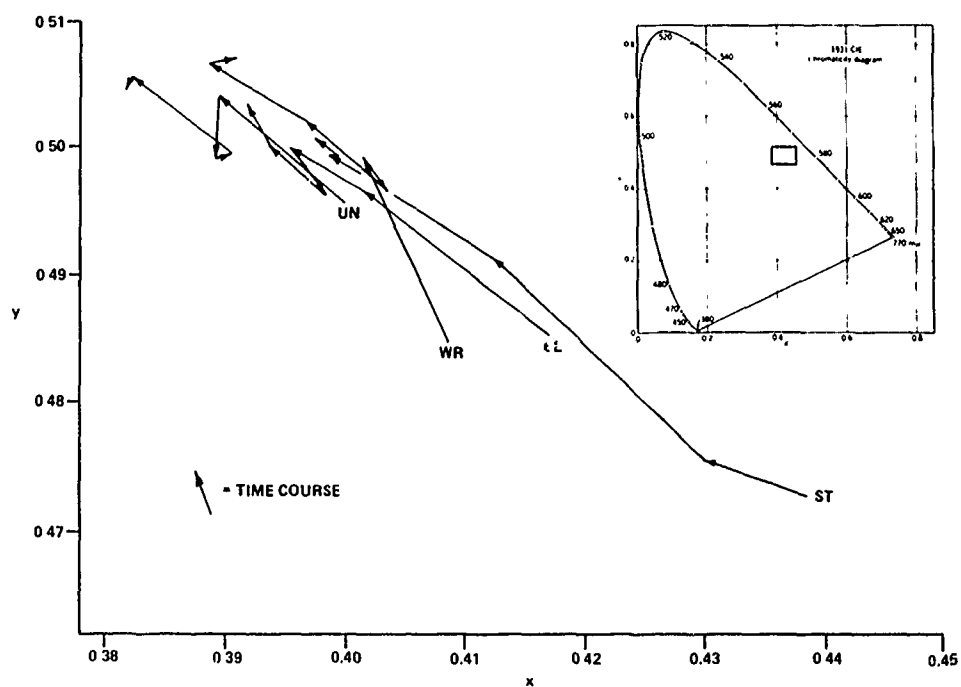


Figure 26 TIME COURSE OF CHROMATICITY COORDINATES FOR FOUR EXPOSED AREAS

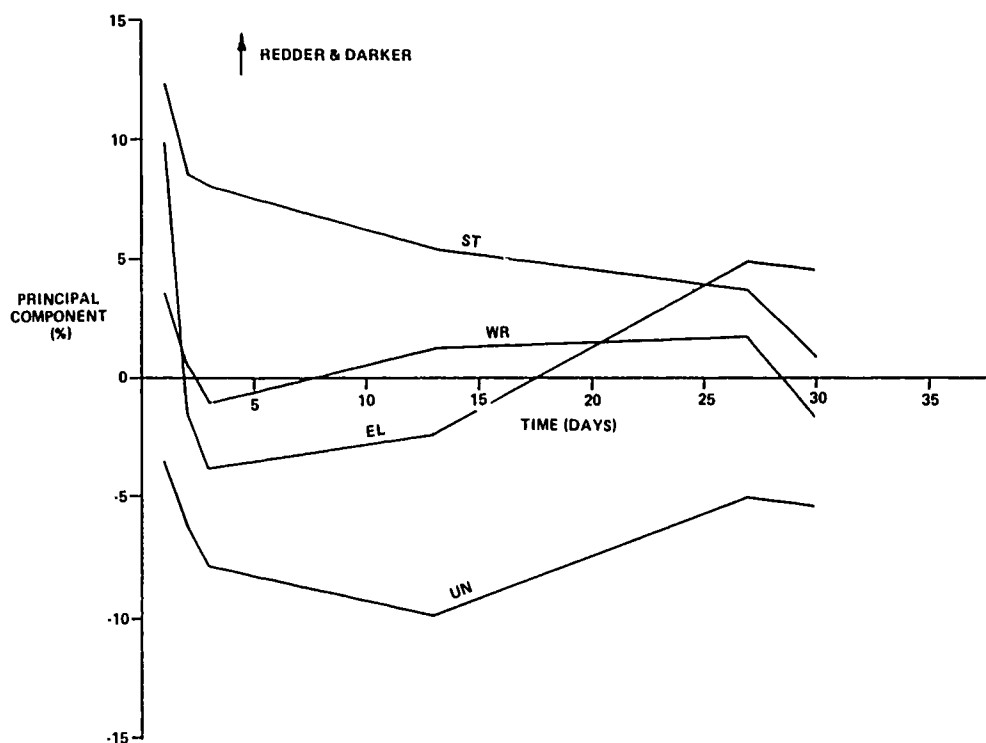


Figure 27 TIME COURSE OF TRISTIMULUS PRINCIPAL COMPONENT FOR FOUR EXPOSED AREAS

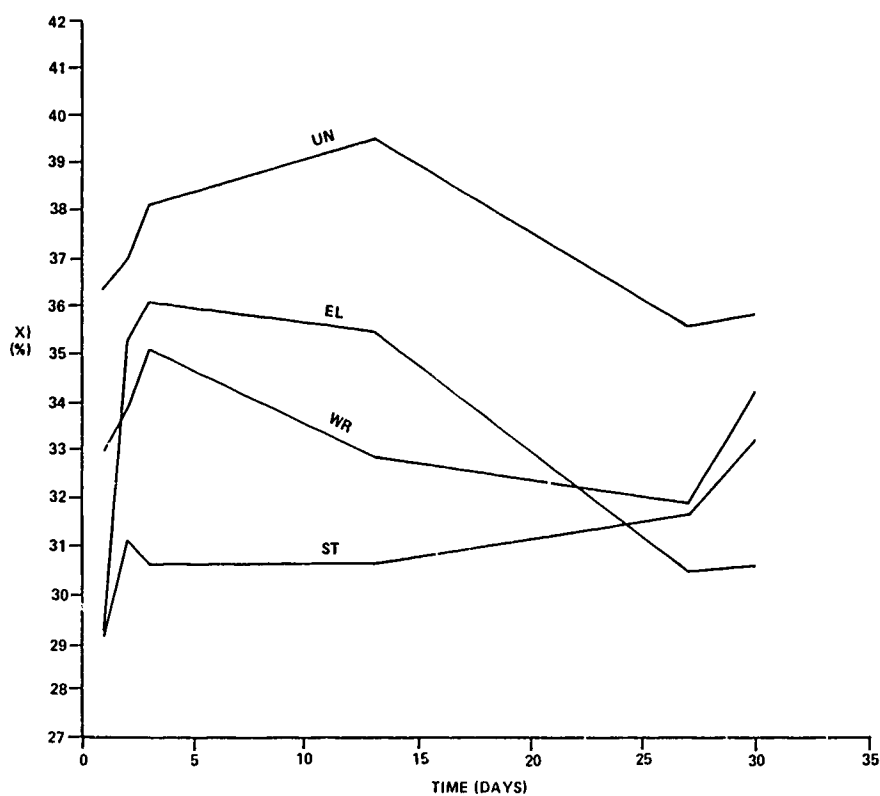


Figure 28 TIME COURSE OF X TRISTIMULUS VALUE FOR FOUR EXPOSED AREAS

inconsistency, since multiple spectral effects can occur in time, in conjunction with an $\bar{r}(\lambda)$ that has significant departure from the red response curve for film. Thus, the "contrariness" probably only begs the definition of erythema.

The following Tables (3 and 4) present two sets of data on erythema; an input data set containing the raw measurements by the Spotmeter, and an output data set containing calibrated color coordinates.

The first line of input data is for the calibration of a secondary standard (#31) from a primary standard (#1). The secondary standard was a piece of colored paper visually chosen as a skin match, and the primary was a visually selected chip from the Munsell color system. Not included in the tables is the note that the selected primary has Munsell designation 10YR 8/8 which under Illuminant A (Tungsten) yields chromaticities of $x = 0.5221$, $y = .4262$ and a luminous reflectance of 59.1%.* The remaining lines in the data set are for skin samples against the secondary standard. For the skin samples, all measurements were taken twice to provide at least a minimum of redundancy for possible error analysis. The two initials in the skin sample identification define the subject, and the first and second digits define the measurement day number and skin area respectively according to the following schedules:

<u>digit</u>	<u>day</u>	<u>digit</u>	<u>area</u>
1	1	0	WR (wrist)
2	2	1	UN (unexposed)
3	3	2	EL (elbow)
4	13	3	ST (stomach)
5	27		
6	30		

The output data set contains, for each input line, the channel scaling multipliers (α, β, γ), the resulting tristimulus values (X, Y, Z) and the chromaticity coordinates (x, y).

FUTURE RESEARCH NEEDS

Objective Characterization of Traumatized Skin

Recognizing the success of these preliminary studies focussed primarily on the objective characterization of erythema, it is now appropriate to attempt to similarly establish objective scientific indices for chemically

* K.L. Kelly and K.S. Gibson, "Tristimulus Specification of the Munsell Book of Color from Spectrophotometric Measurements, "JOSA 33, 7 July 1943)
p 355 ff

TABLE 3
INPUT DATA SET FOR ERYTHEMA

IDENTIFICATION OF SAMPLE	IDENTIFICATION OF STANDARD	FIRST MEASUREMENT						SECOND MEASUREMENT					
		SAMPLE			STANDARD			SAMPLE			STANDARD		
		B	R	P	B	R	P	B	R	P	B	R	P
31	1	6.72	34.7	42.7	6.80	50.5	40.1						
RB10	31	8.25	22.2	28.1	6.72	34.7	42.7	8.28	22.5	25.3	6.88	34.6	43.1
RB11	31	9.21	24.6	30.8	6.85	34.4	42.9	9.25	24.5	30.8	6.89	34.6	43.0
RB12	31	6.71	20.0	23.4	6.88	34.7	43.0	6.66	19.7	23.2	6.88	34.2	42.9
RB13	31	5.79	19.9	21.5	6.87	34.2	42.7	5.69	19.7	21.2	6.87	34.5	42.7
RB20	31	8.10	22.5	28.4	6.76	33.4	41.6	8.02	22.5	28.1	6.82	34.3	42.7
RB21	31	9.80	24.2	31.5	6.74	33.6	41.6	9.96	24.4	32.0	6.84	33.8	42.2
RB22	31	8.78	23.5	29.7	6.79	33.7	42.1	8.40	23.0	28.5	6.75	33.7	41.9
RB23	31	6.57	20.8	23.7	6.77	33.9	42.7	6.57	21.1	23.0	6.82	34.3	42.4
RB30	31	7.80	23.0	29.0	6.47	33.3	41.8	8.00	22.6	28.2	6.40	33.1	41.6
RB31	31	10.04	25.1	32.4	6.44	34.1	41.8	9.97	25.0	32.3	6.46	33.4	41.4
RB32	31	8.55	23.0	29.7	6.37	33.0	41.0	8.71	23.7	30.0	6.40	33.2	41.3
RB33	31	6.41	20.0	23.6	6.47	34.4	41.9	6.40	20.5	24.0	6.43	34.2	41.7
RB40	31	8.13	21.9	27.6	6.97	34.0	42.5	8.25	22.5	28.6	6.8	34.9	42.2
RB41	31	10.8	26.2	34.0	6.98	34.4	42.8	10.86	26.5	34.4	6.83	34.1	42.4
RB42	31	9.27	23.6	30.3	6.91	34.2	42.9	8.95	23.6	29.5	6.79	33.8	42.1
RB43	31	7.49	20.3	25.6	6.83	34.2	42.8	7.60	21.5	26.6	6.8	34.8	42.6
RB50	31	8.71	22.3	28.9	7.08	35.7	43.9	8.38	22.0	28.7	6.91	35.4	43.2
RB51	31	10.27	24.4	32.6	7.02	35.7	43.7	10.51	24.8	32.5	7.03	35.4	43.3
RB52	31	8.25	21.4	26.8	7.02	35.3	43.1	8.02	20.7	26.5	6.97	35.3	43.2
RB53	31	7.84	21.6	26.8	6.92	35.2	43.1	8.02	22.1	27.6	6.96	35.3	43.2
RB60	31	8.85	23.4	30.2	6.99	34.9	42.7	8.86	23.6	30.5	6.99	35.3	43.3
RB61	31	10.52	24.7	32.5	6.98	35.3	43.0	10.64	24.5	32.5	7.04	35.3	43.3
RB62	31	8.02	21.2	27.0	6.99	34.9	43.0	8.14	20.7	26.8	7.00	35.2	43.1
RB63	31	8.54	23.1	29.2	6.94	35.0	43.1	8.17	22.5	28.1	6.93	35.0	42.9

TABLE 4
OUTPUT DATA SET FOR ERYTHEMA

IDENTIFICATION OF SAMPLE	IDENTIFICATION OF STANDARD	SPOTMETER CHANNEL SCALINGS			TRISTIMULUS VALUES (% REFLECTANCE)			CHROMATICITY COORDINATES	
		α	β	γ	x	y	z	x	y
31	1	1.4099	1.4738	1.0543	50.11	62.93	7.08	0.4171	0.5239
RB10	31	1.4120	1.4609	1.0419	33.00	39.17	8.61	0.4085	0.4849
RB11	31	1.4181	1.4652	1.0313	36.40	45.13	9.52	0.3998	0.4956
RB12	31	1.4201	1.4652	1.0298	29.34	34.14	6.88	0.4170	0.4852
RB13	31	1.4243	1.4734	1.0313	29.19	31.47	5.92	0.4384	0.4726
RB20	31	1.4453	1.4930	1.0434	33.92	42.18	8.41	0.4014	0.4991
RB21	31	1.4518	1.5020	1.0434	37.00	47.69	10.31	0.3895	0.5020
RB22	31	1.4518	1.4984	1.0465	35.25	43.60	8.99	0.4013	0.4964
RB23	31	1.4347	1.4790	1.0426	31.20	34.53	6.85	0.4299	0.4758
RB30	31	1.4736	1.5092	1.1010	35.05	43.16	8.70	0.4033	0.4966
RB31	31	1.4496	1.5128	1.0984	38.15	48.94	10.99	0.3890	0.4990
RB32	31	1.4781	1.5293	1.1096	36.11	45.65	9.58	0.3954	0.4998
RB33	31	1.4264	1.5055	1.0984	30.06	35.83	7.04	0.4122	0.4913
RB40	31	1.4201	1.4860	1.0290	32.93	41.76	8.43	0.3962	0.5024
RB41	31	1.4284	1.4773	1.0260	39.50	50.52	11.11	0.3905	0.4996
RB42	31	1.4389	1.4898	1.0343	35.53	44.27	9.42	0.3982	0.4962
RB43	31	1.4059	1.4738	1.0396	30.69	38.47	7.84	0.3986	0.4995
RB50	31	1.3762	1.4450	1.0128	31.93	41.62	8.65	0.3834	0.5063
RB51	31	1.3762	1.4467	1.0085	35.60	47.09	10.48	0.3821	0.5054
RB52	31	1.3860	1.4584	1.0128	30.55	38.87	8.24	0.3934	0.5005
RB53	31	1.3879	1.4584	1.0209	31.68	39.67	8.10	0.3988	0.4993
RB60	31	1.3938	1.4635	1.0136	34.25	44.42	8.98	0.3908	0.5063
RB61	31	1.3860	1.4584	1.0107	35.88	47.40	10.69	0.3818	0.5044
RB62	31	1.3958	1.4618	1.0128	30.61	39.32	8.18	0.3918	0.5034
RB63	31	1.3978	1.4635	1.0216	33.30	41.93	8.54	0.3975	0.5006

traumatized skin. It is expected that some of the noninvasive techniques will be more suitable than others. In Table 5 the various techniques are listed, along with questions that reflect the possible "traumatized" skin relevance of the techniques.

Coincident dermatologic observations will be necessary, and it is important that medical research personnel participate in those observations. One anticipated problem area is the effect that increased blood flow (through exercise, etc.) may have on the techniques that utilize the visible spectrum.

Protective Lotion Effectiveness

Using selected techniques, it is apparent that the effects of candidate protective lotions on skin can be quickly evaluated. Are the lotions acting as moisture barriers or by some other mechanism? It is also important to ascertain the possible effects of lotion "glint" (i.e., specular reflection) on the analytical sensitivity of the optical techniques. Subjects should be observed through a predetermined period of time and at specific intervals. Three types of experiments should be carried out: lotion-only controls, lotion + skin, and skin-only controls. Profiling the skin with various types of internal reflection prisms is expected to be helpful here.

Although some preliminary experiments have been carried out with "spectrum subtraction," it is now necessary that a definitive determination be made as to whether the moisture content of the skin can be separated from that of the protective lotions. In addition to the infrared spectroscopy, surface tension analysis and replication of the skin will be useful to evaluate the effectiveness of different protective skin treatments.

Differentiation of Traumatized States

Using methods similar to those outlined above for the characterization of burned skin, it is clear that objective spectroscopic records can be obtained for decidedly different skin states, and that these states also be observed clinically. It is likely that some of the techniques can be used to rapidly differentiate chemically traumatized skin states and, perhaps, offer data that could supplement medical judgments prior to making treatment decisions.

Image Processing for Skin Texture Analysis

Images can be collected photographically and reduced for computer input by two-dimensional digitization. Calspan has access to a unique image reduction facility capable of reducing imagery up to 20 x 36 inches at a resolution of 20-50 micrometers.

The reduced images, residing on magnetic tape, can undergo any of a variety of formal analyses, for the purpose of finding a summary measure that strongly correlates with skin damage. Of course, for such a correlation to be established it is also necessary for a clinical scale of trauma to exist.

TABLE 5
OBJECTIVE CHARACTERIZATION OF TRAUMATIZED SKIN

Technique	Possible Relevance
Critical Surface Tension	Does skin roughness have an effect on the surface tension of the skin? Does the absence of hydration or any other component have an effect on the surface tension?
IR Internal Reflection Spectroscopy	How does traumatized skin differ from normal skin with respect to hydration and other chemical components of the skin? (It is suggested that the skin profile be obtained using internal reflection prisms having different angles of incidence.)
Spot Meter, Photogrammetry (Visible)	Are there differences in reflectance with respect to sample-spot size? Are the techniques sensitive to dry skin flakes and scales?
Photogrammetry (IR)	Is this technique sensitive to differences in damaged skin? Is "water" content the main factor in prevention of skin "burning"?
Replication and Scanning Electron Microscopy	Do the different degrees of roughness parallel changes in the skin that are observed by other techniques? Where is the greatest stress in traumatized skin - the epidermal crevices or the skin pads?

Spectral Record Analysis

Collection and interpretation of optical and infrared spectral densities for both emitting and reflecting sources is in routine practice. Principally the interpretation is confined to visual inspection; e.g., the presence or absence of various spectral absorption lines is indicative of the presence or absence of responsible species, with magnitudes of peaks giving a rough idea of concentrations. The time is ripe, and the techniques are available, for pursuing "eyes off" analytic procedures to collaborate present state-of-the-art interpretation. Although it would be presumptuous to suggest visual interpretation can be replaced by machine decision, it is nonetheless desirable to proceed in that direction.

Standard analytic techniques should be applied to dichotomize spectral records into concentrations of predetermined members of a library. A comparison of predicted concentrations with those of true "unknowns" together with an inspection of the unpredicted spectral residual will indicate the degree of success.

This effort, which can begin immediately, would have direct application to IR spectra collected on traumatized skin. Beyond this, there is potential application to skin color changes resulting from burning, blistering, and erythema. This latter application may be especially interesting since hemoglobin/melanin concentrations may be predicted in a situation where strong spectral lines do not occur.

APPENDIX

A. Photometric Theory

Exposure on film is defined as light intensity x time and is commonly expressed as Watts-second/square centimeter. A sensitometric wedge consists of a series of 21 steps each incremented by $.15 \times \log (E)$ where E is the lowest exposure on the wedge. Therefore, the exposure of any step may be found simply by the number of steps it is from the first step (i.e., $E_N = N \times .15 \log (E)$).

The optical density of the film is the log of the transmission of light (in percent) through the film. This is the density read on the Macbeth densitometer. The density is also a function of the log (exposure) of the film. This Density-log (Exposure) relationship is established by the use of the wedge and is a function of film type, exposure and processing. Thus, given the relationship developed through the wedge and the density of any spot on the film, the exposure (intensity x time) can be found.

Reflectance is defined as the ratio of ENERGY RETURNED TO INCIDENT ENERGY (i.e., percentage of REFLECTED ENERGY TO INCIDENT ENERGY). Every object has a reflectance ranging from zero to one. This returned energy, in photography, causes the film to be exposed. Therefore, the exposure of the film as it images an object is related to the reflectivity of that object.

However, lighting conditions, camera flare, transmission between object and camera and other factors also affect the exposure of the film. Therefore, it is necessary to calibrate the film to obtain actual reflectivity of an object.

B. Color Analytics

This section presents the analytic tools required for color specification from Spotmeter measurements. First, some basic relations that are important to understanding certain metrics of human color vision are laid down, and second, equations that link these measures to raw Spotmeter measurements are presented.

Trichromatism:

Human color vision is trichromatic; there exist only three degrees of freedom. Spectral stimuli, which can be regarded to possess infinite degrees-of-freedom (the intensity at each wavelength is independent of every other wavelength) map into the visual cortex as three dimensional "color-brightness" sensations. For our purpose here, we can regard the visual system as performing three different spectral integrals over the spectrum.

The three integrals involve three weighting functions ("distribution coefficients"), and a set compatible with human color vision is shown in Figure 29.* (In this, and the measures to follow, data consistent with a "standard observer" defined in 1931, as well as standard spectral illuminants, will be employed.) These functions are used to obtain the tristimulus values (X, Y, Z) of a stimulus $S(\lambda)$ according to:

$$\begin{aligned} X &= \int \bar{x}(\lambda) S(\lambda) d\lambda \\ Y &= \int \bar{y}(\lambda) S(\lambda) d\lambda \\ Z &= \int \bar{z}(\lambda) S(\lambda) d\lambda \end{aligned} \quad \text{A-1}$$

The tristimulus values, as a set, define the color-brightness sensation. It is noted that $\bar{y}(\lambda)$ is the luminosity function of the eye, and therefore Y can be equated to luminous reflectance.

It should now be clear that different stimuli can yield the same sensation X, Y, Z. Spectral functions that do this are known as "metamers," and an example is shown in Figure 30. The importance of this concept is that within the comparative radiometry employed in this study, the visual similarity (or relationship) between a sample and a standard under a given illuminant may not be retained should the spectral character of the illuminant change.

Before proceeding to the equations that describe the Spotmeter performance, one last colorimetric representation is useful; the chromaticity diagram. Understanding that color-brightness space is three-dimensional, the

* This and what is to follow is standard form, and can be found in Judd & Wyszecki, "Color in Business, Science, and Industry," Wiley (1963)

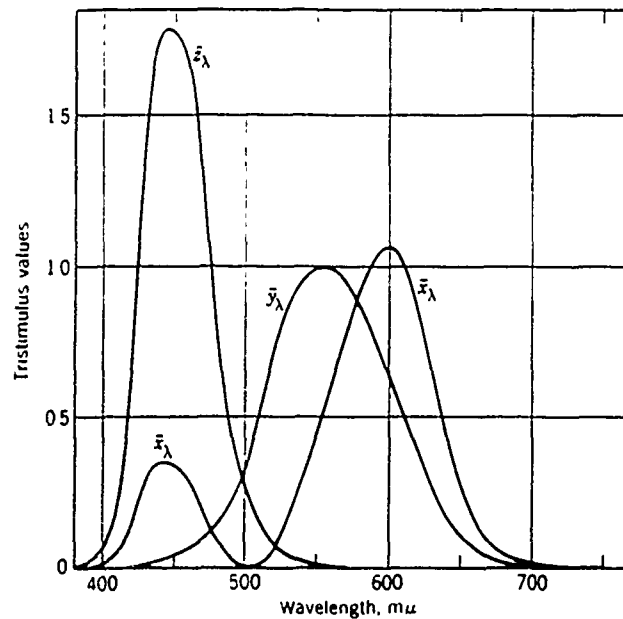


Figure 29 DISTRIBUTION COEFFICIENTS FOR THE CIE 1931 STANDARD OBSERVER. THESE ARE THE SPECTRAL WEIGHTING FUNCTIONS THAT YIELD THE TRISTIMULUS VALUES X, Y AND Z. (AFTER JUDD AND WYSZECKI (1963))

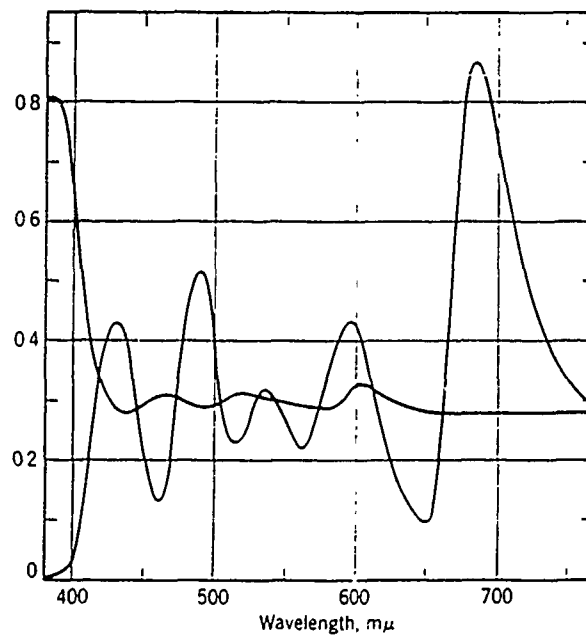


Figure 30 A METAMERIC PAIR - TWO SPECTRAL REFLECTANCES THAT ARE VISUALLY INDISTINGUISHABLE UNDER BOTH DAYLIGHT (STANDARD ILLUMINANT "C") AND TUNGSTEN (ILLUMINANT "A"). (AFTER JUDD AND WYSZECKI (1963)) THIS ILLUSTRATES A BASIC LIMITATION OF HUMAN COLOR VISION IN SPECTRAL SENSITIVITY

data are reduced to two-dimensions by eliminating brightness as a degree-of-freedom. The standard procedure is through the chromaticity coordinates (x,y) defined by

$$x = \frac{X}{X + Y + Z} \quad A-2$$

$$y = \frac{Y}{X + Y + Z}$$

Now y vs x yields the color map of Figure 31 where "intensity" is no longer an issue. The curved outer boundary is the spectrum locus and the straight line connecting the short and long wavelength endpoints is known as the "line of purples." Various mixtures of different wavelengths yield all inner points within the closed boundary.

Spotmeter:

The derivation of color coordinates from raw Spotmeter readings involves two further considerations. First, the three spectral filters incorporated within the Spotmeter (R - red, P - photopic, B - blue) correspond to $\bar{x}(\lambda)$, $\bar{y}(\lambda)$ and $\bar{z}(\lambda)$ of Figure 29 respectively with the exception that R does not include the short wavelength mode of $\bar{x}(\lambda)$. Rather, the X tristimulus value is simulated by including a fraction of $\bar{z}(\lambda)$ according to:

$$X = X_R + 0.167Z \quad A-3$$

where X_R = component of X due to long wavelength mode of $\bar{x}(\lambda)$.

Secondly, the R, P, B channels of the Spotmeter possess only an arbitrary multiplicative relationship thereby requiring scaling constants α, β, γ according to

$$\begin{aligned} X_R &= \alpha R \\ Y &= \beta P \\ Z &= \gamma B \end{aligned} \quad A-4$$

These constants are determined through the measurement of the standard (x,y, Y known) and the inversion of Equations A-3 and A-4,

$$\begin{aligned} \alpha &= \frac{X - 0.167Z}{R} \\ \beta &= \frac{Y}{P} \\ \gamma &= \frac{Z}{B} \end{aligned} \quad A-5$$

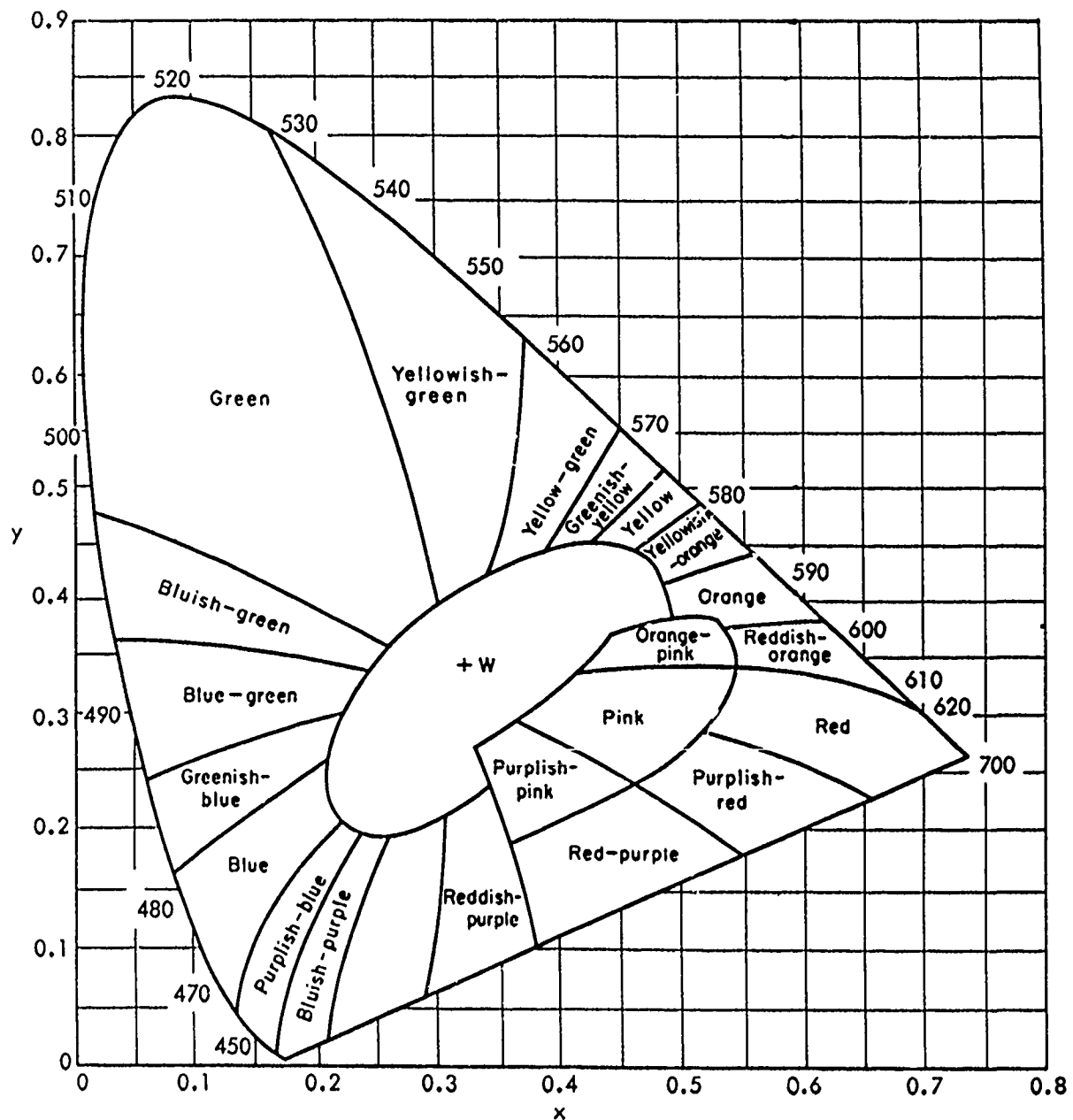


Figure 31 CHROMATICITY DIAGRAM FOR THE 1931 STANDARD OBSERVER. THIS IS THE TWO-DIMENSIONAL COLOR MAP THAT REMAINS AFTER BRIGHTNESS (LUMINOSITY) IS REMOVED AS A DEGREE-OF-FREEDOM FROM THE TRISTIMULUS VALUES, X, Y, AND Z (AFTER SHEPPARD (1966))

With Equations A-2

$$X = \left(\frac{x}{y} \right) Y$$

A-5

$$Z = \left(\frac{1 - x - y}{y} \right) Y.$$

With α , β and γ determined, the tristimulus values and chromaticity coordinates of the unknown are computed from R, P, B measurements using A-4, A-3 and A-2 directly.

THE USE OF HUMAN LEUKOCYTES AS A MODEL FOR STUDYING
THE BIOCHEMICAL EFFECTS OF CHEMICAL WARFARE (CW) AGENTS

by

Henry Louis Meier, Clark L. Gross,
Bruno Papirmeister, and Julia E. Daszkiewicz

US Army Medical Research Institute of Chemical Defense
Aberdeen Proving Ground, Maryland 21010

At Johns Hopkins School of Medicine, I was studying bullous pemphigoid, which is a disease that produces blisters similar to the blisters which occur after mustard gas, HD, exposure. Since blistering diseases are very rare, the availability of an agent such as mustard gas, which causes blistering in humans about 4 hours after contact, greatly enhances our ability to study the mechanism by which blisters are produced. Figure 1 is an illustration of this laboratory's hypothesis of the mechanism by which HD causes pathology. This laboratory and others have shown that cells treated with HD undergo DNA modification, which results in DNA breaks. The hypothesis postulates that these breaks initiate the activation of poly ADPR polymerase, a chromatin-bound enzyme which hydrolyses NAD in order to ADP ribosylate cellular proteins, which in turn would cause the depletion of NAD in the cell. This depletion of NAD would inhibit glycolysis, causing the activation of the hexose monophosphate shunt (which has been shown to cause protease release) and culminate, eventually, in the pathology which could lead to blister formation in human skin.

In order to test this hypothesis, a model relevant to humans was needed because of the differences between existing animal models and man (listed in Figure 2). The number of hair follicles is greatly enhanced in animals, they have no sweat glands, and there is a difference in the skin thickness. Men and mice also differ in their cellular proteases, protease inhibitors, inflammatory responses, and in their ability to synthesize NAD from precursors, which is very pertinent in this hypothesis. Mice do not form blisters. Therefore, a new model which employed human leukocytes was developed, enabling us to study the mustard-induced injury at the cellular level.

Figure 3 shows the cellular composition of circulating human leukocyte. Human peripheral leukocytes are approximately 55-65 percent neutrophils, which are inflammatory end cells capable of secreting potent proteases. Lymphocytes comprise between 30-45 percent of the circulating leukocytes and are capable of reproducing when stimulated by either exogenous or endogenous mitogens. Of special importance for this model is that lymphocytes are the circulating cells known to contain poly ADPR polymerase. Monocytes and granulocytes comprise 1-5 percent of the remaining circulating leukocytes. Basophils are granulocytes which contain potent classical chemical mediators, such as histamine, slow-reacting substance of anaphylaxis (SRS), and potent inflammatory proteases. Figure 4 shows why leukocytes were chosen for study. They are easy to obtain by bleeding a normal volunteer. They represent multiple cell types. They can be purified to relative homogeneity for detailed studies of specific effects. Multiple determination from a single source can be performed. From 100 mls of blood, we can carry out 100 individual points in a given experiment and repetitive samples can be obtained from the same individuals. Most importantly, leukocytes represent a primary target tissue in systematic human HD exposures. This is emphasized in Figure 5, which shows excerpts from a recent UN report on the investigation of Iranian chemical warfare (CW) casualties. Over 50 percent of those patients examined 5 days after exposure to HD demonstrated marked changes in their leukocyte content and, most dramatically, a change in their lymphocyte content. As can be seen from the example of these three soliders, there was a marked lymphocytopenia, indicating that HD either causes the depletion or the sequestering of

lymphocytes in exposed victims. Figure 6 shows how the model is used. Between 50-100 mls of blood was obtained from normal human volunteers and sedimented on a EDTA-dextrose solution, washed in Tyrode's Buffer. Then the red blood cells were lysed with distilled water. Both the washing and the lysing were repeated, so there were no red cells present. The cells were then aliquotted and incubated under varying conditions in the presence of the agent to be studied. Following the incubation, the cells were centrifuged at 14,000 g for one minute and the supernatant and cell pellet were separated. The cellular changes produced by agent exposure can be determined in the cell pellet. The secretion of mediators, as well as the leakage of cell lysis material, can be measured in the supernatants.

The remainder of this paper will deal with the results obtained from both the cell pellet and the cell supernatant. The first part will involve how leukocytes were used to validate our model of HD injury and the latter will discuss the effects of soman on leukocytes. Figure 7 shows a dose-dependent decrease in NAD levels of the cells after exposure to mustard for 4 hours. As can be seen, doses of 10^{-6} molar and higher of HD cause a dose-dependent decrease in NAD levels. This NAD decrease plateaus around 40 percent of the control when cells are exposed to mustard concentrations higher than 10^{-4} molar. HD treatment of human cells does, indeed, cause a decrease in the cellular content of NAD, which is consistent with this hypothesis. The leveling off of the NAD loss at 40 percent probably reflects the fact that only lymphocytes contain poly ADPR polymerase and, thus, are the only cell type affected by NAD depletion as a result of HD exposure. This assumption will be investigated further using purified cell populations.

In order to determine whether NAD levels would be a good early marker for HD injury, the time course of the NAD decrease was determined. Figure 8 demonstrates the level of NAD in both the HD-treated and control cells remains the same for the first 90 minutes of the reaction. By 4 hours, HD causes a decrease in NAD levels, indicating that this biochemical change is an early event and precedes the development of overt pathology.

In order to determine whether the decrease in NAD was due to the activation of poly ADPR polymerase, we pretreated the cells for 10 minutes with nicotinamide (shown in Figure 9). This slide shows that nicotinamide blocked the NAD decrease. Cells that were treated with 10^{-3} M HD for 4 hours, without any nicotinamide present, showed a 25-percent drop in NAD as compared to controls, but those cells that were exposed to nicotinamide at 10^{-6} M or higher demonstrated higher levels of NAD. NAD levels peaked at 10^{-4} molar nicotinamide at almost 200 percent of control. Therefore, it was shown that nicotinamide, an inhibitor of poly ADPR polymerase and a substrate for NAD synthesis, was capable of not only blocking NAD decreases, but also of increasing synthesis of NAD. Preliminary studies with 3-methoxybenzamide, a specific inhibitor of poly ADPR polymerase, suggest that it decreases the HD-induced NAD loss. It was necessary to know if this therapeutic intervention required pretreatment of the cells before exposure to HD or whether intervention would also be effective if initiated after HD exposure.

Figure 10 is an extremely complicated graph that demonstrates the time course of the effects of nicotinamide. These cells were put in culture for

5 hours. Solid line and solid points represent cells that were exposed to HD 1 hour after the cells were put in culture. The cells were incubated in the presence of 10^{-4} M for the amount of time shown on the abscissa. The NAD levels of cells incubated for 5 hours with nicotinamide are shown as 300-minute samples, while cells that had no nicotinamide added are shown as zero time samples. Figure 10 indicates that levels of NAD in HD-treated cells are higher than in control cells when both groups are treated with nicotinamide, even as late as 2 hours postexposure. This increase has been termed superinduction of NAD. This superinduction indicates that nicotinamide is not only an effective pretreatment for blocking the fall of NAD, but is also effective in preventing NAD depletion as late as 2 hours after exposure.

Figure 11 schematically illustrates the biochemical hypothesis for the development of pathology in HD-induced injury and indicates potential sites for therapeutic intervention. The activity of poly ADPR polymerase appears to be required for the ligation of the repaired DNA breaks. Although the use of poly ADPR polymerase inhibitors (such as nicotinamide), prevent the biochemical changes, they also inhibit the repair of the DNA required for recovery.

Therefore, we studied the effect of niacin (which does not inhibit poly ADPR polymerase, but acts as a precursor of NAD) to determine if it was effective in blocking the NAD drop induced by HD exposure. Figure 12 shows the effect of niacin. Niacin prevented the HD-induced drop in NAD. Cells treated with HD, but not with niacin, had a 40-percent drop in their NAD levels. The addition of niacin to the incubation mixture at concentrations greater than 10^{-6} M resulted in an increase in the cellular NAD level. The highest increase in NAD levels resulted from the use of 10^{-5} M niacin, which is about 1/10,000 of the LD50 of niacin. Summarized in Figure 13 are the conclusions from the HD treatment of human leukocytes. They are: 1. In human leukocytes there is a dose-dependent decrease in NAD upon exposure to sulfur mustard. 2. There is sufficient time for therapeutic intervention before a significant decrease in NAD levels occurs. 3. Inhibitors of poly ADPR polymerase and NAD precursors can intervene and block the decrease in NAD. Niacin, though it does not inhibit poly ADPR polymerase, has greater therapeutic potential because it acts solely as an NAD precursor and will block the NAD depletion without blocking the DNA repair, which is essential for recovery. 4. Clinical observations demonstrate that the human leukocytes, especially lymphocytes, are a sensitive target tissue. 5. Both the data and the clinical observations agree with our hypothesis.

Now it is time to consider the effect of soman on human leukocytes. Two effects of soman on human leukocytes were studied, including changes in cellular NAD levels and secretion of histamine. Figure 14 shows the dose-dependent decrease in NAD levels of the cells after exposure to soman for only 1 hour. This figure demonstrates that soman causes a dose-dependent decrease in the level of NAD beginning at 7×10^{-5} M. At concentrations of soman greater than 4×10^{-4} M, the NAD levels decreased to 10 percent of controls.

Next, the soman-induced fall in NAD levels was characterized. Nicotinamide, which inhibits poly ADPR polymerase and acts as a substrate for NAD synthesis, failed to block the NAD decrease. The cells were studied to

determine whether the NAD was converted to NADH and whether the reoxidation of NADH to NAD was blocked by soman. Figure 15 shows that soman caused a dose-dependent decrease in both NAD and NADH levels. The time course of the soman-dependent decrease in NAD is shown in Figure 16. These results indicate that the drop in NAD due to soman exposure takes place within 10 minutes following exposure, and levels off by 30 minutes, unlike the HD-induced decrease. Thus, the processes by which soman and HD decrease NAD appear to be accomplished by different mechanisms. In order to demonstrate that the soman-induced decrease in NAD was not due to a cell lysing process, the effects of incubation temperature on the NAD decrease were studied and the supernatants for the appearance of intracellular enzyme LDH were checked. Temperature experiments show that only cells incubated at approximately 37°C demonstrated a decrease in NAD, suggesting that the fall in NAD was due to an enzymatic process. There was no increase in the supernatant LDH content of soman-exposed cells. Both the temperature effect and the supernatant content indicate that the soman effect on NAD is by physiological processes and not due to cell lysis. Next, the effect of soman on histamine release was investigated.

Diisopropylfluorophosphonate (DFP), contrary to some published reports, causes the release of histamine from human basophils. This work was extended to determine if soman would have a similar effect. Figure 17 demonstrates a dose-dependent release of histamine by soman. This figure illustrates sharp dose-dependent release of histamine, which was maximal at 2×10^{-4} molar soman. By demonstrating the requirements for the divalent cations needed for secretion to occur, it was shown that the release of histamine by soman from basophils was also not due to a lytic process. Histamine release induced by soman was inhibited by treating the cells with EDTA, shown in Figure 18, or by lowering or raising the temperature from the 37°C optimum. This suggests that the release was the result of a physiological process. The release of histamine had previously been reported to be calcium dependent. Here, the findings with soman are consistent with this property (Figure 19). Another parameter of histamine release by known physiological releasers, such as anti-IgE, antigen, and C5A, is a well-defined temperature optimum at 37°C. Figure 20 shows this temperature dependence was also exhibited by soman-induced histamine release. Human leukocytes were exposed to soman at 0, 22, 37, and 46°C for 1 hour. Human leukocytes showed a tight temperature dependent soman-induced histamine release, since only the cells incubated at 37°C demonstrated significant histamine release.

The summary, shown in Figure 21, illustrates the following conclusions: 1. Leukocytes are a target tissue for vesicant agents, such as mustard, and nerve agents, such as soman; 2. The leukocytes are easy to obtain in large numbers for human volunteers and they can be obtained repeatedly; 3. The leukocytes demonstrate biochemical changes due to CW agent exposure and these changes are easily quantified, since you are dealing with a single cell suspension; 4. Leukocytes can be used to investigate the mechanism of CW agent actions and can also be employed to develop and measure the effectiveness of therapeutic interventions.

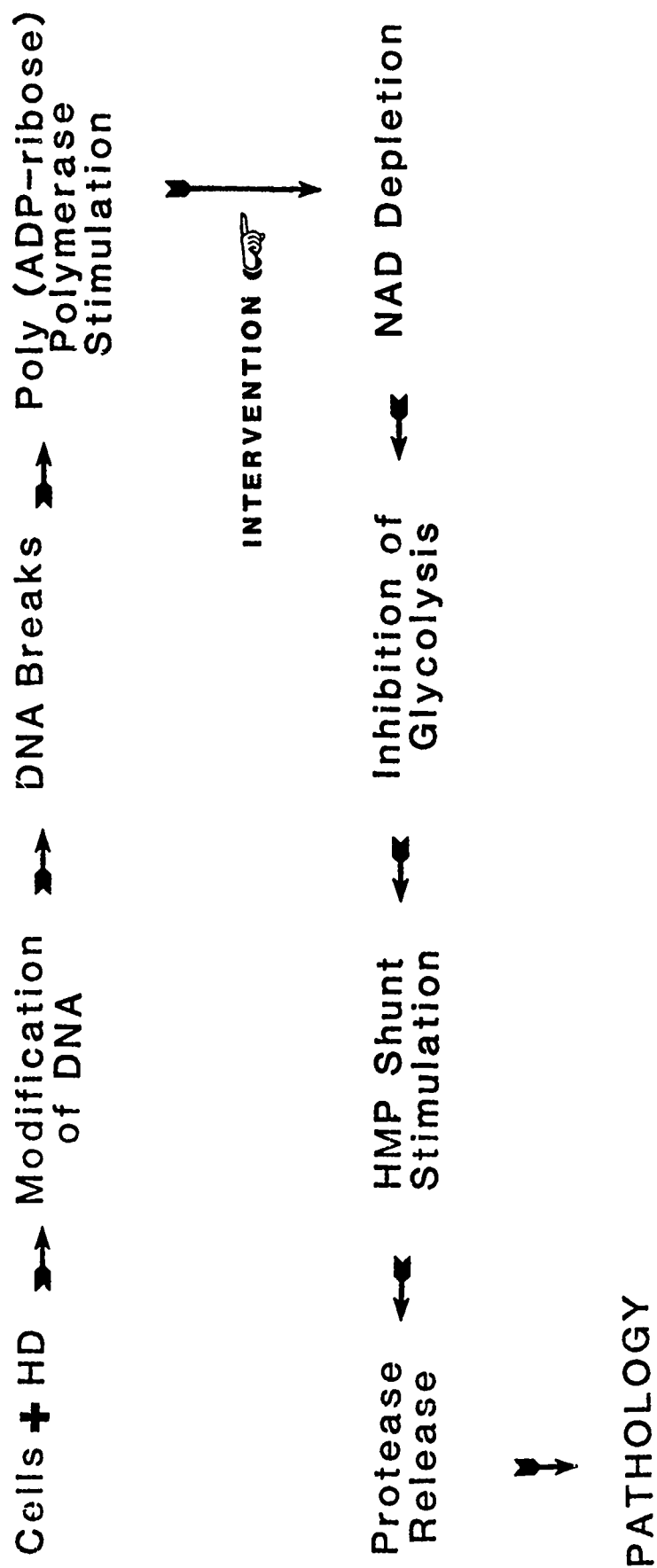


Figure 1

DIFFERENCES BETWEEN MAN AND MOUSE

1. Skin Physical Properties
 - a. number of hair follicles
 - b. sweat glands
 - c. thickness
2. Cellular Proteases
3. Inhibitors
4. Inflammatory Response
5. Synthesis of NAD
6. Blister Formation

Figure 2

LEUKOCYTES

Neutrophils

Lymphocytes

Monocytes

Granulocytes

Figure 3

WHY LEUKOCYTES?

1. Easy to Obtain
2. Represent Multiple Cell Types
3. Purification of Cell Types
4. Multiple Determinations from A Single Source
5. Repetitive Sampling
6. TARGET TISSUE

Figure 4

UNITED NATIONS REPORT OF IRANIAN PATIENTS

5 DAYS AFTER HD EXPOSURE

1. Soldier A

On the day of the observation, the patient had 2,500 leukocytes with 6 lymphocytes.

2. Soldier B

On the day of the observation, the patient had 6,400 leukocytes with no lymphocytes.

3. Soldier C

On the day of the observation, the patient had 300 leukocytes. The patient died the same night.

Figure 5

EXPERIMENTAL PROCEDURE

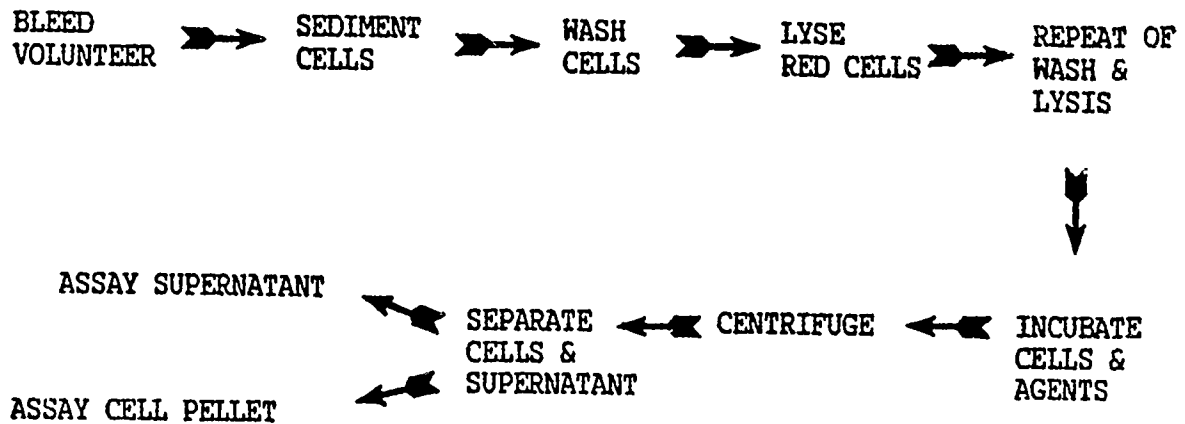


Figure 6

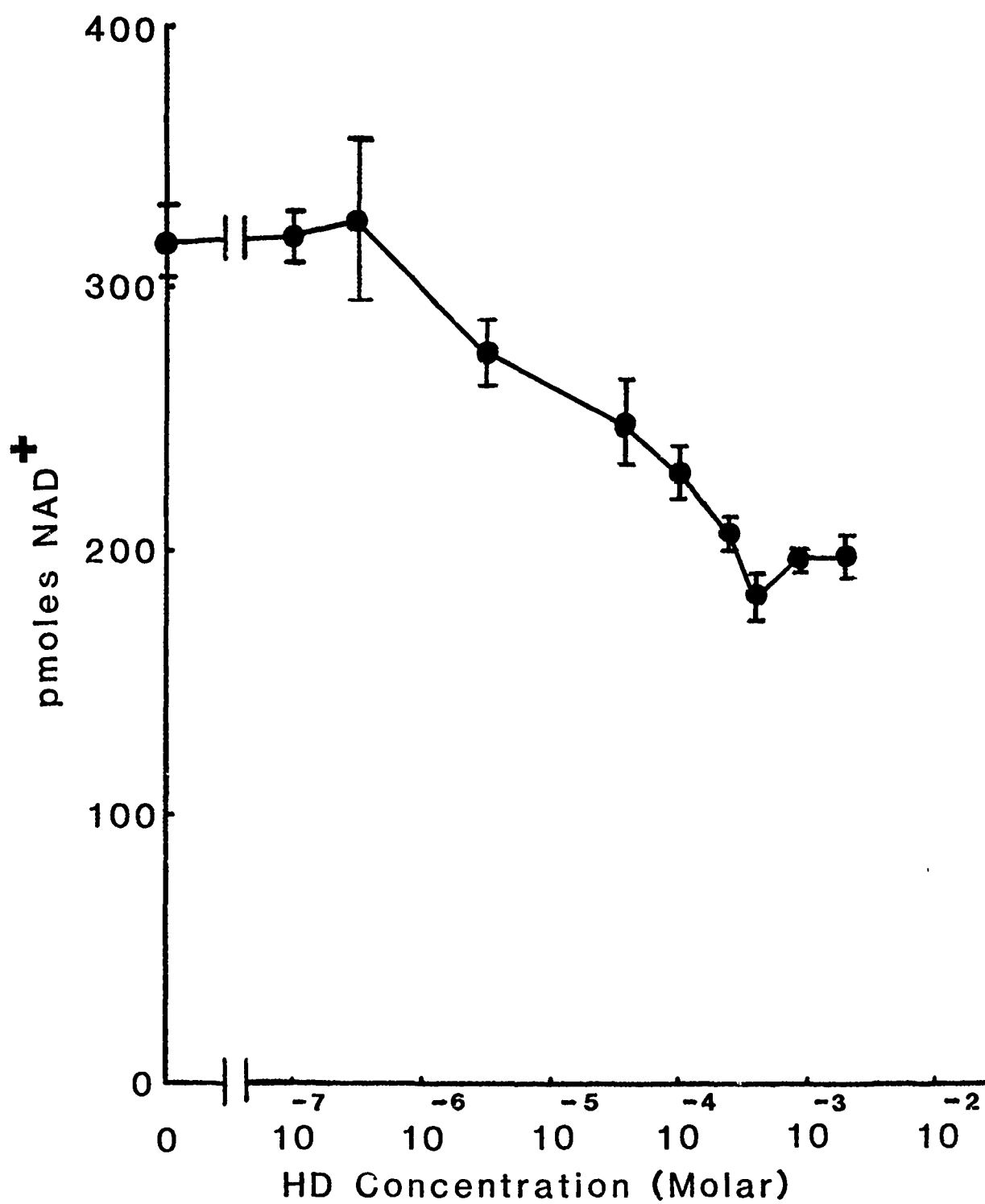


Figure 7

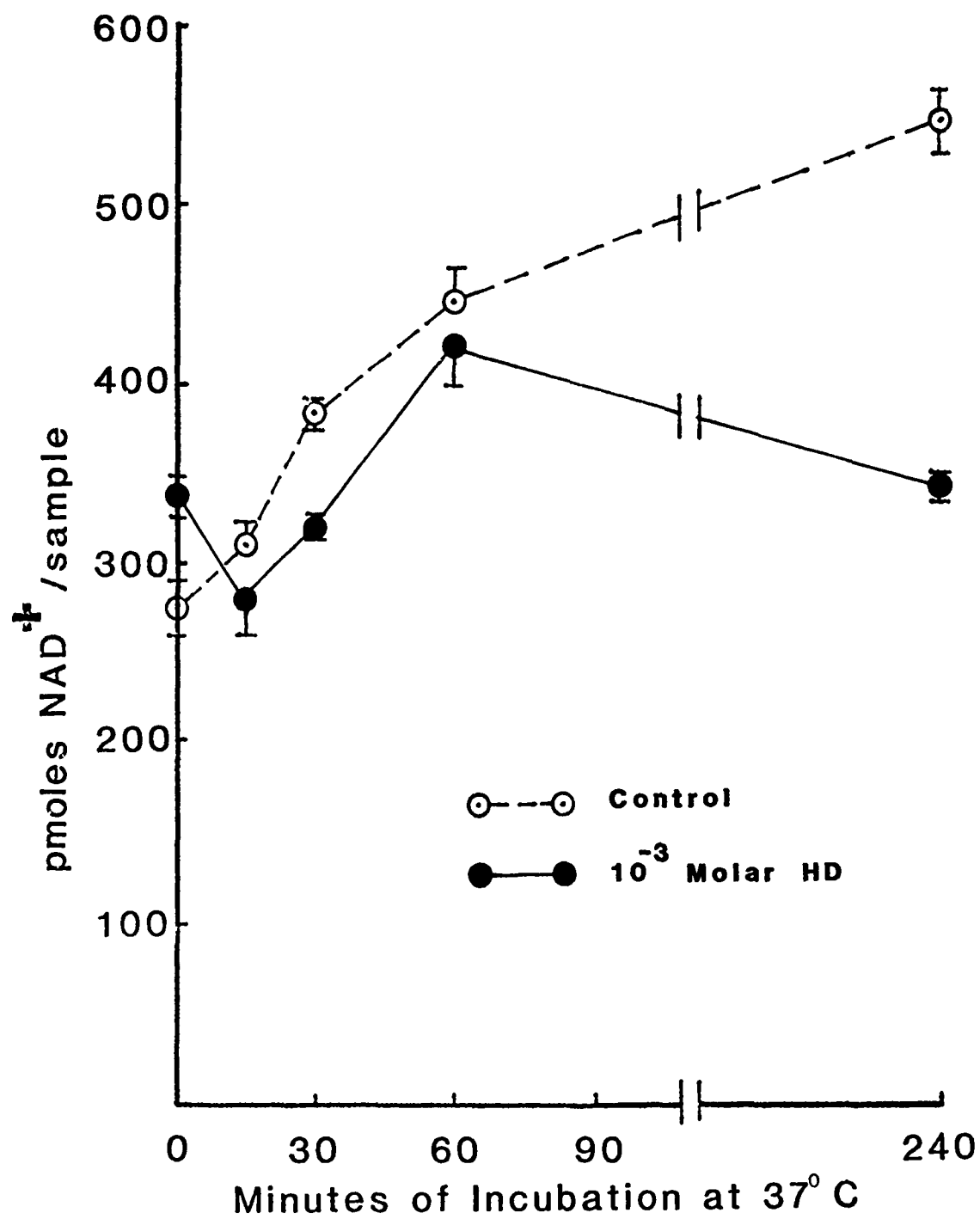


Figure 8

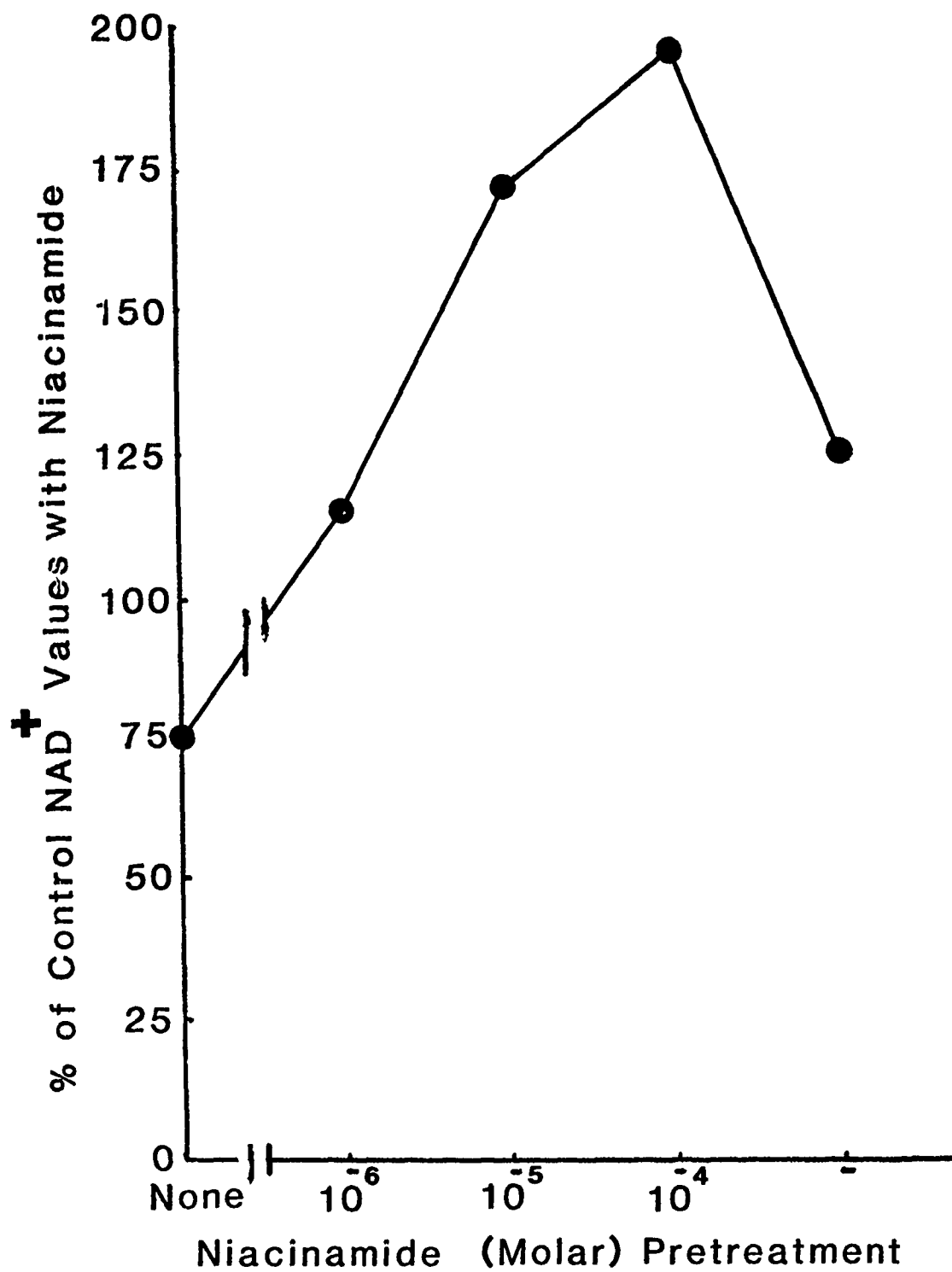


Figure 9

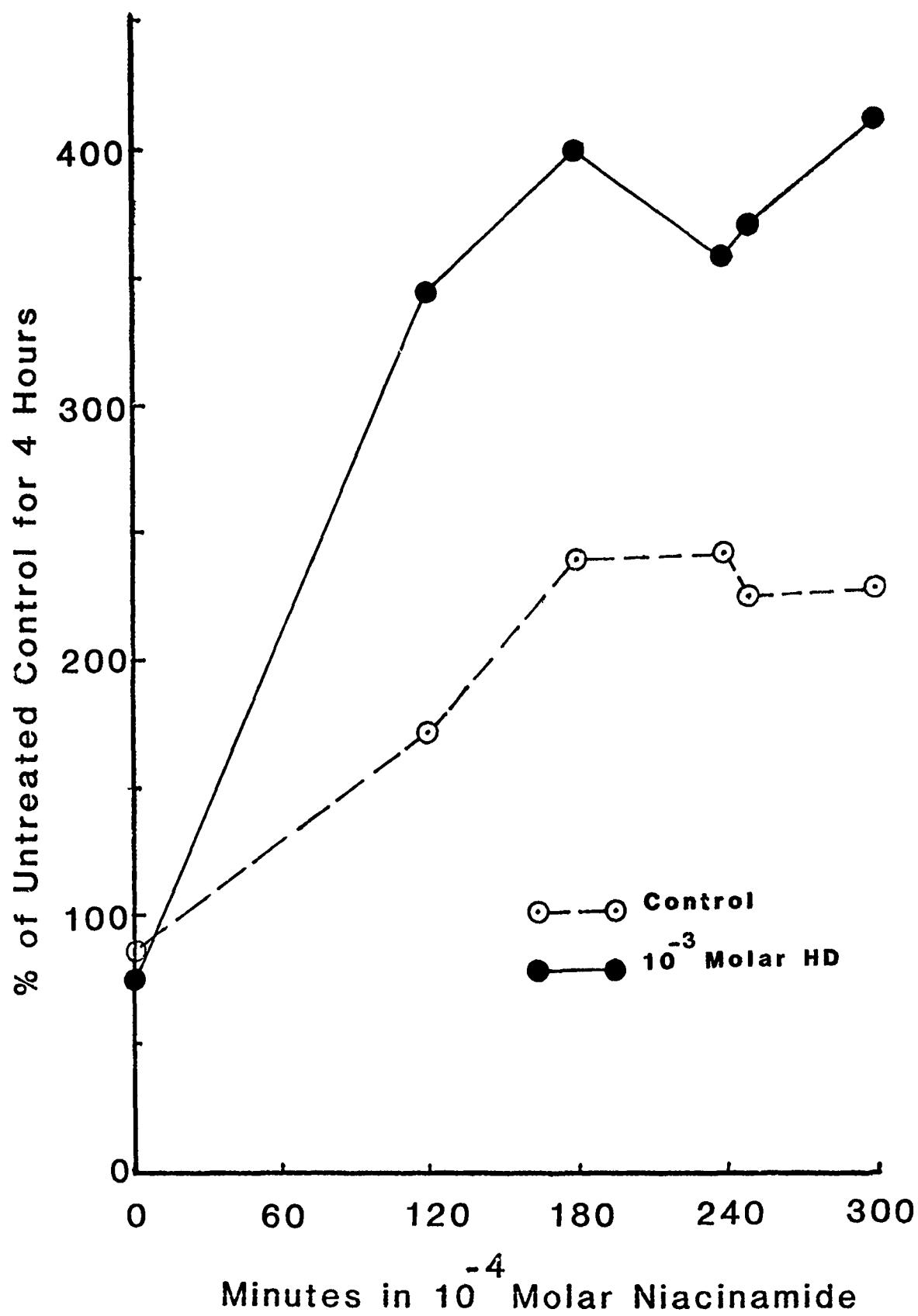


Figure 10

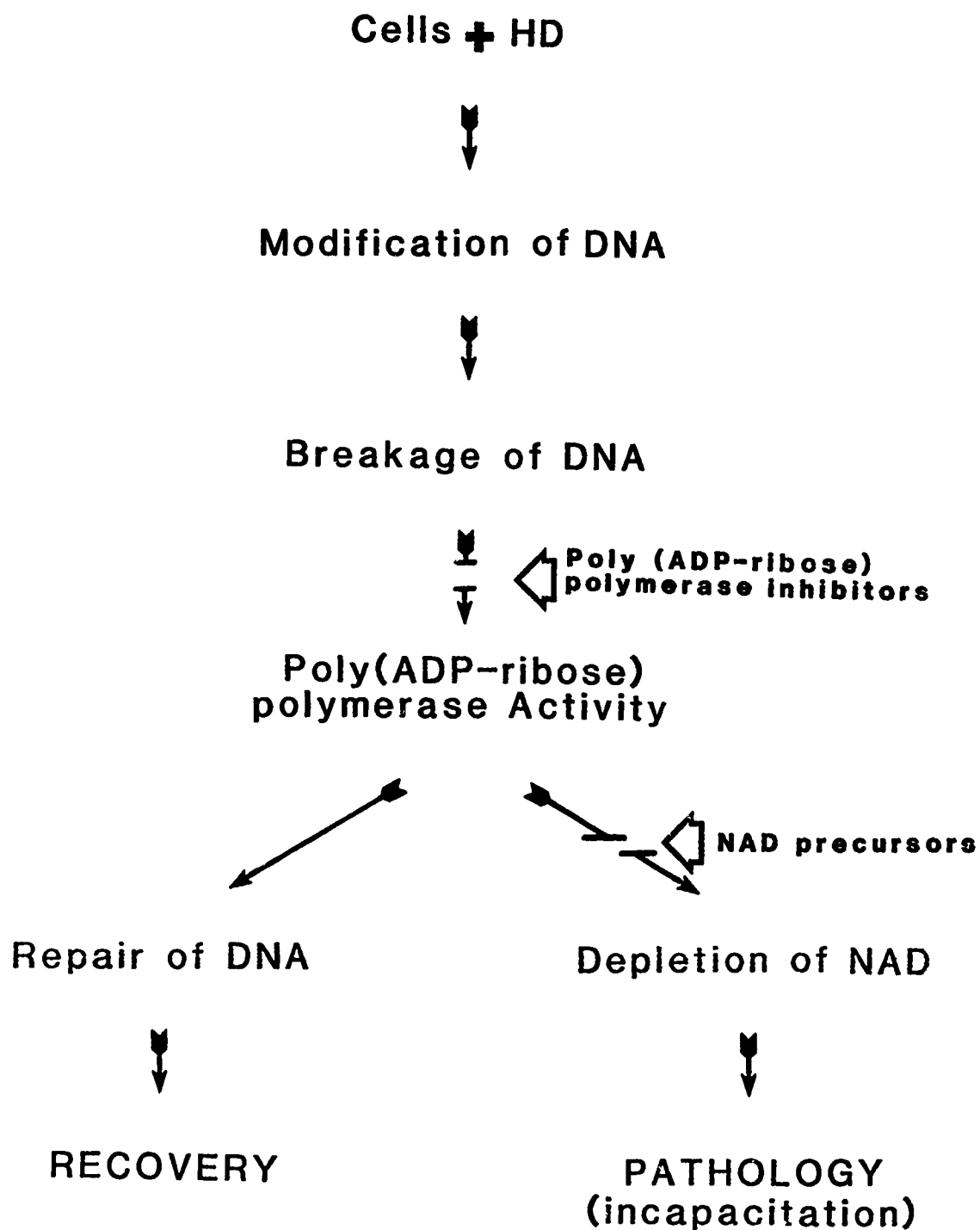


Figure 11

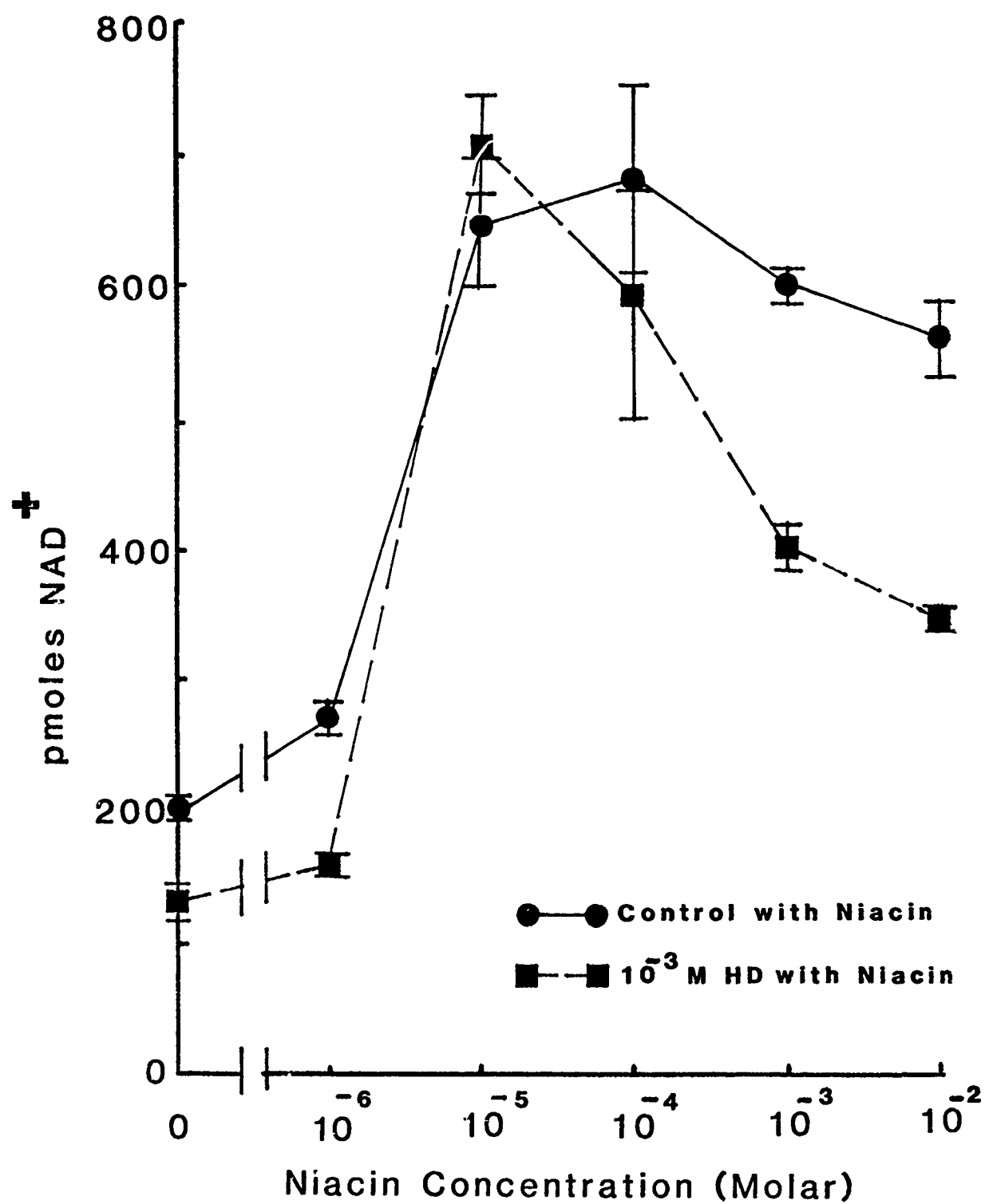


Figure 12

HD SUMMARY

1. HD treatment of leukocytes causes a dose-dependent decrease in NAD.
2. There is sufficient time for therapeutic intervention before the decreases in NAD levels occur.
3. Inhibitors of PADPRP and NAD precursors can intervene and block the decrease in NAD levels.
4. The clinical observations demonstrate that human leukocytes are sensitive target tissues.
5. Both the data and the clinical observations agree with our hypothesis.

Figure 13

EFFECT OF SOMAN ON NAD^+ LEVELS IN LEUKOCYTES

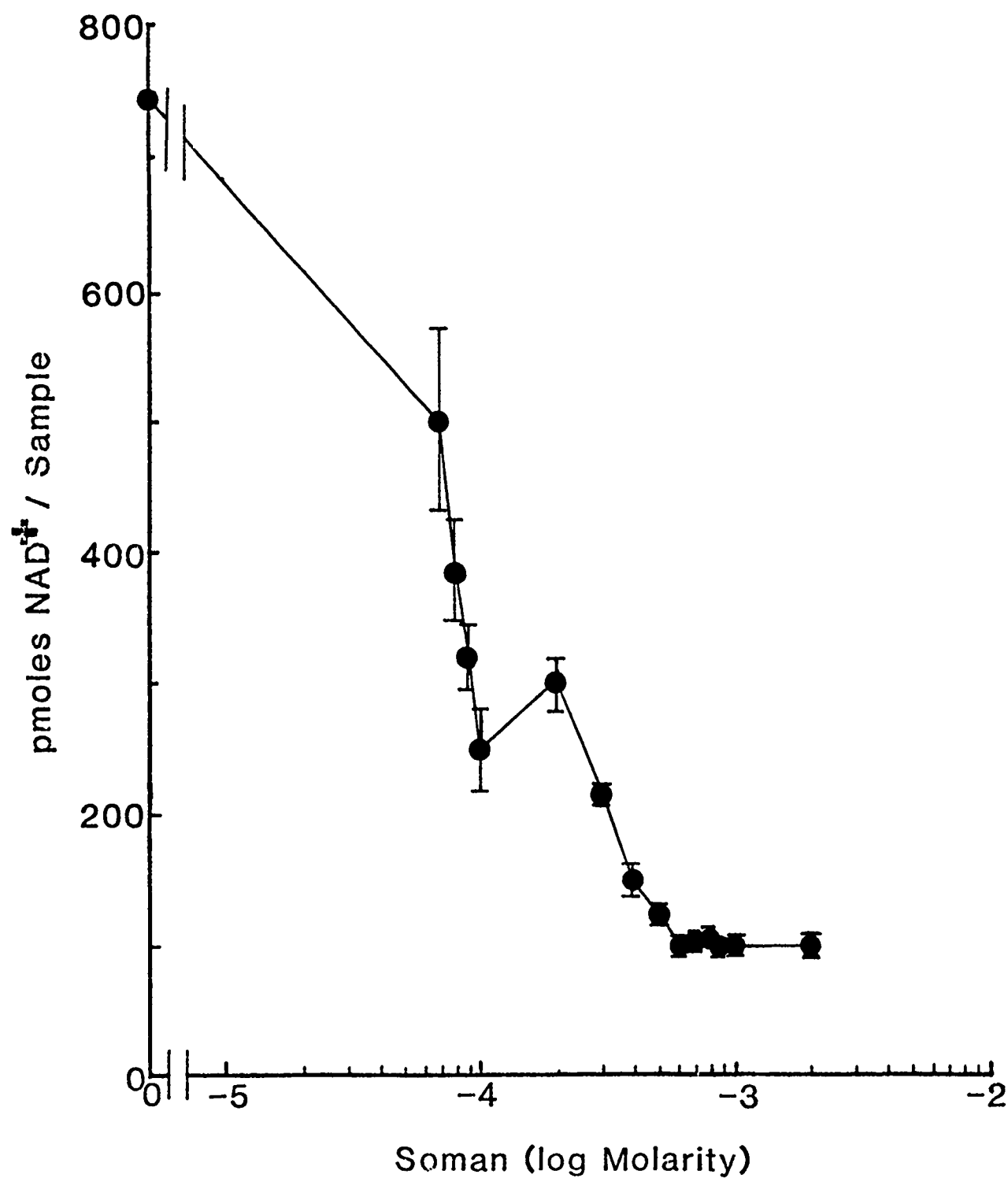


Figure 14

EFFECT OF SOMAN ON NAD⁺ LEVELS IN LEUKOCYTES

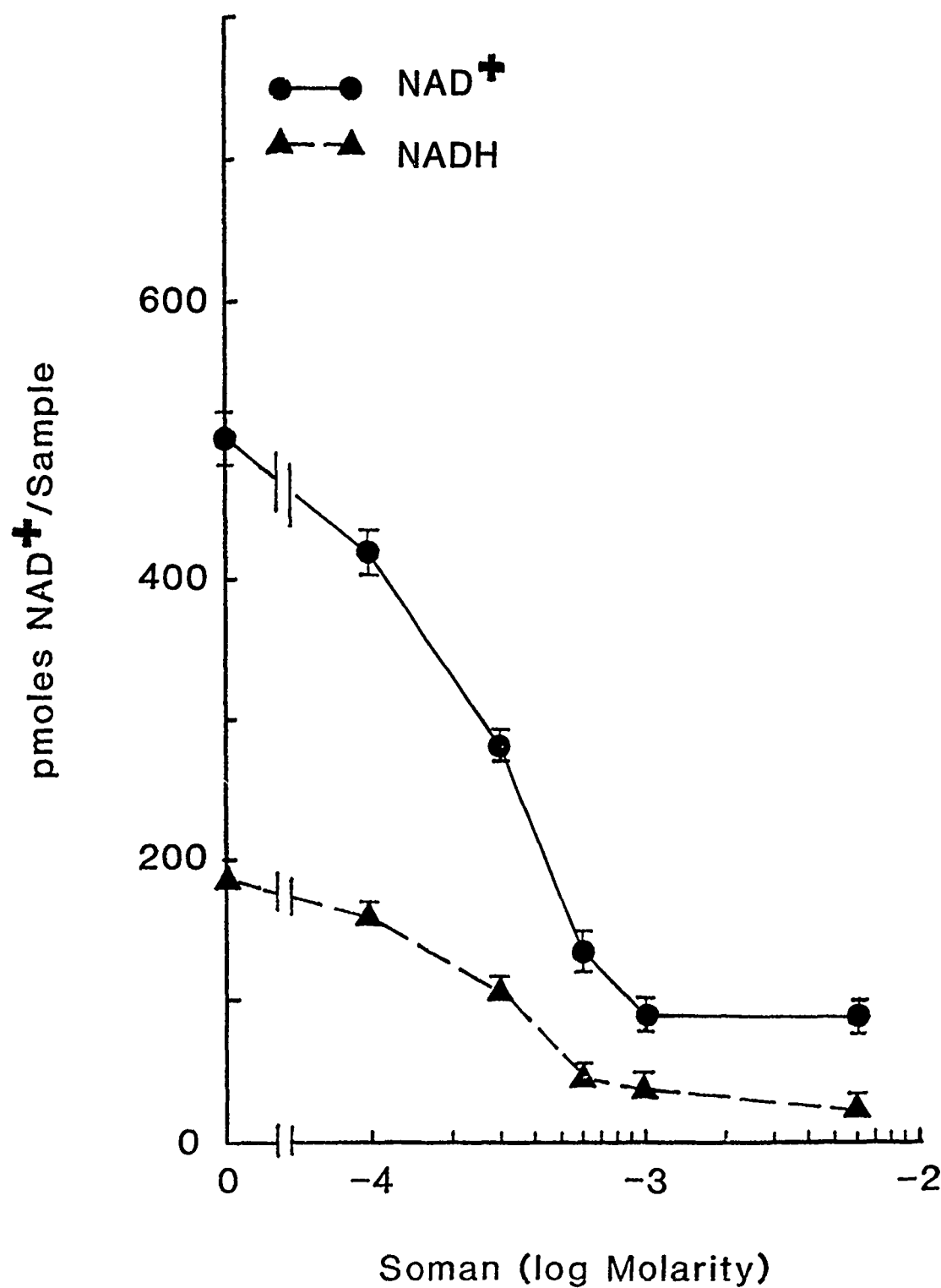


Figure 15

TIME COURSE FOR SOMAN-INDUCED NAD^+ LOSS IN HUMAN LEUKOCYTES

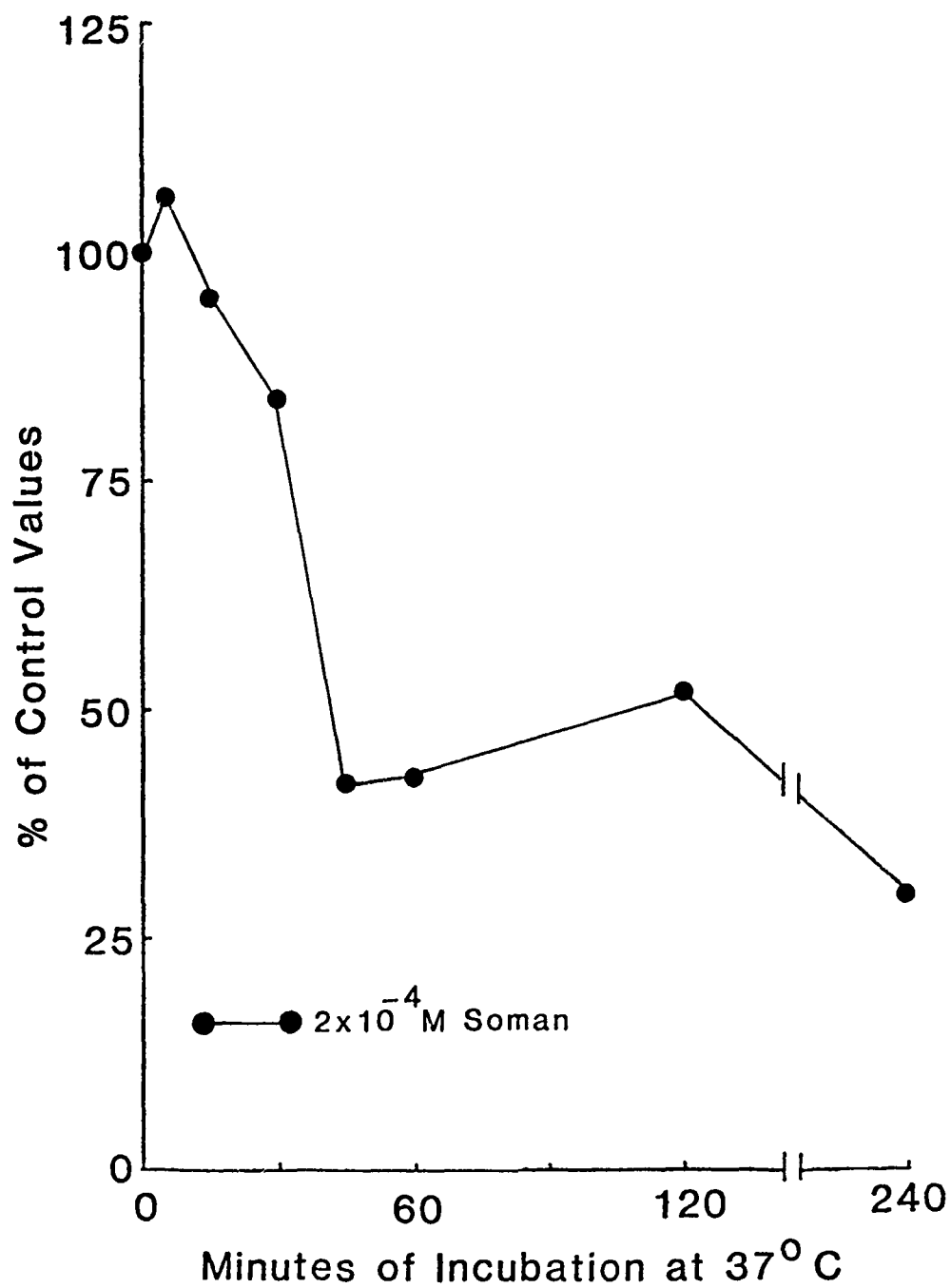


Figure 16

EFFECT OF TEMPERATURE ON NAD⁺ LEVELS IN SOMAN TREATED LEUKOCYTES

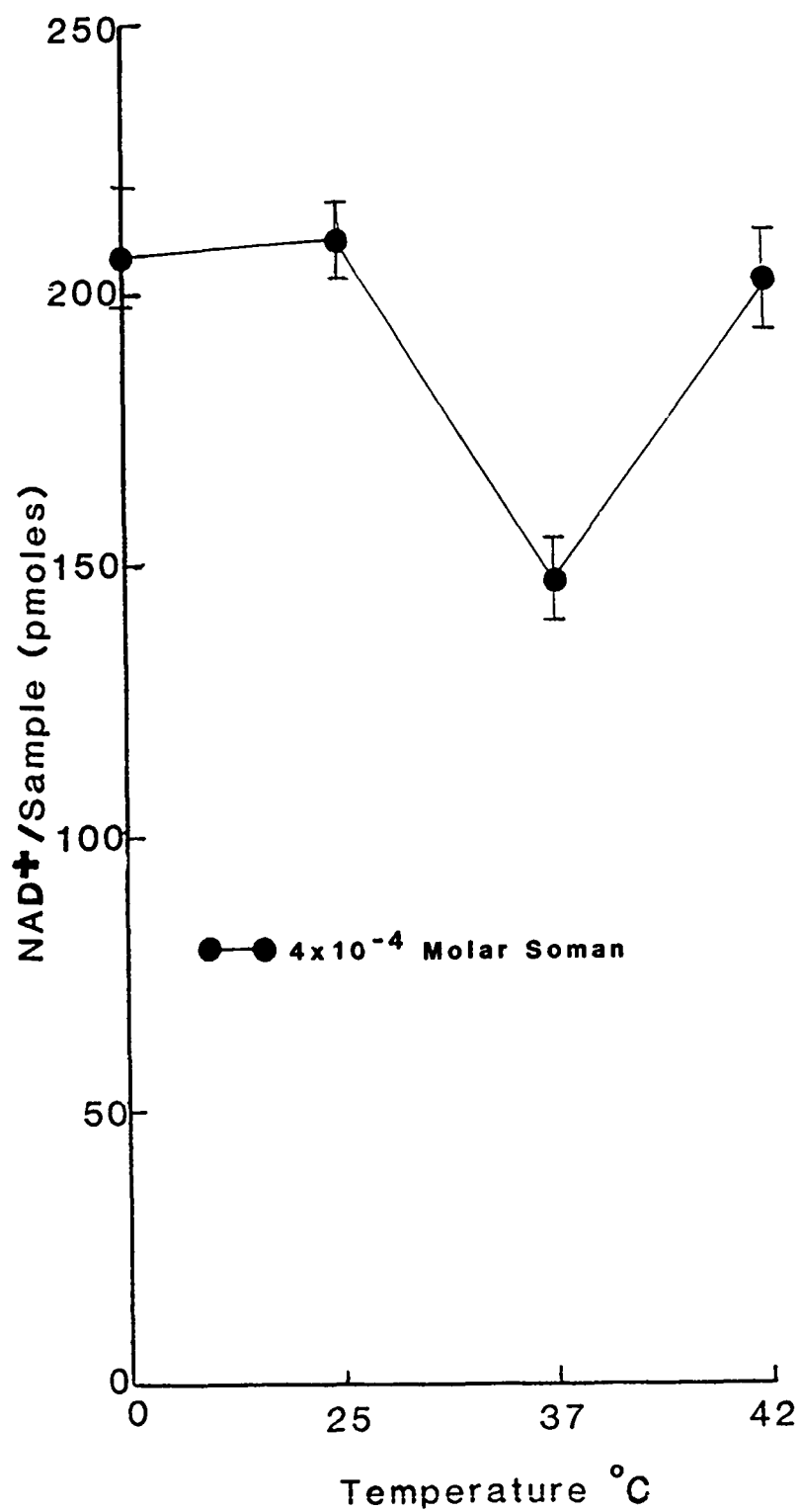


Figure 17

EFFECT OF SOMAN ON HISTAMINE RELEASE FROM LEUKOCYTES

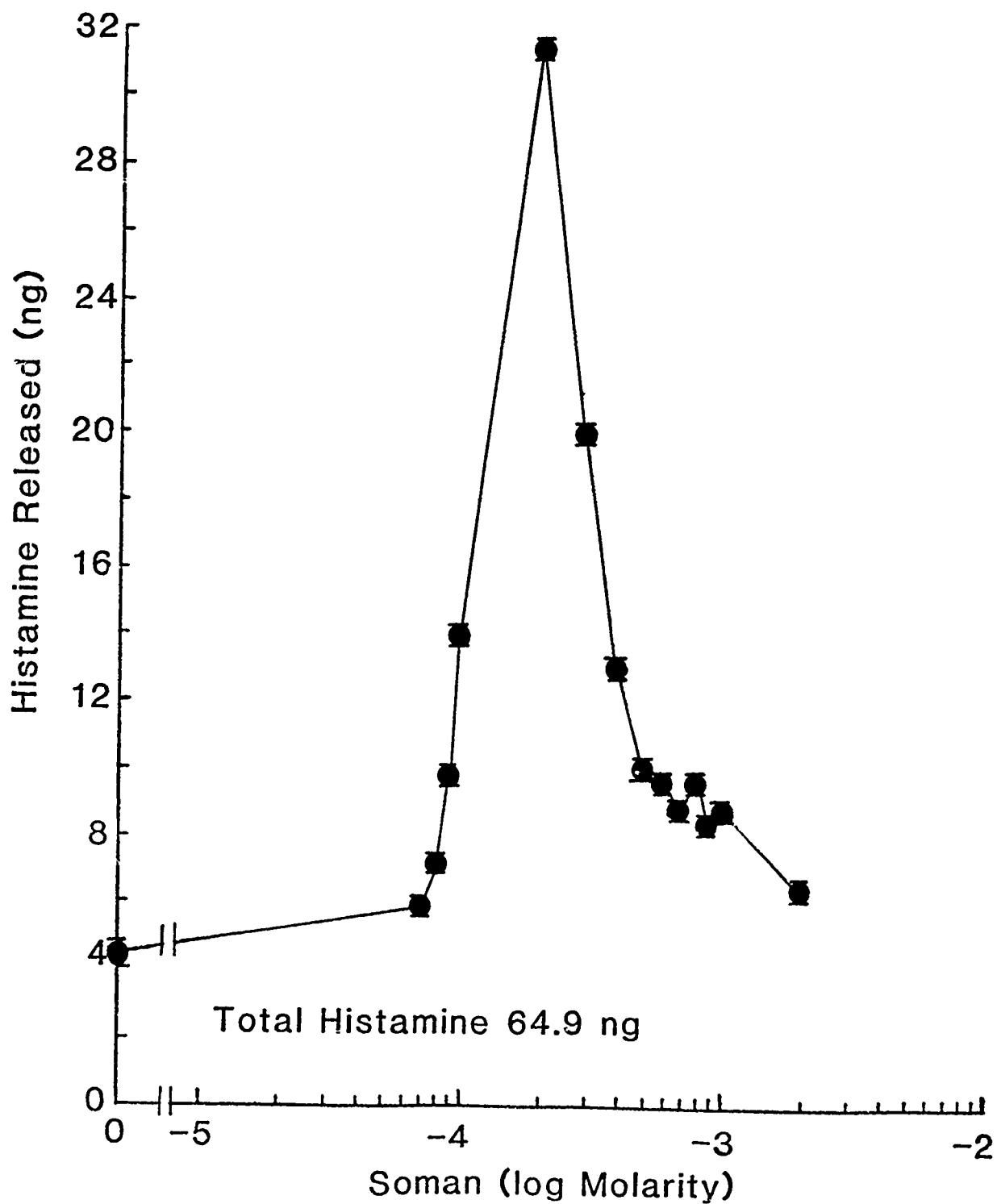


Figure 18

EDTA INHIBITION OF HISTAMINE RELEASE INDUCED BY SOMAN

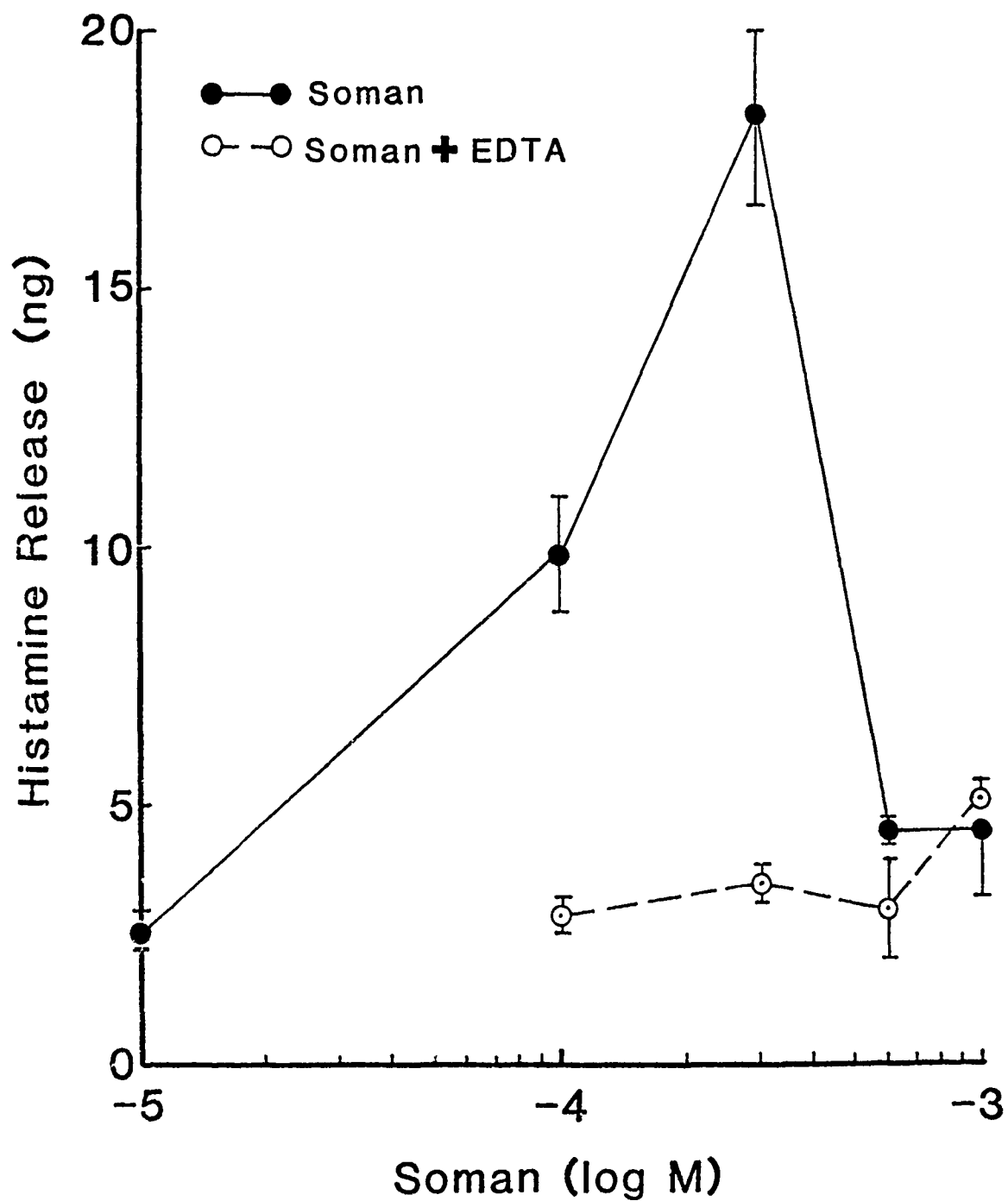


Figure 19

EFFECTS OF TEMPERATURE ON SOMAN INDUCED HISTAMINE RELEASE FROM HUMAN LEUKOCYTES

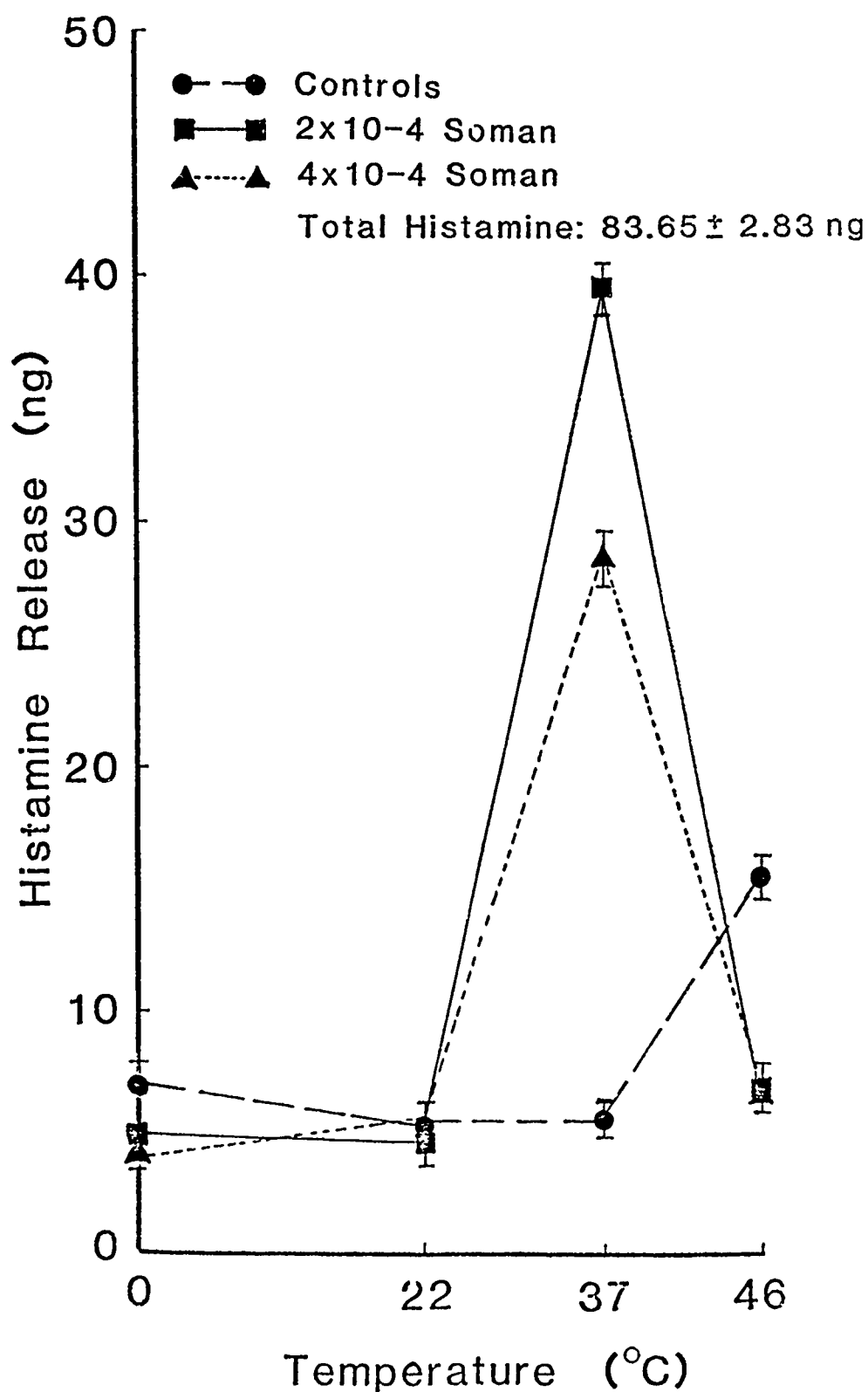


Figure 20

SUMMARY

1. Leukocytes are target tissues for both vesicant and nerve agents.
2. Leukocytes are easily obtained from human blood.
3. Leukocytes demonstrate biochemical changes due to chemical warfare (CW) agent exposure, which are easy to quantify.
4. Leukocytes can be used to investigate mechanisms of action of CW agents as well as to develop a means of intervention.

Figure 21

Solution Hydrolysis and Sorption Kinetics of Chemical Warfare (CW) Agents by
Polymeric Resins: Evaluation for
Decontamination Applications

P.S. Hammond, J. Forster, M. Michie, and S. Kelly

US Army Medical Research Institute of Chemical Defense,
Aberdeen Proving Ground, Maryland 21010

E.J. Langenmayr and R.B. Steigerwalt

The Rohm and Haas Company
727 Norristown Road
Spring House, Pennsylvania

and

A.E. Grow

Midwest Research Institute
Kansas City, Missouri

Existing chemical agent decontamination procedures are effective, but they present considerable potential hazards for human decontamination applications due to the irritative and/or toxic nature of the solutions required. In addition, no prophylactic protection against percutaneous exposure can be provided by those decontamination methods. A rapid, effective, and safe decontamination method, coupled with a suitable skin protectant against chemical agent exposure, could be of use for various military applications.

To address this problem, a USAMRDC contractor has produced a series of polymeric resins capable of hydrolytic and/or sorptive activity against chemical agents. These resins include both simple polymeric, nonfunctionalized (sorptive) resins and polymeric resins containing a variety of functional groups.

Slide 1 shows the steps being taken to evaluate a resin's potential for applications against chemical warfare agents. To conduct these evaluations, we have established a series of in vitro and in vivo tests to assess efficacy against both organophosphorus agents and vesicants. In these tests, resins have been compared to standard, currently available decontamination measures, i.e., for powdered resins, comparison was made to Fuller's earth or carbon while for aqueous suspensions, the M-258 Al kit was used for comparison. The results from these tests are used to evaluate both a resin's prophylactic potential, as well as its decontamination potential.

Based on previous results indicating that resins with both hydrolytic and sorptive activity were available as commercial resins, initial efforts were directed towards screening a range of these resins for desired activity. As summarized in slide 2 our goals were to choose 5 or 6 resins or resin combinations for further testing. These resins or resin blends would be prepared in lots large enough for efficacy studies in both the in vitro and in vivo test systems. In addition, they would be examined in formulation studies and in animal toxicology studies for toxicity level determinations.

Slide 3 lists the general types of resins currently under examination for hydrolytic or sorptive activity, as well as those planned for future testing. These include resins with reactive functionality, sorbent polymers, carbonaceous adsorbents and blends of sorbent and reactive resins.

Summarized on slide 4 are some specific types of resins currently undergoing testing. These include resins with sulfonic acid moieties (strong acid resins), resins which contain quaternary amine functionalities in the hydroxide form (these are termed strong base resins), as well as sorbent resins and resins that contain other, miscellaneous functional groups. As indicated previously, these types of resins were chosen since they are ones for which production processes are currently available.

The two in vitro tests outlined in Slide 5 have been used to assess the activity of these types of resins against organophosphorus compounds. For decomposition and/or removal of these compounds from aqueous and nonaqueous suspensions of resin, the kinetics of inactivation have been studied using an ultrafiltration cell system. To examine the effects of resins as dry powders or as aqueous suspensions, the Franz diffusion cell has been used. In all cases, dry powder resins were compared to Fuller's earth or carbon, while aqueous suspensions were compared to the M-258 Al kit or aqueous suspensions of carbon. Resins performing near the level of the "standard" treatment would then be selected for further in vivo efficacy testing using, as a preliminary screen, rabbit toxicity following agent exposure and resin decontamination.

Slide 6 shows the apparatus used for in vitro testing of a resin's ability to remove or decompose diisopropyl fluorophosphate (DFP), soman, and sarin from aqueous and nonaqueous suspensions. After addition of the

organophosphorus compound, resin and solvent to the reservoir followed by equilibration and stirring at 25°C, samples of filtered solvent are removed for analysis from the lower exit port. Periodically, samples of the resin-solvent suspension are also removed from the reservoir for analysis. Using a fluoride-specific electrode to assay samples of filtrate and resin-solvent suspensions, the parameters shown in Slide 7 are obtained. It is of particular importance to note that this analysis provides the capability to measure both free organophosphorus compound in filtrate, as well as that sorbed on the resin. Since the ratio of resin functionality to organophosphorus compound is high in all studies, plots of agent or DFP concentration in filtrate versus time provide pseudo first-order kinetics for decomposition of the organophosphorus compound. A typical data set analysis for decomposition of DFP is shown on Slide 8. The pseudo first-order rate constant for the reaction k_{obs} , is given by the slope of the line. The second-order rate constant, k_2 , is obtained by dividing k_{obs} by the theoretical concentration of reactive species (for example hydroxide, proton, or other active functionality) as if these were freely soluble in solution.

As a preliminary screen, a series of commercially available resins were evaluated for their ability to decompose the organophosphorus compound DFP from aqueous and nonaqueous solutions using this ultrafiltration cell system. Results for each type of active resin, as compared to solution 1 of the M-258 Al kit, are summarized in the next slide (Slide 9). For strong acid functionalized resins and resins containing the pyridinium aldoxime functionality, less than 0.1 percent and 2 percent of the M-258 Al activity were found, respectively. Strong base resins, that is those containing quaternary amine moieties in the hydroxide form, showed from 2 to 41 percent of the M-258 Al activity, while mixtures of strong base and strong acid resins gave 4 to 34 percent of the M-258 Al activity. Nonaqueous solvents, such as polyethylene glycol, polydimethyl siloxane, and isopropanol, caused substantial decreases in resin activity. For example, strong base-strong acid resin mixtures showed only 2 to 6 percent of the M-258 Al activity in nonaqueous solvents compared to 4 to 34 percent of that activity for aqueous suspensions. Thus, in summary, even the most active functionalized resins of that initial group, in those solvents examined, decomposed DFP at only 41 percent of the rate found for solution 1 of the M-258 Al kit.

In addition to these results for functionalized resins, the time required to adsorb 95 percent of the available DFP from aqueous and thickened aqueous suspensions was determined for both a carbonaceous and polymeric sorbent resin. Comparison of these times for 95 percent sorption of DFP to the same index of activity for carbon in aqueous and thickened aqueous suspensions is made in the next slide (Slide 10). For these resins, the carbonaceous sorbent removes 95 percent or more of the DFP from aqueous mixtures in 5 minutes while, carbon required 22 minutes to achieve the same level of sorption. Both ionic and nonionic thickening agents substantially increased the time required to remove DFP from aqueous mixtures for both the carbonaceous resin and carbon. The polymeric sorbent resin tested showed activity approximately equal to that found for carbon in aqueous suspension.

Based on the results for these resins with DFP, rates of decomposition and sorption of the chemical agent soman (GD) were examined, as is shown in the next slide (Slide 11). For these studies, decomposition of soman by solution 1 of the M-258 Al kit was compared to sorption or decomposition of soman by resins demonstrating high activity against DFP. One should note that the rate of decomposition of soman by solution 1 of the M-258 Al kit was found to be much faster than the comparable rate for DFP, with all available soman decomposed by this solution in 5 seconds or less. This rate was found to be

much faster than that for either a strong base resin alone or a mixture of a strong base and strong acid resin. These resins required 30 min to decompose 97 percent or 57 percent respectively, of the available soman. However, when a carbonaceous resin was added to the strong base-strong acid resin mixture, sorption of 95% or more of the available soman occurred within 3 minutes. We see, therefore, that while the M-258 Al kit caused an extremely fast rate of decomposition, addition of the carbonaceous resin to the strong acid-strong base resin mixture can compensate, at least in part, for the slower decomposition rates found for these active resins.

Based on these initial soman results, six combinations of strong base-strong acid resins, strong base-strong acid-carbonaceous resins, and a carbonaceous-sorbent resin mixture were chosen for further testing. A comparison of the rate of decomposition of soman by solution 1 of the M-258 Al kit and decomposition and/or sorption of soman by these resin mixtures are shown in Slide 12. Again, solution 1 of the M-258 Al kit decomposed soman at a rate much faster than that found for the strong base-strong acid resin mixture alone. However, two of the strong base-strong acid-carbonaceous resin mixtures gave appreciable decomposition rates and removed 99 percent of the available soman by sorption and decomposition in 4 minutes or less. It is of note that the sorbent resin mixture alone removed 99 percent of the available soman in 4 minutes or less through sorption of the agent.

Similar results were obtained with these same resin mixtures when sarin was used as the organophosphorus compound. These results are shown in Slide 13. As was found with DFP and soman, a strong base-strong acid resin combination alone decomposed sarin at a much slower rate than that found for solution 1 of the M-258 Al kit, with 48 percent decomposed in 36 minutes for the resin mixture compared to 99 percent or greater in 5 seconds for M-258. Addition of a carbonaceous resin or a polymeric sorbent resin to this resin mixture gave much faster removal with 99 percent or greater sarin lost in 4 minutes or less. As expected from previous results, the sorbent resin mixture also removed sarin rapidly from aqueous suspensions.

It should be noted that when these same resins were tested against sarin and soman with polyethylene glycol as solvent, all sorptive activity was eliminated. In these studies, resin mixtures showed only decomposition of the agent with rates similar to those shown in Slides 12 and 13. Thus, while these first generation resin mixtures appear to hold promise as decontaminants, formulations in nonaqueous solvents could present serious problems for prophylactic applications.

As previously indicated, we have used a second in vitro technique to evaluate resins for their ability to reduce membrane penetration by chemical agents or by the organophosphorus compound diisopropyl fluorophosphate (DFP). Slide 14 shows the Franz Diffusion Cell apparatus used to carry out these evaluations. For these diffusion tests, a radiolabeled organophosphorus compound is applied to the membrane or skin and allowed to penetrate for a standard period of time. Assay of the isotonic saline solution for the radiolabel provides an assessment of penetration with no decontamination. Through application of decontamination procedures to the membrane, following organophosphorus compound exposure, the effectiveness of various decontamination procedures may be determined. In the studies summarized on Slide 15, a Latex semipermeable membrane acted as the barrier with [14 C] DFP used as the test organophosphorus compound. Decontaminants evaluated were M-258 Al (solution 1), active and sorbent resins, carbon, and Fuller's earth. Following application of [14 C]-DFP, decontamination as indicated was effected at 8 minutes past exposure, with radiolabel penetration evaluated at 3 hours posttreatment. It appears from these results that the strong base resin

tested in aqueous solution, the carbonaceous resin as both a dry powder and as an aqueous suspension, and carbon in aqueous suspension all reduce penetration of radiolabel to a larger extent than M-258 Al (solution 1). It should be noted that the nature of the penetrating material, that is, whether the species penetrating was DFP or hydrolyzed DFP was not determined. It is clear, however, that penetration is greatly reduced by the carbonaceous resin and that this resin is much more effective than Fuller's earth at reducing DFP transmembrane migration. Further tests of resins with skin samples are currently underway.

Preliminary toxicology testing of some of the resins have already been carried out. The results of these tests are shown in the last slide (Slide 16). Those resins examined thus far showed virtually no acute oral toxicity in the rat, were nonirritating to rabbit skin, and showed only slight to moderate eye irritation in the rabbit.

On the basis of these toxicity results and the ability of resin mixtures to rapidly remove agent from aqueous suspensions, in vivo testing of these compounds seems warranted. In addition, further in vitro tests with other organophosphorus agents and vesicants are planned. These tests should provide answers to whether resins will prove effective in agent decontamination or prophylactic applications.

Slide 1

RESIN EVALUATION

1. Establish in vitro and in vivo evaluation models.
2. Assess efficacy against vesicants and OP agents.
3. Test resins against standards
 - a. Powder - Fuller's Earth
 - b. Aqueous suspension - M-258 Al
4. Evaluate prophylactic and decontamination potential.

Slide 2

RESIN DEVELOPMENT: INITIAL GOALS

1. Screen available resins.
2. Identify 5 or 6 resins for further testing.
3. Synthesize lots large enough for:
 - a. Efficacy studies
 - b. Formulation studies
 - c. Toxicology studies
4. Examine 2 or 3 formulations for each resin.

Slide 3

TYPES OF RESINS EVALUATED

1. Reactive Polymers (polystyrene backbone cross-linked with divinyl benzene).
 - a. Covalently bound nucleophiles.
 - b. Covalently bound oxidants.
 - c. Radically bound reactive groups.
 - d. Covalently bound nucleophilic catalysts.
2. Sorbent Polymers
 - a. High surface area.
 - b. Gelular
3. Carbonaceous Adsorbents
4. Reactive/Sorbent Blends

Slide 4

RESIN FUNCTIONAL GROUPS UNDER CONSIDERATION

1. Strong Acid Resins
 - SO_3H Functionality
2. Strong Base Resins
 - $\text{NR}_3^+ \text{OH}^-$ Functionality
3. High Surface Area Sorbent
4. Carbonaceous Sorbent
5. Miscellaneous Resins
 - Other Functionality

Slide 5

INITIAL EFFICACY TESTING OF RESINS
(Dry Powder or Aqueous and Non-Aqueous Suspensions)

1. In Vitro Tests

- a. Kinetics of Inactivation - Ultrafiltration Cell
- b. Dermal Penetration - Franz Diffusion Cell

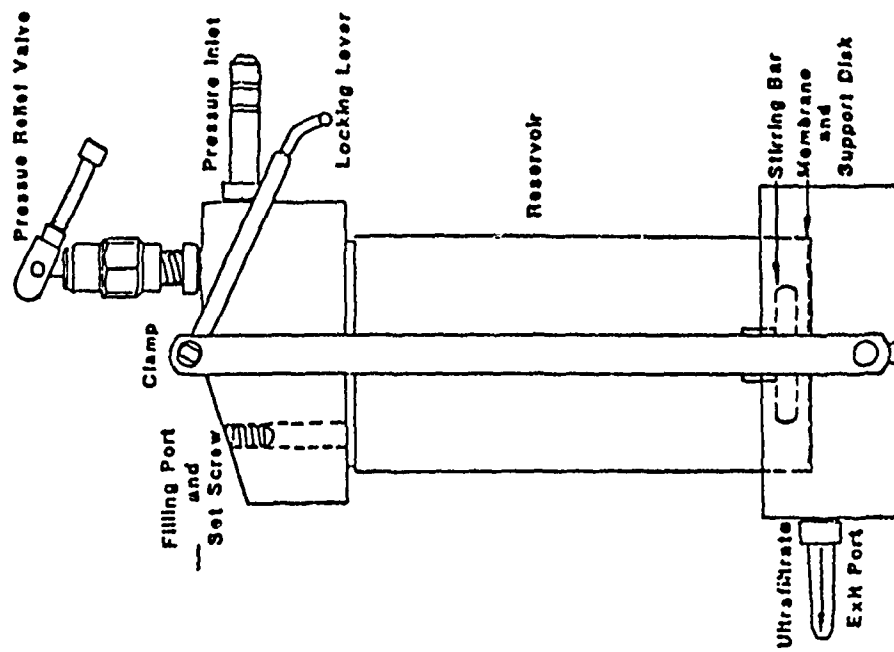
Those Resins with Efficacy \geq Reference Standard

2. In Vivo Tests

- a. Preliminary Screen - Toxicity in Rabbits
- b. Definitive Toxicity Testing with Formulated Materials

Slide 6

ULTRAFILTRATION CELL SYSTEM



Stirred Cell

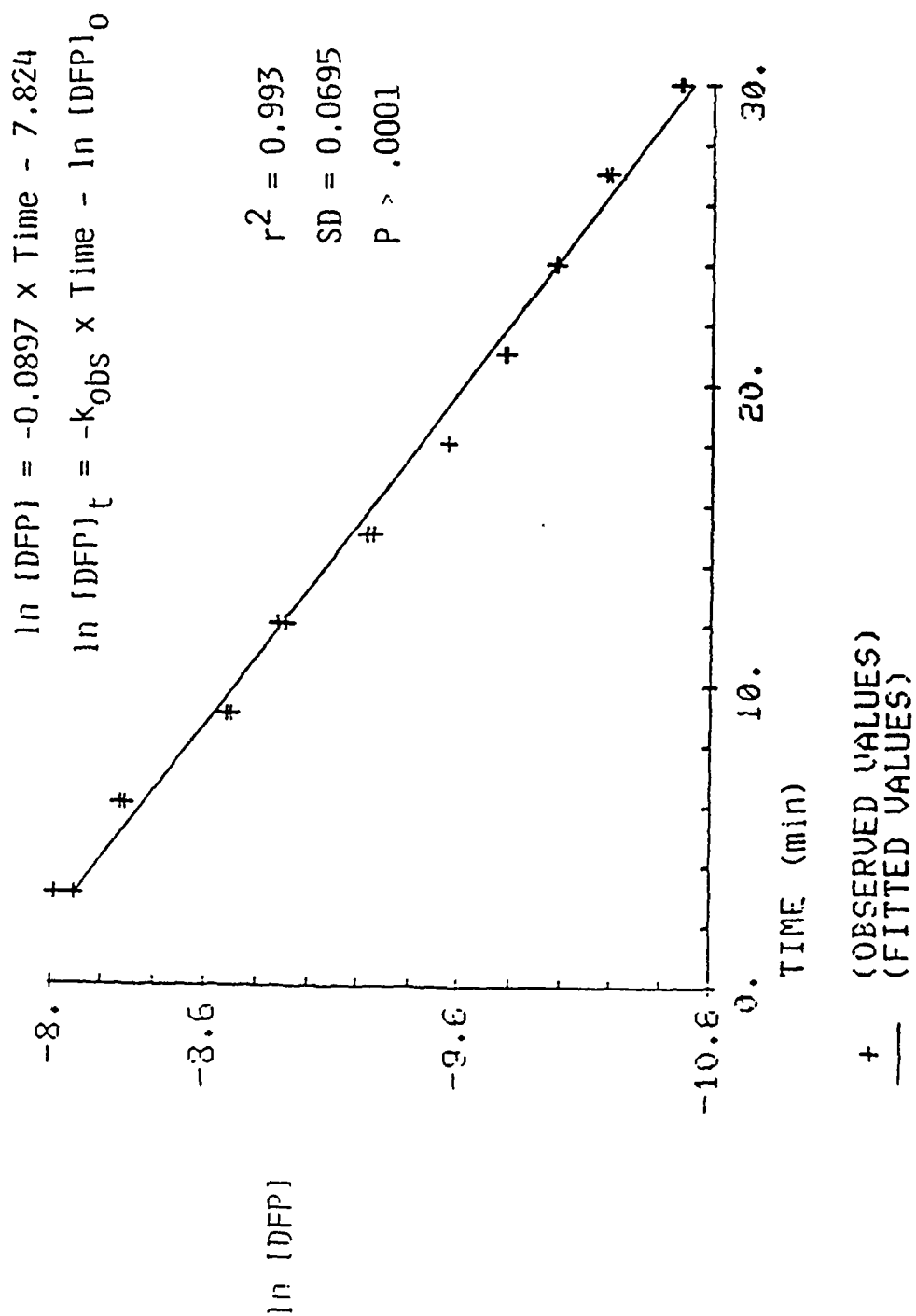
Slide 7

ULTRAFILTRATION CELL DATA EVALUATION

1. Free Fluoride in Filtrate
2. Free Organophosphorus Compound in Filtrate
3. Fluoride on Resin
4. Organophosphorus Compound on Resin

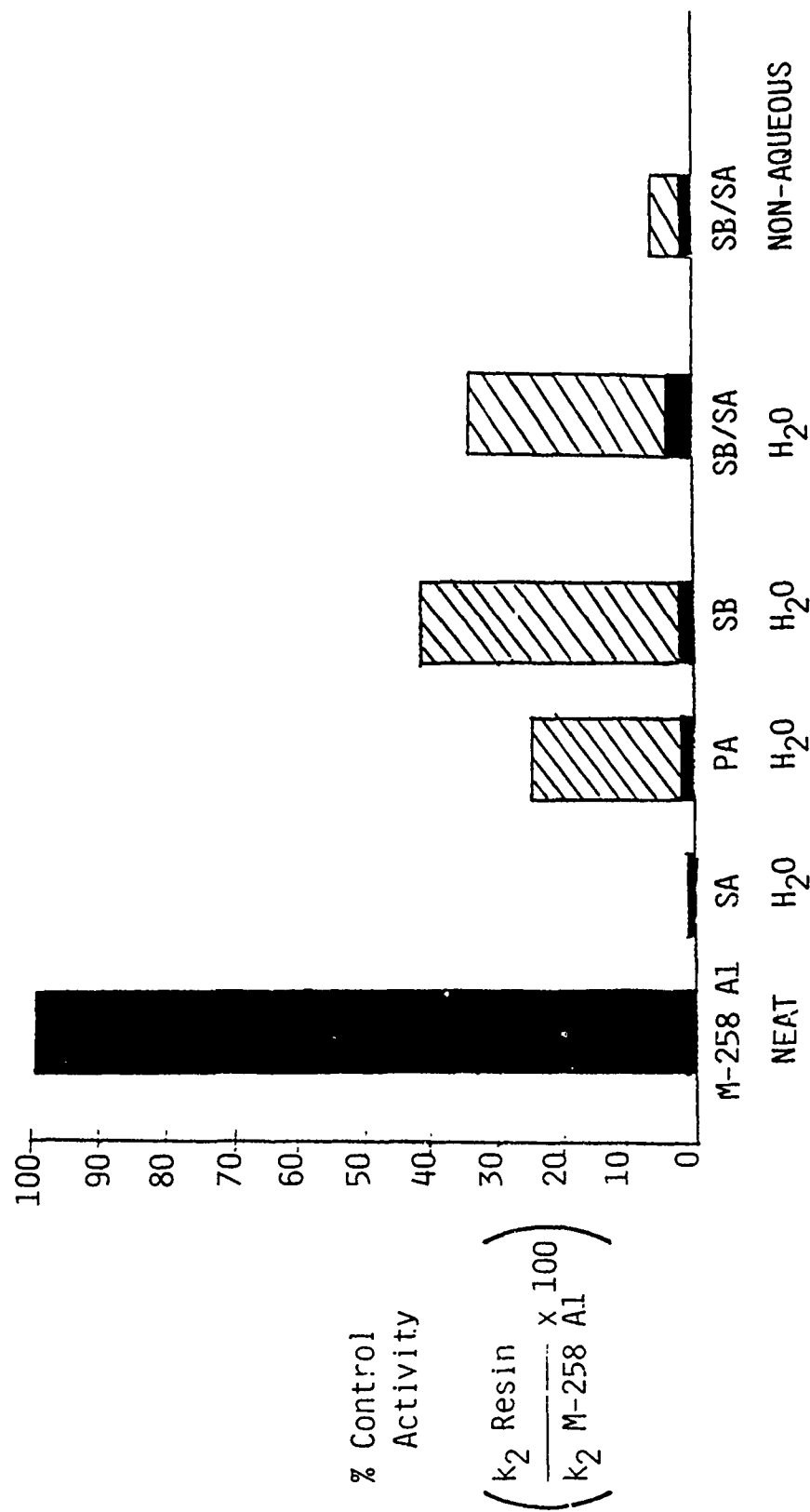
Slide 8

Kinetics of DFP Loss by Incubation with Strong Base/Strong Acid Resin



**RATES OF DECOMPOSITION OF THE ORGANOPHOSPHORUS COMPOUND
DIISOPROPYL FLUOROPHOSPHATE IN NON-AQUEOUS AND AQUEOUS MIXTURES**

RELATIVE TO M-258 A 1



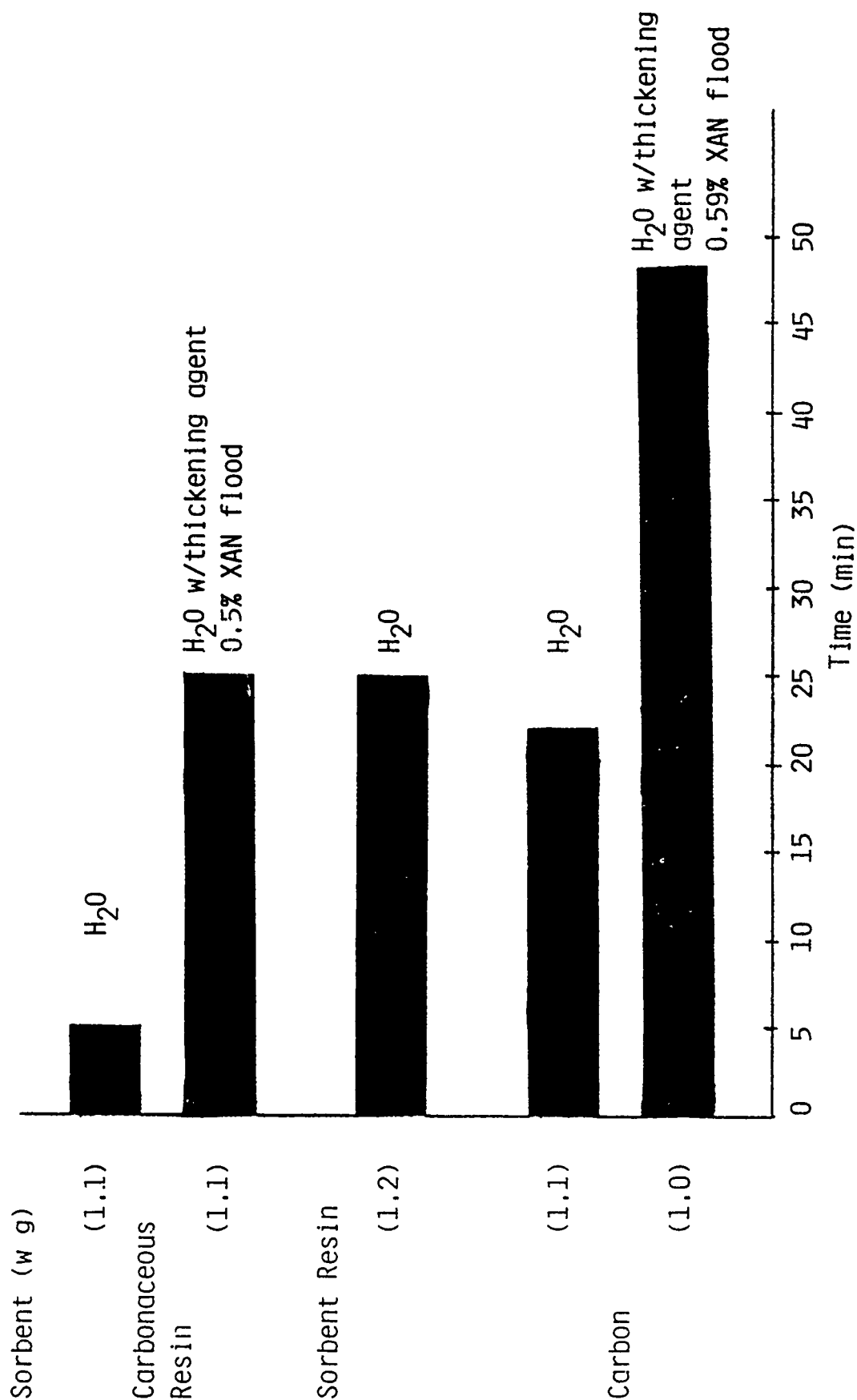
SA = STRONG ACID

PA = PYRIDINIUM ALDOXINE

Slide 10

TIME TO 95% SORPTION OF DFP (DIISOPROPYL FLUOROPHOSPHATE)

BY AQUEOUS AND THICKENED-AQUEOUS SUSPENSIONS



Slide 11

COMPARISON OF SOMAN LOSS BY M-258 A (SOLN I) AND
AQUEOUS RESIN SUSPENSIONS (1-2% W/V)

<u>Test Material</u>	<u>Decomposition Rate</u> k_2 ($M^{-1}min^{-1}$)	<u>Time</u>	<u>% Soman Decomposed (D) or Sorbed (S)</u>
M-258 A (Soln I)	≥ 50	5 Sec	99 (D)
Strong Base Resin	1.7	30 Min	97 (D)
Strong Base Resin w/ Strong Acid Resin (1:1)	1.0	30 Min	57 (D)
Strong Base Resin w/ Strong Acid Resin w/ Carbonaceous Resin (1:1:1)	No Decomp.	≤ 3 Min	95 (S)

Slide 12

COMPARISON OF SOMAN LOSS BY M-258 A (SOLN I) AND
AQUEOUS RESIN SUSPENSIONS (1-3% W/V)

<u>Test Material</u>	<u>Decomposition Rate k_2 ($M^{-1}min^{-1}$)</u>	<u>Time</u>	<u>% Soman Decomposed (D) or Sorbed (S)</u>
M-258 A (Control)	≥ 50	5 Sec	99 (D)
SB/SA (1:1)	1.0	24 Min	55 (D)
SB/SA/Carbonaceous (1:1:1) or (2:1:1)	0.08 to 4.4	≤ 4 Min	99 (D & S)
Carbonaceous Resin w/ Sorbitive Resin (1:1)	No Decomposition	≤ 4 Min	99 (S)

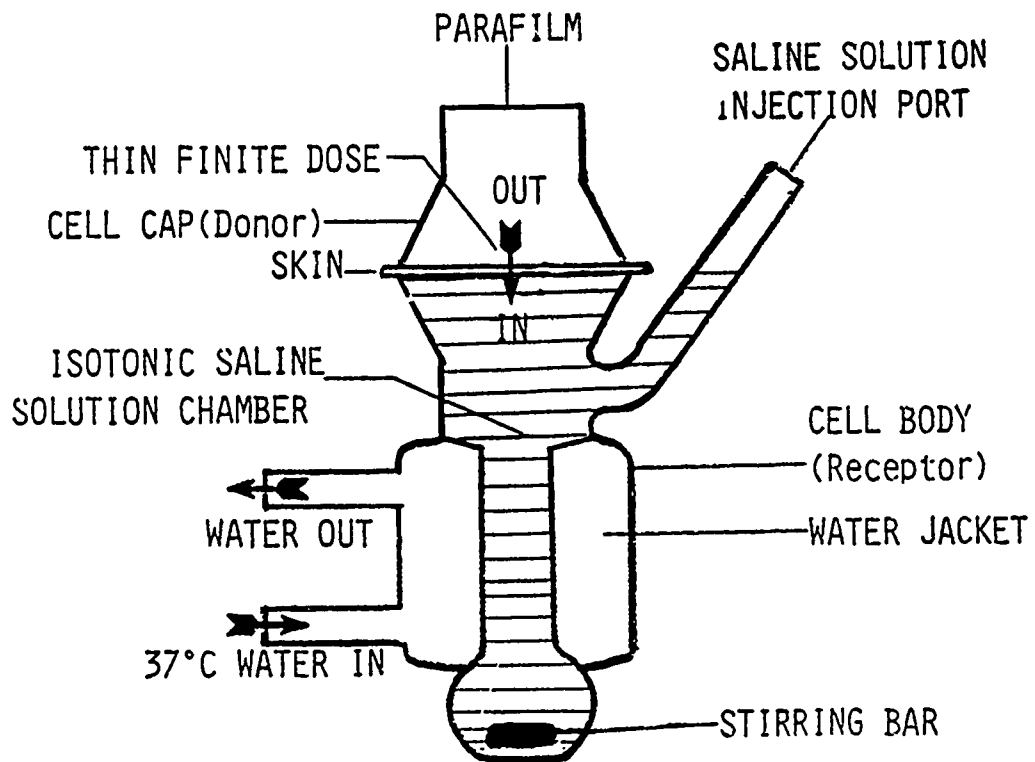
Slide 13

SARIN SORPTION/DECOMPOSITION BY M-258 A (SOLN I) AND
AQUEOUS RESIN SUSPENSIONS (1-2% W/V)

<u>Test Material</u>	<u>Decomposition Rate k_2 ($M^{-1}min^{-1}$)</u>	<u>% Sarin Decomposed (D)</u>	
		<u>Time</u>	<u>Sorbed (S)</u>
M-258 A (Control)	≥ 50	5 Sec	99 (D)
SB/SA (1:1)	0.8	36 Min	48 (D)
SB/SA Carbonaceous or SB/SA/Sorbent (2:1:1) or (1:1:1)	No Decomposition to 0.6	4 Min	99 (S)
Carbonaceous Resin W/ Sorptive Resin	Slow Decomposition	4 Min	99 (S)

FRANZ DIFFUSION CELL

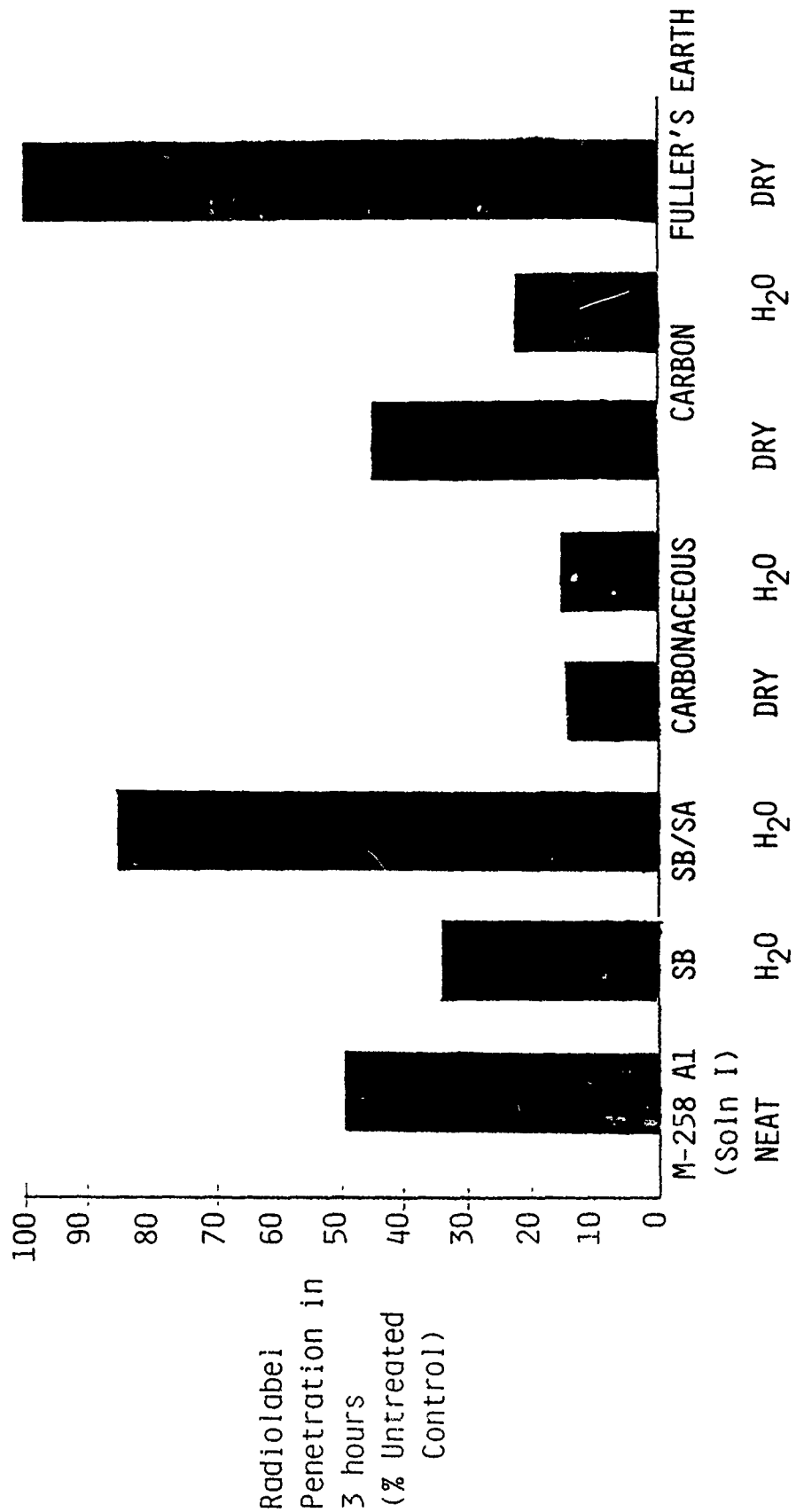
SCHEMATIC



278

Slide 15

**FRANZ CELL EVALUATION OF DFP PENETRATION THROUGH SEMIPERMEABLE
MEMBRANE FOLLOWING STANDARD OR RESIN DECONTAMINATION PROCEDURES**



Slide 16

TOXICOLOGY OF RESINS

- Preliminary Range-Finding Data

<u>Test</u>	<u>Result</u>
Acute Oral LD 50 - Rat	Greater than 5 gm/kg
Acute Skin Irritation - Rabbit	Practically Non-Irritating
Acute Eye Irritation - Rabbit	Slight to Moderate

MODIFICATION OF DNA BY THE SULFUR MUSTARDS

David B. Ludlum

Department of Medicine
Division of Oncology
Albany Medical College
Neil Hellman Medical Research Building
Albany, New York 12208

INTRODUCTION

Sulfur mustards and the closely related nitrogen mustards have a wide range of important biological activities including cytotoxicity, mutagenicity, carcinogenesis, and teratogenesis. There is fairly general agreement that all of these biological activities relate to modification of cellular DNA by the mustards, and it seems probable that different kinds of DNA modification are responsible for these different results (1).

In pursuing this work further, our objectives are: (1) to relate specific DNA lesions to the biological effects caused by sulfur mustards, and (2) to determine how the cell can be protected from this damage.

In what follows, the known reactions of sulfur mustard with DNA will be reviewed briefly. Then, some newer information on the way in which related antitumor agents modify DNA will be presented and the possible significance of this information to sulfur mustard-induced modification of DNA will be described.

Figure 1 shows the familiar structure of sulfur mustard together with its monofunctional analogs, hemisulfur mustard and chloroethyl ethyl sulfide, abbreviated here as CEES. Next are two nitrogen mustards used in cancer chemotherapy, one of which is very closely related to sulfur mustard, while the other (phosphoramidate mustard) is a more distant relative, a metabolite of the antitumor agent, cyclophosphamide. At the bottom is a representative of a much newer class of antitumor agents, bis-chloroethyl nitrosourea, abbreviated here as BCNU.

Studies carried out 10 to 20 years ago on both the sulfur and nitrogen mustards indicated that the N-7 position of guanine is the most readily attacked position in DNA and that interstrand crosslink formation occurs when two guanines are linked together through this position (2). Other base positions which are known to be modified include the N² position of guanine, and the N-1, N-3, and N⁶ positions of adenine (2-4). Recent work with carcinogens has shown that all of the nitrogens and oxygens in the DNA bases can be alkylated (5), and it seems likely that this is true for the mustards as well, although the extent of alkylation at some sites may be small.

DNA interstrand crosslinking and depurination followed by chain scission seem to be related to cytotoxicity while certain monofunctional base modifications seem to be responsible for mutagenesis and carcinogenesis. In particular, alkylation of guanine in the 6 position has been suggested as a mutagenic lesion by Papirmeister and his colleagues (6), but this DNA modification has not been demonstrated previously. We began our own investigations of sulfur mustard-modified DNA's by proving that this lesion was present in CEES-treated DNA as described below (7). DNA modifications like this one which change the configuration of normal base-pairing positions are particularly apt to be mutagenic since they interfere with the informational content of DNA.

RECENT ADVANCES IN THE MOLECULAR BIOLOGY OF ANTITUMOR AGENTS

Previous studies from several laboratories have established the conclusions that: 1. Cytotoxicity is caused by interstrand crosslinking of DNA or by depurination followed by chain scission, and that, 2. Mutagenicity and carcinogenicity are initiated by certain monofunctional alkylations (8). Recent studies of DNA-modifying antitumor agents have indicated, however, that other mechanisms of cytotoxicity may also be important (9). Thus, crosslinks other than those between the N-7 positions of guanine may be involved in interstrand crosslinking of DNA, and chemical instability of certain modified bases may also be significant.

Examples of these principles are shown in the next few figures. The mechanism by which the antitumor agent, BCNU, crosslinks DNA is shown in Figure 2 (10). Here, the initial attack is by a chloroethyl group on the 6 position of guanine. It might be supposed that this lesion would be mutagenic, but instead, an internal rearrangement occurs, and a cyclized intermediate, N¹,O⁶-ethanoguanine, is formed. This intermediate then has the capacity to form an interstrand crosslink with the cytosine moiety in the opposite strand of DNA. This reaction actually illustrates several points: that cytotoxicity can start with an attack on the 6 position of guanine, that internal rearrangement of a substituent group which is attached to a DNA base can occur, and that lethal crosslinks can involve positions other than the N-7 position of guanine.

Figure 3 indicates that the toxicity of BCNU can be prevented by a repair enzyme, O⁶-alkylguanine alkyltransferase, which is known to be present in mammalian cells (11). This enzyme is the same one that we are investigating because it may protect cells from the mutagenicity and carcinogenicity of sulfur mustards (7). Here, the repair enzyme is shown transferring the chloroethyl group from guanine in DNA modified by BCNU to a cysteine moiety within its own structure. This action restores the modified base to its original configuration, and thereby prevents the toxicity of this antitumor agent. Ironically, this is a problem to the chemotherapist who is intentionally trying to kill cells because tumors become resistant to the cytotoxicity of BCNU in this way (11).

If there were a mechanism by which the sulfur mustards could cause crosslinking in a similar manner, this repair enzyme might also be important in preventing the cytotoxicity of the sulfur mustards. Actually, such a mechanism can be visualized. Sulfur mustards are now known to introduce alkylthioethyl groups onto the O⁶ position of guanine, and the same mechanism of crosslinking shown in Figure 2 might occur following this modification of DNA. For this to happen, the alkylthiol group (or oxidized forms of the alkylthiol group) introduced by the sulfur mustard would play the role of the Cl atom shown in Figure 2.

Another newer mechanism by which DNA-modifying agents can cause cytotoxicity is illustrated by the reaction of phosphoramidate mustard with DNA. This agent forms the adduct with deoxyguanosine whose structure and mass spectrum are shown in Figure 4. Although the structure of this adduct is essentially what would have been predicted, its marked instability was unexpected. Figure 5 shows the rate at which this adduct decomposes at

neutral pH and 37° in contrast to the much slower decomposition of N-7 methyl deoxyguanosine (12). Since the sulfur mustard-modified DNA bases are remarkably unstable as described below, this could also prove to be a factor in their cytotoxicity.

REACTIONS OF CEES WITH DNA

Our first objective in this study was to determine whether a model sulfur mustard, CEES, alkylated guanine in the O⁶ position. The first step was to synthesize the expected derivative, O⁶-ethylthioethyldeoxyguanosine, by an unambiguous route so that it would be possible to recognize this derivative if it appeared as a product. This synthesis went smoothly as described previously (7).

Deoxyguanosine (1 mg/ml) was then reacted with CEES (approx. 35 umoles/ml) in pH 7 buffer at 37° and the reaction mixture was separated by high pressure liquid chromatography on a C₁₈ reverse phase column as shown in Figure 6. A peak appeared at the correct retention time for O⁶-ethylthioethyldeoxyguanosine as indicated in that Figure. (The peak indicated as "marker" in this Figure is another compound added as a control on the chromatographic procedure). Proof that this derivative was actually O⁶-ethylthioethyldeoxyguanosine came from comparison of this material with the known compound in several chromatographic systems (7).

The major product from the reaction between deoxyguanosine and CEES is N-7 ethylthioethyldeoxyguanosine (2-4), and the major peak shown in Figure 6 has the correct ultraviolet spectra for this derivative. Acid hydrolysis of material from this chromatographic peak yields, as the major product, a derivative with the reported properties of N-7 ethylthioethylguanine.

Many other alkylation products also appear in Figure 6, but these have not been completely characterized. As will become apparent, however, some of these probably represent decomposition and rearrangement products of O⁶-ethylthioethyldeoxyguanosine, suggesting that DNA containing this lesion would undergo further intracellular changes.

Presumably, O⁶-ethylthioethyldeoxyguanosine has not been detected previously in DNA treated with CEES because acid depurination has generally been used to release modified bases from DNA treated with this agent. As shown in Figure 7, O⁶-ethylthioethyldeoxyguanosine decomposes rapidly, even under mildly acidic conditions, to deoxyguanosine.

When O⁶-ethylthioethyldeoxyguanosine is incubated under neutral or basic conditions, other derivatives appear with retention times of 50 to 60 minutes in this chromatographic system. Two of the major products have ultraviolet spectra very similar to O⁶-ethylthioethyldeoxyguanosine. In view of previous reports that ethylthioethyl groups are easily oxidized (13), O⁶-ethylthioethyldeoxyguanosine was treated in the cold with a dilute solution of NaIO₄. The resulting mixture was again separated by HPLC as shown in Figure 8. The new peaks which appear at 53 and 56 min are probably the sulfone and the sulfoxide, respectively, of O⁶-ethylthioethyldeoxyguanosine, but it is uncertain what structures the other peaks represent.

Figure 9 summarizes these findings, illustrating the structure of O^6 -ethylthioethyldeoxyguanosine, and its known reactions in acidic and oxidizing solutions.

Our next objective in determining whether mammalian cells contain an activity capable of removing O^6 -ethylthioethyldeoxyguanosine from DNA was to prepare a suitably modified DNA for repair studies. Conditions were sought which would produce a DNA with a few pmols of O^6 guanine alkylation per mg. The level of modification achieved, in comparison with CCNU-treated DNA, is shown below. (CCNU, chloroethyl cyclohexylnitrosourea, is closely related to BCNU and acts on DNA by a similar mechanism.)

DNA Modifier	Concentration	Total Alkylation	O^6 Alkylation
CCNU	0.05 mg/ml	0.2 nmol/mg	20 pmol/mg
CEES	0.04	9.2	2200

It is apparent that, at comparable concentrations, CEES is a much more potent DNA modifier than the antitumor agent, CCNU. Furthermore, CEES produces much more O^6 guanine alkylation than CCNU.

The CEES-modified DNA described above was digested to the deoxynucleoside level and separated by HPLC as shown in Figure 10. This Figure shows the locations of the unmodified deoxynucleosides, deoxycytidine (dCR), deoxyguanosine (dGR), deoxythymidine (dTR), and deoxyadenosine (dAR) as well as the two derivatives, N-7 ethylthioethylguanine (N-7 ethylthioethyl G) and O^6 -ethylthioethyldeoxyguanosine (O^6 -ethylthioethyl dGR). Other derivatives are apparent in the front of this chromatogram, and several small peaks which may correspond to decomposition or rearrangement products are seen in the 50 to 60 min region. These appear more clearly in the magnification of this region shown in Figure 11.

This substrate should be a satisfactory one for investigating the protective action of liver cell extracts in repairing these DNA modifications, but in order for the assay to be feasible, radiolabelled CEES must be used. This material has just been received from custom synthesis, and we are currently in a position to determine whether repair occurs.

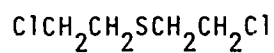
In summary, then, we can state that: 1) CEES modifies DNA extensively at moderate doses, attacking guanine in the O^6 position as well as in other positions. 2) This finding supports earlier biological data which suggest that substitution in the O^6 position of guanine would be mutagenic. 3) CEES-modified bases undergo further reactions which probably contribute to the lethal action of this agent. 4) Mammalian cells probably possess activities which offer protection from DNA modification.

REFERENCES

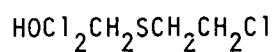
1. Ludlum, D.B., Alkylating Agents and the Nitrosoureas. In: Cancer, A Comprehensive Treatise, Vol. 5, F.F. Becker (ed.), Plenum Press, New York, 1977, pp. 285-307.
2. Lawley, P.D., Lethbridge, P.A., Edwards, P.A., and Shooter, K.V., Inactivation of Bacteriophage T7 by Mono- and Difunctional Sulphur Mustards in Relation to Cross-linking and Depurination of Bacteriophage DNA. *J. Mol. Biol.* 39, 181-198 (1969).
3. Sack, G.H. Jr., Fenselau, C., Kan, M.N., Kan, L.S., Wood, G.W., and Lau, P.Y. Characterization of the Products of Alkylation of 2'-Deoxyadenosine and 2'-Deoxyguanosine by Chloroethyl Ethyl Sulfide. *J. Org. Chem.*, 43, 3932-3936 (1978).
4. Kirchner, M. and Brendel, M. DNA Alkylation by Mustard Gas in Yeast Strains of Different Repair Capacity. *Chem.-Biol. Interactions* 44, 27-39 (1983).
5. Singer, B. and Grunberger, D. Reactions of Directly Acting Agents with Nucleic Acids. Molecular Biology of Mutagens and Carcinogens, Plenum Press, New York, 1983, Chapter IV.
6. Gilbert, R.M., Rowland, S., Davison, C.L., and Papirmeister, B., Involvement of Separate Pathways in the Repair of Mutational and Lethal Lesions Induced by a Monofunctional Sulfur Mustard. *Mutat. Res.*, 28, 257-275 (1975).
7. Ludlum, D.B. Protection Against the Acute and Delayed Toxicity of Mustards and Mustard-Like Compounds. Annual Summary Report, DAMD17-83-C-2203, 1 September 1983.
8. Calabrese, P., and Parks, R.E., Jr., Alkylating Agents, Antimetabolites, Hormones and Other Antiproliferative Agents. In: The Pharmacological Basis of Therapeutics, 6th Edition, A.G. Gilman, L.S. Goodman, and A. Gilman (eds.), MacMillan, New York, 1980, pp. 1256-1313.
9. Hemminki, K. and Ludlum, D.B. Covalent Modification of DNA by Antineoplastic Agents. *J. Natl. Cancer Inst.*, in press.
10. Tong, W.P., Kirk, M.C., and Ludlum, D.B. Formation of the Crosslink, 1-(N³-Deoxycytidyl),2-N¹-Deoxyguanosinyl)-ethane, in DNA Treated with N,N'-Bis(2-Chloroethyl)-N-Nitrosourea (BCNU). *Cancer Res.* 42, 3102-3105 (1982).
11. Brent, T.P. Suppression of Cross-Link Formation in Chloroethyl-nitrosourea-treated DNA by an Activity in Extracts of Human Leukemic Lymphoblasts. *Cancer Res.* 44, 1887-1892 (1984).

12. Mehta, J.R., Przybylski, M., and Ludlum, D.B. Alkylation of Guanosine and Deoxyguanosine by Phosphoramidate Mustard. *Cancer Res.* 40, 4183-4186 (1980).
13. Brookes, P. and Lawley, P.D. The Reaction of Mustard Gas with Nucleic Acids in vitro and in vivo. *Biochem. J.* 77, 478 (1960).

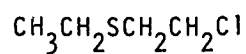
DNA MODIFYING AGENTS



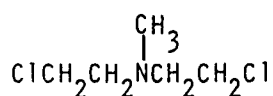
Sulfur Mustard



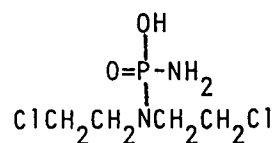
Hemisulfur Mustard



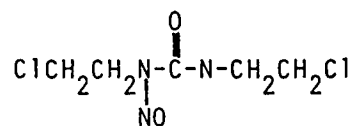
CEES



Nitrogen Mustard



Phosphoramidate Mustard



BCNU

Figure 1: Chemical structures of sulfur mustard and related compounds.

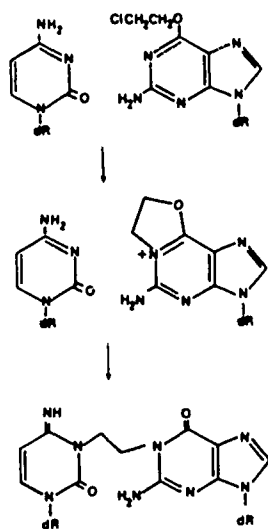


Figure 2: DNA crosslinking by the antitumor agent, BCNU.

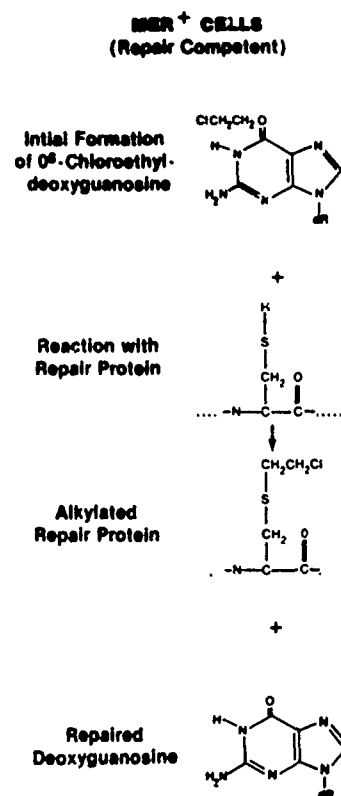


Figure 3: Repair of O⁶-alkylguanine in DNA.

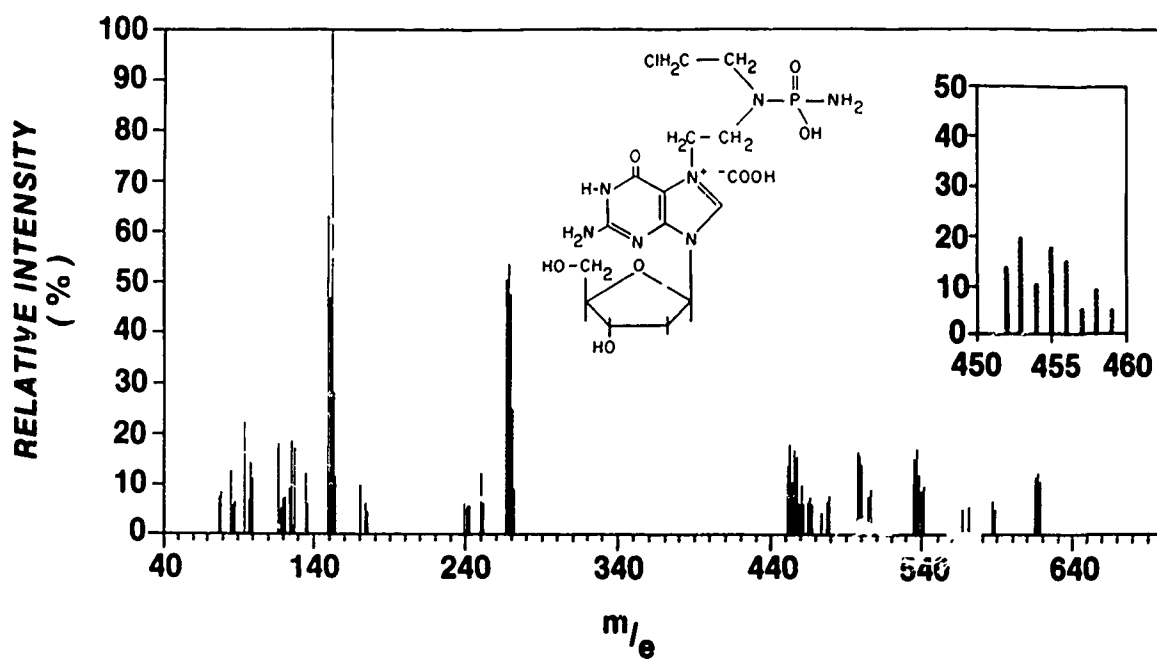


Figure 4: Structure of an unstable derivative of guanine resulting from reaction with phosphoramidate mustard.

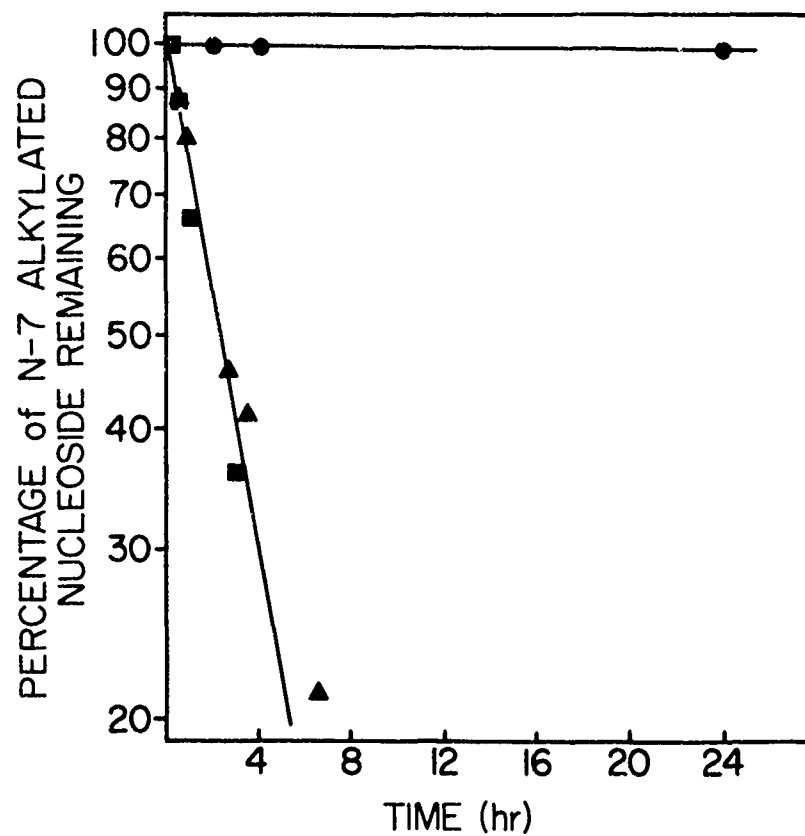


Figure 5: Decomposition of the adduct shown in Figure 4 (▲), of the corresponding deoxyguanosine adduct (■), and of 7-methylguanosine (●) at 37° and pH 7.4.

HPLC Separation of CEES-Deoxyguanosine Reaction Products

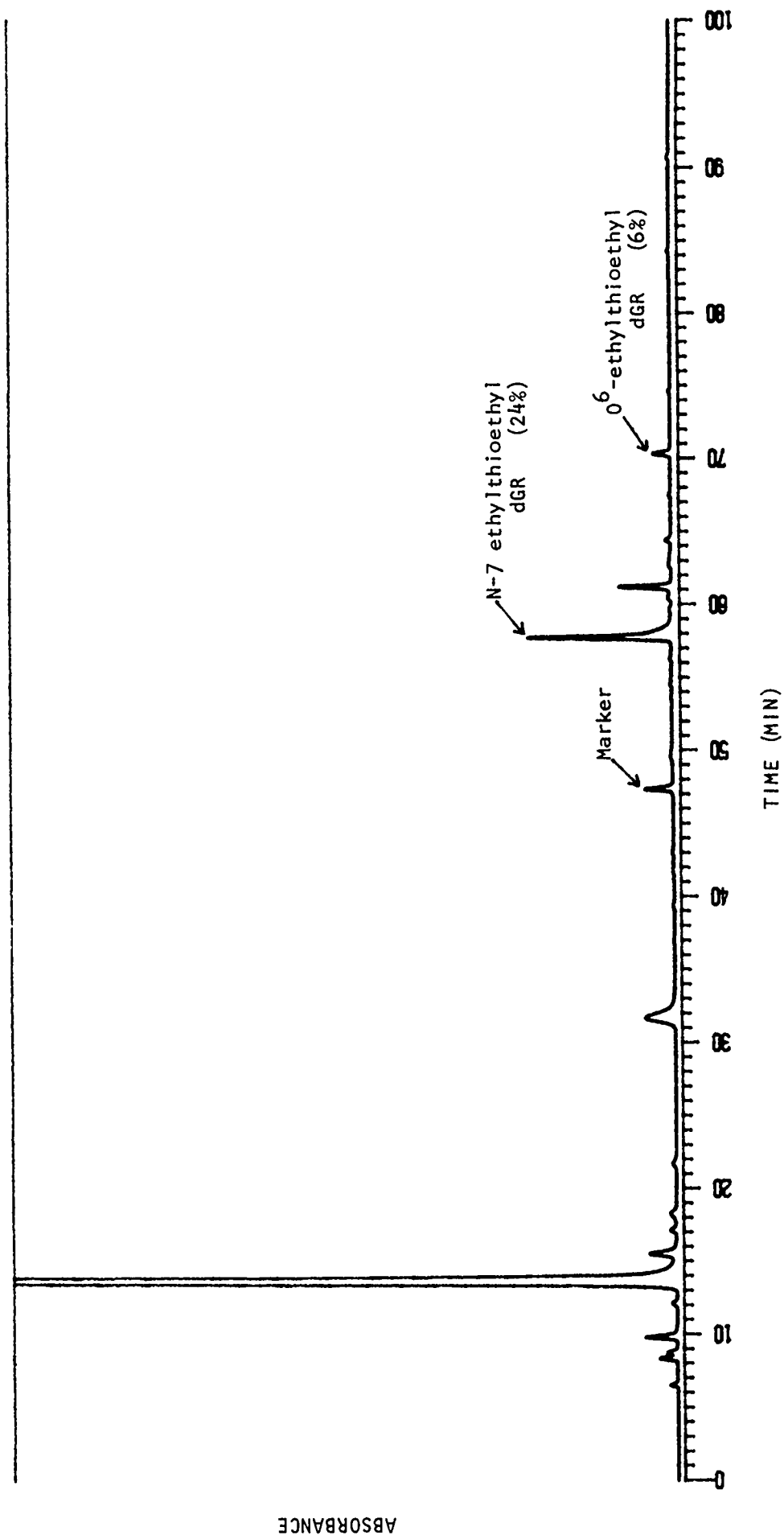
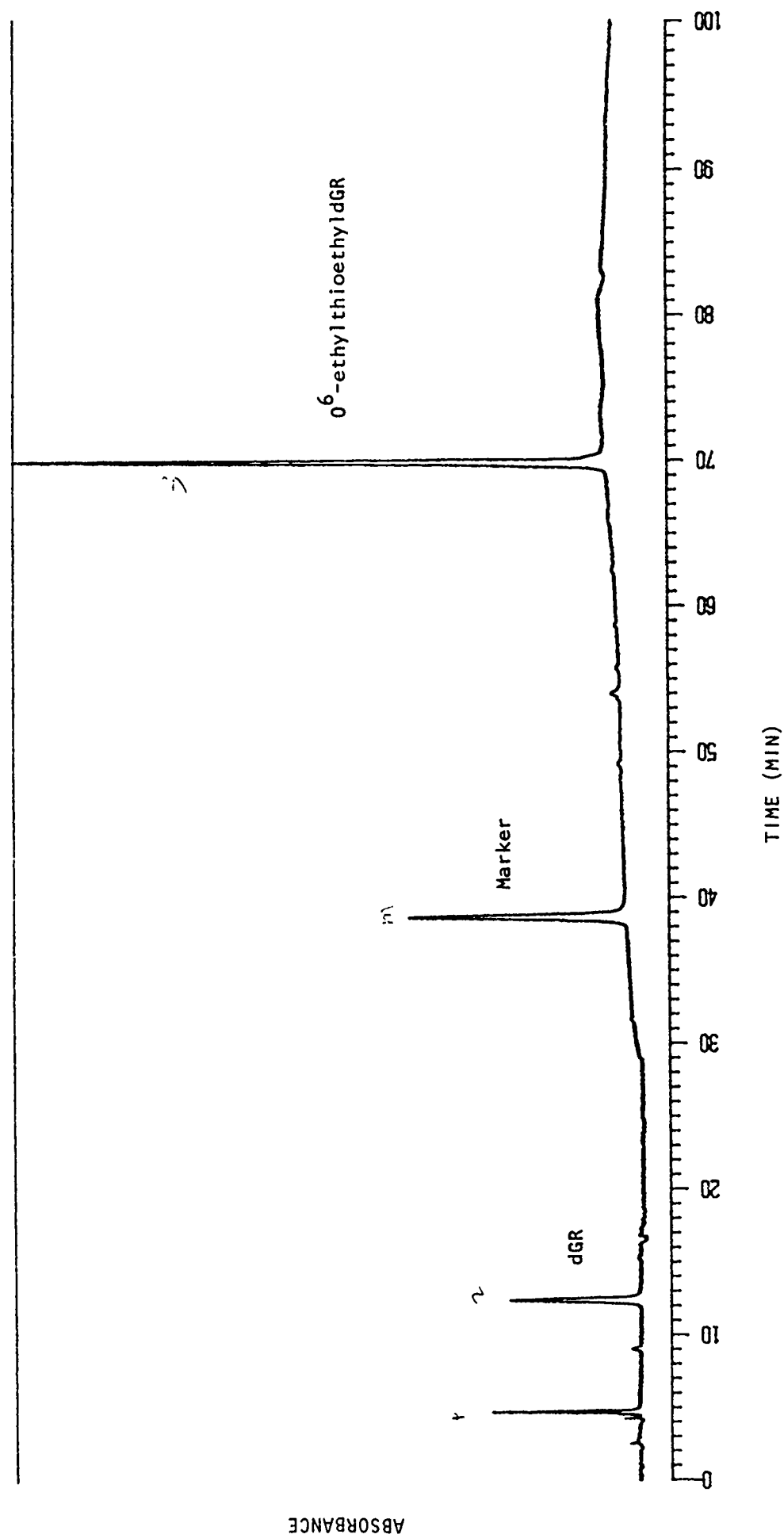


Figure 6: HPLC separation of CEES-deoxyguanosine reaction products.

Decomposition of 0^6 -Ethylthioethyl dGR after 18 hrs at pH 5.8 and 37°



file 351

Figure 7: Decomposition of 0^6 -ethylthioethyl dGR after 18 hrs at pH 5.8 and 37° .

Separation of NaIO_4 -Treated 0^6 -EthylthioethylDGR

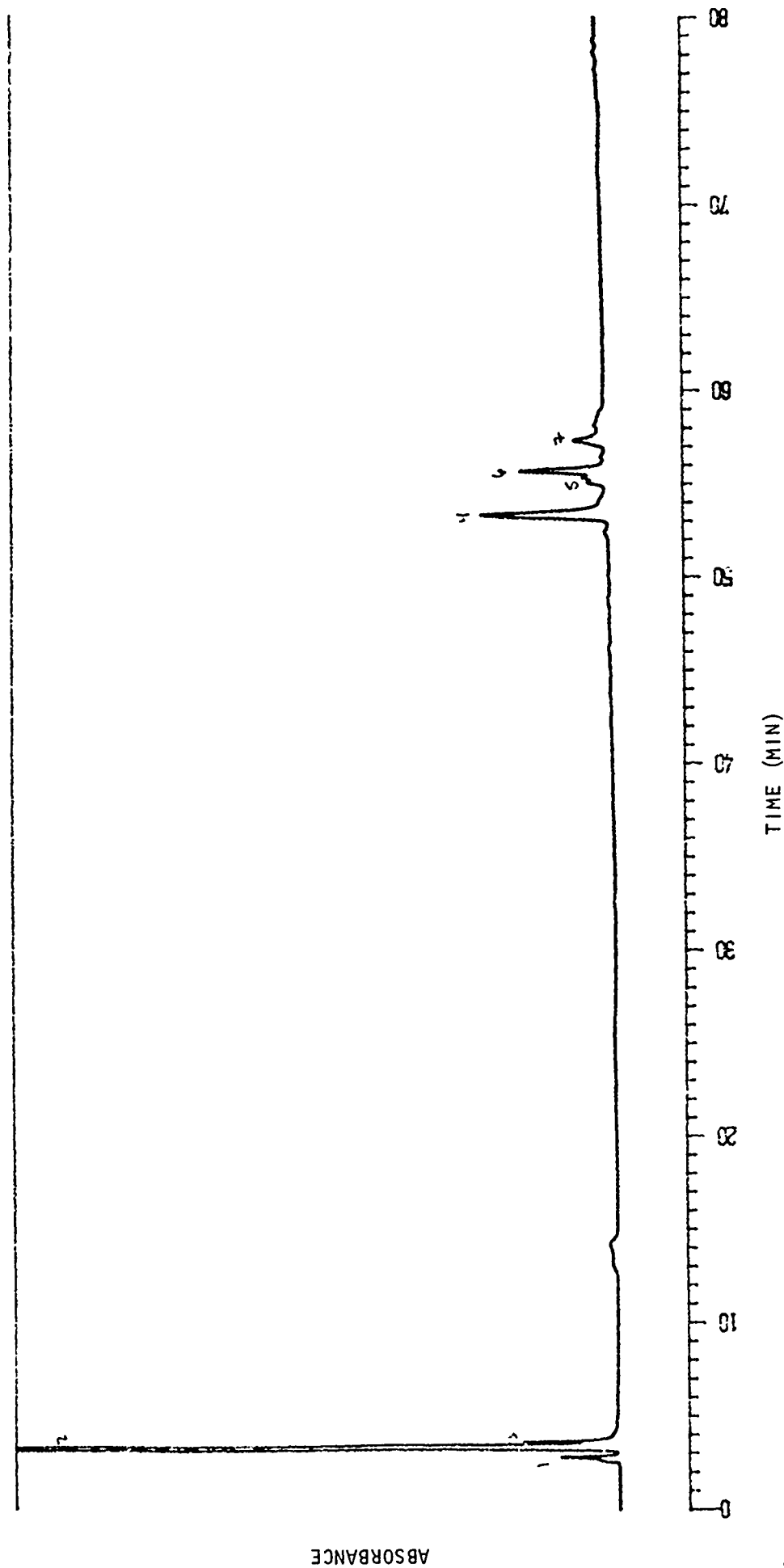


Figure 8: Separation of NaIO_4 -treated 0^6 -ethylthioethylDGR.

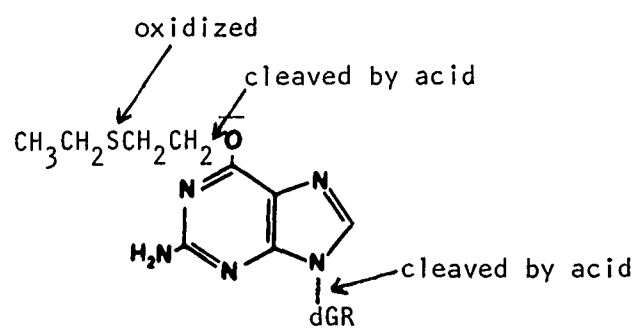


Figure 9: Reactions of 0⁶-ethylthioethylAdR.

Digest of DNA Treated with 0.04 mg/ml CEES

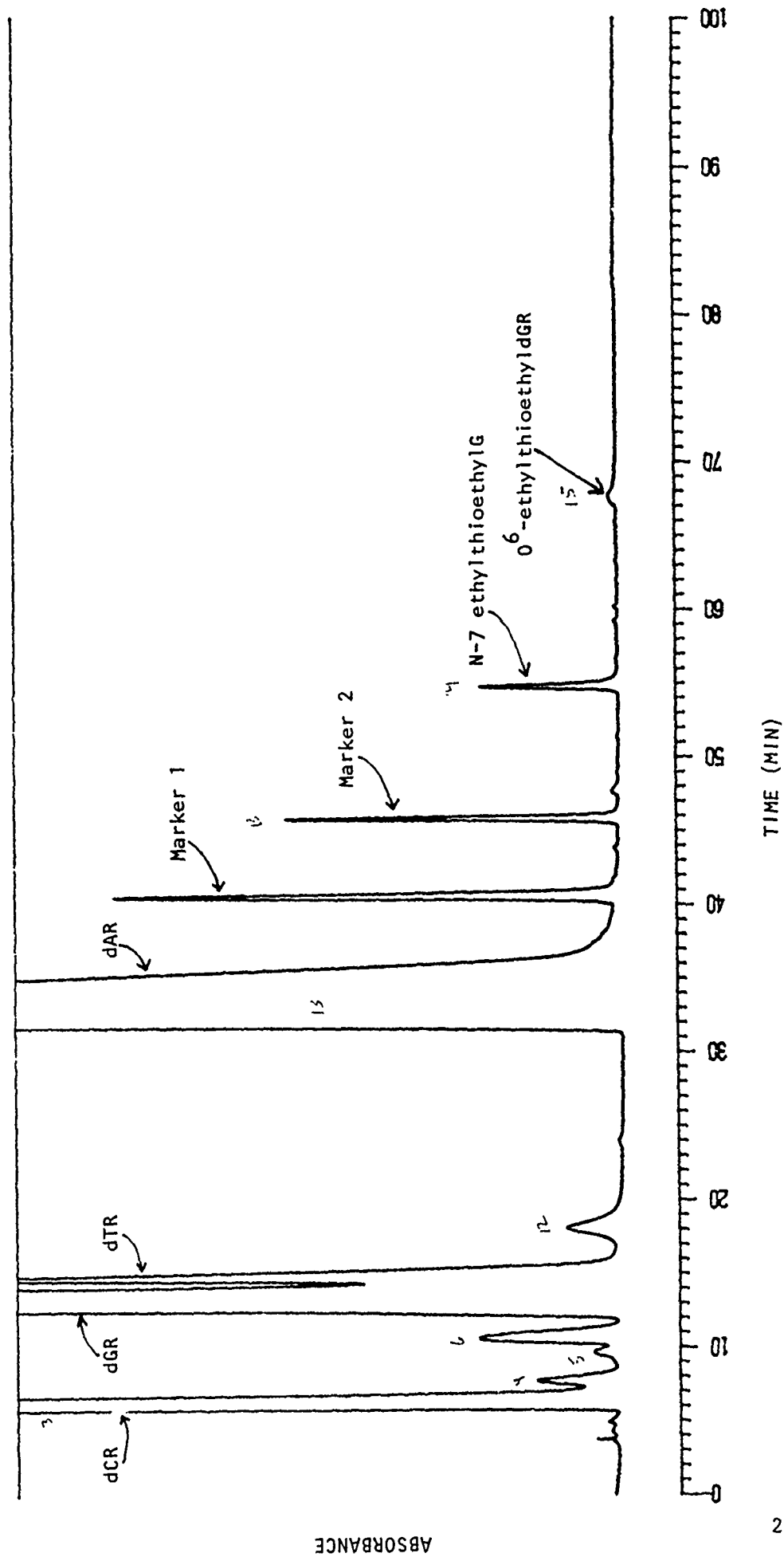


Figure 10: Digest of DNA treated with 0.04 mg/ml CEES.

file 333

Digest of DNA Treated with 0.04 mg/ml CEES (expanded scale)

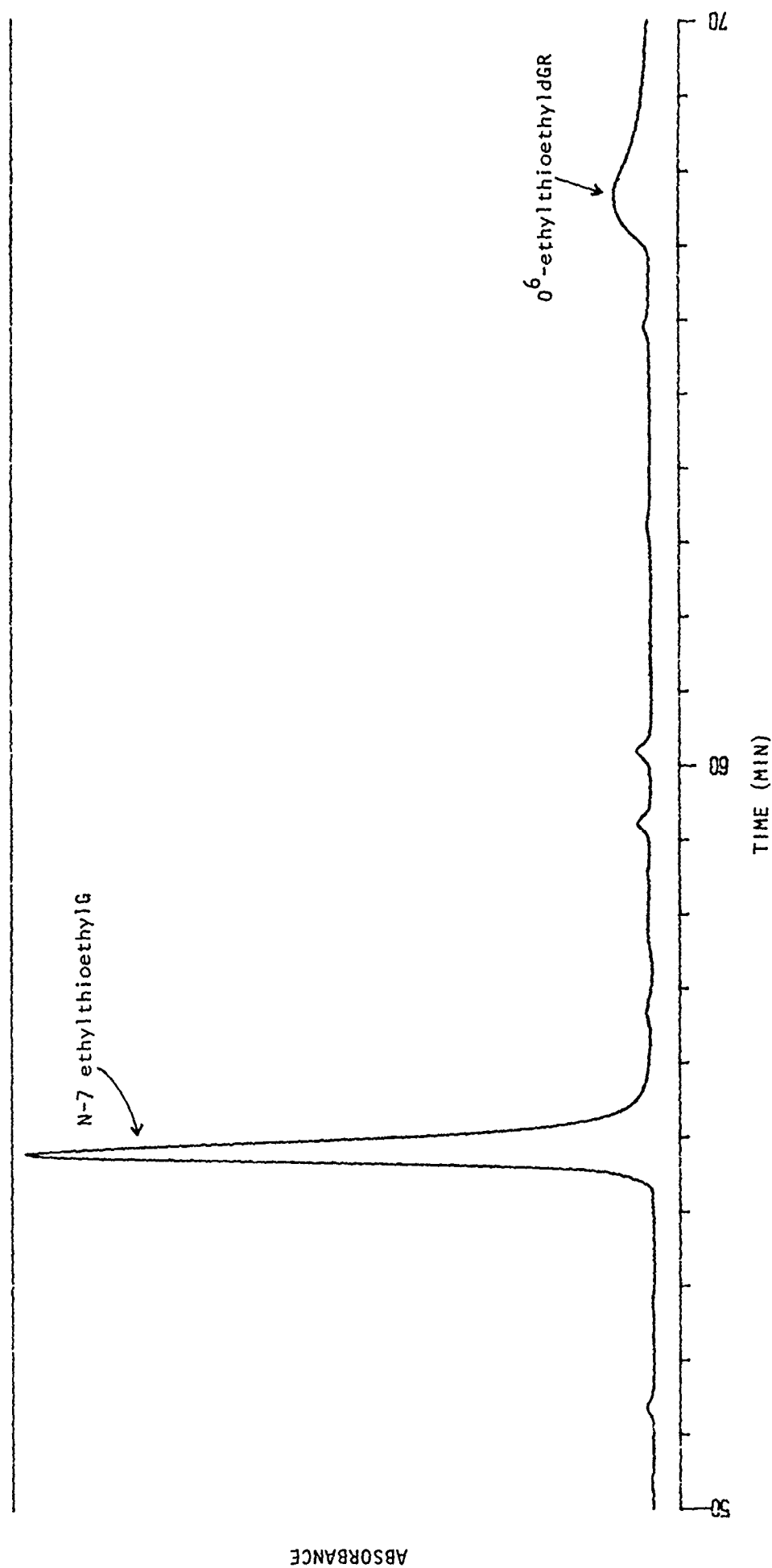


Figure 11: Digest of DNA treated with 0.04 mg/ml CEES (expanded scale).

file 333

IV. Biotechnology: Advances in Molecular Biology

MOLECULAR CLONING OF ACETYLCHOLINE RECEPTOR

James Patrick

Molecular Neurobiology Laboratory
The Salk Institute
P.O. Box 85800
San Diego, CA 92138

Acetylcholine is the neurotransmitter at the vertebrate neuromuscular junction. When an action potential invades the terminal of a motorneuron the resultant depolarization activates voltage dependent Ca^{++} channels. The influx of Ca^{++} promote release of acetylcholine stored in the nerve terminal. The released acetylcholine diffuses across the synaptic cleft where it binds to an acetylcholine receptor. When acetylcholine binds to this receptor a channel permeable to cations opens. The resulting ionic current depolarizes the muscle membrane leading to muscle contraction. In a competing reaction, the enzyme acetylcholinesterase hydrolyzes free acetylcholine ensuring that transmission between nerve and muscle occurs as a discrete event (for review see 1).

The acetylcholine receptor in the post-synaptic membrane of the vertebrate neuromuscular junction is an integral membrane glycoprotein. The best studied acetylcholine receptor is purified from the electric organ of the ray Torpedo where it represents about 10% of the extractable protein. Receptor purified from this tissue contains four different polypeptides, α , β , γ and δ of apparent molecular weights of 40, 50, 60 and 65 kilodaltons respectively. The receptor is a pentamer composed of two α chains and one each of the other three chains. The α chains are thought to carry the binding site for acetylcholine. Each of the four polypeptides span the membrane with about 50% of the total mass on the extracellular side, 30% of the mass on the cytoplasmic side and about 20% buried within the membrane. The four polypeptides are arranged in a circle such that the two α chains are not contiguous. The center of the circle appears to form a hole and may represent the ion channel. Although acetylcholine receptors appear to act independently they are often purified as dimers due to a disulfide bond between the δ subunits of two receptors (2,3,4).

Determination of the sequence of the polypeptide chains that compose the receptor was begun using chemical techniques to sequence the purified protein. The results of these studies showed that the polypeptides were related, probably encoded by genes derived from a single ancestral sequence (5). We have approached the problem in a different way. We have isolated cDNA clones coding for acetylcholine receptor subunits and determined the nucleotide sequence of these clones. From the nucleotide sequence we deduce the sequence of the polypeptide chains. We now have a sequence of the α subunit of Torpedo acetylcholine receptor (6,7) and 80% of the sequence of the α subunit (unpublished). Other laboratories have deduced sequences for the α (8,9,10), β and δ subunits (11). We now have the complete sequence, derived from cDNA clones, of all four subunits of Torpedo acetylcholine receptor. The following paragraphs will discuss properties of the receptor which we have surmised based upon analysis of these sequences.

Acetylcholine Receptor Subunits Are Homologous

The four polypeptide chains of acetylcholine receptor show considerable sequence homology. The results in Figure 1 show the amino acid sequence of each subunit with shared amino acids indicated. Several things are apparent in this figure. Over 20% of the amino acid residues are identical in all four polypeptide chains. In 23% the same amino acid is present in three out of four polypeptides. In many of these instances the dissimilar residue is structurally related. More important however is the fact that the homologies are clustered. There is a region near the amino terminus of the protein in which 9 out of 13 residues are identical and another region in which 10 out of 15 residues are identical in all four subunits. In contrast, the carboxy terminal sequences seem to be less well

conserved. The extensive conservation in specific regions suggests that these regions play a role in specific receptor functions. We have tried, by analysis of the sequence of individual receptor polypeptide chains, and by examination of regions of homology, to identify specific portions of the sequence with known physiological and biochemical properties of the receptor.

Acetylcholine Receptor Contains Identifiable Membrane Spanning Regions

We analyzed the sequence of the gamma subunit using the SOAP program devised by Kyte and Doolittle (12). This program makes a running average of the hydropathy of seven amino acid stretches of sequence. Regions of the protein which contain predominately hydrophobic amino acids can be identified with this program. This analysis revealed five stretches of hydrophobicity in the primary structure (Figure 2). The first stretch was found at the amino terminus and corresponded to the leader or signal peptide that presumably inserts the amino terminal portion of the protein through the membrane. This sequence is removed during processing of the protein since it is not found in the mature protein. The remaining four stretches of extended hydrophobicity are each sufficiently long and sufficiently hydrophobic to span the membrane bilayer.

If these sequences are within the bilayer, and if the amino terminus is extracellular, then the distribution of protein across the membrane must be as indicated in Figure 3. This figure shows about 50% of the protein is extracellular, 30% is intracellular and 20% is buried within the membrane. This model is therefore consistent with results obtained from X-ray diffraction (13) immunoelectron microscopy (14) and neutron scattering (15). Interestingly, the regions which we identified as membrane spanning are among the sequences which are conserved between the polypeptide chains. The portions of the sequence indicated as I, II, III and IV in Figure 1 correspond to the four membrane spanning regions. It is interesting to speculate on why membrane spanning regions of a protein should be conserved. At first glance, any hydrophobic amino acid could function as part of a sequence buried within the lipid bilayer. The fact that these sequences are conserved suggests that they interact with each other in the bilayer, perhaps by close interaction of helices. In this case conservation of sequence is required since changing a residue in one helix requires a precise and coincident change in the residue in the other interacting helix. The probability of obtaining requisite mutations in both helices at the same time is not large. This idea predicts that we might identify which helices interact and which do not based upon their conservation. Clearly membrane spanning regions I and II are highly conserved while membrane spanning regions III and IV are much less conserved. This suggests that membrane spanning regions I and II form bilayer spanning helices that interact with other protein sequences while membrane spanning regions III and IV interact predominately with the lipid in the bilayer.

The four membrane spanning regions we have identified are hydrophobic. If the receptor is to function as a cation channel it may be important to include ionizable groups in the membrane spanning sequences. Stroud (16) has identified a sequence which can form an amphipathic helix. This sequence will form a helix in which amino acids in which ionizable side chains are found on one side of the helix and amino acids with hydrophobic side chains are found on the other side of the helix. Thus, the helix has one face which is compatible with the lipid bilayer and one face which could donate ionizable groups to a putative channel.

All four polypeptide chains have the same general structure. The results in Figure 2 show that all four polypeptides have the same distribution of hydrophobic sequences and consequently are likely to partition their sequences across the membrane in the same way. The amphipathic helix can also be formed from homologous sequences in each subunit. A general structure of the receptor multimer emerges in which the five subunits contribute either 20 or 25 membrane spanning regions. The amino terminus and the bulk of the protein is extracellular. Depending upon whether there are four or five membrane spanning regions, the carboxy terminal sequences are either extracellular or intracellular respectively. The location of the carboxy terminal sequences will help determine whether or not the amphipathic helix actually spans the membrane. In fact, we can infer the location of these sequences from existing data. The δ chains are known to be linked by a disulfide which is found in the carboxy terminal portion of the protein. There is only one cysteine in the carboxy terminal third of the protein and this cysteine is the penultimate residue. Since it is known that disulfide bonds rarely form in the cytoplasm due to the reducing potential of glutathione this cysteine is probably extracellular. This would argue that the carboxy terminus is extracellular and that there are only four membrane spanning regions.

A Potential Acetylcholine Binding Site Is Conserved Among Subunits

The acetylcholine binding site is located on the α subunit and is probably on the portion of the α subunit that is extracellular. Acetylcholine is known to contain a disulfide bond that can be reduced and then alkylated with the affinity alkylating reagent MBTA (17). This places a disulfide bond, and hence two cysteines, at or near the acetylcholine binding site. The portion of the α subunit which is extracellular has 4 cysteine residues, two of which are contiguous. It is unlikely that contiguous cysteine residues both participate in the same disulfide bond. There are two other cysteine residues separated by 13 amino acids. This 15 amino acid residue sequence is highly conserved between subunits; 10 out of the 15 residues are identical in all four chains. This region appears to be a good candidate for an acetylcholine binding site. Analysis of the sequence reveals a β pleated sheet structure with a β turn at the proline which falls midway between the 2 cysteines. We have constructed a model of this region of the protein using Corey-Pauling-Koltun space filling models and find that the two cysteine residues can be placed in a position appropriate for the formation of a disulfide bond. The remainder of the residues between the cysteines stack together forming a hydrophobic pocket and a cationic region that accomodates an acetylcholine molecule. This region also accomodates the affinity labeling reagent MBTA in a configuration that promotes reaction with the reduced disulfide. The photographs in Figure 4 show the CPK models of the region of the alpha subunit that we think constitutes the acetylcholine binding site. In each case the receptor is shown in the top photo with the ligand in the appropriate orientation to fit into the binding site, and in the bottom photo with the ligand inserted into the site. These observations may be completely fortuitous or they may be first steps in providing a molecular model of the interaction of acetylcholine with its receptor. The utility of the approach lies in the possibility of testing the model. We have synthesized peptides corresponding to the two sides of the putative acetylcholine binding site and use these peptides, coupled to a carrier, to raise antibodies in rabbits. We predict that these sequence specific antibodies will block binding of acetylcholine to receptor and interfere with activation of receptor. If the acetylcholine binding site is also the toxin binding site we would expect that toxin, or even acetylcholine, might block binding of the antibodies.

It is interesting that this potential acetylcholine binding site is conserved in all four polypeptide chains. The apparent homology however breaks down in two important instances. The α chain has charged residues, glutamate and histidine, in positions where the other three chains have polar groups. The homology in the other residues may reflect homologous functions for the β , λ and δ subunits. This would be consistent with data suggesting additional agonist binding sites on the receptor molecule (18). Alternatively, the conservation of sequence could reflect the necessity of packing the two sides of the loop. If the amino acid residues on both sides must interact closely to form a stable structure it might be difficult to change a residue on one side of the loop without a compensating change on the other side. As mentioned above, the probability of getting compensating mutations at the same time is low. Consequently the conservation may, as was suggested for the membrane spanning regions, identify sequences that interact.

Acetylcholine Receptor Is Glycosylated

Each of the four polypeptide chains of acetylcholine receptor can be found in a glycosylated form (2,3) and the γ subunit polypeptide may have as many as three sites at which carbohydrate is attached (19). It is the case that the sequences surrounding sites of asparagine-linked glycosylation are the same in many proteins (20). The amino acid sequence of the γ subunit of Torpedo acetylcholine receptor has 5 such canonical glycosylation sites. Since glycosylation is found uniquely on the extracellular portions of membrane proteins it is important that three of the five glycosylation sites be found in the portion of the γ sequence we predict is extracellular. In fact the appropriate glycosylation sites are found not only in γ but on the other three polypeptide chains.

There is a glycosylation site which is conserved among all four receptor polypeptide chains. This site flanks the putative acetylcholine binding site on the α subunit and is found flanking the homologous sequences in the other three polypeptides. It is probable that this site is in fact used as a glycosylation site since it is the only canonical glycosylation site in the α subunit and we know that an α polypeptide is glycosylated. It is not the case, however, that we know that both of the two α chains are glycosylated. In fact there is accumulating evidence that only one of the two α chains is glycosylated (21). This may account for the known differences in antagonist binding by the two α chain sites (22).

Acetylcholine Receptor Is Phosphorylated

Torpedo acetylcholine receptor can be phosphorylated on the λ and δ subunit polypeptide chains (23). Since phosphorylation normally occurs due to cytoplasmic kinase activity we expect to find potential phosphorylation sites on the cytoplasmic sequences of the γ and δ but not the α and β subunit sequences. The identification of phosphorylation sites is much less clear than the identification of glycosylation sites but it is generally true that more than one basic residue is followed by more than one serine or threonine, one of which is phosphorylated. Both the γ (arg-arg-arg-ser-ser) δ (arg-arg-ser-ser-ser) subunits have the appropriate sequences in what we predict will be the cytoplasmic regions of the protein. These sequences are not found in the δ and β subunit polypeptide chains.

These observations are all consistent with the model in which there are four membrane spanning regions with the amino terminal and carboxy terminal

sequences extracellular. The observations do not, however, rule out the model with the additional amphipathic helical membrane spanning region. The addition of a membrane spanning moves the carboxy terminal from the extracellular to the cytoplasmic side of the membrane but does not change the distribution of relevant phosphorylation or glycosylation sites.

The Acetylcholine Binding Site Is Conserved in Evolution

Figure 5 shows the amino acid and nucleotide sequences corresponding to the acetylcholine binding sites of Torpedo, human (24) and mouse (25) acetylcholine receptor α subunits. Although it is interesting from an evolutionary point of view that the sequences are highly conserved, the cross-species comparison may have other uses. For example, one advantage of having recombinant DNA clones that code for receptor is that we can introduce specific changes in the sequence to produce receptor with altered function. By appropriate choice of the changes we can test specific aspects of our model of receptor structure or our model of the acetylcholine binding site. Alternatively we can look at the changes that have been acceptable throughout evolution. If any of these changes introduce amino acid side chains into portions of our model that would prohibit function then our model is probably wrong.

SUMMARY

The application of recombinant DNA technology to the study of acetylcholine receptor allowed the isolation of cDNA clones containing sequences that code for receptor polypeptide chains. Determination of the nucleotide sequence of these clones revealed the amino acid sequence of the receptor polypeptides. Analysis of the primary structure of acetylcholine receptor led us to propose specific models for the way in which the receptor polypeptides are partitioned across the membrane and for the structure of the portion of the sequences that binds receptor ligands. We also propose ways in which these models can be tested.

REFERENCES

1. Katz, B. (1966) Nerve, Muscle and Synapse. McGraw-Hill, New York.
2. Conti-Tronconi, B.M. and Raftery, M.A. (1982) The nicotinic cholinergic receptor: correlation of molecular structure with functional properties. *Ann. Rev. Biochem.* 51:491-530.
3. Karlin, A. (1980) Molecular properties of nicotinic acetylcholine receptors. *Cell Surface Rev.* 6:191-260.
4. Changeux, J-P. (1981) Harvey Lecture Series 75, Academic Press.
5. Raftery, M.A., Hunkapiller, M.W., Strader, C.B. and Hood, L.E. (1980) Acetylcholine receptor: complex of homologous subunits. *Science* 208:1454-1457.
6. Ballivet, M., Patrick, J., Lee, J. and Heinemann, S. (1982) Molecular cloning of cDNA coding for the gamma subunit of Torpedo acetylcholine receptor. *Proc. Nat. Acad. Sci.* 79:4466-4470.

7. Claudio, T., Ballivet, M., Patrick, J. and Heinemann, S. (1983) Nucleotide and deduced amino acid sequence of Torpedo californica acetylcholine receptor gamma-subunit. Proc. Nat. Acad. Sci. 80:1111-1115.
8. Sumikawa, K., Houghton, M., Emtage, J.S., Richards, B.M. and Barnard, E.A. (1981) Active multi-subunit ACh receptor assembled by translation of heterologous mRNA in Xenopus oocytes. Nature 292:862-864.
9. Devillers-Thiery, A., Giraudat, J., Rentaboulet, M. and Changeux, J-P. (1983) Complete mRNA coding sequence of the acetylcholine binding alpha-subunit from Torpedo marmorata acetylcholine receptor: a model for the transmembrane organization of the polypeptide chain. Proc. Nat. Acad. Sci. (in press).
10. Noda, M., Takahashi, H., Tanabe, T., Toyosato, M., Furutani, Y., Hirose, T., Asai, M., Inayama, S., Miyata, T. and Numa, S. (1982) Primary structure of alpha-subunit precursor of Torpedo californica acetylcholine receptor deduced from cDNA sequence. Nature 299:793-797.
11. Noda, M., Takahashi, H., Tanabe, T., Toyosato, M., Kikuyotani, S., Hirose, T., Asai, M., Takashima, H., Inayama, S., Miyata, T. and Numa, S. (1983) Primary structures of beta- and delta-subunit precursors of Torpedo californica acetylcholine receptor deduced from cDNA sequences. Nature 301:251-255.
12. Kyte, T. and Doolittle, R.F. (1982) A simple method for displaying the hydropathic character of a protein. J. Mol. Biol. 157:105-132.
13. Ross, M.J., Klymkowsky, M.W., Agard, D.A. and Stroud, R.M. (1977) Structural studies of a membrane-bound acetylcholine receptor for Torpedo californica. J. Mol. Biol. 116:635-659.
14. Klymkowsky, M.W. and Stroud, R.M. (1979) Immunospecific identification and three-dimensional structure of a membrane-bound acetylcholine receptor from Torpedo californica. J. Mol. Biol. 128:319-334.
15. Wise, D.S., Schoenborn, B.P. and Karlin, A. (1981) Structure of acetylcholine receptor dimer determined by neutron scattering and electron microscopy. J. Biol. Chem. 256: 4124.
16. Fairblough, R.M., Finer-Moore, J., Love, R.A., Kristofferson, K., Desmeuks, P.J. and Stroud, R.M. (1983) Subunit organization and structure of an acetylcholine receptor. Cold Spring Harbor Symposium, 48:9-21.
17. Karlin, A. and Cowburn, D.A. (1973) Proc. Natl. Acad. Sci. 70:3636-3640.
18. Conti-Tronconi, B.M., Dunn, S. and Raftery, M. (1982) Independent sites of low and high affinity for agonists on Torpedo californica acetylcholine receptor. Biochem. Biophys. Res. Comm. 107:123-129.
19. Anderson, D.J. and Blobel, G. (1981) In vitro synthesis, glycosylation, and membrane insertion of the four subunits of Torpedo acetylcholine receptor. proc. Nat. Acad. Sci. 78:5598-5602.

20. Struck, D.K. and Lennarz, W.J. (1980) In The Biochemistry of Glycoproteins and Proteoglycans (ed. Lennarz, W.J.), Ch. 2, pp 35-83.
21. Conti-Tronconi, B.M., Hunkapiller, M.W. and Raftery, M.A. (1984) Molecular weight and structural nonequivalence of the mature alpha subunits of Torpedo californica acetylcholine receptor. Proc. Nat. Acad. Sci. 81 (in press).
22. Sine, S. and Taylor, P. (1980) J. Biol. Chem. 255:10144-10156.
23. Huganir, R.L. and Greengard, P. (1983) cAMP-dependent protein kinase phosphorylates the nicotinic acetylcholine receptor. Proc. Nat. Acad. Sci. (in press).
24. Noda, M., Furutani, Y., Takahashi, M., Toyosato, M., Tanabe, T., Shimizu, S., Kikuyotani, S., Kayano, T., Hirose, T., Inayama, S. and Numa, S. (1983) Cloning and sequence analysis of calf cDNA and human genomic DNA encoding α -subunit precursor of muscle acetylcholine receptor. Nature 305:818-823.
25. Boulter, J., Evans, K., Ballivet, M., Goldman, M., Luyten, W., Martin, G., Mason, P., Stengelin, S., Ueno, S., Heinemann, S. and Patrick, M. (1984) Isolation of a clone coding for the alpha subunit of a mouse acetylcholine receptor (in press).

Figure 1

Acetylcholine Receptor

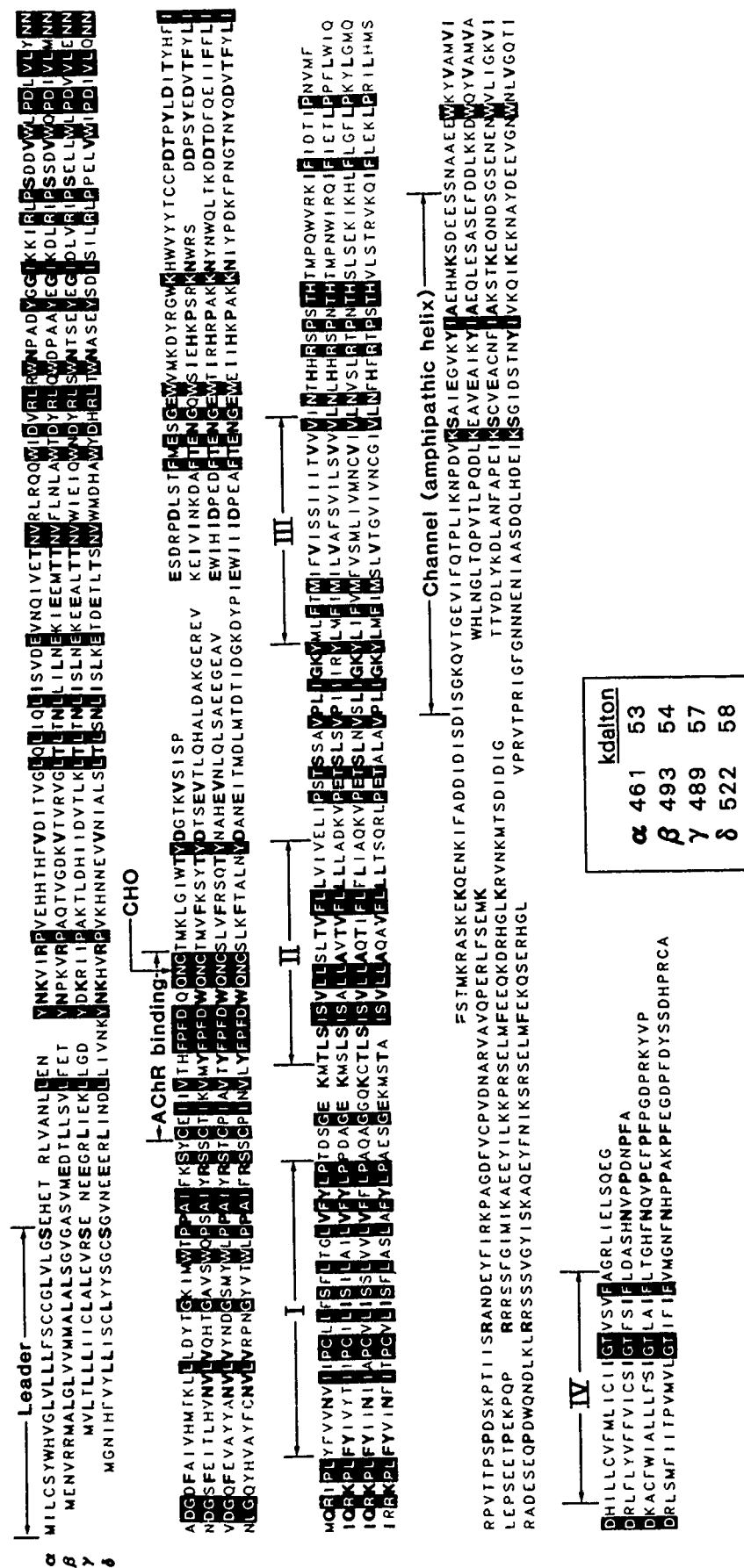


Figure 2

HYDROPATHY INDICES OF ACETYLCHOLINE RECEPTOR SUBUNITS

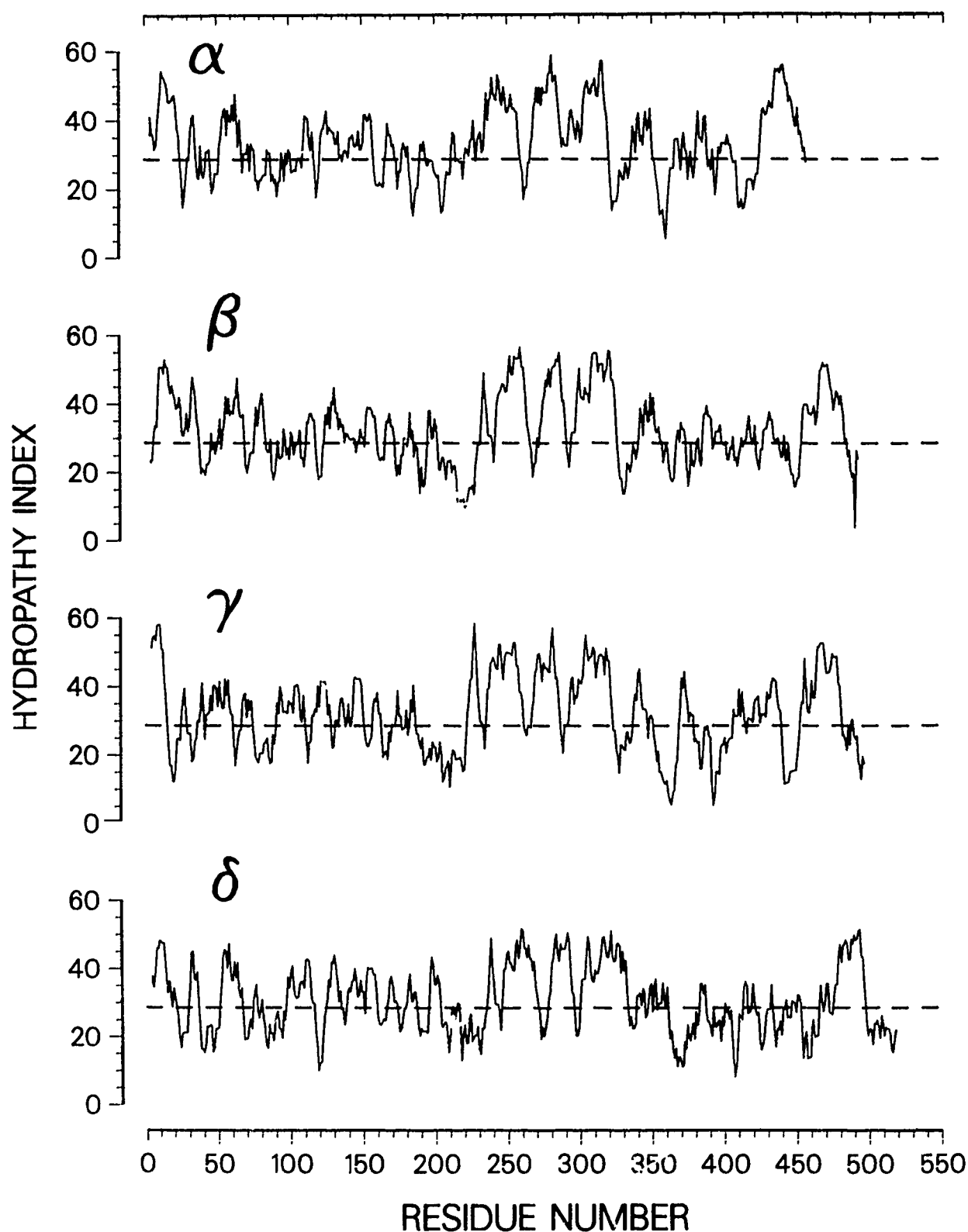
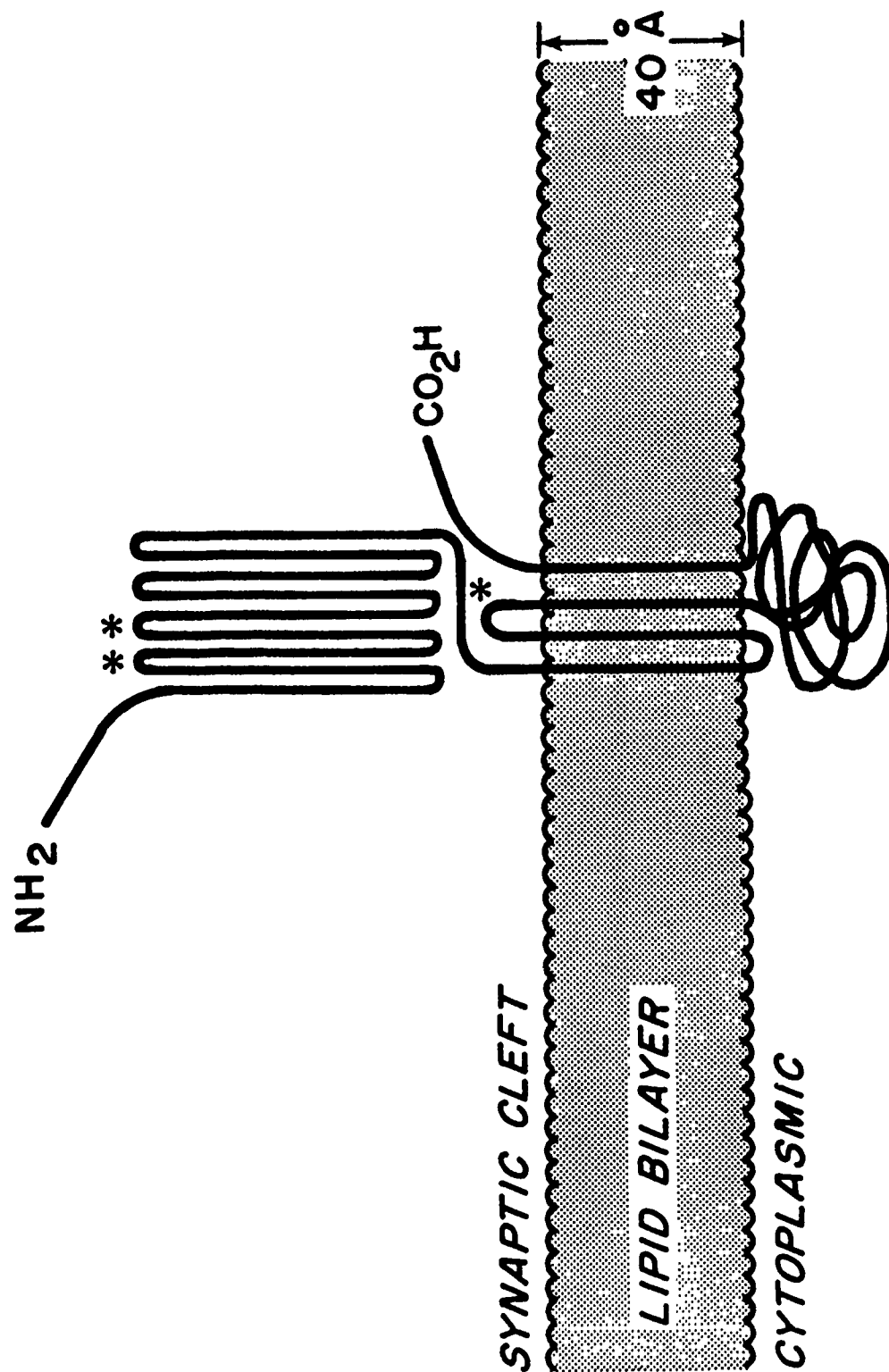


Figure 3

ACETYLCHOLINE RECEPTOR: γ -SUBUNIT



*N-X- (S/T)

Figure 4

Acetylcholine



MBTA

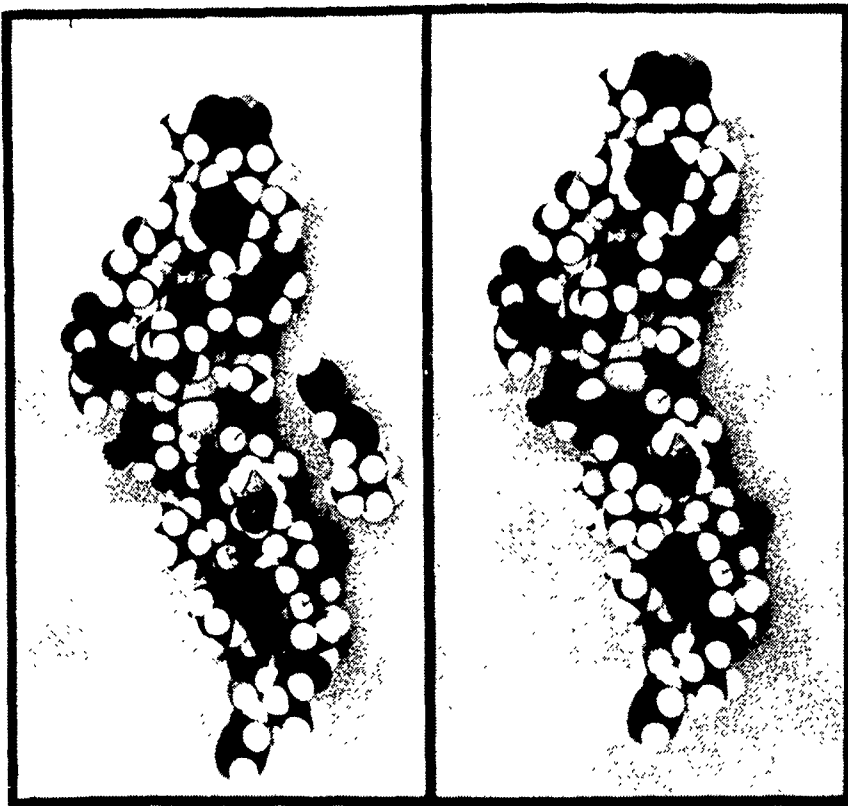


Figure 5

ACETYLCHOLINE BINDING SITE SEQUENCES

Torpedo	-Cys-Glu-Ilu-Ilu-Val-Thr-His-Phe-Pro-Phe-Asp-Gln-Gln-Asn-Cys-
Human	-Cys-Glu-Ilu-Ilu-Val-Thr-His-Phe-Pro-Phe-Asp-Glu-Gln-Asn-Cys-
Mouse	-Cys-Glu-Ilu-Ilu-Val-Thr-His-Phe-Pro-Phe-Asp-Glu-Gln-Asn-Cys-
Torpedo	TGT GAA ATT ATT GTA ACA CAT TTC CCA TTT GAT CAA CAA AAT TGC
Human	TGT GAG ATC ATC GTC ACC CAC TTT CCC TTT GAT GAA CAG AAC TGC
Mouse	TGT GAG ATC ATT GTC ACT CAC TTT CCC TTC GAT GAG CAG AAC TGC

**EXPRESSION OF ACETYLCHOLINESTERASE GENE(S)
IN HUMAN BRAIN TISSUES**

**Hermona Soreq
Department of Neurobiology
The Weizmann Institute of Science
Rehovot 76100, Israel
tel. 972-54-82995**

I. Introduction

Cholinesterases found in the human nervous system (ChEs) are scarce proteins, capable of rapidly degrading the neurotransmitter acetylcholine. ChEs occur in multiple molecular forms, which exhibit different substrate specificities and are localized in various cell types and subcellular sites in the nervous tissue (1). ChEs can be distinguished by their substrate specificity to acetylcholinesterase (acetylcholine hydrolase, EC 3.1.1.7, AChE) and nonspecific cholinesterase, or pseudocholinesterase (acylcholine acylhydrolase, EC 3.1.1.8, ψ ChE). ψ ChE is also known as butyrylcholinesterase, because of its high catalytic activity towards butyrylcholine (which is scarcely hydrolyzed by AChE). The two enzymes differ not only in their substrate specificity, but also in their susceptibility to various inhibitors, which can be used to differentiate between them (2).

There are secreted, cytoplasmic and membrane-associated forms of ChEs in the mammalian nervous system. This indicates that different forms contain distinct domains responsible for their subcellular localization. On the other hand, pharmacological studies and enzyme kinetic analyses suggest that the different forms of AChE possess nearly identical catalytic sites (3). It is not yet clear whether the molecular heterogeneity of nervous system AChEs has a multiple gene origin, or whether it is derived from post-transcriptional and/or post-translational processing events.

Complete inhibition of AChE (i.e., by administration of organophosphorous (OP) poisons) is lethal (4). This inhibition is achieved by formation of a stable stoichiometric (1:1) covalent conjugate with the active site serine (5). Treatment of OP poisoning has involved various prophylactic and therapeutic approaches, including protection against the OP agent with reversible ChE inhibitors (6). Another approach is the reactivation of the inhibited enzyme with active-site directed nucleophiles (e.g., quaternary oximes) which detach the phosphoryl moiety from the hydroxyl group of the active site serine (7). This latter therapeutic approach is often hampered by a parallel competing reaction, termed "aging," which transforms the inhibited ChE into a form that cannot be regenerated by the commonly used reactivators (5). The aging process is believed to involve dealkylation of the covalently bound OP group (5) and renders therapy of intoxication by certain organophosphates, such as sarin, DFP, and Soman, exceedingly difficult (8).

Modifications in both the level (9) and the composition of molecular forms (10) of human brain AChE have been reported in several neurological or genetic disorders, such as Alzheimer disease (11) or Down's syndrome (12). The tetrameric form of AChE, sedimenting as 10S, appears to be most vulnerable to these alterations (10). In addition, neural tube defects in human embryos are clinically characterized by secretion of AChE into the amniotic fluid (for recent reports see 13-16). In this case as well, it is the tetrameric 10S form that is secreted (17).

The clinical detection of alterations in the level and in the isoform composition of AChE is currently carried out by rather laborious procedures. These include sucrose gradient fractionation of brain extracts or blood samples, followed by enzymatic assays of substrate hydrolysis (10,17). Alternatively, amniotic fluid samples are separated by gel electrophoresis and AChE activity detected by specific staining (13,15). Missing, and particularly desirable, are simple selective procedures to determine the level of specific AChE forms. It is our belief that elucidation of the active site topography and the amino acid sequence of AChE would open up new approaches for the development of rapid, simple clinical methods to detect poisoning- or disease-related changes in AChEs. This could be done, for example, by radioimmunoassay, using monospecific antibodies elicited against peptide domains that are specific to the 10S form. Furthermore, this

knowledge is required for the development of therapeutic approaches of OP poisoning. The reversible protection of the active site of AChE, reactivation of the OP-blocked enzyme or its protection against "aging," all require a detailed understanding of the catalytic mechanism, active site topography and the amino acid sequence of AChE.

The enzymatic turnover rate of AChEs is exceptionally fast, as might be expected for a neurotransmitter-hydrolyzing enzyme (18). Hence, very small quantities of catalytically active AChE are sufficient for correct termination of impulse transmission. Indeed, AChE only comprises about 0.001% of the total protein content, even in a rich source like the brain tissue (19). The enzyme is more abundant in the electric organ of electric eel, and AChE has been purified from this tissue by affinity chromatography (20). However, electric fish are phylogenetically remote from man, and there is ample evidence in the literature that the active site of electric eel AChE, although similar in overall features to that of higher vertebrates, often differs in its detailed specificity, whether towards organophosphate inhibitors or quaternary reactivators.

The ideal AChE for devising therapeutic strategies for dealing with OP intoxication of humans is, obviously, human AChE. AChE has been purified from human erythrocytes (21), but not in amounts sufficient for amino acid sequencing. Also, no large-scale purification of human nerve or muscle has yet been reported. Although this task is not impossible, it is difficult to envisage the availability of sufficient amounts of post-mortem material for routine large-scale purification of the enzyme. The scarcity of ChEs in mammalian tissues therefore complicates the investigation of the detailed properties of these important enzymes. Thus, both the primary sequence and the three-dimensional structure of AChE are still unknown.

In order to investigate in detail the structural properties of human nervous system AChE, we initiated, about three years ago, the study of AChE biosynthesis. Our aim is to replicate the active gene(s) coding for human brain AChE in bacterial plasmids. Since DNA sequencing is by now technically much easier than polypeptide sequencing, the amino acid sequence for human AChE could thus be obtained. If, subsequently, gene expression could be achieved, this would eventually lead to production of sizeable amounts of catalytically active AChE. The purified enzyme could be employed in biochemical studies on structure-function relationships of the enzyme with substrates and putative inhibitors and reactivators. It could also serve for preparation of monospecific antibodies against particular domains of the enzyme molecule. This can lead to development of the radioimmunoassay described above. The availability of ample pure AChE might also permit crystallization, leading, eventually, to elucidation of the three-dimensional structure of human nervous system AChE.

II. Polymorphism of ChEs in human brain tissues

Recent histochemical studies revealed that in the primary visual cortex of the monkey, localization of ψ ChE rivals that of AChE in terms of specificity (22). This implied that the expression of ψ ChE in the central nervous system may be unrelated to that of AChE. In order to first examine this issue at the tissue protein level, we investigated both the properties and the regulation of the expression of ChEs *in vivo*, in tissues derived predominantly of single cell types. Primary brain tumors provided us with such sources.

For this purpose, levels and molecular forms of ChEs were studied in gliomas, meningiomas and embryonic human brain. All of these tissue types contained substantial amounts of ChE activity. In both normal forebrain and meningiomas, AChE accounted for almost all of the ChE activity, but in almost all gliomas, elevated levels of ψ ChE could be detected. The ChE activity of both normal forebrain and gliomas migrated on sucrose gradients as a major component of 10-11S,

together with a minor component of 4-4.5S. In meningiomas, only a light 4.5S component could be detected (23). This implied that if indeed different forms of ChE are translated from distinct mRNA species, primary brain tissues should exhibit variations also at the level of ChEmRNAs.

III. Fluorometric measurement of minute ChE activities

To increase the sensitivity of ChE detection, a highly sensitive microfluorometric assay for ChEs was developed. Enzymatic activity was measured by monitoring the thiocholine produced by specific hydrolysis of acetylthiocholine. This was carried out by reacting the thiocholine formed, with the fluorogenic compound, N-(4'7 diethylamino-4 methyl-coumarin-3-yl) phenyl) maleimide (CPM), to yield an intensely fluorescent product. The assay is linear over a range extending from a few picomoles to nanomoles of thiocholine. The specificity and accuracy of this microfluorometric assay were examined using microgram quantities of rat brain tissue as a source for ChEs. The specific activities and the k_m values determined by this new method for both AChE and ψ ChE were identical to those reported earlier, using the less sensitive spectrophotometric and radiometric methods. The background emission caused by non-enzymatic hydrolysis of the substrate is relatively low, and does not exceed background values encountered in other methods. The assay may be used for monitoring the kinetics of enzymatic activities in microscale reaction mixtures, providing a linear determination of the thiocholine produced over a period of at least 30 hr at room temperature (24).

IV. Expression of heterogeneous AChEmRNAs in micorinjected *Xenopus* oocytes

Labeling techniques or *in vitro* translation assays are not sensitive enough to detect scarce mRNA sequences or their translation products. To study the post-transcriptional regulation of AChE biosynthesis, we developed an "in ovo" bioassay, where we use microinjected *Xenopus* oocytes as a translation system, in which AChEmRNA(s) are expressed into biologically active AChEs (25).

Xenopus oocytes have been extensively used as an expression system for a variety of microinjected mRNAs (26-28). They efficiently perform the translation, processing, and various post-translational modifications (28). In the case of mRNAs directing the synthesis of secretory proteins, they secrete the correct translation products (28-30), in a fashion that can be regulated by microinjection of a synthetic leader peptide (31).

In the oocytes, injected mRNAs are being translated into biologically active and correctly sequestered protein products (32-34). An impressive example is the synthesis of a functional acetylcholine receptor. The biosynthesis of such receptors from microinjected unfractionated (35) or hybrid-selected (36) mRNA involves glycosylation, assembly of 4 different subunits and insertion, in the correct orientation, into the oocyte membrane.

Samples of poly(A)⁺RNA from post-mortem embryonic brain and from biopsies of meningioma and glioblastoma all exhibited the ability to induce the production of catalytically active ChE when injected into *Xenopus* oocytes (37). In general, the content of ChEmRNA within the injected mRNA populations appeared to be in the same range as that observed using mRNA from the rat cerebellum (38). However, pronounced variations could be observed from experiment to experiment. These could initially be attributed to several causes, such as variability of cell type composition between different specimens, changes in the efficiency of extraction of intact mRNA chains, seasonal differences at the post-translational level between different batches of oocytes (28) or interference with ChE determinations.

Several control experiments were carried out in an attempt to distinguish between these

possibilities:

- a. Deviations in the results of repeated injections of the same mRNA preparations revealed that the variabilities were not due to different cell type compositions and/or changes in mRNA extraction.
- b. Injection of the frogs with human chorionic gonadotropin, which induces oocyte maturation, increased the general efficiency of translation in the oocytes, but did not improve the signal/background ratio.
- c. Removal of the follicle layer prior to the microinjection caused damage to part of the oocytes, particularly in long incubations.

Based on these observations, we concluded that the procedure for ChE determination in oocyte samples should be improved. For this purpose, an appropriate mixture of protease inhibitors was developed. This mixture (37) protects ChE activity in oocyte homogenates and incubation medium. The selected inhibitors were added, both to the oocyte incubation medium, following microinjection, and to the homogenization buffer used to prepare the extracts. Under these conditions, the enzymatic release of acetate was found to be linear in time and with quantity of oocytes added, whether examined by the radiometric technique (39) or the microfluorometric one (24). This improved ChE determination was then employed to reveal whether the polymorphism of brain ChEs also extends to the level of mRNA.

RNA was prepared from primary gliomas, meningiomas and embryonic brain, each of which expresses ChE activity with distinct substrate specificities and molecular forms (23). Sucrose gradient fractionation of dimethylsulfoxide-denatured poly(A)⁺RNA from these tissue sources revealed three size classes of ChE-inducing mRNAs, the major one sedimenting at about 32S, and two additional ones of 20S and 9S. The quantitative segregation between these different size classes of ChE-inducing mRNAs varied between the three tissues examined. To distinguish between ChEs having different sensitivities to specific inhibitors, the ChE activity of the oocytes was determined in the presence of such inhibitors (2). Both AChE and ψ ChE multimeric activities were found to be produced in the mRNA-injected oocytes. Moreover, different size distributions were observed for human brain mRNAs inducing AChE and ψ ChE activities, indicating that different mRNAs might be translated into various types of ChEs. These findings implied that the heterogeneity of ChEs in the human nervous system is not limited to the post-translational level, but rather extends to the level of mRNA as well (37).

V. Strategy for molecular cloning of the human gene(s) coding for brain acetylcholinesterase

The polymorphism of ChEmRNAs implied that it would not be possible to enrich these scarce mRNAs by size fractionation without losing several species. This made the cDNA cloning approach, and, particularly, the screening of a very large number of cDNA clones, rather impractical. In order to obtain a specific DNA probe, with which such screening would become more simple, we decided to search first for genomic DNA sequences encoding the synthesis of human brain ChE. For this purpose, we employed a cloned fragment from the *Ace* locus in *Drosophila melanogaster*.

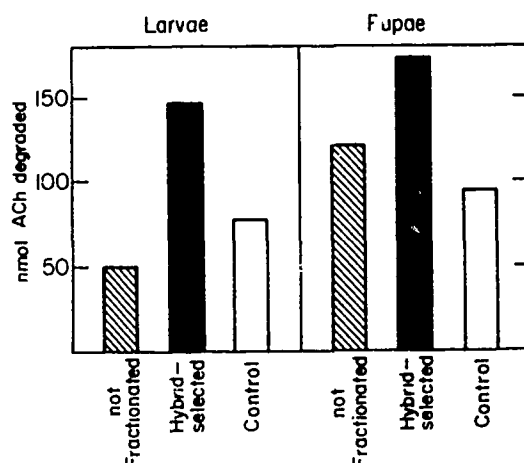
The genetics of the nervous system in *Drosophila* is well-characterized, and various mutants are available in which the expression of specific neurotransmitter-hydrolyzing enzymes is defective (for a recent review, see ref. 40). The *Ace* locus, regulating the biosynthesis of AChE, was first found to be located on the 3rd chromosome by construction of aneuploid flies (41). Mutations

in this locus are lethal in homozygots and cause the complete absence of AChE activity in the nervous system, indicating that the *Ace* locus regulates the expression of AChEmRNA(s). In a recent series of studies, P. Spierer and co-workers investigated the chromosomal organization of the *Ace* locus (42), mapped genetic and chromomeric units in this region (43) and characterized the transcripts of 315Kb in *Ace* (44). Induction of RNA synthesis in ecdysone-treated *Drosophila* cells in culture, in which AChE is inducible (45), suggested that a specific 10.5Kb sequence included in this region is directly involved with AChE synthesis (P. Spierer, unpublished). This Sall fragment has been cloned into pBR322 and was employed in our research as a specific probe for the AChE gene(s).

VI. Expression of *Ace* locus in *Drosophila*

In collaboration with P. Spierer, we mapped the Sall fragment. Enzymatic restriction and hybridization to blotted poly(A)⁺RNA indicated that different parts in this sequence are transcribed into several mRNAs. Oocyte microinjection of gradient-fractionated mRNA, followed by AChE bioassay, revealed that *Drosophila* AChEmRNA is enriched in the 28S fraction, which includes two transcripts (5.2Kb and 4.5Kb) of the *Ace* locus. The DNA region which hybridized with these transcripts was therefore selected as the best candidate to be transcribed into AChEmRNA (46). This region (an EcoRI-cut fragment of 2.0Kb in length) was then bound to nitrocellulose filters and hybridized with poly(A)⁺RNA from *Drosophila* larvae or pupae. The hybrid-selected mRNA, when subsequently eluted, induced AChE biosynthesis in oocytes (Fig. 1). This indicated that the 2.0Kb DNA fragment hybridizes with AChEmRNA and could serve as an appropriate probe to search for homologous human sequences.

Figure 1. Hybridization-selection of *Drosophila* AChE-inducing mRNAs by the filter-bound 2.0Kb DNA fragment from *Drosophila Ace*.



Oocytes were injected with the following mRNA preparations: Not fractionated-total

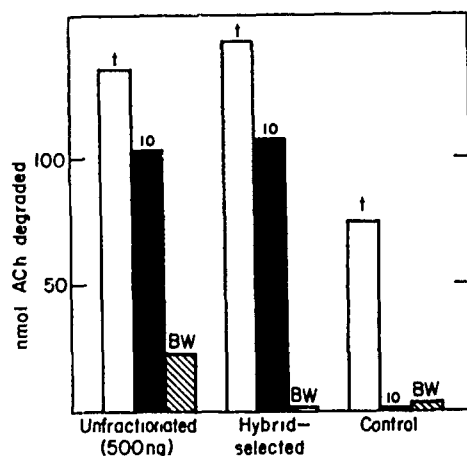
poly(A)⁺RNA from *Drosophila* larvae or pupae (500ng per sample); Hybrid-selected-mRNA eluted from filter-bound 2.0Kb EcoRI DNA (see text), out of 20 μ g poly(A)⁺RNA in each case; Control-mRNA eluted from filter-bound pBR322 DNA under the same conditions. AChE activity was determined as described (37).

VII. Isolation of *Hu.AChE1*, a human genomic sequence homologous to *Drosophila Ace*

The 2.0Kb EcoRI *Drosophila* DNA fragment described above cross-hybridized, under relaxed conditions (indicating partial homology) with a human brain mRNA species of ca. 7.0Kb, which was very faint in the AChE-deficient human epidermoid carcinoma (37). The major species of oocyte-translatable AChEmRNA from embryonic human brain displayed a similar 7.0Kb size, indicating that the *Drosophila Ace* DNA fragment hybridized with human brain AChEmRNA. This fragment was therefore employed to screen a human genomic DNA library.

Three genomic equivalents (7x10⁵ plaques) of human DNA fragments cloned in Charon 4a phages were screened and 6 of these hybridized, under relaxed conditions, with the *Drosophila Ace* 2.0Kb probe. One of these, designated *Hu.AChE1*, was purified and further characterized. This 13.5Kb-long fragment was found to be complementary to a 7.0Kb human brain mRNA species, which, when selected by hybridization, induced AChE biosynthesis in microinjected oocytes (Fig. 2).

Figure 2. Hybridization-selection of human brain AChE-inducing mRNAs using filter-bound DNA from *Hu.AChE1*.



Oocytes were injected with 500ng of unfractionated poly(A)⁺RNA from post-mortem human (21y) parietal cortex, with hybrid-selected mRNA eluted from filter-bound 2.6Kb EcoRI DNA from *Hu.AChE1*, out of 20 μ g poly(A)⁺RNA, or with control mRNA, eluted from filter-bound λ DNA under the same conditions. AChE activity was determined in oocyte extracts and incubation medium as described (37). Iso-OMPA (tetraisopropyl pyrophosphamide) and BW284C51

(1,5-bis(4-allyldimethylammonium-phenyl) pentan-3-one dibromide), which selectively inhibit ψ ChE and AChE, respectively (2), were both used at 10^{-5} M final concentrations.

We employed 20 μ g poly(A)⁺RNA in each hybridization-selection mixture. Assuming a $\geq 0.1\%$ abundance for hybridizable RNA, we could select up to 7ng of AChE-inducing mRNA. One-third of the selected RNA (about 7ng) selectively induced AChE activity, resistant to iso-OMPA, and sensitive to BW284C51. This AChE degraded ca. 100 nmol acetylcholine, similar to the AChE induced by 500ng of unfractionated poly(A)⁺RNA. These results, shown in Fig. 2, reveal a selective enrichment of translationally active AChEmRNA in the hybridization-selection experiments. In contrast, the activity displayed by control oocytes was sensitive to both inhibitors, as expected from the endogenous *Xenopus* enzyme (28). Based on the above described experiments, we have concluded that the DNA fragments selected from *Drosophila* and man represent part of the AChE genes of the two species, since:

- (a) Both fragments hybridize with blotted RNA species in the size range which shows greatest enrichment for AChE-inducing mRNA, as measured in microinjected oocytes.
- (b) The human mRNA hybridizing with both DNA fragments is found in much lower quantities in the AChE-deficient carcinoma than in brain, and in AChE-positive brain tumors.
- (c) Both fragments hybridize specifically with RNA molecules which, on subsequent elution, induce AChE biosynthesis in oocytes.

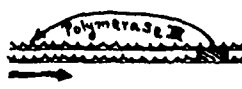
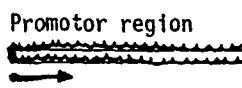
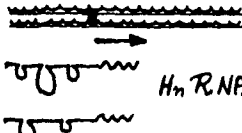
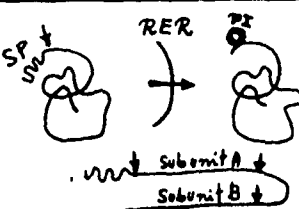
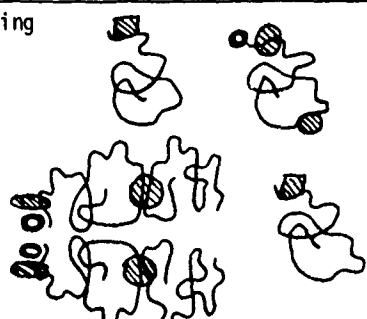
The detailed biochemical and immunological properties of the oocyte-induced AChE are currently being investigated. In addition, the 2.6Kb *Hu.AChE1* fragment was employed to re-screen the human genomic library. Up to 40 positive plaques were selected. Restriction analysis and DNA blotting indicated that these include at least 8 different DNA fragments. In addition, a cDNA library of about 40,000 independent colonies was prepared from mRNA from human embryonic brain (18 weeks gestation), where AChE is expected to be expressed both in morphogenetically migrating cells and in cholinergic neurons. About 40 colonies displayed positive hybridization signals with the *Hu.AChE1* probe. Several of these were amplified for further characterization. All appear to hybridize to the same major 7.0Kb mRNA species as *Hu.AChE1*.

VIII. Conclusive remarks

Our observations imply that the polymorphism of AChEs may originate at multiple steps through the pathway of gene expression. Some of these possibilities are presented schematically in Fig. 3.

At the level of Genome organization, the finding of several independent *Hu.AChE1* -homologous DNA sequences in the human genome suggests that more than one gene encodes the synthesis of AChE. Multigene families for single proteins, particularly polymorphic ones, have been described in the literature (for a review see ref. 47). Regulation of transcription could then determine the tissue-specific expression of particular AChE gene(s). Very recently, it has been suggested that brain-specific polymeraseIII transcription of particular "identifier" sequences, abundant in brain transcripts, activates polymeraseII transcription and leads to the production of brain-specific mRNAs and proteins (48). Alternatively, or in addition, more than one mRNA could be transcribed from a single AChE gene. This could either occur by differential splicing or by alternative transcription. Two mRNAs generated by differential splicing were reported in several cases, e.g. calcitonin and human growth hormone (49,50). If alternative transcription is assumed, the use of more than one promotor within the gene must be postulated.

All of these alternatives would result in the formation of heterogenous mRNAs for AChE, as recently detected by size fractionation and oocyte microinjection (37).

BIOSYNTHESIS OF BRAIN ACETYLCHOLINESTERASES			
Site in the Cell	Step in Gene Expression Pathway	Molecules Involved	Possibilities for Creation of Polymorphism
Nucleus	- Genome organization	DNA: AChE gene(s)	<ul style="list-style-type: none"> - multigene family - brain-specific regulatory sequences - alternate transcription
	- Regulation of transcription		
	- " " "		
	- Production of heterogenous mRNAs		<ul style="list-style-type: none"> - differential splicing - transcription of different genomic sequences
Rough endoplasmic reticulum	- Cotranslational processing		<ul style="list-style-type: none"> - cleavage of signal peptide - formation of lipid anchorage sites - splitting of high m.w. precursor
RER + Golgi	- Post-translational processing		<ul style="list-style-type: none"> - isoform-specific processing steps (i.e., glycosylation, S-S bond formation) - selective production of subunit assembly domains
?	- Assorting of AChE multiple forms		

Cotranslational processing events direct many eukaryotic proteins to their correct subcellular sites. Cotranslational cleavage of the NH₂-terminal signal peptide (for example ref. 31) is a necessary prerequisite to the biosynthesis of most membrane and secretory proteins and their translocation into the lumen of the rough endoplasmic reticulum (RER). The hydrophobic forms of AChE (for a review see ref. 1) would have to include membrane anchorage sites. These could be contributed by an interaction involving phosphatidyl-inositol, as was recently observed by Futerman et al. (51) for the hydrophobic dimer of AChE from *Torpedo* electric organ. Alternatively, membrane anchorage sites could be created by a small hydrophobic peptide, as suggested recently by Rosenberry and co-workers (52).

It is not yet clear whether the various subunits of the different isoforms of AChE are similar in their amino acid sequence, and whether each of these is translated from a discrete mRNA species. For example, it is possible that one large mRNA (such as the 7.0Kb-long mRNA hybridized with *Hu.AChE1*) would include a coding sequence for a putative pro-AChE precursor, to be subsequently cleaved into two similar, but not identical subunits. Such a case has been found very recently for another human serine esterase, urokinase (53). It is also possible that various AChE mRNAs would code for different precursor proteins, all destined to yield the active enzyme. Examples for this phenomenon are glucagon (54), kininogen (55) and albumin (56).

Post-translational processing events of AChE precursors take place in the RER and the Golgi apparatus, as was recently shown by Rotundo (57). These include isoform-specific processing steps, such as glycosylation, and perhaps, formation of S-S bonds. The assorting of AChE multiple forms into their correct subcellular localization would follow the assembly of multisubunit AChE forms. The assembly process itself may involve a selective production of subunit assembly domains, also depending on the amino acid sequence of the specific forms.

Each of these steps would increase the polymorphism of the end product, the catalytically active AChE. Our observations can therefore be added to those recently reviewed by Massoulié and co-workers (58) as explaining additional levels for the creation of such polymorphism. Continuation of the above described research approach can answer at least part of the questions that were raised regarding the regulation of AChE biosynthesis. In addition, the findings should prove valuable in both basic and clinical research of these important enzymes.

This research was supported by the United States Army Medical Research and Development Command (contract no. DAMD 17-82-C-2145). The contribution of D. Zevin-Sonkin, A. Avni, P. Spierer, L.H.C. Hall, I. Silman, I. Pecht, N. Razon, R. Parvari, H. Zakut and R. Zisling in different parts of these studies is gratefully acknowledged.

References

1. Massoulié, J. and Bon, S. (1982). *Ann. Rev. Neurosci.* 5, 57-106.
2. Austin, L. and Berry, W.K. (1953). *Biochem. J.* 54, 695-700.
3. Vigny, M., Gisiger, V. and Massoulié, J. (1978). *Proc. Natl. Acad. Sci. USA* 75, 2588-2592.
4. Koelle, G.B. (1963). In: "Handbuch der Experimentellen Pharmakologie" Vol.XV, Springer-Verlag, Berlin.
5. Aldridge, W.N. and Reiner, E. (1972). In: "Enzyme Inhibitors as Substrates." North-Holland Publishing Co., Amsterdam.
6. Wills, J.H. (1970). In: "International Encyclopedia of Pharmacology and Therapeutics" Section 13, Vol.I, Anticholinesterase agents. A.G. Karczmar, ed., Pergamon Press, Oxford, pp. 357-469.
7. Hobbiger, F. (1963). In: Cholinesterases and Anticholinesterase Agents. G.B. Koelle, ed. Springer, Berlin, pp. 921-988.
8. Loomis, T.A. (1963). *Toxicol. Appl. Pharmacol.* 5, 489-499.
9. Spokes, E.G.s. (1980). *Brain* 103, 179-183.
10. Atack, J.R., Perry, E.K., Bonham, J.R., Perry, R.H., Tomlinson, B.E., Blessed, B. and Fairbairn, A. (1983). *Neuroscience Lett.* 40, 199-204.
11. Coyle, J.t., Price, D.L. and DeLong, M.R. (1983). *Science* 219, 1184-1190.
12. Yates, C.M., Simpson, J., Maloney, A.F.J., Gordon, A. and Reid, A. H. (1980). *Lancet* 2, 979.
13. Barlow, R.D., Cuckle, H.S. and Waid, N.J. (1982). *Clinical Chimica Acta* 119, 137-142.
14. Webb, B.A., Richardson, S.J., Garry, R. and Atkins, J. (1983). *Ann. Clin. Biochem.* 20, 159-162.
15. Brock, D.J.H. and Bader, P. (1983). *Clin. Chim. Acta* 127, 419-422.
16. Hay, D.L., Ibrahim, G.F. and Horacek, I. (1983). *Clin. Chem.* 29, 1065-1069.
17. Bonham, J.R. and Atack, J.R. (1983). *Clin. Chim. Acta* 135, 233-237.
18. Silver, A. (1974). *The Biology of Cholinesterases*. North-Holland Pub. Co., Amsterdam.
19. Leong, S.F., Lai, J.C.K., Lim, L. and Clark, J.B. (1981). *J. Neurochem.* 37, 1548-1556.
20. Dudai, Y., Silman, I., Shinitzky, M. and Blumberg, S. (1971). *Proc. Natl. Acad. Sci. USA* 69, 2400-2404.
21. Ott, P., Jenny, B. and Brodbeck, U. (1975). *Eur. J. Biochem.* 57, 469-480.
22. Graybiel, A.M. and Ragsdale, C.W. (1982). *Nature* 299, 439-441.
23. Razon, N., Soreq, H., Roth, E., Bartal, A. and Silman, I. (1984). *Exp. Neurol*, in press.
24. Parvari, R., Pecht, I. and Soreq, H. (1983). *Anal. Biochem* 133, 450-456.
25. Soreq, H., Parvari, R. and Silman, I. (1982). *Proc. Natl. Acad. Sci. USA* 79, 830-835.
26. Gurdon, J.B., Lane, C.D., Woodland, H.R. and Marbaix, G. (1971). *Nature* 233, 177-182.

27. Lane, C.D. (1983). *Curr. Topics in Dev. Biol.* 18, 89-119.
28. Soreq, H. (1984). *CRC critical reviews in biochem.*, in press.
29. Colman, A. and Morser, J. (1979). *Cell* 17, 517-526.
30. Valle, G., Besley, H. and Colman, A. (1981). *Nature* 291, 338-340.
31. Koren, R., Burstein, Y. and Soreq, H. (1983). *Proc. Natl. Acad. Sci. USA* 80, 7205-7209.
32. Labarca, c. and Paigen, K. (1977). *Proc. Natl. Acad. Sci. USA* 74, 4462-4465.
33. Long, E.O., Grass, N., Wake, C.T., Mach, H.P., Carrel, S., Accalla, R. and Mach, B. (1982). *The EMBO Journal* 1, 649-654.
34. Richter, J.D. and Smith, D.L. (1981). *Cell* 27, 183-191.
35. Barnard, E.A., Miledi, R. and Sumikawa, K. (1982). *Proc. R. Soc. Lond. B.* 215, 241-246.
36. Mishina, M., Kurosaki, T., Tobimatsu, T., Morisoto, Y., Noda, M., Yamamoto, T., Terao, M., Lindstrom, J., Takahashi, T., Kuno, M. and Numa, S. *Nature* 307, 604-608. (1984)
37. Soreq, H., Zevin-Sonkin, D. and Razon, N. (1984). *The EMBO Journal* 3, in press.
38. Parvari, R., Silman, I. and Soreq, H. (1984). In: *Cholinesterases - Fundamental and Applied Aspects*. M. Brzin, T. Kianta and E.A. Barnard, eds. Walter de Gruyter and Co., Berlin, in press.
39. Johnson, C.D., and Russell, R.L. (1975). *Anal. Biochem.* 64, 229-238.
40. Hall, J.c. (1982). *Quarterly Rev. Biophys.* 15, 223-479.
41. Hall, J.C. and Kankel, D.R. (1976). *Genetics* 83, 517-535.
42. Bender, W., Spierer, P. and Hogness, D.S. (1983). *J. Mol. Biol.* 168, 17-33.
43. Spierer, P., Spierer, A., Bender, W. and Hogness, D.S. (1983). *J. Mol. Biol.* 168, 31-40.
44. Hall, L.H.C., Mason, P.J. and Spierer, P. (1983). *J. Mol. Biol.* 169, 83-96.
45. Cherbas, P.T., Cherbas, L. and Williams, C.M. (1977). *Science* 197, 275-277.
46. Soreq, H., Zevin-Sonkin, D., Avni, A., Hall, L.H.C. and Spierer, P. (1984). In: *Physiological and Pharmacological Control of Nervous System Development*. F. Cacigli, ed. Elsevier, Amsterdam, in press.
47. Long, E.D. and David, I.B. (1980). *Ann. Rev. biochem.* 49, 727-764.
48. Sutcliffe, J.G., Milner, R.J., Gottesfeld, J.M. and Lerner, R.A. (1984). *Nature* 308, 237-241.
49. Rosenfeld, M.G., Amara, S.G., Ross, B.A., Ong, E.S., and Evans, R.M. (1981). *Nature* 290, 63-65.
50. Evans, R.M., Amara, S.G. and Rosenfeld, M.G. (1982). *DNA* 1, 323-328.
51. Futerman, A.H., Low, M.G. and Silman, I. (1983). *Neurosci. Lett.* 40, 85-89.
52. Rosenberry, T.L., Scoggin, D.M., Dutta-Choudhury, T.A. and Haas, R. (1984). In: *Cholinesterases - Fundamental and Applied Aspects*. M. Brzin, T. Kianta and E.A. Barnard, eds. Walter de Gruyter and Co., Berlin, in press.

53. Verde, P., Stoppelli, M.P., Galeffi, P., Di Docera, P. and Blasi, F. (1984). *Proc. Natl. Acad. Sci. USA*, in press.
54. Lund, P.K., Goodman, R.H. and Haberner, J.F. (1981). *J. Biol. Chem.* 256, 6515-6518.
55. Nawa, H., Kitamura, N., Hirose, T., Asai, M., Inayama, S. and Nakanishi, S. (1983). *Proc. Natl. Acad. Sci. USA* 80, 90-94.
56. Schoenberg, D.R. (1981). *Nucl. Acids Res.* 9, 6669-6688.
57. Rotundo, R.L. (1984). *Proc. Natl. Acad. Sci. USA* 81, 479-483.
58. Massoulié, J., Bon, S., Lazar, M., Grassi, J., Marsh, D., Meflah, K., Toutant, J.P., Vallette, F. and Vigny, M. (1984). In: *Cholinesterases - Fundamental and Applied Aspects*. M. Brzin, T. Kianta and E.A. Barnard, eds. Walter de Gruyter and Co., Berlin, in press.

Monoclonal Antibody Affinity Purification
of Human Acetylcholinesterase

J. T. August
Department of Pharmacology and Experimental Therapeutics
Johns Hopkins University School of Medicine
Baltimore, MD 21205

INTRODUCTION

Acetylcholinesterase is associated chiefly with cells involved in cholinergic synaptic transmission and is also found in a few non-neuronal cells like erythrocytes. The enzyme exists in a variety of aggregation states with a monomer unit of about 75,000 Mr (Shafai and Cortner, 1971; Wright and Plummer, 1973; Ott and Brodeck, 1978). Two general classes have been distinguished: asymmetric forms that contain catalytic units covalently linked to a collagenous tail and globular forms which are assemblies of catalytic units devoid of the collagenous component (Bon et al., 1979). In the plasma membrane of the erythrocyte the enzyme exists as a globular dimer of a 180,000 Mr. In the central nervous system a membrane-bound tetrameric form predominates. In skeletal muscle, globular forms (monomeric, dimeric, and tetrameric) occur both as soluble and tightly membrane-bound molecules, and some globular forms are secreted. In addition, skeletal muscle contains complex asymmetric forms in which up to three tetramers are covalently linked to a collagenous tail. The occurrence of these asymmetric forms often correlates with innervation, and in most species asymmetric forms are located primarily in the area of innervation and constitute a major fraction of the esterase at neuromuscular junctions. This localization appears to be mediated by the interaction of the collagen-like tail structure with the extracellular basement membrane matrix (Hall and Kelly, 1971; Betz and Sakmann, 1973; McMahan et al., 1978).

All of the molecular species of acetylcholinesterase appear to have the same enzymatic sites. Fambrough, et al. (1982), prepared five monoclonal antibodies that bound to purified human erythrocyte acetylcholinesterase, each reacting with different antigenic sites on the acetylcholinesterase molecule. All of these antibodies crossreacted with human and monkey neuromuscular junctions. It was concluded that a high degree of homology exists between the acetylcholinesterase of erythrocytes and neuromuscular junctions.

The most available source of human acetylcholinesterase is the erythrocyte. It is an integral part of the red blood cell membrane (Bellhorn et al., 1970; Heller and Hanahan, 1971) and is one of the most active of known catalytic agents with a turnover number of about 6×10^5 moles/min/active site. Purification of human erythrocyte acetylcholinesterase has been reported by several workers (Sihotang, 1974; Ott et al., 1975). For example, Ott et al. (1975) solubilized the human erythrocyte enzyme by Triton X-100 and used acridinium affinity chromatography to obtain a fraction with 3800 IU per mg protein specific activity. The purified enzyme appeared as a single polypeptide of 80,000 Mr on SDS-gel electrophoresis. Rosenberry and Scoggin (1984) used a similar procedure for a large scale purification yielding about 5 mg of enzyme from 10 liters of erythrocytes.

Herein we report the purification of human erythrocyte acetylcholinesterase by monoclonal antibody affinity chromatography.

RESULTS

Enzyme Preparation

Acetylcholinesterase Extraction From Human Erythrocytes - Packed human erythrocytes from 10 to 20 day old collections of blood obtained from the central blood bank of the Johns Hopkins Hospital were used as the starting material for the purification of acetylcholinesterase. Red cells were washed 3 times with equal volumes of isotonic buffer (5 mM sodium phosphate, pH 7, 0.9 percent NaCl). Cells were lysed in 40 volumes of hypotonic buffer (5 mM sodium phosphate, pH 7). Ghosts were prepared according to the procedure of Rosenberry et al (1981) using a Millipore pellicon high-volume molecular filtration apparatus. A single modification of the procedure was the use of a Duripore filter (0.45 μ m) in place of the PTKH 100,000 filter. Triton X-100, 1 percent final concentration, was added to solubilize the membrane proteins, and the suspension was centrifuged at 100,000 x g. The 100,000 x g supernatant was diluted 1:5 with 5 mM sodium phosphate buffer, pH 7, and passed through a 30 ml Sepharose-4B column to remove any non-specifically absorbed proteins. The soluble enzyme was then purified by immuno-affinity chromatography as described below.

Monoclonal Antibody Affinity Column Purification of Acetylcholinesterase - Hybridoma cells secreting monoclonal antibody AE-4, specific for human acetylcholinesterase, were obtained from Dr. D. Fambrough, Carnegie Institute (Fambrough, et al, 1982). Large amounts of immunoglobulin were obtained by growing cells as ascites tumors. Mice were injected intraperitoneally with 0.5 ml of pristane (2,6,10,14-tetramethylpentadecane), and 1 week later were injected with 1 to 2 x 10⁷ hybridoma cells. Ascites fluids were inactivated at 56°C for 30 min, and clarified by centrifugation at 100,000 x g for 1 hr.

Purification of the AE-4 antibody was carried out by ammonium sulfate precipitation and ion exchange chromatography (Hughes and August, 1982; Hughes, Colombatti, and August, 1983). All procedures were carried out at 1 to 4°C. Solid ammonium sulfate was added to ascites fluid at a final concentration of 45 percent. The precipitated protein was collected by centrifugation at 20,000 x g for 20 min, suspended in 10 mM sodium phosphate buffer, pH 8.0, and dialyzed for 36 h in 2,000 ml of the same buffer with 6 changes of dialysate. After centrifugation at 100,000 x g for 1 h, the protein solution was applied to a 2.5 x 9-cm DEAE-cellulose (Whatman DE-23) column equilibrated in 10 mM sodium phosphate buffer, pH 8.0. The unabsorbed material contained 5 to 10 mg of immunoglobulin per ml of ascites; the immunoglobulin was greater than 95 percent pure by sodium dodecyl sulfate-polyacrylamide gel electrophoretic analysis of reduced and non-reduced material.

The purified monoclonal antibody was dialyzed against a buffer solution containing 500 mM NaCl and 200 mM sodium citrate, pH 6.5, and coupled to cyanogen bromide-activated Sepharose CL-4B (200 mg of cyanogen bromide/ml of packed beads) at a ratio of 3 mg of protein/ml of packed beads, as previously described (Hughes and August, 1982; Hughes, Colombatti, and August, 1983). The protein content of the filtrates indicated that 96 percent of the antibody preparation was coupled. A 1.5 cm x 10 cm column containing approximately 30 mg of AMF-14 antibody coupled to 10 ml of Sepharose CL-4B beads was treated with 1) 50 ml of 100 mM diethylamine, pH 11.5, 2) 50 ml of 1 M Tris-HCl, pH 7.6, and 3) 50 ml of 5 mM Tris, pH 7.6, before applying the extract.

Approximately 2300 ml of the diluted 100,000 x g supernatant was applied to the antibody column at a rate of 2 ml/min. Most of the protein in the extract was not retained by the column. After the protein sample was loaded, the column was washed with 150 ml of the column buffer, followed by 150 ml of a borate-salt buffer, pH 8.5 (1 M NaCl, 100 mM boric acid, 15 mM sodium borate, 0.2 percent (w/v) Triton X-100) in order to remove components adsorbed non-specifically to the column. The column was then eluted at a rate of 0.5 ml/min with 100 ml of 100 mM diethylamine, pH 11.5, containing 0.2 percent (w/v) Triton X-100, and 20 percent glycerol. Fractions of 2 ml were collected in tubes containing 0.5 ml of neutralizing buffer (2 M Tris-HCl, pH 7.6). The antigen eluted in 32 ml as a single, sharp peak of antigenic activity corresponding to a small protein peak. Analysis by polyacrylamide gel electrophoresis of the individual fractions of the enzyme showed that the concentration of this eluted protein was proportional to enzyme activity (data not shown). The active fractions were pooled and concentrated to 1.5 ml by use of a negative pressure dialysis-concentrating apparatus (Micro-Pro Di Con; Bio-Molecular Dynamics, Beaverton, OR) in 2000 ml of a buffer solution containing 20 mM sodium phosphate, 100 mM NaCl, 0.1 percent (w/v) Triton X-100, pH 8.0, and 20 percent glycerol at 4°C.

The summary of a typical procedure starting with 60 ml of packed red blood cells is shown in Table 1. An apparent 44-fold purification and recovery of 40 percent was obtained by preparing the red cell ghost fraction. The crude hemolysate activity assay is ambiguous, however, since the cells likely contain other contaminating esterase activities. Thus, there is probably greater recovery of activity and greater purification than is shown. Antibody affinity chromatography resulted in 500-fold purification with 30 percent recovery of enzyme activity. The final yield was 750 µg with a overall purification of at least 20,000-fold.

Characterization

³H-diisopropylfluorophosphate (DFP) Labeling and Polyacrylamide Gel Electrophoresis - The purified enzyme analyzed by sodium dodecyl sulfate - polyacrylamide gel electrophoresis (SDS-PAGE) showed a single major polypeptide stained by the silver reduction procedure or with Coomassie brilliant blue. The apparent molecular weight was 75,000.

This polypeptide was proven to be the acetylcholinesterase by DFP labeling. The conditions for DFP labeling were characterized by treating the purified AChE (5×10^{-2} pmoles) with varying amounts of DFP (0-20 pmoles) in 0.1 M Tris-HCl pH 7.5 containing 2 percent propylene glycol in final volume of 10 µl. After 20 min at room temperature, enzyme activity was estimated by the Ellman procedure (1961).

The enzyme was almost totally inhibited (90 percent) by a 400:1 molar ratio of DFP:AChE. Based on these results, enzyme was labeled by reacting 7.5 pmoles of AChE with 3000 pmoles of ³H-DFP. After 30 min, the [³H]DFP-AChE adduct was precipitated with 10 volumes of acetone at -20°C for 15 hrs. After centrifugation at 12,000 x g for 30 min, the pelleted protein was solubilized and analyzed by SDS-PAGE (Figure 1). The gel, analyzed both by silver stain and autoradiography, revealed a single radiolabeled polypeptide corresponding to the purified protein of 75,000 daltons.

High-performance Liquid Chromatography - The purity of the fraction is also demonstrated by size-exclusion on a TSK-SW3000 silica-supported hydrophilic polymer column. A single major protein peak detected by ultra-violet absorbance at 280 nm is present (Figure 2). This peak corresponded perfectly to the enzyme activity of the fractions and to the elution of ^{125}I -labeled AChE.

REFERENCES

- Bellhorn, M.B., Blumenfeld, O.O., and Gallop, P.M. *Biochem. Biophys. Research Comm.* **39**:267-273, 1970.
- Betz, W., and Sakmann, B. *J. Physiol. (Lond.)* **230**:673-688, 1973.
- Bon, S., Vigny, M., and Massoulie, J. *Proc. Natl. Acad. Sci. USA* **76**:2546-2550, 1979.
- Ellman, G.L., Courtney, K.D., Andres, V., Jr., Featherstone, R.M. *Biochem. Pharmacology* **7**:88-95, 1961.
- Fambrough, D.M., Engel, A.G., Rosenberry, T.L. *Proc. Natl. Acad. Sci. USA* **79**:1078-1082, 1982.
- Hall, Z.W., and Kelley, R.B. *Nat. New Biol.* **232**:62-63, 1971.
- Heller, M., and Hanahan, D.J. *Biochim. Biophys. Acta* **255**:251-272, 1971.
- Hughes, E.N., and August, J.T. *J. Biol. Chem.* **257**:3970-3977 (1982).
- Hughes, E.N., Colombatti, A., and August, J.T. *J. Biol. Chem.* **258**:1014-1021 (1983).
- McMahan, U.J., Sanes, J.R., and Marshall, L.M. *Nature (Lond.)* **271**:172-174, 1978.
- Ott, P., and Brodbeck, U. *Eur. J. Biochem.* **88**:119-125, 1978.
- Ott, P., Jenny, B., and Brodbeck, U. *Eur. J. Biochem.* **57**:469-480, 1975.
- Rosenberry, T.L., Chen, J.F., Lee, M.M.L., Moulton, T.A., and Onigman, P. *J. Biochem. Biophys. Methods* **4**:39-48, 1981.
- Rosenberry, T.L., and Scoggin, D.M. *J. Biol. Chem.* **259**:5643-5652, 1984.
- Shafai, T., and Cortner, J.A. *Biochim. Biophys. Acta* **236**:612-618, 1971.
- Sihotang, K. *Biochim. Biophys. Acta* **370**:468-476, 1974.
- Wright, D.L., and Plummer, D.T. *Biochem. J.* **133**:521-527, 1973.

TABLE 1

Purification of Human Erythrocyte Acetylcholinesterase^a

Purification Step	Volume (ml)	Total Protein (mg)	Total Activity ^b (ΔA/min)	Activity Recovery (%)	Specific Activity (ΔA/min/mg)	Fold Purification
HEMOLYSATE	24,000	264,000	233,000		0.9	1
RED CELL GHOSTS	540	2,100	94,000	40	44	49
100,000 x g SUPERNATANT	465	1,023	94,000	40	91	100
ANTIBODY AFFINITY	1.5	0.75	17,000	7	23,000	26,000

^a Purification was performed as described in the text.^b Enzyme activity was measured as described by Ellman *et al.* (1961).

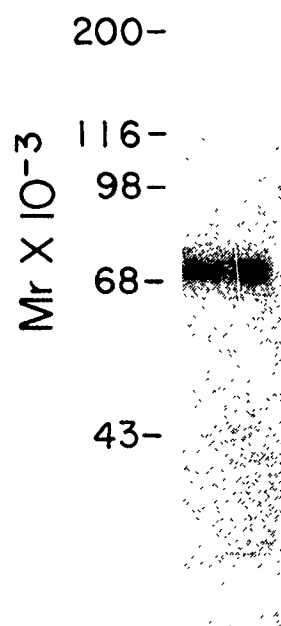


Figure 1. Purified AChE was labeled with ^3H -DFP as described in the text.

HPLC SIZE EXCLUSION CHROMATOGRAPHY PURIFIED AChE

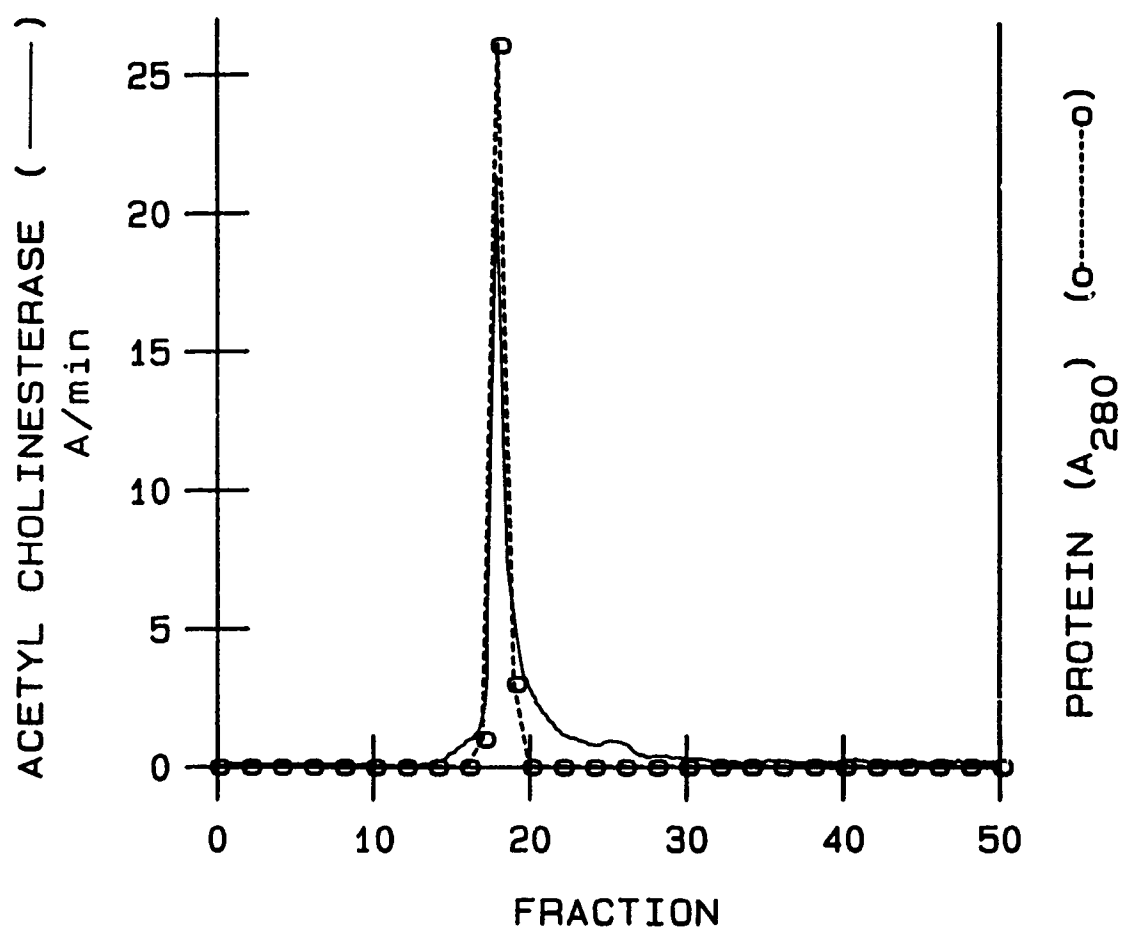


Figure 2. The concentrated affinity purified fraction of AChE (20 μ l, 10 μ g) was placed in a 7.5 mm X 30 cm TSK-SW3000 column. The column was eluted with 5 mM Tris-HCl, pH 7.5, at 0.5 ml/min. The fraction volume was 0.5 ml. The tracing is absorbance at 280 nm with a setting of 0.02 absorbance units full scale. The peak fraction corresponded exactly to enzyme activity and to radioactivity of 125 I-acetylcholinesterase (0.01 μ g, 1.3×10^6 cpm) added as an internal marker.

Anti-Soman Monoclonal Antibodies; Structural
and Stereochemical Specificity

D.E. Lenz, A.A. Brimfield*, H.P. Benschop#, L.P.A. deJong#,
K.W. Hunter*, Tran Chanh" and Jerry Sadoff'

USAMRICD, APG, MD 21001, USA, *USUHS, Bethesda, MD 20014, USA,
#Prins Maurits Laboratorium, TNO, Rijswijk, The Netherlands,
"Georgetown University, School of Medicine,
Washington, D.C. 20007, USA, 'WRAIR,
Washington, D.C. 20307

There are two recurring problems that need to be addressed (Fig. 1). The first difficulty is in identifying the site of action of organophosphorus poisons, which is a problem that has plagued researchers for the past several decades. Secondly, current therapy or prophylaxis regimens are not particularly effective against soman due to the fact that when acetylcholinesterase is inhibited, it is rapidly dealkylated, leading to the phenomenon known as "aging." Aged acetylcholinesterase is not susceptible to treatment by oxime. In addressing these two issues, the techniques of immunology were used. In the first case, we felt that specific antibodies might prove to be useful immunocytochemical reagents; that is, they might be utilized to identify the depot of soman reported by the researchers at the TNO Laboratories in the Netherlands. Secondly, if antibodies could be produced that would demonstrate some *in vitro* competition with acetylcholinesterase for the binding of soman, then a reexamination of these antibodies in an *in vivo* situation might prove to be fruitful. We recently reported on our efforts in this vein in FEBS Letters, 149, 147, 1982; wherein the approach for making monoclonal hapten-specific antisoman antibodies was described. The approach that we used in carrying out the production of these antibodies is shown in Fig. 2. Soman was modified with a p-aminophenyl group in place of the fluorine. This was subsequently attached to a protein carrier, either bovine serum albumin or keyhole limpet hemocyanin (KLH). These modifications were necessary because soman or its p-aminophenyl derivative alone will not elicit an immune response. The soman protein conjugate was used as an immunogen and produced monoclonal antibodies in mice, using the Milstein technique. These antibodies were then subsequently screened for their ability to bind to soman, using a competitive inhibition enzyme immunoassay (CIEIA).

In this technique (Fig. 3), a plastic well is coated with the hapten-protein conjugate. The specific antibody is allowed to react with free hapten under conditions of varying concentrations of free hapten. These solutions are then transferred onto the coated plate and a new equilibrium established between the free hapten, the mouse antihapten antibody, and the hapten-protein conjugate. The greater the concentration of the free hapten, the less likelihood of the antihapten antibody binding to the coated plate. After equilibrium is established, all unbound reagents are washed away and the material remaining is then visualized using an anti-antibody which has attached to it some reporter group (in this case, the enzyme, alkaline phosphatase). The unbound material is again washed away, the substrate p-nitrophenylphosphate is added, and the hydrolysis product, p-nitrophenol, is measured spectrophotometrically. The greater the amount of anti-hapten antibody bound to the coated plate, the greater the optical density due to the amount of p-nitrophenol produced. If the antibody has a greater affinity for the hapten, less will be bound to the coated plate and the optical density will be reduced. Typical results are shown in Fig. 4, wherein the log of the soman concentration on the x-axis and the absorbance of material in the well on the y-axis has been plotted. As soman concentration increases, the absorbance decreases, indicating less and less antibody bound to the coated plate. Data of this type are in the form of a titration curve and, if we can measure the concentration that produces 50 percent inhibition of binding of antibody to coated plate, we can express this as the IC₅₀. This number is convenient because it is directly related to the thermodynamic binding constant. If a series of reactions are carried out, varying only the hapten concentration and keeping other reagents constant, the comparison of the IC₅₀ values gives an immediate comparison of the binding constants of the antibody for each hapten studied. In a preliminary investigation, we showed

the antibody had high specificity for soman, but very little for related haptens.

On the basis of this information, the antibody and its ability to retard the inhibition of acetylcholinesterase by soman was evaluated (Fig. 5). The rate of inhibition of acetylcholinesterase by C+P- isomer of soman was examined. In the absence of antibody, there was a rapid inhibition of the enzyme by this soman isomer. In the presence of 1.4 or 11.2 micromolar antibody, there was a concentration dependent decrease in the rate of inhibition of acetylcholinesterase by soman, indicating that the antibody can compete effectively. Based on this information, this antibody was used in a passive immunization, where the antibody was administered to mice two hours before challenge by soman. Unfortunately, under these conditions, the antibody was not able to compete effectively with the soman and there was no change in the LD50 of soman in mice treated with antibody versus controls treated with saline. Results of these efforts have recently appeared in *Fundamental and Applied Toxicology*, 4, S156, 1984. It was puzzling that an antibody which apparently had specificity for soman and had an ability to retard in vitro inhibition of the enzyme acetylcholinesterase, offered no in vivo protection.

In an attempt to understand these data, we undertook a series of studies in which we examined the fine specificity of this antibody for its hapten (Fig. 6). This was accomplished by altering, in a systematic fashion, the various functional groups attached to the phosphorus atom of the hapten. Here we see the general formula for soman. There is a P double bond Y group, usually an oxygen; a P-Z group, Z usually being the fluorine leaving group; an OR group, where R is usually pinacolyl alcohol; and, finally, an R', which is usually a methyl group. The results which we are presenting in the rest of the talk were obtained by altering each of these four functional groups, one at a time, in a systematic attempt to determine the relative importance of each of these to the hapten antibody binding phenomenon. First, we will examine the P double bond Y, then alterations in the pinacolyl or R group. We shall then examine the alterations in the Z leaving group and finally, alterations in R'. When examining the data to be shown, bear in mind that an increase in IC50 indicates reduced binding affinity. The term NI means that there was no measurable interaction of the antibody with the hapten. Here we see (Fig. 7) the binding differences when the P double bond O is substituted with a P double bond S; that is, the change from soman to thiosoman. The resultant change is largely an electronic one and when that takes place, there is no binding of the antibody with hapten with either of the two antisoman monoclonal antibodies that were developed, designated BE2 or CCl. The difference in these antibodies lies in the compound chosen in the initial screen. In the case of BE2, the screening compound was dipinacolylmethylphosphonate and in the case of CCl, the screening compound was soman itself.

The structure of the pinacolyl group has been altered in a systematic fashion (Fig. 8) using a homologous series of haptens starting with soman and going to sarin. Compound I shows that the removal of the α -methyl group on soman results in a marked change in the IC50. A hundredfold increase in the case of CCl indicates a hundredfold reduction in avidity of the antibody for the hapten. In the case of compound II, upon removal of the β -methyl group, the antibody no longer binds to this hapten analog. Compound III has 2 β -methyl groups removed and, in compound IV, all three of the β -methyl groups have been removed, thereby producing sarin. In neither case does the hapten bind to the

antibody. We removed both the α -methyl and β -methyl group in Compound V and, again, neither antibody will bind to this hapten. In compound VI, the α -methyl group was restored and a methylene spacer inserted between the former α -carbon and the new γ -carbon. Here we see a tenfold reduction in the affinity of the antibody CCl for this hapten. In the homolog, where the α -methyl group is removed (Compound VII), there is a hundredfold decrease compared to soman in the avidity of the antibody for this hapten. The last alteration in this series was the removal of an α -methyl group and replacement of the β -methyls by ethyl groups. This resulted in only a tenfold reduction binding. This is probably attributable to the fact that the ethyl group can now structurally occupy some of the space above the α -carbon normally filled by the β -methyl group. It is important to note the fact that very small changes, such as the removal of one carbon atom, can cause a dramatic decrease in affinity of an antibody for a hapten; e.g. a change of two orders of magnitude or greater.

A series of compounds, wherein the leaving group Z was altered by replacing fluorine with a variety of alcohol derivatives, is shown in Fig. 9. The substitutions were p-aminophenyl (I), followed by pinacolyl alcohol (II), n-propyl alcohol (III), ethyl alcohol (IV), and methyl alcohol (V). In the case of CCl, substitution for this fluorine had little or no effect on the ability of the antibody to bind to these haptens. It bound to them all equally well and it bound to all of them as well as it bound to soman. This is not surprising, given the fact that this was the end of the molecule closest to the protein backbone and the least important in deciding the antigenic determinant. When we replaced the fluorine by a hydroxyl group (Compound VI - hydrolyzed soman), there was no binding of the antibody to this hapten. This result can be explained by the same rationale used to explain the data on the first slide of this series, where we examined the difference between soman and thiosoman. A large change in the electronic structure on the phosphorus atom causes very large changes in binding. In this instance we have a phosphorus with both a double and single bond oxygen, the hydrogen being ionized. In essence, this is a phosphorus atom with two equivalent oxygens with a full, formal, negative charge. This change in electronic structure, compared to soman itself, is sufficiently great to explain the lack of binding.

In the last series of alterations (Fig. 10), we examined the importance of the R' group. The data here indicate the R' group is not particularly sensitive, as long as it contains some sort of hydrophobic group. For instance, replacement of ethyl for methyl on soman makes no alteration in the affinity of the antibody for the hapten. However, if you compare compounds I and III, where the methyl group has been replaced with hydrogen, we see, in the case of both BE2 and CCl, a marked decrease in the binding of the antibody with this hapten. Compound IV, methyl phosphonic acid, is one of the cleavage products of soman, but it was not bound by the antibody.

Having examined structural features, studies examining changes in the spatial features of the soman molecule were pursued. To do this, we employed the four stereoisomers of soman (Fig. 11). As can be seen, the P-C⁺, P-C⁻ isomers of soman (the more toxic isomers of soman) are bound more strongly by the antibody than are the P⁺ C⁺, P⁺ C⁻ (nontoxic) isomers of soman. Admittedly the change in affinity constant is not large across these four stereoisomers (only one order of magnitude), but the differences in each case are real.

In summary (Fig. 12), we have produced antibodies which have an in vitro activity as determined by their ability to reduce the rate of inhibition of acetylcholinesterase by soman. Unfortunately, these antibodies did not alter the soman LD50 when administered passively to mice. Upon examination of the structural features necessary for binding of the antibody to these haptens, it was found that the antibodies have the following binding specificity: $P=O > \beta-CH_2 > \alpha-CH_2 > R' > Y$, with the exception of when Y is a hydroxyl group. The message from these studies is that one must design an immunogen with great care. One must have present all the important structural features of the hapten so that the resulting antibody will have the desired specificity. As we have seen, very small changes which might be thought to be insignificant under normal conditions, may turn out to have dramatic effects upon the ability of the antibody to recognize a hapten of interest. Cognizant of these facts, we have designed two new haptens which contain the fluorine group itself or a group of the same size, as well as as many of the other structural features of soman that we can incorporate (Fig. 13). As can be seen in the top compound, a methoxy group has been substituted for fluorine. The philosophy here being that methoxy is roughly the same size as a fluorine group. In this case, we have put an amine on one of the terminal methyl groups of the pinacolyl, so that the antibody that is developed will have these specific determinants: a $P=O$, a fluorine, an R' , and finally, a pinacolyl group. The second compound is an immunogen which has fluorine itself present. The drawback to this immunogen, designed by COL Sadoff of WRAIR and synthesized at this Institute by Dr. Clarence Broomfield, is that the α -methyl group is missing.

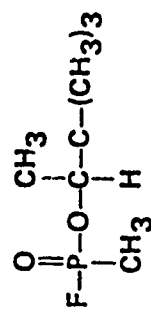
Future goals are summarized in Fig. 14. Both these immunogens have been used in the Milstein technique to produce monoclonal antibodies. We have screened the clones produced and we have found that some clones are capable of cross reacting with soman. Those that test positive will be examined further to determine their IC50 values in much the same way that was done for CCl with soman. These results will be compared with the CCl antibody which will now be a benchmark. The best of these new antibodies will then be tested for their ability to retard acetylcholinesterase inhibition in vitro. Those that show the most promise in chat screen will subsequently be tested in vivo using a passive immunization technique.

Figure 1

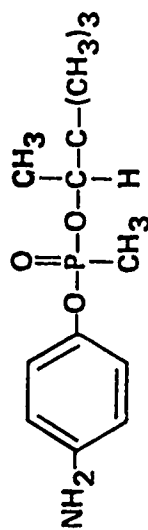
INTRODUCTION

- TWO RECURRING PROBLEMS
 - 1) DIFFICULTY IN IDENTIFYING THE SITE OF ACTION OF ORGANOPHOSPHORUS POISONS.
 - 2) CURRENT THERAPY/PROPHYLAXIS IS NOT VERY EFFECTIVE AGAINST SOMAN DUE TO AGING.
- SOUGHT TO ADDRESS THESE TWO ISSUES THROUGH IMMUNOLOGY
 - 1) SPECIFIC ANTIBODIES MIGHT BE A USEFUL IMMUNOCYTO-CHEMICAL REAGENT.
 - 2) IF IN VITRO COMPETITION COULD BE SHOWN, THEN RE-EXAMINATION OF ANTIBODIES IN AN IN VIVO SITUATION MIGHT BE USEFUL.

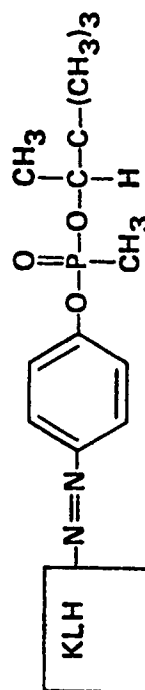
Figure 2



GD



p-AMINOPHENYLPIINACOLYL METHYLPHOSPHONATE

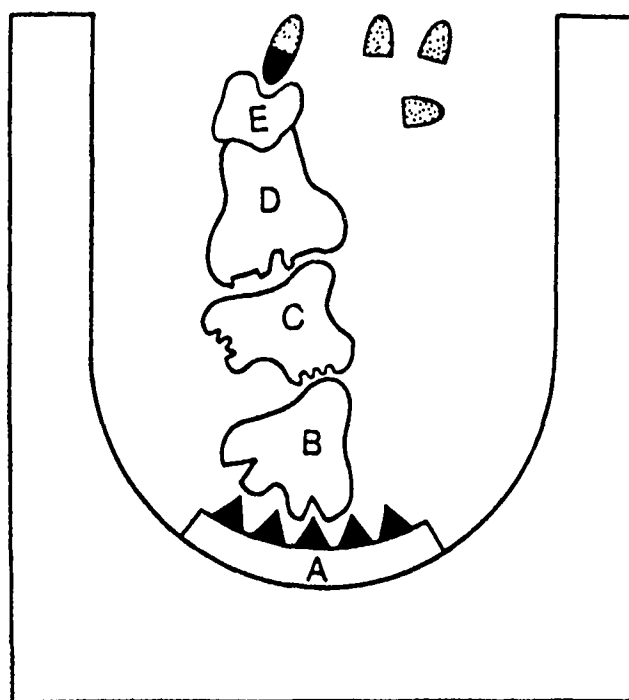


D-IMMUNOGEN

Figure 3

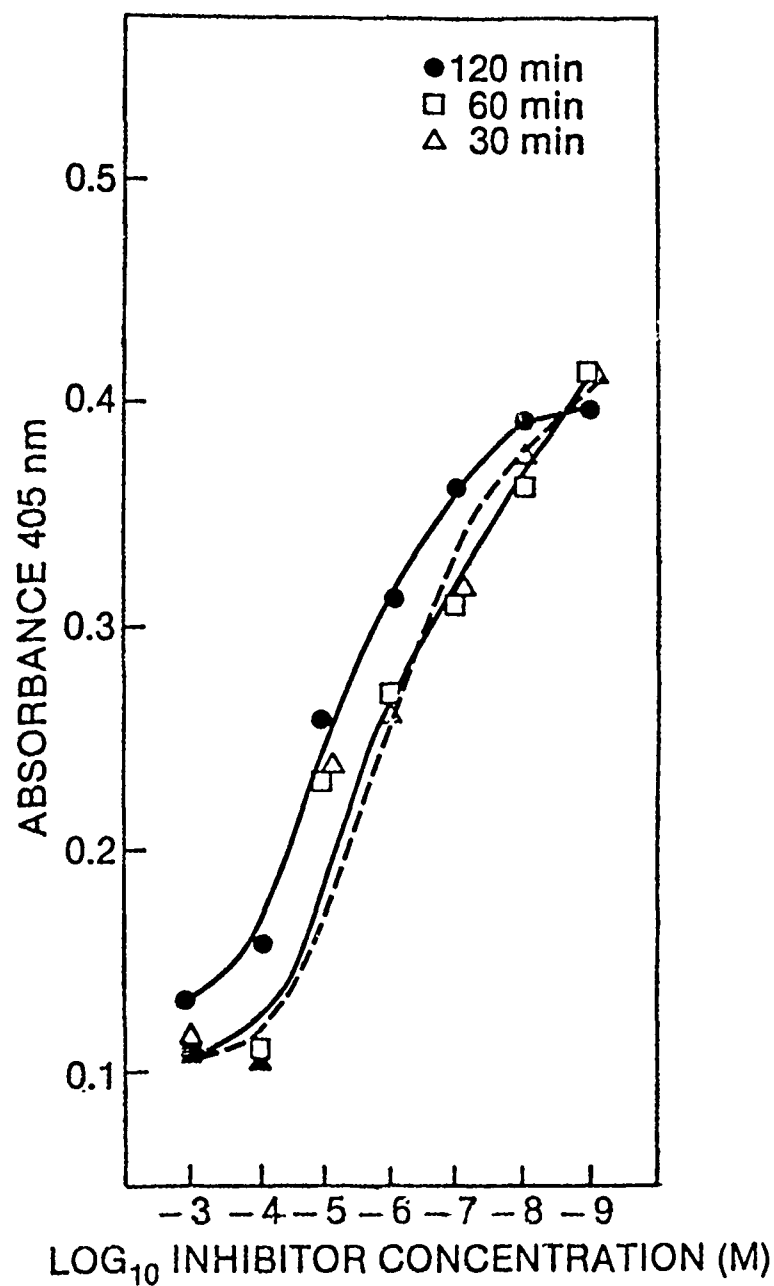
ENZYME IMMUNOASSAY

- A BSA or KLH
- ▲ GD hapten
- B mouse monoclonal anti-GD
- C rabbit anti-mouse kappa
- D goat anti-rabbit IgG
- E alkaline phosphatase
- p-nitrophenyl phosphate
- ▲ p-nitrophenol



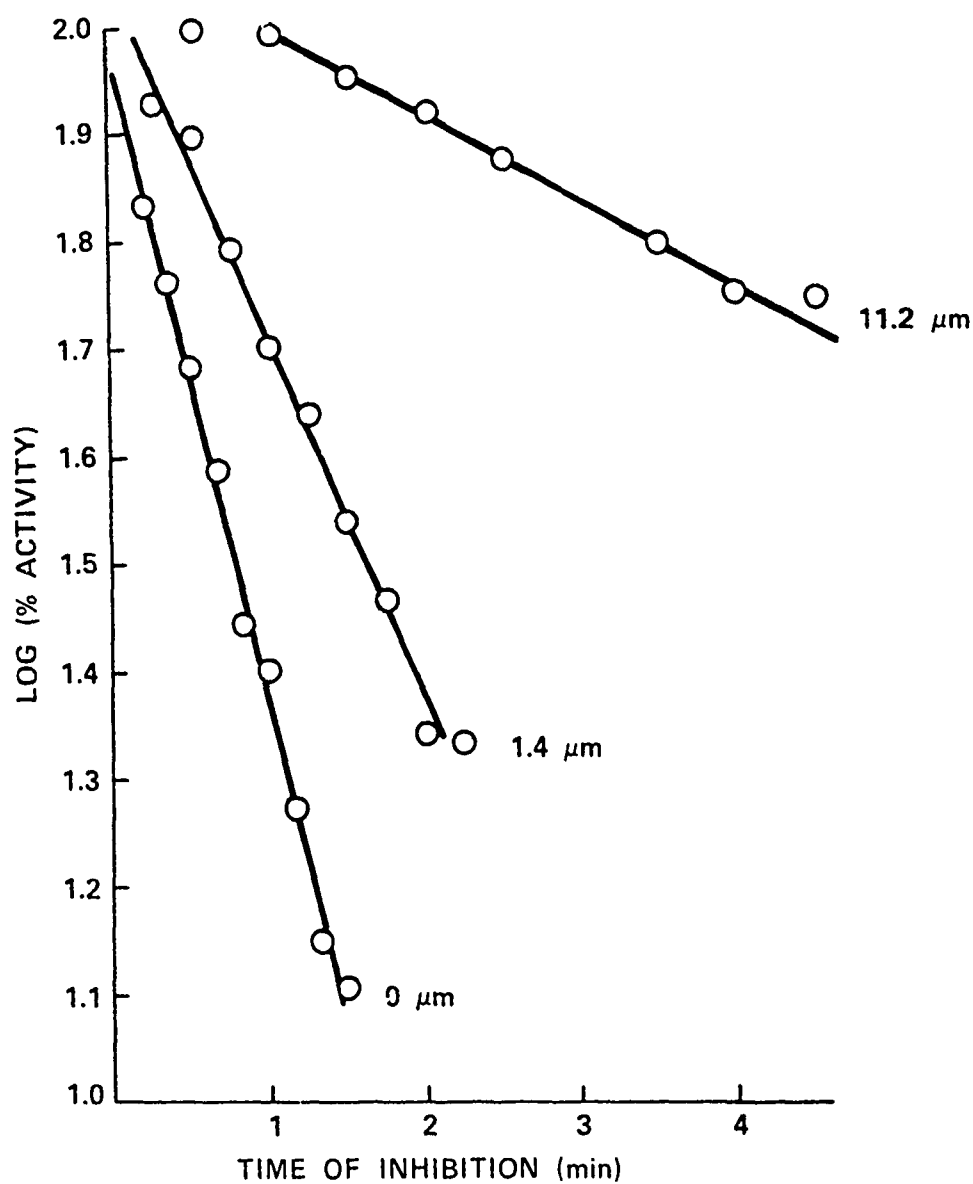
Diagrammatic representation of the components of the enzyme immunoassay system as they might appear after substrate (p-nitrophenyl phosphate) addition.

Figure 4



Determination of the necessity for full equilibration in the CIEIA. It is evident from the curves above that 30, 60 and 120 min incubations yield essentially the same results.

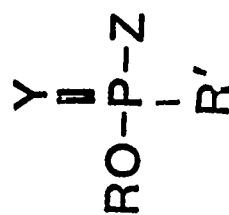
Figure 5



INHIBITION OF ELECTRIC EEL AChE (0.6nM) BY C(+)/P(-) SOMAN (6.1nM) IN PBS, pH 7.4 WITHOUT OR WITH ADDED ANTIBODY (FROM CLONES SELECTED WITH SOMAN) OF FINAL CONCENTRATION OF 1.4 AND 11.2 nM.

Figure 6

EXAMINATION of FINE SPECIFICITY of ANTI-SOMAN ANTIBODIES



GENERAL FORMULA

SHALL ALTER THE FOUR FUNCTIONAL GROUPS, ONE AT A TIME, IN A
SYSTEMATIC FASHION TO DETERMINE THE RELATIVE IMPORTANCE
OF EACH TO THE ANTIBODY-HAPTEN BINDING

- 1) $\text{P}=\text{Y}$
- 2) R
- 3) P-Z
- 4) R'

INCREASE IN IC_{50} INDICATES REDUCED BINDING AFFINITY.

"N.I." MEANS NO MEASURABLE INTERACTION

Figure 7

P=O vs P=S



#	Compound Name	R	Y	R'	Z	IC ₅₀ BE250	(μ M)† CCI
I	SOMAN	$\begin{array}{c} \text{C} \quad \text{C} \\ \quad \\ \text{C}-\text{C}-\text{C}- \\ \quad \\ \text{C} \quad \text{C} \end{array}$	0	Me	F	84.0	6.5
II	THIO-SOMAN	$\begin{array}{c} \text{C} \quad \text{C} \\ \quad \\ \text{C}-\text{C}-\text{C}- \\ \quad \\ \text{C} \quad \text{C} \end{array}$	S	Me	F	NI	NI

Figure 8

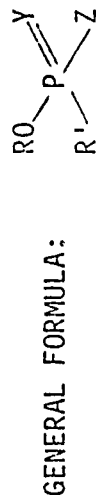
EFFECT OF ALTERATIONS IN PINACOLYL MOIETY



#	Compound Name	R	Y	R'	Z	IC ₅₀ (μ M)†	
						BE250	CC1
I			0	Me	F	790.0	780.0
II			0	Me	F	>1000.0	NI
III			0	Me	F	NI	NI
IV	SARIN		0	Me	F	NI	NI
V			0	Me	F	NI	NI
VI			0	Me	F	43.0	70.0
VII			0	Me	F	600.00	420.0
VIII			0	Me	F	60.0	40.0

Figure 9

EFFECT OF SUBSTITUTION FOR FLUORINE



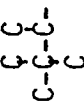
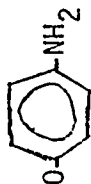
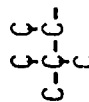
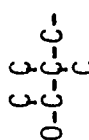
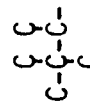
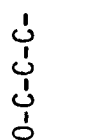
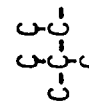

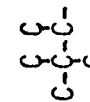

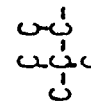
#	Compound Name	R	Y	R'	Z	$\frac{IC_{50}(\mu M)^\dagger}{BE2}$	$\frac{IC_{50}(\mu M)^\dagger}{CC1}$
I			0	Me		4.9	4.5
II			0	Me		3.8	1.8
III			0	Me		6.2	4.4
IV			0	Me		5.6	6.2
V			0	Me		5.5	7.8
VI	"HYDROXY"-SOMAN		0	Me	OH	720.0	NI

Figure 10

EFFECT OF ALTERATIONS IN P-R' GROUP



#	R	Y	R'	Z	BE2	IC ₅₀ (μ M)†	CC1
I	$\begin{array}{c} \text{C} \quad \text{C} \\ \diagdown \quad \diagup \\ \text{C}-\text{C}-\text{C} \\ \diagup \quad \diagdown \\ \text{C} \end{array}$	O	Me	$\begin{array}{c} \text{C} \quad \text{C} \\ \diagdown \quad \diagup \\ \text{O}-\text{C}-\text{C}-\text{C} \\ \diagup \quad \diagdown \\ \text{C} \end{array}$	3.8	1.8	
II	$\begin{array}{c} \text{C} \quad \text{C} \\ \diagdown \quad \diagup \\ \text{C}-\text{C}-\text{C} \\ \diagup \quad \diagdown \\ \text{C} \end{array}$	O	Et	F	18.0	3.5	
III	$\begin{array}{c} \text{C} \quad \text{C} \\ \diagdown \quad \diagup \\ \text{C}-\text{C}-\text{C} \\ \diagup \quad \diagdown \\ \text{C} \end{array}$	O	H	$\begin{array}{c} \text{C} \quad \text{C} \\ \diagdown \quad \diagup \\ \text{O}-\text{C}-\text{C}-\text{C} \\ \diagup \quad \diagdown \\ \text{C} \end{array}$	130.0	100.0	
IV	H	O	Me	OH	NI	NI	NI

Figure 11

SPECIFICITY AND AFFINITY OF THE ANTIBODIES

FOR THE PURE STEREOISOMERS OF SOMAN

Configuration At The Chiral Centers of Soman		Affinity Constant BE2	Affinity Constant (Liter/Mol) CC1
C(+)	P(-)	$2.5 - 5.0 \times 10^3$	$5.9 (\pm .01) \times 10^5$
C(-)	P(-)	$1.0 - 2.5 \times 10^3$	$3.8 (\pm .05) \times 10^5$
C(-)	P(+)	$\underline{\quad} 10^3$	$1.2 (\pm 0.1) \times 10^5$
C(+)	P(+)	$\underline{\quad} 10^3$	$5.2 (\pm 0.8) \times 10^4$

Figure 12

SUMMARY

- 1) ANTIBODIES HAVE IN VITRO ACTIVITY - CAN REDUCE RATE OF INHIBITION OF AChE BY SOMAN
- 2) ANTIBODIES DO NOT ALTER SOMAN LD50 WHEN GIVEN PASSIVELY
- 3) BINDING SPECIFICITY: $P=O$, β -CH₃, α -CH₃, R' EFFECT, P-Y (EXCEPT FOR HYDROXY-SOMAN)

CONCLUSIONS

- 1) MUST DESIGN IMMUNOGEN WITH GREAT CARE, i.e. MUST HAVE PRESENT ALL IMPORTANT STRUCTURAL FEATURES OF THE HAPTEN
- 2) HAVE DESIGNED NEW HAPTENS WHICH HAVE THE F ITSELF OR A GROUP OF THE SAME SIZE AS WELL AS ALL OTHER STRUCTURAL FEATURES

Figure 13

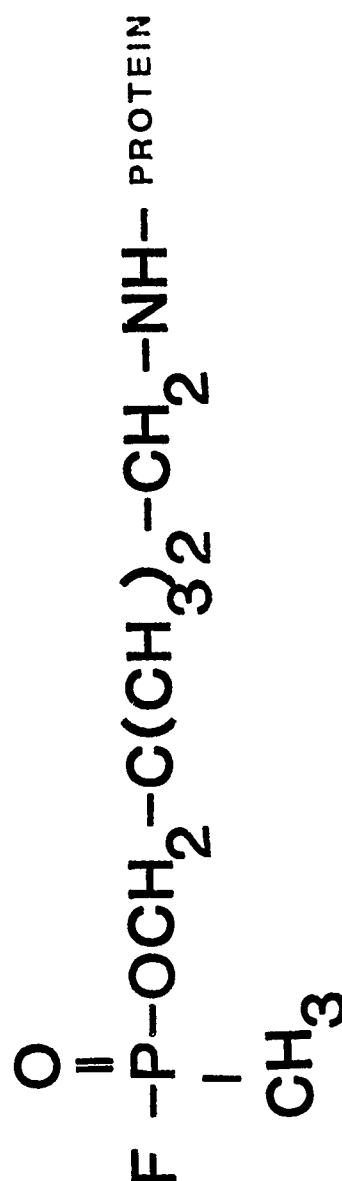
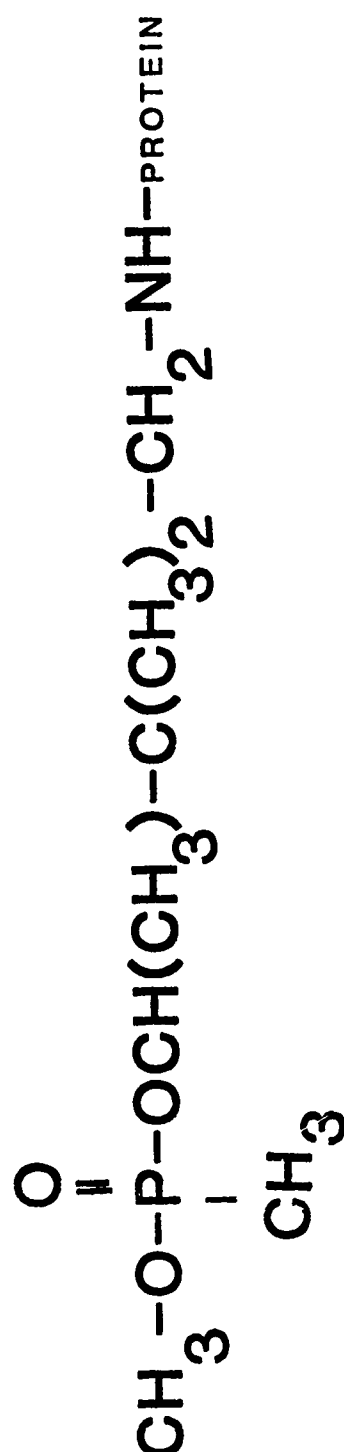


Figure 14

FUTURE

- 1) HAVE SCREENED CLONES DERIVED FROM NEW IMMUNOGENS
- 2) THOSE WHICH WERE POSITIVE WILL BE EXAMINED FURTHER
TO DETERMINE IC50
- 3) THE BEST WILL BE TESTED FOR ABILITY TO RETARD
AChE INHIBITION IN VITRO
- 4) MOST PROMISING WILL BE TESTED IN VIVO
VIA PASSIVE IMMUNIZATION

Design and Synthesis of Peptides Mimicking the Active Site Of A
Serine Esterase With Covalent Binding To Organophosphorus Inhibitors

M. Zouhair Atassi

Marrs McLean Department of Biochemistry, Baylor College of Medicine, Texas
Medical Center, Houston, Texas 77030

ABSTRACT

From the x-ray co-ordinates of bovine trypsin and its complexes with substrate analogues (benzamidine) and with soybean trypsin inhibitor, a peptide (TP) was designed and synthesized by surface-simulation synthesis, a concept previously introduced by this laboratory, to mimic the binding site of trypsin. Also, a control peptide (CTP) was synthesized which contained all the amino acids present in the TP peptide, except that their order was randomized. The radiiodinated TP peptide bound specifically to adsorbents of benzamidine, whereas the control CTP peptide exhibited no binding activity. Conjugates to succinyl lysozyme of the TP peptide, control CTP peptide and other unrelated peptides were examined by a radiometric binding assay for their ability to bind soybean trypsin inhibitor and human α_1 -antitrypsin. Conjugates of the peptides exhibited considerable binding activity to adsorbents of soybean trypsin inhibitor or α_1 -antitrypsin. None of the other peptide conjugates possessed any binding activity. Action of the active-site directed reagents, phenylmethylsulfonyl fluoride and diisopropylfluorophosphate, on free TP and CTP peptides resulted in the modification of a serine residue in the TP peptide while the CTP peptide remained unaltered. The TP peptide, either in the free form or as a conjugate on succinyl lysozyme, had no enzymatic activity on protein substrates or on tosylarginine methyl ester. These findings indicated that the binding activity of an enzyme was well mimicked by the surface-simulation peptide but that reproduction of the catalytic activity was not obtained.

INTRODUCTION

Previously, this laboratory introduced the concept of "surface-simulation" synthesis (Atassi, et al., 1976; Lee and Atassi, 1976) which was subsequently further well developed (Lee and Atassi, 1977a, 1977b; Atassi and Lee 1978a, 1978b; Atassi and Zablocki, 1977, Atassi, 1978, 1979). In this concept, the spatially adjacent residues constituting a protein binding site are linked directly via peptide bonds with appropriate spacing and directionality into a single peptide that does not exist in the protein but mimics a surface region of it. This has proved to be a powerful concept in protein molecular recognition and has provided a new dimension of unlimited versatility for synthetic mimicking of protein binding sites (for review, see Atassi, 1980). In fact, binding sites representing antibody combining sites have been mimicked into single surface-simulation synthetic peptides which bind the antigen and effectively compete with the antibody for the antigen (Atassi and Zablocki, 1977; Twining and Atassi, 1978; Kazim and Atassi, 1980).

The surface-simulation synthesis of the substrate binding site of an enzyme has not been reported. The present work examines the application of this concept to an enzyme binding site. Bovine trypsin is selected here to test



the feasibility of the approach. The substrate binding site of trypsin is mimicked by surface-simulation synthesis into a single peptide comprising the essential contact residues with appropriate spacing. The ability of this peptide to bind substrate analogues and organic and protein inhibitors of trypsin is reported.

MATERIALS AND METHODS

Bovine trypsin was obtained from Worthington Diagnostic Systems Inc. (Freehold, N.J.). The Merrifield resin (0.8 mequiv of Cl/g) and the N^α-t-butyloxycarbonyl amino acid derivatives were from Vega Fox Biochemicals (Tucson, Az). The side chain protecting groups used were; arginine, nitroguanidinium; serine, O-benzylether; tryosine, 2,6-dichlorobenzylether; histidine, im-dinitrophenyl; lysine, ε-chlorocarbobenzoxy; aspartic acid, β-benzylester, while the t-butoxycarbonyl was employed for the protection of all α-amino groups. The purity of all the amino acid derivatives was confirmed by thin layer chromatography. All organic solvents employed for peptide synthesis were of spectroscopic grade and were again dehydrated and further purified by fractional distillation.

Synthesis and purification of the peptides

The peptides were synthesized by the solid phase method according to previously described procedures (Koketsu and Atassi, 1973, 1974), except that in the present work, the t-boc group was removed by treatment with trifluoroacetic acid in CH₂Cl₂ (Gutte and Merrifield, 1971). The peptides were cleaved from the resin by HF at -10° for 30 min (Gutte and Merrifield, 1971). The dinitrophenyl protecting group on the imidazole side chains was removed by thiolation. The peptides were purified by gel filtration on Sephadex G-25 in 30% dimethylformamide, followed by chromatography on Sephadex LH-20 in dimethylformamide and finally by ion-exchange chromatography on CM-Sephadex C-50 (Koketsu and Atassi, 1973, 1974a, 1974b,) in buffers containing 30% dimethylformamide. Peptide purity was checked by peptide mapping (Atassi and Saplin, 1968), high pressure liquid chromatography (HPLC) on an analytical C18 column and amino acid analysis.

Preparation of Sepharose Adsorbents

Coupling of trypsin inhibitor to CNBr-activated (March et al., 1974) Sepharose CL-4B was carried out under the optimum conditions for the preparation of active adsorbents (Twining and Atassi, 1979). Adsorbents of unrelated proteins (bovine serum albumin, sperm-whale Mb and human Hb A) and synthetic peptides [myoglobin 132-153 (Young and Atassi, 1983), human hemoglobin 1-15 (Kazim and Atassi, 1980) and CTP peptide synthesized here] were used as controls to determine non-specific background binding. The adsorbents contained 1-1.5 mg of protein per ml of packed volume.

Preparation of adsorbents of para- and meta-aminobenzamidine

An aliquot (1 ml) of p-ABA or m-ABA (10 mg) in 0.2 M Na₂HCO₃, pH 9.5 was coupled overnight at 4°C to CNBr-activated Sepharose CL-4B. After coupling, the sepharose was washed to remove free uncoupled ligand (checked by reading Absorbance of the washing at 280 nm). The adsorbent was then masked by incubation at 4°C (with gentle rotation) with 1M 2-aminoethanol (1 ml per ml of packed volume). This was followed by the following series of washes (three times each): 0.1 M sodium acetate in 0.5 M NaCl, pH 10; 2M urea in 0.5 M NaCl; 0.1 M Na₂HCO₃ in 0.5 M NaCl, pH 9.0; and finally PBS. Sepharose

adsorbents were stored at 4°C in an equal volume of PBS containing merthiolate.

Coupling of Peptides to Protein Carrier

Because of the hydrophobic nature of the trypsin cavity the surface-simulation peptides were found to possess very low solubility in aqueous solvents. Therefore, in order to conveniently monitor their binding to trypsin inhibitors and substrates, we resorted to coupling them to very soluble carriers. For this purpose, succinylated lysozyme was mostly used. Synthetic peptides were coupled to succinyl lysozyme after activation of the carrier carboxyl groups by conversion to the p-nitrophenylester groups (Atassi et al., 1981). The reaction is performed in DMF and has therefore proved to be convenient for the TP and CTP peptides because they are soluble in DMF. The extent of coupling was determined by amino acid analysis of acid hydrolysates of the peptide-protein conjugates.

Radiolabelling of Proteins and Peptides

Trypsin inhibitor, antibodies, protein A, peptides or peptide-protein conjugates (e.g. TP-Su lysozyme) were radiolabelled with ^{125}I (Amersham Corp., Arlington Heights, IL) using the chloramine-T method (Hunter and Greenwood, 1962). Unbound ^{125}I was separated from the radiolabelled sample by gel filtration on Sephadex G-15 (Pharmacia Fine Chemicals, Piscataway, NJ). Protein-associated ^{125}I was assayed by precipitation with 10% trichloroacetic acid (v/v).

Adsorbent Binding Studies

Quantitative adsorbent binding studies were performed with fixed amounts of adsorbents (50 μl) and increasing amounts of soluble ^{125}I -labelled peptide-protein conjugate in glass tubes by the procedures described previously (Twining and Atassi, 1979). The solvent for the titration studies was 0.1% BSA or sperm-whale myoglobin in phosphate-buffered saline. Adsorbents of unrelated proteins and peptides and of the carrier protein (Su-lysozyme, when peptide-protein conjugates were titrated) were used as controls for background binding.

Peptide binding to soybean trypsin inhibitor and α_1 -antitrypsin by plate assay

We have developed a convenient assay for rapid screening of the synthetic peptides that are designed to mimic the binding site of trypsin. The assay is a variation of a solid phase RIA previously described (Sakata and Atassi, 1981; Schmitz et al., 1982). Briefly the assay is carried out as follows: Polyvinyl RIA plates (Costar, Cambridge, MD) are incubated with trypsin inhibitor (5 μg in 50 μl of PBS) for 1 hr at 37°C. Following washing with PBS (6 times) the plates are incubated with 2% BSA (100 μl per well) for 1 hr at 37°C. The plates are then washed (6 times) and incubated with a peptide-Sulysozyme conjugate (5 μg) in 0.1% BSA in PBS (50 μl) for 3 hr at 37°C. After washing (6 times) mouse anti-lysozyme (1:1000 dilution in 0.1% BSA in PBS) is added (50 μl) and incubated for 2 hr at 37°C. The plates are then washed (6 times) with PBS and incubated with rabbit anti mouse IgG (50 μl of 1/1000 dilution in 0.1% BSA in PBS) for 2 hr at 37°C. Finally, the plates are washed (6 times), incubated with ^{125}I -labelled protein A (2×10^5 cpm in 50 μl 0.1% BSA in PBS) for 2 hr at room temperature, washed (6 times), dried, cut into individual wells and counted on a γ -counter. Plates coated with BSA and with Sulysozyme (instead of trypsin inhibitor) are used as controls. Also Sulysozyme conjugates of unrelated peptides were used as additional controls.

Reaction of the TP peptides with diisopropylfluorophosphate

For reaction with DFP, the TP peptides were used in their free form because it is easier to determine, in amino acid analysis, the change in the amino acid composition when the free peptides are employed. Because the TP peptides are not soluble in aqueous solvents, DMF (at least 15%) was required in the reaction solvent.

For reaction with DFP, the TP peptide (0.5 mg) was mixed with 10 molar excess of DFP (0.5 mg) in 15% DMF-0.1M phosphate buffer, pH 8.0. The total reaction volume was 250 μ l. The solution was stirred magnetically for 3 hr at room temperature. The peptide was then precipitated with cold (0°C) ether (3.0 ml), centrifuged, washed with ether five times on the centrifuge and subjected to hydrolysis and amino acid analysis. Reaction with PMSF was carried out in an identical manner.

Analytical Methods

Completed synthetic peptides, partial synthetic products at selected stages during synthesis, conjugates to carriers, products of reaction with DFP of free peptides were all checked by amino acid analysis. For amino acid analysis, protein or peptide samples (0.05 mg) were dissolved in 0.5 ml each of constant boiling HCl (triple distilled), flushed with nitrogen, evacuated, sealed, heated at 110°C for 22, 48 or 72 hr. The hydrolysates were then freed of excess HCl on a rotary evaporator. Amino acid analyses were performed on a Beckman System 6300 high performance analyzer. The values of serine were obtained by extrapolation to zero hydrolysis time. Careful determination of the serine value is critical because it is an essential active site residue and is the site of covalent attachment of fluorophosphate compounds (e.g. see reaction with DFP). Tryptophan was determined by amino acid analysis of hydrolysates with p-toluenesulfonic acid containing 0.2% 3-(2-aminoethyl)-indole (Liu and Chang, 1971). The hydrolysates were assayed on a Beckman Model 6300 amino acid analyzer. Purity of synthetic peptides was checked by high voltage (3000 volt, 1 hr) paper electrophoresis in pyridine-acetate at pH 3.65, chromatography on an analytical size HPLC C₁₈ columns in acetonitrile-0.5% H₃PO₄ (pH 2.3) gradient, and amino acid analysis.

RESULTS

Purity of the Synthetic Peptides

After purification, the peptides were homogeneous by high voltage electrophoresis and analytical HPLC and had amino acid compositions that were in full agreement with those expected from their respective covalent structures (see Table 3).

Binding of the peptides to trypsin inhibitor and to benzamidine adsorbents

Benzamidine has been employed extensively in binding studies as a substrate analogue of trypsin. The binding of free peptides to benzamidine was studied on adsorbents of benzamidine. However, since benzamidine has no reactive functional group by which to attach it to Sepharose, we used two derivatives for that purpose i.e. p-aminobenzamidine and m-aminobenzamidine. Both the para- and the meta- aminobenzamidine derivatives were used in order to examine whether the point of attachment to the Sepharose anchor relative to the amidine group influences the binding of the peptides. Because of the insolubility of the peptides, they were labelled with ¹²⁵I and titrated with adsorbents using as solvents 20% DMF in 1.6% glycine-PBS. Previously, it was determined

using different protein-free solvents and carrier that this was the most adequate solvent. Results of such a titration are summarized in Table 1.

It is evident from these results that binding of labelled TP peptide to the substrate and to trypsin inhibitor adsorbents did occur and that it was specific since labelled CTP peptide exhibited no binding to these adsorbents. However, the low amount of label bound, relative to the amount of label added, indicated that the conditions of the binding needed to be improved. The difficulty most likely stemmed from the insolubility of these peptides and that the solvent conditions of the experiment were unsatisfactory for binding. It was apparent that a different experimental strategy had to be found and we resorted to coupling the peptides to a soluble protein carrier.

Binding of peptide-Succinyl lysozyme conjugates to trypsin inhibitor

For a soluble carrier, hen lysozyme was selected because of its convenient size and high solubility. The solubility was further improved by extensive succinylation of the protein (Su lysozyme) prior to employing it as a carrier. Obviously carriers of other proteins or amino acid polymers could be used but we have not yet employed them in this work. The peptide-Su lysozyme conjugates were completely soluble in PBS.

For convenience, we developed a rapid plate binding assay (see Experimental) to monitor the binding of the peptides to trypsin inhibitor. In this assay, trypsin inhibitor is bound to the wells. This is followed with the peptide-Su lysozyme conjugate, then with mouse anti-lysozyme (1:1000, v/v), then with ^{125}I -labelled protein A. The results are summarized in Table 2. It can be seen in Table 2 that the TP peptide-conjugate exhibited considerable binding to trypsin inhibitors. The specificity of the binding is indicated from the finding that the control CTP-peptide conjugate or conjugates of other unrelated peptides to Su lysozyme, or Su lysozyme alone, exhibited no binding activity.

Table 1. Binding of ^{125}I -peptides to adsorbents of benzamidine and of soybean trypsin inhibitor

^{125}I -peptide bound when the following amounts were added^a

Adsorbent	Peptide:	120x10 ³		200x10 ³		300x10 ³		500x10 ³	
		TP	CTP	TP	CTP	TP	CTP	TP	CTP
Soybean trypsin inhibitor		1,060	0	1,650	0	2,950	710	7,830	0
p-Aminobenzamidine		1,500	0	1,580	0	3,650	0	7,600	0
m-Aminobenzamidine		1,310	0	1,770	0	2,310	0	5,440	0

⁺Results represent the average of triplicate analyses which varied + 1.5% or less and they have been corrected for non-specific binding (0.35-0.38% of total label) of the labelled peptides to uncoupled Sepharose.

Table 2. Binding of peptide-Su lysozyme conjugates to soybean trypsin inhibitor and human α_1 -antitrypsin.

Protein or conjugate added	Protein coated to well:	Amount of anti-lysozyme bound (cpm) ^a	
		Soybean trypsin inhibitor	Human α_1 -antitrypsin
TP-Su lysozyme		19,110	18,540
CPT-Su lysozyme		410	400
(Nonsense peptide)- Su lysozyme ^b		460	420
Su lysozyme ^b		430	410

^aValues represent the average of triplicate analyses which varied + 1.3% or less. These values have not been corrected for the non-specific binding of the negative control.

^bThe conjugate of nonsense peptide to Su lysozyme or Su lysozyme itself do not bind to trypsin inhibitor, therefore they serve as negative controls for the binding of peptide-Su lysozyme conjugates. For positive control, Su lysozyme was bound directly to the well (instead of trypsin inhibitor) and was followed (after appropriate washing) by 0.2% BSA (instead of protein-peptide conjugate). The amount of anti-lysozyme antibodies bound to Su lysozyme was 19,760 cpm. This served as an appropriate positive control for the antisera and the reagents and also gave an estimate of the maximum amount of label expected to be bound in the assay.

Table 3. Amino acid composition of TP and CTP peptides and the products of their binding with phenylmethylsulfonyl fluoride (PMSF) or diisopropylfluorophosphate (DFP).

Amino acid composition (residues/mole) ^a								
Amino Acid	TP Peptide				CTP Peptide			
	Expected	Found	Product with PMSF	Product with DFP	Expected	Found	Product with PMSF	Product with DFP
Asp	3	3.21	2.99	2.90	3	3.13	3.04	3.02
Ser ^b	3	2.96	1.89	1.73	3	3.16	3.00	3.01
Glu	1	0.88	0.78	0.82	1	0.76	0.98	1.00
Gly	10	10.2	10.3	9.62	10	9.47	10.30	9.90
Ala	2	1.95	3.11	3.02	2	1.85	2.05	1.98
Val	1	1.02	1.10	1.16	1	0.90	1.14	1.15
Leu	1	0.99	0.98	1.11	1	1.36	1.07	1.38
Tyr	1	1.18	1.25	1.02	1	1.33	0.84	0.97
Phe	1	1.35	1.16	0.94	1	0.86	1.11	0.99
Trp	1	0.90	nd	nd	1	1.00	nd	nd
His	2	2.00	2.00	1.98	2	1.97	1.95	2.01

Results represent the average of triplicate analyses of acid hydrolysates at 22h and 48hr. Tryptophan values were derived from duplicate hydrolyses with p-toluenesulfonic acid containing 0.2% aminoethylindole. Values of serine have been obtained by extrapolation to zero hydrolysis time.

^bNote that the serine content in the PMSF and the DFP products decreased by one residue, implicating a serine as the site of attachment to these compounds. The hydrolysis product of the inhibitor-serine adducts co-elutes with alanine, hence the alanine value is increased by one residue.

Binding of phenylmethylsulfonyl fluoride and diisopropylfluorophosphate to TP and CTP peptides

To determine whether the TP peptide will mimic the binding activity of trypsin to its inhibitors, it was allowed to react with PMSF and DFP. The reactions of CTP with both compounds were done concurrently as controls. Since the peptides are insoluble in aqueous solvents, binding studies were done (3 hrs, room temperature) using as a solvent 15% DMF in 0.1 M phosphate buffer, pH 8.0 (see Experimental Section). Following reaction, the peptides were isolated from the mixture and subjected to acid hydrolysis and amino acid analysis.

The results showed that binding of PMSF and DFP to TP peptide afforded a stable conjugate in which a covalent bond was formed between the inhibitor and a serine residue on the TP peptide (Table 3). The specificity of the binding (and the ensuing reaction) was indicated from the finding that the control CTP peptide suffered no covalent alterations under the same conditions (Table 3.) We have not determined which of the three serine residues in the TP peptide is the point of attachment to the inhibitor, but it is not unreasonable to suggest that this may be the residue corresponding to Ser-195 (i.e. residue 7 in the peptide). However, this requires verification. But regardless of which serine residue is involved in the attachment to the inhibitor, the fact remains that the TP peptide bound irreversibly to the inhibitor forming in the process a stable covalent bond.

Enzymic activity of the TP peptide

The finding that the TP peptide exhibited specific binding activity with α_1 -antitrypsin, soybean trypsin inhibitor, substrate analogues, and the serine esterases irreversible inhibitors PMSF and DFP posed the intriguing question whether the TP peptide possessed enzymatic activity. The TP peptide was incubated at pH 8.5 and 37°C with protein substrates (globin of human hemoglobin, apomyoglobin) for two days. Examination of the mixture by peptide mapping revealed that no free fragments were generated from the protein. However, because of the low solubility of the peptide in aqueous solvents, the reaction by necessity was a heterogeneous reaction (the protein substrate was in solution but the peptide was in fine suspension) and it was therefore re-examined with soluble TP peptide-Su lysozyme conjugate. The TP peptide conjugate exhibited no enzymatic activity with protein substrates.

Also, the soluble TP conjugate had no hydrolytic activity (pH 8.1, room temperature) on N^{α} -p-tosyl-L-arginine methylester, a substrate commonly used to monitor trypsin enzymatic activity. Thus, it was evident that the TP peptide, generated by surface-simulation, expressed the binding activity of trypsin with substrates and inhibitors but not its catalytic activity.

DISCUSSION

The three-dimensional structure of bovine trypsin, DIP-trypsin and complexes with trypsin inhibitor and benzamidine substrate analogues are known in detail (Stround et al., 1974; Chambers and Stround, 1977; Huber and Bode, 1978). It is, therefore, possible to design surface-simulation peptides that will mimic the binding site of a serine esterase. The studies described in this report were aimed at mimicking the substrate binding site of bovine trypsin into a surface simulation peptide that expresses the binding activity of the enzyme molecule with substrates and inhibitors. Trypsin was chosen as the model for these studies because its x-ray structure is known in fine detail. The struc-

Surface-simulation synthesis of the trypsin binding site

A	B	C
Contact residues and distances	Surface-simulation synthetic peptides (TP)	Control synthetic peptide (CTP)
Asp-189	Asp (N)	Trp (N)
Ser-190	Ser	His
4.9 Å	Gly	Gly
Gln-192	Gln	Asp
Gly-193	Gly	Gly
Asp-194	Asp	Asp
Ser-195	Ser	Val
8.5 Å	Gly	Ala
Val-213	Gly	Gly
Ser-214	Val	Gln
Trp-215	Ser	Phe
8.5 Å	Trp	Ser
Leu-99	Gly	Gly
5.5 Å	Gly	Gly
Asp-102	Leu	Asp
5.3 Å	Gly	His
Ala-55	Asp	Gly
Ala-56	Gly	Ser
His-57	Ala	Gly
5.0 Å	His	Gly
Cys-42	Gly	Ala
Phe-41	Gly	Gly
His-40	Phe	Leu
Tyr-39	His	Gly
	Tyr (C)	Tyr (C)

Figure 1. Design of the surface-simulation peptide mimicking the substrate binding site of trypsin. (A) This column identifies the contact residues in the binding cavity of the enzyme and the distances (from C^α-to-C^α, in Å) separating appropriate residues. (B) The surface-simulation synthetic peptide (TP) designed to mimic the binding site. (C) A control peptide (CTP) which has all the essential residues of the binding site except that they are randomized. The peptides are written with the N-terminus on the top and the C-terminus on the bottom.

ture of diisopropylfluorophosphate-inhibited trypsin, initially determined by Stroud et al. (1971, 1974), was subsequently refined to 1.5 Å resolution (Chambers and Stroud, 1977). Also, the binding of trypsin to soybean trypsin inhibitor afforded the making of a convenient assay by which the surface-simulation peptides could be screened for binding activity.

The substrate binding site of trypsin in complex with substrate analogues (benzamidine) and with trypsin inhibitor is known in great detail at 1.9 to 1.5 Å (Huber and Bode, 1978; Chambers and Stroud, 1977; Bode and Schwager, 1975; Huber et al., 1974, 1975). The following summarizes the amino acids that have been identified as the contact residues of the trypsin binding site. Try-39 hydrogen bonds with trypsin inhibitor. His-40 is buried in the trypsin-inhibitor complex and participates in polar interaction with arginine 17 of trypsin inhibitor. The residues Phe-41, Ala-55, Ala-56, His-57, Tyr-94 and Leu-99 are all buried in the trypsin inhibitor complex. Phe-41 participates in hydrogen bonding with trypsin inhibitor while Asp-189 participates in interaction with benzamidine and with ϵ -amino or guanidino groups of lysine or arginine in the substrate. Ser-190 is buried in the trypsin-inhibitor complex and participates in the binding to benzamidine. Cys-191 also resides in the binding pocket to benzamidine. The residues Gln-192, Gly-193, Ser-195, Ser-214, Trp-215 and Gly-216 all form hydrogen bonds with trypsin inhibitor and are buried in the inhibitor-trypsin complex. Also, Trp-215 forms the hydrophobic part of the benzamidine binding site. Finally, His-57, Asp-102 and Ser-195 are important residues in the catalytic center of the enzyme. The distances (C^{α} -to- C^{α}) separating the residues of the trypsin binding site are given in Figure 1.

From the x-ray coordinates and taking into account the participation of the residues listed above in the function of the enzyme, a peptide (TP) was designed by surface simulation synthesis to mimic the binding site of trypsin. It should be emphasized that this peptide does not exist in trypsin but rather mimicks the topographic arrangement of the residues in its substrate-binding cavity. The elements of the design which is based on spatial and distance considerations, are shown in Figure 1. A control peptide was also prepared which incorporated all the contact and spacing residues but in random fashion (CTP). The control peptide was crucial in order to confirm, should binding activity be found in the TP peptide, that such binding is indeed specific and not caused by some unusual charge or hydrophobic effects.

The finding that the radiolabelled TP peptide was able to bind to benzamidine and trypsin inhibitor adsorbents, whereas the control CTP peptide exhibited no binding activity, was encouraging and suggested that the peptides must have mimicked the architecture of the site. The relatively low amount of label bound, which was of concern, may have been due to the fact that the binding studies were carried out in the presence of 20% dimethylformamide because of the insolubility of both peptides in purely aqueous solvents. The presence of such an organic solvent would be expected to interfere in the binding of the peptide which involves predominantly hydrophobic interactions on the peptide.

To avoid the aforementioned complications stemming from peptide insolubility, it was decided to couple the peptide to a soluble carrier. We have used here fully succinylated lysozyme as a carrier, because of its high solubility, but clearly any soluble carrier should serve equally as well. The coupling procedure (Atassi et al., 1981) which involves activation of the carboxyl side chains on the carrier by conversion to their p-nitrophenylester groups, avoids

carrier-carrier cross-linking (due to prior succinylation of all the amino acid groups on the protein) and peptide polymerization side reactions since the activated carboxyl groups reside only on the carrier and the reactive nucleophile is the α -amino group of the peptide. Having obtained soluble peptide conjugates, we investigated their abilities to bind to trypsin inhibitor. The binding of the TP peptide conjugates both to soybean trypsin inhibitor and to α_1 -antitrypsin and the absence of any binding activity in the CTP peptide conjugates confirmed the correction of the peptide design.

We have also investigated the action of other inhibitors known to react at the substrate binding site. The action of PMSF and DFP on acetylcholinesterase, chymotrypsin, trypsin and other serine proteases has been well studied (e.g. Fahrney and Gold, 1967; Turini et al., 1969; Singer, 1967; Morgan et al., 1972). In each case, the binding between the enzyme and inhibitor results in the formation of a covalent bond via the active serine of the enzyme. It was gratifying, and at the same time quite surprising, to find that the TP peptide reacted with both PMSF and DFP, the reaction in each case taking place at a serine residue in the peptide. Again the lack of reaction with the CTP peptide confirmed the specificity of reaction with the TP peptide. Although it is tempting to speculate that the reaction may have occurred with the serine residues at the 7th position in the peptide (i.e. the residue representing Ser-195 in the mimicked structure), we have not yet determined which of the three serine residues on the peptide participate in the reaction with PMSF or DFP.

The peptides exist in solution in a conformational equilibrium, the time average of which will be random, and there will exist at any given time conformational states that are energetically favored at appropriate energy minima and whose mode of folding approximate that required for binding (Atassi and Saplin, 1968). Those species are able to bind with the target molecule and are thus removed from the equilibrium which should then shift in their favor (Atassi and Saplin, 1968). It should also be noted that since peptides in the conjugates are attached only via their α -amino end, they would be able to fulfill the requirement of conformational flexibility for proper wrapping around the small ligands or assuming folding that is favorable for binding with protein inhibitors. Appropriate peptide conformation can also be induced by the binding molecule (Atassi, 1975).

The absence of enzymatic activity in the TP peptide was disappointing but was not entirely unexpected. The exact mechanisms of enzymatic catalysis are not really fully understood in spite of the voluminous literature on the subject. Catalysis is also subject to very stringent conformational and distance requirements and, since the distances and conformational relationships of the residues in a surface-simulation synthetic peptide do not precisely duplicate the corresponding parameters in the intact molecule, it is not surprising that only binding but not catalysis are duplicated. Whether catalysis can be obtained by improvement in design and employment of other synthetic strategies is yet to be determined.

The foregoing background information affords a strategy of approach for an effective drug design against organophosphate poisoning. These organophosphorus compounds act via phosphorylation (forming a covalent bond with a serine residue) of the esteratic site of acetylcholinesterase (Koelle, 1981). The inactivation of the enzyme causes accumulation of endogenous acetylcholine at the receptors of the postjunctional sites. The outcome of this is

lethal due to disturbance of the respiratory system. These nerve gases have an estimated lethal dose ranging from 0.4 mg (for agent VX) and 1 mg (for agent GB) (Meselson and Robinson, 1980). Protective equipment, although quite effective, is cumbersome, and we estimate that its large scale application to major population centers is perhaps not feasible in a surprise attack. The structural information presently available on acetylcholinesterase is insufficient to attempt the design of peptides that will mimic the binding site of the enzyme. However, other serine esterases, whose three-dimensional structures are available (e.g. trypsin, chymotrysin), are known to bind to organophosphate compounds. For example, diisopropylfluorophosphate (DFP) was shown to inhibit a number of esterases due to alkyl-phosphorylation of a unique serine residue (Schaffer et al., 1954). Thus, the success reported here in synthetically mimicking the active site of trypsin should afford an important peptide agent against organophosphate poisoning. Undoubtedly, the peptide design reported here may have to be refined in order to improve its affinity to organophosphate agents so that reaction could take place extremely rapidly. The work towards this goal is in progress.

References

- Atassi, M.Z. (1978) Immunochemistry **15**: 909.
- Atassi, M.Z. (1979) Crit. Revs. Biochem. **6**:371.
- Atassi, M.Z. (1980) Mol. Cell Biochem. **32**: 21.
- Atassi, M.Z. (1983), to be published
- Atassi, M.Z. and Koketsu, J. (1975) Immunochemistry **12**:741.
- Atassi, M.Z. and Lee, C. -L. (1978a) Biochem. J. **171**:419.
- Atassi, M.Z. and Lee, C. -L. (1978b) Biochem. J. **171**:429.
- Atassi, M.Z. and Zablocki, W. (1977) J. Biol. Chem. **251**:1653.
- Atassi, M.Z., Lee, C. -L. and Pai, R. -C. (1976) Biochim. Biophys. Acta **427**:745.
- Atassi, M.Z., Kazim, A.L. and Sakata, S. (1981) Biochim. Biophys. Acta **670**:300.
- Bode, W. and Schwager, P. (1975) J. Mol. Biol. **98**:693.
- Chambers, J.L. and Stroud, R.M. (1977) Acta Cryst. **B33**:1824.
- Fahrney, D.E. and Gold, A.M. (1963) J. Am. Chem. Soc. **85**:997.
- Feiser, L.F. (1965) Experiments in Organic Chemistry, p. 284, D.C. Heath, Boston.
- Gutte, B. and Merrifield, R.B. (1971) J. Biol. Chem. **246**:1922.
- Hawk, P.B., Oser, B.L. and Summerson, W.H. (1954) Practical Physiological Chemistry, p. 955, 13th Edition, Blakiston.
- Huber, R. and Bode, W. (1978) Acc. Chem. Res. **11**:114.
- Huber, R., Dukla, D., Bode, W., Schwager, P., Bartels, K., Deisenhofer, J. and Steigmann, W. (1974) J. Mol. Biol. **89**:73.
- Huber, R., Bode, W., Kukla, K., Kohl, U. and Ryan, C.A. (1975) Biophys. Struct. Mech. **1**:189.
- Hunter, W.M. and Greenwood, F.C. (1962) Nature, London **194**:495.
- Kazim, A.L. and Atassi, M.Z. (1980) Biochem. J. **187**:661.
- Koelle, G.B. (1981) Fundamental and Appl. Toxicol. **1**:129.
- Koketsu, J. and Atassi, M.Z. (1973) Biochim. Biophys. Acta **328**:289.
- Koketsu, J. and Atassi, M.Z. (1974a) Immunochemistry **11**:1.

- Koketsu, J. and Atassi, M.Z. (1974b) Biochim. Biophys. Acta 342:21.
- Lee, C. -L. and Atassi, M.Z. (1976) Biochem. J. 159:89.
- Lee, C. -L. and Atassi, M.Z. (1977a) Biochim. Biophys. Acta 495:354.
- Lee, C. -L. and Atassi, M.Z. (1977b) Biochem. J. 167:571.
- Liu, T. -Y. and Chang, Y.H. (1971) J. Biol. Chem. 246:2842.
- March, S.C., Parikh, I. and Cuatrecasas, F. (1974) Anal. Biochem. 60:149.
- Meselson, M. and Robinson, J.P. (1980) Scientific Amer. 242:38.
- Morgan, P.H., Robinson, N.C., Walsh, K.A. and Neurath, H. (1972) Proc. Natl. Acad. Sci. U.S.A. 69:3312.
- Sakata, S. and Atassi, M.Z. (1981) Mol. Immunol. 18:961.
- Schaffer, N.K., May, S.C. and Summerson, W.H. (1954) J. Biol. Chem. 206:201.
- Schmitz, H.E., Atassi, H. and Atassi, M.Z. (1982) Mol. Immunol. 19:1699.
- Singer, S.J. (1967) Adv. Prot. Chem. 22:1.
- Stewart, J.M. and Young, J.D. (1969) "Solid Phase Peptide Synthesis", W.H. Freeman and Company, San Francisco.
- Stroud, R.M., Kay, L.M. and Dickerson, R.E. (1971) Cold Spring Harbor Symp. Quant. Biol. 36:125.
- Stroud, R.M., Kay, L.M. and Dickerson, R.E. (1974) J. Mol. Biol. 83:185.
- Turini, P., Kurooka, S., Steer, M., Corbascio, A.N. and Singer, T.P. (1969). J. Pharmacol. Exp. Therap. 167:98.
- Twining, S.S. and Atassi, M.Z. (1978) J. Biol. Chem. 253:5259.
- Twining, S.S. and Atassi, M.Z. (1979) J. Immunol. Methods 30:139.
- Westall, F.C., Scotcher, J. and Robinson, A.B. (1972) J. Org. Chem. 37:3363.

Molecular and Structural Bases for the
Polymorphic Forms of Acetylcholinesterase

Palmer Taylor¹, Shelley Camp¹, Kathy MacPhee¹, Mark Schumacher¹,
Gabi Amitai¹, Susan S. Taylor¹, Mary Kay Gentry² and B.P. Doctor²

¹ Division of Pharmacology, M-013 H
University of California, San Diego
La Jolla, California 92093

² Division of Biochemistry
Walter Reed Army Institute of Research
Washington, D.C. 20012

Abstract

Both the elongated species of acetylcholinesterase which is confined to the basal lamina and the hydrophobic, dimeric species which associates with plasma membranes are present in sufficient abundance in the Torpedo electric organ to obtain comparative information on the primary structures of the catalytic subunits. Although high pressure liquid chromatography of the corresponding tryptic peptides reveals substantial homology between the two forms, at least two of the non-oligosaccharide-containing tryptic peptides appear unique to each enzyme. Chromatographic separation of the tryptic and cyanogen bromide peptides has allowed us to identify the active site peptide, the oligosaccharide-containing peptides, the N-terminal residues and surface peptides of the peripheral anionic site which react with the photoaffinity label, azidopropidium. Monoclonal antibodies have been prepared to both forms of the enzyme and while the majority show nearly equivalent reactivity with both forms of the enzyme, one shows a 100-fold selectivity for the catalytic subunit of the hydrophobic, dimeric species. Thus structural studies and the immunologic reactivity suggest that the acetylcholinesterase forms arise either as separate gene products or from distinct RNA translation products.

Introduction

Acetylcholinesterase in various tissues is found to exist as two general classes of molecular forms (1). The first class consists of dimensionally asymmetric forms composed of multiple catalytic subunits disulfide-linked to a collagen-like tail unit and, in some cases, a noncollagenous structural subunit (1-4). These forms are found in highest abundance in synaptic areas and their biosynthesis is controlled by synaptogenesis (1). The second class consists of simple oligomers of the catalytic subunits. These forms are often hydrophobic, associate with membranes, and show a wide tissue distribution extending to both excitable and non-excitable tissue (5,6). In muscle, these forms are present in both junctional and extrajunctional areas (1).

In Torpedo, both forms of the enzyme have been identified and are present in near-equal quantities (6-8). The elongated forms from Torpedo exist primarily as 17S and 13S species (2,9,10) and contain a noncollagenous structural subunit of 100,000 daltons in addition to the multiple catalytic subunits of 80,000 daltons and the smaller collagen-containing subunits (9,10). The catalytic and structural subunits are linked by disulfide bonds. The simpler globular form in Torpedo is a dimer of subunits with a sedimentation constant of 5.6S. It aggregates in the absence of detergent (6).

Three explanations which are not mutually exclusive might be put forward as the bases for variegation in acetylcholinesterase molecular structure. The acetylcholinesterases may be expressed as a multigene family where the primary sequences of the catalytic subunits of the molecular forms differ. Second, the structural differences could arise from a single gene and alternative m-RNA processing would cause the structural diversity. Third, differences in structure could arise from post-translational modifications giving rise to different extents of glycosylation, fatty acid acylation and subunit assembly.

To distinguish these possibilities, we have undertaken an analysis of the structures and functional sites of acetylcholinesterase using protein chemistry and immunologic techniques. We have purified the catalytic subunits

from the elongated (17S + 13S) forms of Torpedo acetylcholinesterase and compared them with the purified hydrophobic dimer or 5.6S species. Selective proteolytic cleavage with trypsin removes the structural subunits from the (17S + 13S) enzymes yielding an 11S species (3,9). Gel electrophoresis indicates that the catalytic subunits remain intact during this procedure. Since the structural subunits are disulfide-linked to the catalytic subunits (3,9), small residual fragments of the structural subunits may remain linked to the catalytic subunit (11), but they can be removed following denaturation, disulfide bond reduction and dialysis.

Structure of the Catalytic Subunits

The catalytic subunits of the two forms show different migration rates upon electrophoresis in the presence of SDS (6). The differences are largest for the dimer of catalytic subunits where we observe that at low acrylamide concentrations, catalytic subunits from the 5.6S species migrate more rapidly than those of the 11S species, while the order of migration is reversed at high acrylamide concentrations (6). Intermediate concentrations can be selected where the catalytic subunits show indistinguishable migration rates. Since this behavior is most notable in the dimers and the carbohydrate content is very similar in the 5.6S and 11S species (6), it is likely that secondary structure contributes substantially, but not solely, to the divergent migration rates.

Following reduction of the catalytic subunits with dithiothreitol, carboxymethylation and digestion with trypsin, the tryptic peptides were separated by high pressure liquid chromatography (Fig. 1). Remarkably similar profiles for the two enzyme species are found (6). The active site peptide was identified by [³H]DFP labeling of the native enzyme followed by aging to remove one of the isopropoxy groups. This peptide is found at position 36 in both catalytic subunits. The active site tryptic peptide has been sequenced in the 11S species and we are in the process of comparing the sequence to that in the 5.6S species. Each enzyme contains seven carboxymethylcysteine-containing peptides in their catalytic subunits which appear at comparable positions. However, the profiles show a few peptides which differ in the two cases. Peptides #10 and #42 appear to be unique to the 11S species while #45 and 47 are found only in the 5.6S enzyme. Qualitative differences are also apparent in several other peptides, but their isolation would be necessary to establish them as unique peptides. Some of the peptides have been sequenced or partially sequenced. This includes the N-terminal peptide. Some of the sequences appear to be good candidates for synthesis of nucleotide probes with minimal coding redundancy.

Identification of tryptic peptides in functional and surface regions of acetylcholinesterase

We have also attempted to identify the peptides which form the surface of the peripheral anionic site. Previous work has indicated that this site is unique to the acetylcholinesterases and in the native structure is greater than 20Å removed from the catalytic serine in the active center (12). To label the peripheral site we have prepared a monoazido analogue of [³H]propidium and examined the profile of labeled peptides following light activation. Most of the labeling occurs in three modified peptides, migrating near positions 8, 18 and 32, with the predominate peak being near position 18. Labeling of more

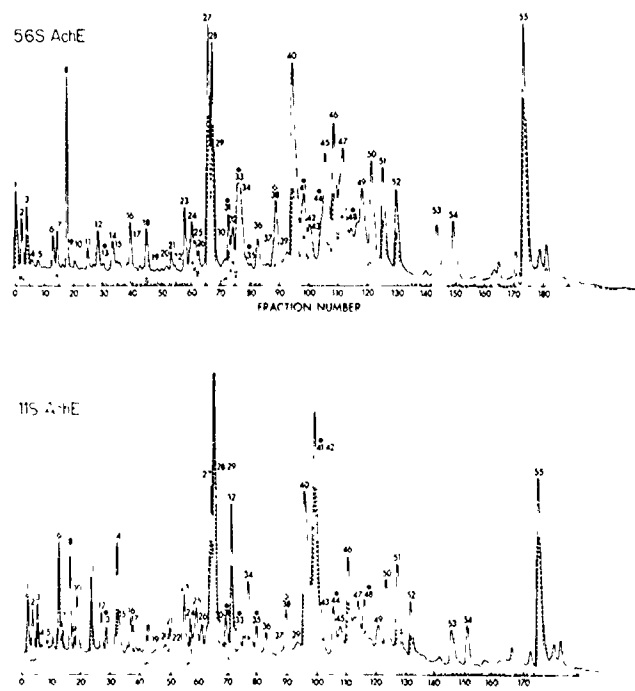


Figure 1. High Pressure Liquid Chromatography of Tryptic Peptides from Top: 5.6S (hydrophobic dimer) and Bottom: 11S Forms of Acetylcholinesterase.

Tryptic peptides were prepared from the reduced, denatured and [14 C]iodoacetate alkylated enzyme. Prior to reduction the enzymes were inhibited with [3 H]DFP and allowed to age by incubation at 25° for 18-24 hours. The tryptic hydrolyzate was placed on a reverse phase microbondapack C_{18} column and eluted with a programmed 0-50% acetonitrile gradient in 0.1% TFA/ H_2O . —, Absorbance 219 nm; ---, Absorbance 280 nm; ●, [14 C]carboxymethyl peptides; ◇, [3 H]diisopropylphosphoryl peptides. Complete details of the digestion and chromatographic procedures are given in reference 14.

than a single peptide is to be anticipated for the peripheral site since the azido group is highly reactive.

Secondly, multiple orientations of the ligand should be possible since previous work on competition of monovalent and divalent inorganic cations with propidium binding to the peripheral site suggest that a matrix of anionic loci may constitute this site (13). Of significance is that the same peptide(s) are not labeled by [3 H]DFP and [3 H]azidopropidium. Since an active site peptide containing more than 45 residues (>5,000 daltons) can be isolated after cyanogen bromide cleavage, a more rigorous test of the non-identity of the active center and peripheral site surfaces should come from CNBr peptide isolation.

The catalytic subunits from the hydrophobic dimer and the elongated species of acetylcholinesterase contain 5-7% carbohydrate and the overall composition would indicate that the oligosaccharides are asparagine N-linked rather than O-linked sugars. To identify the oligosaccharide-containing peptides, we have adsorbed the tryptic peptides on to columns of wheat germ agglutinin, ricin-I and pea lectin linked to Sepharose. Several peptides have been tentatively

identified as oligosaccharide-containing. Differences in the profiles of tryptic peptides appear in regions where we have been unable to detect oligosaccharides. A more complete analysis of the oligosaccharide-containing peptides is underway (A. Drotar, A.N. Miller and P. Taylor) since elucidation of the post-translational modifications of acetylcholinesterase will be critical to future considerations on the structure and biosynthesis of the enzyme.

Antigenic differences in the molecular forms of acetylcholinesterase

Our early studies with polyclonal antibodies did not uncover a significant antibody titer which was selective for the structural subunits of the asymmetric (17 + 13S) species of acetylcholinesterase (2). In contrast, monoclonal antibody production has yielded clones with the requisite specificity for studies on the localization and structure of the various acetylcholinesterase forms (14). Although most of the antibodies showed little difference in reactivity, one denoted as 4F-3 was selective for the asymmetric (17 + 13S) species (Fig. 2) and its reactivity was lost following treatment of the enzyme with collagenase or trypsin. Western blots show slight reactivity with the position of the tail subunits (~48,000 daltons), although the antibody also reacts with a lower molecular weight fraction.

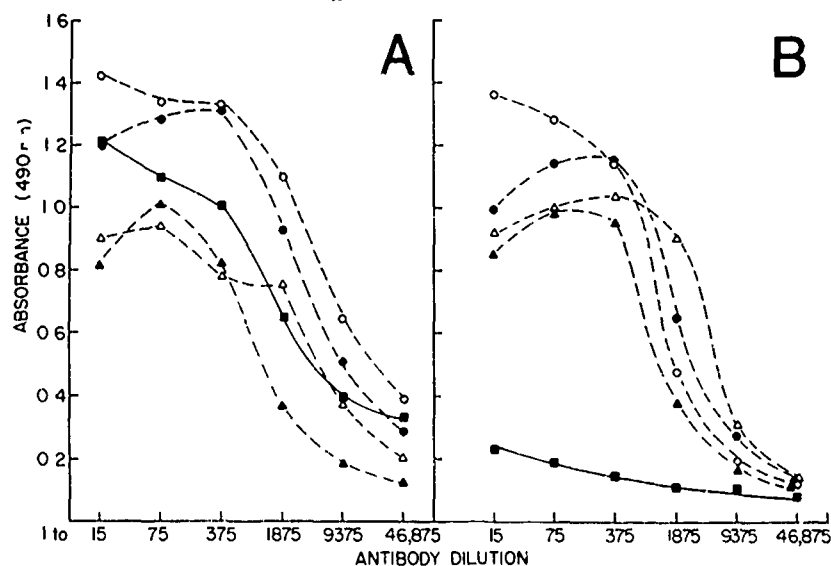


Figure 2. Specificity of Five Monoclonal Antibodies Raised against a Mixture of (17 + 13)S and 5.6S Acetylcholinesterase:

The monoclonal antibodies were obtained from the culture supernatant of the hybridoma cell lines and partially purified by $(\text{NH}_4)_2\text{SO}_4$ precipitation. Assay was done by the enzyme-linked immunoadsorbent method using peroxidase coupled rabbit antimouse IgG + IgM as the second antibody. Panel A: Reaction with (17 + 13)S acetylcholinesterase. Panel B: Reaction with 5.6S acetylcholinesterase: ○, 4E7; ●, 4D1; △, 4G1; ▲, 2C8; ■, 4F3. Note that 4F3 shows a selectivity for the asymmetric forms of acetylcholinesterase. See reference 14 for details on the isolation of the antibodies.

A second antibody, 4E-7, exhibits a 100-fold selectivity for the catalytic subunits of the hydrophobic, dimeric (5.6S) species (Fig. 3). Immunoblots also show reactivity with the migration positions of the 5.6S enzyme. Since the specificity of the antibody for the 5.6S enzyme is also retained after

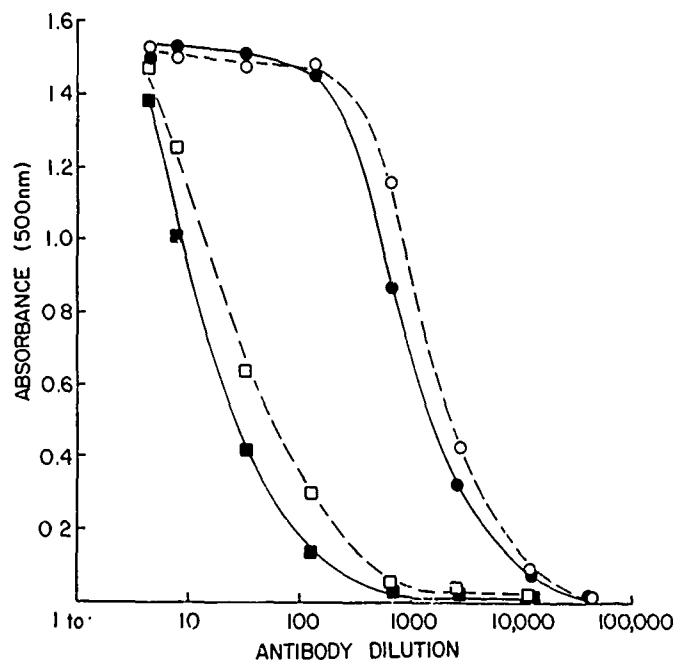


Figure 3. Specificity of Monoclonal Antibody, 4E7 for the 5.6S (hydrophobic dimer) and 11S (lytic form derived from the elongated species) Acetylcholinesterase.

Denaturation of acetylcholinesterase was carried out in 6 M guanidine HCl and the sample dialyzed: ■, native 11S; □, denatured 11S; ●, native 5.6S; ○, denatured 5.6S. The assay procedure was identical to that in Fig. 2.

denaturation, the monoclonal antibodies should prove useful in the identification of domains of primary structure within the catalytic subunits that differ between the two forms.

Structural differences between the molecular forms of acetylcholinesterase

Our studies with antibody selectivity and peptide mapping indicate that the various molecular forms of acetylcholinesterase do not arise solely from different assembly processes for identical catalytic subunits. Rather, we should consider regulatory steps occurring at levels of transcription and translation. The forms of acetylcholinesterase could arise as separate gene products. Alternatively, through message processing a single gene could give rise to acetylcholinesterase species with distinct, but closely homologous, sequences (15). Isolation of the m-RNA and c-DNA species should enable one to distinguish between these alternatives.

The study of the biosynthesis and assembly of acetylcholinesterase

Future studies on the biosynthesis of acetylcholinesterase can be expected to include two complementary approaches. The first would employ cell culture systems that secrete acetylcholinesterase where precursor-labeled amino acids can be followed through formation of the nascent chains, the post-translational processing steps and export from the cell (16). The chief advantage of this approach is that it employs an intact cellular system. However, since acetylcholinesterase is in low abundance in the known cell lines and primary

cultures, characterization of the enzyme forms and isolation of the appropriate m-RNA's will provide formidable obstacles.

Alternatively, biosynthesis could be examined in the electric organ where quantities of the enzyme are large and the gene products can be characterized. Since these electrocyte cells have not been maintained in cultures, the examination of precursor-product relationships will be limited by cell viability. However, biosynthesis and post-translational processing can still be approached using an in vitro protein synthesis system. With acetylcholinesterase in high abundance, both the gene products and the corresponding m-RNA's should be amenable to characterization (17). Torpedo provides an ideal system for in vitro protein synthesis work since both forms of the enzyme are present in substantial quantities and in near equal abundance.

Over the past decade, the multiple forms of acetylcholinesterase have been characterized and their location in various tissues documented. Moreover, their dispositions are under precise regulatory control and factors such as synapse formation, denervation, muscle activity and development all affect the disposition and relative abundance of the enzyme forms. In the coming years, we can expect that the tools of molecular biology and protein chemistry will enable us to examine the mechanism of regulation of biosynthesis and cellular disposition of this enzyme.

References

1. Massoulie, J. and Bon, S.: *Ann. Rev. Neurosciences* 5, 57-106 (1982).
2. Lwebuga-Mukasa, J., Lappi, S. and Taylor, P.: *Biochemistry* 15, 1425-1434 (1976).
3. Rosenberry, T.L. and Richardson, J.M. *Biochemistry* 16, 3550-3558 (1977).
4. Anglister, L. and Silman, I. *J. Mol. Biol.* 125, 293-311 (1978).
5. Ott, P. and Brodbeck, U. *Eur. J. Biochem.* 88, 119-125 (1978).
6. Lee, S.L., Camp, S.J. and Taylor, P.: *J. Biol. Chem.* 257, 12302-12309 (1982).
7. Viratelli, O.M. and Bernhard, S.A.: *Biochemistry* 19, 4999-5007 (1980).
8. Bon, S. and Massoulie, J. *Proc. Natl. Acad. Sci. USA* 77, 4464-4468 (1980).
9. Lee, S.L., Heinemann, S., and Taylor, P.: *J. Biol. Chem.* 257, 12283-12291 (1982).
10. Lee, S.L. and Taylor, P.: *J. Biol. Chem.* 257, 12292-12301 (1982).
11. Mays, C. and Rosenberry, T.L. *Biochemistry* 20, 2810-2817 (1981).
12. Berman, H.A., Yguerabide, J. and Taylor, P. *Biochemistry* 19, 2226-2235 (1980).

13. Taylor, P. and Lappi, S. *Biochemistry* 14, 1989-1997 (1975).
14. Doctor, B.P., Camp, S., Gentry, M.K., Taylor, S.S. and Taylor, P. *Proc. Natl. Acad. Sci. USA* 18, 5767-5771 (1983).
15. Early, P., Rogers, J., Davis, M., Calame, K., Bond, M., Wall, R. and Hood, L.: *Cell* 20, 313-319 (1980).
16. Rotundo, R. in Proceedings of the 2nd International Conference on Cholinesterases, M. Brzin and E.A. Barnard, Eds., Walter de Gruyter & Co., Berlin, in press.
17. Taylor, P., Camp, S., MacPhee, K., Schumacher, M., Amitai, G., Taylor, S.S., Gentry, M.K. and Doctor, B.P. in Proceedings of the 2nd International Conference on Cholinesterases, M. Brzin and E.A. Barnard, Eds., Walter de Gruyter & Co., Berlin, in press.

V. Organophosphates: CNS Toxicity and Therapeutic Approaches

INTRAVENOUS SOMAN INTOXICATION OF AWAKE CATS - MODEL
DEVELOPMENT, LABORATORY FINDINGS, AND NEUROPATHOLOGY

James B. Moe, LTC, VC, James S. Nelson, COL, MC, USAR, Isaac J. Hayward, CPT, VC, Dennis E. Jones, MAJ, VC, and Donald G. Harrington, LTC, VC

Walter Reed Army Institute of Research, Washington, D.C. and the U.S. Army Medical Research Institute of Chemical Defense, Aberdeen Proving Ground, MD.

Introduction

Diagnosis and monitoring of nerve agent casualties in a battlefield setting will present a unique challenge to medical personnel. The clinical symptoms seen, especially in milder cases of nerve agent intoxication can be quite characteristic, but are not necessarily specific for organophosphate toxicity. For example, nerve agent casualties may be confused with anxiety states or combat exhaustion, conditions which must be separated from nerve agent intoxication in order to effectively manage casualties. While testing of blood acetylcholinesterase (ACHE) levels would provide definitive evidence of organophosphate intoxication, this test must be run at a relatively sophisticated laboratory located, in many cases, remote from the sites of primary casualty care. Furthermore, relatively little can be learned about the pathophysiology of nerve agent intoxication from the study of ACHE activity in plasma.

During the design of this pilot study, the hypothesis was developed that a distinctive pattern of biochemical or enzymatic changes would occur in blood of experimental animals intoxicated with nerve agent. If these changes involved relatively conventional laboratory tests, for example, blood glucose, then there, might be an opportunity to confirm a diagnosis of nerve agent intoxication at a relatively unsophisticated medical laboratory located close to the site of primary casualty care. Additionally, by doing a complete battery of laboratory tests on blood and cerebrospinal fluid (CSF) a change, or set of changes, in laboratory parameters might be found which would correlate with the clinical observations, eventual survival or death of the individual, and neuropathologic findings.

The primary impetus for developing this experiment was the observation of changes in the levels of glucose, potassium, and several enzymes (SGOT, LDH, and CPK) in the blood and CSF of dogs during the acute phase of Soman intoxication. These findings were obtained from dogs on neuroanatomy studies and only involved a few animals. Because the changes were somewhat unique, a decision was made to extend these studies using cats. Domestic cats were chosen as the experimental animal for this experiment because of the extensive experience in working with this species and the ready availability of neurophysiological and neuroanatomical data.

Materials and Methods

Specific-pathogen-free (SPF) domestic short haired cats of either sex weighing 2-4 kg, were examined for clinical evidence of abnormality and the medial surfaces of both rear legs were prepared for minor surgery. An 18-gauge, 3.8 cm thinwall needle containing a 21 gauge, 28 cm catheter (Venocath Abbott Laboratories) inserted through the skin into the medial saphenous vein slightly proximal to the tarsal joint. The catheter was then threaded proximally into the femoral vein, the needle retracted and the catheter hub anchored to the skin using adhesive tape. The cats were then placed in a restraining stand in the standing position. A tube containing the solution to be infused was connected to the hub of the catheter. Infusion was accomplished by using a roller pump injecting at the rate of approximately 0.4 ml/minute, adjusted appropriately for the weight of the subject. The solution consisted of sterile physiologic saline solution containing 5.0 ug/ml of Soman for the principals and sterile physiologic saline alone for the controls. The infusion rate was adjusted to achieve a dose of 1 ug/kg/minute. Infusion was continued until classical signs of organophosphate intoxication (salivation, licking, muscle fasciculations, piloerection, etc.) were detected or until a total dose of 15ug/kg was delivered. The infusion apparatus was disconnected, the catheter capped and secure, and the cat removed from the restraint stand and placed in a cage for observation. Blood samples were collected immediately prior to infusion, 30 minutes after completion of infusion, and immediately prior to death. Cerebrospinal fluid samples were obtained from the foramen magnum immediately prior to necropsy.

Complete necropsies were performed on each of the 21 experimental cats and on six control cats which had received intravenous saline instead of Soman. Tissues were fixed with 10% phosphate buffered formalin by perfusion or immersion. Paraffin sections of all major viscera, cerebral hemispheres, brainstem, cerebellum, spinal cord, peripheral nerve, and skeletal muscle were examined by light microscopy. The following stains were used: Hematoxylin and Eosin (H & E); Luxol Fast Blue-PAS (LFB-PAS-Myelin); Sevier-Munger (Axons); PAS with and without diastase (glycogen); and aldehyde fuchsin (pancreatic beta cells). Semi thick plastic sections of sciatic nerves and branches were stained with basic dyes and examined by light microscopy.

Results

The most common clinical signs of Soman intoxication were muscle fasciculations or tremors, licking, salivation, limb flexion or extension, pupillary dilatation, loss of equilibrium, chewing and seizures (See Table 1). The first signs to appear, in most cats, were pupillary dilatation, licking, and muscle fasciculations or tremors. Loss of equilibrium and seizure appeared to be triggered in several instances by the physical activity associated with removal of the cats from the restraint stands and placement in the observation cages. In a few cases, the cats returned to a relatively normal state within a few hours and were eating and drinking within 12 hours after

INTRAVENOUS SOMAN INTOXICATION - Moe, et al

intoxication. Other cats remained in a semicomatose state for 12 hours or more; some of these gradually return to normal while the condition of other grew worse until they either died or were euthanized when judged to be in a moribund state. Animals which failed to gain the ability to maintain equilibrium within 12 hours were given supportive care in the form of frequent turning, parenteral fluid administration and assistance with eating and drinking. Nine cats died or were euthanized when judged to be moribund within 48 hours of intoxication (Table 2). One cat return to a relatively normal state within 48 hours of intoxication, was observed to have a seizure on day 4, and died later that same day. Eleven cats recovered to a relatively normal state and survived until the scheduled day for euthanasia. Overall, the mortality rate for cats intoxicated with Soman according to the regimen described above was 48 per cent. The mean time to spontaneous death for the six cats which never recovered from the acute effects of intoxication was 2 hours, 57 minutes.

A precipitous decrease in plasma ACHE levels to less than 10 percent of preintoxication levels was seen in virtually all cats intoxicated (Table 3). There was no perceptible difference in the degree of ACHE depression at 30 minutes postintoxication between the group of cats which died and those which ultimately survived. In the 3 cats which survived to 24-48 hours postintoxication, the mean ACHE activity was approximately 25 per cent of preintoxication values. ACHE activity was close to the preintoxication values in all cats examined at the 6-13 day intervals and later.

Blood glucose levels were generally increased in cats intoxicated with Soman (Table 4). Those which survived had a somewhat greater (81%) mean increase in blood glucose than those which died or were euthanized in a moribund state (53%). Blood glucose levels remained elevated in the terminal blood samples of the dying/moribund cats, but had returned to the normal range at later intervals.

Serum potassium concentrations were elevated above the normal range at the 30 minute postoxinoculation interval in the group of cats which eventually died and were at extremely high mean values in these cats at the terminal interval (Table 5). Mean serum potassium values were slightly higher at the 30 minute postintoxication interval for the cats which ultimately survived the Soman exposure than in those Which died.

Creatine phosphokinase (CPK) activities in blood of all groups of cats, including controls, were elevated at the 30 minute postintoxication interval. The CPK activities were elevated at the terminal sampling for cats which died (24-48 hours postintoxication) and for those which survived into the 6-13 day interval. Cerebrospinal fluid CPK levels were elevated somewhat proportionately to those in the blood. Isoenzyme analyses of CPK from both blood and CSF failed to reveal a selective or greater increase in one isoenzyme over the others.

INTRAVENOUS SOMAN INTOXICATION - Moe, et al

Lactic dehydrogenase (LDH) enzyme activity in blood was increased to approximately 300 percent of preintoxication values by 30 minutes postintoxication in all exposed cats, regardless of eventual outcome (Table 7). At 6-13 days and ensuing intervals, LDH activity had returned to the normal range. There were no discernible patterns of specificity in the LDH isoenzyme analyses. The LDH values in CSF were not elevated to the same extent as those in blood.

There were mild increases in serum glutamic oxaloacetic transaminase (SGOT) and serum glutamic pyruvic transaminase (SGPT) activities in intoxicated cats 30 minutes postintoxication and more marked increases in terminal samples from cats dying during the first few days after intoxication (Tables 8 & 9). The SGOT activity was also increased in terminal CSF samples of cats which died during the first few days after intoxication.

There were no significant or extensive parenchymal lesions in sections of the heart, lungs, liver, kidney or adrenals from any of the 21 Soman intoxicated cats. Acute congestion of myocardium, liver, and kidney, decreased stainable liver glycogen, normal pancreatic beta cell granulation, occasional foci of pulmonary atelectasis, and intraluminal accumulations of cellular and amorphous debris in a few small caliber bronchioles were evident in animal dying or killed within 48 hours after intoxication.

Parenchymal alterations with histologic and topographic features indicative or characteristic of ischemic parenchymal injury were present in each of the 9 animals dying or killed within 48 hours after intoxication and in 6 animals killed 9-48 days after intoxication. The earliest lesions seen 2-3 hours following exposure consisted of multiple foci of vacuolated cerebral cortical neuropil within the boundary zones between the anterior and middle cerebral arteries. Within 24-48 hours frank eosinophilic neuronal necrosis accompanied by reactive glial and mesodermal changes was evident within the boundary zones, the cortex over the cerebral convexities, the basal ganglia, and the pyramidal cell layer of the hippocampus. Obvious neuron loss and reactive fibrillary astrocytosis was apparent at these same sites in cats killed 3 weeks or more following Soman exposure.

There was no unequivocal evidence of axonal lesions characteristic or delayed organophosphate neurotoxicity in sections of spinal cord or sciatic nerve from the Soman exposed cats. In some intoxicated cats, however, there appeared to be increased numbers of astrocytic nuclei in the dorsal columns. Alterations suggestive of axonal degeneration were present in sections of sciatic nerve from 1/4 experimental and 1/3 control cats examined.

INTRAVENOUS SOMAN INTOXICATION - Moe, et al

Discussion

The slow intravenous infusion of Soman into cats, as described in this experiment, provided a reliable model of nerve agent intoxication in mammals. A relatively uniform clinical expression was produced and the mortality rate approximated the 50 percent value desired in the experimental design. Transcutaneous placement of an intravenous catheter facilitated repeated blood sampling and infusion of agent solution without requiring excessive preliminary manipulation. In this model, which did not involve specific resuscitative measures, it was apparent that most individuals which spontaneously recover and survive past 4 days postintoxication will survive with few grossly detectable functional deficits. These survivors do, however, express pathological evidence of residual damage in the brain. Acetylcholinesterase activity was reliably depressed to approximately 5-10 percent of the normal value by the treatment regimen used.

The ACHE values at 30 minutes postintoxication were of no value in predicting the eventual outcome of the individual animals at the LD 50 level of exposure used. These interpretation of the ACHE values, as well as other laboratory duties, suffers from absence of periodic samples in the 48 hour time frame immediately following the 30 minute postintoxication interval. There was evidence of partial recovery of ACHE activity in the plasma of cats bled when in a moribund condition at 24-48 hours postintoxication. Comparison of the recovery curves of ACHE activity in survivors versus nonsurvivors at the 6 and 12 hours intervals might reveal a difference which would be of prognostic value.

Glucose concentrations were increased in the blood of intoxicated cats, probably as a result of the stress and hyperactivity associated with the intoxicated state. The glucose concentrations in blood of intoxicated cats may have a great deal of biological significance for intoxicated individuals. Hyperglycemia has been associated with more severe neuropathologic manifestations during experimentally induced ischemia of the brain in cats. Greater amounts of carbohydrate energy sources probably enhance the concentration of lactate in the brain under the anaerobic metabolic conditions associated with the ischemic state. At lactate concentrations greater than 16 m mole/kg of the brain there is necrosis of endothelial cells and astrocytes, resulting in edema of the brain, further diminishing the oxygen supply to the tissue. Although the blood glucose concentrations in these cats did not correlate with eventual survival observations, the potential for reducing organic brain damage by decreasing the blood glucose concentration during the acute phase of intoxication deserves to be investigated.

INTRAVENOUS SOMAN INTOXICATION - Moe, et al

The increased concentrations of potassium in the extracellular fluids (blood and CSF) of intoxicated cats was the factor most likely related to the acute deaths. Electrocardiographic abnormalities are detectable when the serum concentration of potassium exceeds 7 mEq/l and death occurs when this ion reaches 10-12 mEq/liter of serum. Additionally, increased concentrations of potassium in the extracellular fluids of the brain can lead to astrocytic swelling, edema, and reduced oxygen perfusion of the brain. Pathologic changes in the brain are probably exacerbated by extracellular potassium which stimulates brain metabolism, increasing requirements for oxygen and energy, and consequently magnifying the effects of ischemia. The cause(s) of increased extracellular potassium concentrations in intoxicated cats were unknown, but possibly resulted from skeletal muscle and other tissue injury associated with seizures, hyperactivity, and hypoxia in the brain.

Increased activities of CPK and LDH in blood at the 30 minute postintoxication interval were probably due to release of these enzymes from skeletal muscle associated with hyperactivity, although distinctive isoenzyme profiles were not identified. Refinement of the CSF collection technique and more complete blood sampling to permit collection of more complete samples should resolve the question of whether specific isoenzyme increases are responsible for increased CPK or LDH activities during Soman intoxication.

Increased activities of SGOT and SGPT somewhat later (24 - 48 hours) in the acute phase of intoxication probably reflected muscle and liver damage, respectively. These same enzymes have been reported to be elevated in both humans and in cattle following intoxication with organophosphates.

The CNS lesions demonstrable in the majority of the soman exposed cats are histologically and topographically identical with those occurring in mammals, including man, as a consequence of spontaneously occurring or experimentally-induced, transient, widespread cerebral ischemia associated with transient cardiorespiratory arrest or profound hypotension. In addition, such lesions are observed in association with prolonged seizures. In this instance, however, the role of ischemia in the pathogenesis of the lesions has been challenged. At present this controversy is unresolved.

No lesions typical of those associated with delayed organophosphate neurotoxicity were present in any of the Soman treated cats. The study, however, was not designed for optimal detection of delayed neurotoxicity. Definitive conclusions regarding chronic neurotoxicity from Soman exposure will require a study with longer animal survival times and the use of sensitive morphologic techniques such as electron microscopy and quantitative fiber spectrum analysis.

TABLE 1. CLINICAL SIGN IN CATS INTOXICATED WITH SOMAN BY SLOW
INTRAVENOUS INFUSION (CALCULATED LD₅₀)

SIGN	NO. AFFECTED	TIME OF ONSET (X MINUTES)
MUSCLE FASCICULATION/TREMORS	21	12.70
SALIVATION	21	-
LIMB FLEXION/EXTENSION	20	-
PUPILLARY DILATATION	20	11.6
LICKING	20	11.9
LOSS OF EQUILIBRIUM	19	-
CHEWING	17	-
SEIZURE	15	-
NYSTAGMUS	5	-
PILOERECTION	3	-
URINATION	3	-
DEFECATION	0	-

TABLE 2. OUTCOME IN CATS INTOXICATED WITH SOMAN BY SLOW
INTRAVENOUS INFUSION (CALCULATED LD₅₀)

OUTCOME	NO. OF CATS	DOSE, $\mu\text{M/kg}$ X
DIED (< 48 HOURS POSTINTOX.)*	6	12.7
DIED (\leq 96 HOURS POSTINTOX.)	1	15.0
EUTHANASIA/MORIBUND (48 HOURS POSTINTOX.)	3	14.7
EUTHANASIA/SCHEDULED (9-48 DAYS POSTINTOX.)	11	13.9
CONTROLS	6	0.0

* MEAN TIME TO DEATH = 2 HRS. 57 MIN.

TABLE 3. PLASMA ACETYLCHOLINESTERASE LEVELS IN CATS INTOXICATED
WITH SOMAN BY SLOW INTRAVENOUS INFUSION ($\mu\text{M}/\text{ml}/\text{Min}$)

GROUP	PRE	30° POST	TERMINAL
DIED/MORIBUND	1.36	0.10	0.40*
SURVIVED (ALL)	1.52	0.11	-
(6 - 13 DAYS)	1.43	0.10	1.26
(14 - 20 DAYS)	1.92	0.11	1.87
(21 - 28 DAYS)	1.53	0.12	1.84
(29 - 48 DAYS)	1.17	0.08	1.83
CONTROLS	1.46	1.35	1.52

* BASED ON DATA FROM 3 CATS EUTHANIZED 24-48 HRS. POSTINTOXICATION

TABLE 4. GLUCOSE IN BLOOD AND CEREBROSPINAL FLUID OF
SOMAN INTOXICATED CATS (mg/dl)

GROUP	BLOOD			CSF
	PRE	30° POST	TERMINAL	TERMINAL
DIED/MORIBUND SACRIFICE	119	182	198	60
SURVIVED (ALL)	116	210	-	-
(6 - 13 DAYS)	116	162	124	69
(14 - 20 DAYS)	133	267	104	53
(21 - 28 DAYS)	90	186	99	68
(29 - 48 DAYS)	127	239	-	-
CONTROLS	134	114	135	61

TABLE 5. POTASSIUM LEVELS IN CATS INTOXICATED BY SLOW
INTRAVENOUS INFUSION OF SOMAN (mEq/l)

GROUP	SERUM			CSF
	PRE	30° POST	TERMINAL	TERMINAL
DIED/MORIBUND	4.2	5.4	8.8	12.4
SURVIVED (ALL)	4.1	5.8	-	-
(6 - 13 DAYS)	4.2	7.9	3.6	3.4
(14 - 20 DAYS)	4.0	4.8	3.9	4.6
(21 - 28 DAYS)	4.0	4.8	3.8	3.3
(29 - 48 DAYS)	4.0	6.2	4.6	3.2
CONTROLS	4.1	4.3	4.2	4.1

TABLE 6. CPK LEVELS IN CATS INTOXICATION BY SLOW
INTRAVENOUS INFUSION OF SOMAN (mU/ml)

GROUP	BLOOD			CSF
	PRE	30° POST	TERMINAL	TERMINAL
DIED/MORIBUND	82	364	800	407
SURVIVED (6-13 DAYS)	126	137	566	742
(14 - 20 DAYS)	96	562	64	180
(21 - 28 DAYS)	104	382	67	6
(29 - 48 DAYS)	62	66	70	157
CONTROLS	118	290	139	62

TABLE 7. LDH LEVELS IN CATS INTOXICATED BY SLOW
INTRAVENOUS INFUSION OF SOMAN (mU/ml)

GROUP	BLOOD			CSF
	PRE	30° POST	TERMINAL	TERMINAL
DIED/MORIBUND	79	246	526	180
SURVIVED (ALL)	93	259	-	-
(6 - 13 DAYS)	82	199	101	100
(14 - 20 DAYS)	67	298	97	36
(21 - 28 DAYS)	122	299	85	-
(29 - 48 DAYS)	100	82	117	14
CONTROLS	102	169	84	267

TABLE 8. SGOT LEVELS IN CATS INTOXICATED BY SLOW
INTRAVENOUS INFUSION OF SOMAN (mU/ml)

GROUP	BLOOD			CSF
	PRE	30° POST	TERMINAL	TERMINAL
DIED/MORIBUND	16	31	607 (n=2)	124
SURVIVED (ALL)	20	44	-	-
(6 - 13 DAYS)	20	37	30	38
(14 - 20 DAYS)	21	52	14	18
(21 - 28 DAYS)	20	38	17	17
(29 - 48 DAYS)	18	28	30	16
CONTROLS	18	22	24	11

TABLE 9. SGPT LEVELS IN CATS INTOXICATED BY SLOW
INTRAVENOUS INFUSION OF SOMAN (mU/ml)

GROUP	BLOOD			CSF
	PRE	30° POST	TERMINAL	TERMINAL
DIED/MORIBUND	44	48	190	7
SURVIVED (ALL)	45	64	-	-
(6 - 13 DAYS)	42	40	26	3
(14 - 20 DAYS)	50	74	38	6
(21 - 28 DAYS)	52	61	41	6
(29 - 48 DAYS)	46	50	59	6
CONTROLS	53	52	57	11

INTRAVENOUS SOMAN INTOXICATION - MOE, et al

References

1. Lemerrier, G., Carpentier, P., Sentenac-Raumanou, H. Morelis, P. Histological and histochemical changes in the central nervous system of the Cat poisoned by an Irreversible Anticholinesterase organophosphorous compound. *Acta. Neuropathol.* 61: 123-129, 1983.
2. Badyugin, I.S., Titova, V.N., Khamitova, R.Y., Makarov, N.Y. Clinical picture of household poisonings and pathogenesis of intoxication caused by anticholinesterase organophosphorous compounds. *Voy-medits zh.* 11:37-40, 1979.
3. Olney, J.W., Gubareff, T., Labruyene, J. Seizure-related brain damage induced by cholinergic agents. *Nature* 301: 522-1983.
4. Cutler, R.W.P., Spertell, R.B. Cerebrospinal fluid: A selective review. *Ann. Neurol.* 11: 1-10, 1983.
5. Pulsinelli, W.A., Waldman, S., Rawlinson, D., Plum, F. Moderate hyperglycemia augments ischemic brain damage: A neuropathologic study in the cat. *Neurol.* 32:1239-46, 1982.
6. Plum, F. What causes infarction in ischemic brain? *Neurol* 33: 222-33, 1983.
7. Raichle, M.E. The pathophysiology of brain ischemia. *Ann. Neurol.* 13: 2-10, 1983.
8. Wright, F.C., Hunt, L.M., Palmer, J.S. The biochemical effects of coumaphos and three oximes on certain enzyme systems and blood proteins in cattle. *Am. J. Vet. Res.* 27: 177-185, 1966.
9. Mcleod, C.G., Singer, A.W., Harrington, D.G. Acute neuropathology in soman poisoned cats. *Neurotoxicology* (In press), 1984.
10. Kramer, J.W. Clinical enzymology In *Clinical Biochemistry of Domestic Animals*, ed. by J.J. Kaneko, Academic Press, New York, 1980. pp 175-200.
11. Duncan, J.R., Prasse, K.W., *Veterinary Laboratory Medicine*, Iowa State University Press, Ames, 1977. pp. 79-119.

INTRAVENOUS SOMAN INTOXICATION - Moe, et al

12. Garcia, J.H. Ischemic injuries of the brain: Morphologic evolution. Arch. Path. 107:;157-161, 1983.
13. Meldrum, B.S. Brierley, J.B. Prolonged epileptic seizures in primates. Arch. Neurol. 28:10-17, 1973.
14. Soderfeldt, B., Kalimo, H., Olsson, Y., Siesjo, B. Pathogenesis of brain lesions caused by experimental epilepsy. Acta Neuropathol. 54:219-231, 1981.

Pathology of Organophosphorus Compounds in Various Animal Species:
Comparison with Seizure-Related Pathology in Man

By:

James S. Nelson, M.D.
Department of Pathology
Washington University School of Medicine
660 South Euclid Avenue
Saint Louis, Missouri 63110



Organophosphate intoxication in mammals including man may cause acute or chronic nervous system disturbances (1,2). The acute disturbance is a form of cholinergic crisis with widespread disruption of synaptic and neuromuscular transmission resulting from virtually irreversible, organophosphate-induced inhibition of acetylcholinesterase in the central and peripheral nervous systems. Signs of acute intoxication include miosis, bronchoconstriction, increased bronchial secretion, salivation, lacrimation, sweating, and peristalsis. Incontinence of urine and feces and bradycardia progressing to heart block may develop. Muscular fatigability and weakness followed by involuntary twitching and fasciculations are present. Central nervous system disturbances include anxiety, restlessness, headache, slurred speech, ataxia, convulsions, and depression of respiratory and circulatory centers. The immediate cause of death is respiratory failure secondary to bronchoconstriction, increased bronchial secretions, weakness of respiratory muscles, and depressed activity of the CNS respiratory center. Little information is available concerning the neuropathologic changes associated with acute fatal organophosphorus intoxication (3). In humans edema and congestion of the brain has been reported. Similar changes were observed by Holmstedt, et al (4) in their study of the pathology of acutely intoxicated experimental animals. Two recently published studies concern the occurrence of ischemic brain lesions observed in soman intoxicated rats (5,6).

Many organophosphorus compounds may, after one or more doses, cause a chronic progressive central and peripheral nervous system disorder (7). This disorder, called "organophosphate-induced delayed neurotoxicity" develops one to three weeks after initial exposure. Experimentally, delayed neurotoxicity has been induced in a number of animal species including birds, laboratory rodents, lambs, sheep, cats, dogs, and primates. Not all species are equally susceptible to development of the disorder. In some species repeated dosages or modification of the route of administration is necessary to induce the chronic disorder (8,9). Delayed organophosphate neurotoxicity has also occurred in humans, most often as a result of accidental ingestion of TOCP. In addition, however, there are reports of the disorder caused by exposure to organophosphate insecticides. In man and other sensitive animals functional disturbances begin in the distal portion of the lower or hind extremities with motor weakness, mild sensory disturbances, depression or loss of reflexes, and eventually paralysis of the lower extremities. The upper or fore-limbs may be affected in a similar fashion. In humans with a relatively mild form of the disorder the possibility of recovery is good. In cases with a severe initial deficit, varying degrees of permanent neurologic disability may occur. In contrast to acute organophosphate neurotoxicity, the neuropathology of delayed organophosphorus neurotoxicity has been extensively studied. All organophosphates which cause delayed neurotoxicity produce similar neuropathologic alterations in the central and peripheral nervous systems. The basic lesion is a symmetrical distal axonopathy involving ascending and descending tracts in the central nervous system and peripheral nerves. Long, large caliber myelinated fibers are selectively affected. The initial lesion is a distal (but not terminal) focus of axonal degeneration. The axonal segment distal to the focus undergoes Wallerian degeneration (10). Ultrastructurally, intra-axonal vacuoles and accumulations of agranular endoplasmic reticulum are observed within affected axons (11).

Pathogenesis of the axonopathy is not fully understood. Development of the disorder is unrelated to inhibition of acetylcholinesterase. Recent studies suggest that development of delayed neurotoxicity may be related to phosphorylation of a membrane-bound neural protein by the organophosphate (9). This protein, because it exhibits esterase activity, is commonly referred to as neurotoxic esterase. The precise role of neurotoxic esterase in the pathogenesis of the axonal degeneration is unclear. The available data, however, do indicate that neurotoxic esterase activity is inhibited selectively by organophosphates which are known to cause chronic neurotoxicity. Organophosphates which do not produce chronic neurotoxicity have little or no effect on neurotoxic esterase activity. These observations suggest that among organophosphates of unknown chronic neurotoxic potential, compounds likely to produce chronic neurotoxicity could be identified by examining their effect on neurotoxic esterase activity.

Our studies of Soman intoxication in the awake cat indicate that consideration must be given to an additional type of acute or chronic neurologic disturbance associated with organophosphorus intoxication. Following Soman intoxication parenchymal lesions including eosinophilic neuronal necrosis were observed in the cerebral cortex (including hippocampus) and thalamus. The histologic development of the lesions was proportional to the duration between exposure and death of the animal. Initial changes involve focal spongy alterations in the cortical neuropil observed at 2-4 hours following intoxication. Within 24 hours after exposure focal frank neuronal necrosis was present within major arterial boundary zones over the cerebral convexities. At 48 hours these changes were more extensive. In animals surviving one week or more foci of nerve cell loss and reactive astrocytosis were seen within the cerebral cortex particularly the arterial boundary zones and the dorsal and medial thalamus.

The available evidence indicates that cerebral ischemia (possibly secondary to the systemic effects of intoxication) is a major factor in the pathogenesis of the neuronal necrosis. In humans lesions with similar histologic and topographic characteristics are regularly observed in cases of profound transient widespread CNS ischemia caused by cardiac arrest and resuscitation or profound hypotension. Controlled, experimental induction of cerebral ischemia in a number of animal species consistently induces such lesions (12,13). Similar changes are also observed in humans and experimental animals following prolonged generalized motor seizures (14). Although some type of relative or absolute degree of ischemia is believed to play the primary role in the development of the parenchymal changes, in these cases as well, this view has not gone unchallenged (15). At present, however, the data are inconclusive.

The development of the awake cat model of Soman intoxication provides a unique opportunity to systematically investigate acute and chronic neuropathologic disorders which may develop as complications of the physiologic and metabolic disturbances induced by acute organophosphorus intoxication. These changes are distinct from the direct toxic effects of the compound and need to be distinguished from them for reasons of prevention, treatment, and prognosis.

References

- 1) Murphy, S.D.: Pesticides. In Casarett and Doull's Toxicology, 2nd ed., J. Doull, C.D. Klaassen, and M.O. Amadur (eds). New York, MacMillan, 1980, Ch 16, pp 365-375.
- 2) Taylor, P.: Anticholinesterase Agents. In Goodman and Gilman's The Pharmacological Basis of Therapeutics. New York, MacMillan, 1980, pp 100-119.
- 3) Koller, W.C. and Klawans, H.L.: Organophosphorus Intoxication. In Intoxications of the Nervous System, Part II. Handbook of Clinical Neurology, Vol 37. P.J. Winken and G.W. Bruyn (eds). Amsterdam, Elsevier, 1979, pp 541-562.
- 4) Holmstedt, B., Krook, L., and Rooney, D.R.: The Pathology of Experimental Cholinesterase-Inhibitor Poisoning. *Acta pharmacol. (Kbh)* 13:337-344, 1957.
- 5) McLeod, C.G., Singer, A.W., Harrington, D.G. and Beattie, R.J.: Pathology of the Nerve Agents Soman and Sarin (Abstract) USAMRDC 3rd Annual Chemical Defense Bioscience Review. June 2-3, 1983.
- 6) Lemerrier, G., Carpentier, P., Sentenac-Roumanon, H. and Morelis, P.: Histological and Histochemical Changes in the Central Nervous System of the Rat Poisoned by an Irreversible Anticholinesterase Organophosphorus Compound. *Acta Neuropathol. (Berl)* 61:123-129, 1983.
- 7) Abow-Donia, M.B.: Organophosphorus Ester-Induced Delayed Neurotoxicity. *Ann. Rev. Pharmacol. Toxicol.* 21:511-548, 1981.
- 8) Davis, C.S. and Richardson, R.J.: Organophosphorus Compounds. In Experimental and Clinical Neurotoxicology. P.S. Spencer and H. Schaumburg (eds). Baltimore, Williams & Williams, 1980, pp 527-544.
- 9) Lotti, M., Becker, C.E. and Aminoff, M.J.: Organophosphate Polyneuropathy: Pathogenesis and Prevention. *Neurology* 34:658-662, 1984.
- 10) Bouldin, T. and Cavanagh, J.B.: Organophosphorus Neuropathy. I. A Teased Fiber Study of Spatio-Temporal Spread of Axonal Degeneration. *Am. J. Pathol.* 94:241-252, 1979.
- 11) Bouldin, T. and Cavanagh, J.B.: Organophosphorus Neuropathy. II. A Fine Structural Study of the Early Stages of Axonal Degeneration. *Am. J. Pathol.* 94:253-270, 1979.
- 12) Garcia, J.H.: Ischemic Injuries of the Brain: Morphologic Evolution. *Arch. Pathol. Lab. Med.* 107:157-161, 1983.
- 13) Plum, F.: What Causes Infarction in Ischemic Brain. *Neurology* 33:222-233, 1983.
- 14) Meldrum, B.S. and Brierley, J.B.: Prolonged Epileptic Seizures in Primates: Ischemic Cell Change and its Relation to Ictal Physiological Events. *Arch. Neurol.* 28:10-17, 1973.
- 15) Soderfeldt, B., Kalimo, H., Olsson, Y. and Siesjo, B.: Pathogenesis of Brain Lesions Caused by Experimental Epilepsy. *Acta Neuropathol. (Berl)* 54:219-231, 1981.

A Study on the Effect of Soman on the Rat Blood-Brain Barrier

John P. Petrali, Donald M. Maxwell, David E. Lenz
and Kenneth R. Mills

United States Army Medical Research Institute of Chemical Defense
Aberdeen Proving Ground, Maryland 21010

INTRODUCTION

The concept of a vascular barrier isolating the central nervous system from the general circulation was introduced at the turn of the century by the fundamental work of Ehrlich and Goldman who described that dyes bound to plasma proteins stained visceral organs the color of the dye while the brain remained conspicuously uncolored (1). The morphological parameters of this barrier were identified later by Brightman (2) and Westergaard (3) as being the cerebral capillary endothelial cell and its tight junction. Investigations on the role of the barrier in disease and toxic processes has led to the conclusion that induced barrier dysfunction-breaching - can complicate the pathologic process by interfering with homeostatic autoregulatory mechanisms normally provided for by an intact barrier or may initiate the added insult of autoimmune responses to nervous system protein.

A continuing division of opinion as to the effects of anticholinesterase compounds on the blood-brain barrier has been maintained for a surprising length of time. Early work on the effects of anticholinesterases suggested that selected inhibition of esterases at the barrier-site probably was responsible for observed barrier leaks to tracer proteins. This was based on the observations that capillaries in brain areas lacking a true barrier, such as the pineal gland, did not contain esterases while capillaries of barriered brain areas did (4). In these experiments the authors noted that the animals presented typical signs of anticholinesterase intoxication including excitation, respiratory distress, muscle fasciculations and paroxysms. More recent work suggests that mechanisms secondary to, or independent of, enzyme inhibition including accompanying seizure, are responsible for barrier opening (5).

Our present study addresses the following questions and objectives on the effects on the rat blood-brain barrier during the first 24 hours of soman acute intoxication. 1) Is the rat blood-brain barrier rendered permeable to Evans blue? 2) Does the blocking of convulsions associated with soman toxicity prevent barrier leaks? 3) Does a soman-induced breach permit entry of quaternary compounds into the CNS and 4) Seek subcellular barrier mechanisms of an induced breach with horseradish peroxidase as a tracer molecule.

MATERIALS AND METHODS

Animals and Soman: The animal for study was the adult male (200-250 grams) Sprague-Dawley rat. Rats surviving a single subcutaneous dose of 0.9 LD50 soman (114 micrograms/kilogram) were processed for study at 15 minutes, 30 minutes, 1 hour and 24 hours following soman.

Tracer Compounds and Drugs: Evans blue dye at a dose of 2 milligrams/kilogram, I.V., of a 2% solution in saline, was used for rapid visual assessments of cerebrovascular permeability. The dye was either injected by tail vein, 5 minutes prior to soman, or, was injected intracardiacally

5 minutes before collection times with the animal under light anesthesia. Horseradish peroxidase (HRP), type VI, at a dose of 35 milligrams/kilogram, I.V., was used to determine subcellular barrier mechanisms of an induced breach and was administered according to the same injection schedules as Evans-blue.

The quaternary compound 3H-hexamethonium (18 Ci/mmol) was mixed 1:1 with cold hexamethonium and given at a dose of 0.71 milligrams/kilogram, I.P., at a final radioactivity of 1.2 million dpm/minute/injection. Animals were injected during peak signs of soman intoxication and were collected 15-30 minutes later. Regions of cerebral cortex, cerebellum and medulla of aldehyde-perfused brains were oxidized in a tri-carb oxidizer and extracted. Tritium was counted in a liquid scintillation counter for 5 minutes. Counts were recorded as dpm/gram of tissue and compared with control levels. Significance was determined by student-t-test.

Sodium pentobarbital (nembutal) was used as a short acting anti-convulsant at a dose of 30-45 milligrams/kilogram I.P. and was injected 10 minutes prior to soman.

Tissue Collection and Processing: Animals receiving Evans-blue were anesthetized with nembutal (65 milligrams/kilogram I.P.) and fixed by perfusion with approximately 300cc of 2% paraformaldehyde and 4% glutaraldehyde in phosphate buffered mammalian ringers (330 mOsm, pH 7.45). Brains were rapidly removed and visual assessments made of dye penetrations.

Animals receiving HRP were fixed by perfusion or by immersion in dilute fixative (1% paraformaldehyde and 2% glutaraldehyde) to maximize HRP activity. Semiadjacent vibratome sections (50 micron) of major regions of HRP brains were cytochemically developed for peroxidase with diaminobenzidine (0.05%) and hydrogen peroxide (0.01%) in Tris-water for 15 minutes. Following extensive buffer washes, sections were osmicated in 1% osmic acid for 30 minutes, dehydrated in graded ethanol and embedded in epoxy resin. Ultrathin sections of breached areas were viewed by electron microscopy without non-specific counter staining to maximize HRP localization.

RESULTS

All convulsing animals showed some degree of barrier penetration to Evans-blue during the first hour of intoxication (Fig 1). The degree of stain was subjectively assessed as 0, no stain; 1+, focal stain; 2+, regional stain; 3+, bilateral stain. Non-convulsing animals and animals treated prophylactically with nembutal as an anticonvulsant were free of stain. Animals surviving for 24 hours and injected with Evans-blue were also free of extravasated dye, although at this time period, inhibition of acetylcholinesterase persisted at 10% and 5% of control levels in brain and blood respectively. The incidence of staining up to 1 hour and at 24 hours is seen in Fig 2. A qualitative ranking of brain areas opened to Evans-blue is seen in Fig 3.

Electron microscopy of breached areas of cerebral cortex and cerebellum demonstrated that the mode of movement of HRP through the endothelium was

apparently by vesicular transport. Vesicles positive for HRP appeared to emanate from the luminal surface and were seen throughout the cytoplasm and in close association with basement membranes. Tight junctions, although only rarely seen, did not appear separated or injected with HRP. Basement membranes were usually positive for HRP and in some cases provided evidence for aggregates of exocytosed HRP. Extracellular spaces adjacent to capillaries were positive for HRP. Occasionally HRP was seen in foot processes of glial cells closely applied to basement membranes. In some endothelial cells a total swamping of the cytoplasm with HRP occurred. This could have been an artifact of fixation or an effect of elevated levels of acetylcholine which may have adverse effects on cell membranes (5). In the instance of swamping, no vesicular activity was noticed.

The quaternary compound ^3H -hexamethonium gained entry to brains of soman treated animals in significantly elevated amounts over control values (Fig 4, 5, 6). Although this compound is not usually used in soman therapy this uptake does demonstrate the receptiveness of the soman-breached brain to blood-borne quaternary drugs.

DISCUSSION

The results of this study provide evidence that a soman-induced breach of the rat blood-brain barrier is convulsive dependent, and occurs early in the course of toxicity. This is consistent with recent reports of organophosphorous effects on brain capillaries (5). The subcellular mechanism of enhanced vesicular transport described in this study is consistent with some and is at variance with other literature accounts where opinions are still polarized as to whether vesicular transport, opening of tight junctions, or both, are operative mechanisms during convulsion (6). No matter what is decided, it is important to note that vesicular transport and an opened barrier do not discriminate between protein types and it is therefore predictable that gammaglobulins may enter the CNS during episodes of seizure with perhaps specific or cross-specific activity against neuronal elements leading to a deepening of cell injury and contributing to long-term effects of soman poisoning.

SUMMARY

Soman was studied for its effect on the rat blood-brain barrier (BBB) during the first 24 hours of toxicity. The results indicate that a soman-induced breach of the rat BBB is convulsive dependent. All convulsing animals showed some degree of extravasation into the CNS of the visual marker Evans-blue albumin during the first hour of toxicity. Nonconvulsing animals and animals treated prophylactically with nembutal were free of extravasations. Extraluminal stain was also absent in 24 hour survivors. The subcellular mechanism of the breach as elaborated with horseradish peroxidase was probably enhanced endothelial vesicular transport. This barrier breakdown to protein allowed increased uptake of the quaternary compound ^3H -hexamethonium which is normally slowed by an intact BBB.

REFERENCES

1. Bradbury, M. (1979) The Concept of a Blood-Brain Barrier. John Wiley & Sons. New York
2. Brightman, M. W. and Reese, R. S. (1969) Junctions Between Intimately Apposed Cell Membranes in Vertebrate Brain. J. Cell Biology, 40.
3. Westergaard, E., and Brightman, M. W. (1973) Transport of Proteins Across Normal Cerebral Arterioles. J. Comp. Neurol, 152.
4. Joo, F. and Varkonyi, T. (1969) Correlation Between Cholinesterase Activity of Capillaries and the Blood-Brain Barrier in the Rat. Acta. Biol. Acad. Sci. Hung., 20, 4.
5. Ashani, Y. and Catravas, G. N. (1981) Seizure-Induced Changes in the Permeability of the Blood-Brain Barrier Following Administration of Anticholinesterase Drugs to Rats. Biochem. Pharm., 30, 18.
6. Rapoport, S. I. (1976) Blood-Brain Barrier in Physiology and Medicine. Raven Press, New York.
7. Wisniewski, H. M. and Kozlowski, P. B. (1982) Evidence for Blood-Brain Barrier Changes in Senile Dementia of the Alzheimer Type. Ann. New York Acad. Sci. 1982.

BBB OPENING TO EVANS-BLUE VS. TIME

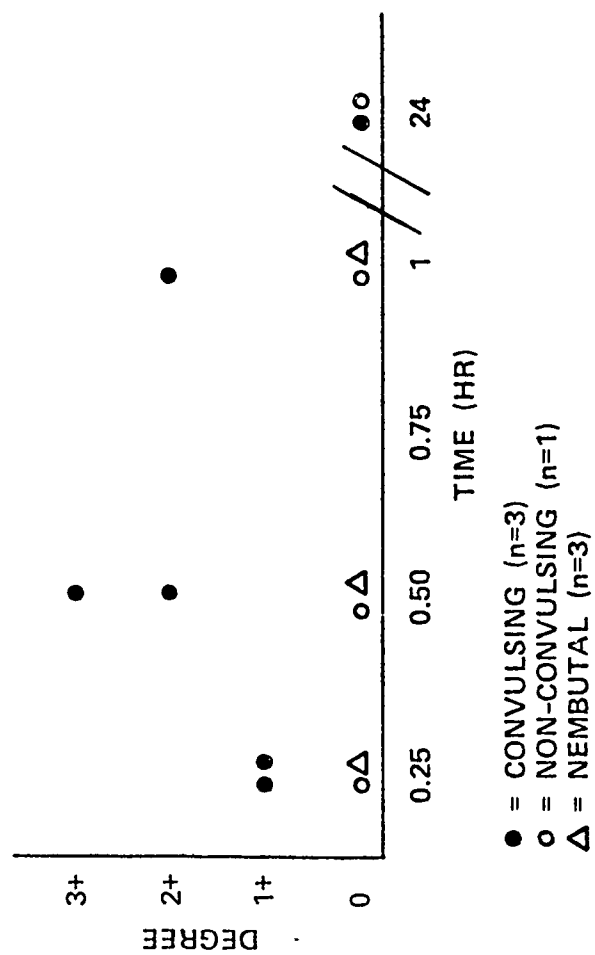


FIGURE 1

INCIDENCE OF BBB OPENING TO EVANS-BLUE

	<u>NON-CONVULSING</u>	<u>CONVULSING</u>	<u>ANESTHETIZED</u>
UP TO 1 HOUR	0/3	15/15	0/9
AT 24 HOURS	0/1	0/3	--

FIGURE 2

**RANKING OF BRAIN REGIONS
TO EVANS-BLUE ALBUMIN**

- CEREBELLUM
- CEREBRAL CORTEX
- HIPPOCAMPUS
- BASAL GANGLIA
- THALAMUS, HYPOTHALAMUS
- BRAIN STEM

FIGURE 3

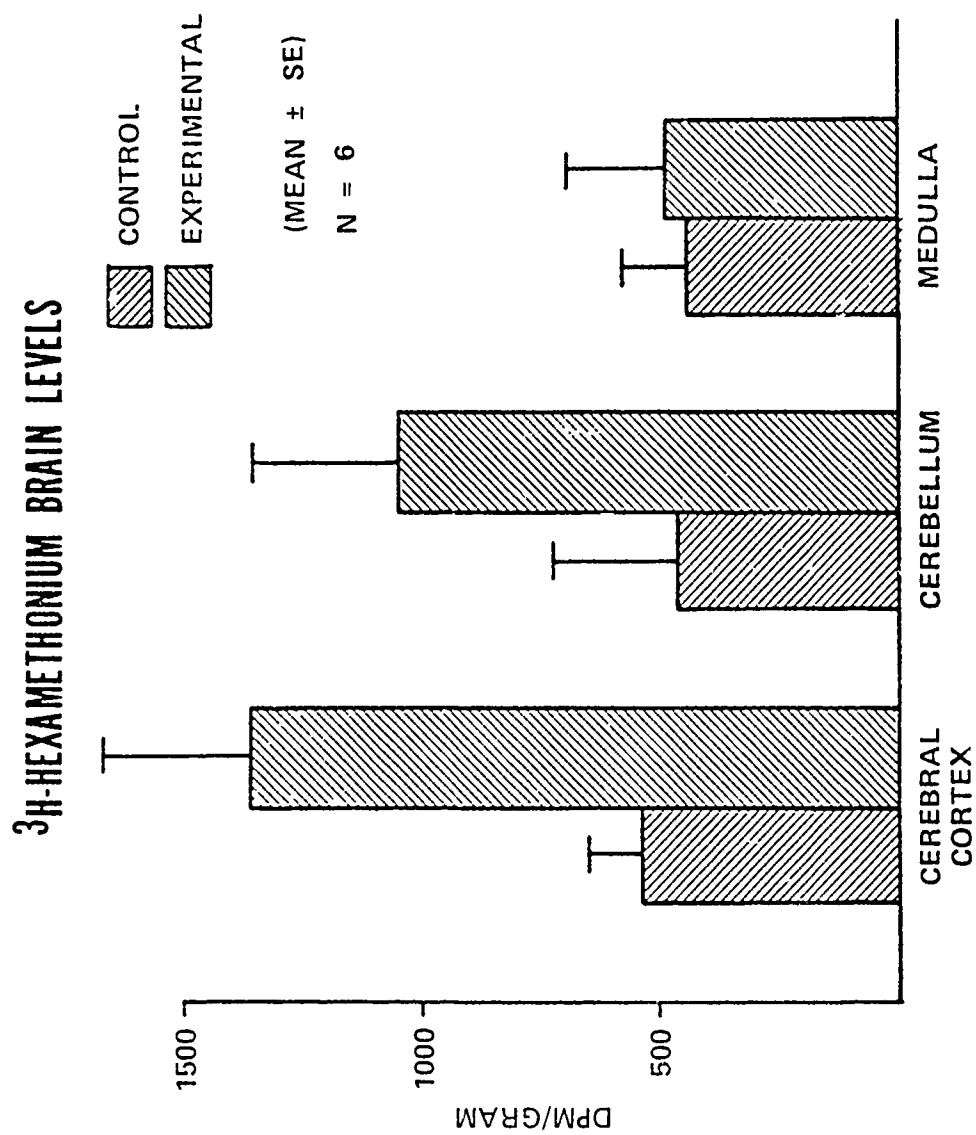


FIGURE 4

CHANGE IN ^3H HEXAMETHONIUM BRAIN LEVELS

<u>BRAIN AREA</u>	<u>N</u>	<u>% CHANGE FROM CONTROL</u>	<u>SIGNIFICANCE</u>
CEREBRAL CTX	6	+155	p0.02
CEREBELLUM	6	+122	p0.20
MEDULLA	6	+9	ns

FIGURE 5

AMOUNTS OF HEXAMETHONIUM IN BRAIN

(pMOLES x 10⁻⁶/GRAM)

<u>BRAIN AREA</u>	<u>UNTREATED</u>	<u>SOMAN</u>
CEREBRAL CTX	5.4	14
CEREBELLUM	4.7	11
MEDULLA	4.5	4.9

FIGURE 6

BRAIN PATHOLOGY INDUCED BY ORGANOPHOSPHATE POISONING WITH THE NERVE AGENT SOMAN

J.M. Petras
Division of Neuropsychiatry
Walter Reed Army Institute of Research
Washington, DC 20307

A number of chemical (3,6,8,12) pharmacological (2,20), physiological (10,11,18) and clinical (8,14) studies have attempted to define the effects of chemical warfare agents, whereas, the pathological effects of these organophosphates has remained largely undocumented. Recent studies have indicated seriously damaging effects upon the brains of rats (16,9,13). The present report reviews our original observations (16) by comparing the results of Soman surviving rats, cats and cynomolgus monkeys.

METHODS

All animals were observed for evidence of neurological signs following Soman or saline injection. Medical treatment was not provided in order to assess the effects of the nerve agents action upon the nervous system in cases uncomplicated by antidote administration. Upon the conclusion of the observation and postinjection experimental period, euthanasia was performed and the central nervous system perfusion fixed. The brains and spinal cords were dissected, removed in toto, and subsequently prepared for processing with specialized neuroanatomical stains. The Nauta(16) and Fink-Heimer(5) techniques were used for degenerated axons and their terminals (Figs 1-3); the Woelke and Weil methods for normal and degenerated myelin (Fig. 4); the Nissl method for normal and chromatolytic nerve cells and for neuroglial proliferation. The conventional method of hematoxylin and eosin was used for nuclear details of cellular infiltrates and inflammatory responses.

*The views of the author do not purport to reflect the position of the Department of the Army or the Department of Defense, (para 4-3, AR 360-5). Reprinted with permission of the 1984 Army Science Conference Proceedings, West Point, N.Y. In conducting the research described in this report, the investigator adhere to the 'Guide for the Care and Use of Laboratory Animals', as promulgated by the Committee on Care and Use of Laboratory Animals of the Institute of Laboratory Animal Resources, National Research Council.



SOMAN INTOXICATED RATS.

Nineteen male rats were available for study.* Four served as uninjected controls while 15 individuals were injected intramuscularly with Soman at dose levels of 79.4-114.8 $\mu\text{g/kg}$. Neurological signs and their severity varied widely. Four animals seized while generalized muscular fasciculations, tremor and limb jerks were observed in four other cases. Localized muscular fasciculations or tremor and head bobbing were present in three additional animals and the remaining four showed no neurological signs. Asymptomatic animals, and those experiencing local signs, were devoid of brain pathology, including infarcts. Brain pathology was found in all animals of the seizure group and three of four animals of the group with generalized tremors, fasciculations and limb movements. Widespread axon degeneration was present in the forebrain and midbrain and could be traced into the hindbrain and spinal cord. The amount of axon degeneration is usually graded qualitatively on a scale such as: none, sparse, moderate, abundant or massive. The damaged sites varied from sparse to massive. The pattern of degeneration was comparable in all affected cases and the changes were bilateral. Axon degeneration was present in the cerebral cortex, basal ganglia, thalamus, subthalamic region, hypothalamus (fig. 3), hippocampus, fornix (figs. 1 & 2), septum, preoptic area, superior colliculus, pretectal area, basilar pontine nuclei, medullary tegmentum and corticospinal tracts.

We cannot specify the mechanism of brain damage on the basis of the neuroanatomical data, but we can state that the pattern of degeneration across brain regions following Soman exposure does not resemble that caused by experimental fetal hypoxia(4) or by the neurotoxicity produced by the organophosphate tri-ortho-cresylphosphate (1, 7).

FIGURES 1-4. If the axon of a nerve cell is surgically cut, the separated axon will undergo a disintegration. Following euthanasia, the brains of Soman survivors were perfused and then removed from the skull. Brain slices were collected in serial order and treated with specialized silver staining methods to reveal, under the lenses of the light microscope, the degenerated axonal debris. Nerve cells and their axons may be killed by poisoning, infection, accidental injury, stroke or metabolic failure. The injured cells may respond in several ways to the insult, i.e., chromatolysis of the cell body, disfigurement of cellular organelles, altered staining properties of the cytoplasmic matrix, demyelination and axonal disintegration (1,4,7,9,13,17,18,20). Axon and myelin degeneration are the focus of the accompanying illustrations. Normal axons are seen in figure 1 and were present in a non-injected control rat. Brain slices were stained in the same way as Soman exposed rats. Degenerating axons of the fornix are seen in figure 2 and were present in a rat surviving single exposure to Soman. The nerve-bundles of the fornix can be followed into a structure named the mammillary bodies of the hypothalamus. The terminal arborizations of degenerating fornix axons within the mammillary bodies are illustrated in figure 3 and were present in a Soman exposed rat. Degenerated myelin (fig. 4 arrows) was present in the corticostriate bundles of a Soman surviving rat.

*The rats were obtained from the study of Elsmore, T.F. (1981) "Circadian Susceptibility to Soman Poisoning," *Fundam. Appl. Toxicol.*, 1:238-241.

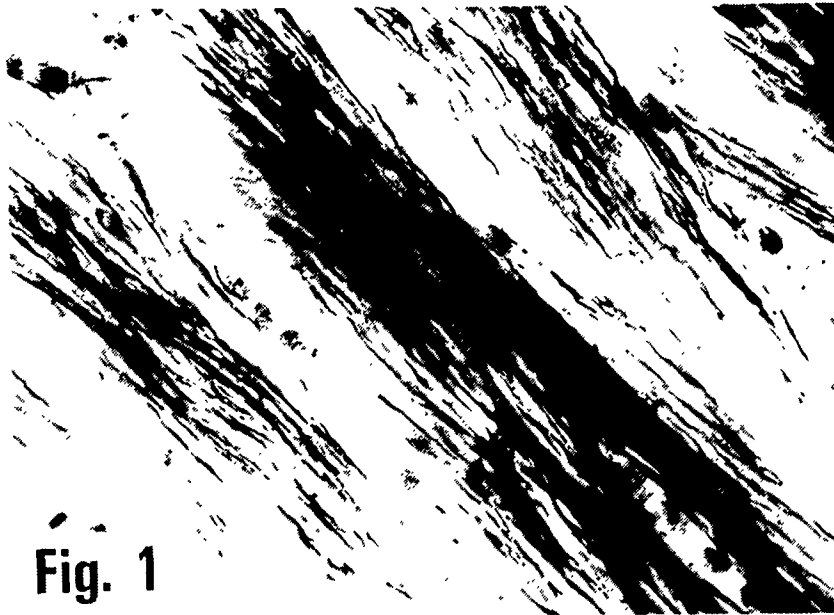


Fig. 1

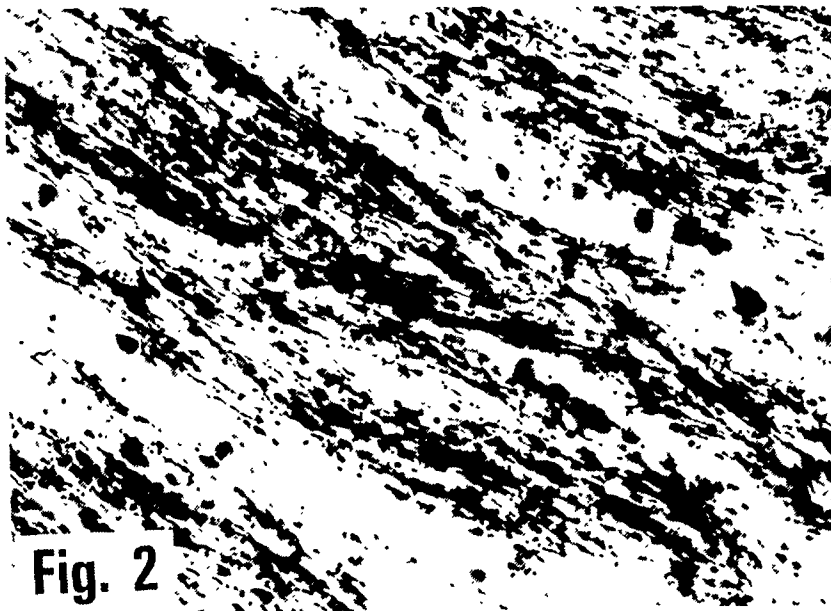


Fig. 2

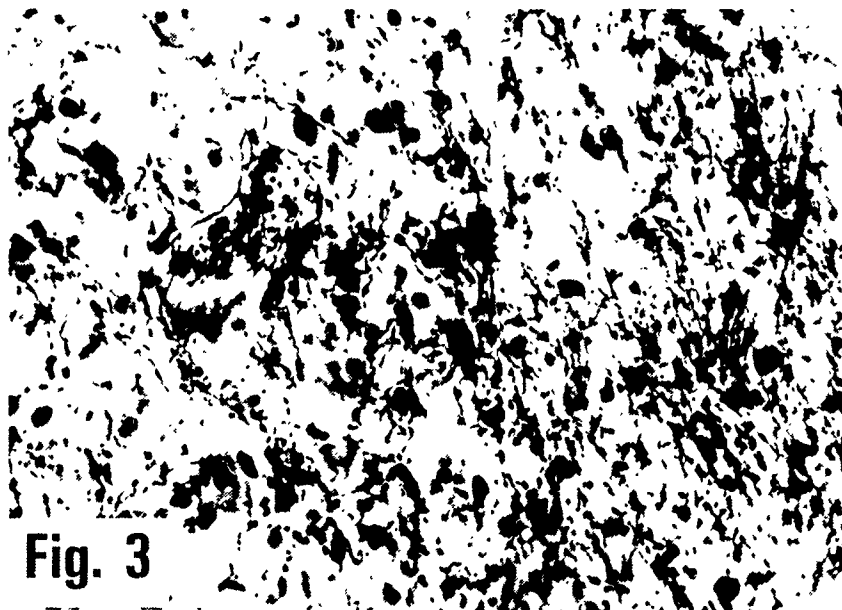


Fig. 3



Fig. 4

SOMAN INTOXICATED CATS.

Sixteen cats of either sex were injected intramuscularly with the nerve agent Soman. The dosage varied from 8.25-13.5 $\mu\text{g/kg}$. Two animals received an intramuscular dose of the saline diluent only. Of 11 survivors, neurological signs were present in one case and the remaining ten cases were asymptomatic. Six asymptomatic animals were selected for a second intoxication at the same dose level as given one week earlier. Of four survivors, neurological signs were present in one case. In summary, one out of 11 surviving one dose showed signs and one of four surviving two doses showed signs.

Pathological changes were found in the single exposure cat with neurological signs. Grand mal seizures and status epilepticus occurred in this cat. Axon degeneration was present in the cerebral cortex, basal ganglia, thalamus, midbrain, hindbrain and spinal cord. Multiple bilateral infarcts of the forebrain were present also.

Among the twice exposed cats, two showed evidence of axon degeneration, one that had shown signs after the second exposure and one that failed to show signs after the first and the second exposures.

From the Soman induced mortality group of cats, one individual survived beyond the 12 hours postexposure criterion. In sharp contrast to the Soman survivors with axon degeneration, this mortality case revealed evidence of cellular pathology in cerebral and cerebellar cortical neurons. These "red cells" contain a glassy or homogenous cytoplasmic matrix which is strongly eosinophilic, thus the name "red cells." The neuronal nuclei are of irregular outline and usually pyknotic. In contrast, "red neurons" were not identified in the brain damaged Soman survivors. The presence of red cells is indicative of cerebral and cerebellar anoxia.

Compared with rats, the limbic system in the affected cats appeared to have been minimally involved; degenerated axons were present in small areas of the cingulate gyrus. By comparison, the affected rats contained abundant axon degeneration in the cingulum, cingulate gyrus, anterior thalamic nuclear group, and fornix.

A comparison of the rat and cat experimental findings led to the following conclusions:

1. Brain damage is not rat specific.
2. Seizures need not occur in rats or in cats for the damage to be present.
3. That species variation may be expected with respect to the presence or severity of damage in different functional regions of the brain.

SOMAN INTOXICATED MONKEYS.

Considering the species differences between rats and cats, it was important to extend the analyses to a species more similar to man. Eight cynomolgus monkeys received intramuscular injections of Soman within a dose range of 3.6-6.4 $\mu\text{g/kg}$. One control subject received the saline diluent alone. Six monkeys survived the intoxication. Two of these experienced grand mal seizures, while the remaining four cases appeared asymptomatic. Three weeks later, two of the clinically asymptomatic monkeys received a second Soman injection at the same dose level. The second intoxication produced generalized muscular fasciculations and tremors, dysmetria, and trunkal ataxia but no grand mal seizures. Multiple bilateral infarcts were found in the

brains of the two monkeys surviving grand mal seizures. The affected areas included, among others, the basal ganglia and associated nuclei, amygdala, anterior commissure, substantia innominata, internal capsule and cerebral peduncle.

The nature of the damage in the affected primates suggests impairment of the vascular supply. In contrast, the findings in rats and cats are not entirely consistent with this interpretation. First, we have found brain damage in a cat which was asymptomatic after both the first and second exposures to the nerve agent. Second, among rats we have found that seizures need not be present for the damage to occur. Third, the pattern of damage in the rat is not similar to that observed after hypoxia. Although the mechanisms of Soman induced pathology are incompletely understood, and the number of animals studied is small, more than one mechanism of pathogenesis may be operable in each of the species.

A number of conclusions may be drawn from these comparative experiments:

1. Extensive and irreparable damage can result from nerve agent exposure.
2. Seizures and neurological signs need not be present for the damage to occur.
3. The region most severely affected is the forebrain.
4. The pattern of damage within the forebrain is not identical in all species.

COMMENTS

The mature brain and spinal cord, unlike other organ systems, does not possess the capacity to produce new nerve cells. Injured neurons are capable of sprouting new processes, but functional recovery is largely prevented by the formation of dense scar tissue at the site of injury. If the number of lost nerve cells comprising a functional population is low, the remaining neurons can subserve the functions of the lost tissue and the impairments will be less severe or of temporary duration.

The nature of the brain damage in rats, cats and monkeys suggests that the damage is both permanent and extensive in many cases. Several functional systems are affected and the severity of the lesions implies for patients multiple impairments both immediate and long-term. One could infer that humans surviving Soman poisoning may have impairments of skilled-movements, posture, locomotion, memory, cognition, autonomic regulation and psychiatric disorders. The overriding conclusion from all these experiments is that extensive and irreparable brain damage can result from nerve agent exposure.

Controlled animal experiments to assess the value of therapy in preventing neuropathology following Soman exposure have not been performed. The military use of nerve agents on the battlefield could produce large numbers of combat casualties. Undoubtedly some will not receive immediate medical attention. Survivors who appear clinically asymptomatic may not completely escape brain damage and those survivors who have seizures may be injured as a result of brain anoxia.

LITERATURE CITED

1. Cavanagh, J.B. and G.N. Patangia (1965) Changes in the central nervous system in the cat as the result of tri-O- cresylphosphate poisoning. *Brain* 88: 165-180.
2. Dirnhuber, P., M.C. French, D.M. Green, L. Leadbeater and J.A. Stratton (1978) The protection of primates against Soman poisoning by pretreatment with pyridostigmine. *J. Pharm. Pharmacol.*, 31: 295-299.
3. Doeblner, J.A., T.M.A. Bocan, R.A. Moore, T-M. Shih and A. Anthony (1983) Brain neuronal RNA metabolism during acute Soman intoxication. *Neurochem. Res.*, 8: 997-1011.
4. Faro, M.D. and W.F. Windle (1969) Transneuronal degeneration in brains of monkeys asphyxiated at birth. *Expt. Neur.*, 24: 38-53.
5. Fink, R.P. and L. Heimer (1967) Two methods for selective silver impregnation of degenerating axons and their synaptic endings in the central nervous system. *Brain Research*, 4: 367-374.
6. Fonnum, F. and S.H. Sterri (1981) Factors modifying the toxicity of organophosphorus compounds including Soman and Sarin. *Fund Appl. Toxicol.*, 1: 143-147.
7. Illis, L., G.N. Patangia and J.B. Cavanagh (1966) Boutons terminaux and tri-ortho-cresylphosphate neurotoxicity. *Expt. Neurol.*, 14: 160-174.
8. Jovic, R.C. (1974) Correlation between signs of toxicity and some biochemical changes in rats poisoned by Soman. *Eur. J. Pharmacol.*, 25: 159-164.
9. Lemerrier, G., P. Carpentier, H. Sentenac-Roumanou and P. Morelis (1983) Histological and histochemical changes in the central nervous system of the rat poisoned by an irreversible anticholinesterase organophosphorus compound. *Acta Neuropathol.*, 61: 123-129.
10. Lipp, J.A. (1968) Cerebral electrical activity following Soman administration. *Arch. Int. Pharmacodyn.*, 175: 161-169.
11. Lipp, J.A. and T.J. Dola (1978) The effects of atropine upon the cerebrovascular system during Soman-induced respiratory depression. *Arch. Int. Pharmacodyn.*, 235: 211-218.
12. McDonough, J.H. Jr., B.E. Hackley, Jr., R. Cross, F. Samson and S. Nelson (1983) Brain regional glucose use during Soman-induced seizures. *Neurotoxicol.*, 4: 203-210.
13. McLeod, C.G., A.W. Singer & D.G. Harrington (1984) Acute neuropathology in Soman poisoned rats. *Neurotoxicol.*, (in the press).
14. Namba, T., C.T. Nolte, J. Jackrel and D. Grob (1971) Poisoning due to organophosphate insecticides. *Amer. J. Med.*, 50: 475-492.

15. Nauta, W.J.H., (1964) Unpublished technique, see Ebbesson, S.O.E. (1970) The selective silver-impregnation of degenerating axons and their synaptic endings in nonmammalian species. In: W.J.H. Nauta and S.O.E. Ebbesson, Eds., "Contemporary Research Methods in Neuroanatomy", pp. 132-161, Springer-Verlag, New York.
16. Petras, J.M. (1981) Soman neurotoxicity. *Fundam. Appl. Toxicol.*, 1: 242.
17. Prineas, J. (1969) The pathogenesis of dying-back polyneuropathies. An ultrastructural study of experimental acrylamide intoxication in the cat. *J. Neuropath. Expt. Neurol.*, 28: 598-621.
18. Sim, V.M. (1975) Anticholinesterase poisoning. In: P.G. Waser, Ed., "Cholinergic Mechanisms," pp. 395-398, Raven Press, N.Y.
19. Spencer, H.H. and H. Schaumburg (1977) Ultrastructural studies of the dying-back-process. III. The evolution of experimental peripheral giant axonal degeneration. *J. Neuropath. Expt. Neurol.*, 36: 276-299.
20. Wolthuis, O.L., F. Berends and E. Meeter (1981) Problems in the therapy of Soman poisoning. *Fundam. Appl. Toxicol.*, 1: 183-192.

ANTICONVULSANT THERAPY FOR OP-INDUCED LETHALITY

D.E. JONES*, I. KOPLOVITZ, D.G. HARRINGTON, D.E. HILMAS
US Army Medical Research Institute of Chemical Defense
Aberdeen Proving Ground, MD 21010

*Mailing Address: Commander
US Army Medical Research Institute
of Chemical Defense
ATTN: SGRD-UV-DD/Major Dennis E. Jones
Aberdeen Proving Ground, MD 21010

ABSTRACT

The gamma-amino butyrate (GABA)-active anticonvulsant, diazepam (DZ), was evaluated for efficacy against soman-induced lethality in the guinea pig. Treatment with DZ alone, DZ plus atropine (ATS), and DZ plus pralidoxime chloride (2-PAM) did not provide protection greater than that afforded by the treatment with ATS plus 2-PAM. DZ, however, in combination therapy with ATS plus 2-PAM, was found to increase the protection afforded by the optimal dose combination of ATS plus 2-PAM. Other GABA-active anticonvulsants were evaluated, both in treatment and pretreatment modes, and found to provide soman antidotal efficacy similar in scope and degree as that provided by DZ. In addition, this class of compounds was found to be efficacious against lethality induced by the organophosphate nerve agent, tabun (GA).

Introduction

The purpose of this presentation is to present data accumulated from testing and evaluation of anticonvulsant therapies against nerve agent-induced lethality. The purpose of those tests has been to screen compounds for efficacy against agent-induced lethality and to determine the full range and limits of that protective efficacy.

When compounds are screened and evaluated for this type of efficacy, the classes of compounds that immediately come to mind are the oximes, the cholinolytics, and, more recently, the pretreatment carbamates. The underlying mechanisms of action for those types of therapies, although by no means conclusive, have at least been well explored and the mechanism of action postulated (1,2,3). Why, then, the concern with a so-called class of compounds referred to as anticonvulsants?

The rationale for this is basically simple. Therapy or treatment of a pathogenic condition, such as nerve agent toxicity, can consist of specific antidotal therapy, such as that supposedly manifested by the oximes, as well as symptomatic treatment of agent-induced effects. Indeed, maintenance or assistance of respiratory function has been shown to be one of the best methods for treatment of agent-induced toxicity (4).

In this regard, since agent-induced convulsions are one of the primary signs of agent toxicity (5), the rationale for symptomatic control of convulsions would, in itself, seem logical.

Indeed, this avenue has been explored in the past and, in fact, has proven valuable. In one of the original studies in this area, Lipp et.al., it was shown that the anticonvulsant, diazepam, was effective in abating soman-induced seizures in rabbits and in rhesus monkeys (6). Since that time, several other investigators have shown diazepam to be effective not only in controlling agent-induced seizures, but to increase both mean survival time and percent survival of agent-challenged animals (7,8). Indeed, the results of these studies have been so encouraging that Boskovic has stated that, based on the results reported in the literature, "Diazepam is the drug of choice in the symptomatic treatment of organophosphate poisoning." (9). For these reasons, we are interested in screening and evaluating anticonvulsants as a potential adjunct therapy to agent poisoning.

against soman (GD) challenge in guinea pigs. We elected to initially evaluate diazepam as a third component BZP, as it is a prototype BZP with extensive literature reports showing efficacy against nerve agents (6,7,8). The methods of this particular third component efficacy screen were outlined previously (15). Briefly, each bar represents a group of 10 animals challenged with an LD90 of GD and treated with the therapy indicated in the figure. As indicated earlier, candidate third components are screened alone and in combination with atropine (ATS), 2-PAM, and ATS plus 2-PAM. One additional problem that is frequently encountered with the BZP compounds is that of extremely poor solubility. The diazepam tested here was in a commercial diazepam vehicle (15), that being the best vehicle we could identify. As the range and limits of acute lethality could not be determined for this compound within physiological dose volumes, the doses tested here indicate the upper limits of diazepam solubility and fractions thereof.

The point that should be noted here is that diazepam alone, or when combined with ATS or 2-PAM, did not provide greater protection against GD than that afforded by the optimal dose of ATS/2-PAM. When diazepam was given in conjunction with the optimal dose of ATS/2-PAM, it provided a dose-related increase in protection, depicted here as an increase in percent survivors. The results here reflect what has been reported in the literature (6,7,8) and tend to validate the methods outlined for evaluating third component anti-convulsants.

As was previously indicated (15), we are also concerned with the efficacy of antidotal compounds against other nerve agents. Figure 3 shows the screening results of diazepam against the nerve agent tabun (GA). Diazepam has also been reported to be efficacious against this agent (7,8) and we see those reports confirmed here. Diazepam provided greater efficacy than the optimal ATS/2-PAM dose when combined as a third component, but not when tested alone or as a singular adjunct to either ATS or 2-PAM.

As was also previously indicated (15), compounds which are identified as being more efficacious than ATS/2-PAM are optimal dose tested to assess their full range and limits of protective efficacy. Figure 4 illustrates these results in GD-challenged guinea pigs. Here we see that diazepam increased protective efficacy in a dose-dependent manner when tested alone, combined with ATS, 2-PAM, or ATS/2-PAM. It should be noted, however, that no dose of diazepam when tested alone, with ATS, or with 2-PAM provided protection equivalent to that provided by the optimal dose of ATS/2-PAM without diazepam. This is shown in Figure 4 as a dose of ATS/2-PAM combined with 0.0 mg/kg diazepam providing a protective ratio (PR) of 3.0. When diazepam is added to ATS/2-PAM therapy, the PR increases from 3.0 to approximately 4.7, an 85 percent relative increase in the PR. It should be further noted that the increase in PR due to addition of diazepam to ATS/2-PAM is greater than the total PR afforded by any dose combination of diazepam alone or combined with ATS or 2-PAM.

With these studies thus validating the premise that the BZP's can, indeed, provide protection against the nerve agents, we were next interested in looking at other BZP's to hopefully identify those which were capable of providing protection similar to or greater than that afforded by diazepam, but with less of the objectionable qualities of diazepam.

As has been previously mentioned, one of the problems with diazepam is its relative insolubility, especially in aqueous vehicles. In addition, diazepam, as prepared in the present commercial valium vehicle, is not compatible to admixing with other compounds (16). This, of course, presents a problem if diazepam were to be considered for combination in an auto-injector with a cholinolytic and/or oxime. Figure 5 illustrates the screening results of the water soluble BZP, midazolam (17), against GD in guinea pigs. The doses tested here represent the upper limits of water solubility and fractions thereof. Here, as with diazepam, midazolam is efficacious when combined with the optimal dose of ATS/2-PAM, but not when tested alone or in combination with either ATS or with 2-PAM.

Again, we were concerned with the ability of compounds to provide protection against the other nerve agents. Figure 6 shows the results of screening midazolam against GA in guinea pigs. Here we see that midazolam is again efficacious when combined with ATS plus 2-PAM, but not alone or in combination with only ATS or 2-PAM.

Figure 7 illustrates the results of a dose optimization study for midazolam against GD in guinea pigs. Here we see that midazolam alone increases the PR only slightly, but when combined with ATS/2-PAM, it increases the PR from 3.00 to approximately 4.10. This figure also clarifies a point about which we had some concern, that of the vehicle effect of the commercial diazepam solvent. The commercial diazepam vehicle consists of 40 percent propylene glycol, 10 percent ethanol, 5 percent benzoic acid, 5 percent sodium benzoate, and 1.5 percent benzyl alcohol (16). Since midazolam is both water soluble to the limits of the doses tested here and extremely soluble in the commercial diazepam vehicle, the opportunity to evaluate the vehicle effects of the commercial diazepam solvent was possible. As can be seen in Figure 7, there is no appreciable difference in response between the aqueous vehicle group and the diazepam vehicle group, indicating no vehicle effect on either response to agent or to therapy. This fact is important in that although many of the compounds of this general class (that we have or intend to evaluate) are not water soluble, most have been found to be reasonably soluble in the commercial diazepam solvent. These findings allow us the opportunity to evaluate water-soluble compounds in a vehicle shown to have minimal effect on both BZP and agent response.

It is important to cover one additional area concerning anticonvulsant therapy for nerve agent poisoning, that area being pretreatment of agent poisoning. An additional interesting characteristic of diazepam is its rapidity of absorption following oral administration. Figure 8, a composite of data published in the British Journal of Anesthesiology (18), illustrates human plasma levels of diazepam following oral and intramuscular (IM) administration. Note that much higher plasma levels are obtained following oral dosing as compared to parenteral dosing and, further, that peak plasma levels occur much more rapidly. This data would indicate that oral treatment may even prove more effective than IM. In addition, many investigators have shown diazepam to be an effective pretreatment compound (7,8,9).

As was also previously stated (19), we are interested in identifying and evaluating effective oral pretreatment antidotes. Figure 10 illustrates the pretreatment efficacy screening results for diazepam given orally. Here,

again, we see confirmation that diazepam is, indeed, efficacious as an oral pretreatment compound when combined with ATS/2-PAM.

Figure 10 shows similar screening results for midazolam efficacy against GD in guinea pigs. Again, we see that midazolam is also efficacious as an oral pretreatment nerve agent antidote.

I do not intend to relate to you the results of all the BZP efficacy studies we have done, but rather show you data accumulated which indicate that the BZP's are as effective as oral pretreatment and parenteral treatment compounds for nerve agent poisoning, especially when used as a third component adjunct to ATS/2-PAM therapy. We are presently in the process of evaluating several proprietary BZP's, which have proven efficacious and which promise to be much less incapacitating than the more traditional BZP anticonvulsants. Our ultimate intent is to identify, develop, and field a third component anticonvulsant, which is capable of providing significantly enhanced protection at nonincapacitating doses.

References

1. Wilson, I.B., J. Biol. Chem., 190:111-117, 1951.
2. Wilson, I.B. and S. Ginsburg, Biochem. Biophys. Acta., 18:168-170, 1955.
3. Gordon, J.J., L. Leadbeater, and M.P. Maidment, Toxicol. and Appl. Pharm., 43:207-216, 1978.
4. Taylor, P., Goodman and Gilman's: The Pharmacological Basis of Therapeutics, 6th. Ed., Macmillan Publishing Co., Inc., New York, New York, 6:100-119, 1980.
5. Johnson, D.D. and W.C. Wilson, European J. Pharmacol., 34:127-132, 1975.
6. Lipp, J.A., Electroenceph. Clin. Neurophysiol., 32:557-560, 1972.
7. Lipp, J.A. and T.J. Dola, Arch. Int. Pharmacodyn., 246:138-148, 1980.
8. Inns, R.H. and L. Leadbeater, J. Pharm. Pharmacol., 35:427-433, 1983.
9. Boskovic, B., Fundamental and Appl. Toxicol., 1:203-213, 1981.
10. Costa, E. and P. Greengard, (eds.), Mechanisms of Action of Benzodiazepines, Raven Press, New York, New York, 1975.
11. Otuska, M., Pharmacology and the Future of Man: Proceedings of the Fifth International Congress on Pharmacology, Vol. 4, Archison, G.N and Bloom, F.E., eds., S. Karger, Basel, 186-201, 1973.
12. Braestrup, C., M. Nielsen, and T. Honore, Advances in Biochem. Psychopharm., 37:237-245, 1983.
13. Zbinder, G. and L.O. Randall, Adv. Pharmac., 5:213-291, 1967.
14. Bennet, D.A. and B. Petrack, Drug Development Res., 4:75-82, 1984.
15. Jones, D.E., I. Koplovitz, D.G. Harrington, D.E. Hilmas, and C.J. Canfield, Presentation, Fourth Annual Chemical Defense Bioscience Review, 30 May-1 June, 1984.
16. Baker, C.E., Jr., Pub., Physicians Desk Reference, 36th Ed., 1623-1625, 1982.
17. Greenblatt, D.J., M. Divoll, D.R. Abernatly, H.R. Ochs, and R.I. Shader, Clinical Pharmacokinetics, 8:233-252, 1983.
18. Kanto, J., Br. J. Anesth., 46:817, 1974.
19. Koplovitz, I., D.E. Jones, D.E. Harrington, D.E. Hilmas, and C.J. Canfield, Presentation, Fourth Annual Chemical Defense Bioscience Review, 30 May-1 June, 1984.

PROPOSED BENZODIAZEPINE (BZP) RECEPTOR LIGANDS

<u>Classification</u>	<u>Binding</u>	<u>Action</u>	<u>Example</u>
I. BZP Agonist	1. Binds to BZP Receptor 2. Binding Affinity Increased by GABA Agonist e.g. GABA/Muscimol	Mimics GABA (anticonvulsive)	Diazepam
II. BZP Antagonist	1. Binds to BZP Receptor 2. Binding Affinity Not Affected by GABA Agonist	1. Are Themselves Inactive 2. Block Activity of BZP such as Diazepam	Roche Compd 15-1788
III. BZP Inverse Agonist	1. Binds to BZP Receptor 2. Binding Affinity Increased by GABA Agonist	Antagonize Effects of GABA (convulsive)	DMCM (β -Carboline)

Figure 1

Initial Efficacy of Diazepam with Atropine/2-PAM Against (4.3xLD50) GD in Guinea Pigs

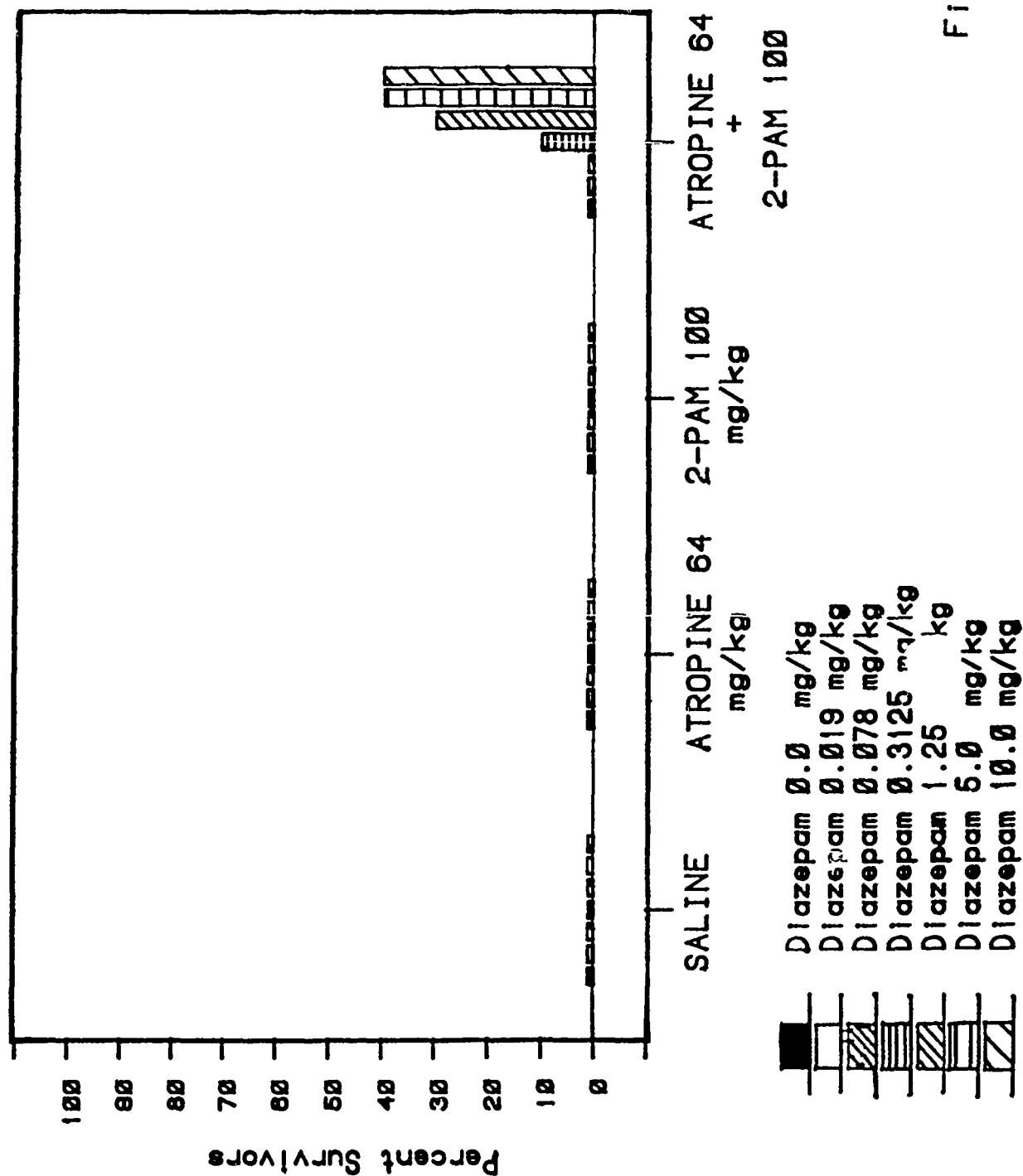


Figure 2

Initial Efficacy of Diazepam and Atropine/2-PAM Against (5.36xLD50) GA in Guinea Pigs

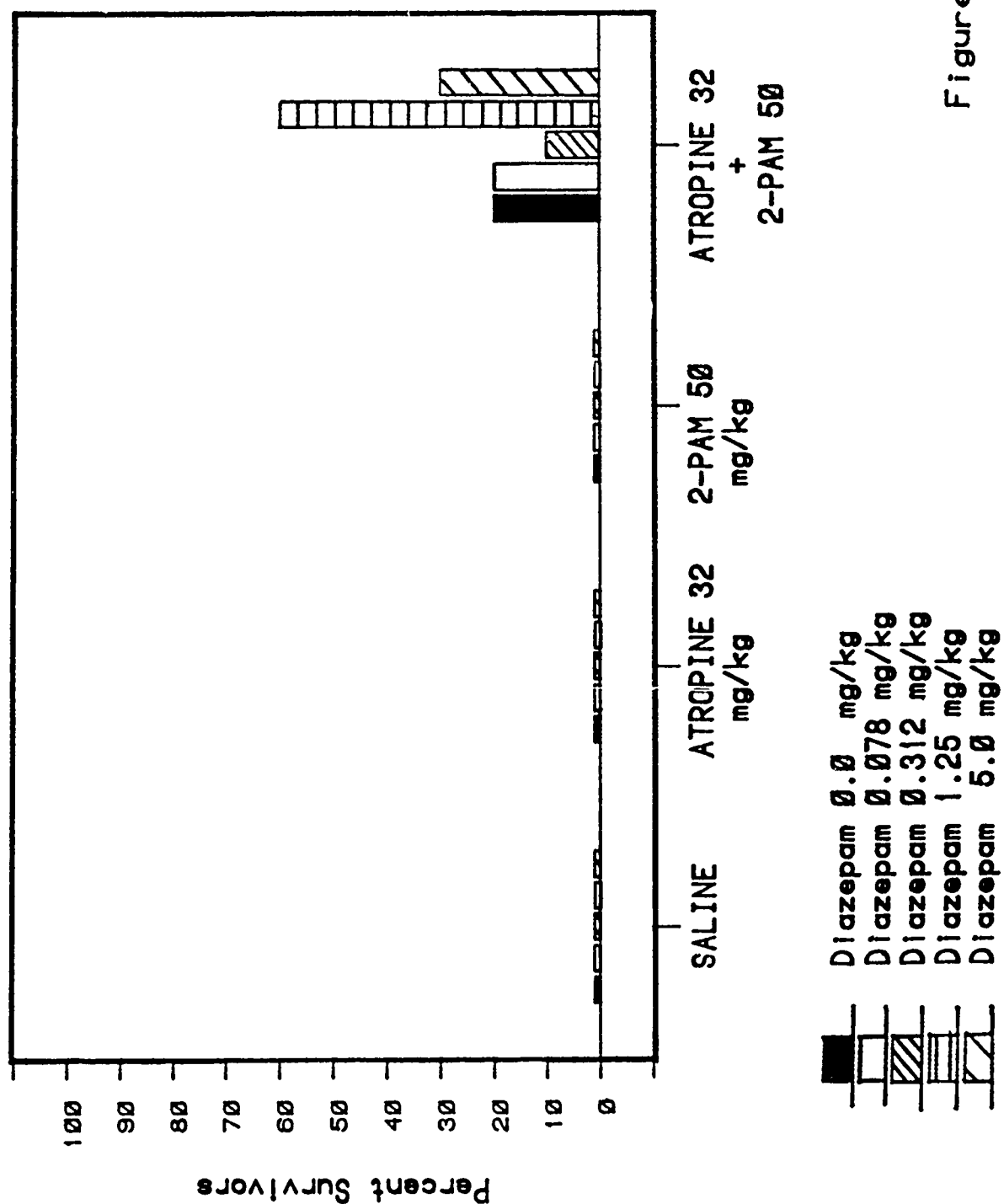
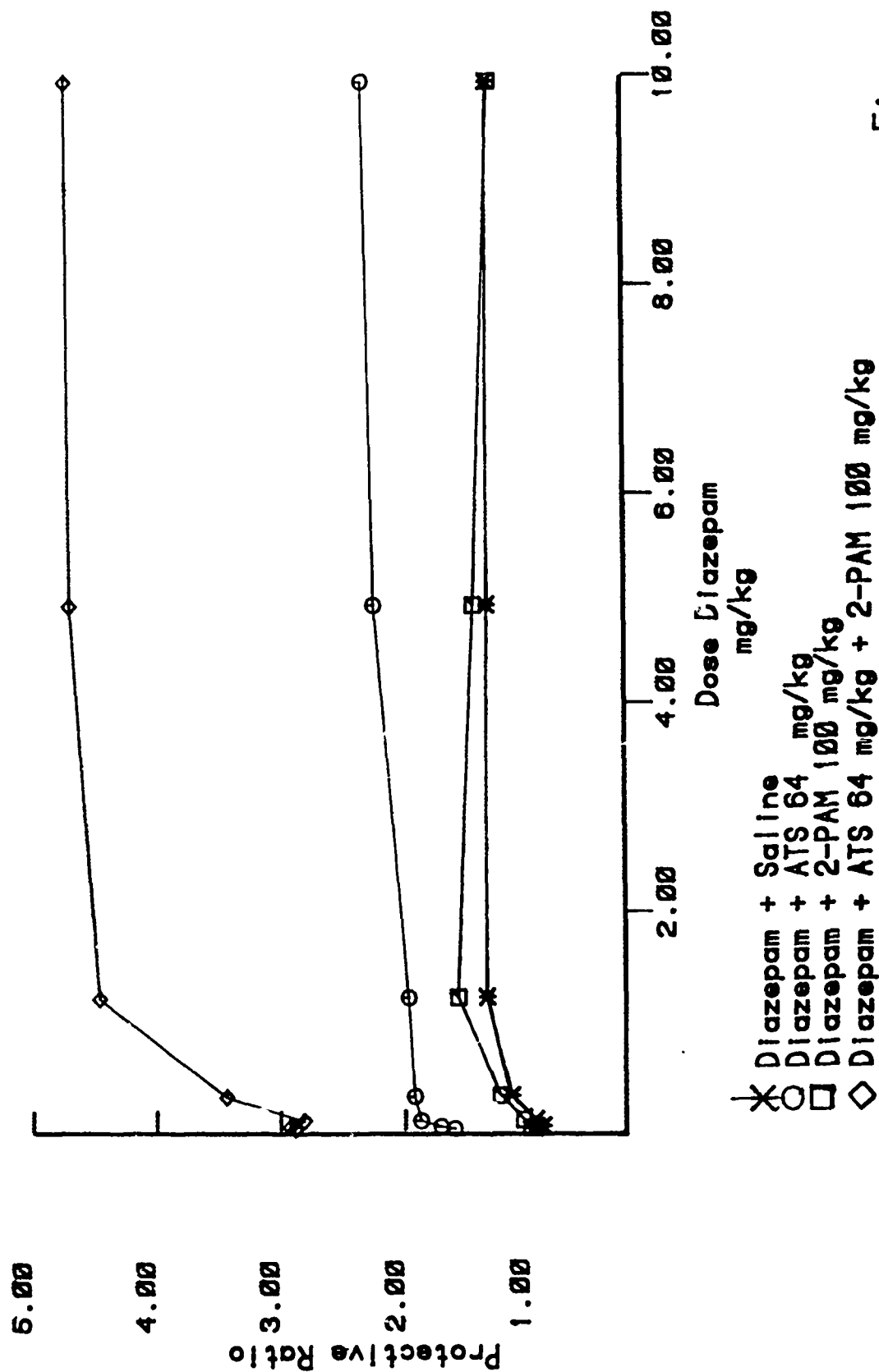


Figure 3

Efficacy of Diazepam Alone and with Atropine/2-PAM CI Against GD in Guinea Pigs



Initial Efficacy of Midazolam with Atropine/2-PAM Against (4.3xLD50) GD in Guinea Pigs

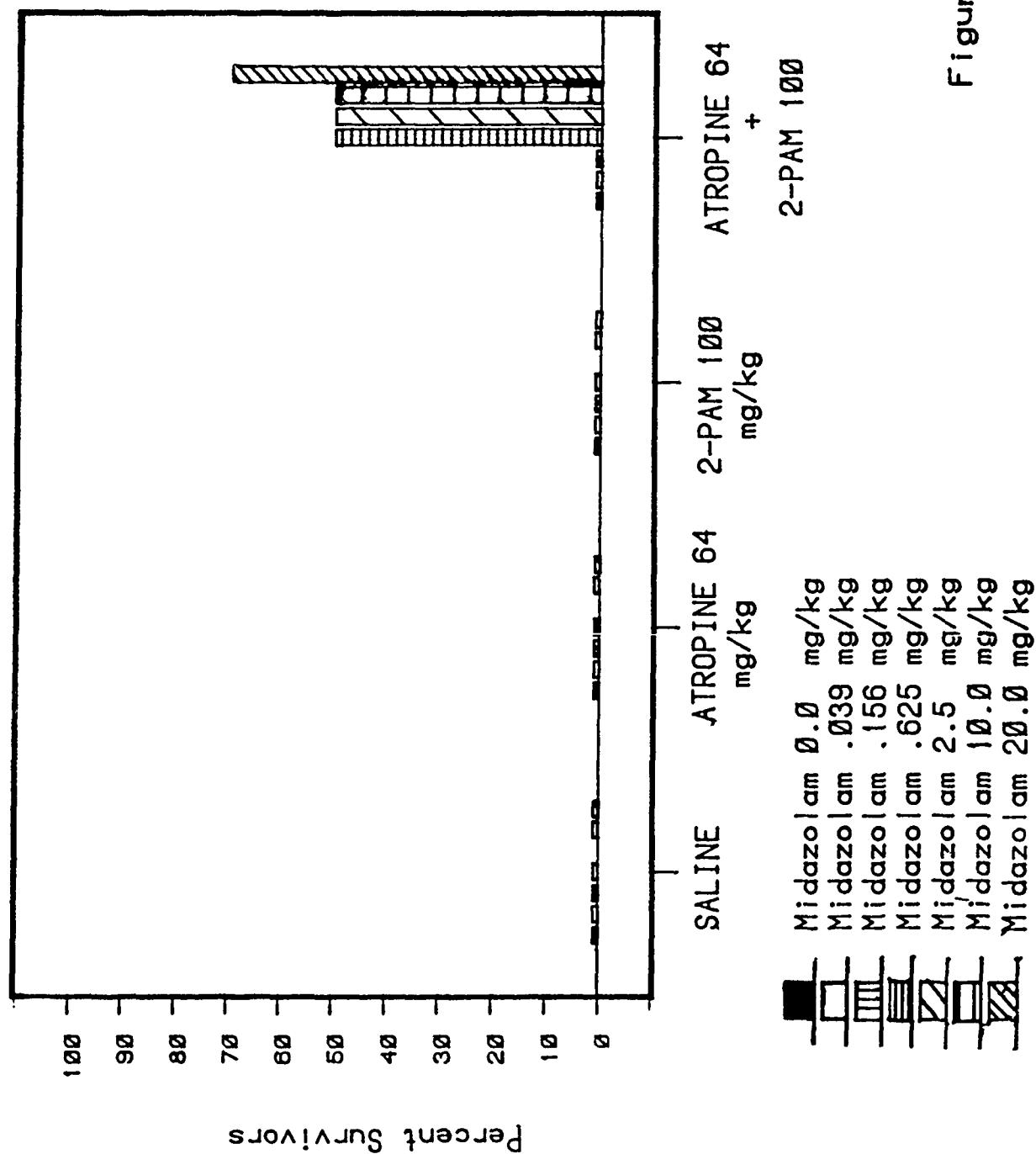


Figure 5

Initial Efficacy of Midazolam and Atropine/2-PAM Against (5.36xLD50) GA in Guinea Pigs

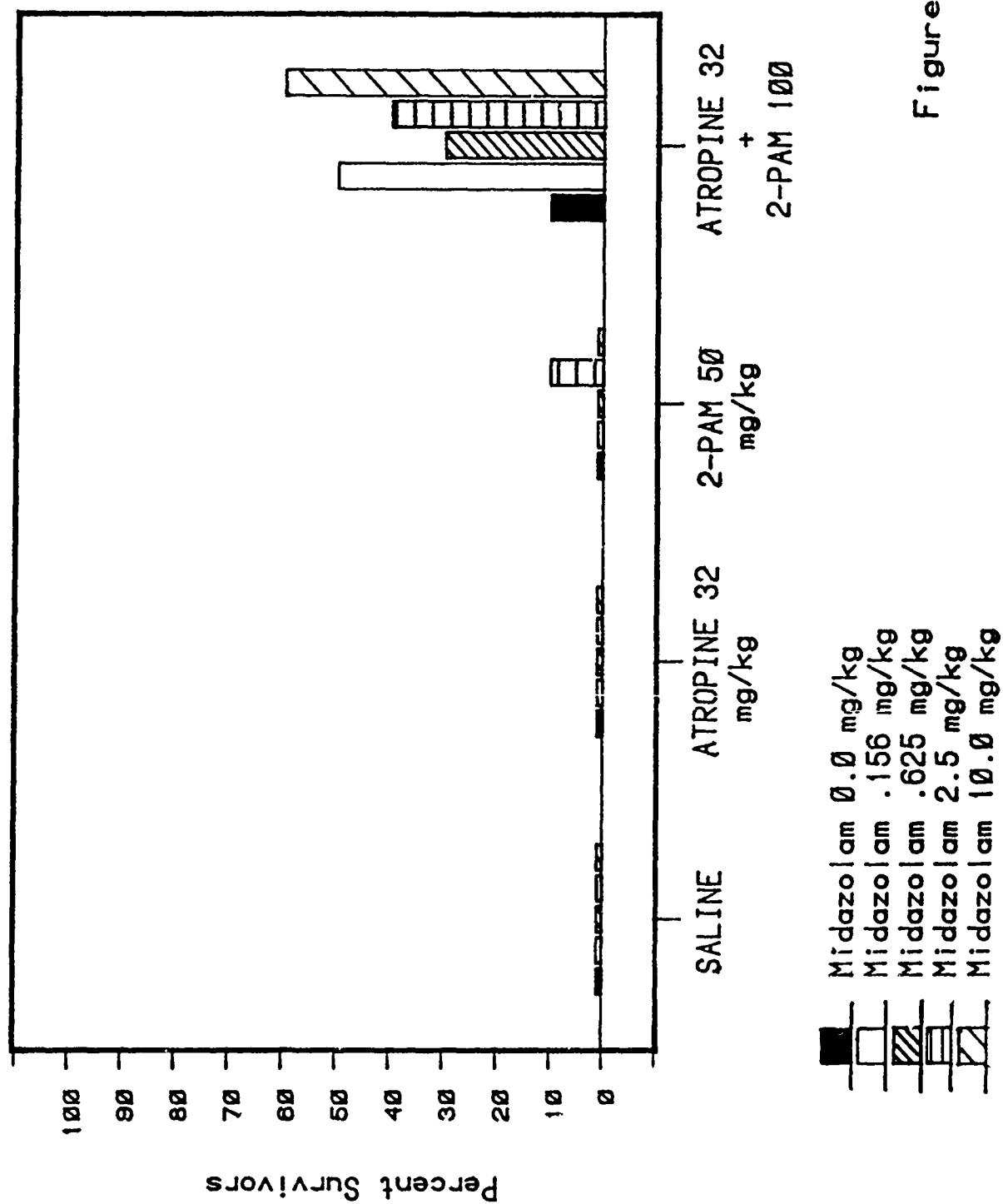


Figure 6

Efficacy of Midazolam Alone and with Atropine/2-PAM Against GD in Guinea Pigs

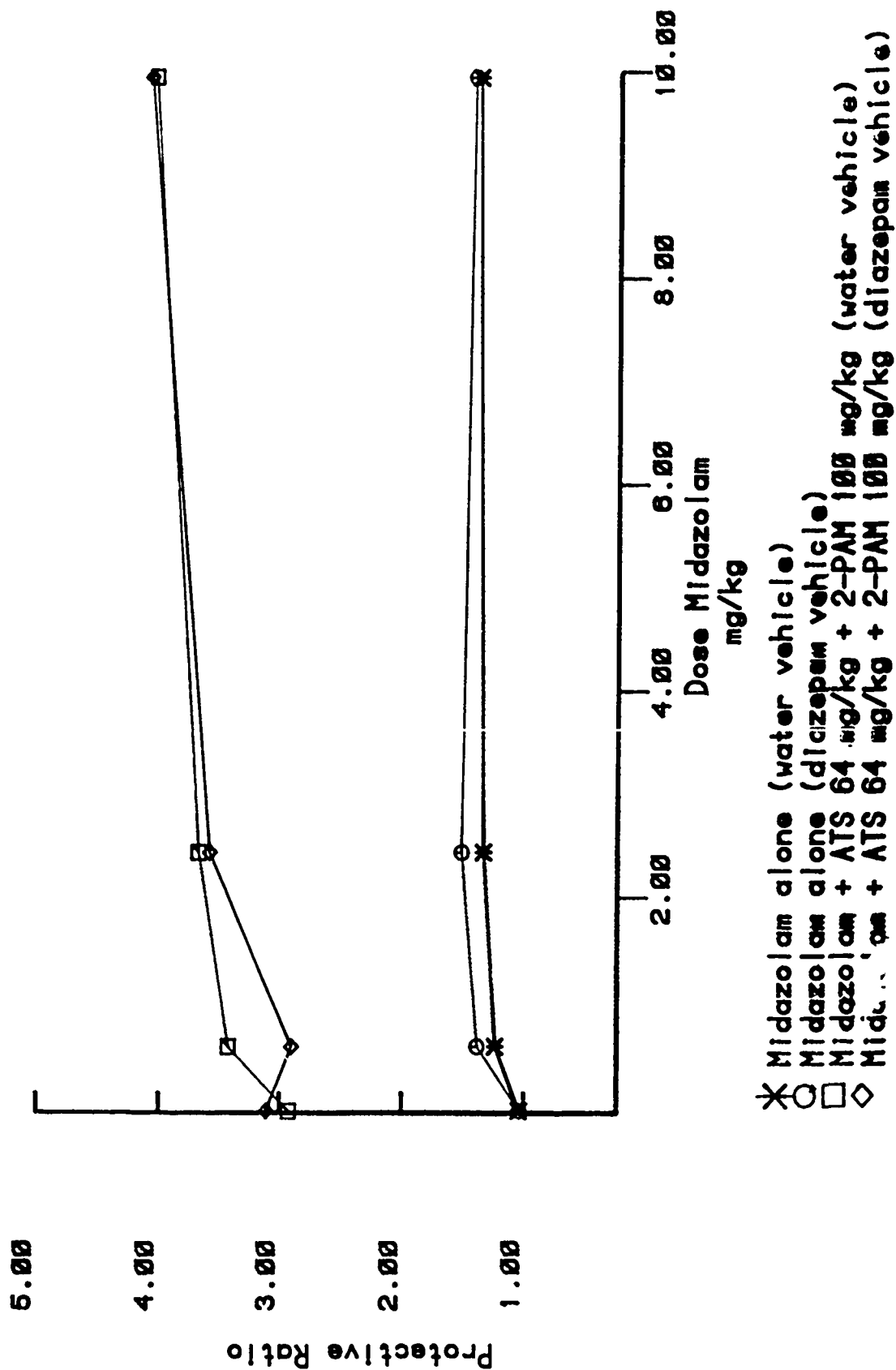


Figure 7

DIAZEPAM HUMAN PLASMA LEVELS*

Diazepam Preparation	Dose	Route of Administration	Peak Plasma Level (ng/ml)	Time to Peak Effect (Hrs)
1. Diapam R	5 mg	intramuscular	170-180	0.5
2. Diapam R	5 mg	oral	90-100	2.0

* Adapted from Kanto, J., Br. J. Anesth., 46: 817, 1974.

Figure 8

Initial Efficacy of Diazepam Oral Pretreatment with Atropine/2-PAM Against (4.3xLD50) GD in Guinea Pigs

430

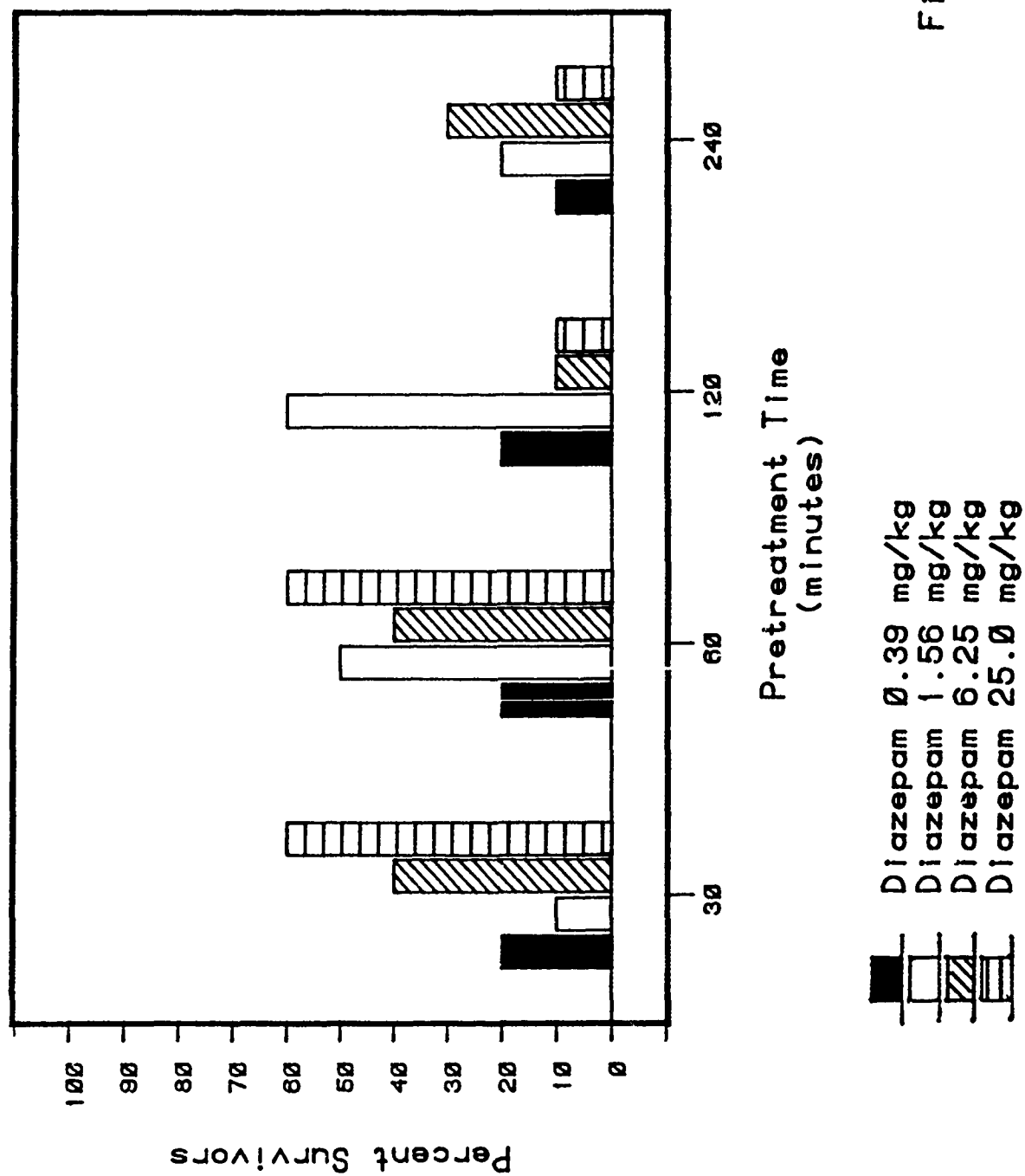


Figure 9

Initial Efficacy of Midazolam Oral Pretreatment (Diazepam Vehicle) with Atropine/2-PAM Against (4.3xLD50) GD in Guinea Pigs

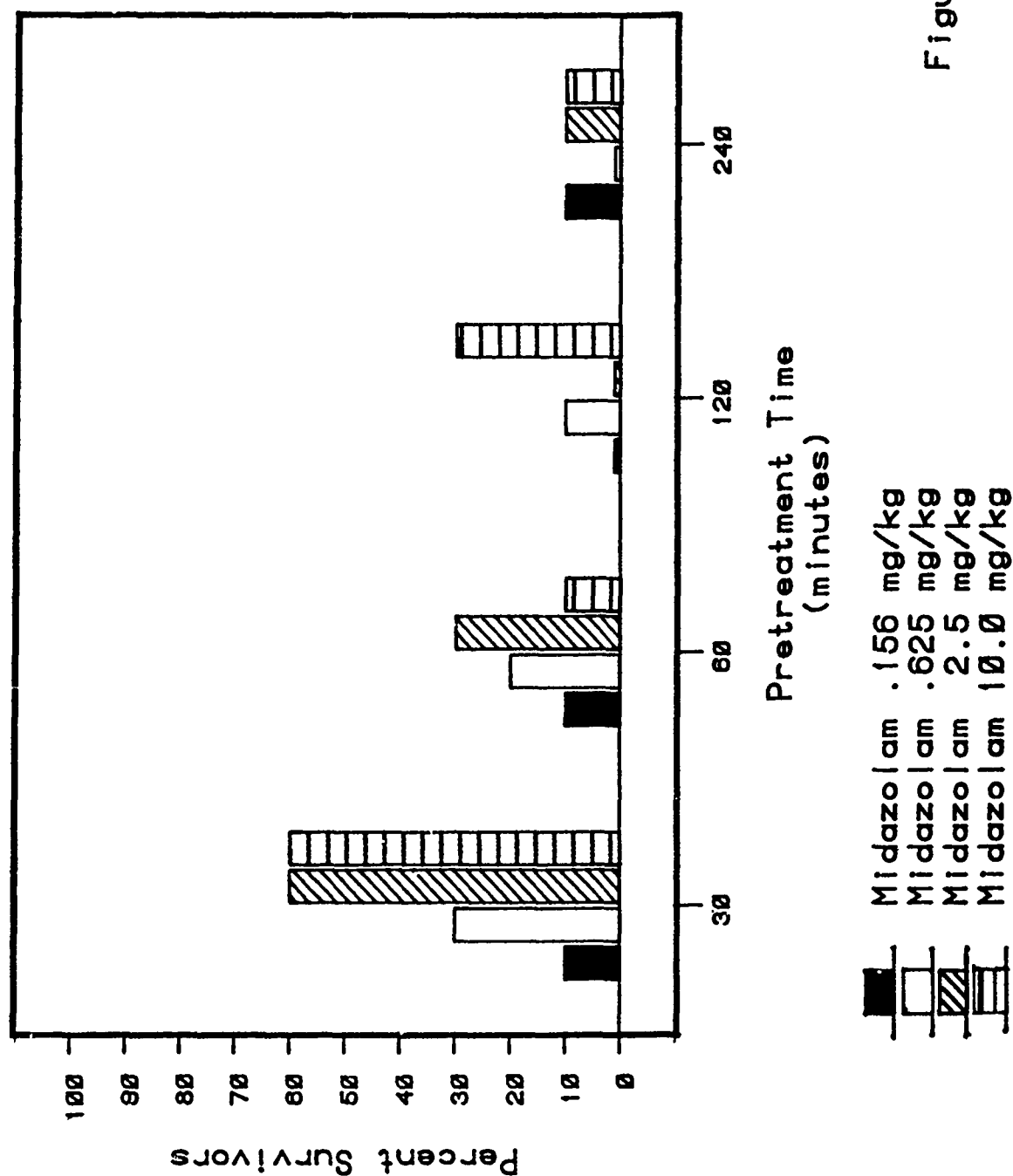


Figure 10

Effect of Valium and Atropine on Soman-
Induced Neuropathology in Guinea Pigs

Allen W. Singer, Theodore W. Slone
and John S. Graham

United States Army Medical Research Institute of Chemical Defense
Aberdeen Proving Ground, Maryland 21010



Effect of Valium and Atropine on Soman-Induced Neuropathology in Guinea Pigs

Previous studies have shown that rats exposed to soman may have microscopic brain lesions consisting of neuronal necrosis in the cortex, hippocampus and thalamus (1,2). The lesions are usually bilaterally symmetrical and are essentially indistinguishable from those described for experimental hypoxia or ischemia (3). Neuronal lesions similar in appearance and distribution have also been described in animals with a history of idiopathic epilepsy (4), and in animals subjected to chemically induced convulsions (5). Since both hypoxia and convulsions have been clinical features of the affected rats in the soman studies (1,2), the pathogenesis of the lesions has remained obscure.

In this study, anticonvulsant doses of Valium were given to groups of guinea pigs either before or after soman intoxication. Atropine sulfate was also given, alone and in combination with Valium, since previous studies with rats have indicated that excessive oral and respiratory secretions have contributed to the soman induced hypoxia. Guinea pigs were randomized and assigned to one of eight experimental groups (Table 1).

Table 1. Experimental design.

<u>Group</u>	<u>N</u>	<u>Treatment</u>
A	4	Saline (1cc/kg, sc)
B	10	Valium (5mg/kg, im)
C	10	Atropine (.4mg/kg, im)
D	20	Soman (30ug/kg, sc; LD50 = 30ug/kg)
E	15	Valium 10 minutes prior to soman
F	15	Soman + Valium at tremor onset
G	15	Soman + Valium and atropine at tremor onset
H	15	Soman + atropine at onset of salivation

Additional therapy was given to subjects in groups E,F,G and H if signs recurred.

Clinical signs were closely monitored and are summarized with 24 hour mortality data in Table 2. Six of the twenty group D (soman) subjects and ten of the fifteen group H (soman/atropine) subjects had clinical convulsions. Only one of the forty-five subjects which received Valium (groups E,F and G) had a clinical convulsion.

Table 2. Clinical signs.

<u>Group</u>	<u>N</u>	<u>Treatment</u>	<u>Signs</u>	<u># dead at 24 hours</u>
A	4	Saline	Normal	0
B	10	Valium	Normal	0
C	10	Atropine	Normal	0
D	20	Soman	Chewing, salivation, hyperactivity, white tears, tremors, convulsions	10
E	15	Valium/soman	Salivation, hyperactivity	0
F	15	Soman/Valium	Chewing, salivation, tremors	4
G	15	Soman/Valium-atropine	Chewing, salivation, tremors, convulsions	0
H	15	Soman/atropine	Chewing, salivation, tremors, convulsions	5

Surviving guinea pigs were randomly selected for euthanasia at 24, 48 and 72 hours post exposure. After pentobarbital anesthesia, they were transcardially perfused with 10% buffered formalin and brains were collected. After trimming, tissues were paraffin embedded, routinely processed and stained with hematoxylin and eosin for light microscopic evaluation. In addition to the 24 hour survivors, six guinea pigs which died between 18 and 24 hours were also included in the light microscopic study (Table 3). Five of these were from group D (soman) and one was from group F (soman/Valium). Guinea pigs which died prior to 18 hours were not examined because prior studies with rats indicate a subject must survive at least 18 hours for lesions to be consistently identified by light microscopy. Two distinctly different morphological diagnoses were made on various sections. Acute neuronal necrosis, with clusters of red shrunken neurons containing pyknotic or faded nuclei, was seen in many animals (Table 3). In addition, five guinea pigs had a multifocal granulomatous meningoencephalitis associated with protozoal cysts compatible with an organism called Encephalitozoon cuniculi. This is an organism which is seen commonly in rabbit brains and rarely in guinea pigs. It causes a characteristic granulomatous reaction which cannot be confused with the soman induced neuronal damage.

Table 3. Histology results.

<u>Group</u>	<u>Treatment</u>	<u>Total Evaluated</u>	<u># with Acute Neuronal Necrosis</u>
A	Saline	4	0
B	Valium	10	0
C	Atropine	10	0
D	Soman	15	12
E	Valium/Soman	15	0
F	Soman/Valium	12	2
G	Soman/Valium-atropine	15	6
H	Soman/atropine	10	10

Twenty-three of the twenty-five group D (soman) or group H (soman/atropine) subjects which were examined had documented tremors or convulsions. All but one of these had areas of brain necrosis. Twenty-one of the thirty group F (soman/Valium) or group G (soman/Valium-atropine) had documented tremors or convulsions. Seven of these twenty-one had small areas of brain necrosis. Only one guinea pig (from group G) without documented tremors had a brain lesion. In addition to lessening the incidence and severity of brain necrosis, Valium also altered the distribution of the lesions. Hippocampal necrosis was found in seventeen of the twenty-two group D or H subjects with lesions. By contrast, hippocampal necrosis was not found in any of the eight guinea pigs with lesions (groups F and G) that had received Valium.

In conclusion, under the conditions of this experiment, Valium prevented tremors and convulsions caused by soman when used as a pretreatment drug, and reduced tremor and convulsion severity when used as post exposure therapy. It also markedly reduced the incidence and severity of brain lesions caused by soman intoxication. Atropine, at low doses which prevent secretions, appears to have no effect on the formation of the brain lesions. This suggests that the pathogenesis of the acute neuronal necrosis seen in soman intoxication is due to excessive neuronal activity (brain seizures) and not simply due to local hypoxia.

References

1. Lemerrier G, Carpentier P, Sentenac-Roumanou, Morelis P. Histological and histochemical changes in the central nervous system of the rat poisoned by an irreversible anticholinesterase organophosphorus compound. Acta Neuropathol (Berl) 1983; 61:123-129
2. McLeod CG Jr, Singer AW, Harrington DG. Acute neuropathology in soman-poisoned rats. Neurotoxicology (accepted for publication, 1983)
3. Brown AW, Brierley JB. The nature, distribution, and earliest stages of anoxic-ischaemic nerve damage in the rat brain as defined by the optical microscope. Brit J Exp Path 1968; 49:87-106
4. Montgomery DL, Lee AC. Brain damage in the epileptic beagle dog. Vet Pathol 1983; 20:160-169
5. Meldrum BS, Brierley JB. Prolonged epileptic seizures in primates. Arch Neurol 1973; 28:10-17

BRAIN REGIONAL ENERGY FLOW: EFFECTS OF PRETREATMENT
WITH VALIUM IN SOMAN-EXPOSED RATS

T. L. Pazdernik, F. E. Samson, R. Cross, M. Giesler,
J. Jackson and S. R. Nelson

Departments of Pharmacology, Toxicology, and
Therapeutics, Anatomy and Ralph L. Smith
Research Center
University of Kansas Medical Center
College of Health Sciences and Hospital
Kansas City, Kansas 66103

Principle Author: T.L. Pazdernik
Department Pharmacology, Toxicology and
Therapeutics
University of Kansas Medical Center
College of Health Sciences
39th & Rainbow
Kansas City, Kansas 66103

Summary

Soman administered to rats at near-lethal doses produces strong, repetitive convulsions for several hours during the acute phase of intoxication. Local cerebral glucose utilization (LCGU) is markedly increased in most brain structures during the seizure phase. Rats which survive soman-induced seizures develop gross damage in amygdala, dorsal thalamus and piriform cortex. This neuropathology is evident 24 to 72 hr post soman exposure and at this time LCGU is suppressed greater than 2-fold in many brain structures. Diazepam (3.2 mg/kg, im) pretreatment protects against overt convulsions and extensive neurotoxicity associated with near-lethal doses of soman. Diazepam pretreatment blocks the increase in LCGU in most brain structures during the seizure phase, however, LCGU is still notably elevated in the globus pallidus, ventral pallidum and substantia nigra reticularis. Likewise, the suppression of LCGU observed 72 hr post-soman exposure was abolished by diazepam pretreatment. We conclude that diazepam blocks the propagation of seizure activity in the limbic system but does not block soman-induced epileptogenic foci in basal ganglia and substantia nigra.

Introduction

Soman (0-1,2,2-trimethylpropyl methylphosphonofluoridate), a potent organophosphate anticholinesterase agent, administered to rats at near-lethal doses, produces strong, repetitive convulsions for several hours during the acute phase of intoxication. During this acute phase of soman intoxication, local cerebral glucose utilization (LCGU), assessed by the 2-deoxyglucose (2-DG) method of Sokoloff *et al.* (1977), increases dramatically in most brain regions (McDonough *et al.*, 1983). This reflects the large increase in neuronal activity associated with overt convulsions. Rats which survive this acute phase of intoxication develop gross damage in amygdala, dorsal thalamus and piriform cortex as well as less obvious damage in other cortical and limbic related areas. Reports by Petras (1981), Lemerrier *et al.* (1983) and McLeod *et al.* (in press) suggested that the development of brain lesions was positively related to the presence of convulsions during soman intoxication, although there could be other contributory factors (Lemerrier *et al.*, 1983).

Twenty-four to 72 hr post soman exposure, the behavior of rats is best described as asthenic but hyperexcitable when handled. At this time, extensive neuropathology is evident in some regions and LCGU is reduced greater than 2-fold in many brain structures (Pazdernik *et al.*; 1984a, submitted). Thus, it appears that prolonged seizures lead to long-term biochemical abnormalities that result in suppression of functional activity (refractoriness) and irreversible neuronal damage in certain vulnerable structures.

In view of the recent interest in diazepam (Valium^R) as a protective agent against soman-induced brain damage, we investigated the impact of diazepam pretreatment on LCGU in soman treated rats during the seizure (15 min after injection of soman) and the pathology phases (72 hr after injection of soman) of intoxication.

Methods

Animals. Adult male rats (Wistar) were purchased from Charles River Breeding Laboratories (Willington, MD). Rats were 250-300 g at time of use.

Experimental Design: Rats were pretreated with either vehicle (ethanol 10%; propylene glycol 40%; 0.67 ml/kg, im) or diazepam (3.2 mg/kg) in vehicle 10 min prior to injection of either saline (0.86 ml/kg, sc) or soman (104-108 µg/kg) in saline. [14 C]-2-deoxyglucose was injected either 15 min (seizure phase) or 72 hr (pathology phase) after injection of saline or soman. Rats were sacrificed 45 min after injection of 2-DG and processed as described below.

Surgical Preparation: After animals were anesthetized with halothane, lidocaine was infiltrated around the incision sites. The femoral vein was cannulated with a 3 cm section of Intramedic PE 50 polyethylene tubing inserted into a 3 cm piece of Dow silastic tubing (0.03" I.D.) attached to a 24 cm section of S-54-HL formulation tygon tubing (0.034" I.D.). By the use of a seven inch stainless steel needle, the venous cannula was threaded subdermally from the hind leg to exit between the ears. The femoral artery was cannulated with a 5 cm section of Intramedic PE 10 polyethylene tubing connected to a 15 cm section of S-54-HL formulation tygon tubing (0.02" I.D.). The arterial cannula reached the aorta and could be cleared by two or three drops of blood. The arterial cannula was passed subdermally behind the leg to exit just rostral to the base of the tail. Each cannula was anchored to the skin with a sleeve of PE 205 Intramedic polyethylene tubing. About 4 cm of each cannula was left protruding and plugged. The rats were allowed to recover from halothane for a minimum of two hours before experiments were begun.

Just prior to the initiation of the 2-DG procedure, 150 units of heparin was injected i.v. into each free roaming animal and control blood samples were taken and iced. The rats were placed in a plastic rodent restraining cage which allowed access to the venous cannula through a hole near the front of the cage. The arterial cannula was accessible at the open end of the cage.

Brain Regional Metabolism Mapping Procedure: The method for regional brain glucose utilization was based on that of Sokoloff *et al.* (1977). 2-Deoxy- [14 C]-glucose (American Radiolabeled Chemicals Inc., St. Louis, MO) was injected i.v. (100 µCi/kg) as a pulse in a 0.9% saline solution via the venous cannula which was immediately flushed with saline (see Experimental Design section for time of injection). During the first minute immediately following the pulse, six timed serial arterial blood samples (0.05-0.07 ml) were collected in heparinized hematocrit tubes. The rat was released from the cage after the one minute blood sampling and allowed to roam freely. Blood samples were taken every five minutes for plasma glucose determinations and 14 C scintillation counting. At the end of the experiment, the rat was decapitated and the brain quickly removed, frozen in freon 12 kept at -70°C and bagged in plastic air tight bags for storage at -70°C .

Five µl of each plasma sample were pipetted into 4 ml of scintillation cocktail (Research Products International Corp, 3a70) and counted in a Hewlett-Packard Tri-Carb Scintillation Counter. Ten µl of plasma were used to determine plasma glucose levels with a Yellow Springs Instrument model 23A glucose analyzer (Yellow Springs, OH).

The brains were sectioned coronally into 20 μm slices at -20°C and immediately dried on a $55-60^{\circ}\text{C}$ slide warmer. Adjacent sections were used for autoradiograms and hematoxylin and eosin (H&E) stains. These sections, along with [^{14}C]-methyl methacrylate standards, were exposed to Kodak Min-R x-ray film for 21 days. The optical density of a given brain structure was determined by video-computer assisted analysis. For each subject the average of several optical density readings per brain area along with the plasma glucose levels and ^{14}C concentrations were used to calculate the rate of brain regional glucose use according to the equation developed by Sokoloff *et al.* (1977).

Expression of data: The rates of glucose use ($\mu\text{mol}/100\text{ g}/\text{min}$) in 36 specific brain regions were calculated according to the Sokoloff equation as described above. The Paxinos and Watson (1982) atlas was used for structure identification. Specific differences ($p < 0.01$) in the rates of glucose use between groups were determined with an ANOVA, planned comparison BMDP statistical package (Keppel, 1973). The data shown in Figs. 2 and 4 are expressed as a percent of control and the standard error of each percentage was calculated as:

$$\text{S.E.} = \frac{100}{\bar{y}} \sqrt{\frac{\text{var}(\bar{x})}{n_1} + \frac{\bar{x}^2}{\bar{y}^2} \cdot \frac{\text{var}(\bar{y})}{n_2}}$$

where \bar{x} and \bar{y} were values of experimental and control groups, respectively, and n_1 and n_2 represented the number of rats in each group.

Results

Seizure Phase:

Four groups of rats (vehicle controls; diazepam pretreatment; soman; diazepam pretreatment plus soman) were treated as described in the experimental design section of Methods: 2-DG was given 15 min after saline or soman and 25 min after vehicle or diazepam. Diazepam pretreatment (3.2 mg/kg, im) alone produced notable ataxia and behavioral depression; a slight reduction in LCGU was observed in most brain structures when 2-DG was injected 25 min after diazepam (Figs. 1 & 2). The greatest reduction in LCGU ($65.8 \pm 17\%$ of control) occurred in the piriform cortex (Fig. 2).

Symptoms during acute soman intoxication (104-108 $\mu\text{g}/\text{kg}$, sc) were similar to those previously reported (McDonough *et al.*, 1983) and to those described as moderate to severe by Jovic (1974). Seizures consisted primarily of continuous repetitive jerking of the head, shoulders and forepaws approximately every 2-3 seconds and often there were brief periods of tonic extension of both fore- and hind-limbs accompanied by Straub tail. These symptoms usually started 5-10 min post soman exposure and persisted throughout the 45 min 2-DG experimental period. Soman-induced seizures caused a pronounced increase in most of the 36 brain structures quantitated (Figs. 1 & 2). Structures that had a greater than 4-fold increase in LCGU included: ventral pallidum, lateral septum, globus pallidus, mediodorsal thalamus, basolateral amygdala, substantia nigra reticularis and lobule 1 of vermis. The only structures quantitated that did not show a significant increase in LCGU were: mammillary body, anterior pretectum,

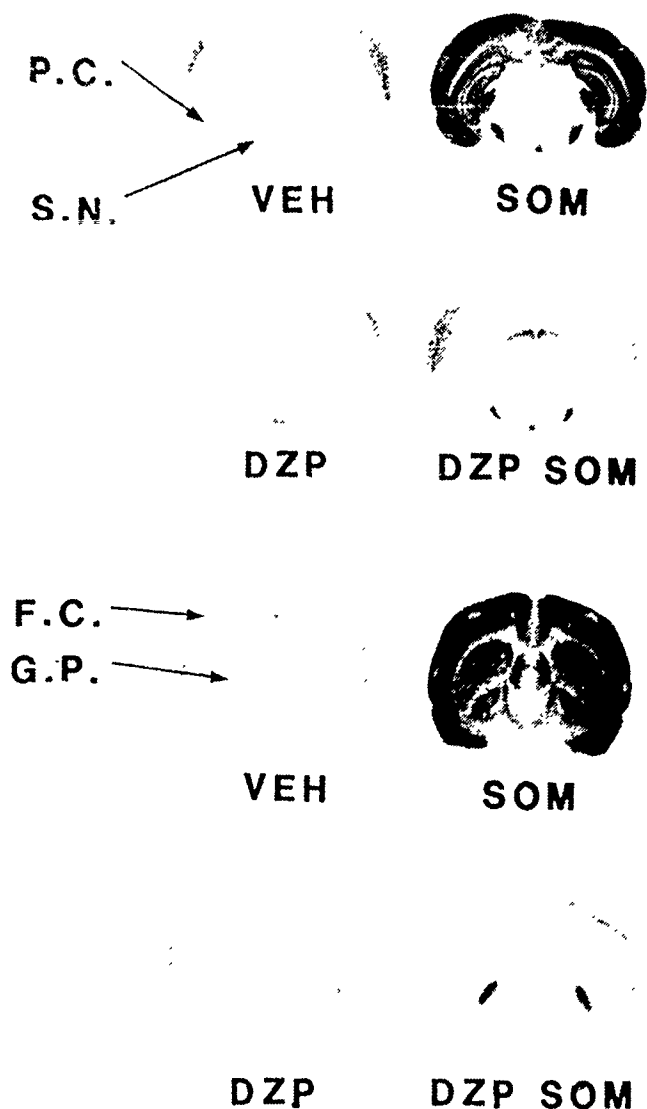


Figure 1. Representative autoradiographs showing local cerebral glucose utilization in coronal sections during the seizure phase. 2-DG was given 15 min after saline or soman and 25 min after vehicle or diazepam as described in Methods. The abbreviations used to describe the four treatment groups are: VEH = vehicle; SOM = soman; DZP = diazepam; DZP SOM = diazepam plus soman. Labeled structures are: P.C. = piriform cortex; S.N. = substantia nigra reticularis; F.C. = frontal cortex; G.P. = globus pallidus.

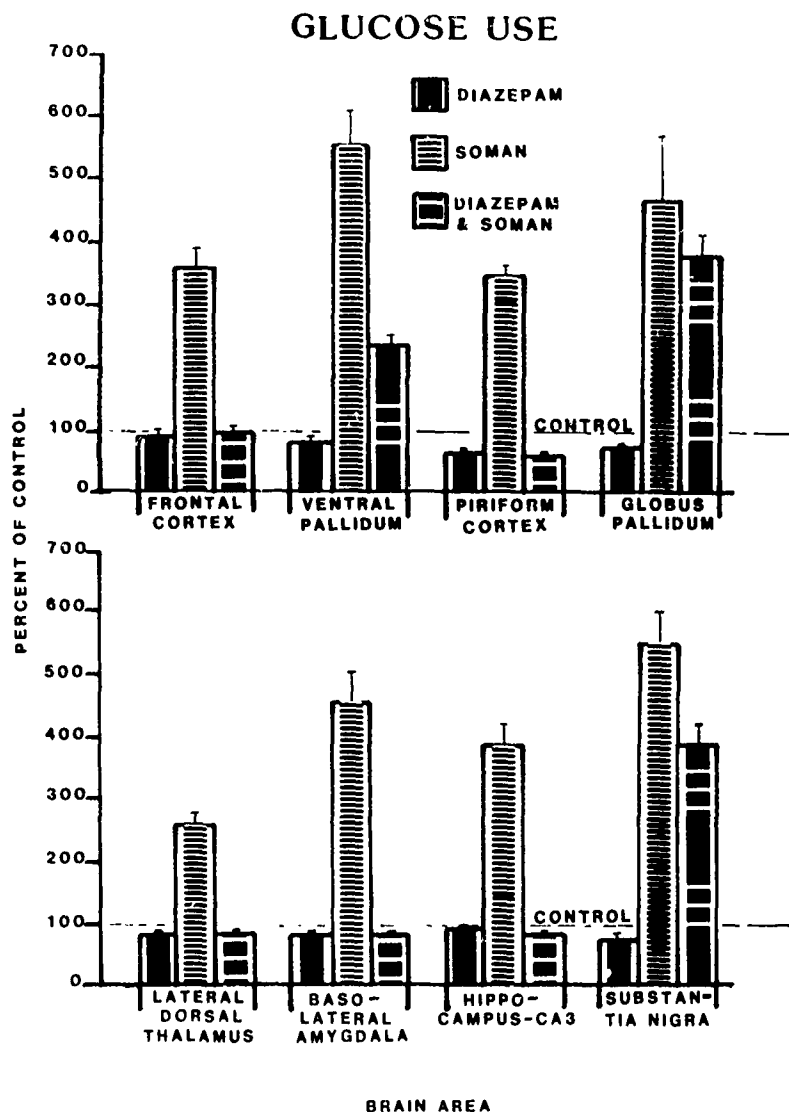


Figure 2. Each bar represents local cerebral glucose utilization of the indicated structure expressed as percent of vehicle control for the designated treatment. Rats were treated as in Fig. 1. All regions shown were significantly greater from control in the soman group, whereas only ventral pallidum, globus pallidus and substantia nigra reticularis were significantly elevated in the diazepam plus soman group.

lateral lemniscus, inferior colliculus, and dorsal lobule of vermis. In general, LCGU was low throughout much of the mid-brain area as illustrated in Fig. 1. There was also a very striking shutdown of LCGU in segments of mid-cortical layers. This inhibition was more prominent in the rostral half of the brain and most noted in the dorsal portion of the cortex.

Pretreatment with diazepam abolished the overt convulsions observed with soman alone but many acute symptoms of soman intoxication were still displayed such as marked salivation, behavioral depression, loss of righting reflex and somewhat dilated, non-responsive pupils. The LCGU pattern in rats pretreated with diazepam prior to injection of soman reflected the absence of soman-induced seizures. In most structures, the rate of LCGU was identical to that in rats pretreated with diazepam alone (Figs. 1 & 2). Interestingly, some key structures still remained significantly elevated in the diazepam pretreatment plus soman group; these structures were: ventral pallidum, globus pallidus, substantia nigra, superior colliculus and lobule 1 of vermis.

Pathology Phase:

Four groups of rats (vehicle control; diazepam pretreatment; soman; diazepam pretreatment plus soman) were again injected as described before but now 2-DG was injected 72 hr post soman or saline injection. Symptoms described for the seizure phase were noted in all groups and subsided within a few hours for all groups except the soman group. After the initial cholinomimetic symptoms subsided, the soman treated rats were profoundly asthenic with occasional brief seizure episodes noted during the next few days. The soman treated rats had reduced food and water intake during this period as substantiated by their marked weight loss. The three day weight changes for each group were as follows: vehicle controls = $+27 \pm 4$ g, diazepam pretreatment = $+15 \pm 5$ g, soman = -61 ± 7 g and diazepam pretreatment plus soman = -36 ± 14 g. Interestingly, the diazepam plus soman rats appeared in good condition (eg. well groomed) compared to the soman rats but did lose weight over the three day period.

The LCGU pattern for the diazepam pretreatment group and diazepam pretreatment plus soman group were similar to the vehicle control group at the 72 hr time period. On the other hand, LCGU in the soman group was markedly suppressed in most brain regions (Figs. 3 & 4) as previously observed (Pazdernik *et al.*, 1984a, submitted). In many structures, the rate of LCGU was suppressed greater than 2-fold. The greatest reduction occurred in structures with the most notable damage such as piriform cortex, basolateral amygdala, and lateral dorsal thalamus (Figs. 3 & 4). Extensive damage in these structures was confirmed by H&E stained sections; this damage was not present in the diazepam pretreatment plus soman group.

Discussion

These studies indicate that pretreatment with diazepam protects against overt convulsions and extensive neurotoxicity associated with near-lethal doses of soman. Furthermore, evidence is provided that diazepam blocks the propagation of seizure activity in the limbic system but fails to block the development of epileptogenic foci in the basal ganglia and substantia nigra reticularis.

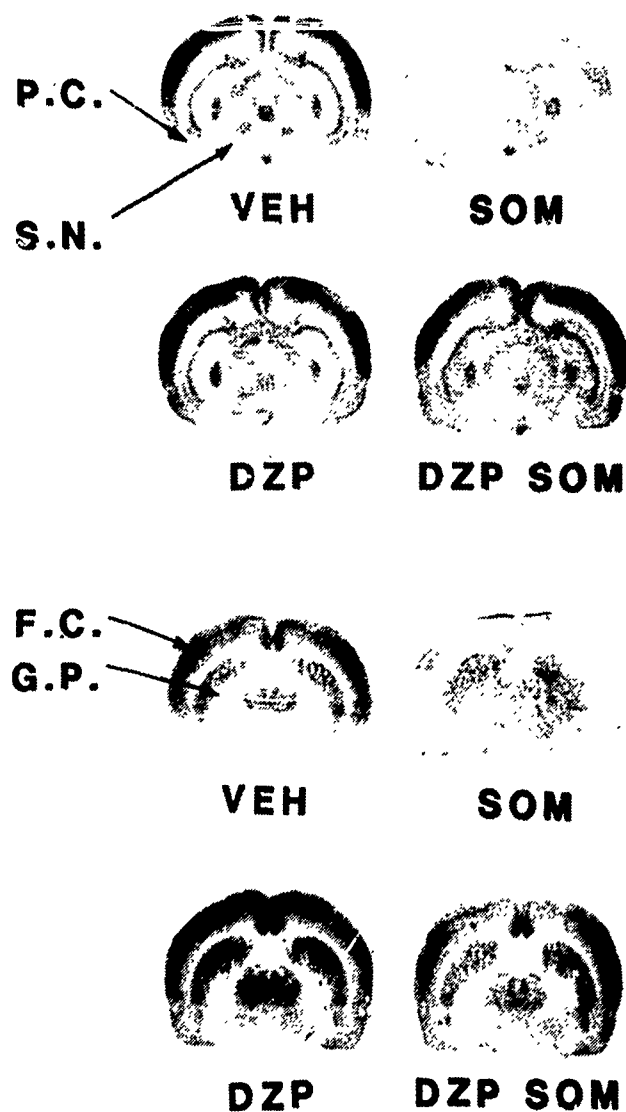


Figure 3. Representative autoradiographs showing local cerebral glucose utilization during the pathology phase. 2-DG was given 72 hr after treatment. Abbreviations are as in Fig. 1.

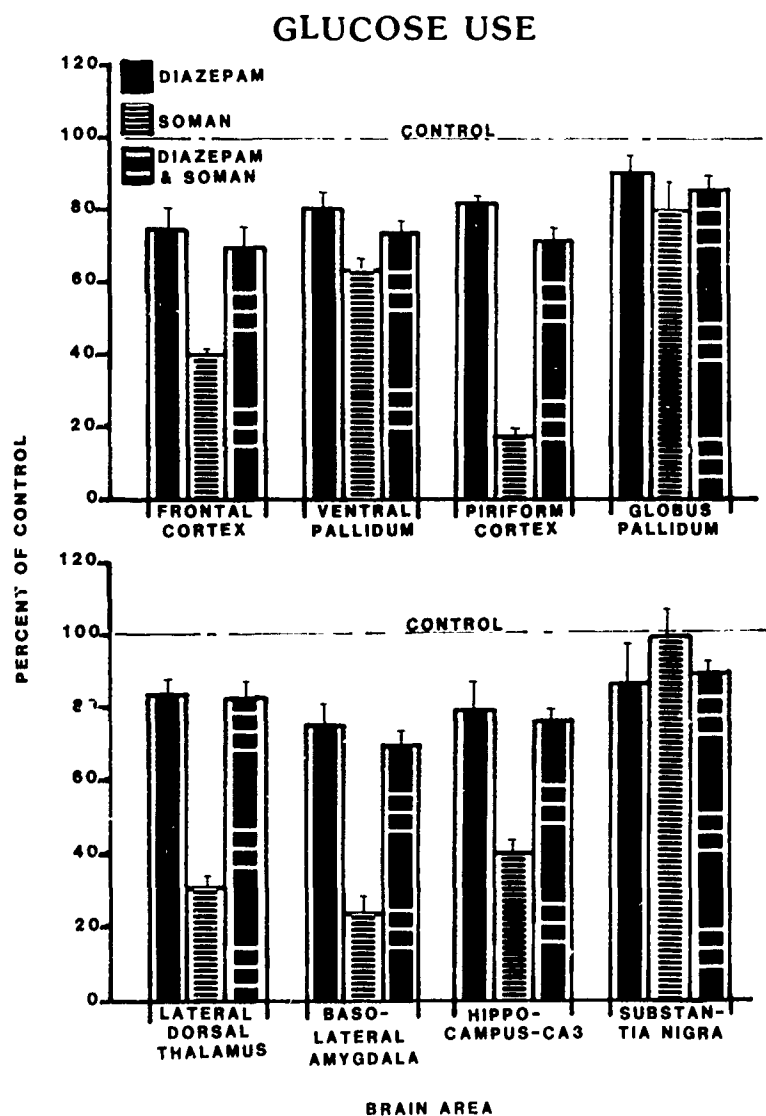


Figure 4. Each bar represents local cerebral glucose utilization of the indicated structure expressed as percent of vehicle control for the designated treatment. Rats were treated as in Fig. 3.

We have previously studied the impact of several convulsants on LCGU assessed by the 2-DG method (Pazdernik *et al.*, 1984b, submitted). From these studies, we concluded that intermittent motor convulsions, such as those observed with pentylenetetrazol or picrotoxin, can be mediated by recurrent electrical inputs from basal ganglia and substantia nigra via the thalamus and cortex. In addition, for status epilepticus to occur, such as observed with soman, intrahippocampal penicillin or kainic acid, a synchronous flow of activity in the limbic system, is needed, probably driven by hippocampal CA₃ epileptogenic pacemaker cells (Pazdernik *et al.*, 1984b, submitted). Diazepam pretreatment abolishes the spread of electrical activity throughout the limbic system and thus, blocks the expression of overt limbic motor seizures.

Our earlier studies with diisopropylfluorophosphate (DFP) failed to produce limbic motor seizures as observed with near-lethal doses of soman. However, we noted (Churchill *et al.*, 1984) transient seizure-like activity in rats peripherally protected with methylatropine bromide (3.0 mg/kg, iv) and then given DFP (2.36 mg/kg, iv). Interestingly, the autoradiograms (Fig. 5) from these rats are similar to those from diazepam pretreatment plus soman rats. Namely, LCGU was markedly elevated in globus pallidus, ventral pallidum



Figure 5. Representative autoradiographs showing local cerebral glucose utilization. DZP-SOM rats were pretreated with diazepam 10 min prior to injection of soman. DFP-MeAt were pretreated with methylatropine bromide 5 minutes prior to injection of DFP. 2-DG was given 15 minutes after soman or DFP. Labeled structures are: S.N. = substantia nigra reticularis; G.P. = globus pallidus.

and substantia nigra reticularis. Thus, these basal ganglia and extrapyramidal structures may represent the epileptogenic initiation sites for seizures induced by cholinergic agents. However, for the expression of limbic motor seizures, as observed with near-lethal doses of soman, synchronous electrical discharges must be propagated through the limbic system; this is abolished by diazepam pretreatment.

We have previously described the delayed metabolic and pathological sequela that follow soman-induced seizures (Pazdernik *et al.*, 1984a, submitted). The metabolic profile is characterized by marked depression of LCGU in many brain areas 24, 48 and 72 hr post soman exposure; this was again observed in the 72 hr post soman group of the present study. At these times, conspicuous neuropathology is also obvious by inspection of the frozen brain sections, H & E stained sections or the 2-DG autoradiograms. Our initial conclusions (Pazdernik *et al.*, 1984a, submitted) that the postictal depression of LCGU and regional delayed neuropathology observed 24 to 72 hr after soman exposure is related to intensive seizure activity is strengthened by the findings in this study that both postictal depression of LCGU (Figures 3 & 4) and regional neuropathology was blocked when limbic seizure activity was attenuated by diazepam pretreatment.

Extensive piriform cortex damage has now been demonstrated in several experimental situations where increased activity occurs in the limbic circuitry. Intra-amygdaloid injections of cholinomimetic agents produced damage in the piriform cortex which was blocked by atropine (Olney *et al.*, 1983). Honchar *et al.* (1983) reported that administration of physostigmine or pilocarpine to lithium pretreated rats produced sustained limbic seizures and brain damage similar to which we observed with soman; this effect was also blocked by atropine. Similar damage to the piriform cortex also occurs with other agents which induce limbic motor seizures, such as kainic acid (Wuerthele *et al.*, 1978; Schwob *et al.*, 1981; Lothman and Collins, 1981; Sperk *et al.*, 1983; our unpublished data) and folic acid derivatives (Olney *et al.*, 1981). Distal damage to the piriform cortex caused by injection of kainic acid or folic acid into the substantia innominata was reduced by scopolamine and to even a greater extent by diazepam (McGeer *et al.*, 1983). Thus, it appears that distal damage to the piriform cortex is mediated via limbic excitatory inputs which involve cholinergic connections.

We suggest that the cholinergic inputs to the piriform cortex are activated by limbic seizures per se and are not epileptogenic foci for cholinergic-induced seizures since the increase in LCGU in the piriform cortex during the seizure phase and the delayed pathology are blocked by diazepam pretreatment. Diazepam also blocks limbic motor seizures induced by kainic acid and the ensuing damage to the amygdala and piriform cortex (Heggle and Malthe-Sorensen, 1982). Recent studies in our laboratory have shown that diazepam blocked the increases in LCGU in all brain structures during the seizure phase except in the hippocampus, a foci of kainic acid induced seizures. Thus, giving further credence to the notion that diazepam blocks the propagation of seizure activity in the brain but not the initiation of epileptogenic foci.

The 2-DG method provides information about the dynamic, vital process of glucose utilization and serves as a "window" to the entire brain for identifying anatomical structures affected by neurotoxins. Using this technique,

we have identified neuroanatomical structures involved in soman-induced seizures (McDonough et al., 1983; Pazdernik et al., 1984b, submitted), as well as in soman's delayed actions (Pazdernik et al., 1984a, submitted). This technique is especially useful for evaluating the efficacy of antidotes for protection against soman's impact on the brain. The calculated rates of LCGU are dependent upon several rigorous requirements that must be fulfilled to provide accurate rates; these have been reviewed by McCulloch (1983). Seizure induced alterations in cerebral tissue such as changes in permeability of the blood brain barrier, changes in cerebral blood flow, changes in plasma/brain glucose ratios and damage in some brain structures can affect constants used in the operational equation.

The present findings indicate that anticonvulsants, such as diazepam may be valuable agents to include in antidotal mixtures for protection against soman intoxication. Studies are now underway to determine the lowest dose of diazepam which will provide protection. The use of anticonvulsant agents may be even more important when a subject is provided with peripheral protection against soman, such as with pyridostigmine, which will allow the subject to survive larger doses of soman. In these subjects it is even more important to provide protection against soman-induced seizures. Thus, it is important to identify combinations of antidotes which will have minimal impact on brain functional activity themselves but will protect against both the acute and delayed effects of soman's action on brain functional activity.

Acknowledgements

Supported in part by U.S. Army DAMD 17-83-C-3242. We wish to thank Dr. Lynn Churchill and A.C. Lawrence for their valuable input, and Rosa Meagher for her secretarial service.

References

- Churchill L, Pazdernik TL, Cross RS, Giesler M, Nelson SR, Samson FE. Impact of DFP on glucose utilization in antidote-pretreated rats. Amer. Soc. Neurochem. 1984; 15:Abst. 188.1.
- Heggle DE, Malthe-Sorensen D. Systemic injection of kainic acid: Effect on neurotransmitter markers in piriform cortex, amygdala complex and hippocampus and protection by cortical lesioning and anticonvulsants. Neuroscience, 1982; 7:1257-1264.
- Honchar MP, Olney JW, Sherman WR. Systemic cholinergic agents induce seizures and brain damage in lithium-treated rats. Science, 1983; 220:323-325.
- Jovic RC. Correlation between signs of toxicity and some biochemical changes in rats poisoned by soman. Europ. J. Pharmacol. 1974; 25:154-164.
- Keppel G. Design and Analysis: A Researchers Handbook, New Jersey, Prentice-Hall, p. 85, 1973.
- Lemercier G, Carpentier P, Sentenac-Roumanou H, Morelis P. Histological and histochemical changes in the central nervous system of the rat poisoned by an irreversible anticholinesterase organophosphorous compound. Acta Neur pathologia 1983; 61: 123-129.

- Lotham EW, Collins RC. Kainic acid induced limbic seizures: metabolic, behavioral, electroencephalographic and neuropathological correlates. Brain Res 1981; 218: 299-318.
- McCulloch J. Mapping functional alterations in the CNS with [14 C] deoxy-glucose. Handbook of Psychopharmacology. 1983; 15: 321-410.
- McDonough JH, Hackley BE, Cross R, Samson F, Nelson S. Brain regional glucose use during Soman-induced seizures. Neurotoxicology 1983; 4:203-210.
- McGeer PL, McGeer EG, Nagai T. Gabaergic and cholinergic indices in various regions of rat brain after intracerebral injections of folic acid. Brain Res, 1983; 260:107-116.
- McLeod CG, Singer AW, Harrington DG. Acute neuropathology in Soman poisoned rats. Neurotoxicology (in press).
- Paxinos G, Watson C. The rat brain in stereotaxic coordinates, New York, Academic Press, 1982.
- Pazdernik TL, Cross R, Giesler M, Nelson SR, Samson F, McDonough J. Delayed effects of soman: Brain glucose use and pathology (1984a, submitted).
- Pazdernik TL, Cross RS, Giesler M, Samson FE, Nelson SR. A comparison of changes in local cerebral glucose utilization induced by soman and other convulsants. (1984b, Submitted).
- Petras JM. Soman neurotoxicity. Fundam. Appl. Toxicol. 1981; 1:242.
- Olney JW, Fuller TA, de Gubareff T. Kainate-like neurotoxicity of folates. Nature, 1981; 292:165-167.
- Olney JW, de Gubareff T, Labruyere J. Seizure-related brain damage induced by cholinergic agents. Nature, 1983; 301:520-522.
- Schwob JE, Fuller T, Price JL, Olney JW. Widespread patterns of neuronal damage following systemic or intracerebral injections of kainic acid: A histological study. Neuroscience 1981; 5:991-1014.
- Sokoloff L, Reivich M, Kennedy C, Des Rosiers MH, Patlak CS, Pettigrew KD, Sakurada O, Shinohara M. The [14 C] deoxyglucose method for the measurement of local cerebral glucose utilization: Theory, procedure, and normal values in the conscious and anesthetized albino rat. J. Neurochem. 1977; 28: 897-916.
- Sperk G, Lassman H, Baran H, Kish SJ, Seitelberger F, Hornykiewicz O. Kainic acid induced seizures: Neurochemical and histopathological changes. Brain Res. 1983; 1301-1315.
- Wuerthele SM, Lovell KL, Jones MZ, Moore KE. A histological study of kainic acid-induced lesions on the rat brain. Brain Res, 1978; 149:489-497.

VI. Cyanide: Intoxication, Prophylaxis, and Therapy

TOXICODYNAMIC BASIS OF CYANIDE INTOXICATION AND ITS ANTAGONISM

Dr. James Leong Way
Department of Medical Pharmacology and Toxicology
Texas A&M University
College of Medicine
Medical Sciences Building
College Station, Texas 77843



I. INTRODUCTION

One of the oldest chemical warfare gases employed is hydrogen cyanide, HC. Napoleon III employed various substances which would liberate hydrogen cyanide as a war gas prior to an attack. During World War I hydrogen cyanide was incorporated in various projectiles and bombs and there is documentation that the French used hydrogen cyanide blended with other toxic gases against the Germans. In World War II the potential efficacy of hydrogen cyanide as a chemical weapon was improved by using larger projectiles so a cooling effect from the heat of vaporization would occur to increase the relative vapor density of hydrogen cyanide. With regard to front line battlefield antidotal kits for the war gases, there are effective therapeutic measures to counteract poisoning from the organophosphorus war gases by the application of 2-PAM-atropine self-injectors. However, with hydrogen cyanide, no such front line antidotal kit is available. Moreover, amyl nitrite, which was formerly issued for front line use has been deferred with regard to its deployment. This, then, places greater emphasis on the development of therapeutic measures which can be employed against hydrogen cyanide similar to what is presently available for the organophosphorus war gases.

Dr. James Blake, who was a student of Dr. Francois Magendie, continued his interest in attempting to elucidate the toxicodynamic action of cyanide. With regard to the relevance of his work to military application, Dr. Blake (1839, 1840) indicated that artificial respiration was quite effective in antagonizing the lethal effects of cyanide. This concept was literally forgotten or ignored until the last few years with regard to the treatment of cyanide poisoning. The mechanism of intoxication by cyanide has been attributed to the production of a histotoxic anoxia by the inhibition of the terminal oxidase of the mitochondrial respiratory electron transport chain, cytochrome oxidase (Keilin, 1929). Although this concept is reasonable from an academic viewpoint, in massive cyanide poisoning as would occur from the use of hydrogen cyanide as a war gas, the cyanide concentration would greatly exceed the amount necessary to inhibit cytochrome oxidase. Under these circumstances the mechanism of the lethal effects of cyanide would be too overly simplistic to be attributed to a single biochemical lesion, as numerous other enzyme systems, especially the metalloenzymes, and certain critical biochemical intermediates, such as Schiff bases, would be involved. Under these circumstances of very high cyanide concentrations, the mechanism for the lethal effects of cyanide would be very complex. Needless to say, it should be pointed out that there are many enzymes which are either more sensitive or equally as sensitive to forming an inhibitory cyanide-enzyme complex (Solomonson, 1982).

II. TOXICODYNAMIC BASIS FOR ANTAGONIZING CYANIDE INTOXICATION

The toxicodynamic basis for antagonizing cyanide intoxication was reported over 150 years ago. Conceptually, the mechanism may be viewed from a different perspective; however, the antidote remains essentially the same with very little improvement. An American by the name of James Blake (1840) was the first to report on the antagonism of cyanide intoxication on a scientific basis. He indicated that artificial respiration would greatly enhance the

protection against cyanide intoxication. Subsequently, an antidotal combination was reported by K.K. Chen (1933) employing amyl nitrite, sodium nitrite and sodium thiosulfate. The toxicodynamic basis to antagonize cyanide intoxication was based on a combination of sequestering cyanide by formation of methemoglobin by nitrite so that it could react with cyanide to form the relatively inert cyanmethemoglobin. Also, an alternative mechanism to sequester cyanide was the formation of a stable cyanide-metallo complex with cobalt. Besides the sequestering of cyanide to a relatively inert compound, another method was to biotransform cyanide to thiocyanate by the use of sulfur donors. The various methods to antagonize cyanide intoxication have been classified into three classes below. However, it should be emphasized that this classification is relatively arbitrary as recent perspectives suggest that these antagonists may be exerting their effect by different or alternative mechanisms.

A. Conversion of Cyanide to Thiocyanate

An enzyme which can convert cyanide to thiocyanate was described over half a century ago. This thiosulfate sulfurtransferase, better known as rhodanese, has been intensively investigated (Sorbo, 1953) and the formal mechanism of enzyme catalysis by this sulfurtransferase is a classic study (Westley, 1977). Actually, there are a few sulfurtransferases which may be involved in the detoxification of cyanide, e.g., thiosulfate and mercaptopyruvate sulfurtransferases. These two sulfurtransferases detoxify cyanide by different enzymic mechanisms, and the organ and subcellular distribution of these two enzymes are quite different, but the net reaction is the same: cyanide is metabolized to thiocyanate.

More recently, Westley and coworkers (Westley *et. al.*, 1983) have proposed an additional hypothesis which adds an intriguing perspective to the mechanism of cyanide detoxification. The proposal for this detoxification reaction was dependent on a sulfur sulfane pool which can react with cyanide. There are various natural substrates in the body which contain a sulfane sulfur and these compounds can rapidly equilibrate within the body. A source of the sulfane sulfur is cysteine which can be metabolized to mercaptopyruvate. This thio compound then reacts either with the sulfurtransferases or can serve as the basis for forming various sulfur sulfane intermediates. Rhodanese, under these circumstances, not only can catalyze the transfer of sulfur to cyanide but also can interconvert various sulfane intermediates in the sulfur sulfane pool (Westley, 1980). The carrier mechanism for the sulfur sulfane was proposed to be albumin and this serum albumin sulfane sulfur complex then reacts with cyanide. Besides *in vitro* data to support this concept, there are *in vivo* pharmacokinetic data from another laboratory which would be consistent with the formation of a serum albumin-sulfane carrier complex as a mechanism for the detoxification of cyanide (Sylvester *et. al.*, 1983). The pharmacokinetic data indicate that the detoxification reaction occurs predominantly in the central compartment of dogs with a volume of distribution which would approximate that of the blood volume. In addition, the rate that the serum albumin-sulfur sulfane carrier complex can convert cyanide to thiocyanate is consistent with the detoxification role of this intermediate.

B. Oxygen

Because cyanide is believed to produce a histotoxic anoxia and block the tissue utilization of oxygen by the inhibition of cytochrome oxidase, it does not seem reasonable to employ oxygen to treat cyanide poisoning. However, studies have indicated that oxygen alone has minimal effects, but when oxygen is employed in combination with sodium nitrite-sodium thiosulfate, a synergistic effect is observed (Way et. al., 1966). This striking enhancement in protecting against cyanide poisoning occurs primarily with the nitrite-thiosulfate combination, as oxygen does not enhance the effects of sodium nitrite and it has much less effect in combination with sodium thiosulfate alone. Even more important, this action of oxygen is observed therapeutically as well as prophylactically (Sheehy and Way, 1968). It should be emphasized that oxygen is not merely adjunct therapy, but has an integral part in the treatment of cyanide poisoning. Besides the antagonism of the lethal effects as the endpoint, the beneficial effect of oxygen over air in antagonizing the toxic effect can also be demonstrated physiologically by reversal of the EEG (Burrows et. al., 1973) and biochemically by reversal of the inhibitory effects of cyanide on cytochrome oxidase (Isom et. al., 1982) and glucose oxidation (Isom and Way, 1974).

C. Sequestration of Cyanide

1. Cobalt-containing Compounds

Cobalt was known to form a stable metal complex with cyanide and had been used in the treatment of cyanide poisoning almost 100 years ago. However, because of its toxicity, the use of cobalt in cyanide poisoning was discarded until only recently when hydroxycobalamin was employed in the treatment of cyanide intoxication. More recently, cobalt-EDTA has been generally considered the preferred cobalt compound to antagonize cyanide poisoning (Paulet, 1958). Conceptually, it was believed that many of the toxic effects of cobalt ion could be minimized by administering cobalt as an EDTA chelate. The use of metal complexes such as cobalt, iron and gold is a reasonable approach to explore in the development of compounds which can antagonize the toxic effects of cyanide during a gas attack, either when it is used prophylactically or therapeutically.

2. "Nitrites"

It has been known for fifty years that cyanide can react with methemoglobin to form cyanmethemoglobin, and methemoglobin can reactivate cyanide-inhibited cytochrome oxidase. Therefore, it seems reasonable to employ nitrites as a cyanide antagonist, as it would generate methemoglobin formation which then can sequester the toxic cyanide as cyanmethemoglobin. The rationale for the use of two nitrites is that amyl nitrite can be inhaled while sodium nitrite was being prepared for intravenous administration. Many questions have arisen with regard to the relatively slow rate of formation of methemoglobin by sodium nitrite and this led to the development of more rapid methemoglobin formers, such as dimethylaminophenol, DMAP (Kiese and Weger, 1969).

More recently, reports have indicated that methemoglobin forming properties of sodium nitrite may play very little, if any, role in the therapeutic antagonism of cyanide intoxication (Holmes and Way, 1982; Way, 1983). Methylene blue is an azo dye which had been used to treat methemoglobinemia. When methemoglobin formation by sodium nitrite was prevented by pretreatment with methylene blue, sodium nitrite, particularly in combination with sodium thiosulfate, was equally as efficacious in protecting against the lethal effects of cyanide. Of course, this does not suggest that methemoglobin formation can not play a role in antagonizing the lethal effects of cyanide, but it does indicate that sodium nitrite does not play an important role in antagonizing the lethal effects of cyanide on a therapeutic basis by the formation of methemoglobin. Conceptually, this is quite important, as if the nitrites are acting by a mechanism other than methemoglobin formation, this would provide an opportunity for developing a new class of cyanide antidotes. The first toxicodynamic mechanism to be explored with regard to sodium nitrite is its vasogenic properties, as the nitrites have been known to be potent vasodilators. As a result of the studies with sodium nitrite, the investigation of numerous alpha adrenergic blocking agents were initiated as potential cyanide antagonists. The alpha adrenergic blocking agent, phenoxybenzamine, when used in combination with sodium thiosulfate, was found to be equally as effective as the classic nitrite-thiosulfate antidotal combination (Burrows and Way, 1976; Burrows et. al., 1977). More important, phenoxybenzamine has no cyanide antidotal properties alone; however, a striking synergism is noted when it is combined with sodium thiosulfate. Of academic interest is the observation that the antidotal effects of phenoxybenzamine can be reversed with an alpha agonist, methoxamine. Of all the classes of autonomic agents and vasodilators examined, only the ganglionic blocking agents and alpha adrenergic blocking agents were observed to antagonize the lethal effects of cyanide, and only when they are administered in combination with sodium thiosulfate. The pharmacologic basis why sodium nitrite, but not many other vasodilators, can protect against the lethal effects of cyanide is being intensively investigated by various laboratories. Chlorpromazine also has been reported to be able to protect against cyanide intoxication by an action almost identical to phenoxybenzamine. The mechanism of action of chlorpromazine was found not to be related to hypothermia, but probably more closely related to the alpha adrenergic blocking properties of this phenolthiazine.

III. TREATMENT

At the present time there is no treatment of cyanide casualties on the front line battlefield. The antidotal combination of nitrite-thiosulfate presently is not available for intramuscular use.

A. Supportive Treatment

Because there are numerous effective cyanide antidotal combinations, the importance of supportive treatment is frequently overlooked. Ventilation and oxygenation is quite effective in the treatment of cyanide poisoning. This may become of considerable importance with improvements and modifications of the chlorate candle for oxygenation and improvements in the Burgin mask so that

ventilation can be conducted in the battlefield. Although cyanide is generally attributed to having a high knockdown potency, it also has been reported to have a slow onset of action in many cases. In other words, the onset of action of cyanide may be dose-dependent. Therefore, in the peripheral area of a gas attack, supportive treatment of military personnel may be of importance as they will be exposed to a lower concentration of hydrogen cyanide. The importance of supportive treatment is best illustrated in a report by Stanford University where a man was unconscious for nine hours and the diagnosis of cyanide poisoning was not established. By supportive treatment and correction of blood chemistry it was possible to protect against 600 mg of potassium cyanide (Graham et. al., 1977). This emphasizes that cyanide poisoning can have a prolonged effect and recovery can occur by supportive treatment alone.

B. Oxygen-Sodium Nitrite-Sodium Thiosulfate

The classic antidotal combination of nitrite-thiosulfate is probably as effective as any antidotal combination in the treatment of cyanide poisoning in spite of the fact that the mechanism of action of these antagonists may be viewed presently from a different perspective. Conceptually, the addition of oxygen to this therapeutic regimen provides a striking potentiation; however, whether modification and improvement of the chlorate candle and the Burgin mask will dictate the practicality of oxygen administration under front line conditions is still debatable. However, it should be emphasized that there does not appear to be any hazard in the employment of oxygen, and this procedure can be lifesaving as it doubles the protection of nitrite-thiosulfate. Therefore, whenever possible, the use of oxygen in cyanide poisoning should be a routine measure when practical. Concerning the use of the antidotal combination of sodium nitrite and sodium thiosulfate it should be pointed out that this antidotal combination has not been developed for front line battlefield use at the present time. The intramuscular administration of sodium nitrite and sodium thiosulfate is clearly highly efficacious in laboratory rodents, both therapeutically and prophylactically; however, hemorrhage, edema and necrosis can occur at the site of injection. Whether the drug delivery biopharmaceutic scientists can minimize this effect is important before this antidotal combination can be considered for use in the front lines by self-injectors or by the buddy system.

Various laboratories, particularly those in Germany, have been critical of the use of nitrite-thiosulfate as an antidotal combination against cyanide intoxication and this is based on the presumably slow onset of action of nitrite based on the rate of methemoglobin formation which we presently know is probably not scientifically valid. There have been various advocates for the use of a more rapid methemoglobin former, such as DMAP, to replace sodium nitrite; however, the clear superiority of DMAP over sodium nitrite has not been very convincing.

Although hydroxocobalamin or cobalt EDTA alone have been employed in cyanide poisoning, the adverse effect of cobalt on the myocardium still remains to be resolved (Naughton, 1974). Also, whether this compound can be administered by the intramuscular route has not been established. The use of cobalt EDTA probably may be of greater value militarily as a prophylactic agent

rather than in the treatment of cyanide casualties. However, the use of cobalt compounds can cause severe cardiac arrhythmias and, unlike the addition of oxygen to the nitrite-thiosulfate combination, the use of cobalt compounds may involve considerable hazard.

IV. PROPHYLAXIS

From a conceptual viewpoint, those personnel subjected to a direct hit will not be expected to survive a cyanide attack. The primary value of prophylactic agents is that those personnel in a peripheral area of a war gas attack will have a higher possibility of survival if an effective prophylactic agent can be developed. The approach to sequester and destroy is applicable to developing a prophylactic agent.

The development of antidote(s) to protect against hydrogen cyanide as a war gas should place a major investigative effort on prophylaxis or pretreatment. This is of particular concern since hydrogen cyanide has been known to have a rapid onset of action. The rationale for prophylaxis is that in an unexpected gas attack there will be a massive number of cyanide casualties and conceptually it would be more practical to try to prevent cyanide casualties than treat them, particularly when medical personnel available in the front line is limited. It should be pointed out that hydrogen cyanide as a war gas is nonpersistent, so that the duration of exposure will be for a relatively shorter period of time than for organophosphorus compounds. The tactic to the development of compounds for the prophylaxis against a cyanide attack should be based on sequester and destroy tactic. This was the approach employed in 1933 by K.K. Chen to sequester cyanide by methemoglobin to form cyanmethemoglobin and then to destroy the cyanide by detoxification to thiocyanate. Also, it should be emphasized that the destroy tactic can also be developed prophylactically. This approach would be to increase the natural substances in the body to destroy cyanide, e.g., by increasing the endogenous level of sulfane sulfur. This combination of approach may provide the opportunity for the combat soldier to have a greater capacity to withstand a cyanide attack, since there is a greater capacity of these individuals to sequester and destroy cyanide.

BIBLIOGRAPHY

1. Blake, J., 1839. Observations on the physiological effects of various agents introduced into the circulation as indicated by the hemodynamometer. *Edin. Med. Surg. J.* 51: 330-345.
2. Blake, J., 1840. Observations and experiments on the mode in which various poisonous agents act on the animal body. *Edin. Med. Surg. J.* 53: 35-49.
3. Burrows, G.E., Liu, D.H.W. and Way, J.L., 1973. Effect of oxygen on cyanide intoxication: V. Physiologic effects. *J. Pharmacol. Exp. Ther.* 184: 739-748.
4. Burrows, G.E. and Way, J.L., 1976. Antagonism of cyanide toxicity by phenoxybenzamine. *Fed. Proc.* 35: 533.
5. Burrows, G.E., King, L., Tarr, S. and Way, J.L., 1977. The protective effect of vasoactive compounds as cyanide antagonists. *Proc. Int. Cong. Tox.* 1: 48
6. Chen, K.K., Rose, C.L. and Clowes, G.H.A., 1933. Methylene blue, nitrites and sodium thiosulfate against cyanide poisoning. *Proc. Soc. Exp. Biol. Med.* 31: 250-252.
7. Graham, D.L., Laman, D., Theodore, J. and Robin, E.D., 1977. Acute cyanide poisoning complicated by lactic acidosis and pulmonary edema. *Arch. Int. Med.* 13: 1051-1055. 46: 793-796.
8. Holmes, R.K. and Way, J.L., 1982. Mechanism of cyanide antagonism by sodium nitrite. *Pharmacologist.* 24: 182.
9. Isom, G.E. and Way, J.L., 1978. Effect of oxygen on cyanide intoxication. VI. Reactivation of cyanide inhibited glucose methabolism. *J. Pharmacol. Exp. Ther.* 189: 871-875.
10. Isom, G.E., Burrows, G.E. and Way, J.L., 1982. Effect of oxygen on the antagonism of cyanide intoxication. Cytochrome oxidase in vivo. *Toxicol. and Appl. Pharmacol.* 65: 250-256.
11. Keilin, D., 1966. "The History of Cell Respiration and Cytochrome". Cambridge University Press, Cambridge.
12. Kiese, M. and Weger, N., 1969. Formation of ferrihaemoglobin with aminophenols in the human for the treatment of cyanide poisoning. *Europ. J. Pharmacol.* 7: 97-105.
13. Naughton, M., 1974. Acute cyanide poisoning. *Anaesth. Intens. Care.* 4: 351-356.

14. Paulet, G., 1958. Intoxication cyanhydrique et chelates de cobalt. *J. Physiol. (Paris)* 50: 438-442.
15. Sheehy, M. and Way, J.L., 1968. Effect of oxygen on cyanide intoxication: III. Mithridate. *J. Pharmacol. Exp. Ther.* 161: 163-168.
16. Solomson, L.P., 1982. Cyanide as a metabolic inhibitor. In "Cyanide in Biology", ed. B. Vennesland, E.E. Conn, C.J. Knowles, J. Westley, F. Wissing. pp. 11-28. Acad. Press, London. 548 pp.
17. Sorbo, B.H., 1953. Crystalline rhodanese. I. Purification and physicochemical examination. *Acta. Chem. Scand.* 7: 1129-1136.
18. Sylvester, D.M., Hayton, W.L., Morgan, R.L. and Way, J.L., 1982. Effect of thiosulfate on cyanide pharmacokinetics in dogs. *Toxicol. Appl. Pharmacol.* 69: 265-271.
19. Westley, J., 1977. Sulfurtransfer Catalysis by Enzymes. In "Bioorganic Chemistry". ed. E.E. van Tamelen. 1: 371-390. Acad. Press, New York.
20. Westley, J., 1980. Rhodanese and the Sulfane Pool. In "Enzymatic Basis of Detoxication". ed. W.B. Jakoby. 2: 245-262. Acad. Press, New York.
21. Westley, J., Adler, A., Westley, L. and Nishida, C., 1983. The sulfurtransferases. *Fund. and Appl. Toxicol.* 3: 377-382.
22. Way, J.L., Gibbon, S.L. and Sheehy, M., 1966. Effect of oxygen on cyanide intoxication. I. Prophylactic protection. *J. Pharmacol. Exp. Therap.* 153: 381-385.
23. Way, J.L., 1983. Cyanide antagonism. *Fund. and Appl. Toxicol.* 3: 383-386.

CHEMOPROPHYLAXIS OF CYANIDE INTOXICATION

David E. Davidson Jr.
David Davis
Craig J. Canfield

Division of Experimental Therapeutics
Walter Reed Army Institute of Research
Washington, D.C. 20307



CHEMOPROPHYLAXIS OF CYANIDE INTOXICATION

David E. Davidson
David Davis
Craig J. Canfield

Division of Experimental Therapeutics
Walter Reed Army Institute of Research
Washington, DC 20307

INTRODUCTION

The current use of intravenously administered sodium nitrite and sodium thiosulfate for the definitive medical treatment of cyanide intoxication is based upon scientific principles developed by K.K. Chen in 1933 (1). This therapy is effective, although it has its limitations. For military use, the major limitation is that it must be administered intravenously. This is not very practicable in forward areas, even though medical aidmen are currently being trained to administer intravenous medications. Intravenous treatment at the battalion aid station or at medical treatment eschelons even further to the rear requires evacuation of casualties, and such treatment is too late to be of optimal benefit against the extremely rapid incapacitating and lethal effects of cyanide. Newer drugs for intravenous therapy which have been introduced in Europe, such as the methemoglobin-former DMAP (4-dimethyl-aminophenol) (2), and the cobalt compounds such as cobalt edetate or hydroxycobalamine (3) have not been licensed for use as cyanide antidotes in the United States.

The use of amyl nitrite for early treatment by self or buddy aid is also founded upon the work of Chen of over 50 years ago (4). This application is based upon the fact that amyl nitrite can be administered by inhalation. Recently, because the operational ability to administer amyl nitrite in therapeutic doses to masked personnel under battlefield conditions has been questioned, the U.S. Air Force has removed amyl nitrite from its supply system, and the U.S. Army is considering a similar course of action.

Currently, no drugs exist for prophylaxis of cyanide intoxication, and the questionable validity of current self and buddy aid suggests that these are the areas in which new drug development efforts ought to be focussed primarily. Definitive medical treatment could be improved, but this wouldn't appear to need the highest priority.

The Division of Experimental Therapeutics at WRAIR began laboratory studies on cyanide antidotes in a small way in 1981, working initially on treatment drugs. Late in 1982, this in-house project was expanded to include a contract program and the priority of emphasis was placed upon pretreatment approaches, which we considered were more relevant to the military requirement. Some of the pretreatment drug candidates developed by this program have already been introduced into formal preclinical and clinical trials.

The goals of the current anti-cyanide drug development program are to deliver drugs to the field which will, when used in conjunction with other defensive measures, reduce the number of casualties, reduce the severity and

duration of incapacitation, increase survival, and improve the ability of the individual and the unit to complete their assigned missions on the chemically contaminated battlefield.

In this presentation, I will describe one class of candidate cyanide pretreatment drugs which we believe shows some promise. The specific compound in this class which is of great interest is WR 2823, S-2[5-(aminopentyl)amino] ethyl phosphorothioic acid, a compound originally synthesized as a radioprotective candidate in 1963 by Piper, et al. (5).

MATERIALS AND METHODS

To support the search for new chemical compounds that might be developed into clinical candidates, a series of in vitro and in vivo laboratory models have been established for screening and evaluation. A simple mouse test system has been established at WRAIR for primary testing of candidate pretreatment compounds.

The mouse pretreatment model utilizes 23-27 gm male Charles River ICR mice from the Walter Reed colony. Candidate compounds to be tested are administered intraperitoneally or orally to test animals 15 or 30 minutes prior to challenge with 2 LD50's (17.6 mg/kg) of potassium cyanide subcutaneously. Mortality is recorded at 1, 3 and 7 days after challenge. The dose of test compound for the primary test is equivalent to one-half the acute LD50 of the compound as determined in a preliminary toxicity test or obtained from historical records. In a primary test, 10 mice receive the test compound followed by cyanide challenge, and 10 mice receive test compound without cyanide challenge as toxicity controls. Three challenge control mice receive 2 LD50 of cyanide alone after administration of the drug vehicle.

Test compounds which provide survival of 30% or more of cyanide challenged mice are subjected to confirmatory test; and, as appropriate, to more extensive testing to include quantitative assessment of dose-response relationships, oral effectiveness, duration of protective effect, protective ratio, and effectiveness in combination with other classes of protective compounds. Compounds with protective activity may also be evaluated for therapeutic properties.

The mouse pretreatment model has been extensively characterized and validated by assessment of a variety of known protective compounds representing several chemical classes. The model is highly sensitive and provides reproducible data which support the drug discovery and development process.

More than 200 sulfur compounds from the inventory of the Division of Experimental Therapeutics have been tested for pretreatment activity in the mouse model. Primarily, these are aminoalkylthiols or aminoalkylthiols with sulfur covering functions. More than 20 of these have exhibited activity with protective ratios of 2 or greater.

RESULTS

The results of testing of a variety of sulfur-containing compounds in the primary mouse pretreatment screen are tabulated in Tables 1-4. Since the

cyanide challenge in this test is 2 LD50's, survival of 50% or more among pretreated mice represents a protective ratio of 2 or more. This has been confirmed for a number of these compounds in more advanced studies, but many of the compounds presented today have not as yet reached this level of testing.

The compounds depicted in Table 1 may all be considered thiol analogs of the thiol amino acid, L-cysteine (WR 348); which, when administered at 400 mg intraperitoneally 15 minutes before cyanide challenge, provided 60% survival. The D-stereoisomer has also been tested, and its activity is virtually identical to that of the L-form. WR 347, 2-mercaptoethylamine (MEA), the simplest analog in the aminoalkylthiol series, was considerably more toxic, and it protected against cyanide challenge, but only at doses which were slightly above the limits of tolerance. Glutathione (WR 351) did not afford protection, even at very high doses, nor did N-acetylmercaptoethylamine (WR 622). The N-acetic acid derivative of MEA (WR 429) did, however, provide 40% survival, and at a dose which was only a small fraction of its toxic dose. WR 651 is an interesting alkyl-branched thiol which was quite toxic, but which afforded 70% survival.

WR 2529, an aminoalkylamino compound, protected 40% at a dose well below its LD50. This compound is also a potent radioprotector and it has beta-adrenergic blocking activity (Davidson, unpublished observation). WR 8146 is N-acetylcysteine. The 60% survival is interesting in view of the earlier observation that the decarboxylated analog (WR 622) was ineffective. A possible reason is the toxicity of the decarboxylated compound which could not be tested above the dose of 175 mg/kg. WR 76842 is an amidinium analog. Tolerance was low, but some survivors were observed at a dose of only 26 mg/kg. WR 250188 is the D-stereoisomer of the amino acid cysteine; which, as was indicated above, had comparable pretreatment activity. WR 606 is an analog of British antilewisite which has 2 thiol groups and no amine. The toxic limitations of this compound, known as dimercaprol, are well known in man from its use as a heavy metal and mustard antagonist.

The pharmacological properties of aminothiols, as well as their toxicity and effectiveness against cyanide challenge, can be markedly modified by addition of substituents on the amine or by incorporating substituents on the carbon backbone. Another versatile means of modifying structure-activity relationships is the addition of substituents on the free sulfhydryl group. In general, these "sulfur-covering" functions are intended to be labile; that is, it is intended that the cover group will be removed in vivo by chemical or enzymatic means to release the free thiol group. The "prodrug" is not generally considered an active form of the drug; rather, the free thiol or some subsequent metabolite is viewed as the active compound. In general, free thiols of the sort that have anti-cyanide activity are highly reactive. They are capable of many chemical reactions, including the formation of mixed disulfides with endogenous non-protein and protein thiols in the plasma or within cells. Table 2 lists some compounds with thiol covering functions that have produced survival in mouse pretreatment tests. Represented are isothiuronium compounds (WR 298 and WR 611), a thioimidazole (WR 116728), and thiosulfonates (WR 361 and WR 1607). The best of these was the thiosulfonate of mercaptoethylamine, which produced 80% survival. Disulfiram (WR 6058), which is used in man for control of alcoholism, produced 70% survival.

A considerable number of disulfides have been tested, but only two have exhibited anti-cyanide activity. WR 352 is cystamine, and WR 1089 is the disulfide or 2-mercaptoethylguanidine. Commonly, disulfides are considerably more toxic than their corresponding thiols.

The most interesting group of aminoalkylthiol prodrugs that we have studied are the phosphorothioates. This was true among radioprotectors (6), and it appears to be true for cyanide pretreatment also. It has been clearly demonstrated in vitro and in vivo that the phosphate group is removed enzymatically through the action of intracellular acid or alkaline phosphatases (7). The phosphate covering function reduces the toxicity of many thiols greatly, increases efficacy, and in some cases increases the biological half-life from minutes to several hours. WR 2721 is the best radioprotective phosphorothioate; it is not the most effective cyanide antagonist.

The anti-cyanide activity of selected phosphorothioates in the mouse pretreatment model is indicated in Table 4. WR 638, the phosphorothioate of mercaptoethylamine was protective, but afforded only 30% survival. WR 2721, WR 2578, WR 2822 and WR 3689 have aminoalkyl substituents on the amino function of the mercaptoethylamine moiety. Survival against cyanide challenge is greatest when alkyl chain length between amines is 3 (WR 2721 and WR 3689). Little or no protection was exhibited by analogs with 2 or 4 carbon chains. Toxicity increases with increasing chain length, with the 4 carbon compound (WR 2822) being appreciably more toxic.

WR 44923, WR 80855 and WR 149023 have aminoalkyl substituents on the amine of the 3 carbon thiol, 3-aminopropanethiol. In this series, also, toxicity increases with increasing carbon chain-length between the amines; however, in this case, anti-cyanide activity increases gradually, but not significantly, as chain length increased. At the bottom of Table 4 are two branched aminoalkyl analogs with anti-cyanide activity and low toxicity.

Data for WR 2823, the best of the phosphorothioates with anti-cyanide activity in the pretreatment mouse model, are presented in Table 5. The structure of WR 2823 is indicated, and its close structural similarity to phosphorothioates shown in Table 4 which have considerably less anti-cyanide activity should be noted. The first line of data on Table 5 corresponds to the screening data shown for other phosphorothioates. The LD50 of WR 2823 is 700 mg/kg, and at half that dose, 350 mg/kg, 100% survival was observed. Lesser survival was observed after pretreatment with one-fourth and one-eighth doses. The duration of the protective effect was assessed by administering WR 2823 at various time intervals before cyanide challenge. Virtually complete protection against lethality was observed at all intervals between 15 minutes and 240 minutes (4 hours). At 5 hours, only 40% survival was observed. The protective ratio of WR 2823 was determined by challenging mice with increasing LD50's of cyanide 30 minutes after administration of 350 mg/kg intraperitoneally. A protective ratio of 3.7 was obtained in this experiment.

As I indicated earlier, phosphorothioates such as WR 2823 are metabolized to the free thiol, and to disulfide. Table 6 indicates the activity of the thiol and disulfide metabolites of WR 2823. Both metabolites are 3 to 4-fold more toxic than the prodrug. The thiol appears to have very weak pretreatment

activity, while the disulfide appears to have a protective ratio of approximately 2.

DISCUSSION

The observation that thiol compounds have anti-cyanide activity is not original to our laboratory. Reports of the activities of L-cysteine, N-acetyl-L-cysteine, mercaptopyruvate, cystine, dimercaprol, and a variety of other thiols have appeared in the published scientific literature and in unpublished reports. The novelty of our approach to the use of thiols for pretreatment against cyanide intoxication rests in the application of thiol prodrugs, which reduce toxicity, enhance efficacy and prolong the duration of the protective effect. Most simple thiols that we and others have studied have protective indices of only 1.5-2.0, and protect for no longer than 15-30 minutes at doses relatively close to toxic levels. WR 2823, the best phosphorothioate prodrug, protects against 3.5 LD50 of cyanide at 30 minutes, and provides 100% survival for up to 4 hours against 2 LD50 of cyanide. Two major limitations of WR 2823 are known from the studies performed to date. First, WR 2823 is ineffective when administered orally. Acid hydrolysis occurs in the acid of the stomach, and the free thiol is poorly absorbed. Special formulation to protect WR 2823 from dephosphorylation in the stomach will be necessary if an orally effective dosage form is to be developed. Second, clinical studies in man with intravenously administered WR 2823 and WR 2721 demonstrate that this group of phosphorothioates are free of dose limiting or irreversible toxic effects at dosages considered to be in the therapeutic range; nevertheless, nausea and vomiting have been common side effects at higher intravenous doses, occurring in up to 50% of individuals. This problem will have to be overcome in oral formulation if these compounds are to have military application.

Little is known about the mechanisms by which aminothiols antagonize cyanide, although these mechanisms are under investigation. Reactive thiols can act as scavengers of cyanide by a direct reaction with cyanide ion forming thiocyanate or a 2-aminothiazoline (8), although the importance of this detoxification reaction in man has been questioned. Thiols can also be metabolized and enter the sulfane pool through the action of a sulfurtransferase other than rhodanese. Thus, they would exert an effect similar to that of thiosulfate, which detoxifies cyanide to thiocyanate through the action of the enzyme rhodanese.

Another feature of WR 2823 which needs to be investigated as a possible factor in its anti-cyanide activity is its alpha-adrenergic blocking activity (9). The alpha blocking activity of WR 2823 is so potent and its affinity for the alpha receptor so specific, that it is currently in clinical trial as a candidate anti-shock compound. Unlike many alpha blockers, WR 2823 has no detectable effect on beta receptors, histamine receptors or cholinergic receptors. In addition to its alpha blocking activity, WR 2823 has a direct action on peripheral vasculature, producing vasodilation. The net effect of these actions is a fall in blood pressure, but an increase in stroke volume and cardiac output with increased perfusion and oxygenation of peripheral tissues. A cause and effect relationship has not been established between these cardiovascular actions of WR 2823 and its anti-cyanide action, but in view of the recent observations of Way, et al. (10), which appear to implicate

the cardiovascular effects of nitrites and chlorpromazine in cyanide antagonism, these phenomena deserve investigation.

We believe that WR 2823, or possibly an analog yet to be discovered, may have potential as a pretreatment drug for prevention of cyanide toxicity.

REFERENCES

1. Chen, K.K., Rose, C.L., and Clowes, G.H.A. (1933). Methylene Blue, Nitrites and Sodium Thiosulfate against Cyanide Poisoning. Proc. Soc. Exp. Biol. Med. 31: 250-252.
2. Kiese, M., and Weger, N. (1969). Formation of Ferrihaemoglobin with Aminophenols in the Human for the Treatment of Cyanide Poisoning. Eur. J. Pharmacol. 7: 97-105.
3. Paulet, G. (1957). Sur une nouvelle mise au point du traitement de l'intoxication cyanhydrique. Presse Med. 65: 573-576.
4. Chen, K.K., Rose, C.L., and Clowes, G.H.A. (1933). Amyl Nitrite and Cyanide Poisoning. J. Am. Med. Assoc. 100: 1920-1922.
5. Piper, J.R., Stringfellow, C.R., Elliott, R.D., and Johnston, T.P. (1969). S-2-(ω -Aminoalkylamino)ethyl Dihydrogen Phosphorothioates as Potential Antiradiation Agents. J. Med. Chem. 12: 236-243.
6. Davidson, D.E., Grenan, M.M., and Sweeney, T.R. (1980). Biological Characteristics of some Improved Radioprotectors. Cancer Management 5: 309-320.
7. Kollmann, G., Martin, D., and Shapiro, B. (1971). The Distribution and Metabolism of the Radiation Protective Agent Aminopentylaminoethylphosphorothioate in Mice. Rad. Res. 48: 542-550.
8. Wood, J.L., and Cooley, S.L. (1956). Detoxication of Cyanide by Cystine. J. Biol. Chem. 218: 449-457.
9. Herman, E.H., Heiffer, M.H., Demaree, G.E., and Vick, J.A. (1971). Alpha-adrenergic Antagonism by a Series of Aliphatic Sulfur-containing Compounds. Arch. Intern. Pharmacodynam. Therap. 193: 102-110.
10. Kong, A., Shen, A., Burrows, G., Sylvester, D., Isom, G.E., and Way, J.L. (1983). Effect of Chlorpromazine on Cyanide Intoxication. Toxicol. and Applied Pharmacol. 7: 407-413.

TABLE 1. ACTIVE THIOLS

COMPOUND		<u>LD₅₀ IP</u>	DRUG DOSE <u>mg/kg</u>	TIME (minutes)	<u>SURVIVAL</u>
WR 347	H ₂ NCH ₂ CH ₂ SH	498	249	15	40% (20% toxic)
WR 348	$\begin{array}{c} \text{COOH} \\ \\ \text{H}_2\text{NCHCH}_2\text{SH} \quad (\text{L}) \end{array}$	1250	400	15	60%
WR 351	Reduced Glutathione	1500	750	15	0%
WR 429	H ₂ OCCH ₂ NHCH ₂ CH ₂ SH	2500	156	15	40%
WR 622	CH ₃ CONHCH ₂ CH ₂ SH	350	175	15	0%
WR 651	$\begin{array}{c} \text{CH}(\text{CH}_3)_2 \\ \\ \text{H}_2\text{NCHCH}_2\text{SH} \end{array}$	163	81.5	15	70%

TABLE 1. ACTIVE THIOLS (CONTINUED)

<u>COMPOUND</u>		<u>LD₅₀ IP</u>	<u>DRUG DOSE</u> mg/kg	<u>TIME</u> (minutes)	<u>SURVIVAL</u>
WR 2529	$\begin{array}{c} \text{O} \\ \parallel \\ \text{H}_2\text{NCCH}_2\text{NHCH}_2\text{CH}_2\text{SH} \end{array}$	>2000	450	15	40%
WR 8146	$\begin{array}{c} \text{COOH} \\ \\ \text{CH}_3\text{CONHCHCH}_2\text{SH} \end{array}$	> 800	400	15	60%
WR 76842	$\begin{array}{c} \text{NH} \\ \parallel \\ \text{H}_2\text{NCCH}_2\text{SH} \end{array}$	52	26	15	30%
WR 250188	$\begin{array}{c} \text{COOH} \\ \\ \text{H}_2\text{NCHCH}_2\text{SH (D)} \end{array}$	1250	400	15	80%
WR 606 (BAL)	$\begin{array}{c} \text{SH} \\ \\ \text{HOCH}_2\text{-CH-CH}_2\text{SH} \end{array}$	150	75	15	80%

TABLE 2. COVERED THIOL FUNCTIONS

COMPOUND		LD ₅₀ IP	DRUG DOSE mg/kg	TIME (minutes)	SURVIVAL
WR 298	$\begin{array}{c} \text{NH} \\ \parallel \\ \text{H}_2\text{NCH}_2\text{CH}_2\text{S}-\text{C}-\text{NH}_2 \end{array}$	450	225	30	30%
WR 611	$\begin{array}{c} \text{NH} \\ \parallel \\ \text{H}_2\text{NCH}_2\text{CH}_2\text{S}-\text{C}-\text{NHCH}_3 \end{array}$	163	81.5	30	40%
WR 116728	$\text{H}_2\text{NCH}_2\text{CH}_2\text{S}-\text{S}-\text{C} \begin{array}{c} \text{NH} \\ \parallel \\ \text{N} \end{array}$	325	162.5	30	30%
WR 361	$\text{H}_2\text{NCH}_2\text{CH}_2\text{SSO}_3\text{H}$	525	262	30	80%
WR 1607	$\text{CH}_3(\text{CH}_2)_9\text{NHCH}_2\text{CH}_2\text{SSO}_3\text{H}$	13	6.5	30	40%
WR 6058 (DISULFIRAM)	$\begin{array}{c} \text{S} \quad \text{S} \\ \parallel \quad \parallel \\ (\text{CH}_3\text{CH}_2)_2\text{N}-\text{C}-\text{S}-\text{C}-\text{N}-(\text{CH}_2\text{CH}_3)_2 \end{array}$	800	400	30	70%

TABLE 3. ACTIVE DISULFIDES

<u>COMPOUND</u>		<u>LD₅₀ IP</u>	<u>DRUG DOSE</u> <u>mg/kg</u>	<u>TIME</u> <u>(minutes)</u>	<u>SURVIVAL</u>
WR 352	NH ₂ CH ₂ CH ₂ S—	225	112	30	30%
WR 1089	$\begin{array}{c} \text{NH} \\ \parallel \\ \text{H}_2\text{N}-\text{C}-\text{NHCH}_2\text{CH}_2\text{S}- \end{array}$	80	40	30	30%

TABLE 4. ACTIVE PHOSPHOROTHIOATES

COMPOUND		LD ₅₀ IP	DRUG DOSE mg/kg	TIME (minutes)	SURVIVAL
WR 638	$\text{H}_2\text{NCH}_2\text{CH}_2\text{SPO}_3\text{HNa}$	800	400	30	30%
WR 2721	$\text{H}_2\text{N}(\text{CH}_2)_3\text{NHCH}_2\text{CH}_2\text{SPO}_3\text{H}_2$	1108	554	30	60%
WR 2578	$\text{H}_2\text{N}(\text{CH}_2)_2\text{NHCH}_2\text{CH}_2\text{SPO}_3\text{H}_2$	1300	650	30	0%
WR 2822	$\text{H}_2\text{N}(\text{CH}_2)_4\text{NHCH}_2\text{CH}_2\text{SPO}_3\text{H}_2$	386	193	30	10%
WR 3689	$\text{CH}_3\text{NH}(\text{CH}_2)_3\text{NHCH}_2\text{CH}_2\text{SPO}_3\text{H}_2$	1450	725	30	60%

TABLE 4. ACTIVE PHOSPHOROTHIOATES (CONTINUED)

COMPOUND	LD ₅₀ IP	DRUG DOSE mg/kg	TIME (minutes)	SURVIVAL
WR 44923	550	275	30	30%
WR 80855	225	112.5	30	40%
WR 149023	120	60	30	60%
WR 179209	>1000	500	30	50%
WR 194423	>1250	625	30	50%

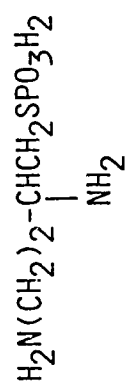
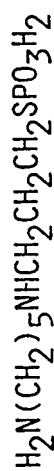
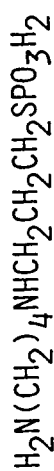
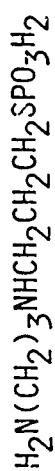




TABLE 5. PROPHYLACTIC CYANIDE TESTING

	mg/kg	TIME	LD ₅₀ CN	SURVIVORS
WR 2823	PHOSPHOROTHIOATE (LD ₅₀ =700 mg/kg)	30	2.0	100%
				80%
				40%
				0%
	350			
	175			
	87.5			
	43.7			
	350	15	2.0	100%
		45		100%
		60		100%
		120		80%
		180		100%
		240		100%
		300		40%
	350	30	2.5	100%
			3.0	80%
			3.5	80%
			4.0	20%
			4.5	0%



TABLE 6. PROPHYLACTIC CYANIDE TESTING

		<u>mg/kg</u>	<u>TIME</u>	<u>LD₅₀ CN</u>	<u>SURVIVORS</u>
WR 149024	DISULFIDE (LD ₅₀ 130 mg/kg)	65	30	2	50%
		32.5	30	2	0%
		16.2	30	2	0%
	THIOL (LD ₅₀ 190 mg/kg)	65	30	2.0	70%
		65	30	3.0	0%
		95	15	2.0	20%

COMPARATIVE ACUTE TOXICITY OF HYDROGEN CYANIDE AND ITS SALTS

BRYAN BALLANTYNE, M.D., D.Sc., Ph.D.

Union Carbide Corporation
Charleston, West Virginia

INTRODUCTION

Hydrogen cyanide and its sodium and potassium salts are known to be absorbed, and produce systemic toxicity, by several routes of exposure. Those which have been described as resulting from accidental or deliberate exposure are summarized in Table 1. Experimental observations on acute lethal toxicity of cyanides, including determination of LD50 and LC50 values, have been undertaken as part of more detailed investigations into the general toxicology of cyanides or the antidotal treatment of acute cyanide poisoning. However, there are few comparative evaluations on acute lethal toxicity of cyanides conducted under controlled conditions. This paper summarizes findings of a study primarily concerned with comparing the acute lethal toxicity of HCN, NaCN and KCN.

METHODS

Animals and Routes

- [1] A comparative study of the acute lethal toxicity as a function of route was conducted in rabbits with particular reference to the following:
 - (a) An investigation into the acute inhalation toxicity of HCN vapor.
 - (b) A determination of the acute lethal toxicity of HCN, NaCN and KCN in aqueous solution by the following routes: intravenous (IV), intramuscular (IM), intraperitoneal (IP), peroral (PO), instillation into the conjunctival sac (CI), and percutaneous (PC).
 - (c) A comparison of the acute toxicity of aqueous solutions of HCN, NaCN and KCN to males and females, given by IM and IP injection.
 - (d) A comparison of the acute lethal toxicity, when instilled into the inferior conjunctival sac, of NaCN as a solution, a solid, and a powder formulation containing 40% (w/w) NaCN and 60% (w/w) kaolin as an inert solid diluent, as contained in many fumigant formulations.
 - (e) A comparison of the acute percutaneous toxicity of aqueous solution of HCN, NaCN and KCN applied to intact or abraded skin.
 - (f) An evaluation of the acute percutaneous toxicity of NaCN under the following conditions:
 - (i) NaCN powder on dry intact skin.
 - (ii) NaCN powder on dry abraded skin.
 - (iii) Solutions of NaCN in water on intact and abraded skin.
 - (iv) A powder formulation, containing 40% NaCN/60% kaolin (w/w), applied to dry intact skin, moist skin, and dry abraded skin.
- [2] Comparative species investigation into the acute lethal toxicity of cyanides as follows:
 - (a) A comparison of HCN, NaCN and KCN given by IP injection to female rabbits, rats, guinea pigs and mice, and PO to rats and rabbits.
 - (b) A determination of the acute lethal inhalation toxicity of HCN vapor to rabbits and rats.
- [3] Measurement of whole blood, serum and tissue cyanide concentrations in rabbits given lethal doses of cyanides by the following routes: IM, IP, PO, CI, PC and inhalation. For noninhalation routes a dose of 8 mg CN/kg was used; for inhalation a 5-min exposure to 3 g/m³ of HCN vapor.

- [4] Measurement of whole blood, serum and tissue cyanide concentrations in rabbits, rats, pigs, sheep and rhesus monkeys given an intramuscular injection of KCN (as 8 mg CN/kg).

Acute Lethal Toxicity Determinations

- [1] For acute inhalation studies with HCN vapor, groups containing between 6 and 10 rabbits or rats were exposed to various concentrations of HCN vapor for different periods of time in order to determine LC50 values for specific exposure periods. For rats the exposure times were 10 sec, 1, 5, 30 and 60 min, and for rabbits 0.75, 5 and 35 min.
- [2] For IV, IP, IM, PO, CI and PC routes of administration, there were 6 to 10 animals for each dose level, and a minimum of 4 dose levels were used for each LD50 determination.
- [3] For abraded skin experiments, sandpaper was gently rubbed over the surface of clipped skin, in order to produce breaks in the stratum corneum.
- [4] LC50 and LD50 values (with 95% confidence limits) were calculated from the dose-mortality data by probit analysis (Finney, 1952).

Measurement of Cyanide Concentrations

- [1] For comparison of cyanide concentrations in rabbits exposed to cyanides by different routes of exposure, there were 6 animals in each group. Immediately after death, blood was taken by cardiac puncture; one portion was used for measurement of whole blood cyanide concentrations, and another for separation of serum for measurement of its cyanide concentration. Samples of liver, kidney, brain, spinal cord, myocardium and lung were taken for measurement of cyanide concentrations.
- [2] For the species comparison, groups containing 6 rats, rabbits, pigs, sheep and rhesus monkeys received 8 mg CN/kg IM, as KCN, and had blood removed for measurement of whole blood and serum cyanide concentrations. Also, liver, kidney, myocardium, brain, lung, and spleen were removed for measurement of cyanide concentrations.
- [3] Cyanide was separated from blood, serum, and saline homogenates of tissues by either a Conway dish (Ballantyne et. al., 1972) or nitrogen aeration procedure (Boxer and Rickards, 1952). Cyanide in the alkaline extract was measured by a modification of the Epstein (1947) procedure (Ballantyne, 1977). Because of the influence of time to sampling and analysis on measured cyanide concentrations (Ballantyne et. al., 1973; Ballantyne et. al., 1974; Ballantyne, 1976), blood and tissues were removed as soon as possible after death and immediately analyzed.

RESULTS

Acute Lethal Toxicity

A. Comparison of Routes in Rabbits

- [1] Values of acute LC50 values for different exposure periods to HCN vapor are shown in Fig. 1 and Table 2. For comparison, L(Ct)50 values are also given. It can be seen that there is a

- disproportionate relationship between the concentration required to cause death at given exposure times for the various exposure periods studied. For the lower atmospheric concentrations of HCN a disproportionately longer time is required to cause mortality than for higher concentrations. This is also reflected in the significantly greater inhalation exposure dosage (Ct) of HCN required for prolonged low concentration exposure than for briefly sustained high concentrations.
- [2] The LD50 values by non-inhalation routes for solutions of HCN, NaCN and KCN are compared in Table 3 (expressed as mg/kg) and Table 4 (expressed on a molar basis). The principal findings were as follows.
- (a) By intravenous injection, although there are differences in toxicity between HCN, NaCN and KCN when expressed on a mg/kg basis, when corrected for the cyanide content by calculating on a molar basis there is little difference in IV lethal toxicity for HCN, NaCN and KCN.
 - (b) By IM injection, HCN is significantly more toxic than NaCN which is significantly more toxic than KCN. There are no differences in acute lethal toxicity between males and females for each cyanide preparation.
 - (c) By IP injection there are no significant differences in acute lethal toxicity, expressed on a molar basis, between HCN, NaCN and KCN. Also, there are no differences between male and female rabbits with respect to acute lethal toxicity for the three cyanide preparations.
 - (d) By gavage, the acute toxicity of aqueous solutions of HCN, NaCN and KCN were similar on a molar basis.
 - (e) When instilled into the conjunctival sac of rabbits, the dose-response relationships allowed the ready calculation of LD50 values for the three cyanides studied. There was no significant difference between NaCN and KCN on a molar basis, but HCN was more toxic by a factor of about 3.
 - (f) By occluded application to intact skin solutions of all three cyanides were lethally toxic. HCN was significantly more toxic than NaCN, which was more toxic percutaneously than KCN. Occluded application of the cyanides to abraded skin resulted in a significant enhancement of percutaneous toxicity. The effect of skin abrasion was particularly pronounced with aqueous HCN, which resulted in a three-fold increase in toxicity based on LD50 estimates.
- [3] The times to onset of signs and death for the solutions of HCN, NaCN and KCN by various routes of exposure to rabbits are shown in Table 5. Times to onset of signs were most rapid with IV injection, followed by the IM, IP, CI and PO routes, and with times to onset by skin contact being significantly delayed. The signs of toxicity included rapid panting breathing, ataxic movements, convulsions, tonic spasms, loss of consciousness, and death. In general the signs of toxicity appeared in this order, but there were variations from animal to animal, and route to route, with respect to the actual order and timing of the signs. Time to death was rapid (<10 min) by the IV, IM, and CI routes, intermediate (<25 min) by IP and PO routes, and prolonged (up to 6 hours) by the PC route. Postmortem features, as found in other studies (Ballantyne, 1973), were few and nonspecific; they included visceral congestion; cerebral, tracheal and pulmonary petechiae; subpleural confluent alveolar hemorrhages.
- [4] LD50 values for the various preparations of NaCN applied to the eye are

shown in Table 6. Although the acute lethal toxicity by CI of the solid is slightly greater than that for the solution, the difference is not statistically significant. Also, the acute toxicity was not significantly modified when NaCN was mixed with the inert material kaolin.

- [5] A comparison of the LD50 values for the various applications of NaCN to skin is given in Table 7. When dry NaCN or NaCN-kaolin were applied to dry intact skin, no deaths occurred up to doses of 200 mg/kg NaCN or 500 mg/kg NaCN-kaolin (= 200 mg/kg NaCN). However, when the skin was moist, death occurred with both solid NaCN and its kaolin formulation; the dose-mortality allowed ready calculation of LD50 values which indicated that the acute percutaneous toxicity on moist skin of NaCN was greater than that of its kaolin formulation (based on NaCN content). When applied to dry abraded skin both the pure NaCN solid and its kaolin formulation caused mortalities, and both had similar percutaneous LD50 values (based on NaCN content). NaCN appeared slightly more toxic by application of the solid to the moist intact skin, than by application of a solution of NaCN to intact skin. For both solution and solid NaCN, there was a significant enhancement of percutaneous toxicity by abrading the skin.

B. Species Comparison.

- [1] The LD50 values for HCN, NaCN and KCN given to different species by IP injection and PO are shown in Table 8. It can be seen that the IP lethal toxicity is similar, for all cyanides examined, when given to rats, guinea pigs and mice; however, the rabbit is more sensitive to cyanides given IP. Additionally, HCN and KCN are more toxic to rabbits than rats when given PO, but such a difference does not exist for NaCN.
- [2] The comparative acute lethal inhalation toxicity data for HCN vapor to rats and rabbits is shown in Table 1, and Figs. 1 and 2. For both species there is a disproportionate relationship between concentration and time to death between high concentration-short duration exposures and prolonged low concentration exposures.

C. Measurement of Cyanide Concentrations in Rabbits Given Cyanides by Different Routes of Exposure.

Concentrations of cyanide in rabbits exposed to lethal doses of cyanide are shown for blood and serum in Table 9, and for tissues in Table 10 (HCN), Table 11 (NaCN) and Table 12 (KCN).

Blood and serum cyanide concentrations are high and diagnostic, but vary with the route of exposure. Highest concentrations are measured following IP, IM, and PO exposures, somewhat lower by PC and CI exposures, and lowest by exposure to HCN vapor.

Tissue concentrations vary significantly with route of exposure. Thus, liver cyanide concentrations are high following IP and PO exposures, intermediate following IM injection, low following PC and CI exposures, and absent by exposure to lethal concentrations of HCN vapor. Kidney and spinal cord levels are consistently low.

Lung, myocardium and brain concentrations of cyanide appear to be diagnostically high and consistently elevated for all the cyanides tested and for all routes of exposure.

D. Species Comparison of Cyanide Concentrations.

Concentrations of cyanide in blood and serum from various species after lethal IM injection of cyanide are given in Table 13, and for various tissues in Table 14.

The blood and serum concentrations were high, of diagnostic significance, and comparable between species. Liver, spleen and kidney concentrations were variable and low in some species. However, cyanide concentrations were high in brain, myocardium and lung.

DISCUSSION

HCN, NaCN and KCN were sufficiently toxic to allow the ready determination of median lethal toxicity values, with narrow 95% confidence limits, by all the various routes of exposure investigated.

Studies on the acute lethal inhalation toxicity of HCN vapor confirmed that a proportionately greater inhalation exposure dose of HCN is required for lethality by prolonged low concentration exposure than by briefly sustained high concentrations. The shape of the LC50-exposure time curve indicates a saturation of the endogenous detoxification mechanisms based on sulfur-transfer processes (Sorbo, 1975).

Given by other routes, HCN, NaCN and KCN were absorbed in amounts sufficient to cause systemic toxicity and death, from which LD50 values with restricted 95% confidence limits could be readily calculated. There were no differences between males and females. Signs typical of acute cyanide poisoning occurred, and their times to appearance appeared to correlate approximately with the anticipated rate of absorption of the materials. With respect to lethality, cyanides were most toxic by the IV and IM routes; intermediate in toxicity were cyanides given IP, PO or CI: and the lowest toxicity was exhibited by cyanides absorbed across intact skin.

Some qualifications are necessary in respect of the above generalizations. For example, HCN by CI has a toxicity only slightly less than that of HCN given by IV injection, both on the basis of LD50 values and times to onset of signs and death. NaCN and KCN by CI, however, have a toxicity equivalent to that given PO. This greater toxicity of HCN, also demonstrated for some of the other routes of exposure, is mainly a function of the lower molecular weight, minimal ionization, and ready diffusibility across biological membranes. Comparison of the LD50 values for NaCN in solution and as a solid revealed no significant differences, and hence within the constraints of the study the physical mode of presentation of NaCN to the eye did not influence potential hazard. Also, when NaCN was mixed with the inert material kaolin, in a powder formulation typical of many fumigant preparations, the decrease in lethal toxicity expressed on a mass basis (mg/kg) was proportional to the kaolin content of the formulation. Hence, the intrinsic toxicity of solid NaCN was not modified by this formulation. The potentially serious hazard from splash contamination of the eye is emphasized by the rapidity of onset of signs of

toxicity and the short latency to death. Biological determinants for the high acute toxicity of cyanides by CI include the vascularity of the conjunctivae, the increase in diffusion area resulting from a promptly induced conjunctival hyperemia, and blepharospasm retaining material in contact with the conjunctiva. Drainage of material into the nasal cavity via the nasolachrymal duct may occur, resulting in absorption of material across the nasal mucosa. A further important determinant of the systemic toxicity of cyanide by transconjunctival absorption is the fact that the material passes directly to the systemic circulation without undergoing first-pass hepatic detoxification. This results in the rapid attainment of toxic blood levels. It follows that contamination of the eye could be a hazardous route of exposure.

HCN, NaCN and KCN in aqueous solution were able to penetrate intact skin in amounts sufficient to cause systemic toxicity and death. In solution, HCN was significantly more toxic than NaCN, which itself was significantly more toxic than KCN. Solid NaCN, as such or in the kaolin powder formulation, was not absorbed in amounts sufficient to cause signs of toxicity or death when applied to dry intact skin. However, when skin was moistened, then systemic toxicity and deaths occurred. Also, formulation with the inert powder kaolin did not alter the systemic toxicity by NaCN by absorption across the skin. Abrasion of skin significantly enhanced toxicity of solutions of HCN, NaCN and KCN, and for solid NaCN and the kaolin powder formulation. These findings emphasize the skin as a potentially hazardous route of exposure to cyanides, particularly if the skin is not intact.

Comparison of the blood cyanide concentrations following the exposure of rabbits by different routes shows that high concentrations of diagnostic significance are produced, although the absolute values vary with the route of exposure. Lowest concentrations, but still of diagnostic significance, were measured following the inhalation of lethal dosages of HCN vapor. Tissue cyanide concentrations vary with route, and some tissues may be inappropriate for analysis. Thus, high cyanide concentrations were measured in liver following IM, IP and PO exposures; concentrations were low by the PC and CI routes; and cyanide could not be detected in liver following exposure to lethal dosages of HCN vapor. Thus, liver may not be appropriate as a tissue for the diagnosis of acute cyanide poisoning by certain routes of exposure. Concentrations of cyanide in kidney and spinal cord were low and also varied with routes of exposure. However, myocardium, lung and brain, had moderately high cyanide concentrations by all the various routes of exposure. The value of myocardium and brain cyanide concentrations for the diagnosis of acute cyanide poisoning was confirmed by the finding that they were also consistently high in various species following exposure by a given route. Additionally, whole blood and serum cyanide concentrations were also high and comparable for the same route of exposure in different species. However, in contrast with the situation in humans (Ballantyne, 1973), spleen cyanide concentrations were generally low following acute cyanide poisoning in various species.

These studies indicate the potential for systemic toxicity by all possible routes of exposure to cyanides. Determinants for toxicity include concentration, exposure time, moisture, and integrity of the absorbing

surface. Whole blood, serum, lung, myocardium and brain are tissues appropriate for a diagnosis of acute cyanide poisoning, providing that sampling and analysis are carried out shortly after death.

SUMMARY

The principal findings and conclusions for the studies presented are as follows:

- (1) For HCN vapor a proportionately greater inhalation dose is required for lethality by prolonged low concentration conditions.
- (2) Acute lethal toxicity by noninhalation exposures, allowing calculation of LD50 values with narrow 95% confidence limits, occurred for the following routes: IV, IM, IP, PO, CI and PC.
- (3) For a detailed study in rabbits, the order of decreasing toxicity was as follows:

HCN:	:	IV = IM > CI > IP > PO > PC
NaCN:	:	IV = IM > IP > CI > PO > PC
KCN	:	IV > IM > IP > PO > CI > PC
- (4) For the different routes, the molar LD50 values for NaCN and KCN were:-
 > HCN for IV, IM, CI and PC
 = HCN for IP and PO
- (5) There were no differences between males and females.
- (6) Times to death were rapid (<10 min) by IV, IM and CI routes; intermediate (<25 min) with IP and PO routes, and prolonged (up to 6 hours) by the PC route.
- (7) For percutaneous toxicity, abrading the skin significantly enhanced toxicity.
- (8) Based on signs, time to death, and LD50 values, instillation into the conjunctival sac was a significant route of exposure for NaCN and KCN, and especially HCN.
- (9) In a study of species differences, the rabbit was significantly more susceptible to the lethal toxicity of cyanides given IP than the mouse, guinea pig and rat; also, cyanides were more toxic perorally to the rabbit than the rat.
- (10) For a given species, blood and serum cyanide concentrations varied with route, but were of diagnostic significance. For the same route with different species, the blood and serum cyanide concentrations were closely comparable between species.
- (11) Cyanide concentrations in brain, lung and myocardium were consistently high for different routes of exposure and different species.
- (12) Liver, spleen and kidney cyanide concentrations were variable with route, and sometimes not diagnostic. For example, liver cyanide concentrations were high by IP, IM and PO routes, but low or absent by PC, CI and inhalation routes.
- (13) Lowest concentrations of cyanide in body fluids and tissues were found following lethal exposures to inhaled HCN.
- (14) HCN, NaCN and KCN can be absorbed in potentially lethal amounts by all possible routes of exposure.

REFERENCES

- Ballantyne, B. (1973). The forensic diagnosis of acute cyanide poisoning. In, *Forensic Toxicology*, Ed. by B. Ballantyne. Wright, Bristol, p. 99.
- Ballantyne, B. (1976). Changes in blood cyanide as a function of storage time and temperature. *J. Forens. Sci. Soc.*, 16; 305.
- Ballantyne, B. (1977). In vitro production of cyanide in normal human blood and the influence of thiocyanate and storage temperature. *Clin. Tox.*, 11; 173.
- Ballantyne, B., Bright, J., Swanston, D.W. and Williams, P. (1972). Toxicity and distribution of cyanides given intramuscularly. *Med. Sci. and Law*, 12; 209.
- Ballantyne, B., Bright, J.E. and Williams, P. (1973). An experimental assessment of decreases in measurable cyanide levels in biological fluids. *J. Forens. Sci. Soc.*, 13; 111.
- Ballantyne, B., Bright, J.E. and Williams, P. (1974). The post-mortem rate of transformation of cyanide. *Forens. Sci.*, 3; 71.
- Boxer, G.E. and Richards, J.C. (1952). Determination of thiocyanate in body fluids. *Arch. Biochem.*, 39, 292.
- Epstein, J. (1947). Estimation of microquantities of cyanide. *Anal. Chem.*, 19; 272.
- Finney, D.J. (1952). *Probit Analysis*. Cambridge University Press, London.
- Sorbo, B. (1975). Thiosulfate sulfur transferase and mercaptopyruvate sulfurtransferase. In, *Metabolism of Sulfur Compounds*. Ed. by D.M. Greenberg, Vol. 7. Academic Press, New York. p. 443.

TABLE 1. Principal Routes of Exposure to Cyanides

ROUTE	PHYSICAL STATE	CAUSE	CIRCUMSTANCES
Inhalation	HCN vapor	Accidental	Industrial processes Fumigation operations
		Intentional	Judicial execution Chemical warfare
Skin contact	Solutions	Accidental	Industrial processes
	Solids Molten NaCN Contaminated clothing High HCN vapor		Fumigation operations
Swallowing	Solids and Liquids	Accidental	Domestic uses
		Intentional	Suicide Homicide

TABLE 2. Comparative Acute Inhalation Toxicity of HCN Vapor

SPECIES	EXPOSURE TIME	MEDIAN LETHAL TOXICITY (95% CONFIDENCE LIMITS)	
		as LC50 (mg/m ³)	as L(Ct)50 (mg min/m ³)
Rat	10 sec	3778 (3771-4313)	631 (562- 719)
	1 min	1471 (664-1471)	1129 (664- 1471)
	5 min	493 (372- 661)	2463 (1861- 3301)
	30 min	173 (159- 193)	5070 (4690- 5497)
	60 min	158 (144- 174)	9441 (8609-10399)
Rabbit	45 sec	2432 (2304-2532)	1824 (1728- 1899)
	5 min	409 (321- 458)	2044 (1603- 2288)
	35 min	208 (154- 276)	7283 (5408- 9650)

TABLE 3. Median Lethal Toxicities for Aqueous Solutions of HCN, NaCN and KCN to Rabbits by Various Routes of Exposure: Expressed as mg/kg.

ROUTE	SEX	CYANIDE	LD50 (95% CONFIDENCE LIMITS) mg/kg
Intravenous	F	HCN	0.59 (0.55-0.65)
		NaCN	1.23 (1.11-1.34)
		KCN	1.89 (1.66-2.13)
Intramuscular	F	HCN	0.50 (0.45-0.55)
		NaCN	1.67 (1.51-1.84)
		KCN	3.27 (2.70-4.10)
	M	HCN	0.52 (0.48-0.56)
		NaCN	1.61 (1.38-1.83)
		KCN	3.06 (2.60-3.60)
Intraperitoneal	F	HCN	1.95 (1.60- 2.60)
		NaCN	2.79 (2.48- 3.09)
		KCN	3.99 (3.40- 4.60)
	M	HCN	1.72 (0.85- 2.00)
		NaCN	2.93 (2.72- 3.35)
		KCN	3.60 (2.71- 4.10)
Peroral	F	HCN	2.49 (2.26- 2.81)
		NaCN	5.11 (4.62- 5.66)
		KCN	5.82 (5.50- 6.31)
Conjunctival instillation	F	HCN	1.04 (0.96- 1.13)
		NaCN	5.06 (4.44- 6.10)
		KCN	7.87 (6.51- 8.96)
Percutaneous (intact skin)	F	HCN	6.89 (6.43- 7.52)
		NaCN	14.62 (13.75-15.35)
		KCN	22.30 (20.40-24.00)
Percutaneous (abraded skin)	F	HCN	2.34 (2.02- 2.61)
		NaCN	11.28 (9.17-12.67)
		KCN	14.30 (13.27-25.09)

TABLE 4. Median Lethal Toxicities for Aqueous Solutions of HCN, NaCN and KCN to Rabbits by Various Routes of Exposure: Expressed as m-mole/kg.

ROUTE	SEX	CYANIDE	LD50 (95% CONFIDENCE LIMITS) m-mole/kg
Intravenous	F	HCN	0.022 (0.020-0.024)
		NaCN	0.025 (0.023-0.027)
		KCN	0.029 (0.026-0.033)
Intramuscular	F	HCN	0.018 (0.017-0.020)
		NaCN	0.034 (0.031-0.038)
		KCN	0.050 (0.042-0.063)
	M	HCN	0.019 (0.018-0.021)
		NaCN	0.033 (0.028-0.037)
		KCN	0.047 (0.040-0.055)
Intraperitoneal	F	HCN	0.072 (0.059-0.096)
		NaCN	0.057 (0.051-0.063)
		KCN	0.061 (0.052-0.071)
	M	HCN	0.064 (0.031-0.074)
		NaCN	0.060 (0.056-0.068)
		KCN	0.055 (0.042-0.063)
Peroral	F	HCN	0.092 (0.081-0.104)
		NaCN	0.104 (0.094-0.116)
		KCN	0.090 (0.085-0.097)
Conjunctival instillation	F	HCN	0.039 (0.036-0.042)
		NaCN	0.103 (0.091-0.124)
		KCN	0.121 (0.100-0.138)
Percutaneous	F	HCN	0.260 (0.240-0.280)
		NaCN	0.298 (0.281-0.313)
		KCN	0.343 (0.314-0.369)
Percutaneous	F	HCN	0.087 (0.077-0.097)
		NaCN	0.230 (0.190-0.259)
		KCN	0.220 (0.204-0.232)

TABLE 5. Times to Onset of Signs of Toxicity and Times to Death with Rabbits Used for the Determination of Acute Median Lethal Toxicities of Solutions of HCN, NaCN and KCN

ROUTE	CYANIDE	TIME TO SIGNS	TIME TO DEATH
Intravenous	HCN	0-17 sec	2.5 - 5.5 min
	NaCN	0-10 sec	2.0 -12.0 min
	KCN	15-30 sec	2.0 - 5.0 min
Intramuscular	HCN	1.75- 3.0 min	3.0 -10.0 min
	NaCN	2.5 - 5.5 min	4.0 -13.0 min
	KCN	3.0 - 6.75 min	4.0 -10.0 min
Intraperitoneal	HCN	1.0 - 2.0 min	2.0 -18.0 min
	NaCN	1.0 - 2.25 min	5.0 -26.0 min
	KCN	1.5 - 4.0 min	5.0 -15.0 min
Peroral	HCN	1.0 - 5.0 min	15.0 -23.0 min
	NaCN	2.0 - 6.5 min	13.0 -26.0 min
	KCN	1.5 - 7.75 min	7.0 -25.0 min
Conjunctival instillation	HCN	0.5 - 1.5 min	3.0 - 7.5 min
	NaCN	2.0 - 2.5 min	4.0 -10.0 min
	KCN	2.0 - 2.5 min	4.5 -11.0 min
Percutaneous (intact skin)	HCN	5.0 -61.0 min	10 min-4.25 hr
	NaCN	1.5 - 4.0 hr	1.75- 5.75 hr
	KCN	0.25- 2.5 hr	0.5 - 5.0 hr
Percutaneous (abraded skin)	HCN	10.0 -20.5 min	15 min-4.75 hr
	NaCN	1.15- 4.0 hr	50 min-6.0 hr
	KCN	20.0 -93 min	30 min-5.75 hr

TABLE 6. Median Lethal Toxicities for Various Preparations of NaCN
Instilled into the Conjunctival Sac of Rabbits.

CYANIDE PREPARATION	LD50 (95% CONFIDENCE LIMITS)	
	as mg/kg	as m-mole/kg
NaCN in aqueous solution	5.06 (4.44- 6.10)	0.103 (0.091-0.124)
Solid NaCN	4.47 (2.47- 5.93)	0.090 (0.060-0.120)
NaCN-kaolin*	9.06 (7.75-11.33)	0.070 (0.060-0.090)**

*60/40 : kaolin/NaCN (w/w)

**Expressed as NaCN content

TABLE 7. Median Lethal Toxicities for Various Preparations of NaCN Applied to the Skin of Rabbits

SKIN CONDITION	CYANIDE PREPARATION	LD50 (95% CONFIDENCE LIMITS)	
		as mg/kg	as m-mole/kg
Dry intact	NaCN powder	> 200	> 4.08
Dry intact	NaCN-kaolin*	> 500	> 4.08**
Moist intact	NaCN powder	11.80 (7.40- 18.90)	0.24 (0.15 -0.39)
Moist intact	NaCN-kaolin*	66.3 (51.3 -130.7)	0.54 (0.42 -1.11)**
Dry intact	NaCN solution	14.62 (13.75- 15.35)	0.298 (0.281-0.313)
Dry abraded	NaCN solution	11.28 (9.17- 12.67)	0.230 (0.190-0.259)
Dry abraded	NaCN powder	7.7 (6.9 - 7.8)	0.160 (0.140-0.170)
Dry abraded	NaCN-kaolin*	21.5 (19.6 - 23.3)	0.180 (0.160-0.190)**

* 40/60 : NaCN/kaolin (w/w)

**Expressed as NaCN content

TABLE 8. Median Lethal Toxicities for Solutions of HCN, NaCN and KCN to various Species by Different Routes of Exposure

ROUTE	SPECIES	SEX	CYANIDE	LD50 (95% CONFIDENCE LIMITS)	
				as mg/kg	as m-mole/kg
Intraperitoneal	Rabbit	F	HCN	1.95 (1.60-2.60)	0.072 (0.059-0.096)
			NaCN	2.79 (2.48-3.09)	0.057 (0.051-0.063)
			KCN	3.99 (3.40-4.60)	0.061 (0.052-0.071)
	Rat	F	HCN	2.23 (1.93-2.59)	0.083 (0.071-0.096)
			NaCN	4.72 (4.42-5.44)	0.096 (0.090-0.111)
			KCN	5.55 (4.84-6.44)	0.085 (0.074-0.099)
	Guinea Pig	F	HCN	2.64 (2.38-2.96)	0.098 (0.088-0.110)
			NaCN	5.51 (4.89-6.23)	0.112 (0.100-0.127)
			KCN	6.49 (5.84-7.21)	0.100 (0.090-0.111)
	Mouse	F	HCN	2.80 (2.70-3.00)	0.103 (0.100-0.111)
			NaCN	4.55 (4.26-4.83)	0.093 (0.083-0.099)
			KCN	6.43 (6.00-7.10)	0.099 (0.091-0.111)
Peroral	Rabbit	F	HCN	2.49 (2.26-2.81)	0.092 (0.081-0.104)
			NaCN	5.11 (4.62-5.66)	0.104 (0.094-0.116)
			KCN	5.82 (5.50-6.31)	0.090 (0.085-0.097)
	Rat	F	HCN	4.21 (3.76-4.95)	0.156 (0.139-0.183)
			NaCN	5.72 (5.23-7.08)	0.117 (0.107-0.144)
			KCN	7.49 (6.68-8.48)	0.115 (0.103-0.130)

TABLE 9. Concentrations of Cyanide in Whole Blood and Serum from Rabbits Exposed to Lethal Doses of HCN, NaCN and KCN by Various Routes (N = 6 for each route).

		CYANIDE CONCENTRATION AS MEAN \pm S.E. (μ g/100 ml)					
FLUID		IP	IM	PO	PC	CI	Inhalation
HCN	Blood	620 \pm 47	746 \pm 121	480 \pm 80	310 \pm 39	552 \pm 51	170 \pm 19
	Serum	279 \pm 30	220 \pm 36	252 \pm 62	144 \pm 30	341 \pm 53	48 \pm 9
NaCN	Blood	390 \pm 52	580 \pm 79	422 \pm 51	248 \pm 13	216 \pm 28	
	Serum	231 \pm 31	330 \pm 54	195 \pm 32	70 \pm 7	80 \pm 16	
KCN	Blood	507 \pm 33	506 \pm 38	524 \pm 20	233 \pm 20	222 \pm 18	
	Serum	209 \pm 25	176 \pm 16	332 \pm 17	69 \pm 5	86 \pm 16	

TABLE 10. Concentrations of Cyanide in Various Tissues Removed from Rabbits Exposed to Lethal Doses of HCN by Various Routes (N = 6 for each route).

CYANIDE CONCENTRATION AS MEAN \pm S.E. (μ g/100 g)						
TISSUE	IP	IM	PO	PC	CI	Inhalation
Liver	691 \pm 130	200 \pm 52	512 \pm 112	26 \pm 12	15 \pm 8	0
Kidney	98 \pm 30	84 \pm 32	82 \pm 18	66 \pm 18	14 \pm 11	6 \pm 4
Brain	167 \pm 37	237 \pm 43	95 \pm 11	97 \pm 22	107 \pm 15	50 \pm 5
Cord	30 \pm 13	86 \pm 18	22 \pm 8	24 \pm 4	29 \pm 8	7 \pm 4
Heart	176 \pm 28	202 \pm 36	104 \pm 14	110 \pm 18	205 \pm 28	62 \pm 4
Spleen	42 \pm 21	26 \pm 8	N.D.*	21 \pm 6	14 \pm 4	6 \pm 3
Lung	182 \pm 28	N.D.*	107 \pm 16	120 \pm 25	225 \pm 51	54 \pm 5

*N.D. = not done.

TABLE 11. Concentrations of Cyanide in Various Tissues Removed from Rabbits Exposed to Lethal Doses of NaCN by Various Routes (N = 6 for each route).

TISSUE	CYANIDE CONCENTRATION AS MEAN \pm S.E. (μ g/100 g)				
	IP	IM	PO	PC	CI
Liver	295 \pm 65	23 \pm 8	306 \pm 71	21 \pm 4	3 \pm 1
Kidney	65 \pm 19	23 \pm 10	37 \pm 8	58 \pm 4	19 \pm 4
Brain	36 \pm 4	43 \pm 6	43 \pm 3	27 \pm 1	29 \pm 4
Cord	36 \pm 3	30 \pm 9	31 \pm 4	19 \pm 3	23 \pm 4
Heart	95 \pm 8	128 \pm 17	70 \pm 6	49 \pm 3	54 \pm 5
Spleen	108 \pm 53	11 \pm 2	397 \pm 91	37 \pm 4	11 \pm 2
Lung	102 \pm 5	175 \pm 25	85 \pm 6	45 \pm 5	49 \pm 8

TABLE 12. Concentrations of Cyanide in Various Tissues Removed from Rabbits Exposed to Lethal Doses of KCN by Various Routes (N = 6 for each route).

TISSUE	CYANIDE CONCENTRATION AS MEAN \pm S.E. (μ g/100 g)				
	IP	IM	PO	PC	CI
Liver	468 \pm 106	7 \pm 3	594 \pm 75	24 \pm 6	0
Kidney	39 \pm 12	22 \pm 10	70 \pm 11	59 \pm 2	18 \pm 5
Brain	92 \pm 11	70 \pm 14	107 \pm 9	29 \pm 5	69 \pm 12
Cord	14 \pm 3	6 \pm 4	37 \pm 11	19 \pm 3	19 \pm 11
Heart	139 \pm 32	131 \pm 10	114 \pm 14	61 \pm 11	73 \pm 11
Spleen	16 \pm 4	0	0	46 \pm 12	8 \pm 4
Lung	133 \pm 13	152 \pm 13	123 \pm 15	51 \pm 7	103 \pm 29

TABLE 13. Concentrations of Cyanide in Whole Blood and Serum from Various Species Given Lethal Intramuscular Injections of KCN (N = 6 for each species).

FLUID	CYANIDE CONCENTRATION AS MEAN \pm S.E. (μ g/100 ml)				
	Rabbit	Pig	Monkey	Rat	Sheep
Blood	444 \pm 58	401 \pm 36	420 \pm 40	402 \pm 20	360 \pm 8
Serum	119 \pm 22	175 \pm 22	156 \pm 25	142 \pm 14	184 \pm 16

TABLE 14. Concentrations of Cyanide in Various Tissues Removed from Different Species Given Lethal Intramuscular Injection of KCN (N = 6 for each species).

TISSUE	CYANIDE CONCENTRATION AS MEAN \pm S.E. (μ g/100 g)				
	Rabbit	Pig	Monkey	Rat	Sheep
Liver	69 \pm 10	86 \pm 25	55 \pm 12	5 \pm 1	285 \pm 41
Kidney	3 \pm 1	155 \pm 46	74 \pm 17	3 \pm 1	133 \pm 20
Brain	118 \pm 18	159 \pm 71	108 \pm 18	120 \pm 14	95 \pm 11
Heart	127 \pm 10	185 \pm 61	126 \pm 18	147 \pm 8	159 \pm 25
Spleen	0	66 \pm 16	19 \pm 3	10 \pm 2	54 \pm 4
Lung	131 \pm 25	112 \pm 50	115 \pm 11	122 \pm 17	138 \pm 19

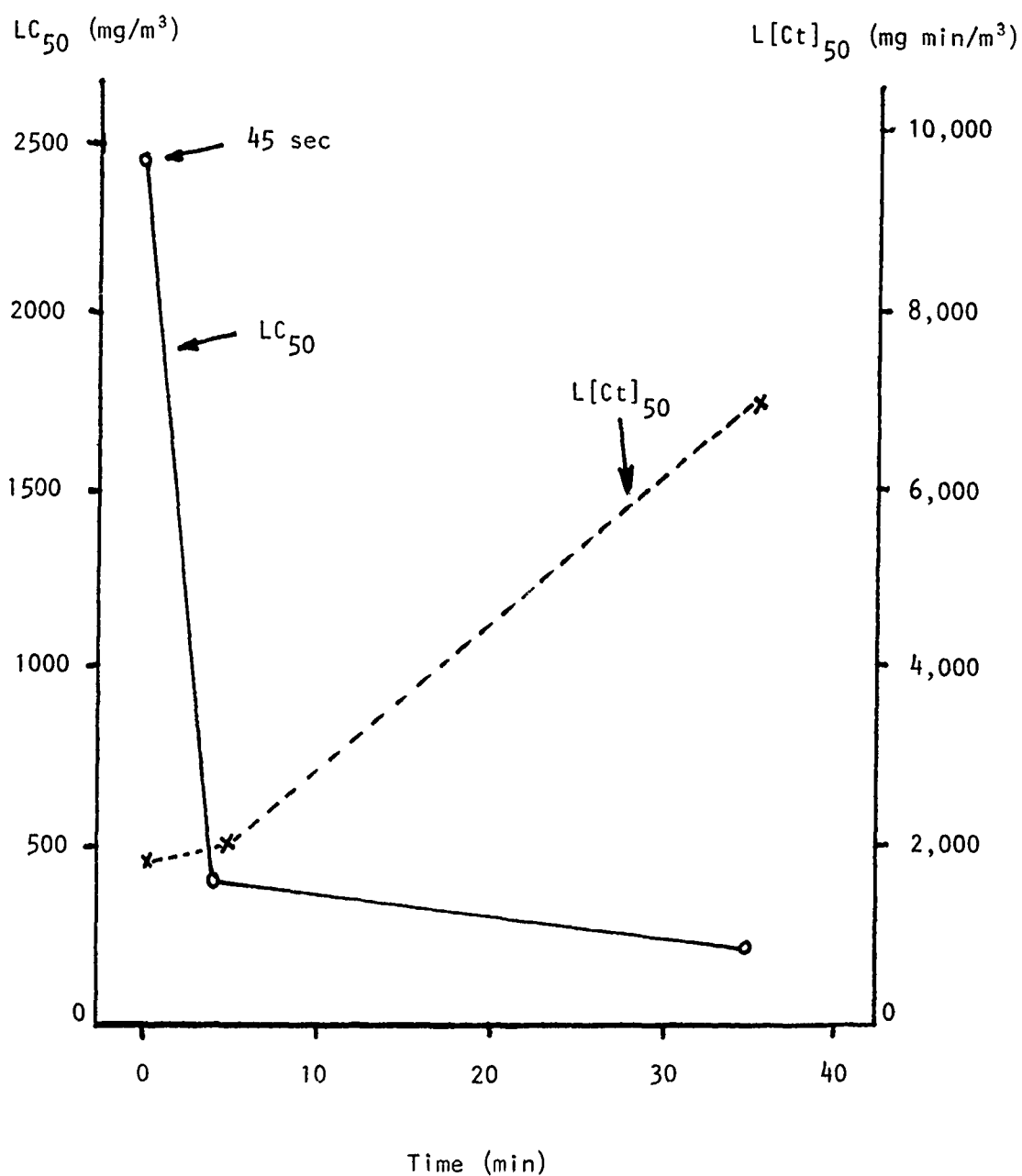


FIGURE 1. LC₅₀ values (connected by continuous lines) and L[Ct]₅₀ values (connected by interrupted lines) for various exposure periods.

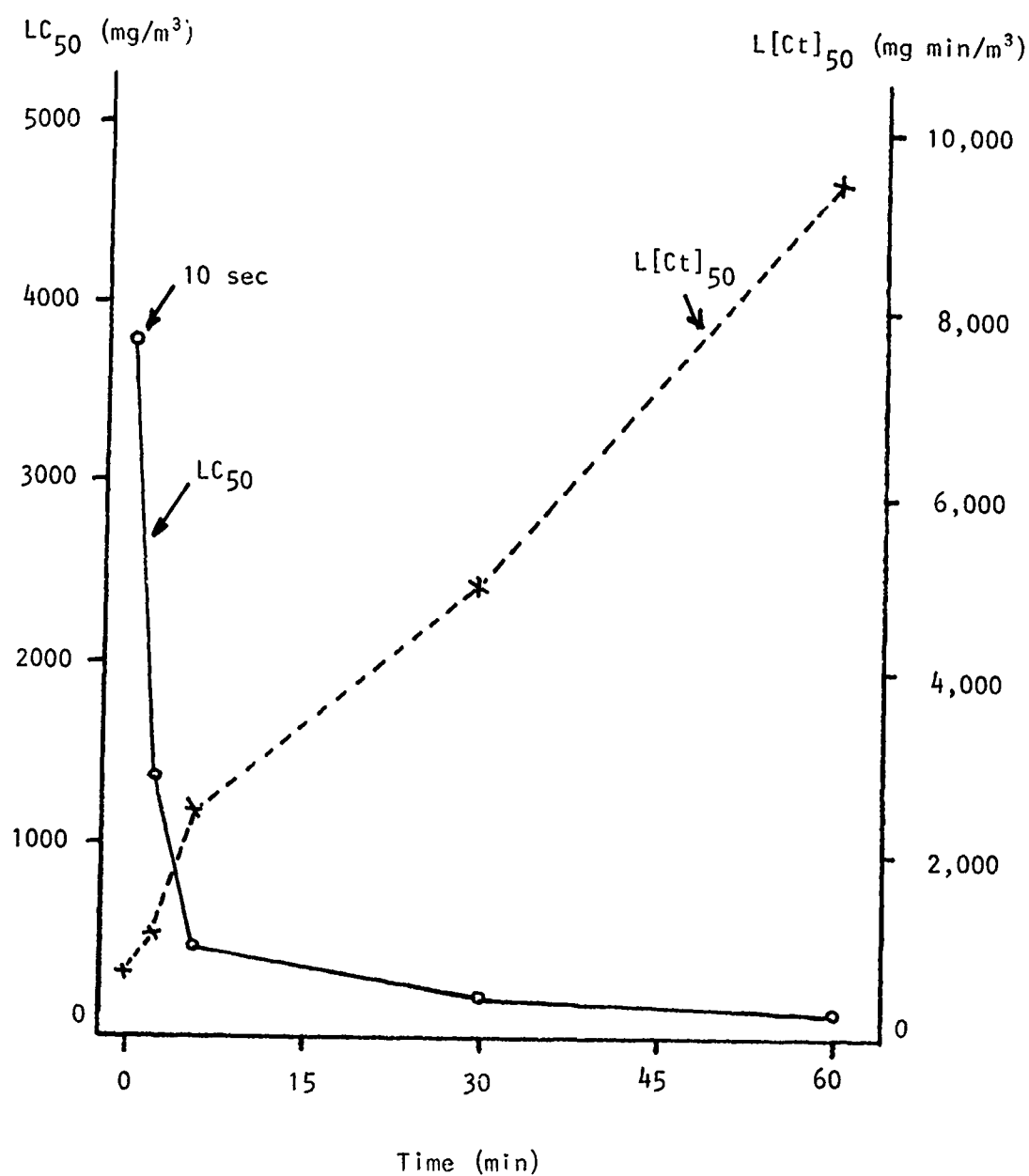


FIGURE 2. LC₅₀ values (connected by continuous lines) and L[Ct]₅₀ values (connected by interrupted lines) for various exposure periods.

Roles of Divalent Sulfur in the Biological
Detoxication of Cyanide

John Westley

Department of Biochemistry, The University of Chicago
920 East 58th Street, Chicago, IL 60637



It has been known for more than half a century that mammalian tissues contain both the enzymes and the substrates necessary for converting cyanide to thiocyanate, which is a very much less toxic material.



Moreover, it was known even earlier that experimental animals given sublethal doses of cyanide excrete most of it as urinary thiocyanate. Thus it has been apparent for a very long time that anyone who wishes to understand cyanide detoxication at the molecular level must be conversant with at least some aspects of the biochemistry of sulfur compounds.

Unfortunately, however, understanding of the relevant areas of sulfur metabolism has been slow to develop and is still rather incomplete. This paper will present a general overview of this area from the perspective of mammalian sulfane biochemistry and then go on to examine some parts of the story in more detail, with an eye to locating other mechanistic roles of divalent sulfur in these processes. Finally, we will report some recent developments that show promise as a basis for future progress.

Sulfane sulfur in metabolism. As will be appreciated from an examination of Fig. 1, which is a kind of map of a part of sulfur biochemistry, we have a quite detailed knowledge of some of the essential features and yet fail to know even the basic facts about others.

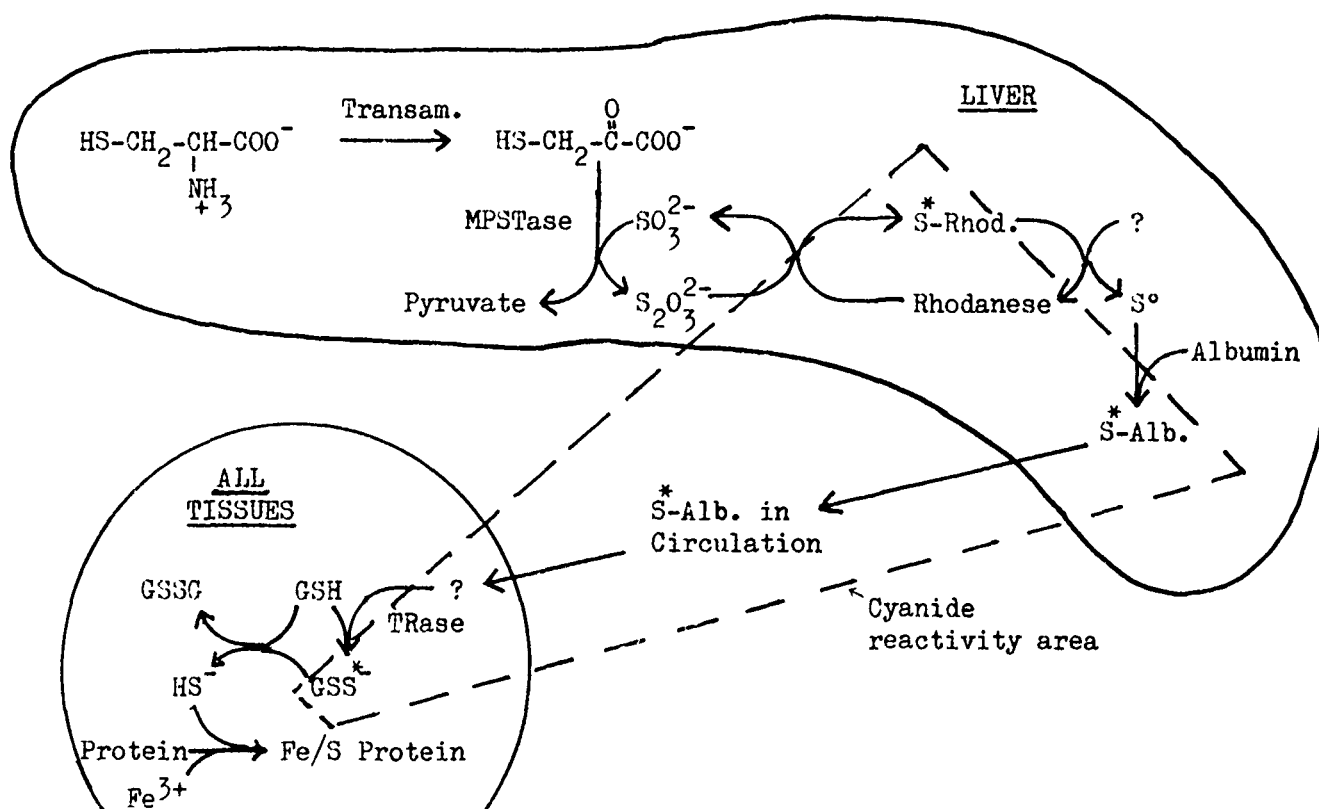


Fig. 1. An explicit hypothesis on the biochemistry of the sulfane pool. The dashed enclosure contains species, denoted by asterisks, known to be highly reactive with cyanide. Compounds not yet definitely identified are indicated by question marks. MPSTase \equiv mercaptopyruvate sulfurtransferase; TRase \equiv thiosulfate reductase.

It is understood that sulfur of the kind that is reactive with cyanide in vivo is derived ultimately from the amino acid cysteine in normal metabolism. Cysteine is transaminated to yield 3-mercaptopyruvate, and the carbon-sulfur bond of this compound is then cleaved by the enzyme mercaptopyruvate sulfurtransferase (EC 2.8.1.2) to pyruvate and a product containing a sulfane sulfur atom. When metabolic sulfite is available (also from cysteine, via a different pathway), this product is inorganic thio-sulfate anion.

Thiosulfate, like other sulfane-containing anions, is a good substrate for the sulfurtransferase known as rhodanese (EC 2.8.1.1), which cleaves the sulfur-sulfur bond of the substrate and forms a sulfur-substituted enzyme that is highly reactive with cyanide. In normal metabolism, however, it appears that some other, as yet unidentified, acceptor substrate removes the sulfane sulfur from sulfur-rhodanese and transfers it as elemental sulfur to serum albumin. The sulfur-albumin is also very reactive with cyanide.

The foregoing hepatic processes result in the formation of sulfane sulfur and also ready it for transport to the peripheral tissues. All tissues utilize inorganic sulfur in the formation of the iron-sulfur proteins of the mitochondrial respiratory assemblies. Sulfane sulfur carried in as elemental sulfur bound to serum albumin becomes available (again we do not know in what molecular form) to the ubiquitous sulfurtransferase known as thiosulfate reductase (EC unassigned). This enzyme catalyzes the reaction of sulfane-level atoms with glutathione to produce glutathione persulfide, which is another sulfane form very reactive with cyanide.

In thiosulfate reductase-catalyzed reactions when cyanide is not present, glutathione persulfide reacts spontaneously with a second molecule of glutathione to yield glutathione disulfide and inorganic sulfur at the level of hydrosulfide. This is the oxidation level of the inorganic sulfur atom in the iron-sulfur centers that are essential components of all mitochondrial respiratory assemblies. Free hydrosulfide is very toxic, but this system of production appears to ensure that it is formed only locally where needed, presumably under some form of metabolic control.

It is our working hypothesis that the molecular mechanisms summarized in Fig. 1 serve two important biological functions. One of these is the detoxication of cyanide, which is a substance encountered with surprising frequency in natural environments and less surprising but more alarming frequency in modern industrial environments. The other is the essential synthesis of iron-sulfur centers by a mechanism that does not involve systemic transport of inorganic sulfide, a material that is as toxic as cyanide.

Molecular mechanisms of enzyme-catalyzed sulfane transfer. From the foregoing discussion it should be understood that the form of divalent sulfur known as sulfane sulfur is required as a substrate in biological cyanide detoxication. What is probably less evident is the fact that there is at least one other major biochemical role of divalent sulfur that appears several times in the reaction sequences of Fig. 1. This is the role of thiophile or sulfur-nucleophile. Cleavage of sulfur-sulfur bonds is of course absolutely crucial to sulfane transfer catalysis. Heading the thiophilicity series (analogous to but not identical to the carbon-nucleophilicity series) is the aliphatic thiolate anion (RS^-). Accordingly, it is no surprise

that, where it is known, the attacking nucleophile that cleaves the sulfur-sulfur bond of sulfane-donor substrates in sulfurtransferase mechanisms is just such an ionized sulphydryl group.

Rhodanese provides the most thoroughly studied example. Fig. 2 displays the established formal mechanism by which this hepatic enzyme catalyzes the transfer of a sulfane sulfur atom from thiosulfate to cyanide.

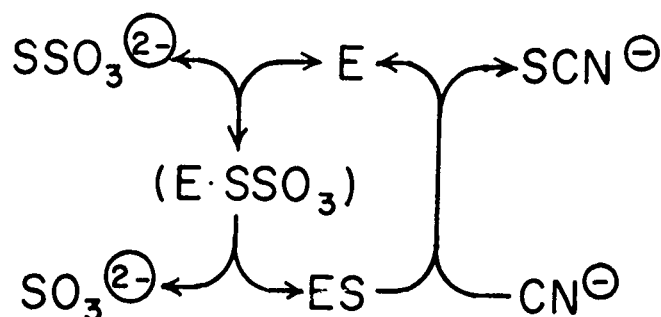


Fig. 2. Formal mechanism of catalysis by rhodanese.

Following the formation of a complex between thiosulfate and the enzyme, the sulfur-sulfur bond of this substrate is cleaved by the enzyme. The product sulfite is then discharged, leaving the sulfur-substituted rhodanese to be attacked by cyanide anion with formation of product thiocyanate and regeneration of the free enzyme (1,2).

The detailed chemical mechanism proposed for the action of rhodanese, on the basis of kinetic and chemical evidence, assigns the role of cleaving thiophile to an enzymic sulphydryl group in its ionized form (3,4). This assignment has since been confirmed by direct chemical studies (5) and is also in accord with the now established primary sequence (6) and high-resolution X-ray crystallographic structure of this enzyme (7,8). The sulfur-substituted rhodanese is thus an enzyme persulfide, and although it is surprisingly stable for a persulfide (stable enough to isolate and crystallize), this form reacts with cyanide anion at a rate approaching the diffusion-controlled limit (3).

Thiosulfate reductase, a sulfurtransferase present in all tissues, makes an interesting contrast with rhodanese in terms of formal mechanism. As shown in Fig. 3, thiosulfate reductase must first form a complex with its sulfur-acceptor substrate, glutathione. Only then can the sulfur-donor

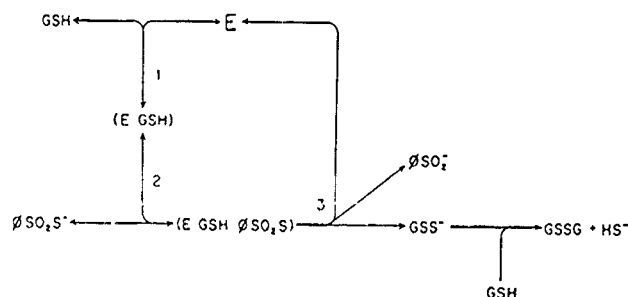


Fig. 3. Formal mechanism of catalysis by thiosulfate reductase.

substrate (here an organic thiosulfonate) enter a complex to be cleaved, with transfer of the sulfane sulfur atom to the acceptor (9). There is no sulfur-substituted enzyme in this catalytic mechanism. Moreover, although the thiosulfate reductase molecule does contain one lone sulfhydryl group, it has been shown that alkylation of this group does not destroy the catalytic activity (10).

It follows that the enzymic sulfhydryl group is not the thiophile that cleaves the donor substrate. That role is taken on instead by the sulfhydryl group of the acceptor substrate glutathione. Again the product is a persulfide but this time glutathione persulfide rather than an enzyme persulfide (9). Nevertheless, glutathione persulfide shares the common persulfide property of being highly reactive with cyanide, and once again divalent sulfur as a sulfhydryl group has played the thiophile role to produce a cyanide-reactive species.

Mercaptopyruvate sulfurtransferase provides a somewhat different kind of example of divalent sulfur participation in the metabolism of sulfane sulfur and cyanide. The sulfur-donor substrate is β -mercaptopyruvate, for which the enzyme seems to be absolutely specific; the acceptor substrate can be any of many thiols, sulfite, or cyanide. As Fig. 4 indicates, the formal mechanism of this enzyme-catalyzed reaction is relatively complex (11).

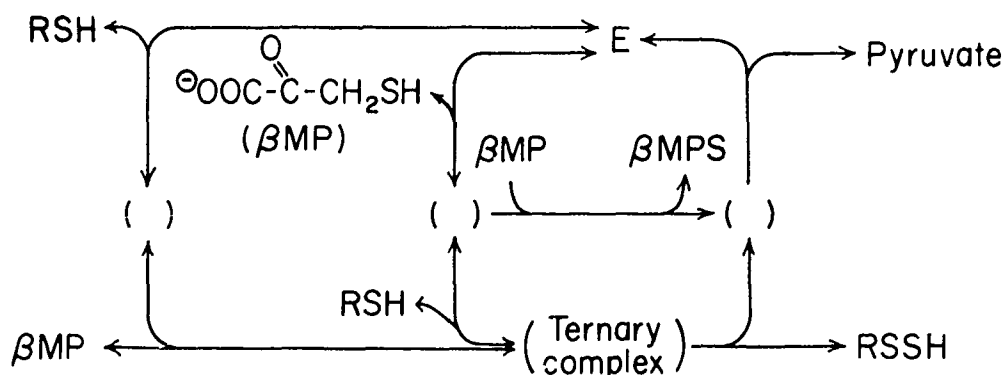


Fig. 4. Formal mechanism of catalysis by mercaptopyruvate sulfurtransferase.

When a thiol is used as acceptor substrate, either the sulfur donor or the acceptor may complex first with free enzyme, followed by the other substrate. Furthermore, since mercaptopyruvate, the donor substrate, is also a thiol, it can also serve as an acceptor substrate -- hence the inner cycle in Fig. 4 that is simply a disproportionation between two molecules of mercaptopyruvate to yield one molecule of pyruvate and one of mercaptopyruvate persulfide. It is to be noted that in the cycles involving RSH, the "intended acceptor," the sulfane sulfur product is also a persulfide, and thus a product having high cyanide reactivity is always produced.

Recent developments. There have been several recent advances that improve our understanding of the systems under discussion here, although they unfortunately also bring additional complexity to the story.

The sulfane pool, a physiological collection of reactive materials containing sulfane sulfur (Fig. 5), is a notion that originated in response to in vivo labeling patterns following administration of radioactive thio-sulfate (12). This concept has been well received, but we are still in the

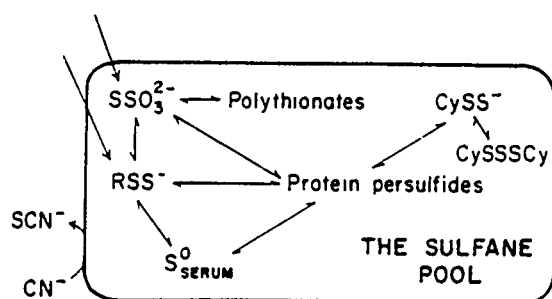


Fig. 5. The physiological pool of sulfane sulfur.

early stages of examining pool components for their quantitative significance in cyanide detoxication. One result that has helped bring the participation of elemental sulfur into better focus was the finding that rhodanese has access to elemental sulfur despite earlier literature reports to the contrary. The key to this observation is the presence in vivo of glutathione, which functions as a cofactor for rhodanese in this reaction. At physiological concentrations, glutathione reacts rapidly with elemental sulfur to form a persulfide, and it is this compound that serves as an efficient sulfur-donor substrate for rhodanese (13). We now understand that the processes within the sulfane pool which result in rapid equilibration of sulfane forms in vivo are the combined result of several reactions, some enzyme-catalyzed and some spontaneous (14).

Sulfur-albumin has provided a further focus for research in this area. Mammalian serum albumins have carrier sites that can be titrated with elemental sulfur (15). Bo Sörbo originally observed that the presence of serum albumin increases the cyanolysis rate of colloidal elemental sulfur (16). Further investigation of this phenomenon has shown that serum albumin recycles exactly like an enzyme and is in fact a perfectly respectable sulfurtransferase for the reaction of sulfur with cyanide (Fig. 6). The most recent

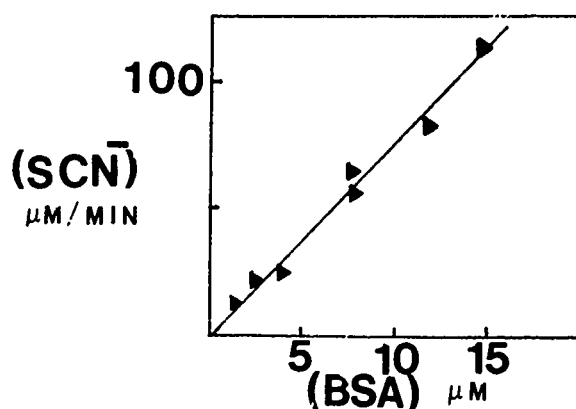


Fig. 6. Bovine serum albumin as a sulfurtransferase.

result from investigations of the albumin catalysis at the molecular level is that in this case, despite the high cyanide reactivity of the sulfur-albumin, intermediate persulfide formation does not seem to be involved. Physiologically, considering the quantity of serum albumin present in the circulation, the albumin-mediated reaction appears to have potential for being the main natural cyanide detoxication buffer in mammals with fully loaded sulfane pools (17).

Several new tools have recently become available for the use of investigators who study the transfer of sulfane sulfur atoms. Two of these are chromogenic substrates for rhodanese and thiosulfate reductase, both shown in Fig. 7. Another tool is the silica gel thin layer chromatography

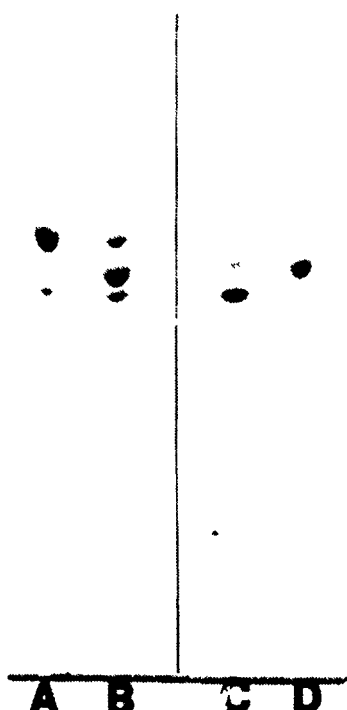


Fig. 7. Thin-layer chromatogram of new sulfurtransferase substrates. A, 4-(dimethylamino)-4'-azobenzene thiosulfonate with a trace of the sulfinates; C, the sulfinates with a trace of the sulfonates; D, the sulfonate (methyl orange) alone; B, a mixture of all three components.

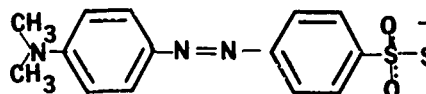


Fig. 8. 4-(dimethylamino)-4'-azobenzene thiosulfonate

system used for these separations and applicable to the examination of thiosulfonates generally (18). The fast-moving compound on these chromatograms is 4-(dimethylamino)-4'-azobenzene thiosulfonate (Fig. 8); the slowest moving is the corresponding sulfinates. Synthesis of these compounds (17) provides, respectively, a sulfur donor substrate for both rhodanese and thiosulfate reductase, used with acceptor cyanide in the one case and acceptor glutathione in the other, and a sulfur-acceptor substrate for rhodanese, used with thiosulfate as donor. Continuous observation of the reactions is at 500 nm, where the thiosulfonate has about one-third more absorption than the sulfinates. The third (middle) compound on the chromatograms is the corresponding sulfonate, which is the common indicator dye methyl orange.

SUMMARY

Most cyanide that enters the mammalian organism, whether by inhalation, injection or ingestion, is detoxified by conversion to thiocyanate, which is excreted in the urine. Investigations concerning the physiological sources of the sulfane sulfur used in this conversion have implicated a rapidly equilibrating pool of potential sulfane donors, including per- and polysulfides, thiosulfonates, polythionates, inorganic thiosulfate, and protein-associated elemental sulfur. This research has thus linked cyanide detoxication to sulfur metabolism in several ways. Moreover, close study of the isolated enzymes that catalyze the formation, interconversion, and cyanolysis of the various physiological materials that contain sulfane sulfur has shown that divalent sulfur also has additional roles in these catalytic mechanisms.

Mammalian liver rhodanese, an enzyme long associated with cyanide detoxication, has an active site sulfhydryl group that serves as the nucleophile which cleaves the sulfur-sulfur bond of the sulfane-donor substrate. A sulfur-substituted rhodanese that is the direct molecular donor to cyanide is an obligatory intermediate in the enzyme-catalyzed reaction. In contrast, the ubiquitous enzyme known as thiosulfate reductase has no sulfur-substituted form but utilizes the sulfhydryl group of the sulfur-acceptor substrate glutathione as an attacking nucleophile, thus producing the cyanide-reactive product glutathione persulfide. In yet another variation on this theme, mammalian β -mercaptopyruvate sulfurtransferase cleaves a carbon-sulfur bond in its thiolic substrate to produce a sulfane-level sulfur atom which may then either be equilibrated with other sulfane forms or reacted directly with cyanide.

Finally, it has also been found that mammalian serum albumins can serve as sulfane carriers, transporting elemental sulfur in a cyanide-reactive form. Strategies for analysis and deliberate manipulation of the cyanide-reactive physiological sulfane pool are currently under investigation.

References

1. Westley, J., *Adv. Enzymol.* 32, 327-368 (1973).
2. Sörbo, B., In *Metabolic Pathways*, Third Edn., Vol. 7 (D. M. Greenberg, ed.) pp. 433-456, Academic Press, New York, 1975.
3. Schlesinger, P., and Westley, J., *J. Biol. Chem.* 249, 780-788 (1979).
4. Westley, J., In *Bioorganic Chemistry*, Vol. 1 (E. E. van Tamelen, ed.) pp. 371-390, Academic Press, New York, 1977.
5. Weng, L., Heinrichson, R. L., and Westley, J., *J. Biol. Chem.* 253, 8109-8119 (1978).
6. Russel, J., Weng, L., Keim, P. S., and Heinrichson, R. L., *J. Biol. Chem.* 253, 8102-8108 (1978).
7. Ploegman, J. H., Drent, G., Kalk, K. H., and Hol, W. G. J., *J. Mol. Biol.* 123, 557-594 (1978).
8. Hol, W. G. J., Lijk, L. J., and Kalk, K. H., *Fundam. Appl. Toxicol.* 3, 370-376 (1983).
9. Chauncey, T. R., and Westley, J., *J. Biol. Chem.* 258, 15037-15045 (1983).
10. Chauncey, T. R., and Westley, J., *Biochim. Biophys. Acta* 744, 304-311 (1983).
11. Jarabak, R., and Westley, J., *Biochemistry* 19, 900-904 (1980).
12. Schneider, J. F., and Westley, J., *J. Biol. Chem.* 244, 5735-5744 (1969).
13. Westley, J., and Adler, H., *Fed. Proc.* 42, #4 (1983). Full report in preparation.
14. Westley, J., and Adler, H., *Fed. Proc.* 42, #7 (1983). Full report in preparation.
15. Vennesland, B., Castric, P. A., Conn, E. E., Solomonson, L. P., Volini, M., and Westley, J., *Fed. Proc.* 41, 2639-2648 (1982).
16. Sörbo, B., *Acta Chem. Scand.* 9, 1656-1660 (1955).
17. Westley, J., Adler, H., Westley, L., and Nishida, C., *Fundam. Appl. Toxicol.* 3, 377-382 (1983).
18. Westley, A., and Westley, J., Submitted for publication.
19. Burrous, M., and Westley, J., Manuscript in preparation.

INTERACTION OF CARBON MONOXIDE AND CYANIDE

Norris, J. C., Moore, S., Fontenot, H. J., Wilson, R. D.
Ho, I. K. and Hume, A. S.

Departments of Pharmacology/Toxicology and
Anesthesiology
University of Mississippi Medical Center
Jackson, Mississippi 39216-4505



INTRODUCTION

The majority of fire fatalities result from inhalation of toxic combustion products (Thomas, 1971; Birky and Clarke, 1981). A study by Birky *et al.* (1979) involved 530 fire cases in which 11% of fire-related deaths were due to burns while 89% were attributed to inhalation of toxic smoke and hot gases. Of these inhalation-related deaths, only 67% were considered the result of carbon monoxide poisoning. In addition, sublethal percentages of carboxyhemoglobin were found in the blood of the other inhalation victims. Other factors such as ethanol and heavy metals were also implicated in these deaths (Birky *et al.*, 1979). However, direct contribution by these factors in these fatalities was discounted and thus, the cause of death was not determined. Data from Teige *et al.*, (1977) reported that 32% of the victims studied had carboxyhemoglobin percentages below lethal levels.

Hydrogen cyanide, a potent toxin, has also been found to be a constituent of fire gases (Mohler, 1975; Anderson and Harland, 1982). Hydrogen cyanide is generated in fires by the thermal degradation of materials containing nitrogen such as wool, silk, polyurethane and polyacrylonitrile (Woolley, 1972; Sumi and Tsuchiya, 1973). Reports have been made showing that, indeed, the blood of fire victims contains cyanide (Wetherell, 1966; Mohler, 1975; Birky and Clarke, 1981). However, the cyanide blood concentrations in these victims were not within the lethal range, so that cyanide could not be positively identified as the lethal agent in these victims.

After studying data from air crash-related fire victims, Mohler (1975) concluded that perhaps the combined sublethal blood levels of carbon monoxide and cyanide could be considered as a cause of death. Such an interaction could provide an explanation for those deaths previously unexplained.

METHODS

Animals and Chemicals

Male ICR mice from Charles River (Wilmington, MA) were used in these experiments. The living conditions (lighting and temperature) of the animals were automatically controlled. Standard laboratory diet and water were provided *ad libitum*. Potassium cyanide was obtained from Aldrich (Milwaukee, WI). Methanol, sodium carbonate and sodium bicarbonate were purchased from J. T. Baker (Philipsburg, NJ). Saponin and potassium ferricyanide were obtained from Fisher Scientific (Fair Lawn, NJ). Toluene was obtained from Mallinckrodt (St. Louis, MO). Dichloromethylsilane was purchased from Kodak (Rochester, NY). Methane (4.75%), air and carbon monoxide were obtained from Lincoln Big Three (Jackson, MS). Molecular sieve 5A column packing material was purchased from Coast Engineering Laboratory (Gardena, CA). Porapak Q-S column packing material and reaction vessels were obtained from Supelco (Bellefonte, PA).

Carbon Monoxide Chamber

A plexiglass chamber was specifically designed for animal exposure to carbon monoxide. The chamber was 16.8 inches long, 12 inches wide and 4.75 inches. The chamber was divided into two compartments by a sliding door. The outer chamber served as a foyer. When the appropriate carbon monoxide concentration was reached the animals were placed in the foyer. After the outer door to the foyer was closed, the sliding door was opened. The animals

entered the inner chamber, then the sliding door was closed. This procedure allowed minimal disturbance to the carbon monoxide concentration. A stable carbon monoxide concentration was insured with intermittent gas sampling. Dead space within the chamber was avoided by installing a fan which maintained a homogenous atmosphere.

Carbon Monoxide Determination

A. Determination of the Level of Carbon Monoxide in Chamber

The procedure of Winek and Prex (1981) was used to determine CO percentages in the chamber. A one milliliter sample of the chamber atmosphere was injected into a Tracor 550 chromatograph equipped with a thermoconductive detector. The column was packed with molecular sieve 5A, 60-80 mesh. Operating conditions of the gas chromatograph were: inlet temperature, 160°C; column temperature, 100°C; detector temperature, 163°C; detector current, 205ma and helium flow 30 ml/min. A Hewlett-Packard 3390A integrator recorded the detector's output and calculated carbon monoxide percentages in the chamber.

B. Determination of Carbon Monoxide in Blood

Blood concentrations of carbon monoxide were determined according to the procedure of Winek and Prex (1981) with some modifications. Blood from each decapitated animal was collected in a tube containing heparin. Fifty μ l of blood was transferred to a one ml reaction vessel which could be capped with a Teflon^R lined septum seal. Before capping the reaction vessel, 450 μ l of saponin solution (100 mg/100 ml) was added. Two hundred and fifty μ l of headspace was removed from the sealed vial and then one hundred μ l of 4.75% methane (95.25% nitrogen) was added for an internal standard. One hundred and fifty μ l of degassing solution (20 g sodium carbonate, 20 g sodium bicarbonate and 15 g potassium ferricyanide/550 ml water and 5 ml Triton X-100) was added, then the vial was shaken for 10 minutes. Five hundred μ l of headspace from the reaction vessel was injected into the gas chromatograph mentioned in the previous section. The concentration of CO contained in the blood was calculated by comparing the peak areas of CO with the peak areas of the known volume of CH₄.

Cyanide Determination

Blood was collected from each animal in a heparinized tube, and was analyzed for cyanide according to the method of McAuley and Reive (1983). Two hundred μ l of blood was placed in a one ml, silanized reaction vessel. After sealing the reaction vessel, one hundred μ l of glacial acetic acid was added, vortexed for 30 sec and then heated in a 60°C water bath for one hour. One hundred μ l of headspace from the reaction vessel was injected into a Hewlett-Packard gas chromatograph equipped with a nitrogen-phosphorus detector. The operating conditions of the gas chromatograph were: inlet temperature, 250°C; carrier gas flow, 30 ml/min; air flow, 56 ml/min; helium-hydrogen flow, 27.5 ml/min. The 6-foot glass column was packed with Porapak Q-S, 80-100 mesh.

LD₅₀ Value of Potassium Cyanide (KCN) in Animals Exposed to Air or Carbon Monoxide (CO)

Animals were subjected to an atmosphere in the chamber containing either

air or CO, 0.63-0.66% for three minutes. After this pretreatment of air or CO, animals were given various doses of KCN, 4-9 mg/kg, i.p. Each dose of KCN was given to 10 animals. From the percentage of dead animals at each KCN dose, the LD₅₀ value of KCN in air and CO-pretreated animals was determined by the method of Litchfield and Wilcoxon (1949).

Carbon Monoxide Lethality in Saline or Potassium Cyanide (KCN) Pretreated Animals

Animals were pretreated with either saline, 0.1 ml/10 g, i.p., or a dose of KCN, 3-6.35 mg/kg, i.p., then placed in the chamber with an atmosphere percentage of CO ranging from 0.325 to 0.375%. Ten animals of both saline and a KCN dose pretreatment were in the chamber at the same time. KCN-pretreated animals were marked so that they could be distinguished from saline-pretreated animals. The time of death was noted by the cessation of respiration. Chi square test was used to determine degree of significance.

Blood Concentrations of Cyanide and Carbon Monoxide in Potassium Cyanide (KCN) Pretreated Animals that were Subjected to a Carbon Monoxide Atmosphere

Groups of ten animals were used in these experiments. Five of these animals received saline, 0.1 ml/10 g, i.p., while five other animals were given KCN, 3.5 mg/kg, i.p. Immediately after these injections, these 10 animals were transferred to the chamber with an atmosphere of CO, 0.325 to 0.375%, for 4 min. After being removed from the CO chamber, animals were sacrificed by decapitation and blood collected. The same procedure was followed for three groups, each containing ten animals which were exposed for time points of 6, 10 and 12 min. Both cyanide and carbon monoxide concentrations from the blood of KCN-pretreated animals were determined. Blood from saline-pretreated animals was analyzed for CO concentrations. Comparison of CO blood concentrations was made between saline- and KCN-pretreated animals. Five animals were pretreated with KCN, 3.5 mg/kg, i.p., and placed in the chamber with an atmosphere of air for 4 min. After removal from the chamber, these animals were sacrificed and blood was collected. The same procedure was followed for three groups, each containing five animals, which were exposed for time periods of 6, 10 and 12 min. Cyanide concentrations in this blood were determined and compared to cyanide blood concentrations from animals in the CO atmosphere. Student's *t* test was used to determine degree of significance.

RESULTS

LD₅₀ Value of Potassium Cyanide (KCN) in Animals Exposed to Air or Carbon Monoxide (CO)

The effect by CO on the LD₅₀ value of KCN was investigated to determine the possibility of an interaction between cyanide and CO. The data demonstrate that animals pretreated with CO did have a significantly lower LD₅₀ value for cyanide than animals pretreated with air (Figures 1 and 2).

Carbon Monoxide Lethality in Saline or Potassium Cyanide (KCN) Pretreated Animals

Effects on CO lethality by administration of sublethal doses of KCN were determined. The two lower doses of KCN (3 and 3.5 mg/kg, i.p.) produced no significant change in CO lethality as compared to CO lethality in saline-pretreated animals (Figures 3 and 4).

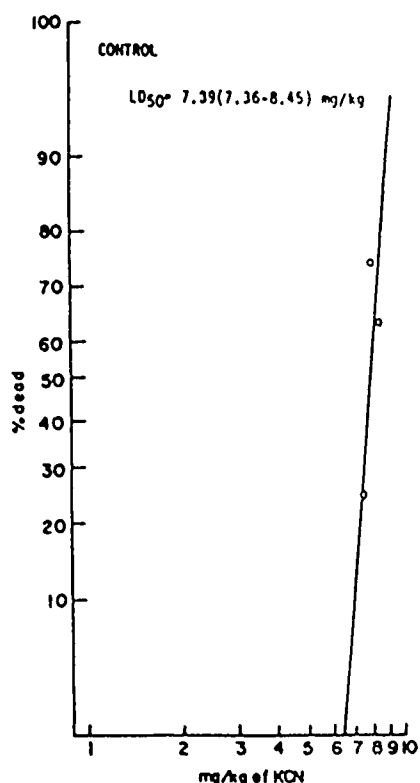


Figure 1. Lethality curve of potassium cyanide for air pretreated animals

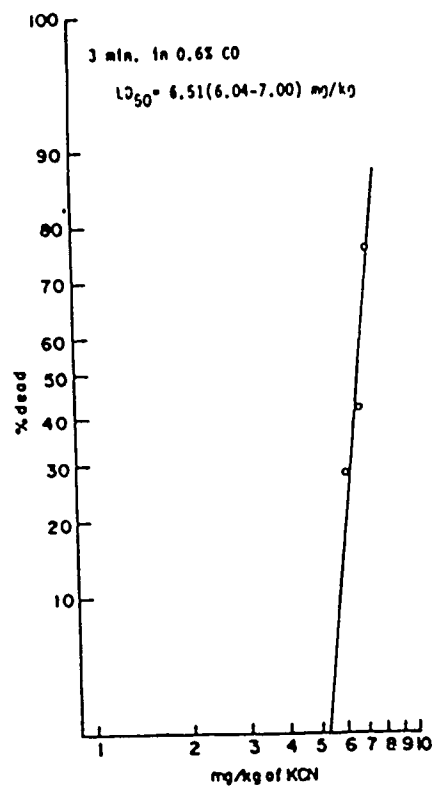


Figure 2. Lethality curve for potassium cyanide for animals pretreated with 0.6% CO for 3 minutes.

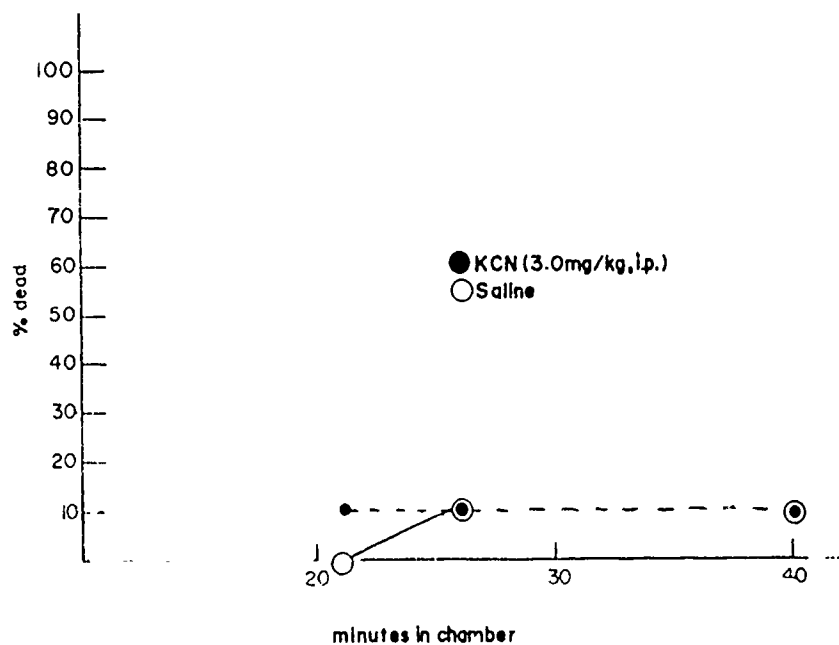


Figure 3. Lethality of animals pretreated with either saline, 0.1 ml/10g, i.p., or KCN, 3.0 mg/kg, i.p., and then placed in the chamber with an atmosphere of CO, 0.325 to 0.375%.

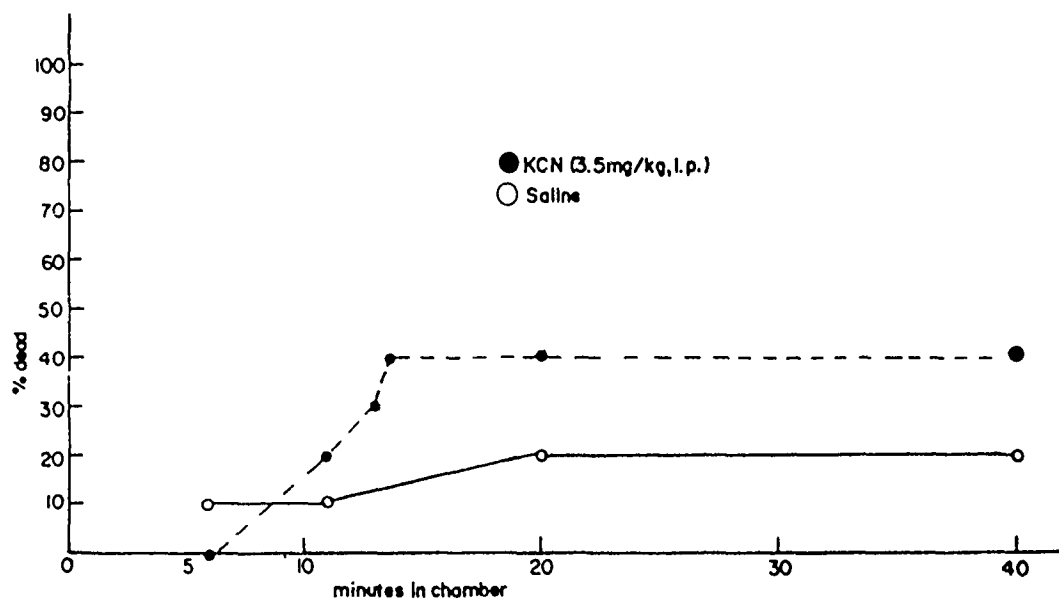


Figure 4. Lethality of animals pretreated with either saline, 0.1 ml/10g, i.p., or KCN, 3.5 mg/kg, i.p., and then placed in the chamber with an atmosphere of CO, 0.325 to 0.375%.

However, animals pretreated with higher doses (3.75, 4, 5.8 and 6.35 mg/kg, i.p.) of cyanide resulted in significantly higher mortalities (70, 80, 100 and 100%, respectively) than animals pretreated with saline in the CO atmosphere (Figures 5, 6, 7 and 8).

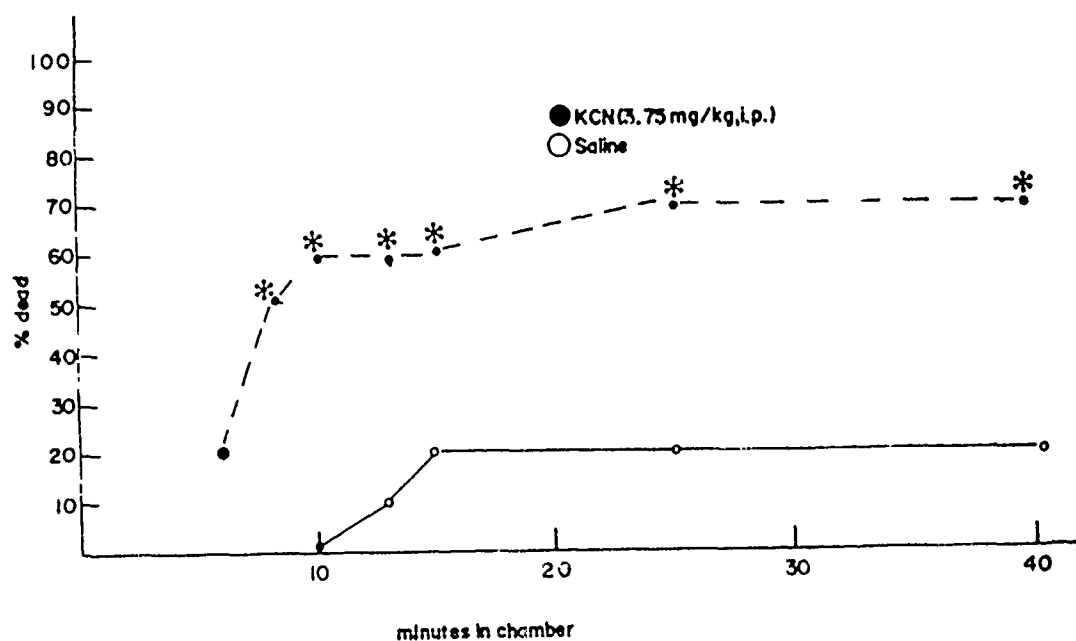


Figure 5. Lethality of animals pretreated with either saline, 0.1 ml/10g, i.p., or KCN, 3.75 mg/kg, i.p., and then placed in the chamber with an atmosphere of CO, 0.325 to 0.375%.

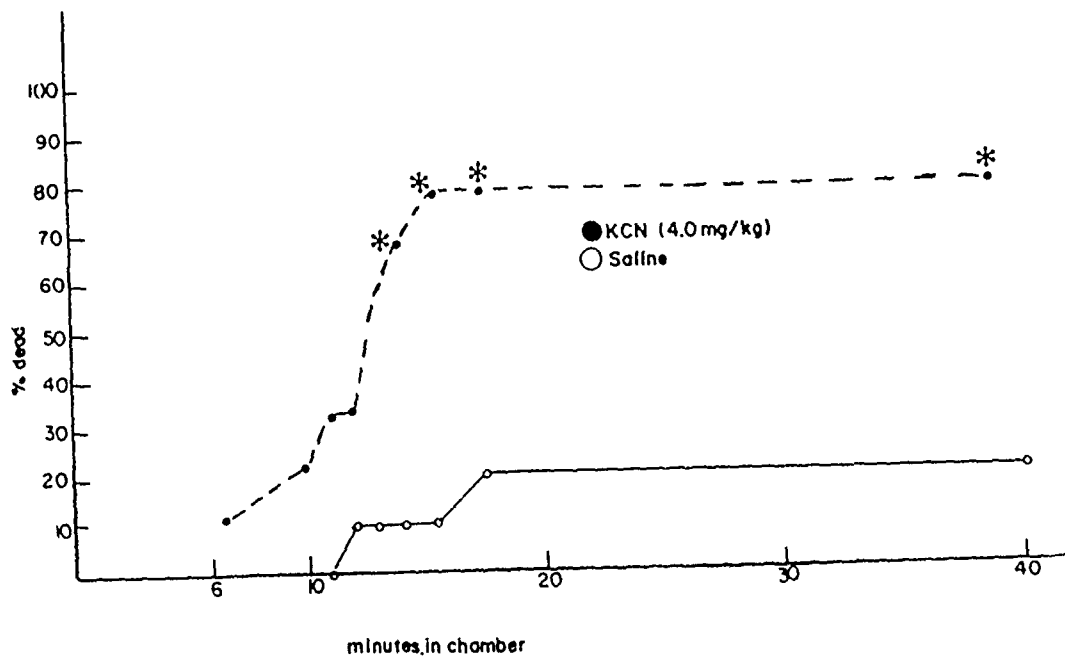


Figure 6. Lethality of animals pretreated with either saline, 0.1 ml/10g, i.p., or KCN, 4.0 mg/kg, i.p., and then placed in the chamber with an atmosphere of CO, 0.325 to 0.375%.

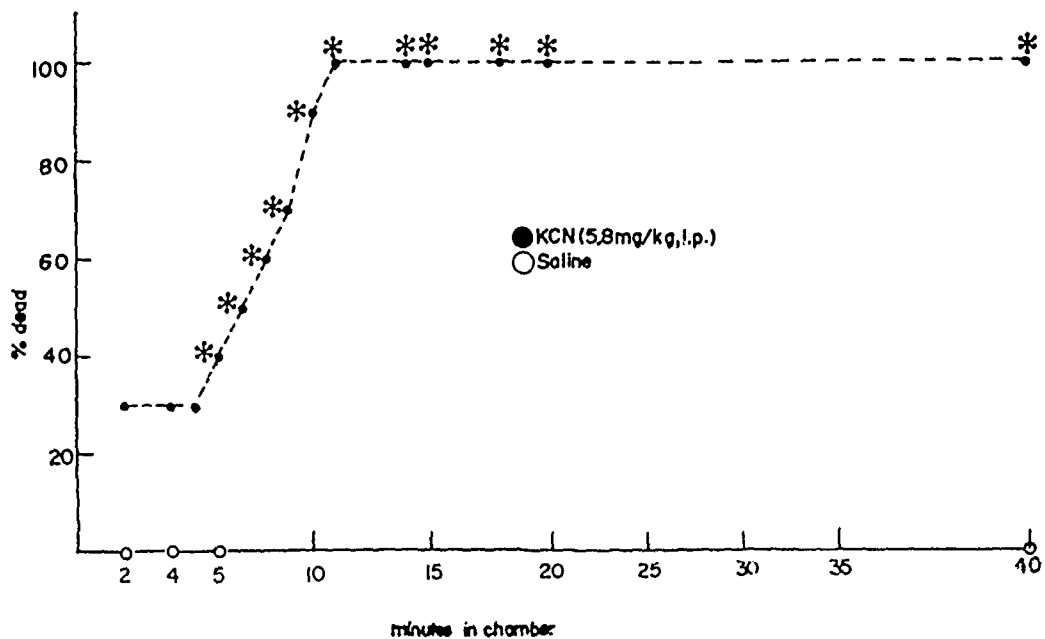


Figure 7. Lethality of animals pretreated with either saline, 0.1 ml/10g, i.p., or KCN, 5.8 mg/kg, i.p., and then placed in the chamber with an atmosphere of CO, 0.325 to 0.375%.

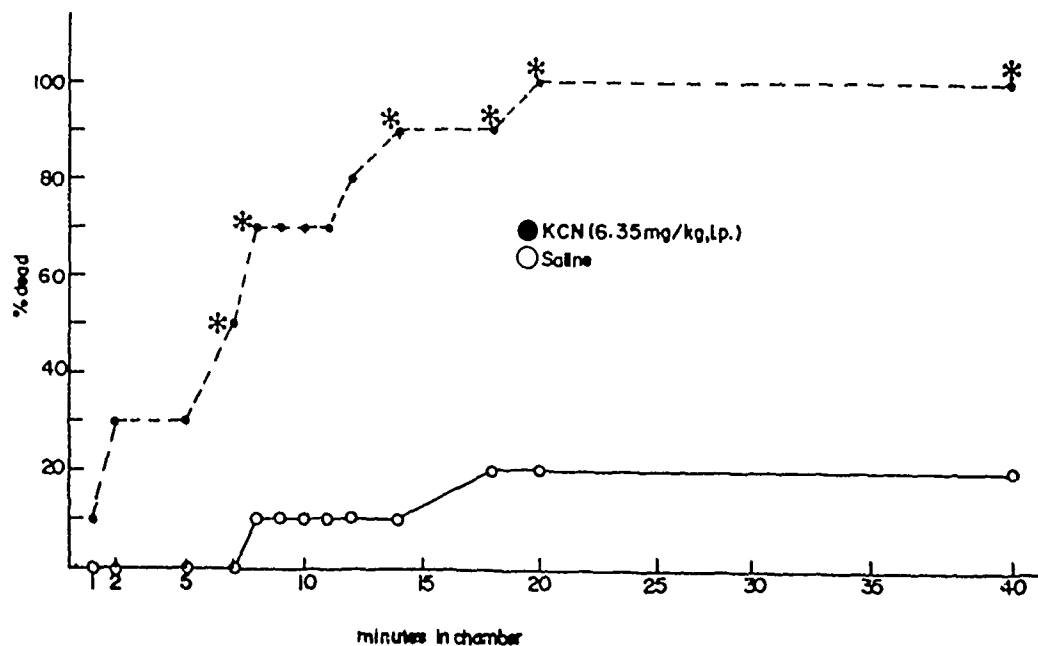


Figure 8. Lethality of animals pretreated with either saline 0.1ml/10g, i.p., or KCN, 6.35 mg/kg, i.p., and then placed in the chamber with an atmosphere of CO, 0.325 to 0.375%.

Blood Concentrations of Carbon Monoxide and Cyanide in Potassium Cyanide (KCN) Pretreated Animals that were Subjected to a Carbon Monoxide Atmosphere

Animals were pretreated with either saline, 0.1 ml/10 g, i.p., or KCN, 3.5 mg/kg, i.p., and then transferred to the chamber with an atmosphere of 0.325 to 0.375% CO. Figure 9 demonstrates that there was no difference in the CO blood concentrations of saline- and cyanide-pretreated animals. Figure 10 illustrates cyanide disappearance from the blood of animals subjected to air or CO. No difference in cyanide concentrations was noted between the two treatment groups.

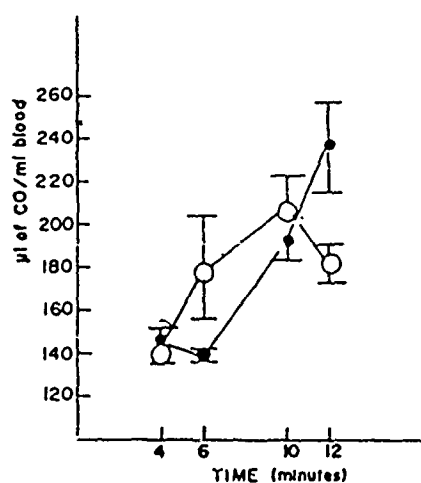


Figure 9. Animals were pretreated with saline (●), 0.1 ml/10g, i.p., or KCN (○), 3.5 mg/kg, i.p., then placed in the chamber with an atmosphere of CO, 0.325 to 0.375%. After 4, 6, 10 or 12 minutes in the chamber, the animals were removed, sacrificed and blood collected.

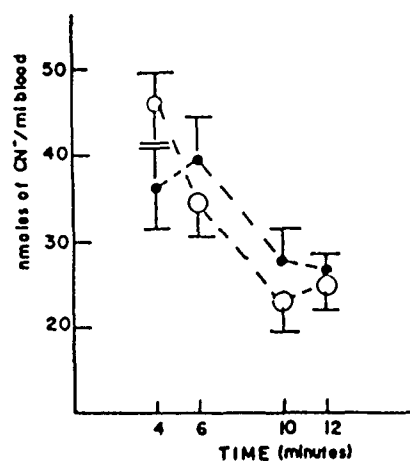


Figure 10. Animals were pretreated with KCN, 3.5 mg/kg, i.p. then placed in a chamber with an atmosphere of air (●) or CO (○), 0.325 to 0.375%. After 4, 6, 10, or 12 minutes in the chamber the animals were removed, sacrificed and blood collected.

DISCUSSION

The possibility of an interaction between carbon monoxide (CO) and cyanide has been studied by other investigators. An interaction was suggested in the work of Smith et al. (1976), Mohler (1975) and Levin (personal communication). Higgins et al. (1972) and Yamamoto (1976), however, observed no interaction between CO and cyanide. Comparison of our LD₅₀ values of potassium cyanide (KCN) demonstrates that CO-pretreated animals had an increased toxicity to cyanide-induced lethality as compared to air-pretreated animals. Based on these results, there is an interaction between CO and cyanide.

Two possible types of interaction proposed by Brown (1981) could exist between CO and cyanide, an additive or potentiation effect. An additive effect would indicate that the mortality of CO-cyanide equals the sum mortality of CO and cyanide give independently. A potentiation effect would be evidenced by a percent mortality of CO and cyanide, concurrently, which is greater than the sum of the respective percent mortalities of CO and cyanide when administered alone.

A series of experiments was designed so that CO-cyanide interaction could be investigated. In these experiments, animals were pretreated with saline or KCN, then subjected to a CO atmosphere. LD₁₀ dose of KCN (6.35 mg/kg, i.p.) was administered to a group of animals. Twenty percent of saline-pretreated animals died. If CO and cyanide exert an additive effect, the expected mortality in KCN-pretreated animals would be 30 percent. However, our data show that this combination of toxins produced 100% mortality, which suggests that the CO-cyanide interaction exhibits potentiation.

It was also of interest to determine the range of sublethal concentrations of CO and cyanide in combination, which would result in a lethality situation. In order to further characterize the interaction of these toxins and to evaluate the potential hazards at lower cyanide concentrations, sublethal KCN doses (3.5 to 5.8 mg/kg, i.p.) were administered to animals prior to CO administration. These results exemplify that even a sublethal KCN dose combined with a low CO concentration can result in a high degree of mortality.

The administration of cyanide results in an initial elevation in rate of respiration (Dreisbach, 1977). The potentiated lethality could be due to an increased breathing rate and intake of CO. To investigate this aspect, blood concentrations of CO and cyanide were measured in animals pretreated with saline (0.1 ml/10 g, i.p.) or cyanide (3.5 mg/kg, i.p.) and then exposed to CO. As anticipated, blood concentrations of CO increased as time in the CO chamber increased. However, comparison of CO blood concentration in saline- and cyanide-pretreated animals showed no significant difference. Cyanide disappearance from blood was also determined in these animals exposed to CO or air. No significant difference in cyanide blood concentrations was found in animals which were exposed to either air or CO. Thus, the potentiated lethality of CO and cyanide could not be explained by altered blood CO or cyanide concentrations.

A study of the interaction between CO and cyanide could aid in the elucidation of mechanism of action of these toxic agents. Both CO and cyanide are known to inhibit cytochrome oxidase (Nicholls, 1978; Ballantyne, 1977). Perhaps this inhibition of cytochrome oxidase is involved in this interaction.

Our data would indicate that the toxicologic interaction between CO and cyanide is greater than the additive effect. Thus, it appears that potentiation does exist in a simultaneous or sequential administration of CO and cyanide. It must be recognized that the combination of CO and cyanide produces an extremely toxic environment.

ACKNOWLEDGEMENT

This research was partially supported by U. S. Army Medical Research Command, Project #DAMD17-83-C-305.

LITERATURE CITED

- Anderson, R. A. and Harland, W. A. (1982). Fire deaths in the Glasgow area: III. The role of hydrogen cyanide. *Med. Sci. Law* 22, 35-40.
- Ballantyne, B. (1977). An experimental assessment of the diagnostic potential of histochemical and biochemical methods for cytochrome oxidase in acute cyanide poisoning. *Cell. Mol. Biol.* 22, 109-123.
- Birky, M. M. and Clarke, F. B. (1981). Inhalation of toxic products from fires. *Bull. N.Y. Acad. Med.* 57, 997-1013.
- Birky, M. M., Halpin, B. M., Caplan, Y. H., Fisher, R. S., McAllister, J. M. and Dixon, A. M. (1979). Fire fatality study. *Fire and Materials* 3, 211-217.
- Brown, V. K. H. (1981). Acute toxicity testing -- a critique. In: *Testing for toxicity*. Ed. J. W. Gorrod, Taylor and Francis, Ltd., pp. 21-27.
- Dreisbach, R. H. (1977). Cyanides, sulfides and carbon monoxide. In: *Handbook of Poisoning*, 9th edition, Lange Medical Publications, Los Altos, CA, p. 241.
- Higgins, E. A., Fiora, V., Thomas, A. A. and Davis, H. V. (1972). Acute toxicity of brief exposures of HF, HCl, NO₂ and HCN with and without CO. *J. Fire Tech.* 8, 12-30.
- Litchfield, J. T. and Wilcoxon, F. (1949). A simplified method of evaluating dose-effect experiments. *J. Pharmacol. Exp. Ther.* 96, 99-113.
- McAuley, F. and Reive, D. S. (1983). Rapid quantitation of cyanide in blood by gas chromatography. *J. Anal. Tox.* 7, 213-215.
- Mohler, S. R. (1975). Air crash survival: Injuries and evacuation toxic hazards. *Avia. Space and Environ. Med.* 46, 86-88.
- Nicholls, P. (1978). A new carbon monoxide-induced complex of cytochrome with oxidase. *Biochem. J.* 175, 1147-50.
- Smith, P., Crane, C., Sander, D., Abbott, J. and Endicott, B. (1976). Effects of exposure to carbon monoxide and hydrogen cyanide. *Physiological and Toxicological Aspects of Combustion Products*, pp. 75-88. Washington, D. C., National Academy of Science.
- Sumi, K. and Tsuchiya, Y. (1973). Combustion products of polymeric materials containing nitrogen in their chemical structure. *J. Fire Flammability* 4, 15-22.
- Teige, B., Lundevall, J. and Fleischer, E. (1977). Carboxyhemoglobin concentrations in fire victims and in cases of fatal carbon monoxide poisoning. *Z. Rechtsmed.* 80, 17-21.

- Thomas, D. M. (1971). The smoke inhalation problem. Proceedings of the Symposium on Occupational Health and Hazards of the Fire Service, Notre Dame University, South Bend, Indiana.
- Wetherell, H. R. (1966). The occurrence of cyanide in the blood of fire victims. J. Forensic Sci. 11, 167-173.
- Winek, C. L. and Prex, D. M. (1981). A comparative study of analytical methods to determine postmortem changes in carbon monoxide concentration. Forensic Sci. International 18, 181-187.
- Woolley, W. D. (1972). Nitrogen-containing products from the thermal decomposition of flexible polyurethane foams. Brit. Polymer J. 4 27-43.
- Yamamoto, K. (1976). Acute combined effects of HCN and CO with the use of the combustion products from PAN (polyacrylonitrile)-gauge mixtures. Z. Rechtsmed. 78, 303-311.

Mechanisms of Cyanide Inhibition by Scavengers

Peter Hambright, Ph.D.*; David R. Franz, DVM, MAJ, VC;
Harold H. Newball, M.D., LTC, MC

US Army Medical Research Institute of Chemical Defense,
Aberdeen Proving Ground, Maryland 21010
*Department of Chemistry, Howard University
Washington, DC 20059

The rapid onset of action of cyanide suggests that, from a military viewpoint, emphasis should be placed on the development of prophylactic rather than therapeutic compounds. However, the main approaches to the problems of cyanide intoxication are currently therapeutic in nature. Nevertheless, consideration of therapeutic approaches gives some insight into the types of molecular systems that might act as prophylactic scavenger compounds (1,2).

The classical framework for understanding the effects of cyanide assumes that cyanide binds to the iron(III) porphyrins of the cytochromes a and a_3 in cytochrome c oxidase, the terminal member of the respiratory chain. This binding of cyanide prevents electron transfer into oxygen, and thus inhibits cellular respiration. Such coordinated cyanide must be removed from cytochrome oxidase by scavengers, and subsequently detoxified.

The current therapy of cyanide in the USA involves the formation of blood methemoglobin (which has iron(III) porphyrins as prosthetic groups) to scavenge cyanide(3). Amyl nitrite and sodium nitrite are administered to oxidize 30 to 40% of the oxygen carrying iron(II) hemoglobin (which has low cyanide binding capacity) into the iron(III) methemoglobin form, which has an avid affinity for cyanide. This high concentration of methemoglobin will remove cyanide from cytochrome oxidase, and absorb any free cyanide remaining in the blood. The nitrite oxidation is relatively slow, and the more rapid methemoglobin former, dimethylaminophenol (DMAP) has been used in place of nitrite with some success (4). In either case, sodium thiosulfate is injected after methemoglobin formation to act as a substrate for the conversion of CN^- into the relative nontoxic thiocyanate (SCN^-); a reaction catalyzed by several sulfur transferases (5). There is evidence that ventilation with oxygen during this treatment has beneficial effects (6,7). The problems with this therapy are: that methemoglobin formation makes the patient even more hypoxic; that the massive amounts of both nitrite and thiosulfate are vasodilators and cause hypotension; and that the procedure itself is impractical under battle-field conditions. In addition, recent experiments by Way (6) indicate that the cyanide LD_{50} 's with nitrite/thiosulfate were not notably different from the cyanide LD_{50} with the same drugs when the reducing agent methylene blue was added to reduce the methemoglobin formed by the nitrite oxidation. Thus methemoglobin may not in fact act as a primary cyanide scavenger in this system, and the effect may be due to vasogenic action of the nitrite itself.

An alternative therapy used in Europe involves the administration of dicobalt (II) EDTA as a cyanide scavenger (8). Cobalt(II) itself reacts extremely rapidly with cyanide at room temperature to form the air sensitive $Co(CN)_5^{3-}$ (and other species), and this reaction can be used as an analytical method for the determination of cobalt(II). However, the aquo cobalt(II) ion has a high cardiotoxicity and therefore, EDTA is used as a complexing agent to bind cobalt(II) and disguise the potentially harmful effects of the free metal ion. Unfortunately, Co_2EDTA itself produces convulsions, hypertension and other adverse effects in patients that do not have cyanide poisoning (9), and as such, cannot act as a prophylactic agent. Toxic after effects due to the Co_2EDTA or its dissociation products with cyanide in cyanide poisoned patients limit the usefulness of this scavenger in a therapeutic sense.

Finally, hydroxocobalamin (Vitamin B_{12} , a cobalt(III) complex of a porphyrin-like molecule called a corrin) has been used as a cyanide scavenger in animals (10). The coordinated cobalt(III) portion of the molecule forms a strong bond with cyanide, thus removing the cyanide from the cytochrome oxidase, and in addition, Vitamin B_{12} has little toxicity in itself. High doses of the drug are required, and the treatment could probably not be

used in a combat situation.

The brief discussion above indicates that a metal ion center (iron(III) in the cytochromes or hemoglobin, cobalt(II) in Co_2EDTA or cobalt(III) in Vitamin B_{12}) is necessary in the scavenger system to coordinate with the cyanide or HCN species. Many metals in the periodic table form cyano complexes, from simple $\text{Zn}(\text{H}_2\text{O})_5\text{CN}^+$ to the more complicated $\text{Mo}(\text{CN})_8^{3-}$. Since low concentrations of many aquo metal ions are toxic (as noted above⁸ for cobalt(II), and cobalt(III) is unstable in water), an organic complexing agent (porphyrins in methemoglobins or the cytochromes, the corrin ring in Vitamin B_{12} , and EDTA in Co_2EDTA) must be present in the scavenger system to carry the metal ion in a form that masks the inherent toxicity of the free metal ion itself. The complexing agent should be nontoxic, should not seriously alter the cyanide affinity of the metal, and stabilize the proper oxidation state of the coordinated ion. The metal-cyanide bond should be inert, that is, the cyanide should remain with the metal or metal complex in a form that does not readily dissociate until after elimination or conversion into SCN^- . Such a prophylactic drug should be administered by an oral route, and have a long half-life in the body. Finally, the drug should be stable, water soluble and inexpensive.

With such considerations in mind, we have initially investigated two classes of cyanide scavengers. The first are water soluble metalloporphyrins, having a wide range of metal ions bound to a variety of positively and negatively charged porphyrin ligands. The second class are members of the class of antiarthritic drugs containing gold(I).

EXPERIMENTAL

For in vitro studies of cyanide binding by scavengers, an autoanalyzer was used (11). Basically, increasing molar concentrations of the scavengers were equilibrated for several minutes with a constant concentration of cyanide at physiologic pH (pH 7.5) in a phosphate buffer. The solutions were then dialyzed such that only the unbound cyanide passed through the membrane, and such cyanide was then measured. From plots of percent bound cyanide versus substrate concentration (Fig. 1), the molar concentration of scavenger required to bind 50% of the total cyanide (BC_{50}) could be determined. For each study, the total KCN concentration was the same, and thus the smaller the BC_{50} for a given compound, the higher its scavenger ability.

METALLOPORPHYRINS AS SCAVENGERS

Figure 2 shows the basic structure of the porphyrin molecule, a cyclic conjugated tetrapyrrole pigment (12). When the two central protons are replaced by a metal ion, the resulting species is known as metalloporphyrin. In nature, iron porphyrin structures are found in hemoglobin, myoglobin, catalases, peroxidases and cytochromes. Magnesium porphyrins occur in chlorophyll, and cobalt porphyrins constitute Vitamin B_{12} . Over sixty five metal ions form complexes with the porphyrin molecule (13). Thousands of different porphyrins have been identified. They differ by the types of side chains attached around the porphyrin framework. Sulfonic acid ($-\text{SO}_3^-$) or carboxylic acid ($-\text{COO}^-$) substituents provide negatively charged water soluble porphyrins. N-methylated pyridines or quinolines and N,N,N-trimethylanilinium groups form positively charged water soluble porphyrin molecules in solution. Table 1 shows the abbreviations and charges of the porphyrin ligands used in this study.

Table 2 is a list of metalloporphyrins with BC_{50} 's greater than 10^{-3} M. They are considered to have minimal rapid scavenger action towards the cyanide levels of interest. The list includes the metal ions nickel(II), vanadium(IV), chromium(III), molybdenum(V), tungsten(V), manganese(III), copper(II), silver(III), zinc(II), aluminum(III), indium(III) and gold(III). In most cases, the results appear to be independent of the charge of the metalloporphyrin. The most notable exception is for iron(III). The negatively charged iron(III) porphyrins have significantly less cyanide affinity than does a positively charged iron porphyrin.

-4 Table 3 is a tabulation of metalloporphyrin compounds having BC_{50} 's $\approx 10^{-4}$ M, making them moderately good cyanide scavengers. The negative porphyrins are complexed with cobalt(III), rhodium(III), silver(II), platinum(II) and palladium(II). The tetranegative sulfonated water soluble phthalocyanine (which has a structure similar to the porphyrin framework (Fig. 3)) as well as the hydroxo form of the cobalt(III) Vitamin B_{12} are also on this list.

The best scavengers having BC_{50} 's $\approx 10^{-5}$ M are also in Table 3. The porphyrin compounds all have positively charged peripheral substituents, and all are complexed to the metal cobalt(III). The iron(III) proteins methemoglobin and metmyoglobin are also in this class, as is dicobalt EDTA (Kelocyanor).

In terms of the porphyrins and phthalocyanines, it appears that the charge on the complex, the identity of the metal ion and the nature of the axial groups above and below the metal ion must be considered in explaining the observed results. With cobalt(III) porphyrins, the positively charged molecules have a greater cyanide affinity than do the negatively charged porphyrins. This effect is predominately electrostatic in nature. The negative cyanide ligand is more stable in a positive porphyrin environment, than is the negative cyanide in a negatively charged porphyrin surrounding.

Cobalt(III), a d^6 low spin metal ion having no unpaired electrons, appears to have the highest affinity for cyanide of any of the first row transition metal ions tested. With cobalt(III), electrons can be placed in orbitals that avoid the electron density of the incoming cyanide group (14). This both decreases the metal-cyanide bond distance, and maximizes the crystal field stabilization energy. Iron(III) is a low spin d^5 metal ion, and while it has one less electron than cobalt(III), the stabilization energy should be similar. In both cases, excess electron density on the metal ion due to cyanide coordination can be removed back into the cyanide using the filled t_{2g} orbitals of the cobalt (or iron), and the empty π antibonding orbitals of cyanide. Insofar as bond strength increases as we go down a column in the periodic table, we find that $(Pt(II), Pd(II)) > Ni(II), Ag(I) > Cu(II)$, and $Rh(III)$ is similar to $Co(III)$ porphyrins in scavenging ability.

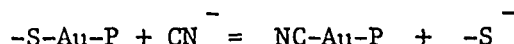
For cobalt(III) and iron(III), the extraplanar axial groups $-OH^-$ and $-OH_2$ are favorable for cyanide binding. As shown in Fig. 4, iron(III) myoglobin(15) and cobalt(III) porphyrins (13) have $-OH$ and/or $-OH_2$ groups at pH 7.5 and are strong cyanide binders. However, simple iron(III) porphyrins at this pH are mainly (13) oxy bridged dimers, $Fe-O-Fe$, and bridge breaking must occur before cyanide complexation can occur. In a similar fashion, $Co(III)$ myoglobin (16) has both axial positions coordinated with nitrogen groups from the proximal and distal histidine imidazoles, $N-Co-N$. Dissociation of the $Co-N$ bond (a slow process) must occur before cyanide complexation can occur. Thus, while $Co(III)$ and $Fe(III)$ have complexing ability in some complexes, this ability can be lost due to unfavorable axial coordination in other molecules.

This brief study of metalloporphyrin complexation reactions with cyanide

indicates the types of reactive groups favoring scavenger action. While many other compounds of this nature can be designed, the present cobalt(III) positive porphyrins scavenge cyanide as well as methemoglobin, and better than hydroxo-Vitamin B₁₂

GOLD DRUGS AS SCAVENGERS

Ore containing metallic gold(0) is treated with cyanide and oxygen leading to oxidation of Au⁰ to Au^I and subsequent complexation of Au^I as Au(CN)₂⁻. This affinity of low oxidation states of gold for cyanide led to studies with the gold(I) containing rheumatoid arthritis drug Auranofin ((2,3,4,6-tetra-O-acetylthio-β-D-glucopyranosato-S) (triethylphosphine)gold(I)). This derivative is basically a sulfur containing sugar with the S bound to one side of the Au and phosphorus on the other (17). We have demonstrated that one mole of cyanide is taken up by one mole of Auranofin in solution, breaking only the S-Au bond:



This reaction is rapid, and gives a BC₅₀ of 2×10^{-5} M, similar to methemoglobin and the positive cobalt(III) porphyrins. Gold(I) thioglucose (Solganol) gives similar results (Table 4). While Auranofin is soluble only in water/alcohol mixtures, the related chlorobis-(Triethylphosphine) gold(I) is fully water soluble, and gives similar BC₅₀'s, as does disodium gold(I) thiomalate. Gold(III) in AuCl₄⁻Na binds cyanide, but this ability is lost in gold(III) porphyrins.

In vivo studies show the BC₅₀ of Auranofin in plasma (4×10^{-5}) or blood (5×10^{-5}) is comparable to its BC₅₀ in a physiologic buffer. In general, Auranofin meets many of the criteria listed above as a potential cyanide prophylactic agent, namely:

- a. It binds cyanide in vitro with a BC₅₀ comparable to methemoglobin.
- b. Animal and human toxicology data show low chronic toxicity (18,19).
- c. It can be absorbed orally, thus there is no need for parenteral administration.
- d. It can probably be used prophylactically since it has a long half-life (20) (10 days in man), thus obviating the need for frequent administration.

In summary, mechanistic data derived from in vitro studies have provided information regarding reactive groups of metals that avidly bind cyanide, and have provided direction for the synthesis of therapeutic and prophylactic scavengers of cyanide for in vivo studies.

REFERENCES

1. Chen, K., C. Rose and G. C. Lowes, Amyl nitrite and cyanide poisoning, JAMA 100:1920-1922, 1933.
2. Chen, K., and C. Rose, Treatment of acute cyanide poisoning, JAMA 162:1154-1157, 1956.
3. Rumack, B. H. Ed., Cyanide poisoning, in Poisindex (R) Emergency Poison Management, Micromedex Inc., Englewood, Colorado, 1984.
4. Weger, N. P., Treatment of cyanide poisoning using 4-DAMP--experimental and clinical overview, Fundamental and Applied Toxicology, 3:387-396, 1983.
5. Westley, J., Rhodanese and the sulfane pool, in Enzymatic Basis of Detoxification, W. B. Jakoby, Ed., 2:245-262, New York Academic Press, 1980.
6. Way, J. L., Mechanism of cyanide intoxication and its antagonism, in Proceedings of the Symposium on the Respiratory Care of Chemical Casualties, McLean, Virginia, H. H. Newball, Ed., 1984.
7. Burrows, G., D. Liu and S. Way, Effect of oxygen on cyanide intoxication. V. physiologic effect, J. Pharmacology and Experimental Therapeutics, 184(3):739-756, 1973.
8. Hillman, B., K. Bardham and J. Bain, The use of dicobalt edetate (Kelocyanor) in cyanide poisoning, Postgrad Med. J. 50:171-174, 1974.
9. Rumack, B. H., Cyanide poisoning, in Proceedings of the Symposium on the Respiratory Care of Chemical Casualties, McLean, Virginia, H. H. Newball, Ed., 1984.
10. Drew, R. H., The use of hydroxocobalamin in the prophylaxis and treatment of nitroprusside induced cyanide toxicity, Vet. Hum. Toxicol., 25:342-344, 1976.
11. Groff, W. A., S. A. Cucinell, P. Vicario, and A. Kaminskis, A completely automated fluorometric blood cyanide method: A specific assay incorporating dialysis and distillation, Clinical Toxicology, 11(2):159-171, 1977.
12. Bonnett, R., Nomenclature, in The Porphyrins, D. Dolphin, Ed., Academic Press, New York, 1:1-27, 1978.
13. Hambright, P., Dynamic coordination chemistry of metalloporphyrins, in The Porphyrins and Metalloporphyrins, K. M. Smith, Ed., Elsevier, Amsterdam, 7:233-278, 1973.
14. Cotton, F., and G. Wilkinson, Advanced inorganic chemistry, 3rd Edition, Interscience Publishers, New York, 1972.
15. Antonini, E., and M. Brunori, Hemoglobin and myoglobin and their reactions with ligands, American Elsevier, New York, 188-234, 1971.
16. Hambright, P., S. LeMelle, K. Alston, P. Neto, S. diStefano and H. Newball, A dissociative mechanism for the dithionite reduction of cobalt(III) myoglobin, Inor. Chem. Acta., 92:42-47, 1984.

17. Sutton, B., Overview and current status of gold-containing antiarthritic drugs, in *Platinum, Gold and Other Metal Chemotherapeutic Agents*, S. Lippard, Ed., ACS Symposium Series 209, Washington, DC, 1983.
18. Kamel, H., D. H. Brown, J.M. Ottaway, and W.E. Smith, A comparison of tissue gold levels in guinea-pigs after treatment with myocrisin injected intramuscularly and triethylphosphine gold chloride and myocrisin administered orally, *Agents and Actions*, Birkhauser Verlag, Basel, 8/5:546-550, 1978.
19. Payne, B.J., The toxicity of three gold-containing compounds in laboratory animals, *Veterinary Pathology*, 15(Supplement 5):1-3, 1978.
20. Walz, D. T., D.E. Griswold, M.J. DiMartino, and E.E. Bumbier, Pharmacokinetics of gold following administration of auranofin (SK&F D-39162) and myochrysine to rats, *Journal of Rheumatology*, 7(6):820-824, 1980.

Table 1. Abbreviations and Ligand Charges

<u>Abbreviation</u>	<u>Name</u>
H_2 -Proto ²⁻	Protoporphyrin-IX
H_2 -Hemato ²⁻	Hematoporphyrin-IX
H_2 -DPS ₂ ⁴⁻	3,8-disulfonated deuteroporphyrin-IX
H_2 -Copro ⁴⁻	Coproporphyrin-I
H_2 -Uro ⁸⁻	Uroporphyrin-III
H_2 -ENP ⁴⁻	3,8,13,17-tetraethylenediamine protoporphyrin-IX
H_2 -TSPH ⁴⁻	tetrasulfonated phthalocyanine
H_2 -TMPyP(X) ⁴⁺	<u>meso</u> -Tetra(N-Methyl-4(3 or 2) Pyridyl)porphyrin [*]
H_2 -TPPS ⁴⁻	<u>meso</u> -Tetra(4-sulfonatophenyl)porphyrin
H_2 -QP(X) ⁴⁺	<u>meso</u> -Tetra(N-Methyl-4(or 3)quinolyl)porphyrin
H_2 -TPPC(X) ⁴⁻	<u>meso</u> -Tetra(4-(or 3) carboxyphenyl)porphyrin
H_2 -TAP ⁴⁺	<u>meso</u> -Tetra(4-N,N,N-trimethylanilinium)porphyrin
H_2 -PF	The water soluble picket fence porphyrin
FeMb ⁺	Iron (III)metmyoglobin
CoMb ⁺	Cobalt(III) sperm whale metmyoglobin
FeHb ⁺	Iron(III)methemoglobin
Co(III)-B12	Hycroxocobalamin form of Vitamin B
Co(II) ₂ -EDTA	Dicobalt(II)-EDTA (Kelocyanor)

*In Figure 1, the 5, 10, 15 and 20 positions are the meso substituents.

Table 2. Metalloporphyrins Having a Low Affinity for Cyanide

$BC_{50} > 10^{-3} \text{ M, pH 7.5}$

METALLOPORPHYRIN

VO(IV)-TMPyP(3)

Cr(III)-TMPyP(3)

Cr(III)-TSPH

O-Mo(V)-TPPS

O-W(V)-TPPS

Mn(III)-TPPS

Mn(III)-TPPC(4)

Mn(III)-TMPyP(4)

Fe(III)-TPPS

Fe(III)-PF

Fe(III)-Proto

Fe(III)-Hemato

Ni(II)-TPPS

Cu(III)-TPPC(4)

Cu(II)-TPPS

Ag(III)-TPPS

Zn(II)-TMPyP(4)

Zn(II)-TSPH

Zn(II)-TPPS

Al(III)-TPPS

In(III)-TPPS

Au(III)-TPPC(4)

Co(III)-Mb⁺

Table 3. Metalloporphyrins with Moderate and High Cyanide Affinities. pH 7.5

MODERATE AFFINITY FOR CYANIDE		HIGH AFFINITY FOR CYANIDE	
Metalloporphyrin	BC (M) 50	Metalloporphyrin	BC (M) 50
Co(III)-Hemato	1×10^{-4}	Co(III)-TMPyP(4)	1×10^{-5}
Co(III)-Proto	1×10^{-4}	Co(III)-TMPyP(2)	1×10^{-5}
Co(III)-TPPS	1×10^{-4}	Co(II) ₂ -EDTA	2×10^{-5}
Co(III)-Copro	1×10^{-4}	Fe(III)-Hb	2×10^{-5}
Co(III)-B ₁₂	1×10^{-4}	Co(III)-TMPyP(3)	3×10^{-5}
Co(III)-DPS ₂	2×10^{-4}	Co(III)-ENP	3×10^{-5}
Ag(II)-TPPS	2×10^{-4}	Co(III)-QP(3)	3×10^{-5}
Pt(II)-Proto	2×10^{-4}	Co(III)-TAP	3×10^{-5}
Pd(II)-Proto	2×10^{-4}	Co(III)-QP(4)	4×10^{-5}
Co(III)-TPPC(3)	3×10^{-4}	Co(III)-PF	6×10^{-5}
Rh(III)-TPPS	3×10^{-4}	Fe(III)-Mb	8×10^{-5}
Co(III)-Uro	4×10^{-4}	Co(III)-TPPC(4)	8×10^{-5}
Co(II)-TSPH	4×10^{-4}		
Fe(III)-TSPH	5×10^{-4}		
Co(III)-TSPH	6×10^{-4}		
Fe(III)-TMPyP(4)	8×10^{-4}		

Table 4. Cyanide Affinities of Gold Compounds

	BC_{50} (M)
Auranofin ^a	2×10^{-5} (Buffer)
	4×10^{-5} (Plasma)
	5×10^{-5} (Blood)
Solganol ^b	2×10^{-5}
Chloroethyl triphosphine (Gold(I))	2×10^{-5}
Myochrisine ^c	3×10^{-5}
$Au(III)Cl_4Na$	3×10^{-5}
Chlorobis(triethylphosphine) (Gold(I))	3×10^{-5}
$Au(III)-TPPC(4)$	$< 10^{-3}$

a Auranofin is (2,3,4,6-tetra-0-acetyl-1-thio- β -D-glucopyranosato-S) (triethylphosphine) (Gold(I))

b Solganal is aurothioglucoase

c Myochrisine is disodium Gold(I) thiomalate

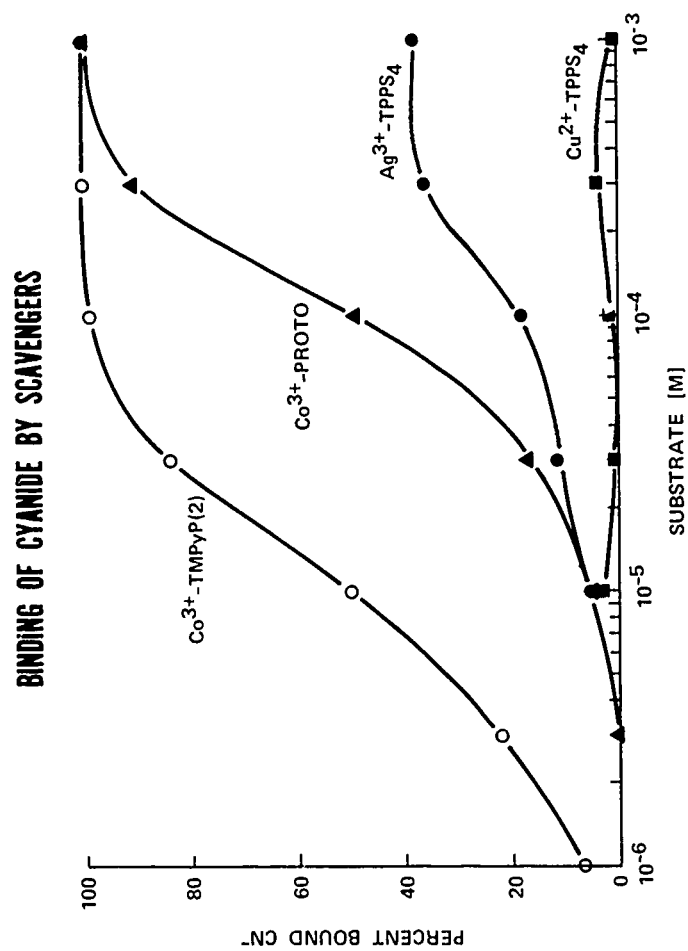


Figure 1. Binding of Cyanide by Metalloporphyrin Scavengers

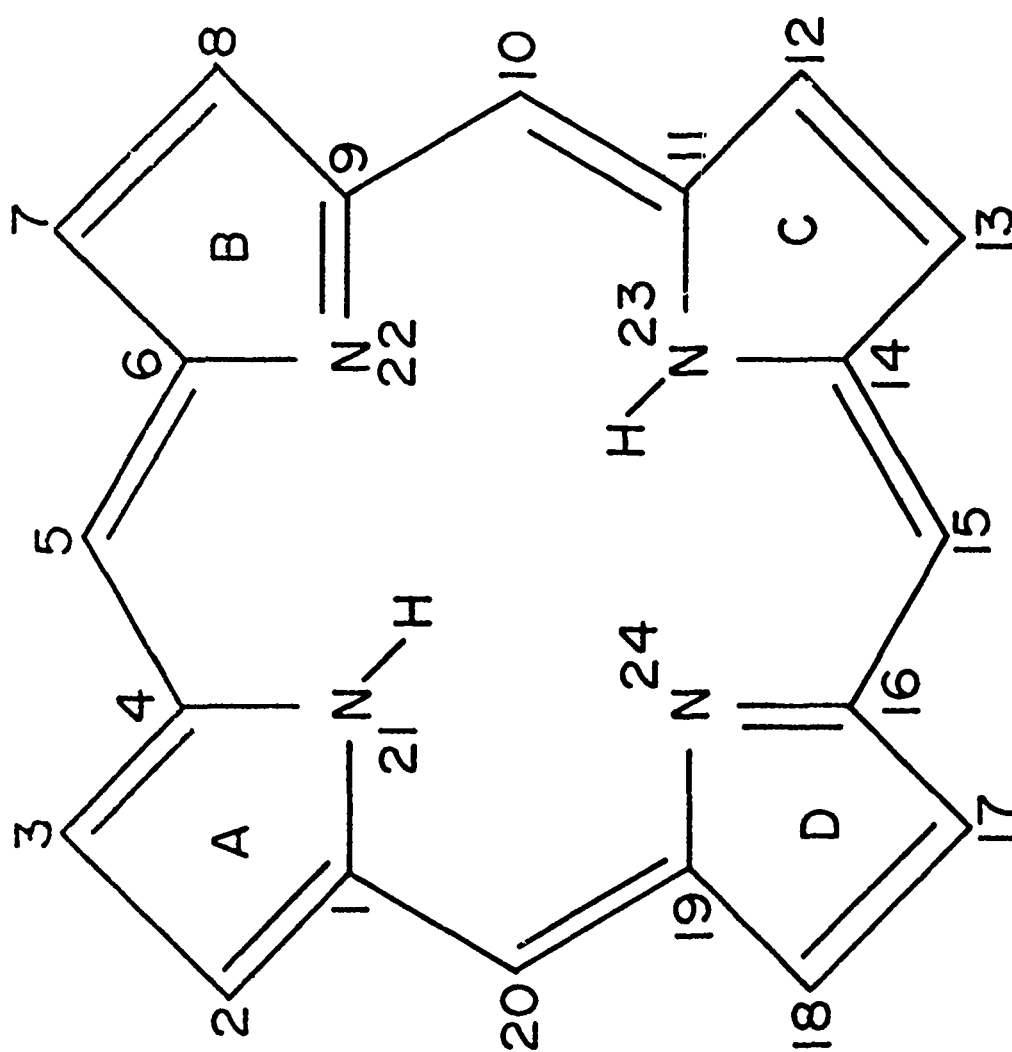


Figure 2. Ring Structure of the Basic Porphyrin Molecule

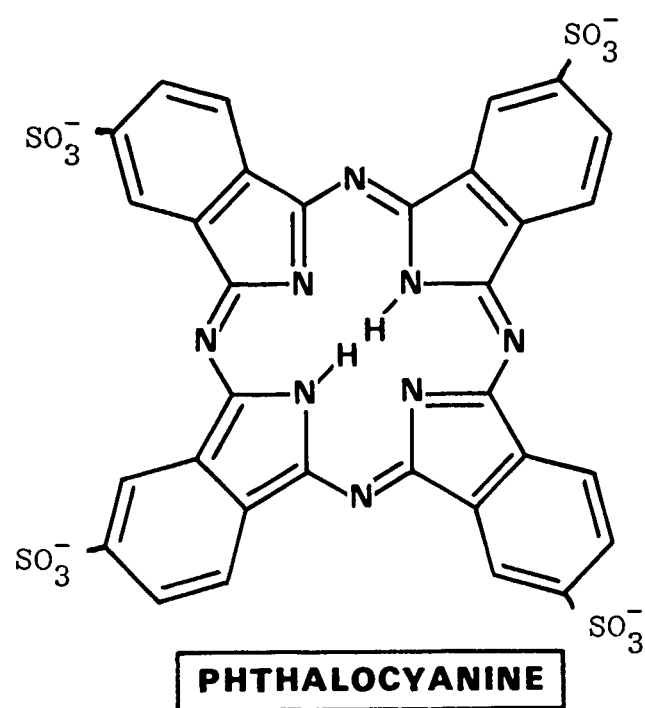


Figure 3. Cyclic Ring System of the Tetrasulfonated Phthalocyanine

BINDING OF CYANIDE BY SCAVENGERS

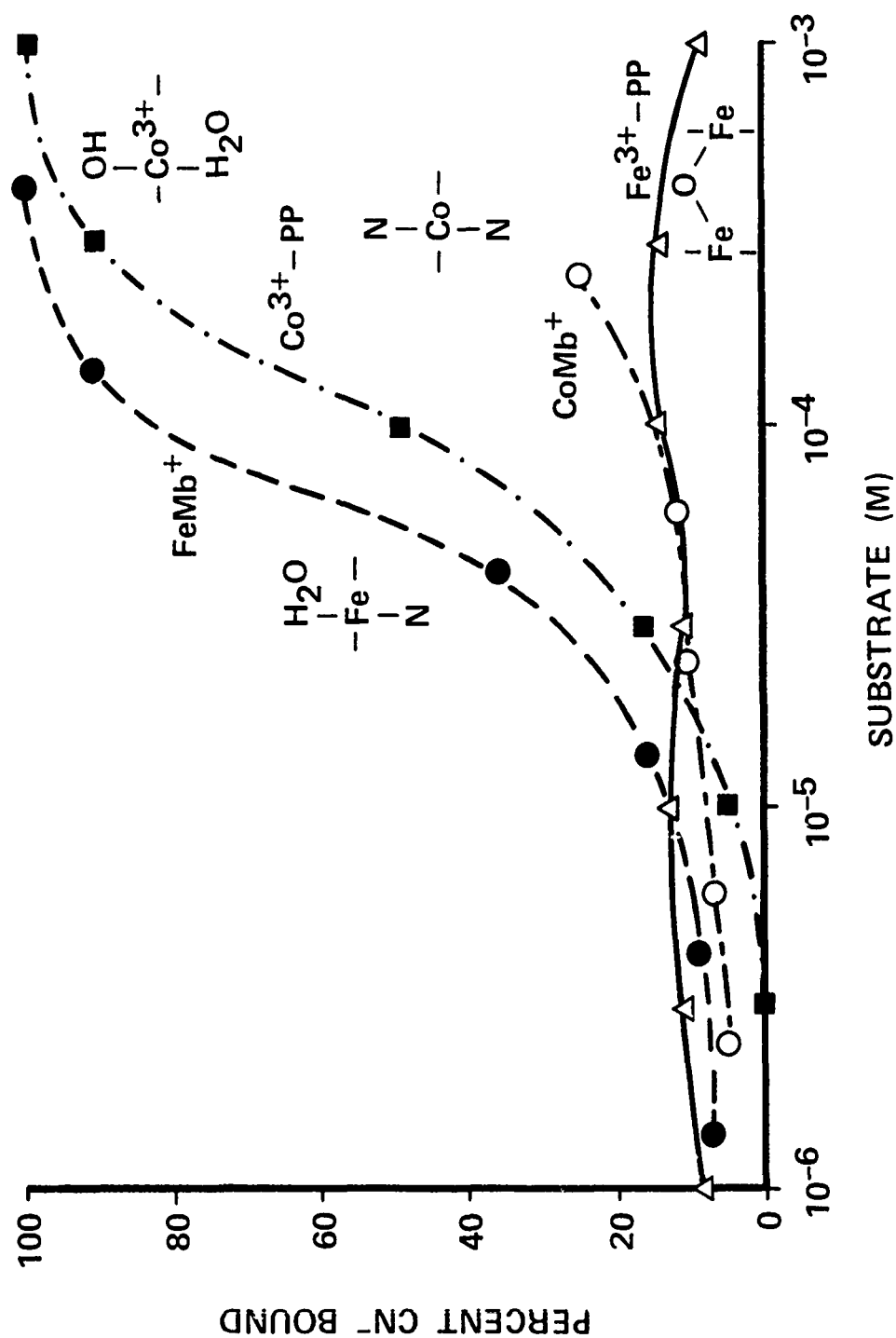


Figure 4. Influence of Axial Groups on the Complexation by Cobalt(III) and Iron(III) Porphyrin and Proteins

USAMRDC Advisory Subcommittee
on Medical Defense
Against Chemical Agents

US Army Medical Research and Development Command (USAMRDC)

ADVISORY SUBCOMMITTEE ON MEDICAL DEFENSE
AGAINST CHEMICAL AGENTS

Dr. Lewis Aronow
Uniformed Services University of
the Health Sciences
Department of Pharmacology
4301 Jones Bridge Road
Bethesda, MD 20814

Dr. Thomas J. Franz
Assistant Professor of Medicine
Division of Dermatology
Room 14
University of Washington
Seattle, WA 98195

Dr. Joseph V. Brady
The Johns Hopkins University
School of Medicine
Division of Behavioral Biology
720 Rutland Avenue
Baltimore, MD 21205

Dr. Alan M. Goldberg
Department of Environmental Health
Sciences
The Johns Hopkins University
School of Hygiene and Public Health
615 N. Wolfe Street
Baltimore, MD 21205

Dr. Frederick L. Eldridge
Department of Physiology
University of North Carolina
School of Medicine
Chapel Hill, NC 27514

Dr. Michael V. Johnston
University of Michigan
Neuroscience Laboratory Building
1103 East Huron
Ann Arbor, MI 48109

Dr. Warren W. Epinette
Department of Dermatology
Indiana University School of
Medicine
1100 W. Michigan Street RG 524
Indianapolis, IN 46223

Dr. Alexander G. Karczmar
Department of Pharmacology
and Therapeutics
Stritch School of Medicine
Loyola University Medical Center
2160 South First Avenue, Suite 3621
Maywood, IL 60153

Dr. Aron Baer Fisher
Department of Physiology
University of Pennsylvania
School of Medicine/G4
Philadelphia, PA 19104

Dr. David Evan Leith
Department of Anesthesia
Brigham and Women's Hospital
75 Francis Street
Boston, MA 01778

Dr. Robert B. Forney
Department of Toxicology
Indiana University School
of Medicine
1100 West Michigan Street
Indianapolis, IN 46223

Dr. Horace H. Loh
Department of Psychiatry and
Pharmacology
University of California School of
Medicine
San Francisco, CA 94143

Dr. Raymond H. Murray
Department of Medicine
Michigan State University
B-220 Life Sciences
East Lansing, MI 48823

Dr. Sumner Robinson
President
St. Louis College of Pharmacy
4588 Parkview Plaza
St. Louis, MO 63310

Dr. James Swarbrick
Professor and Chairman
Division of Pharmaceutics
School of Pharmacy
Beard Hall, 200H
University of North Carolina
Chapel Hill, NC 27514

Dr. David Terrian
Research Neurochemist
Neurosciences
USAF School of Aerospace Medicine
ATTN: USAFSAM/NGNS
Brooks Air Force Base, TX 78235

Dr. John S. Urbanetti
Lawrence Memorial Hospital
155 Montauk Avenue
New London, CT 06320

Registrants

US Army Medical Research and Development Command (USAMRDC)

FOURTH ANNUAL CHEMICAL DEFENSE BIOSCIENCE REVIEW
Post Theater, Aberdeen Proving Ground (Edgewood Area), Maryland
30 May - 1 June 1984

Registrants

Dr. Peter H. Abbrecht
Professor of Medicine and Physiology
Uniformed Services University of
the Health Sciences
School of Medicine
4301 Jones Bridge Road
Bethesda, MD 20814

LTC William Amos
Chief, Department of Chemical
Information Systems
Walter Reed Army Institute of
Research
ATTN: SGRD-UWM-A
Washington, DC 20307

Dr. Edson X. Albuquerque
Professor and Chairman
Department of Pharmacology and
Experimental Therapeutics
University of Maryland
School of Medicine
660 W. Redwood Street
Baltimore, MD 21201

Dana R. Anderson
Research Biologist
Drug Assessment Division
US Army Medical Research Institute
of Chemical Defense (USAMRICD)
ATTN: SGRD-UV-D
Aberdeen Proving Ground, MD 21010

Dr. Michael Adler
Principal Investigator
Neurotoxicology Branch
US Army Medical Research Institute
of Chemical Defense (USAMRICD)
ATTN: SGRD-UV-YN
Aberdeen Proving Ground, MD 21010

MAJ Gary L. Andersen
Chief, Department of Comparative
Pathology
Walter Reed Army Institute of
Research
Washington, DC 20307

LTC William A. Alter, III
Assistant Professor
Department of Physiology and
Military Medicine
Uniformed Services University of
the Health Sciences
4301 Jones Bridge Road
Bethesda, MD 20814

Dr. George K. Anderson
Chief, Medical Readiness Division
Directorate of Medical Plans and
Research
Headquarters, US Air Force
Office of the Surgeon General
ATTN: HQUSAF/SGHR
Bolling Air Force Base, DC 20332

Dr. Rebecca Anderson
Group Leader, Neurological Diseases
Warner-Lambert Company
2800 Plymouth Road
Ann Arbor, MI 48105

Dr. Robert S. Anderson
Physical Scientist
Toxicology Branch, Research Division
Chemical Research and Development
Center
ATTN: DRSMC-CLB-TA(A)
Aberdeen Proving Ground, MD 21010

Dr. M. Mouhair Atassi
Professor of Chemistry and
Biochemistry
Department of Biochemistry
Baylor College of Medicine
1 Baylor Plaza, Room 213E
Texas Medical Center
Houston, TX 77030

Dr. Adam Anthony
Professor of Physiology
Pennsylvania State University
418 Mueller Building
University Park, PA 16802

Dr. William S. Augerson
Arthur D. Little, Inc.
Acorn Park
Cambridge, MA 02140

Dr. Antonio Anzueto
Research Fellow
University of Texas Health Sciences
Center at San Antonio
7703 Floyd Curl Drive
San Antonio, TX 78240

Dr. J. Thomas August
Professor and Director
Department of Pharmacology and
Experimental Therapeutics
The Johns Hopkins University
725 N. Wolfe Street
Baltimore, MD 21205

Robert D. Armstrong
Pharmacologist
Toxicology Branch, Research Division
Chemical Research and Development
Center
ATTN: DRSMC-CLB-TC(A)
Aberdeen Proving Ground, MD 21010

Ruth V. Ault
Chief, Services Department
Logistics Division
Walter Reed Army Institute of
Research
ATTN: SGRD-UWC-D
Washington, DC 20307

Mark Arnold
Mechanical Engineer
US Army Medical Bioengineering
Research and Development Laboratory
Building 568
Fort Detrick
Frederick, MD 21701

Dr. Robert E. Baier
Staff Scientist
Environmental Science Department
Calspan Corporation/Advanced
Technology Center
P.O. Box 400
Buffalo, NY 14225

William P. Ashman
Research Biologist
Physics Branch, Research Division
Chemical Research and Development
Center
ATTN: DRSMC-CLB-PC(A)
Aberdeen Proving Ground, MD 21010

Dr. Bryan Ballantyne
Director of Applied Toxicology
Union Carbide Corporation
P.O. Box 8361
South Charleston, WV 25303

Dr. Louis E. Banderet
Research Physiologist
US Army Research Institute of
Environmental Medicine
ATTN: SGRD-UE-HP
Natick, MA 01760

Dr. Guy R. Banta
Chief, Biomedical Assessment Division
Code 21
Naval Aerospace Medical Research
Laboratory
Pensacola, FL 32508

Elliot Bartner
Vice President
Survival Technology, Inc.
8101 Glenbrook Road
Bethesda, MD 20814

Dr. Steven I. Baskin
Pharmacologist
Physiology Branch
US Army Medical Research Institute
of Chemical Defense (USAMRICD)
ATTN: SGRD-UV-YP
Aberdeen Proving Ground, MD 21010

Edgar L. Bateman
Material Developer
US Army Medical Bioengineering
Research and Development Laboratory
ATTN: SGRD-UBE-L
Fort Detrick
Frederick, MD 21701

Dr. Wes Baumgardner
Chief, Chemical Defense Branch
US Air Force School of
Aerospace Medicine
ATTN: USAFSAM/VNC
Brooks Air Force Base, TX 78235

Dr. Howard T. Bausum
Assistant Manager
Chemical Systems Research
US Army Medical Bioengineering
Research and Development Laboratory
ATTN: SGRD-UBG-M
Fort Detrick
Frederick, MD 21701

MAJ Wallace B. Baze
Chief, Department of Ultrastructural
Studies
Division of Pathology
Walter Reed Army Institute of
Research
ATTN: SGRD-UWP-C
Washington, DC 20307

COL Robert J. Beattie
Chief, Veterinary Medicine and
Laboratory Resources Support
Division
US Army Medical Research Institute
of Chemical Defense (USAMRICD)
ATTN: SGRD-UV-V
Aberdeen Proving Ground, MD 21010

Dr. Clifford D. Bedford
Manager, Chemical Defense Program
SRI International
333 Ravenswood Avenue
Menlo Park, CA 94025

CPT Everette T. Beers
Principal Investigator
Neurotoxicology Branch
US Army Medical Research Institute
of Chemical Defense (USAMRICD)
ATTN: SGRD-UV-YN
Aberdeen Proving Ground, MD 21010

Dr. William R. Beisel
Special Assistant to the Surgeon
General for Biotechnology
US Army Medical Research and
Development Command
ATTN: DASG-RDB
Fort Detrick
Frederick, MD 21701

Dr. Helen C. Benet
Research Specialist
US Armed Forces Medical Intelligence
Center
ATTN: AFMIC/SA
Fort Detrick
Frederick, MD 21701

LTC Josh Berman
Parasitologist
Division of Experimental Therapeutics
Walter Reed Army Institute
of Research
ATTN: SGRD-UWM-B
Washington, DC 20307

Dr. William O. Berndt
Dean for Graduate Studies and
Research and Professor of
Pharmacology
University of Nebraska Medical Center
42nd and Dewey Avenue
Omaha, NE 68105

Dr. Rajendra S. Bhatnagar
Professor of Biochemistry
School of Dentistry, HSW-604
University of California
San Francisco, CA 94143

Amy Blitstein
Biological Laboratory Technician
Analytical Chemistry Branch
US Army Medical Research Institute
of Chemical Defense (USAMRICD)
ATTN: SGRD-UV-VA
Aberdeen Proving Ground, MD 21010

Brenda Bolden
Chemist
Uniformed Services University of
the Health Sciences
4301 Jones Bridge Road
Bethesda, MD 20814

Dr. Ronald T. Borchardt
Professor and Chairman, Department of
Pharmaceutical Chemistry
The University of Kansas
3006 Malott Hall
Lawrence, KS 66045

CPT Bob Borowski
US Army Institute of Dental Research
Walter Reed Army Medical Center
ATTN: SGRD-UDR-C
Washington, DC 20307

Dr. Karl F. Bowman
Assistant Professor of Veterinary
Surgery
School of Veterinary Medicine
North Carolina State University
4700 Hillsborough Street
Raleigh, NC 27606

Dr. Alan Bcyne
Associate Professor
Department of Pharmacology and
Experimental Therapeutics
University of Maryland
School of Medicine
660 W. Redwood Street
Baltimore, MD 21201

Ronald J. Bradley
Professor, Neurosciences Program
University of Alabama in Birmingham
P.O. Box 190, University Station
Birmingham, AL 35294

Emil Braun
Physicist
Center for Fire Research
National Bureau of Standards
Washington, DC 20234

Dr. Henry Brezenoff
Professor of Pharmacology
University of Medicine and Dentistry
of New Jersey
100 Bergen Street
Newark, NJ 07103

Dr. Alan A. Brimfield
Research Assistant Professor
Uniformed Services University of
the Health Sciences
4301 Jones Bridge Road
Bethesda, MD 20814

Floyd B. Brinkley
Research Biologist
Skin Protection and Decontamination
Branch
US Army Medical Research Institute
of Chemical Defense (USAMRICD)
ATTN: SGRD-UV-CP
Aberdeen Proving Ground, MD 21010

CPT Nina L. Brokaw
Project Officer
MLSD, DCD
USACMLS
ATTN: ATZN-CM-CS
Fort McClellan, AL 36205

Dr. Neville Brookes
Associate Professor
Department of Pharmacology and
Experimental Therapeutics
University of Maryland
School of Medicine
660 W. Redwood Street
Baltimore, MD 21201

Clarence A. Broomfield
Research Chemist
Basic Pharmacology Branch,
US Army Medical Research Institute
of Chemical Defense (USAMRICD)
ATTN: SGRD-UV-PB
Aberdeen Proving Ground, MD 21010

CPT Danley Brown
Research Biochemist
Division of Combat Casualty Care
Letterman Army Institute of Research
ATTN: SGRD-UL-CCC
Presidio of San Francisco, CA 94129

Dr. Harry D. Brown
Professor, Biochemistry Department
Lipman Hall
Rutgers University
New Brunswick, NJ 08903

MAJ Larry D. Brown
Toxicologist
Toxicology Working Group
Letterman Army Institute of Research
ATTN: SGRD-ULV-T
Presidio of San Francisco, CA 94129

Nesbitt D. Brown
Research Chemist
Division of Biochemistry
Walter Reed Army Institute of
Research
Washington, DC 20307

Dr. Thomas M. Brown
Associate Professor
Clemson University
Clemson, SC 29631

Dr. Howard J. Bryant
Assistant Professor of Physiology
Uniformed Services University of the
Health Sciences
4301 Jones Bridge Road
Bethesda, MD 20814

MAJ Charles K. Burdick
Acting Chief, Drug Assessment
Division
US Army Medical Research Institute
of Chemical Defense (USAMRICD)
ATTN: SGRD-UV-DB
Aberdeen Proving Ground, MD 21010

Dr. David R. Burt
Associate Professor of Pharmacology
University of Maryland
School of Medicine
660 W. Redwood Street
Baltimore, MD 21201

COL Donald E. Butkus
Director, Division of Medicine
Walter Reed Army Institute of
Research
ATTN: SGRD-UWH
Washington, DC 20307

Susan K. Cameron
Department of Pharmacology and
Therapeutics
University of Maryland
660 West Redwood Street
Baltimore, MD 21201

Dr. Robert J. Campbell
Chief, Pharmacology Branch
Chemical and Biological Sciences
Division (DRXRO-CB)
US Army Research Office
P.O. Box 12211
Research Triangle Park, NC 27709

Nicholas S. Capasso
Consultant
IIT Research Institute
10 West 35th Street
Chicago, IL 60616

Dr. Yale Caplan
Toxicologist
Office of the Chief Medical Examiner
State of Maryland
111 Penn Street
Baltimore, MD 21201

Dr. Homer. W. Carhart
Head, Combustion and Fuels Branch
Naval Research Laboratory
4555 Overlook Avenue, SW
Washington, DC 20375

Dr. Mickey C. Castle
Associate Professor
Eastern Virginia Medical School
P.O. Box 1980
Norfolk, VA 23501

Dr. Joy Cavagnaro
Staff Scientist
Hazleton Biotechnologies Corporation
9200 Leesburg Turnpike
Vienna, VA 22180

F.-C. Tony Chang
Neurotoxicology Branch
US Army Medical Research Institute
of Chemical Defense (USAMRICD)
ATTN: SGRD-UV-YN
Aberdeen Proving Ground, MD 21010

CDR Raymond L. Chaput
Program Element Manager
Office of Naval Technology
MAT 0723
800 N. Quincy Street
Arlington, VA 22217

Dr. Peter K. Chiang
Research Chemist
Division of Biochemistry
Walter Reed Army Institute of
Research
ATTN: SGRD-UWG
Washington, DC 20307

Dr. George C.Y. Chiou
Professor and Head, Department of
Medical Pharmacology
Texas A&M University
Medical School
College Station, TX 77843

COL Martin Chipman
Medical Science Liaison Officer,
USAMRDC
Hadassah-Hebrew University Medical
Center
US Defense Attache Office
American Embassy Israel
APO NY 09672

Dr. Edward Chou
Research Chemist
Analytical Chemistry Branch
US Army Medical Research Institute
of Chemical Defense (USAMRICD)
ATTN: SGRD-UV-VA
Aberdeen Proving Ground, MD 21010

Dr. Ho Chung
Chief, Biochemical Pharmacology
Division of Experimental Therapeutics
Walter Reed Army Institute of
Research
ATTN: SGRD-UWM-C
Washington, DC 20307

James H. Clark
Research Biologist
Applied Pharmacology Branch
US Army Medical Research Institute
of Chemical Defense (USAMRICD)
ATTN: SGRD-UV-DA
Aberdeen Proving Ground, MD 21010

Offie E. Clark, III
Biological Technician
Basic Pharmacology Branch
US Army Medical Research Institute
of Chemical Defense (USAMRICD)
ATTN: SGRD-UV-PB
Aberdeen Proving Ground, MD 21010

Dr. Ronald E. Clawson
Pharmacologist, Medical Chemical
Defense Research Program
US Army Medical Research and
Development Command (USAMRDC)
ATTN: SGRD-PLE
Fort Detrick
Frederick, MD 21701

Dr. J.G. Clement
Chief, Pharmacology
Defense Research Establishment
Suffield
Ralston, Alberta
Canada T0J 2N0

Dr. Daniel R. Coleman
Head, Biochemical Engineering Section
Southern Research Institute
2000 9th Avenue South
Birmingham, AL 35255-5305

John J. Cuculis
Physical Science Administrator
Operations and Liaison Branch
Administrative Division
US Army Medical Research Institute of
Chemical Defense (USAMRICD)
ATTN: SGRD-UV-AO
Aberdeen Proving Ground, MD 21010

Dr. Jack C. Dacre
Toxicologist and
Manager, Chemical Weapons
Health Effects Research Division
US Army Medical Bioengineering
Research and Development Laboratory
ATTN: SGRD-UBG-M
Fort Detrick
Frederick, MD 21701

Nicholas F. Dalessandro
Biological Science Assistant
US Army Institute of Dental Research
Walter Reed Army Medical Center
ATTN: SGRD-UDR-C
Washington, DC 20307

COL Bruce A. Dalton
Occupational Health Consultant
Office of the Surgeon General
Professional Services
ATTN: DASG-PSP-O
The Pentagon
Washington, DC 20310

Dr. David R. Dalton
Professor of Chemistry
Temple University
Philadelphia, PA 19122

Dr. Arthur M. Dannenberg, Jr.
Professor, Experimental Pathology
The Johns Hopkins University
School of Hygiene and Public Health
615 N. Wolfe Street
Baltimore, MD 21205

Dr. Yehuda L. Danon
Head, Division of Pediatric
Immunology
Beilinson Medical Center
Beilinson, Israel 40601

Julia E. Daszkiewicz
Biological Laboratory Technician
Skin Toxicity Branch
US Army Medical Research Institute
of Chemical Defense (USAMRICD)
ATTN: SGRD-UV-CT
Aberdeen Proving Ground, MD 21010

COL David E. Davidson, Jr.
Chief, Department of Biology
Division of Experimental Therapeutics
Walter Reed Army Institute of
Research
ATTN: SGRD-UWM-D
Washington, DC 20307

Dr. David Davis
Research Biologist
Division of Experimental Therapeutics
Walter Reed Army Institute
of Research
Washington, DC 20307

Edward G. Davis
Research Physical Scientist
Physics Branch, Research Division
Chemical Research and Development
Center
ATTN: DRSMC-CLB-PB(A)
Aberdeen Proving Ground, MD 21010

COL Rudolph H. de Jong
US Army Medical Research Institute
of Chemical Defense (USAMRICD)
ATTN: SGRD-UV-ZB
Aberdeen Proving Ground, MD 21010

Dr. John De Lorge
Head, Bioenvironmental Sciences
Department
Naval Aerospace Medical Research
Laboratory
Naval Air Station
ATTN: 04 NAMRL
Pensacola, FL 32508

Ignatius Dembure
Biological Science Assistant
Basic Pharmacology Branch
US Army Medical Research Institute
of Chemical Defense (USAMRICD)
ATTN: SGRD-UV-PB
Aberdeen Proving Ground, MD 21010

Dr. Sharad S. Deshpande
Research Assistant Professor
Department of Pharmacology and
Experimental Therapeutics
University of Maryland
School of Medicine
660 W. Redwood Street
Baltimore, MD 21201

Dr. William L. Dewey
Professor, Department of Pharmacology
Medical College of Virginia
Virginia Commonwealth University
P.O. Box 613, MCV Station
Richmond, VA 23298-0001

Dr. Garrett S. Dill
Manager, Pathology and Animal
Resources
Battelle Columbus Laboratories
505 King Avenue
Columbus, OH 43201

Dr. Bhupendra P. Doctor
Director, Division of Biochemistry
Walter Reed Army Institute
of Research
ATTN: SGRD-UWG
Washington, DC 20307

Dr. Lester R. Drewes
Professor
Department of Biochemistry
University of Minnesota
School of Medicine
Duluth, MN 55812

Dr. Jeffrey Doeblner
Professor of Physiology
Pennsylvania State University
418 Mueller Building
University Park, PA 16802

CPT Michael J. Dunne, Jr.
Naval Flight Surgeon/Pathologist
Naval Aerospace Medical Research
Laboratory
Naval Air Station
Pensacola, FL 32508

Dr. Edward F. Domino
Professor of Pharmacology
Department of Pharmacology
University of Michigan
M6414 Medical Science Building I
Ann Arbor, MI 48109

Dr. Walter Ehrlich
Associate Professor
The Johns Hopkins University
School of Hygiene and Public Health
615 N. Wolfe Street
Baltimore, MD 21205

CPT Patricia Lynn Donaldson
Research Physiologist
Neurotoxicology Branch
US Army Medical Research Institute
of Chemical Defense (USAMRICD)
ATTN: SGRD-UV-YN
Aberdeen Proving Ground, MD 21010

Dr. Antoine El-Hage
Research Pharmacologist
Basic Pharmacology Branch
US Army Medical Research Institute
of Chemical Defense (USAMRICD)
ATTN: SGRD-UV-PB
Aberdeen Proving Ground, MD 21010

CPT Bruce A. Donzanti
Behavioral Pharmacologist
Biomedical Model Development Branch
US Army Medical Research Institute
of Chemical Defense (USAMRICD)
ATTN: SGRD-UV-DB
Aberdeen Proving Ground, MD 21010

Dr. Robert Ellin
Analytical Chemistry Branch
US Army Medical Research Institute
of Chemical Defense (USAMRICD)
ATTN: SGRD-UV-VA
Aberdeen Proving Ground, MD 21010

Dr. Peter H. Doukas
Professor of Molecular Pharmacology
Temple University School of Pharmacy
3307 North Broad Street
Philadelphia, PA 19140

Dr. Everett H. Ellinwood, Jr.
Professor of Psychiatry and
Pharmacology
Director of Behavioral
Neuropharmacology Section
Duke University Medical Center
Box 3870
Durham, NC 27710

Dr. William Y. Ellis
Chief, Chemical Handling and
Data Analysis Branch
Division of Experimental Therapeutics
Walter Reed Army Institute of
Research
ATTN: SGRD-UWMA
Washington, DC 20307

Dr. Julie Elmund
Assistant Professor
Department of Anatomy
Colorado State University
Fort Collins, CO 80523

Dr. Timothy F. Elsmore
Chief, Physiology and Behavior
Branch
Department of Medical Neuroscience
Division of Neuropsychiatry
Walter Reed Army Institute of
Research
Washington, DC 20307

Dr. Jerry M. Farley
Assistant Professor
Department of Pharmacology and
Toxicology
University of Mississippi Medical
Center
2500 North State Street
Jackson, MS 39216-4505

Dr. Joseph Feeney
Research Chemist
Toxicology Branch Research Division
Chemical Research and Development
Center
ATTN: DRSMC-CLB-TE(A)
Aberdeen Proving Ground, MD 21010

MAJ Henry G. Fein
Research Internist
Department of Clinical Physiology
Walter Reed Army Institute
of Research
ATTN: SGRD-UWH-D
Washington, DC 20307

Dr. Margaret G. Filbert
Pharmacologist
Neurotoxicology Branch
US Army Medical Research Institute of
Chemical Defense (USAMRICD)
ATTN: SGRD-UV-YN
Aberdeen Proving Ground, MD 21010

Lawrence Fleckenstein
Research Pharmacologist
Department of Pharmacology
Division of Experimental Therapeutics
Walter Reed Army Institute
of Research
Washington, DC 20307

Jeffrey S. Forster
Biological Lab Technician
Skin Toxicity Branch
US Army Medical Research Institute
of Chemical Defense (USAMRICD)
ATTN: SGRD-UV-CT
Aberdeen Proving Ground, MD 21010

Jeffrey Foster
Biological Lab Technician
Drug Testing and Evaluation Branch
US Army Medical Research Institute
of Chemical Defense (USAMRICD)
ATTN: SGRD-UV-DD
Aberdeen Proving Ground, MD 21010

Dr. Robert E. Foster
Research Physiologist
Neurotoxicology Branch
US Army Medical Research Institute
of Chemical Defense (USAMRICD)
ATTN: SGRD-UV-YN
Aberdeen Proving Ground, MD 21010

Dr. Sophia S. Fotopoulos
Director
Assistant to the Senior
Vice-President for Life Sciences
Midwest Research Institute
425 Volker Boulevard
Kansas City, MO 64110

Dr. Ralph P. Francesconi
Research Chemist
US Army Research Institute of
Environmental Medicine
ATTN: SGRD-UE-HR
Natick, MA 01760

MAJ David R. Franz
Chief, Physiology Branch
US Army Medical Research Institute
of Chemical Defense (USAMRICD)
ATTN: SGRD-UV-YP
Aberdeen Proving Ground, MD 21010

COL Nicholas F. Frattaroli
Commander
Kirk US Army Health Clinic
ATTN: HSXR-APG-Z
Aberdeen Proving Ground, MD 21005

Joe Frijia
Biological Lab Technician
Physiology Branch
ATTN: SGRD-UV-YP
Aberdeen Proving Ground, MD 21010

Harry L. Froehlich
Pharmacologist
Physiology Branch
US Army Medical Research Institute
of Chemical Defense (USAMRICD)
ATTN: SGRD-UV-YP
Aberdeen Proving Ground, MD 21010

CPT Donald E. Furry
Executive Officer
Naval Aerospace Medical Research
Laboratory
Naval Air Station
ATTN: Code 00A
Pensacola, FL 32508

Dr. Bruce Paul Gaber
Research Chemist
Naval Research Laboratory
Code 6510
Washington, DC 20375

Dr. Benedict Gallo
Research Microbiologist
Science and Advanced Technology
Laboratory
US Army Research and Development
Center
Natick, MA 01760

Emily M. Gause
Associate Research Scientist
Southwest Foundation for Biomedical
Research
West Loop 410 at Military Drive
San Antonio, TX 78284

COL Jay D. Gensler
Chief, Health and Veterinary Services
Office
Chemical Research and Development
Center
ATTN: DRSMC-CLM(A)
Aberdeen Proving Ground, MD 21010

Mary Kay Gentry
Research Chemist
Division of Biochemistry
Walter Reed Army Institute
of Research
ATTN: SGRD-UWG
Washington, DC 20307

MAJ David T. George
Staff Officer, Medical Chemical
Defense Research Program
US Army Medical Research and
Development Command (USAMRDC)
ATTN: SGRD-PLE
Fort Detrick
Frederick, MD 21701

LTC Dennis W. Gilstad
Chief, Aeromedical Systems Functions
Chemical Defense Branch
US Air Force School of Aerospace
Medicine
ATTN: USAFSAM/VNC
Brooks Air Force Base, TX 78235

MAJ John F. Glenn
Chief, Neurotoxicology Branch
US Army Medical Research Institute of
Chemical Defense (USAMRICD)
ATTN: SGRD-UV-YN
Aberdeen Proving Ground, MD 21010

CPT Glenn A. Goddard
Pharmacologist
Research and Development
US Air Force School of
Aerospace Medicine
ATTN: USAFSAM/RZV
Brooks Air Force Base, TX 78235

LTC Dennis N. Gold
Medical Readiness Manager
Directorate of Medical Plans
and Resources
Office of the Surgeon General
ATTN: SGHR
Bolling Air Force Base, DC 20332

Dr. Marvin Goldman
Director, Energy Lab
US Department of Energy
Davis, CA 95616

Dr. Barry D. Goldstein
Assistant Professor
Department of Pharmacology and
Toxicology
Medical College of Georgia
Augusta, GA 30912

Dr. Claudia Golenda
Research Entomologist
Department of Entomology
Walter Reed Army Institute of
Research
Washington, DC 20307

Alan Goodman
Chemist
Chemical/Biological Detection
and Alarms Division
Chemical Research and Development
Center
ATTN: DRSMC-CLC-C(A)
Aberdeen Proving Ground, MD 21010

Dr. Richard K. Gordon
Research Chemist
Division of Biochemistry
Department of Applied Biochemistry
Walter Reed Army Institute
of Research
Washington, DC 20307

Harold L. Gotoff
Assistant Chief, Physical
Protection Division
Chemical Research and Development
Center
ATTN: DRSMC-CLW(A)
Aberdeen Proving Ground, MD 21010

Dr. Charles Graham
Principal Experimental Psychologist
Midwest Research Institute
425 Volcker Boulevard
Kansas City, MO 64110

John S. Graham
Biological Lab Technician
Comparative Pathology Branch
US Army Medical Research Institute
of Chemical Defense (USAMRICD)
ATTN: SGRD-UV-VC
Aberdeen Proving Ground, MD 21010

PFC Lisa M. Graham
Biological Assistant
US Army Medical Research Institute of
Chemical Defense (USAMRICD)
ATTN: SGRD-UV-CM
Aberdeen Proving Ground, MD 21010

Dr. Allan P. Gray
Manager, Biotechnology Department
Dynamac Corporation
11140 Rockville Pike
Rockville, MD 20852

R. Richard Gray
Research Chemist
Division of Biochemistry
Walter Reed Army Institute of
Research
ATTN: SGRD-UWG
Washington, DC 20307

MAJ(P) Martin D. Green
Chief, Applied Pharmacology Branch
US Army Medical Research Institute
of Chemical Defense (USAMRICD)
ATTN: SGRD-UV-DA
Aberdeen Proving Ground, MD 21010

MAJ Judith J. Greenamyre
Research Veterinarian
Chemical Defense Branch
US Air Force School of
Aerospace Medicine
ATTN: USAFSAM/VNC
Brooks Air Force Base, TX 78235

Linda Grimm
Research Associate
Radiopharmaceutical Chemistry
George Washington University
2300 Eye Street, NW
Washington, DC 20037

Dr. James D. Grissett
Head, Medical Sciences Department
Naval Aerospace Medical Research
Laboratory
ATTN: 02
Pensacola, FL 32508

Clark L. Gross
Chemist
Skin Toxicity Branch
US Army Medical Research Institute
of Chemical Defense (USAMRICD)
ATTN: SGRD-UV-CT
Aberdeen Proving Ground, MD 21010

Dr. Tamara Gund
Assistant Professor
New Jersey Institute of Technology
323 High Street
Newark, NJ 07102

Dr. Joshua L. Gurman
Research Associate
American Iron and Steel Institute
1000 16th Street, NW
Washington, DC 20036

Dr. Peter Hambright
Professor of Chemistry
Chemistry Department
Howard University
525 S. College Street, NW
Washington, DC 20059

Dr. Philip S. Hammond
Research Chemist
Skin Toxicity Branch
US Army Medical Research Institute
of Chemical Defense (USAMRICD)
ATTN: SGRD-UV-CT
Aberdeen Proving Ground, MD 21010

Dr. Dan W. Hanke
Pharmacologist
Biomedical Model Development Branch
US Army Medical Research Institute
of Chemical Defense (USAMRICD)
ATTN: SGRD-UV-DB
Aberdeen Proving Ground, MD 21010

LTC Donald G. Harrington
Chief, Cutaneous Hazards Division
US Army Medical Research Institute
of Chemical Defense (USAMRICD)
ATTN: SGRD-UV-C
Aberdeen Proving Ground, MD 21010

Dr. Gerald Hiatt
Toxicologist
Toxicology Group
Letterman Army Institute of Research
ATTN: SGRD-ULZ-T
Presidio of San Francisco, CA 94129

Larrel W. Harris
Research Chemist
Applied Pharmacology Branch
US Army Medical Research Institute
of Chemical Defense (USAMRICD)
ATTN: SGRD-UV-DA
Aberdeen Proving Ground, MD 21010

Elaine Hickey
Librarian, Technical Library
Chemical Research and Development
Center
ATTN: DRSMC-CLJ-IL(A)
Aberdeen Proving Ground, MD 21010

Troy Hawkins
Biological Lab Technician
Physiology Branch
ATTN: SGRD-UV-YP
Aberdeen Proving Ground, MD 21010

CPT Joseph L. High
Chief of Inpatient Services
Madigan Army Medical Center
Tacoma, WA 98431

CPT Isaac J. Hayward
Staff Pathologist
Division of Pathology
Walter Reed Army Institute of
Research
ATTN: SGRD-UWP
Washington, DC 20307

COL Duane E. Hilmas
Commander
US Army Medical Research Institute
of Chemical Defense (USAMRICD)
ATTN: SGRD-UV-ZA
Aberdeen Proving Ground, MD 21010

Dr. Ralph A. Heasley
Manager, Aerosol Research and
Development
3M-Riker Company
3M Center, Building 270-4S-02
St. Paul, MN 55144

MAJ Clifford J. Hixson
Veterinary Pathologist
Comparative Pathology Branch
Veterinary Medicine and Laboratory
Research Support Division
US Army Medical Research Institute
of Chemical Defense (USAMRICD)
ATTN: SGRD-UV-VC
Aberdeen Proving Ground, MD 21010

Dr. Frederick W. Hegge
Research Psychologist
Department of Behavioral Biology
Walter Reed Army Institute
of Research
ATTN: SGRD-UWI-C
Washington, DC 20307

Dr. Ing K. Ho
Professor and Chairman
Department of Pharmacology and
Toxicology
University of Mississippi
Medical Center
2500 N. State Street
Jackson, MS 39216-4505

COL Richard A. Hodder
Deputy Director
Division of Medicine
Walter Reed Army Institute
of Research
Washington, DC 20307

Daniel A. Holterman
Laboratory Technician
Hazleton Biotechnologies Corporation
9200 Leesburg Turnpike
Vienna, VA 22180

Dr. Gerlof Homan
Vice President
Pharmaceutical Division for
Research and Development
Survival Technology, Inc.
8101 Glenbrook Road
Bethesda, MD 20814

CPT William M. Houk
Commanding Officer
Naval Aerospace Medical Research
Laboratory
Naval Air Station
ATTN: 00
Pensacola, FL 32508

COL William E. Houston
Director, Medical Chemical Defense
Research Program
US Army Medical Research and
Development Command (USAMRDC)
ATTN: SGRD-PLE
Fort Detrick
Frederick, MD 21701

Dr. Luke Hsiao
Principal Investigator
Starks Associates, Inc.
1280 Niagara Street
Buffalo, NY 14213

Dr. Fu-Lian Hsu
Research Chemist
Analytical Branch, Research Division
Chemical Research and Development
Center
ATTN: DRSMC-CLB-R(A)
Aberdeen Proving Ground, MD 21010

Dr. C. Sue Hudson
Research Assistant Professor
Department of Pharmacology and
Experimental Therapeutics
University of Maryland
School of Medicine
660 W. Redwood Street
Baltimore, MD 21201

Dr. Arthur S. Hume
Associate Professor
Department of Pharmacology and
Toxicology
University of Mississippi Medical
Center
2500 N. State Street
Jackson, MS 39216

MAJ Steven R. Hursh
Chief, Department of Medical
Neurosciences
Walter Reed Army Institute
of Research
ATTN: SGRD-UWI-B
Washington, DC 20307

Matthew I. Hutton
Operations Research Analyst
Systems Development Division
Chemical Research and Development
Center
ATTN: DRSMC-CLY-A(A)
Aberdeen Proving Ground, MD 21010

CPT August C. Ibay
US Army Institute of Dental
Research
Walter Reed Army Medical Center
ATTN: SGRD-UDR-C
Washington, DC 20307

Dean Irino
Biological Aid
Drug Testing and Evaluation Branch
US Army Medical Research Institute
of Chemical Defense (USAMRICD)
ATTN: SGRD-UV-DD
Aberdeen Proving Ground, MD 21010

CPT Warren W. Jederberg
Chief, Skin Protection and
Decontamination Branch
US Army Medical Research Institute
of Chemical Defense (USAMRICD)
ATTN: SGRD-UV-CP
Aberdeen Proving Ground, MD 21010

COL George W. Irving, III
US Air Force Liaison Officer for
Medical Chemical Defense Research
Program
US Army Medical Research and
Development Command (USAMRDC)
ATTN: SGRD-PLE
Fort Detrick
Frederick, MD 21710

Dr. Donald J. Jenden
Professor and Chairman
Department of Pharmacology
Center for Health Sciences
University of California
School of Medicine
Los Angeles, CA 90024

Louis Isaacson
Geo-Centers
4710 Auth Place
Suitland, MD 20746

1LT Gary W. Jepson
Research Chemist
Air Force Aerospace Medical Research
Laboratory
ATTN: AFAMRL/THB
Wright-Patterson Air
Force Base, OH 45433

Samuel E. Jackson, Jr.
Engineering Psychologist
US Army Human Engineering Laboratory
ATTN: DRXHE-IS
Aberdeen Proving Ground, MD 21005

CPT Vernon R. Jimmerson
Pharmacology Division
US Army Medical Research Institute
of Chemical Defense (USAMRICD)
Aberdeen Proving Ground, MD 21010

MAJ Willis H. Jacob
Product Manager, Headquarters
US Army Medical Research and
Development Command
ATTN: SGRD-DTM
Fort Detrick
Frederick, MD 21701

Deadre J. Johnson
Research Chemist
Department of Hematology
Walter Reed Army Institute of
Research
Washington, DC 20307

MAJ James J. Jaeger
Analytical Chemistry Branch
US Army Medical Research Institute
of Chemical Defense (USAMRICD)
ATTN: SGRD-UV-VA
Aberdeen Proving Ground, MD 21010

Dr. Donald E. Johnson
Director
Southwest Research Institute
P.O. Drawer 28510
6500 Culebra Road
San Antonio, TX 78284

LTC Howard C. Butch Johnson
Contracting Officer's Technical
Representative, USAMRICD
Battelle Columbus Division
MREF (JM-3)
505 King Avenue
Columbus, OH 43201

Tracey A. Justus
Biological Lab Technician
Comparative Pathology Branch
US Army Medical Research Institute
of Chemical Defense (USAMRICD)
ATTN: SGRD-UV-VC
Aberdeen Proving Ground, MD 21010

LTC John P. Johnson
Chief, Department of Nephrology
Division of Medicine
Walter Reed Army Institute of
Research
ATTN: SGRD-UWH-A
Washington, DC 20307

Andris Kaminskis
Research Biologist
Analytical Chemistry Branch
US Army Medical Research Institute
of Chemical Defense (USAMRICD)
ATTN: SGRD-UV-VA
Aberdeen Proving Ground, MD 21010

Dr. Ronald L. Joiner
Manager
Applied Medical Sciences
Battelle Columbus Laboratories
505 King Avenue
Columbus, OH 43201

Lynda V. Kane
Biological Lab Technician
Drug Testing and Evaluation Branch
US Army Medical Research Institute
of Chemical Defense (USAMRICD)
Aberdeen Proving Ground, MD 21010

Dr. David J. Jones
Associate Professor
Department of Anesthesiology
University of Texas Health
Sciences Center
7703 Floyd Curl Drive
San Antonio, TX 78284

Dr. Jean Karle
Chemist
Department of Pharmacology
Walter Reed Army Institute of
Research
Washington, DC 20307

MAJ Dennis E. Jones
Chief, Drug Testing and
Evaluation Branch
US Army Medical Research Institute
of Chemical Defense (USAMRICD)
ATTN: SGRD-UV-DD
Aberdeen Proving Ground, MD 21010

Dr. Frederick C. Kauffman
Professor of Pharmacology and
Experimental Therapeutics
University of Maryland
School of Medicine
660 W. Redwood Street
Baltimore, MD 21201

R. Douglas Jones
Research Psychologist
US Army Human Engineering Laboratory
ATTN: DRXHE-IS
Aberdeen Proving Ground, MD 21005

Leo Kazyak
Division of Biochemistry
Walter Reed Army Institute of
Research
ATTN: SGRD-UWG
Washington, DC 20307

COL John J. Kearney
Ophthalmologist
Division of Ocular Hazards
Letterman Army Institute of
Research
ATTN: SGRD-UL-OH
Presidio of San Francisco, CA 94129

Alan David Knapton
Biological Lab Aide
Drug Testing and Evaluation Branch
US Army Medical Research Institute
of Chemical Defense (USAMRICD)
ATTN: SGRD-UV-DD
Aberdeen Proving Ground, MD 21010

Susan Kelly
Biology Lab Technician
US Army Medical Research Institute
of Chemical Defense (USAMRICD)
Aberdeen Proving Ground, MD 21010

Dr. Margaret A. Kolka
Research Physiologist
US Army Research Institute of
Environmental Medicine
ATTN: SGRD-UE-MEP
Natick, MA 01760

Dr. Bruce J. Kelman
Associate Manager
Biology and Chemistry Department
Battelle, Pacific Northwest
Laboratories
P.O. Box 999
Richland, WA 99352

Dr. Irwin Koplovitz
Pharmacologist
Drug Testing and Evaluation Branch
US Army Medical Research Institute
of Chemical Defense (USAMRICD)
ATTN: SGRD-UV-DD
Aberdeen Proving Ground, MD 21010

Dr. Sylvia J. Kerr
Associate Professor
Biochemistry, Biophysics, Genetics
University of Colorado Health
Sciences Center
4200 E. 9th Avenue
Denver, CO 80262

MAJ Don W. Korte, Jr.
Chief, Toxicology Group
Letterman Army Institute of
Research
ATTN: SGRD-ULV-T
Presidio of San Francisco, CA 94129

Dr. Albert W. Kirby
Neuropharmacologist
US Army Aeromedical Research
Laboratory
P.O. Box 577
ATTN: SGRD-UAS-SN
Fort Rucker, AL 36362

Dr. Joe W. Kosh
Professor
College of Pharmacy
University of South Carolina
Columbia, SC 29208

Dr. Judith P. Kitchell
Manager, Biosystems Programs
Dynatech R/D Company
99 Erie Street
Cambridge, MD 02139

Dr. Walter S. Koski
Professor of Chemistry
The Johns Hopkins University
Baltimore, MD 21218

Diane M. Kotras
Physical Scientist
Toxicology Branch
Chemical Research and Development
Center
ATTN: DRSMC-CLB-TA
Aberdeen Proving Ground, MD 21010

Dr. Michael Krausz
Haddasah Medical Center
Jerusalem, Israel

William H. Kraybill
Microbiologist
Chemical/Biological Detection and
Alarms Division
Chemical Research and Development
Center
ATTN: DRSMC-CLC-B(A)
Aberdeen Proving Ground, MD 21010

Robert A. Lamontagne
Research Chemist
Naval Research Laboratory
Code 6682
4555 Overlook Avenue, SW
Washington, DC 20375

Dr. Michael R. Landauer
Research Scientist
Toxicology Branch, Research Division
Chemical Research and Development
Center
ATTN: DRSMC-CLB-TC(A)
Aberdeen Proving Ground, MD 21010

Dr. Milton Landowne
Medical Advisor
US Army Research Institute of
Environmental Medicine
ATTN: SGRD-UEZ-A
Natick, MA 01760

Lawrence A. Landry
President
Associate Consultants, Inc.
1701 K Street, NW, Suite 501
Washington, DC 20006

Dr. Eric J. Langenmayr
Senior Scientist
Rohm and Haas Company
Northtown and McKean Roads
Spring House, PA 19477

Charlotte Lattin
Biological Lab Technician
Analytical Chemistry Branch
US Army Medical Research Institute
of Chemical Defense (USAMRICD)
ATTN: SGRD-UV-VA
Aberdeen Proving Ground, MD 21010

Dr. K. Ronald Laughery
President
Micro Analysis and Design
9132 Thunderhead Drive
Boulder, CO 80302

LTC Marvin A. Lawson
Chief, Basic Pharmacology Branch
US Army Medical Research Institute
of Chemical Defense (USAMRICD)
ATTN: SGRD-UV-PB
Aberdeen Proving Ground, MD 21010

Dr. Frank J. Lebeda
Assistant Professor
Baylor College of Medicine
Department of Neurology
Houston, TX 77030

MAJ William E. Legg
Environmental Science Officer
Directorate of Combat Developments
US Army Academy of Health Sciences
ATTN: HSHA-CDM
Fort Sam Houston, TX 78234

W. James Lenné
Pharmacologist
Applied Pharmacology Branch
US Army Medical Research Institute
of Chemical Defense (USAMRICD)
ATTN: SGRD-UV-DA
Aberdeen Proving Ground, MD 21010

Dr. J. Michael Lentz
Chief, Vestibular Science Division
Naval Aerospace Medical Research
Laboratory
ATTN: Code 22
Pensacola, FL 32508

Dr. David E. Lenz
Research Chemist
Basic Pharmacology Branch
US Army Medical Research Institute
of Chemical Defense (USAMRICD)
ATTN: SGRD-UV-PB
Aberdeen Proving Ground, MD 21010

CPT John R. Leu
Research Psychologist
Department of Medical Neurosciences
Walter Reed Army Institute of
Research
Washington, DC 20307

Dr. Barbara C. Levin
Head, Fire Toxicology
Center for Fire Research
National Bureau of Standards
Washington, DC 20234

James H. Lewis
Research Biologist
Physics Branch, Research Division
Chemical Research and Development
Center
ATTN: DRSMC-CLB-PC(A)
Aberdeen Proving Ground, MD 21010

Claire N. Lieske
Research Chemist
Applied Pharmacology Branch
Drug Assessment Division
US Army Medical Research Institute
of Chemical Defense (USAMRICD)
ATTN: SGRD-UV-DA
Aberdeen Proving Ground, MD 21010

COL Richard E. Lindstrom
Associate Director
Research Contracts Management
US Army Medical Research Institute
of Chemical Defense (USAMRICD)
ATTN: SGRD-UV-CM
Aberdeen Proving Ground, MD 21010

MAJ James S. Little
Chief of Biochemistry Services
Madigan Army Medical Center, Box 99
Tacoma, WA 98431

Florence F. Liu
Operations Research Analyst
CSD
US Army Materiel Systems Analysis
Activity
ATTN: DRXSY-CR
Aberdeen Proving Ground, MD 21010

COL Craig H. Llewellyn
Chairman and Professor
Department of Military Medicine
Uniformed Services University of
the Health Sciences
School of Medicine
4301 Jones Bridge Road
Bethesda, MD 20814

Dr. Richard H. Lovely
Neurosciences Group Leader
Biology and Chemistry Department
Battelle-Northwest
P.O. Box 999
Richland, WA 99352

Susan K. Luckan
International Research and
Development Program Manager
US Army Medical Research Institute
of Chemical Defense (USAMRICD)
ATTN: SGRD-UV-AO
Aberdeen Proving Ground, MD 21010

Dr. David B. Ludlum
Professor of Medicine and
Pharmacology
Department of Medicine
Albany Medical College
Neil Hellman Medical Research
Building
47 New Scotland Avenue
Albany, NY 12208

Dr. Robert E. Lyle
Vice President Division of Chemistry
Chem. Eng.
Southwest Research Institute
6220 Culebra Road
P.O. Drawer 28510
San Antonio, TX 78230

Dr. Raymond A. Mackay
Chief, Chemical Branch
Research Division
Chemical Research and Development
Center
ATTN: DRSMC-CLB-C(A)
Aberdeen Proving Ground, MD 21010

Ellen Kushner MacKenzie
Biological Scientist
Contract Management Office
US Army Medical Research Institute
of Chemical Defense (USAMRICD)
ATTN: SGRD-UV-CM
Aberdeen Proving Ground, MD 21010

Dr. Jeannine A. Majde
Program Manager, Cellular Biosystems
Office of Naval Research
300 North Quincy Street
Code 441CB
Arlington, VA 22217

Jerome W. Malek
Technical Advisor, Field Materiel
Development Division
US Army Medical Bioengineering
Research and Development Laboratory
ATTN: SGRD-UBE
Fort Detrick
Frederick, MD 21701

R.S. Malooley
Assistant to the Chairman
Survival Technology, Inc.
8101 Glenbrook Road
Bethesda, MD 20814

Dr. Noel K. Marshall
Research Psychologist
US Army Medical Research Institute
of Chemical Defense (USAMRICD)
ATTN: SGRD-UV-YN
Aberdeen Proving Ground, MD 21010

Dr. Billy R. Martin
Associate Professor
Medical College of Virginia
Box 613
Richmond, VA 23298

Dr. Samuel P. Massie
Professor of Chemistry
US Naval Academy
Annapolis, MD 21402

Donald M. Maxwell
Research Chemist
Basic Pharmacology Branch
US Army Medical Research Institute
of Chemical Defense (USAMRICD)
ATTN: SGRD-UV-PB
Aberdeen Proving Ground, MD 21010

MAJ John H. McDonough
Chief, Behavioral Toxicology Branch
US Army Medical Research Institute
of Chemical Defense (USAMRICD)
ATTN: SGRD-UV-PT
Aberdeen Proving Ground, MD 21010

Michael McGee
Physical Scientist
Weapons Effects Division
Army Nuclear and Chemical Agency
Building 2073
7500 Backlick Road
ATTN: MONA-WE
Springfield, VA 22150

Dr. Evelyn L. McGown
Chief, Analytical Chemistry Group
Letterman Army Institute of
Research
ATTN: SGRD-ULV-AC
Presidio of San Francisco, CA 94129

Bernie McHugh, Jr.
Research Psychologist
Neurotoxicology Branch
US Army Medical Research Institute
of Chemical Defense (USAMRICD)
ATTN: SGRD-UV-YN
Aberdeen Proving Ground, MD 21010

CPT Roger G. McIntosh
Occupational Medicine Officer
US Army Environmental Hygiene Agency
ATTN: HSHB-OM
Aberdeen Proving Ground, MD 21010

LTC Charles G. McLeod, Jr.
Chief, Comparative Pathology Branch
US Army Medical Research Institute
of Chemical Defense (USAMRICD)
ATTN: SGRD-UV-VC
Aberdeen Proving Ground, MD 21010

James McNeil
Division of Medicine
Walter Reed Army Institute
of Research
Washington, DC 20307

Dr. Henry Louis Meier
Research Chemist
Skin Toxicity Branch
US Army Medical Research Institute
of Chemical Defense (USAMRICD)
ATTN: SGRD-UV-CT
Aberdeen Proving Ground, MD 21010

Dr. Millard M. Mershon
Research Pharmacologist
Skin Protection and Decontamination
Branch
US Army Medical Research Institute
of Chemical Defense (USAMRICD)
ATTN: SGRD-UV-CP
Aberdeen Proving Ground, MD 21010

Mark Michie
Biologist
Skin Protection and Decontamination
Branch
US Army Medical Research Institute
of Chemical Defense (USAMRICD)
ATTN: SGRD-UV-CP
Aberdeen Proving Ground, MD 21010

Dr. David B. Millar
Head, Biochemistry Branch
Transplant Research Program Center
Naval Medical Research Institute
Mail Stop 36
National Naval Medical Center
Bethesda, MD 20814

Robert A. Miller
Research Chemist
US Army Institute of Dental Research
ATTN: SGRD-UDR-C
Walter Reed Army Medical Center
Washington, DC 20307

LTC Joseph E. Milligan
Chief, Chemical Defense Division
US Air Force Aerospace Medical
Division
ATTN: HQAMD-RDTK
Brooks Air Force Base, TX 78235

Dr. Richard M. Millis
Chief Science Officer
Associate Consultants, Inc.
1701 K Street, NW, Suite 501
Washington, DC 20006

Kenneth R. Mills
Biologist
Comparative Pathology Branch
US Army Medical Research Institute
of Chemical Defense (USAMRICD)
ATTN: SGRD-UV-VC
Aberdeen Proving Ground, MD 21010

Dr. Robert Mioduszewski
Research Biologist
Physics Branch, Research Division
Chemical Research and Development
Center
ATTN: DRSMC-CLB-PC(A)
Aberdeen Proving Ground, MD 21010

CDR William A. Monaco
Chief, Vision Sciences Research
Division
Naval Aerospace Medical Research
Laboratory
Naval Air Station
ATTN: Code 023
Pensacola, FL 32508

George Miura
Biological Science Assistant
Division of Biochemistry
Walter Reed Army Institute of
Research
ATTN: SGRD-UWG
Washington, DC 20307

COL Richard D. Montrey
Chief, Veterinary Resources Branch
US Army Medical Research Institute
of Chemical Defense (USAMRICD)
ATTN: SGRD-UV-VV
Aberdeen Proving Ground, MD 21010

Dr. Thomas W. Mix
President
Merix Corporation
192 Worcester Street
Wellesley, MA 02181

Dr. Edward Montz
Research Associate
Naval Medical Research Institute
Bethesda, MD 20814

Dr. Bert A. Mobley
Associate Professor of Physiology
and Biophysics
University of Oklahoma College of
Medicine
Oklahoma City, OK 73190

Dr. Gary T. Moore
Manager, Laboratory Animal Sciences
Southwest Research Institute
6220 Culebra Road
San Antonio, TX 78284

MAJ William Mobley
Research Neurologist
Department of Medical Neurosciences
Walter Reed Army Institute of
Research
ATTN: SGRD-UWI
Washington, DC 20307

CPT Earl W. Morgan
Toxicologist
Toxicology Group
Letterman Army Institute of Research
ATTN: SGRD-ULV-T
Presidio of San Francisco, CA 94129

LTC James B. Moe
Director, Division of Pathology
Walter Reed Army Institute of
Research
ATTN: SGRD-UWP
Washington, DC 20307

Dr. Arnold T. Mosberg
Principal Research Scientist
Battelle Columbus Laboratories
505 King Avenue
Columbus, OH 42301

Dr. Robert H. Mosebar
Medical Officer
Directorate of Combat Developments
US Army Academy of Health Sciences
ATTN: HSHA-DCD
Fort Sam Houston, TX 78234

Dr. Rudy H. Moyer
Geomet, Incorporated
1801 Research Boulevard
Rockville, MD 20850

Dr. Michael R. Murphy
Project Manager, Senior Scientist
Systems Research Laboratories, Inc.
ATTN: SAM-RZV
Brooks Air Force Base, TX 28235

Dr. H.A. Mat Musallam
Chief Technical Monitor
Department of Medicinal Chemistry
Walter Reed Army Institute of
Research
ATTN: SGRD-UWM-A
Washington, DC 20307

Dr. Krishen L. Nagpal
Physical Scientist
Program Management Research Division
Chemical Research and Development
Center
ATTN: DRSMC-CLR-P(A)
Aberdeen Proving Ground, MD 21010

Catherine Nalls
Biological Aid
Drug Testing and Evaluation Branch
US Army Medical Research Institute
of Chemical Defense (USAMRICD)
ATTN: SGRD-UV-DD
Aberdeen Proving Ground, MD 21010

Dr. James S. Nelson
Professor and Head, Neuropathology
Department of Pathology
Washington University School
of Medicine
660 S. Euclid Avenue
St. Louis, MO 63110

Dr. Stanley Nelson
Chairman, Department of Anatomy
University of Kansas Medical Center
39th and Rainbow Boulevard
Kansas City, KS 66103

LTC Harold H. Newball
Chief, Physiology Division
US Army Medical Research Institute
of Chemical Defense (USAMRICD)
ATTN: SGRD-UV-Y
Aberdeen Proving Ground, MD 21010

Dr. Robert W. Newburgh
Head, Biological Sciences Division
Office of Naval Research
Code 441
800 North Quincy Street
Arlington, VA 22217

MAJ Carl Johann Nielsen
Research Pharmacologist
Department of Pharmacology
Division of Experimental Therapeutics
Walter Reed Army Institute
of Research
ATTN: SGRD-UWC
Washington, DC 20307

Dr. Howard E. Noyes
Associate Director, WRAIR
Office of Research Management
Walter Reed Army Institute of
Research
ATTN: SGRD-UWZ-C
Washington, DC 20307

CPT Vincent M. O'Donnell
Research Psychologist
Department of Military Medical
Psychophysiology
Walter Reed Army Institute of
Research
ATTN: SGRD-UWI-C
Washington, DC 20307

Dr. Eugene J. Olajos
Pharmacologist, Toxicology Branch
Chemical Research and Development
Center
ATTN: DRSMC-CLB-T(A)
Aberdeen Proving Ground, MD 21010

Dr. Hugh J. O'Neill
Manager, Chemistry Research
IIT Research Institute
10 West 35th Street
Chicago, IL 60616

Dr. John J. O'Neill
Chairman, Department of Pharmacology
Temple University School of Medicine
3420 N. Broad Street
Philadelphia, PA 19140

Dr. Joseph V. Osterman
Director of Programs and Scientific
Advisor
Naval Medical Research and
Development Command
Naval Medical Command, National
Capital Region
ATTN: Code-40
Bethesda, MD 20814

LCDR Jerry M. Owens
Head, Psychological Sciences
Department
Naval Aerospace Medical Research
Laboratory
Naval Air Station
ATTN: Code 03
Pensacola, FL 32508

Maya Paabo
Research Chemist
Center for Fire Research
National Bureau of Standards
Washington, DC 20234

LTC Charles L. Pamplin, III
Assistant Chief
Department of Pharmacology
Walter Reed Army Institute of
Research
ATTN: SGRD-UWM-C
Washington, DC 20307

Dr. Bruno Papirmeister
Acting Chief, Skin Toxicity Branch
US Army Medical Research Institute
of Chemical Defense (USAMRICD)
ATTN: SGRD-UV-CT
Aberdeen Proving Ground, MD 21010

Dr. James W. Patrick
Senior Member
Molecular Neurobiology Laboratory
The Salk Institute
P.O. Box 85800
San Diego, CA 92138

Dr. Arthur S. Paul
Assistant Professor
Howard University
2300 6th Street, NW
Washington, DC 20059

Dr. Thomas L. Pazdernik
Associate Professor, Pharmacology,
Toxicology, and Therapeutics
University of Kansas Medical Center
39th and Rainbow Boulevard
Kansas City, KS 66103

COL Carl C. Peck
Director, Division of Clinical
Pharmacology
Professor of Medicine and
Pharmacology
Uniformed Services University of
the Health Sciences
4301 Jones Bridge Road
Bethesda, MD 20814

H. Herbert Peel
Manager, Biomedical Engineering
Southwest Research Institute
6800 Culebra Road
San Antonio, TX 78284

Patricia Pepin
Chief, Library Branch
Wood Technical Library
US Army Medical Research Institute
of Chemical Defense (USAMRICD)
ATTN: SGRD-UV-AW
Aberdeen Proving Ground, MD 21010

Barbara Perrone
Research Psychologist
Neurotoxicology Branch
US Army Medical Research Institute
of Chemical Defense (USAMRICD)
ATTN: SGRD-UV-YN
Aberdeen Proving Ground, MD 21010

LTC Ray H. Perry
Chemical and Biological Warfare
Staff Officer
Office of the Surgeon General
ATTN: HQDA-DASG-HCD
The Pentagon
Washington, DC 20310

Dr. John P. Petrali
Research Anatomist
Comparative Pathology Branch
US Army Medical Research Institute
of Chemical Defense (USAMRICD)
ATTN: SGRD-UV-VC
Aberdeen Proving Ground, MD 21010

Dr. James Petras
Neuroanatomist
Department of Medical Neurosciences
Division of Neuropsychiatry
Walter Reed Army Institute of
Research
ATTN: SGRD-UWI
Washington, DC 20307

Ronda R. Pindzola
Research Psychologist
Neurotoxicology Branch
US Army Medical Research Institute
of Chemical Defense (USAMRICD)
ATTN: SGRD-UV-YN
Aberdeen Proving Ground, MD 21010

Dr. Colin G. Pitt
Director for Physical Sciences
Research Triangle Institute
P.O. Box 12194
Research Triangle Park, NC 27709

Dr. Robert D. Platz
Senior Scientist
Dynamac Corporation
11140 Rockville Pike
Rockville, MD 20852

Dr. Gordon A. Plishker
Assistant Professor
Department of Neurology
Baylor College of Medicine
One Baylor Plaza
Houston, TX 77030

CPT Garrett D. Polhamus
USAF Aerospace Medical Division
Liaison to USAMRICD
Neurotoxicology Branch
US Army Medical Research Institute
of Chemical Defense (USAMRICD)
ATTN: SGRD-UV-YN
Aberdeen Proving Ground, MD 21010

LTC Michael C. Powanda
Chief, Division of Cutaneous Hazards
Letterman Army Institute of Research
ATTN: SGRD-UL-CH
Presidio of San Francisco, CA 94129

Dr. Edward J. Poziomek
Chief, Research Division
Chemical Research and Development
Center
ATTN: DRSMC-CLB(A)
Aberdeen Proving Ground, MD 21010

Dr. S.N. Pradhan
Department of Pharmacology
Howard University
College of Medicine
2400 6th Street, NW
Washington, DC 20059

Dr. Richard G. Priest
Research Physicist
Naval Research Laboratory
Code 6510
4555 Overlook Avenue, SW
Washington, DC 20375

MG Garrison Rapmund
US Army Medical Research and
Development Command (USAMRDC)
ATTN: SGRD-ZA
Fort Detrick
Frederick, MD 21701

Lawrence R. Procell
Biological Lab Technician
Physiology Branch
US Army Medical Research Institute
of Chemical Defense (USAMRICD)
ATTN: SGRD-UV-YP
Aberdeen Proving Ground, MD 21010

Dr. Radharaman Ray
Research Chemist
Basic Pharmacology Branch
US Army Medical Research Institute
of Chemical Defense (USAMRICD)
ATTN: SGRD-UV-PB
Aberdeen Proving Ground, MD 21010

CPT Harry J. Quebbeman
Research Physiologist
Physiology Branch
US Army Medical Research Institute
of Chemical Defense (USAMRICD)
ATTN: SGRD-UV-YP
Aberdeen Proving Ground, MD 21010

BG Frank A. Ramsey
Deputy Commander
US Army Medical Research and
Development Command
ATTN: SGRD-ZB
Fort Detrick
Frederick, MD 21701

Marilee H. Quesada
Research Biologist
Naval Medical Research Institute
Bethesda, MD 20814

LCDR Gary G. Reams
Senior Flight Surgeon
2nd MAW
Marine Corps Air Station
Naval Hospital
Cherry Point, NC 28533

Dr. K.S. Rajan
Science Advisor, Chemistry Division
IIT Research Institute
10 West 35th Street
Chicago, IL 60616

LTC Bryce G. Redington
Director, Grants Management
Uniformed Services University of
the Health Sciences
4301 Jones Bridge Road
Bethesda, MD 20814

Dr. John Ralston
National Research Council Research
Associate
Division of Biochemistry
Walter Reed Army Institute
of Research
Washington, DC 20307

Dr. Frances Mae Reid
Veterinary Medical Research Officer
Drug Testing and Evaluation Branch
US Army Medical Research Institute
of Chemical Defense (USAMRICD)
ATTN: SGRD-UV-DD
Aberdeen Proving Ground, MD 21010

Dr. Kandala V.N. Rao
Research Toxicologist
IIT Research Institute
10 West 35th Street
Chicago, IL 60616

Dr. Louis Reiss
Research Chemist
Research Division
Chemical Research and Development
Center
ATTN: DRSMC-CLB-CO
Aberdeen Proving Ground, MD 21010

MAJ Daniel L. Rickett
Staff Officer, Medical Chemical
Defense Research Program
US Army Medical Research and
Development Command (USAMRDC)
ATTN: SGRD-PLE
Fort Detrick
Frederick, MD 21701

LTC William E. Ridder
Department of Biology
Division of Experimental Therapeutics
Walter Reed Army Institute of
Research
ATTN: SGRD-UWM
Washington, DC 20307

Dr. William K. Riker
Professor and Chairman, Department
of Pharmacology (SOM)
Oregon Health Sciences University
3181 SW Sam Jackson Park Road
Portland, OR 97201

Dr. Jim E. Riviere
Associate Professor Pharmacology and
Toxicology
School of Veterinary Medicine
North Carolina State University
Raleigh, NC 27606

Dr. Susan E. Robinson
Assistant Professor of Pharmacology
Medical College of Virginia
Box 613, MCV Station
Richmond, VA 23298

Dr. Richard Roblin
Executive Staff Scientist
Genex Corporation
16020 Industrial Drive
Gaithersburg, MD 20877

Dr. James A. Romano, Jr.
Biotechnology Liaison Officer
US Air Force School of Aerospace
Medicine
ATTN: USAFSAM/RBV
Brooks Air Force Base, TX 28235

Dr. Barry H. Rumack
Associate Professor of Pediatrics
Director, Rocky Mountain Poison
Center
645 Bannock Street
Denver, CO 80204-4507

Dr. Robert S. Rush
Research Chemist
Division of Biochemistry
Walter Reed Army Institute
of Research
Washington, DC 20307

Matthew Sacher
Biological Lab Technician
Skin Protection and Decontamination
Branch
US Army Medical Research Institute
of Chemical Defense (USAMRICD)
ATTN: SGRD-UV-CP
Aberdeen Proving Ground, MD 21010

LTC (P) Jerald C. Sadoff
Task Area Manager
Molecular Biology and Immunology
Division of Communicable Disease
and Immunology
Walter Reed Army Institute
of Research
Washington, DC 20307

James R. Sampson
Chief, Life Cycle Management Branch
(Equipment Specialist)
US Army Medical Bioengineering
Research and Development Laboratory
ATTN: SGRD-UBE-L
Fort Detrick
Frederick, MD 21701

Dr. Frederick Samson
Director, Ralph L. Smith Research
Center
University of Kansas Medical Center
39th and Rainbow Boulevard
Kansas City, KS 66103

Dr. Stanley J. Sarnoff
President and Chairman of the Board
Survival Technology, Inc.
8101 Glenbrook Road
Bethesda, MD 20814

Dr. John M. Sarvey
Assistant Professor
Department of Pharmacology
Uniformed Services University
of the Health Sciences
4301 Jones Bridge Road
Bethesda, MD 20814

Dennis P. Schaefer
Deputy Database Administrator
Associate Consultants, Inc.
1701 K Street, NW, Suite 501
Washington, DC 20006

Dr. Stephen A. Schaub
Research Area Manager, Field
Sanitation and Water
Health Effects Research Division
US Army Medical Bioengineering
Research and Development Laboratory
ATTN: SGRD-UBG-M
Fort Detrick
Frederick, MD 21701

Dr. Eli D. Schmel
Program Manager, Molecular Biology
Office of Naval Research
Code 441MB
800 N. Quincy Street
Arlington, VA 22217

Dr. Richard L. Schowen
Professor of Chemistry
Center for Biomedical Research
University of Kansas
Lawrence, KS 66045-2112

CPT Allan C. Schroeder
Chief, Analytical Methods Development
Branch
Department of Pharmacology
Division of Experimental Therapeutics
Walter Reed Army Institute of
Research
ATTN: SGRD-UWM-C
Washington, DC 20307

Dr. John Schrot
Research Psychologist
Environmental Stress Program Center
Naval Medical Research Institute
Bethesda, MD 20814

Jonathan Seidenberg
Biological Lab Technician
Physiology Branch
US Army Medical Research Institute
of Chemical Defense (USAMRICD)
ATTN: SGRD-UV-YP
Aberdeen Proving Ground, MD 21010

Dr. Barbara Seiders
Research Chemist
Physics Branch
Chemical Research and Development
Center
ATTN: DRSMC-CLB-PC(A)
Aberdeen Proving Ground, MD 21010

John Seigh
Chief, Systems Analysis Branch
Chemical Research and Development
Center
ATTN: DRSMC-CLY-A(A)
Aberdeen Proving Ground, MD 21010

Dr. Lawrence C. Sellin
Research Physiologist
Pathology Division
US Army Medical Research Institute
of Infectious Diseases
Fort Detrick
Frederick, MD 21701

Dr. Herbert Seltzman
Senior Chemist
Research Triangle Institute
Research Triangle Park, NC 27709

Helen Settles
Safety Officer
Safety Office, Logistics Division
Walter Reed Army Institute
of Research
ATTN: SGRD-UWC-D
Washington, DC 20307

Alan M. Shefner
Associate Director of Research, Life
Sciences
IIT Research Institute
10 West 35th Street
Chicago, IL 60616

Dr. Ronald S. Sheinson
Research Chemist
Chemistry Division, Code 6180
Naval Research Laboratory
Washington, DC 20375

Ming Shih
Chemist
Analytical Chemistry Branch
US Army Medical Research Institute
of Chemical Defense (USAMRICD)
ATTN: SGRD-UV-VA
Aberdeen Proving Ground, MD 21010

Dr. Tony Shih
Pharmacologist
Basic Pharmacology Branch
US Army Medical Research Institute
of Chemical Defense (USAMRICD)
ATTN: SGRD-UV-PB
Aberdeen Proving Ground, MD 21010

Dr. Michael Thomas Shipley
Associate Professor of Neurobiology/
Cell Biology
Department of Anatomy/Cell Biology
Mail Loc #521
University of Cincinnati
College of Medicine
Cincinnati, OH 45267

Dr. Donald J. Sibbett
Vice President
Geomet, Incorporated
1801 Research Boulevard
Rockville, MD 20850

Dr. Karin Sikora-VanMeter
Assistant Professor
University of Maryland
School of Medicine
660 West Redwood Street
Baltimore, MD 21201

Dr. Thomas C. Simmons
Chief, Organic Chemistry Section
Research Division
Chemical Research and Development
Center
ATTN: DRSMC-CLB-CO(A)
Aberdeen Proving Ground, MD 21010

MAJ Allen W. Singer
Veterinarian Pathologist
Comparative Pathology Branch
US Army Medical Research Institute
of Chemical Defense (USAMRICD)
ATTN: SGRD-UV-VC
Aberdeen Proving Ground, MD 21010

LTC Robert W. Sjogren, Jr.
Gastroenterologist
Department of Gastroenterology
Walter Reed Army Institute of
Research
ATTN: SGRD-UWH-C
Washington, DC 20307

Dale W. Sloop
Operations Research Analyst
Systems Development Division
Chemical Research and Development
Center
ATTN: DRSMC-CLY-A(A)
Aberdeen Proving Ground, MD 21010

LTC Robert C. Smallridge
Chief, Department of Clinical
Physiology
Division of Medicine
Walter Reed Army Institute of
Research
ATTN: SGRD-UWH-D
Washington, DC 20307

Dr. Dennis H. Smith
Manager, Research Applications
Lederle Laboratories
Building 105/107
Pearl River, NY 10965

Donna Corkey Smith
Librarian, Technical Library
Chemical Research and Development
Center
ATTN: DRSMC-CLJ-IL(A)
Aberdeen Proving Ground, MD 21010

2LT Mark A. Smith
HPSP Medical Student
Behavioral Toxicology Branch
US Army Medical Research Institute
of Chemical Defense (USAMRICD)
ATTN: SGRD-UV-PT
Aberdeen Proving Ground, MD 21010

Dr. Satu M. Somani
Professor of Pharmacology and
Toxicology
Department of Pharmacology
Southern Illinois University
School of Medicine
P.O. Box 3926
Springfield, IL 62708

Harold Z. Sommer
Chief, Analytical Branch
Research Division
Chemical Research and Development
Center
ATTN: DRSMC-CLB-R(A)
Aberdeen Proving Ground, MD 21010

Dr. Hermona Soreq
Associate Professor
Department of Neurobiology
Weizmann Institute of Science
Rehovot 76100
Israel

Phyllis Spector
Librarian
Chemical Research and Development
Center
ATTN: DRSMC-CLJ-IL(A)
Aberdeen Proving Ground, MD 21010

LTC Donald Spoon
Chief, Medical Operations Division
Aeromedical Casualty Systems
Program Office
Headquarters, AMD/RDSMM
Brooks Air Force Base, TX 78235

Dr. George R. Spratto
Professor of Pharmacology and
Associate Dean
School of Pharmacy and Pharmacal
Sciences
Purdue University
West Lafayette, IN 47907

Patric Stanton
Graduate Student
Department of Pharmacology
Uniformed Services University of
the Health Sciences
4301 Jones Bridge Road
Bethesda, MD 20814

John S. Svalina
Industrial Hygienist
DARCOM
Office of the Surgeon General
ATTN: DRCSG-I
5001 Eisenhower Avenue
Alexandria, VA 22333

William C. Starke
Pharmacologist
Chemical Research and Development
Center
ATTN: DRSMC-CLB-TC(A)
Aberdeen Proving Ground, MD 21010

COL Dennis R. Swanson
Deputy Commander
US Army Medical Research Institute
of Chemical Defense (USAMRICD)
ATTN: SGRD-UV-ZB
Aberdeen Proving Ground, MD 21010

Dr. Fred Starks
Project Director
Starks Associates, Inc.
1280 Niagara Street
Buffalo, NY 14213

Brian Talbot
Research Biologist
Applied Pharmacology Branch
US Army Medical Research Institute
of Chemical Defense (USAMRICD)
ATTN: SGRD-UV-DA
Aberdeen Proving Ground, MD 21010

Douglas M. Stavert
Life Science Technician
Los Alamos National Laboratory
Box 1663, Group LS-1
Mail Stop 880
Los Alamos, NM 87544

Dr. Lily C. Tang
Research Pharmacologist
Division of Experimental Therapeutics
Walter Reed Army Institute
of Research
ATTN: SGRD-UWM
Washington, DC 20307

Dr. Fred W. Stemler
Physiology Branch
US Army Medical Research Institute
of Chemical Defense (USAMRICD)
ATTN: SGRD-UV-YP
Aberdeen Proving Ground, MD 21010

Dr. Palmer Taylor
Professor of Medicine and Head
Division of Pharmacology
Department of Medicine M-013H
University of California, San Diego
La Jolla, CA 92093

Dr. James F. Stubbins
Professor of Medicinal Chemistry
Virginia Commonwealth University
MCV Station, Box 581
Richmond, VA 23298

LTC Philip Taylor
Research Biochemist
US Army Aeromedical Research
Laboratory
Box 577
ATTN: SGRD-UAB-CB
Fort Rucker, AL 36362

Dr. Walter E. Sultan
Pharmacologist
Drug Assessment Division
US Army Medical Research Institute
of Chemical Defense (USAMRICD)
ATTN: SGRD-UV-D
Aberdeen Proving Ground, MD 21010

Dr. Kenneth E. Thames
Physical Scientist
Chemical and Biological Detection
and Alarms Division
Chemical Research and Development
Center
ATTN: DRSMC-CLC-B(A)
Aberdeen Proving Ground, MD 21010

Dr. John R. Thomas
Head, Behavior Technology Branch
Naval Medical Research Institute
Bethesda, MD 20814

Dr. Sandra Thomson
Research Biologist
Research Division
Chemical Research and Development
Center
ATTN: DRSMC-CLB-TE(A)
Aberdeen Proving Ground, MD 21010

Dr. Debra J. Trantolo
Senior Staff Scientist
Dynatech R/D Company
99 Erie Street
Cambridge, MA 02139

CDR Patrick A. Truman
Program Manager, Naval Medical
Chemical Warfare Defense
Naval Medical Research and
Development Command
Naval Medical Command
National Capital Region
ATTN: NRMDC-407
Bethesda, MD 20814

F. Steven Tucker
Microbiologist
Comparative Pathology Branch
US Army Medical Research Institute
of Chemical Defense (USAMRICD)
ATTN: SGRD-UV-VC
Aberdeen Proving Ground, MD 21010

MAJ George Turner
Assistant Chief, Pharmacy Services
P.O. Box 10
Letterman Army Medical Center
ATTN: HSHH-G
San Francisco, CA 94129

Dr. Charles A. Tyson
Director, Biochemical Toxicology
Program
SRI International
Menlo Park, CA 94025

CPT John Van Hamont
US Army Institute of Dental Research
Walter Reed Army Medical Center
ATTN: SGRD-UDR-C
Washington, DC 20307

Dr. William Van Meter
Research Pharmacologist
Neurotoxicology Branch
US Army Medical Research Institute
of Chemical Defense (USAMRICD)
ATTN: SGRD-UV-YN
Aberdeen Proving Ground, MD 21010

Dr. R. Venkatarghavan
Manager, Research Applications
Lederle Labs
Pearl River, NY 10965

LTC Jurgen D. Von Bredow
Chief, Pharmacology Division
US Army Medical Research Institute
of Chemical Defense (USAMRICD)
ATTN: SGRD-UV-P
Aberdeen Proving Ground, MD 21010

Dr. Randall J. von Wedel
Research Scientist
Bio-Response, Inc.
1978 West Winton Avenue
Hayward, CA 94545

Dr. Clarence W.R. Wade
Research Chemist
Health Effects Research Division
US Army Medical Bioengineering
Research and Development Laboratory
ATTN: SGRD-UBG-M
Fort Detrick
Frederick, MD 21701

Dr. James L. Way
Shelton Professor of Pharmacology
and Toxicology
Department of Medical Pharmacology
Texas A&M University
School of Medicine
Medical Sciences Building
College Station, TX 77843

LTC Henry G. Wall
Veterinary Pathologist
Comparative Pathology Branch
US Army Medical Research Institute
of Chemical Defense (USAMRICD)
ATTN: SGRD-UV-VC
Aberdeen Proving Ground, MD 21010

Dr. Robert J. Werrlein
Biomedical Model Development Branch
US Army Medical Research Institute
of Chemical Defense (USAMRICD)
ATTN: SGRD-UV-DB
Aberdeen Proving Ground, MD 21010

LTC Gerald Wannarka
Product Manager
Development and Production
Management Directorate
US Army Medical Research and
Development Command (USAMRDC)
ATTN: SGRD-DPM
Fort Detrick
Frederick, MD 21701

CPT Lynn F. Westberg
Instructor, NBC Branch
Preventive Medicine Division
US Army Academy of Health Sciences
ATTN: HFHA-IPM
Fort Sam Houston, TX 78234

Dr. F. Prescott Ward
Chief Scientist, Research Division
Chemical Research and Development
Center
ATTN: DRSMC-CLB(A)
Aberdeen Proving Ground, MD 21010

Dr. John L. Westley
Professor, Department of Biochemistry
University of Chicago
920 East 58th Street
Chicago, IL 60637

Dr. Jordan E. Warnick
Associate Professor
Department of Pharmacology and
Experimental Therapeutics
University of Maryland
School of Medicine
660 W. Redwood Street
Baltimore, MD 21201

MAJ Tim Weyandt
Occupational Medicine Officer
US Army Environmental Hygiene Agency
ATTN: HSHB-O
Aberdeen Proving Ground, MD 21010

Dr. Thomas Whaley
Staff Member
Los Alamos National Laboratory
Group LS-1 MS M880
Los Alamos, NM 87545

CPT Christopher E. Whalley
Physiologist
US Army Institute of Dental Research
ATTN: SGRD-UDR-C
Fort George G. Meade, MD 20755

Dr. William E. White, Jr.
Physical Scientist
Research Division
Chemical Research and Development
Center
ATTN: DRSMC-CLB-TA(A)
Aberdeen Proving Ground, MD 21010

Nancy E. Whorton
Research Physiologist
Walter Reed Army Institute of
Research
Washington, DC 20307

COL George Thomas Wier
IMA to HQ USAF/SGN
ATTN: HQ USAF/SGN
Bolling Air Force Base, DC 20332

Gersham Wilkerson
Biological Lab Technician
Physiology Branch
US Army Medical Research Institute
of Chemical Defense (USAMRICD)
ATTN: SGRD-UV-YP
Aberdeen Proving Ground, MD 21010

Dr. Carl E. Williams
Naval Aerospace Medical Research
Laboratory
Naval Air Station
ATTN: NAMRL Code 24
Pensacola, FL 32508

Harold L. Williams
Supervisory Research Chemist
Department of Hematology
Walter Reed Army Institute of
Research
Washington, DC 20307

Dr. Andrew Williamson
Research Assistant
Department of Pharmacology
Uniformed Services University
of the Health Sciences
4301 Jones Bridge Road
Bethesda, MD 20814

Michael L. Williamson
Physical Scientist
Chemical and Biological Detection
and Alarms Division
Chemical Research and Development
Center
ATTN: DRSMC-CLC-B
Aberdeen Proving Ground, MD 21010

Dr. J. Henry Wills
Visiting Professor, Department of
Pharmacology
Uniformed Services University
of the Health Sciences
4301 Jones Bridge Road
Bethesda, MD 20814

CPT Robert A. Wirtz
Research Entomologist
Department of Entomology
Walter Reed Army Institute
of Research
Washington, DC 20307

Dr. Donald T. Witiak
Professor of Medicinal Chemistry
Director of the Pharmaceutical and
Toxicological Research Institute
The Ohio State University
441 McCampbell Hall
1580 Cannon Drive
Columbus, OH 43210-1205

Dr. Alan D. Wolfe
Biochemist
Division of Biochemistry
Walter Reed Army Institute of
Research
ATTN: SGRD-UWG
Washington, DC 20307

Dr. Otto L. Wolthuis
MD PLD
TNO Medical Biological Lab
Lange Kleiweg 139
Rijswijk (2M)
The Netherlands

Dr. Arthur A. Woodward, Jr.
Research Physiologist
US Army Human Engineering Laboratory
ATTN: DRXHE-IS
Aberdeen Proving Ground, MD 21005

Dr. Daniel L. Wu
Physical Scientist
Systems Development Division
Chemical Research and Development
Center
ATTN: DRSMC-CLY-A(A)
Aberdeen Proving Ground, MD 21010

Ronald E. Yates
Research Physiologist, HEG
US Air Force Aerospace Medical
Research Laboratory
ATTN: AFAMRL/HEG
Wright-Patterson Air Force
Base, OH 45433

Dr. Homer Ren Yeh
Research Chemist
Chemical and Biological Detection
and Alarms Division
Chemical Research and Development
Center
ATTN: DRSMC-CLC-B(A)
Aberdeen Proving Ground, MD 21010

Dr. Edmund Yodlowski
Assistant Professor
Department of Anesthesiology
University Physicians Foundation,
Inc.
956 Court Street
Coleman Building, Room 2C24
Memphis, TN 38103

Diane Zehupfennig
Reference Librarian
Wood Technical Library
US Army Medical Research Institute
of Chemical Defense (USAMRICD)
ATTN: SGRD-UV-AW
Aberdeen Proving Ground, MD 21010

Distribution

Names	Copies	Names	Copies
Commander US Army Medical Research and Development Command Fort Detrick Frederick, MD 21701	2	Commander US Army Medical Research Institute of Infectious Diseases Fort Detrick Frederick, MD 21701	1
HQDA(DASG-HCD) WASH DC 20310	1	Commander US Army Research Institute of Environmental Medicine Natick, MA 01760	1
Superintendent Academy of Health Sciences ATTN: AHS-COM Fort Sam Houston, TX 78234	1	Commander US Army Medical Bioengineering Research & Development Laboratory Fort Detrick, MD 21701	1
Assistant Dean Inst & Rsch Support Uniformed Services University of Health Sciences 6917 Arlington Road Bethesda, MD 20014	1	Commander US Army Aeromedical Research Laboratory Fort Rucker, AL 36362	1
US Army Research Office ATTN: Chem & Bio Sci Div P.O. Box 1221 Research Triangle Park, NC 27709	1	Commander Letterman Army Institute of Research Presidio of San Francisco, CA 94129	1
Biological Science Division Office of Naval Research Arlington, VA 22217	1	Commander Naval Medical Research Institute National Naval Medical Center Bethesda, MD 20014	1
Director of Life Sciences USAF Office of Scientific Research (AFOSR/C) Bolling AFB WASH DC 20332	1	Commander USAF School of Aerospace Medicine Aerospace Medical Division Brooks AFB, TX 78235	1
Director Walter Reed Army Institute of Research WASH DC 2037	1	Commander US Army Training and Doctrine Command ATTN: ATMD Fort Monroe, VA 23651	1
Commander US Army Chemical School ATTN: ATZN-CM-AS/J. Swisher Fort McClellan, AL 36205	1		

Names	Copies	Names	Copies
Commander	1	Commander	1
Naval Air Development Center		US Army Nuclear and Chemical	
ATTN: Dr. R. Helmbold (Code		Agency	
2012)		Fort Belvoir, VA 22060	
Warminster, PA 18974			
Commander	1	US Army Research and	1
Chemical Research and		Standardization Group (Europe)	
Development Center		ATTN: DRXSN-UK-RC	
ATTN: DRDAR-CLB	1	Box 65	
ATTN: DRDAR-CLB-C	1	FPO New York 09510	
ATTN: DRDAR-CLC	1		
ATTN: DRDAR-CLD	1	Defense Technical	12
ATTN: DRDAR-CLJ-L	1	Information Center	
ATTN: DRDAR-CLP	1	ATTN: DTIC-DDA-2	
ATTN: DRDAR-CLY	1	Cameron Station, Bldg 5	
		Alexandria, VA 22314	
Commander	1		
US Army Medical Research		Commander	1
Institute of Chemical Defense		US Army Armament Research	
ATTN: SGRD-UV-ZB	1	and Development Command	
ATTN: SGRD-UV-XO	1	ATTN: DRDAR-TSS	
ATTN: SGRD-UV-AO	10	Dover, NJ 07801	
ATTN: SGRD-UV-AW	1		
ATTN: SGRD-UV-CM	1	Director	1
ATTN: SGRD-UV-D	1	US Armed Forces Medical	
ATTN: SGRD-UV-P	1	Intelligence Center	
ATTN: SGRD-UV-V	1	Fort Detrick	
ATTN: SGRD-UV-Y	1	Frederick, MD 21701	
(AUTHOR COPIES)	5		
Office of Under Secretary	1	Director	1
For Defense (R&E)		US Army Material Systems	
ATTN: Mr. T. Dashiell		Analysis Agency	
Pentagon		Aberdeen Proving Ground, MD 21005	
Wash DC 20301			